ECSS-E-HB-32-20 Part 3A
20 March 2011

Space engineering

Structural materials handbook - Part 3: Load transfer and design of joints and design of structures

NOTE:
This pdf-file does not contain automatic cross-references. To make use of the cross-references please use the MS Word version of this document.

ECSS Secretariat
ESA-ESTEC
Requirements & Standards Division
Noordwijk, The Netherlands

Foreword

This Handbook is one document of the series of ECSS Documents intended to be used as supporting material for ECSS Standards in space projects and applications. ECSS is a cooperative effort of the European Space Agency, national space agencies and European industry associations for the purpose of developing and maintaining common standards.

This handbook has been prepared by the ECSS-E-HB-32-30 Working Group, reviewed by the ECSS Executive Secretariat and approved by the ECSS Technical Authority.

Disclaimer

Published by: ESA Requirements and Standards Division
ESTEC, P.O. Box 299,
2200 AG Noordwijk
The Netherlands

Change log

ECSS-E-HB-32-20 Part 3A 20 March 2011	First issue

Table of contents

Figures

Tables

Introduction

The Structural materials handbook, ECSS-E-HB-32-20, is published in 8 Parts.

A glossary of terms, definitions and abbreviated terms for these handbooks is contained in Part 8.

The parts are as follows:

Part 1	Overview and material properties and applications	Clauses 1 - 9
Part 2	Design calculation methods and general design aspects	Clauses 10 - 22
Part 3	Load transfer and design of joints and design of structures	Clauses 23 - 32
Part 4	Integrity control, verification guidelines and manufacturing	Clauses 33 - 45
Part 5	New advanced materials, advanced metallic materials, general design aspects and load transfer and design of joints	Clauses 46 - 63
Part 6	Fracture and material modelling, case studies and design and integrity control and inspection	Clauses 64 - 81
Part 7	Thermal and environmental integrity, manufacturing aspects, in-orbit and health monitoring, soft materials, hybrid materials and nanotechnoligies	Clauses 82 - 107
Part 8	Glossary	

23
Inserts

23.1 Introduction

An insert is a fixation device for honeycomb sandwich panel structures. A conventional or standard potted insert system consists of three main components:

Insert + Sandwich structure + Potting mass

Non-standard types of inserts have also been developed, Ref. [23-3].

This chapter provides an introduction to the various types of inserts along with some basic guidelines for their use. It does not provide detailed design information, because this is available in a separate handbook.

[See: ECSS-E-HB-32-22 - Insert design handbook]

23.2 Features of inserts

23.2.1 Basic description

An insert is a fixation device which enables joining of:

- Honeycomb sandwich structures,
- Other structural parts, e.g. frames, profiles, brackets.
- Equipment, e.g. mounting of boxes, feed lines, cable ducts.

A conventional 'standard' insert system has three main components:

- Removable part: a screw or another threaded element.
- Insert: a nut like part fixed to the honeycomb structure.
- Potting compound: a means of coupling the insert to the honeycomb structure; normally an epoxy-based compound.

[See: ECSS-E-HB-32-22 - Insert design handbook]

23.2.2 Types of inserts

23.2.2.1 General

There are three types of insert which are distinguished by the method of integration into the honeycomb sandwich structure; as shown in Table 23.2.1. These are:

- Group A for simultaneous bonding during sandwich production;
- Group B for fixing into an existing sandwich using a thermosetting resin, e.g.:
  - usual potting process of standard inserts.
  - an equivalent bonding procedure for non-standards inserts, e.g. for carbon-fibre tube inserts.
- Group C for mechanical clamping or screwing into an existing sandwich.

Table 23.2-1 - Types of inserts

Type	Shape	Diameter (mm)	Material	Potting Considerations	Torque Locking	Thread Locking	Floating Nut Exchange Capability	Standards	Comments
Type A: Bonding during sandwich manufacture									
1	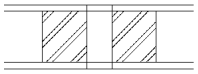	17 to 30	Al	Full bonded with core filler	None or square shape	e.g. Locktite	No	-	The bore hole is drilled after sandwich bonding. Only for small core height.
Type B: Potting (or equivalent non-standard procedure)									
2	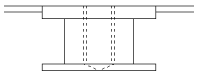	11 to 22	Al (St) (Ti)	Partially or fully potted	Planes or riffles	Deformation of tread	No	NAS 1832 NSA 5135 PA 3825 ENN 3GG/386	Al insert can be used with St or Ti screws. Most common type.
3	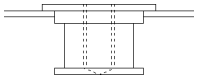	11 to 22	Al (St) (Ti)	Partially or fully potted	Planes or riffles	Deformation of tread	No	-	Rarely used
4	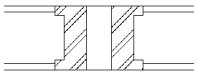	11 to 14	Al	Fully potted only	Planes or riffles	e.g. Locktite	No	NAS 1832 TAN 16489 PAN 3827 NSA 5071	Available with and without thread.
5	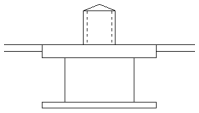	6 to 14	St Ti	Partially or fully potted	Planes or riffles	e.g. Locktite	No	ERNO No. R 000/095.00 0	Rarely used.
6	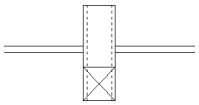	3 to 6	St Ti	Partially or fully potted	Planes or riffles	e.g. Locktite	No	-	Only for very low loads. Rarely used.
7	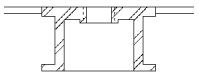	19 to 70	Al	Partially or fully potted	Planes or riffles	e.g. Locktite	No	-	For high loads
8	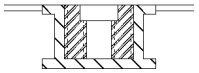	19 to 25	Al: Insert Ti: Nut	Partially or fully potted	Planes or riffles	Deformation of thread	Yes	NAS 1835 PAN 3829 ENN 379 NSA 5072	Extended and heavy type for applying floating nuts and exchanging capacity.
9		7 to 20	CFRP / Al	Carbon fibre tube bonded into core	N/A	e.g. Locktite, helicoils.	No	No	Carbon fibre tube inserts
10	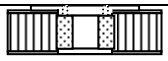	-	-	-	-	-	-	-	Bonded flange inserts
Type C: Mechanically clamped or screwed									
11	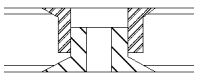	14 to 22	Al (St) (Ti)	-	Adhesive bonding	Deformation of thread	No	TAN 16485	Low pull-out strength, if no connection with core.
12	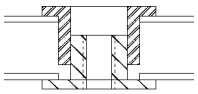	14 to 22	Al (St) (Ti)	-	Adhesive bonding	-	No	-	-

Key: St: steel; Ti: titanium; CFRP: carbon fibre-reinforced plastic

23.2.2.2 Type A: Bonding during sandwich manufacture

These inserts are used only in thin sandwich structures, i.e. small core height, and can be applied only where there is no particular locking requirement. Furthermore, it is difficult to precisely place the insert for connection purposes. Therefore, a greater diameter insert is generally selected to allow for drilling and thread cutting within a margin of 3 mm to 6 mm from the insert axis.

23.2.2.3 Type B: Potting into an existing sandwich

Inserts potted by curing of epoxy resin are the most important group and are widely used in space structures.

Non-standard alternatives, in which the normal potting is replaced by an equivalent bonding procedure, are also available, e.g. carbon-fibre tube inserts developed by DLR and used for the Rosetta Lander.

23.2.2.4 Type C: Mechanical fastening into an existing sandwich

Mechanically fastened inserts have significant disadvantages:

- no direct connection with the sandwich core giving low load-carrying capability.
- an individual adapted size for each core height.
- torque can be transferred by adhesive bonding only.

23.2.3 Inserts for honeycomb sandwich structures

23.2.3.1 General

The majority of inserts used in sandwich panels are standard commercially-available items. Non-standard inserts are used to meet a particular project demand, such as the strict mass budget on Rosetta Lander. Other non-standard types of inserts also exist, [See also: 26.8].

Figure 23.2.1 compares a standard potted insert with an example of a non-standard ‘carbon-fibre tube insert’.

A: Standard potted insert:

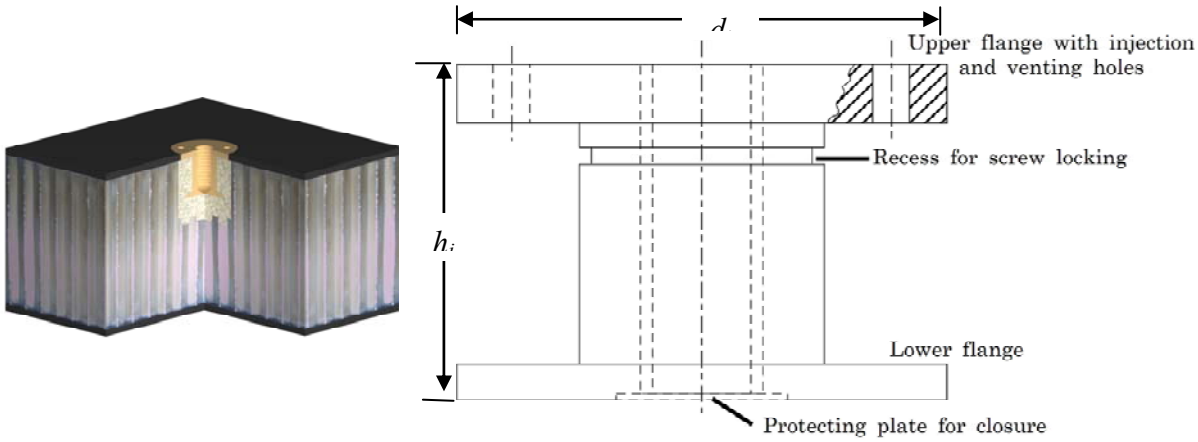

B: Non-standard insert (example):

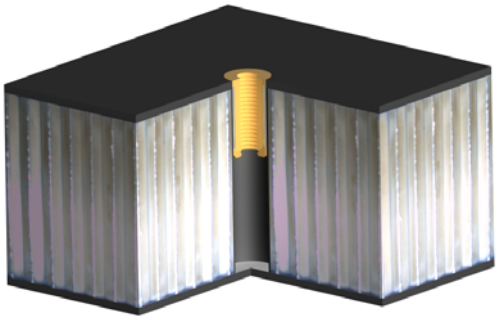

Carbon-fibre tube insert (developed by DLR)

Figure 23.2-1 - Inserts for honeycomb sandwich structures

23.2.3.2 Standard potted inserts

The standard configuration consists of a hollow cylindrical body closed by two discs (flanges) at both ends. Both the flanges provide a form- locking connection with the resin. Applied loads are transferred only by adhesion shear forces between the resin and insert. The upper flange has two bore holes, one for the injection of the potting resin and the other for venting purposes. The cylindrical section and the lower flange have a riffled surface, or the lower flange is faced on two opposite sides. Both features increase the shear load capability when the insert is subjected to a torsional moment. A thin circular sheet in the lower flange protects the thread from resin penetration during the potting procedure. A recess in the upper region of the cylindrical body enables the thread to deform by applying local compression forces on two opposite sides. This is to assure self locking of the mated screw.

23.2.3.3 Non-standard 'carbon-fibre tube inserts'

Developed by DLR for use on the Rosetta Lander, in 2003-04 they were investigated more thoroughly in the course of an ESA-funded study, Ref. [23-3].

The load introduction from the metallic insert part into the sandwich is not performed by conventional epoxy resin potting, but by means of an extremely stiff, thin-walled carbon fibre tube which fits exactly between the face sheets and is bonded to the honeycomb core by a epoxy adhesive layer. This adhesive layer can be relatively thin. Only a small amount of resin is needed to ensure good contact with the surrounding cell walls of the honeycomb core. However, the full length of the (extremely stiff) carbon fibre tube actively contributes to the shear load transfer into the (much softer) honeycomb core, because the tube always goes through the whole sandwich thickness. The form-locking contact under both face sheets makes the sandwich in the vicinity of the insert practically incompressible.

The carbon fibre tube contains unidirectional high-modulus carbon fibres and is slit lengthways during manufacture. This enables folding or overlapping to reduce the diameter for feeding it through the borehole in the face sheet. After placement, the carbon fibre tube is spread and aligned by means of a simple tool, so that the ends of the tube fit just underneath the face sheets. The inner radius of the tube is identical with the bore hole radius of the face sheets.

After curing of the adhesive, the carbon fibre tube is ready for fitting of one or two metallic insert caps. There are two basic developed types, i.e. replacement for conventional through-the-thickness insert or for the conventional potted insert, Ref. [23-3].

23.2.4 Sizes of inserts

23.2.4.1 General

There are a wide variety of sizes, shapes and dimensions available because inserts were developed separately in various countries by different companies. The products can be grouped as:

- Commercially available, which are standard specified items, e.g. Shur-lok range.
- Non-standard, which are designed and manufactured ‘in-house’ for a particular project applications.

23.2.4.2 Standards

Many inserts have been qualified to meet company standards, project-related standards or, after approval by national airworthiness authorities, national standards. Examples of some of the standards are given in Table 23.2.2

Table 23.2-2 - Summary list of standcrds for inserts

National Aerospace Standard	NAS	1832 1833 1835 1836 1837
Deutsches Institut für Normung	DIN	65187 65188 65189 65190 65191 65192 65193
Transall-Norm	TAN	16487 16488 16489 16490
Panavia-Standard	PAN	3825 3826 3827 3828 3829
Deutsche Airbus-Norm	DAN	214
Normalisation Sud Aviation	NSA	5345 5074
ERNO-Norm	ENN	366 377 379 386 398

23.2.5 Design parameters

The most important parameters to consider for strength are:

- Insert overall diameter (d_i)
- Insert overall height (h_i)

Insert diameter and height are stated in manufacturers' product literature. Figure 23.2.2 shows standardised insert heights plotted as a function of standardised insert diameters. The dashed lines denote examples of linear dependencies.

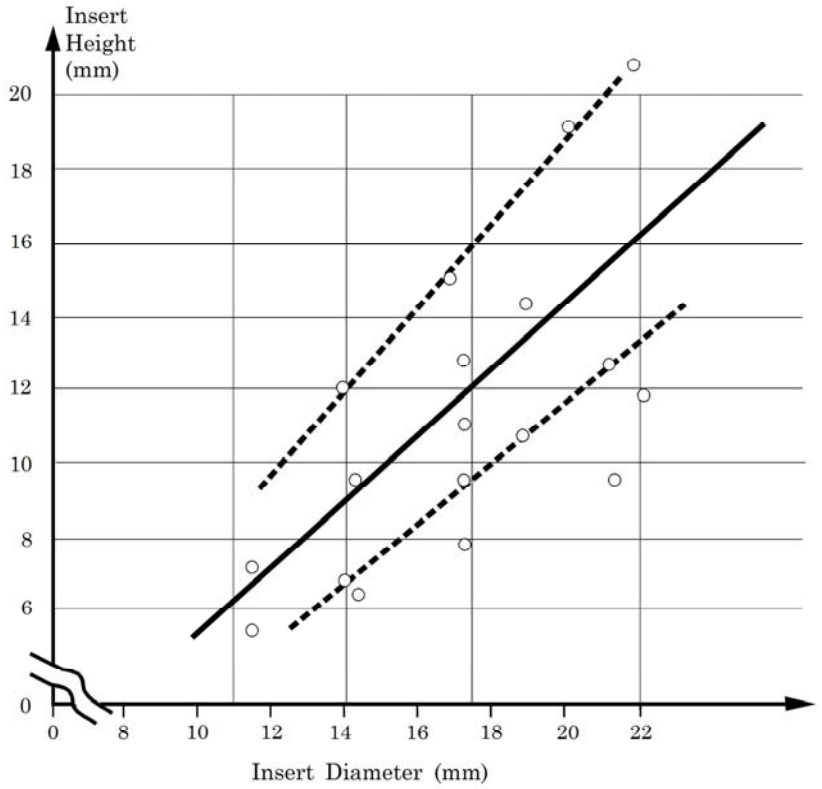

Figure 23.2-2 - Determining the preferred insert height

To determine a recommended insert height, first select the appropriate diameter. The height, in whole millimetres, is taken from the value where the straight line crosses the chosen diameter.

23.2.6 Typical insert materials

23.2.6.1 Aluminium alloys

Inserts are usually made from aluminium alloy 2024 (DIN AlCuMg2) in T4 or T6 condition, i.e. solution heat-treated and naturally or artificially aged. Some comparable material designations are shown in Table 23.2.3.

Table 23.2-3 - Insert material: Aluminium alloys specifications

Germany	3.1354 -T42 or -T62	Werkstoff-Leistungsblatt
USA	2024-T4	QQ-A-200/3D
	2024-T6 or -T62	QQ-A-225/6D
U.K.	3L65	BS
France	A-U4G1	Air 9050/C
Italy	PAC 4,5 GM	UNAVIA 811-02

[See: Table 23.2.4 for other materials]

23.2.6.2 Other materials

Where improved strength or special locking properties are needed, Ti-6Al-4V titanium alloy is used in a solution treated and aged condition.

Steel inserts also exist but are always cadmium plated and as such are not permitted in spacecraft structures due to sublimation problems which can arise in thermo vacuum, [See: ECSS-Q-70-71]. Therefore, carbon steels are replaced by austenitic stainless steels, e.g. AISI 303 or 1.4305 (DIN 17007).

Table 23.2.4 lists some typical insert materials.

Table 23.2-4 - Typical insert materials

Insert Materials			
Designation	**Applicable Specifications**	**Applied Surface Protection**	**Characteristic Properties**
Aluminium Alloys			
AlCuMg2: Condition:T4 or T6 (heat treated and aged naturally or artificially)	3.1354. Condition:T42 or T62 Werkstoff Leistungsbiatt	Anodised e.g. LN 9368 Code 20205 MIL-A-8625C	
	2024-T4. Condition:T4, T6 or T62 QQ-A-200/30		
AlMgSiCu soft annealed temper	AA 6051	Chromated	
Titanium Alloys			
TiAl6V4 solution treated and aged		Normally not necessary. For special cases anodised	
Steel			
Carbon steel	AISI 1137	Cadmium plated	Not allowed in spacecraft structures †
Stainless steel	AISI 303	Passivated LM 9368	

Key: † Sublimation of cadmium in space environment.

Other factors to consider are:

- The use of materials with better temperature resistance than aluminium provides no advantage if the insert is potted using an epoxy resin, i.e. the resin fails at temperatures much lower than the insert can withstand.
- It is also unreasonable to select an insert material of higher strength than aluminium, since the strength of the system is limited by the strength of the epoxy.
- Inserts with changeable floating nuts offer the possibility to apply a higher strength material for the nut operating in the aluminium housing.
- On the bottom side of the lower flange, the bore with the internal thread is closed by a thin flat shim or a cup both made out of aluminium alloy AlMgSiCu, i.e. AA 6061, in a soft annealed temper.

23.2.7 Surface protection for inserts

23.2.7.1 General

All inserts need surface protection to avoid corrosion. This protection is especially important for inserts in a honeycomb sandwich structure with CFRP facings.

23.2.7.2 Anodising of aluminium inserts

The housings made from 2024 aluminium alloy (AlCuMg2) are treated by an anodising process such as that specified, for example, in LN 9368, Code No. 202 or MIL A8625 C.

By a galvanic treatment in a sulphuric acid bath, a 10µm to 15µm thick aluminium oxide layer is produced which is hard, electrically non conductive and protects the insert from corrosive attack.

The housing, plug and nut of inserts with floating and removable nuts are treated in the same manner. Covers closing the bore hole are chromated, as per MIL C 5541, Class 1A. When a cup is applied for closure purposes, both inner and outer surfaces are chromated.

23.2.7.3 Titanium insert parts

Any titanium parts are normally used without surface treatment because they develop a protective oxide layer after machining.

To increase the protection against corrosion an additional coating can be applied by an anodising treatment; as given in LN 9368, Code No. 2500.

23.2.7.4 Stainless steel inserts

Stainless steel inserts are passivated according to LN 9368, Code No. 1200.

23.3 Insert design for non-metallic sandwich components

23.3.1 Basic design parameters

Generally, the procedures provided in ECSS-E-HB-32-22 - 'Insert design handbook', are considered relevant to both metallic and non-metallic sandwich elements.

For inserts used in non metallic sandwich panels, the designed mechanical properties depend on the intended loading conditions.

Different aspects relevant to the design process are summarised in Figure 23.3.1 and Table 23.3.1.

The related design principles are given in ECSS-E-HB-32-22 and Ref. [23-2].

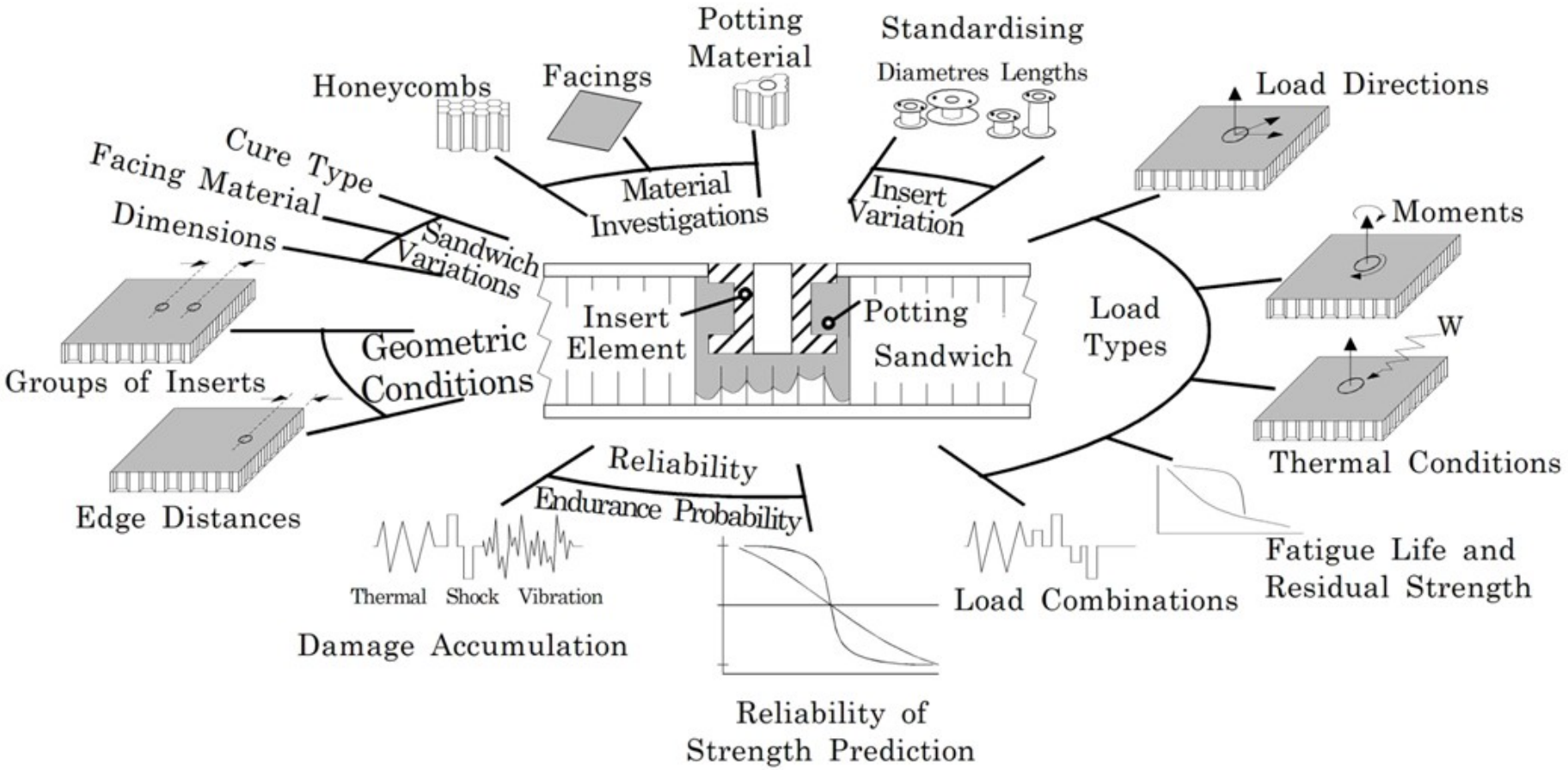

Figure 23.3-1 - Basic aspects of insert design, analysis and testing

23.3.2 Areas of concern with respect to analysis

23.3.2.1 General

In order to establish the capabilities of inserts in non metallic sandwich elements, the material data of the components of the sandwich panel to be used need to be determined as inputs to the analytical model.

The influence of the different sandwich panel elements on the insert load-carrying capability is summarised in Table 23.3.2. This shows that the different elements are not dependent on each other as regards their sensitivity to certain loads.

Table 23.3-1 - Summary of the basic insert design parameters

Geometry	Material	Loads	Primary Failure Mode	Special Conditions
Face sheet thickness	Face sheet: - aluminium - GFRP - CFRP	Mechanical loads Short time/ long time	Strength/ stability Life/remaining life	Reliability: - design - manufacture - control - testing
Core: - height - size - foil thickness	Core: - foam - Al honeycomb (e.g. 5052, 5056) - GFRP honeycomb - Nomex	Static load: - tensile - shear - torsion - bending - magnitude - direction	Core failure: - shear - normal tension - buckling by compression	
Inserts: - diameter - height - height/core†	Insert: - aluminium - steel - titanium	Dynamic load: - shock - vibration - quasi-static cycling	Face sheet failure: - shear buckling - exceedences - radial cracks by crimping	
Insert to edge distance	Potting: - glass-bubble epoxy	Conditions: - amplitude - exceedences - sequence - direction	Insert failure: - insert flange fracture - thread or screw failure	
Insert to insert distance: - same load - different load direction		Preload by: - temperature - mounting stress	Potting failure: - resin fracture (basic plane) - shear failure on cylinder	
		Thermal load: - quasi-static - dynamic		
		Physical load: - radiation - vacuum - humidity		

Key: † Height relative to core height

Table 23.3-2 - Contribution of sandwich elements to insert load carrying capability

Loading		Sandwich Elements		
Type	Direction	Core	Facing	Potting Adhesive
Load normal to plane of facings	Tension Compression	major major	little little	very little very little
Load in plane of facings	all	very little	major	very little
Moments normal to plane of facings	all	important	little	important
Moments in plane of facings	all	major	little	little

23.3.2.2 Perforated and non-perforated cores

The ultimate shear strength of perforated and non perforated core is identical in specification. Experience shows that the fatigue life of a structural element is significantly reduced if it contains defects such as cracks. Furthermore, the impact of core perforations upon fatigue life behaviour should be considered, along with the degradation of residual strength with increasing fatigue life; as shown in Figure 23.3.2, Ref. [23-2].

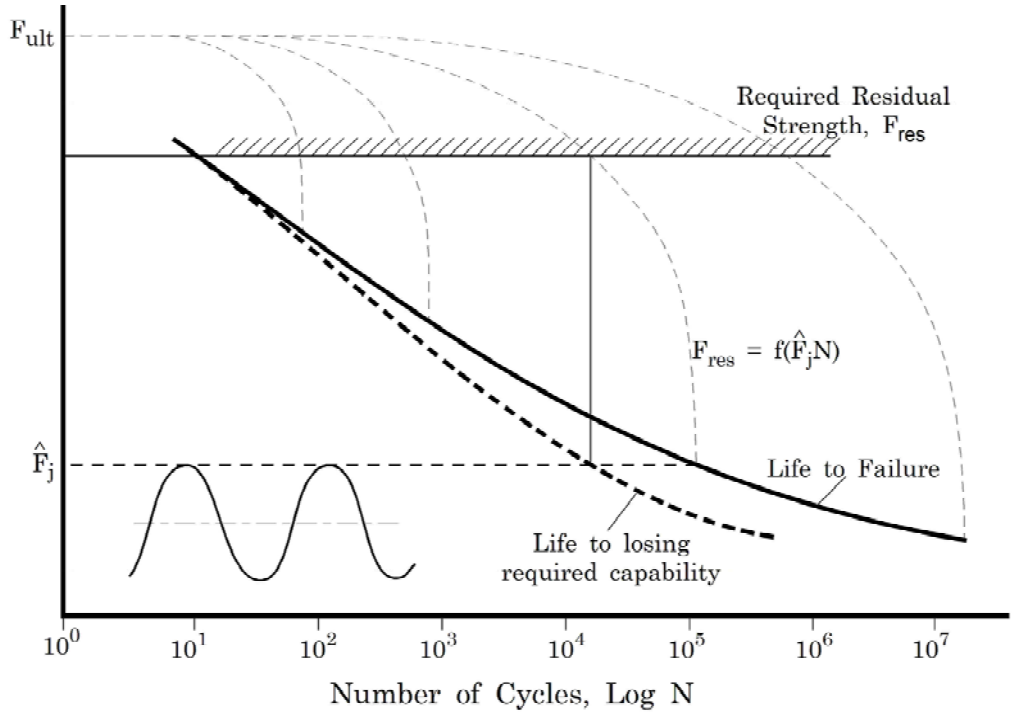

Figure 23.3-2 - Insert design: Decrease of the residual strength with life

23.3.2.3 Thermal loads

In order to decide on the acceptability of thermal loads superimposed on forces normal to the plane, an evaluation of the thermal degradation of potting strength with increasing temperature is necessary.

23.3.2.4 Torsion

The assumption that torsion applied to an insert is transferred via the core cells coupled only in a ring zone is conservative. Therefore the tolerable shear forces between the potting and the facing for insert torsion have to be considered.

23.4 Insert analysis for sandwich components

23.4.1 General

The insert itself has little effect on the performance of inserts. The load capabilities are usually limited by the:

- mechanical properties of honeycomb core, or
- face skin of the sandwich panel.

The use of non metallic materials for one or both of these sandwich elements results in different load-carrying capabilities.

23.4.2 Inserts loaded normal to the plane of facing

23.4.2.1 Stresses in the core

The load-carrying capability of inserts loaded normal to the plane is mainly determined by the core shear strength. The analytical model generated by Paul, Ref. [23-2], shows that depending upon the related stiffness of core and facings, most of the load is carried by the core. The stresses in the core created in a circular panel with a concentric insert by a load normal to the plane of the facing are shown in Figure 23.4.1.

23.4.2.2 Stresses in the facing

Owing to the small contribution of facings to the load-carrying capability of inserts under normal loads, facing stresses are not as relevant for practical applications. This is, however, limited to loads normal to plane of the facing, [See: Inserts loaded in plane of the facing].

Figure 23.4-1 - Fully potted insert: Shear stress distribution in the core depending upon radius *r*

23.4.2.3 Stresses in potting

Stresses in the potting body are usually so low that they do not become the weak link in insert design. Therefore a simplified treatment is acceptable.

The only significant stress is determined in a partially potted insert beneath the insert flange. The local stress at the edge of the lower flange is shown by a stress concentration factor K_t. This is determined by test, Ref. [23-1].

In the capability plots of ECSS-E-HB-32-22, this failure mode is marked by a cross; as shown in Figure 23.4.2. This applies only in the case of severe combinations of:

- partial potting, i.e. insert height is less than the height of core,
- small potting diameter,
- core of relatively high density.

Under elevated temperatures, the strength of the resin can degrade more rapidly than that of the aluminium core. Under those circumstances the potting can creep. The stress distribution is then expected to become smoother.

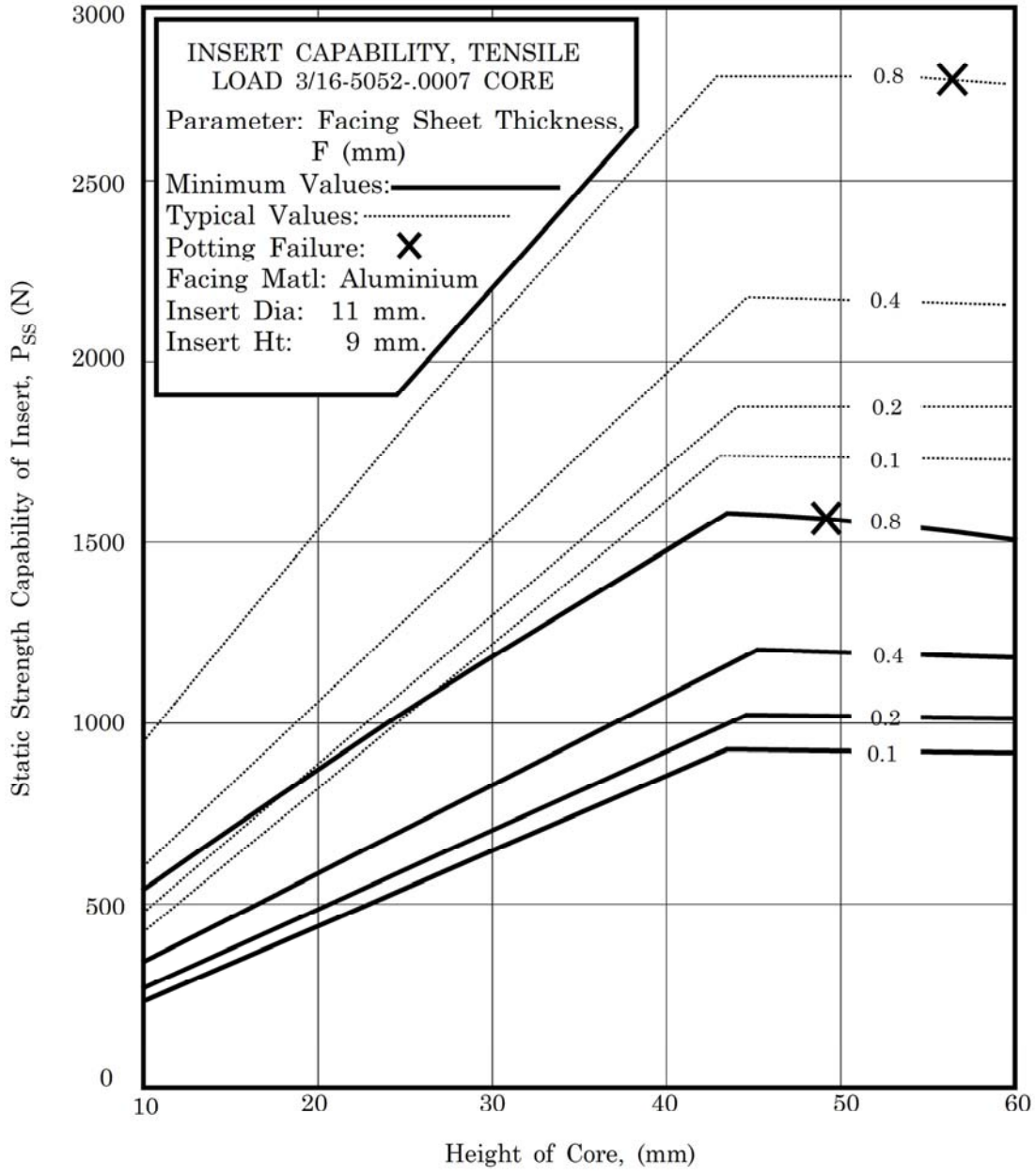

Figure 23.4-2 - Design plot from ECSS-E-HB-32-22: The relevance of failure modes

23.4.3 Inserts loaded in plane of the facing

Assuming that a panel with width w, height of core h_c, facing thickness $t_1 = t_2 = t$, containing an insert of diameter $2b_i$ (as shown in Figure 23.4.3), has the load acting on the upper facing. It is assumed to be introduced by a bearing pressure P of the insert flange against the wall of the hole in the facing.

Any coupling by the adhesive and any load introduction by tension loading on the backside of the flange of the insert are ignored.

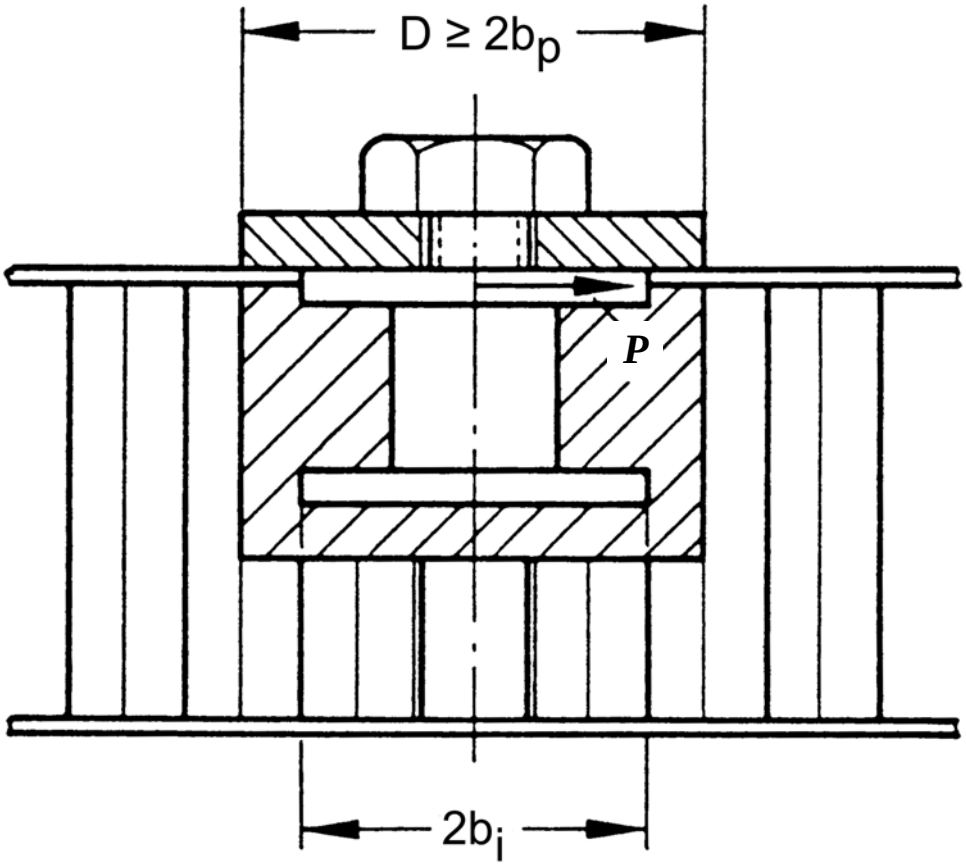

Figure 23.4-3 - Insert under in plane loading

The failures modes which should be considered are:

- Tensile failure,
- Shear-out failure,
- Dimpling failure,
- Bearing failure.

Figure 23.4.4 and Figure 23.4.5 show the results obtained by Paul, Ref. [23-1] for the ratios P/P_{test} for dimpling, bearing and net section tensile failure. Both the tensile and the compressive values are presented. The failure modes of the different laminate structures are characterised. Values greater than 1.0 indicate a margin against failure.

Figure 23.4.4 also shows that the relationships between failure modes are correct in general. The prediction of the ultimate value of the applicable failure criteria is good for laminates with fibres in 0°

direction. For laminates without 0° fibres, the criteria give values below the real failure loads. This discrepancy is extreme in the case of +45°/ 45° laminates.

Figure 23.4.5 shows the results of the failure criteria for +45°/ 45° samples. In addition the values resulting from a load resolving are plotted, Ref. [23-1]. The diagram illustrates that a clear statement in the case of multi directional laminates without 0° fibres is only possible after an exact examination of the stress distribution in front of the hole.

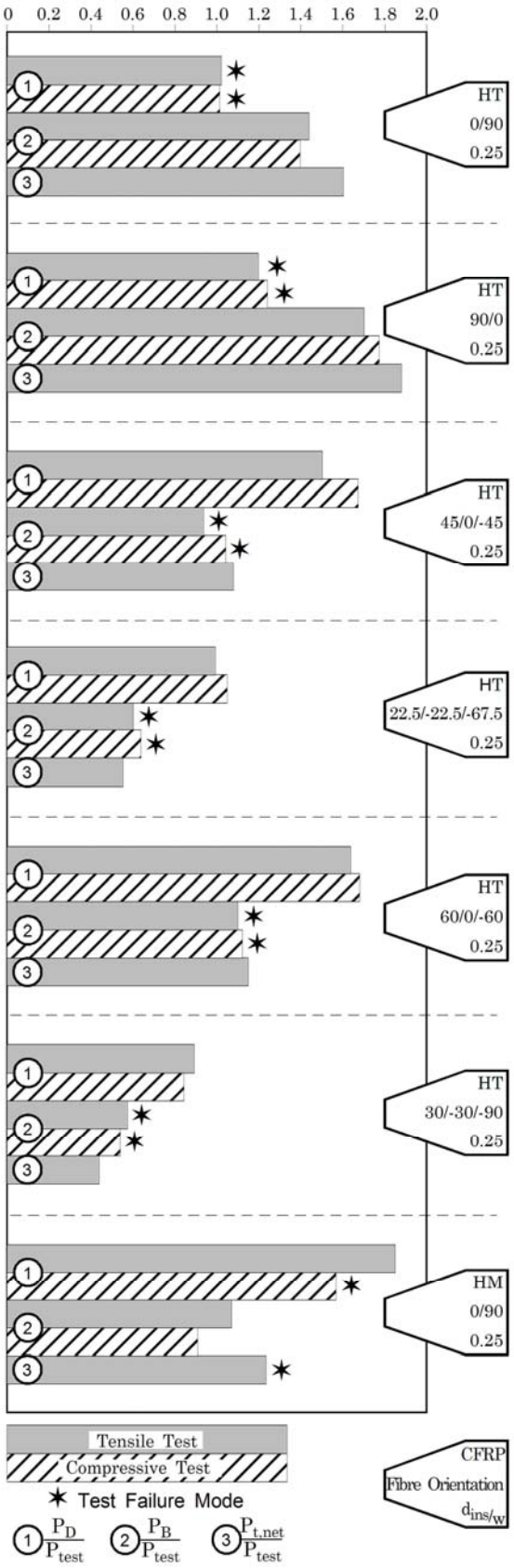

Figure 23.4-4 - Insert analysis: Predictions of the failure criteria

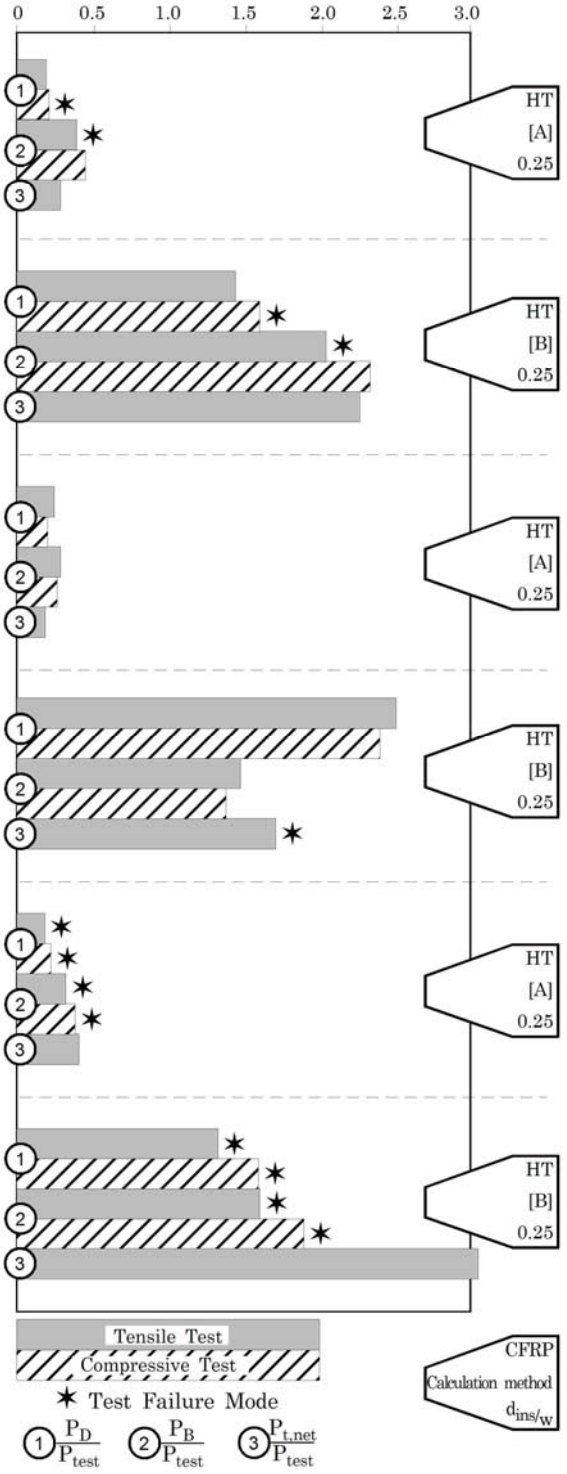

Key: Method A: See: Figure 23.4.4

Method B: with load resolved in the fibre direction.

Most of the HM samples and some of the HT compressive samples with $d_{ins}/W = 0.25$ failed by shear-out.

Figure 23.4-5 - Insert analysis: Predictions of the failure criteria for samples with fibre orientations +45°/-45°

23.5 References

23.5.1 General

[23-1] W. Hertel, W. Paul & D. Wagner
'Standardisation program on design, analysis and testing of inserts'
Final report ESA CR(P)-1498, February 1981

[23-2] W.H. Paul, D. Wagner & J. Bischoff
'Standardisation program on design, analysis and testing of inserts in non-metallic sandwich components: Final report'
ESA CR(P)-1585, December 1981

[23-3] J. Block, R. Schütze, T. Brander, K. Marjoniemi, L. Syvänen, M. Lambert: DLR Braunschweig/Helsinki Univ. Technology/Patria/ESA/ESTEC
'Study on Carbon Fibre Tube Inserts'
ESTEC Contract No. 16822/02/NL/PA, (2004)

23.5.2 ECSS documents

[See: ECSS website]

ECSS-E-HB-32-22	Insert design handbook; previously ESA PSS-03-1202
ECSS-Q-70-71	Data for the selection of space materials and processes; previously ESA PSS-01-701

24
Load introduction elements

24.1 Introduction

24.1.1 Composite links

A good example of the use of such links is their application as the suspension chain for the support of a helium tank used in the GIRL 'German Infrared Laboratory' satellite, Ref. [24-5].

[See: 24.2]

24.1.2 Shear load elements

Spider elements are used as structural elements for the introduction of loads into light sandwich structures, e.g. solar generator panels.

[See: 24.4]

24.2 Composite links

24.2.1 Basic description

24.2.1.1 Materials

The composite links described are either:

- Homogeneous, comprising of one type of reinforcement fibre, i.e. GFRP (E glass), CFRP (HT or HM fibres) or ARP (aramid).
- Hybrid, having more than one type of reinforcement, i.e. an outer layer of CFRP (HT or HM) with an inner layer of GFRP.

24.2.1.2 Tensile and compressive behaviour

The static behaviour of some unidirectional fibre/epoxy links under tensile and compressive loads is considered for the external-to-internal radius ratio, R_o/R_i of 1.2, 1.35, 1.55, 2.0, 2.5 and 3.0.

Figure 24.2.1 provides a definition of terms.

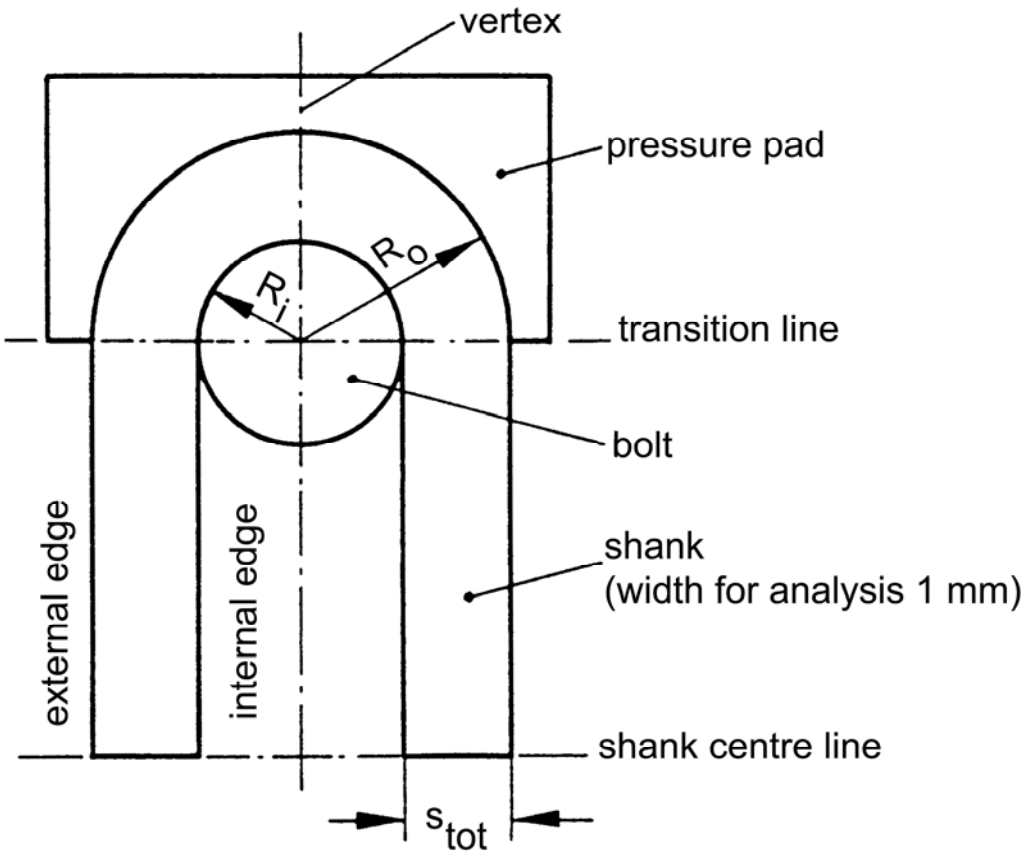

Figure 24.2-1 - Composite link: Tensile or compression loaded

Depending on the radius ratio, the stress concentration factors on the internal and external edge of the link are plotted. Furthermore, tension and compression loaded hybrid links are considered for different radius ratios.

Links and modified links are also detailed in Ref. [24-1], [24-2], [24-3], [24-4].

24.3 Analysis of composite links

24.3.1 Analytical notation

R_o external radius of the link

R_i internal radius of the link

s thickness of internal layer (hybrid links)

s_{tot} total thickness

Δ_x displacement in shank centre

σ_{max} maximum tangential stress

σ_1 normal stress in the unidirectionally reinforced laminate parallel to the material axis (x^1).

σ_m $$\text{average stress} = \frac{\text{tensile (or compression) load}}{\text{cross - sectional area}}$$

U $$\text{stress concentration factor} = \frac{\text{maximum tangential stress } (\sigma_{\max})}{\text{average stress } (\sigma_m)}$$

E_1 Young's modulus of a ply in fibre direction

E_2 Young's modulus of a ply transverse to fibre direction

G_{12} in-plane shear modulus of the ply

ν_{12} Poisson's ratio of ply (when loaded in x-direction)

P_f ultimate strength of tensile-loaded link

24.3.2 Stress distribution in unidirectional composite links

24.3.2.1 General

Table 24.3.1 lists elastic moduli used for the static analysis by a finite element method.

Table 24.3-1 - Composite link analysis: Unidirectional properties of fibre reinforced plastics

Material	E_1 Nmm^{-2}	E_2 Nmm^{-2}	G_{12} Nmm^{-2}	ν_{12}
GFRP (E-Glass)	46 100	13 100	4 360	0.290
AFRP (Aramid: Kevlar 49)	81 200	5 540	3 600	0.368
CFRP (HT) (Toray T 300 A)	139 000	9 690	4 640	0.308
CFRP (HM) (Thornel 75S)	331 000	4 920	3 970	0.356

Key: Fibre/epoxy volume fraction (Vf): 60%

The load is introduced by a bolt for the tensile loaded link, and by a pressure pad for the compression loaded link, [See: Figure 24.2.1]. The friction between bolt or pressure pad and link is not considered.

24.3.2.2 Homogeneous links

Calculation shows that for links with a high radius ratio, R_o/R_i, which show high radial loading in the region of the load introduction, a substantial strength increase can be reached by an efficient lateral support in the area of high radial pressure, e.g. by shims. This prevents a premature failure due to delamination.

For the tensile- and compression loaded links consisting of only one material, very high stress concentrations, U, are found for large radius ratios, R_o/R_i, especially if stiff fibres, i.e. high E_1/E_2, are used. Therefore high loads can be carried by these links only if the radius ratio, R_o/R_i, is reduced.

The tangential stress distribution of composite links are shown in Figure 24.3.1 for tensile loaded links; Figure 24.3.2 for compression loaded links and Figure 24.3.3 for tensile- and compression-loaded links.

[See also: Figure 24.3.6 for stress concentration factors under tensile loading and Figure 24.3.7 for stress concentration factors under compression loading]

The load capacity of the compression loaded link is higher than for tensile links. Only links with aramid fibre, Kevlar™ 49, are an exception, because of the poor compression strength of this fibre.

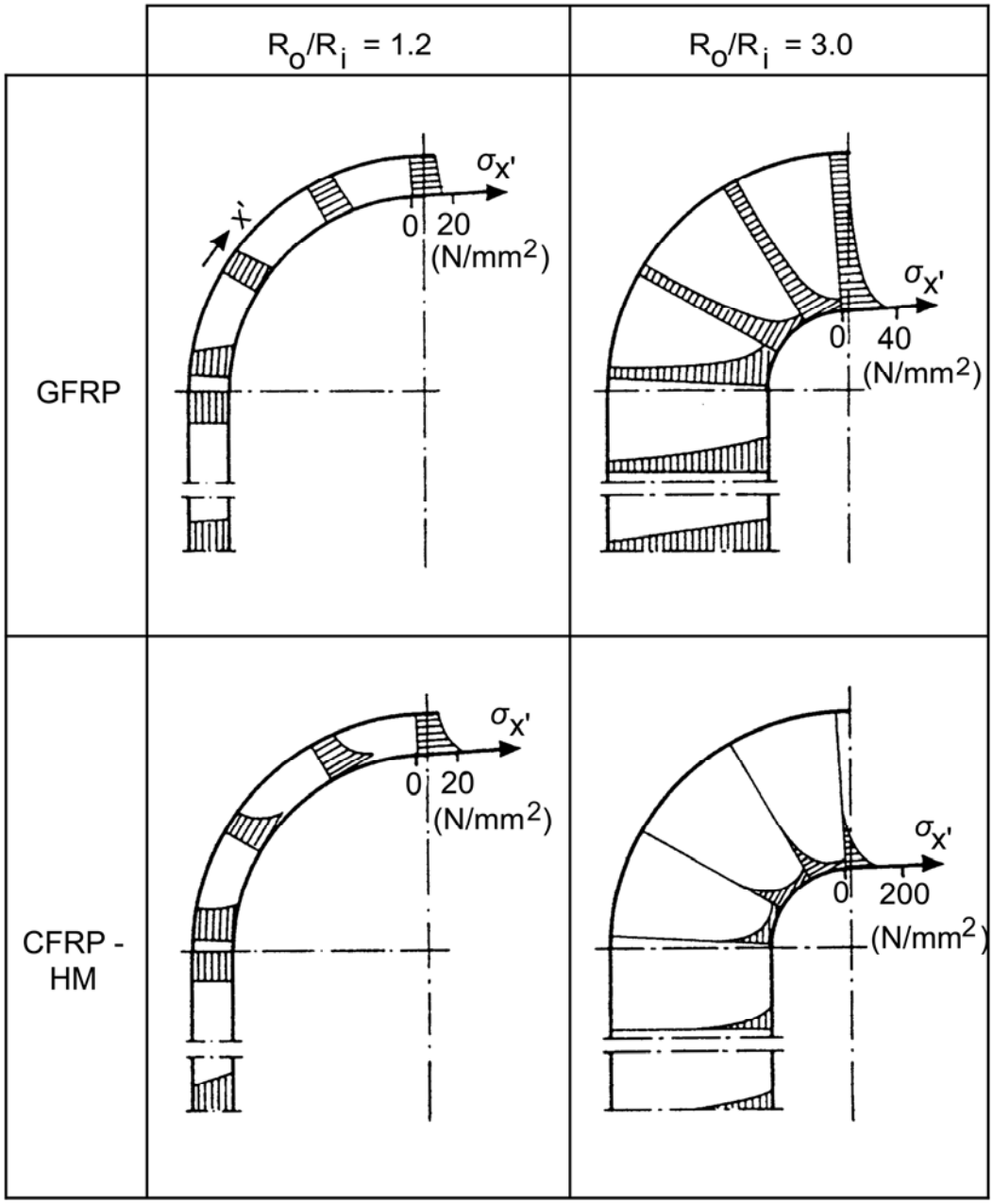

σ_m = 15 N mm^{-2}

Figure 24.3-1 - Composite links: Tangential stress distribution of tensile loaded GFRP and CFRP HM

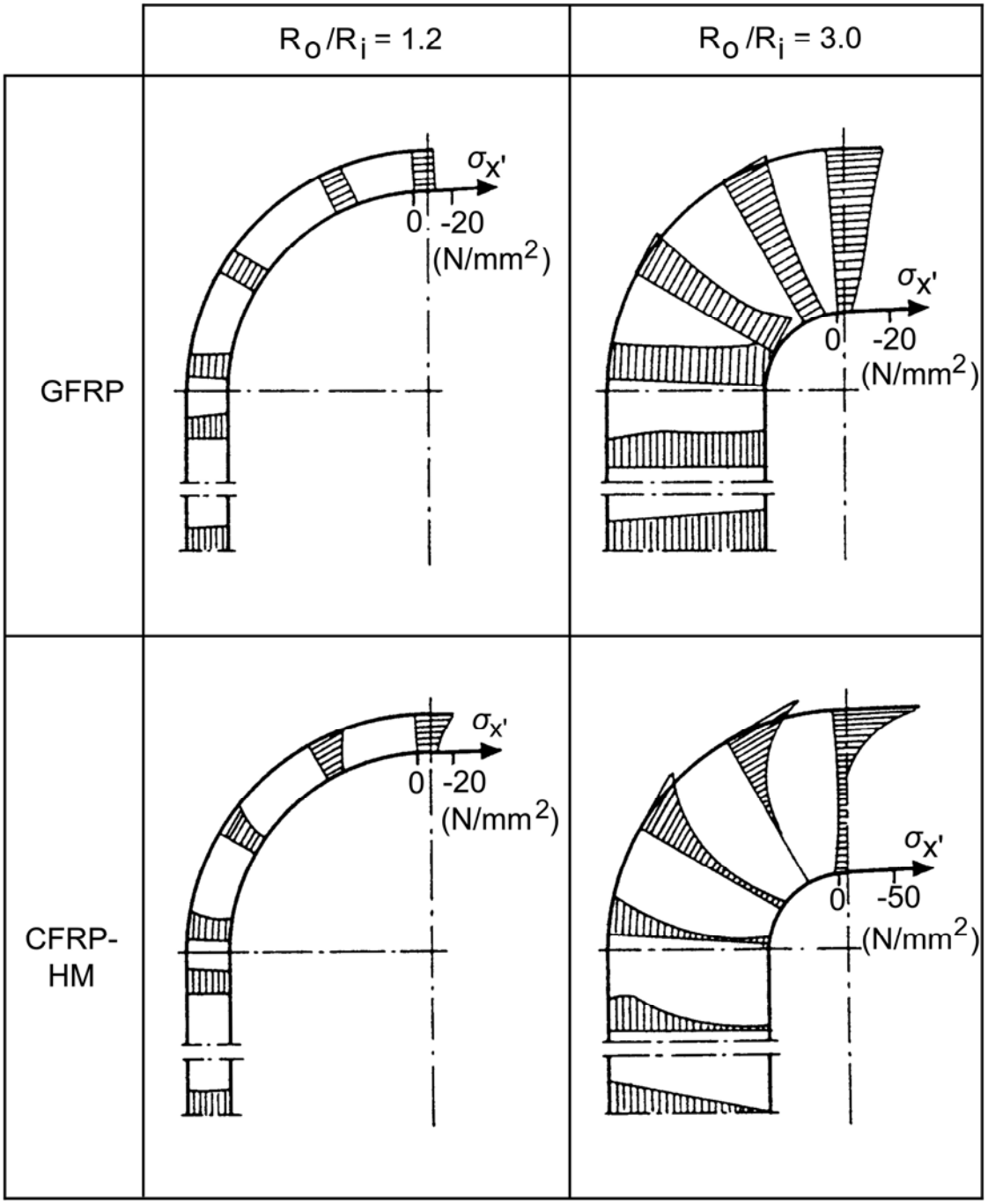

Figure 24.3-2 - Composite links: Tangential stress distribution of compression loaded GFRP and CFRP HM

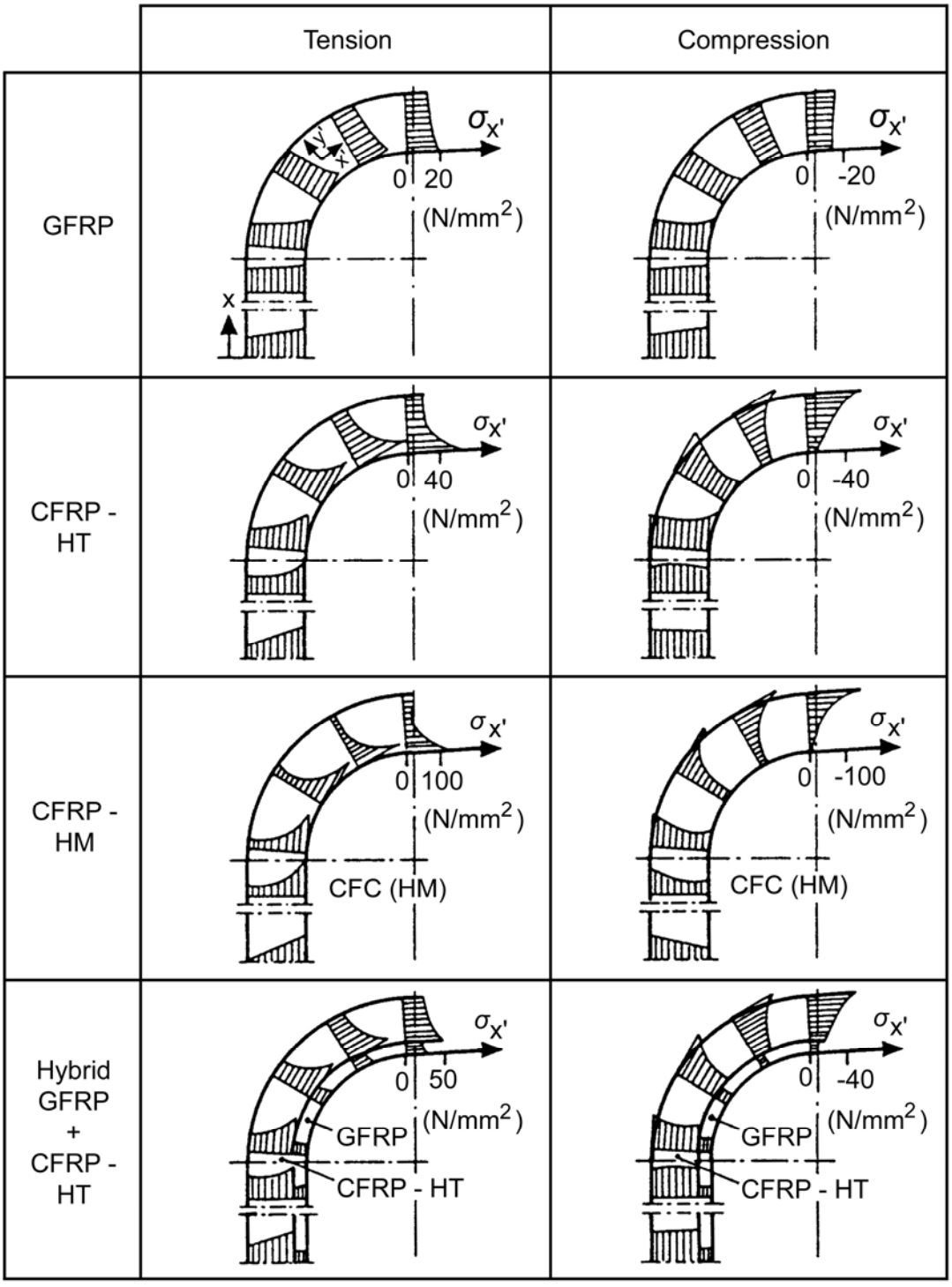

R_o/R_i = 1.55; Δ_x = -03 mm

Figure 24.3-3 - Composite links: Tangential stress distribution of tensile and compression loaded links

24.3.2.3 Hybrid links

In order to increase the tensile load capacity for a highly-stressed link with constant radius ratio R_o/R_i, fibres with low E_x are placed at the internal edge to reduce the high tension. The portion of the internal layer is expressed by the thickness relation S/S_{tot}.

The hybrid construction is especially useful for links with stiff fibres and high radius ratios. Depending on radius ratio and fibre type, there is a distinct thickness ratio which yields the highest possible load-carrying capacity. These optimal thickness ratios of different material combinations are shown in Figure 24.3.4.

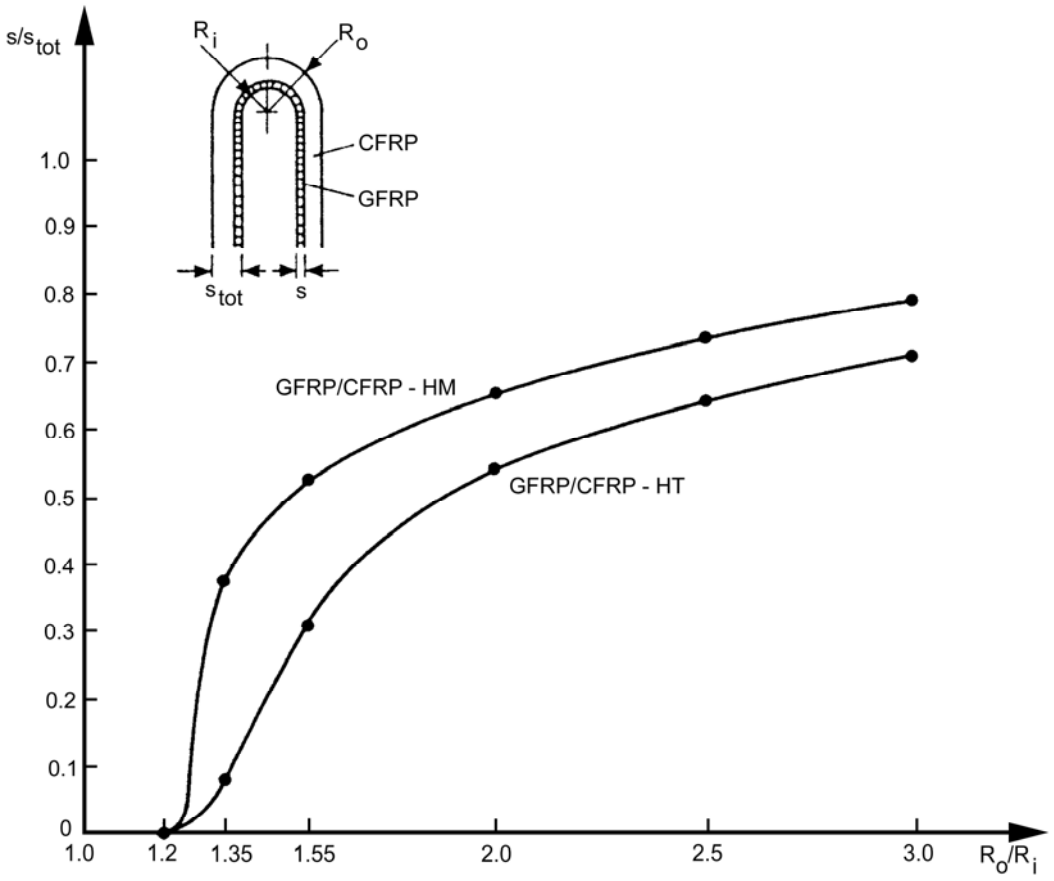

Figure 24.3-4 - Hybrid composite links: Optimal thickness relation under tensile loading

The optimal thickness ratio increases with the stiffness of the fibre and with the radius ratio. A substantial increase of tensile load capacity is reached for links with high radius ratios. The decrease of the compression load capacity and compression stiffness due to this hybrid lay-up is small.

The ultimate strengths of tensile-loaded CFRP links are compared with those of hybrid links with an optimal thickness relation in Figure 24.3.5.

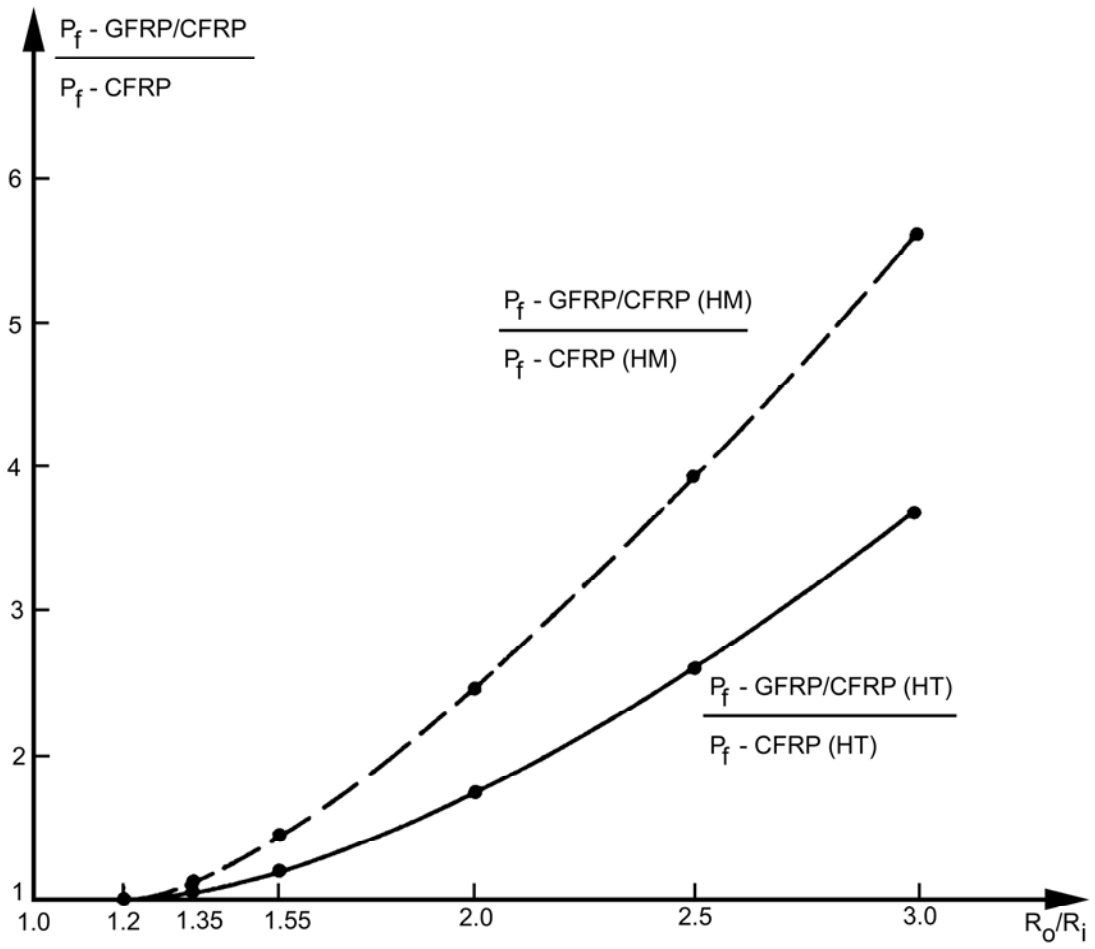

Figure 24.3-5 - Composite links: Ultimate strength ratios of tensile loaded links with optimal thickness relation compared with homogeneous (single material) links

For static loading, a good correspondence was reached between calculation and test results. For the computation of rupture load, the stress concentration factors of Figure 24.3.6 were used. These factors are not sufficient for dynamic loads, because there is a high shear stress due to friction between bolt and link. Therefore a premature failure is to be expected.

For the hybrid links, a premature failure due to thermal loads is possible, where the difference in thermal coefficient of the fibres is too high. High thermal loads are possible during manufacturing (curing) and during use.

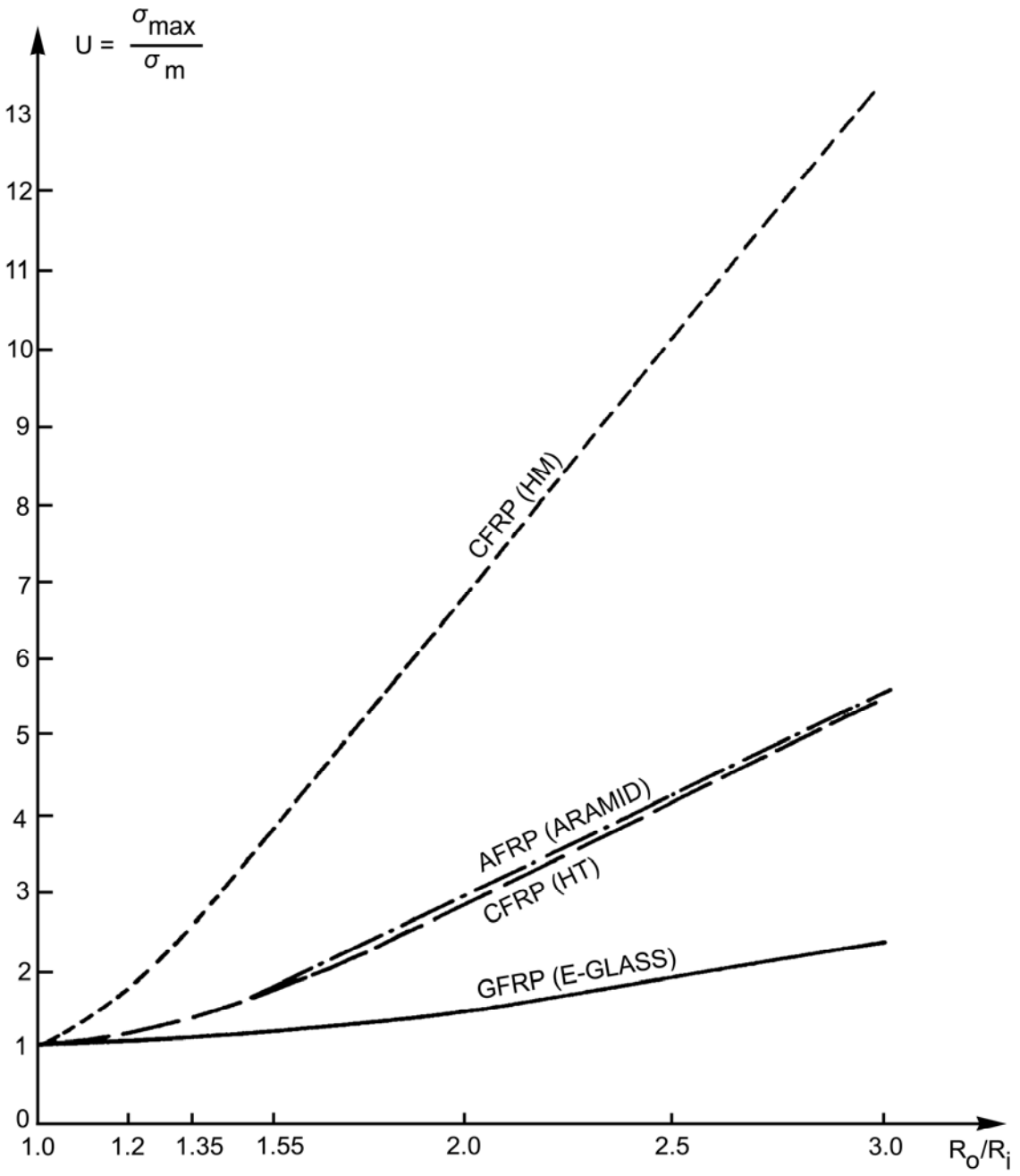

Figure 24.3-6 - Composite links: Stress concentration factors for tensile loading

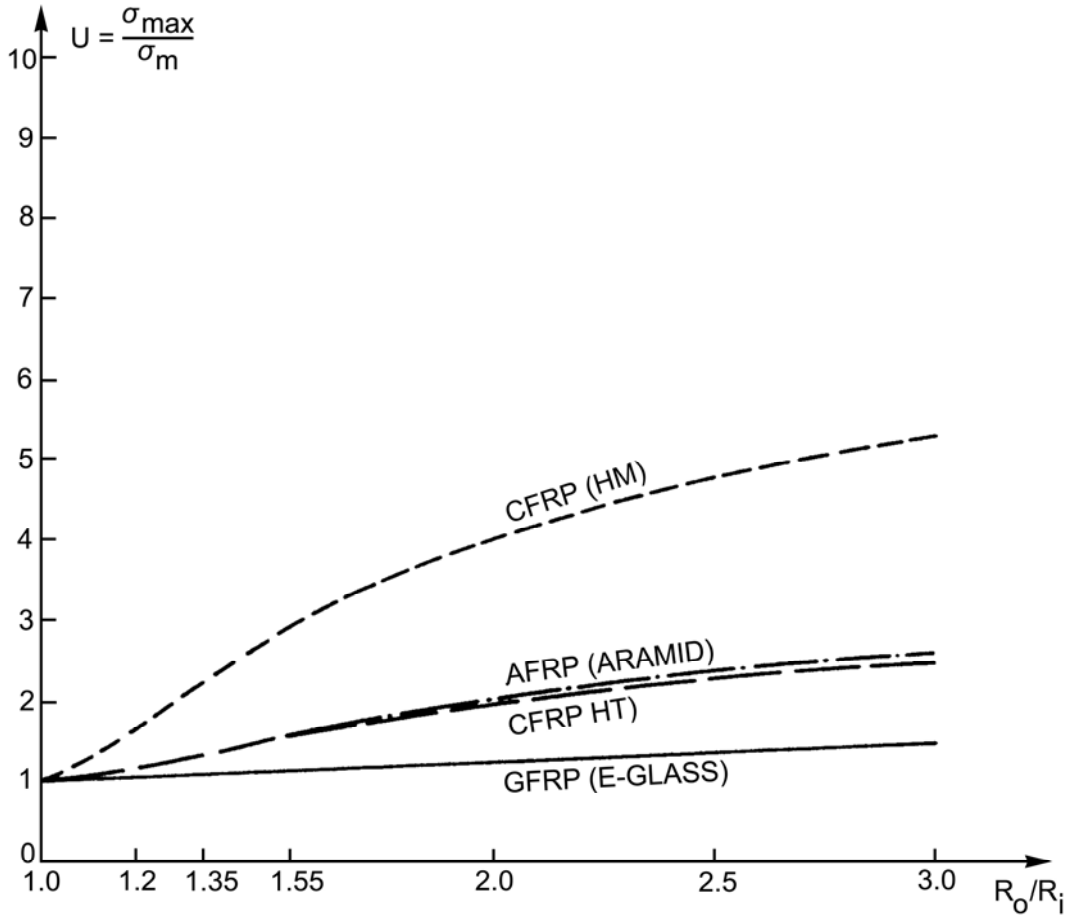

Figure 24.3-7 - Composite links: Stress concentration factors for compression loading

24.4 Shear load elements

24.4.1 The 'Spider' element

24.4.1.1 Basic description

Spider elements are used as structural elements for the introduction of loads into light sandwich structures, e.g. solar generator panels.

As shown in Figure 24.4.1, the shear loads are introduced into the titanium bush by clamping, and passed on to the massive filler block in the middle of the insert. The transmission of the shear loads from the filler block in the centre to the inner webs is ensured by bonding. Each inner web branches into outer webs. This means that the resistance to shear and torsional loads of each web decreases towards the outside.

All webs are coated with splice adhesive and bonded to the light honeycomb panel. The octagonal plane through which the webs run transmits the shear load into the honeycomb of the sandwich laminate.

The inner webs are backed by a doubler in a [±45°] arrangement to avoid face wrinkling at the compression side, and to increase the extensional stiffness when axial loads are introduced.

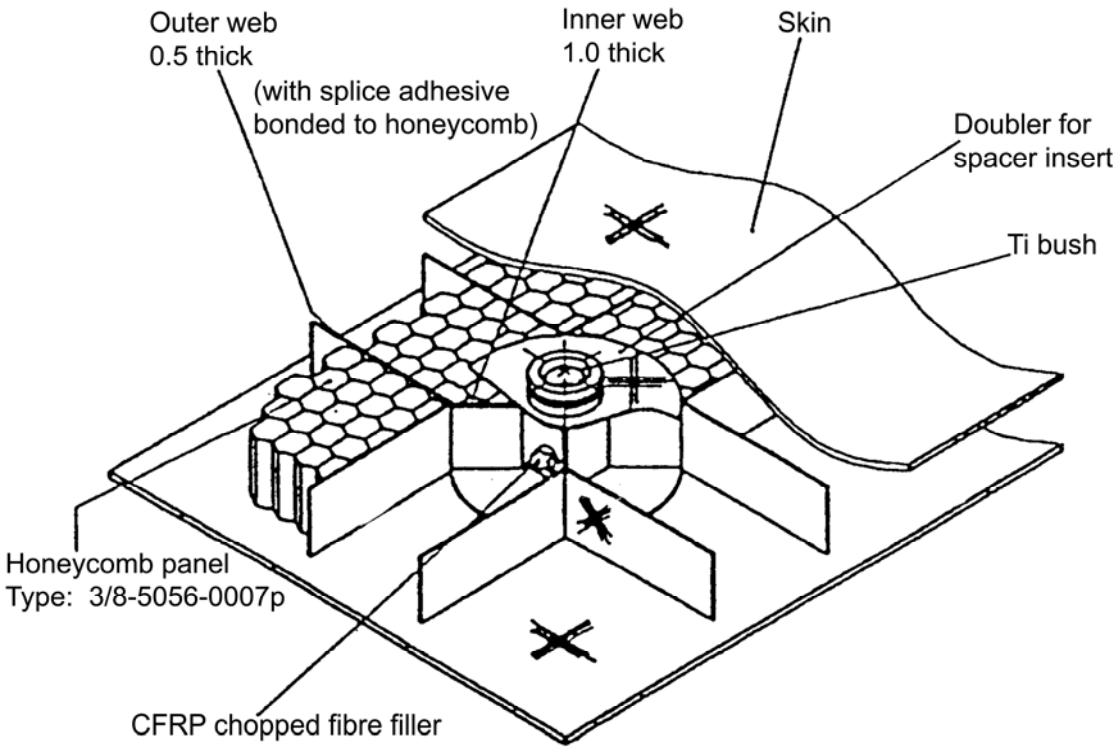

Figure 24.4-1 - Shear load 'Spider' element: Structural components and assembly into a sandwich panel

24.4.1.2 Calculation of the properties

The shear loads are transmitted by the filler blocks to the webs and by these to the honeycomb core. This transmission is ensured by adhesives and (between web and honeycomb) splice adhesives.

The average shear stress is calculated by means of:

$$\tau = \frac{\text{shear load}}{\text{area to be bonded}} \qquad [24.4\text{-}1]$$

The four sides of the filler block constitute the area to be bonded. The bonding sides of the webs correspond to their total surface.

If additional bending loads occur, it is assumed that the tensile loads acting inside the skins are the dimensioning factors. The critical section is a strip in each skin, which is as wide as the filler block. These sections have to transmit the tensile loads resulting from both the bending load and the core thickness.

24.4.1.3 Laminate structure and manufacturing process

[See: Figure 24.4.1 for definition of components]

The filler block can consist of:

- CFRP chopped fibres, or
- Cut from a sufficiently thick quasi-isotropic CFRP laminate.

The webs (as shear-load-transmitting elements) are made of laminates with [±45°] fibre orientation. Such laminates can be produced by filament winding or from CFRP prepregs.

The manufacturing process consists of:

- Winding of the tubular CFRP skin.
- Cutting and laying of the webs and the lower doubler.
- Filling the centre space with a mixture of CFRP chopped fibres and epoxy resin.
- Pressing and curing.
- Assembly of the webs against the honeycomb core using splicing adhesive.
- Assembly of doubler against the sandwich core and skin using adhesive foils.
- Drilling, using a CFRP jig.
- Insertion of the titanium bushes.

A single cure cycle is used to consolidate the assembly.

24.5 References

24.5.1 General

[24-1] U. Hütter
'Probleme der Krafteinleitung in Glasfaser-Kunststoff Bauteile'
Kunststoffe, Bd. 56, Heft 12, 1966

[24-2] H. Conen
'Deformation und Versagen von GFK-Strangschlaufen'
Kunststoffe, Bd. 56, Heft 9, 1966

[24-3] R. Wörndle und H. Bansemir: MBB GmbH
'Beitrag zur statischen Berechnung von Krafteinleitungselementen aus faserverstärkten Werkstoffen (FVW)'
DGLR Symposium München, DGLR Nr. 76 231, 1976

[24-4] R. Wörndle und W. Daschner: MBB GmbH
'Spannungstheoretische Untersuchungen von Kraftein und-Kraftüberleitungselementen'
Bericht UD 225 77, ZTL FAGs, 1977

[24-5] H. Bansemir and W. Weiß
'Fibre composites for aerospace structures subject to low temperatures'
Cryogenic Engineering Conference, Colorado Springs, USA,
August 1983

[24-6] H. Bansemir and W. Buchs
'Leichtbaustrukturen aus CFK für Satellitensolargeneratoren verschiedener Größe'
DGLR-Vortrag Nr. 81-080, Aachen 1981

25
Design of struts

25.1 Introduction

25.1.1 General

Struts are a good example of the application of fibre-reinforced plastics. CFRP is especially appropriate for use in such items, given optimisation of the fibre directions, because:

- Struts are generally axially loaded, so the fibre reinforcement can be oriented mainly in load direction (0° direction), [See: 30.7].
- In addition to high tensile strength, struts made of CFRP exhibit longitudinal stiffness and stability (column buckling), despite of their low mass.
- Under compression loading, the local buckling behaviour also should be considered. Consequently, struts have also to be reinforced in the circumferential direction with:
  - 90° layers to produce higher circumferential stiffness, and
  - 45° layers to increase the torsional stiffness.
- The ±45°layers are generally more effective in ensuring buckling stability than 90° layers. Buckling stability is less important than mass optimisation of struts, Ref. [25-1].

The calculation method described is related to a CFRP strut having 90°/0°/90° reinforcement with the majority of the layers in 0° direction, [See: 25.3].

25.1.2 Design aspects

Buckling is a major consideration for the global design of struts made of composite materials. Other global considerations, such as stiffness and strength, can usually be analysed using the approaches described elsewhere in this handbook. Other design aspects for the practical applications of composite struts include:

- Design of end-fittings, e.g. CTE mismatch between metal end-fittings and composite tubes.
- Bonding materials and processes to connect the end-fitting to the composite tube, e.g. [See: Chapter 21; 30.10; ECSS-E-HB-32-21].

25.2 Analytical notation for strut optimisation

E_1	Young's modulus in fibre direction (UD ply).
E_2	Young's modulus perpendicular to fibre (UD ply).
E_x	Young's modulus in load direction (laminate).
F	area.
L	length of strut.
t	thickness of laminate.
r	radius of strut.
P	load.
K	characteristic value.
k	buckling coefficient.
W	weight.
γ	specific weight.
σ_N	nominal stress.
σ_C	critical stress (Euler column buckling).
σ_B	critical stress (local buckling).

25.3 Theoretical evaluation

25.3.1 Method

Figure 25.3.1 defines the notation for a compression-loaded strut, [See also: 25.2].

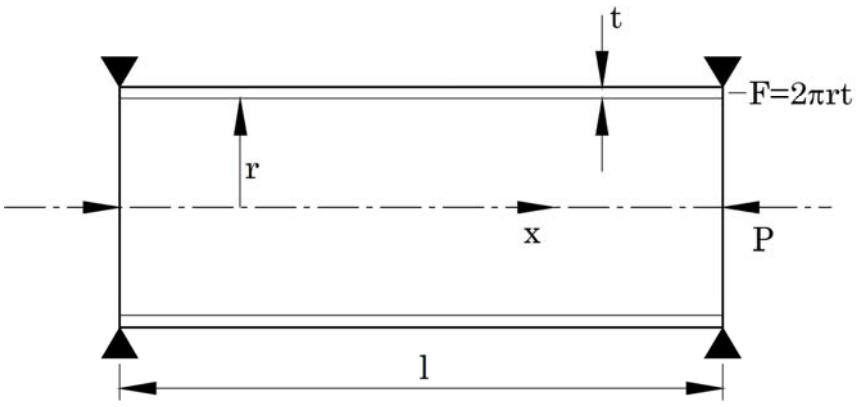

Figure 25.3-1 - Notation: Compression loaded strut

According to the optimisation methods in Ref. [25-2], [25-3], the radius, laminate thickness and optimal fibre ply angle for a compressively loaded strut can be shown as a function of the strut length, *l*, and the compression load, *P*:

$$K = P/l^2 \qquad [25.3\text{-}1]$$

The resulting stress in any cross-section of the strut is:

$$\sigma_N = P/F = Kl^2/F = Kl^2/2\pi rt \qquad [25.3\text{-}2]$$

To obtain a weight-optimised strut, failure occurs at σ_N together with column instability and local buckling, i.e.:

$$\sigma_N = \sigma_C = \sigma_B \qquad [25.3\text{-}3]$$

With:

$$\sigma_C = \frac{\pi^2}{2} E_x (r/l)^2 \qquad [25.3\text{-}4]$$

for Euler column buckling, and:

$$\sigma_B = k\sqrt{E_1 E_2}\, t/r \qquad [25.3\text{-}5]$$

for the local buckling of 90°/0_n°/90° laminates, Ref. [25-1].

In practice, a coupling of column buckling and local buckling should be avoided.

The validity of Equation [25.3-3] means that for this special case, the cross-section area of the strut has its minimum for:

$$\sigma_N = \sigma_{\max} \qquad [25.3\text{-}6]$$

Assuming that σ_{max} can be described as a function of the characteristic value *K* (Equation [25.3-7]), Equation [25.3-8] gives the optimised cross section (r_{opt} and t_{opt}) when inserted in Equation [25.3-4] and Equation [25.3-5] for $\sigma_C = \sigma_{max}$ and $\sigma_B = \sigma_{max}$.

$$\sigma_{\max} = (\sigma_N \sigma_C \sigma_B)^{1/3} \qquad [25.3\text{-}7]$$

$$\sigma_{\max} = \left(\frac{\pi}{4} K E_x k \sqrt{E_1 E_2} \right)^{1/3} \qquad [25.3\text{-}8]$$

The specific weight of an optimised strut is determined by:

$$\left(W/L^3\right)_{\min} = \gamma K / \sigma_{\max} = \gamma \left[\frac{4K^2}{\pi E_x k \sqrt{E_1 E_2}} \right]^{1/3} \qquad [25.3\text{-}9]$$

The buckling coefficient has been verified, by experiment Ref. [25-1].

For 90°/0$_n$°/90° CFRP composites, the factor used is be:

k = 0.25 or less

At the lower limit, k seems to be independent of the relation of axial and circumferential reinforcements.

The k factor already contains the influences of pre- and post-buckling.

A detailed determination of the buckling coefficient k in relation to the reinforcements and the ratio of radius to thickness is certainly possible but not useful, because of the fact that the coefficient becomes $k^{1/3}$ in Equation [25.3-9], i.e. only a small influence on the optimum weight.

This preliminary design method does not consider shear effects or bending effects (column beam). For a method including these factors, [See: 25.4 for optimisation of compression tubes].

25.3.2 Evaluation example

25.3.2.1 Strut optimisation preliminary design

Theoretical values are illustrated for:

- Maximum compression strength, σ_{max}, in Figure 25.3.2.
- 'Specific weight' of strut: $(W/l^3)_{min}$ in Figure 25.3.3.
- Optimised values of cross-section radius and thickness in Figure 25.3.4 $(r/l)_{opt}$ and Figure 25.3.5 $(t/l)_{opt}$.

These are shown as a function of the characteristic value $K = P/l^2$ (or load P for a strut length of l).

The material properties of CFRP and, for comparison, aluminium alloy 2024 are shown in Table 25.3.1.

A comparison of the optimised values for a CFRP and an aluminium strut are given in Table 25.3.2.

Table 25.3-1 - Strut optimisation: Material properties

Optimised Property	Value
E_1	18000 daN/mm²
E_2	700 daN/mm²
E_x	14000 daN/mm²
E_{Al}	7400 daN/mm²

[See: Figure 25.3.2; Figure 25.3.3; Figure 25.3.4; Figure 25.3.5]

Table 25.3-2 - Comparison of optimised values for a CFRP and aluminium strut

l	1000 mm	
P	1000 daN	
K	10^{-3} daN/mm	
	CFRP	**Aluminium**
W_{min}	81 x 10^{-3} kg	132 x 10^{-3} kg
t_{opt}	0.47mm	0.33 mm
r_{opt}	17 mm	24 mm

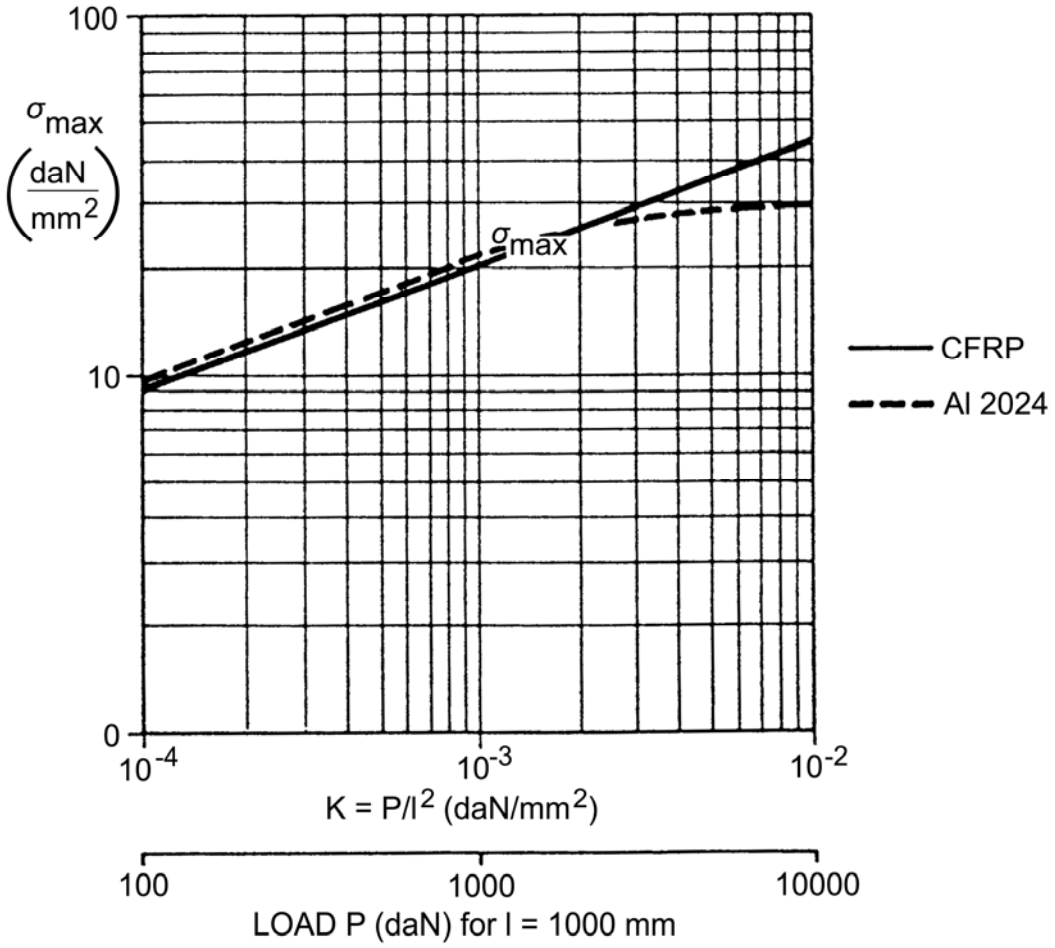

Figure 25.3-2 - Strut optimisation: Maximum compressive strength

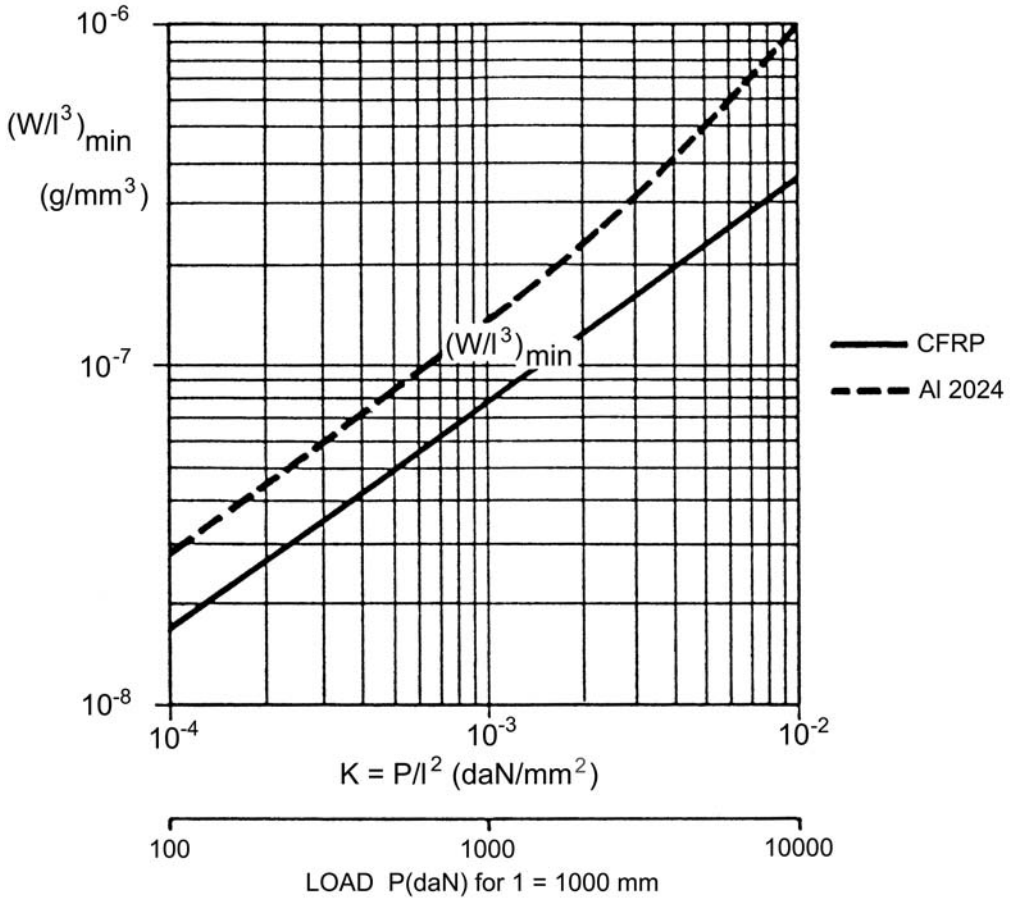

Figure 25.3-3 - Strut optimisation: Minimum specific weight

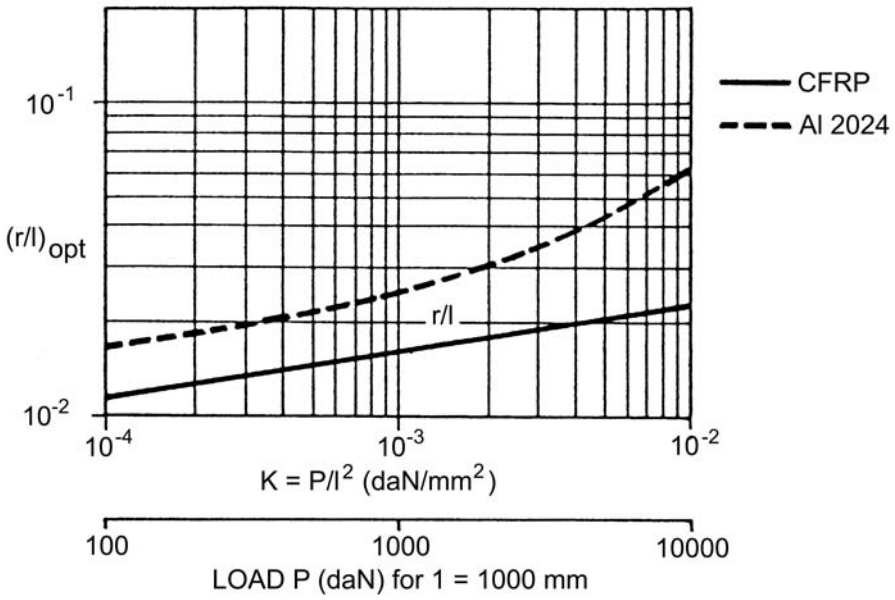

Figure 25.3-4 - Strut optimisation: Optimum radius

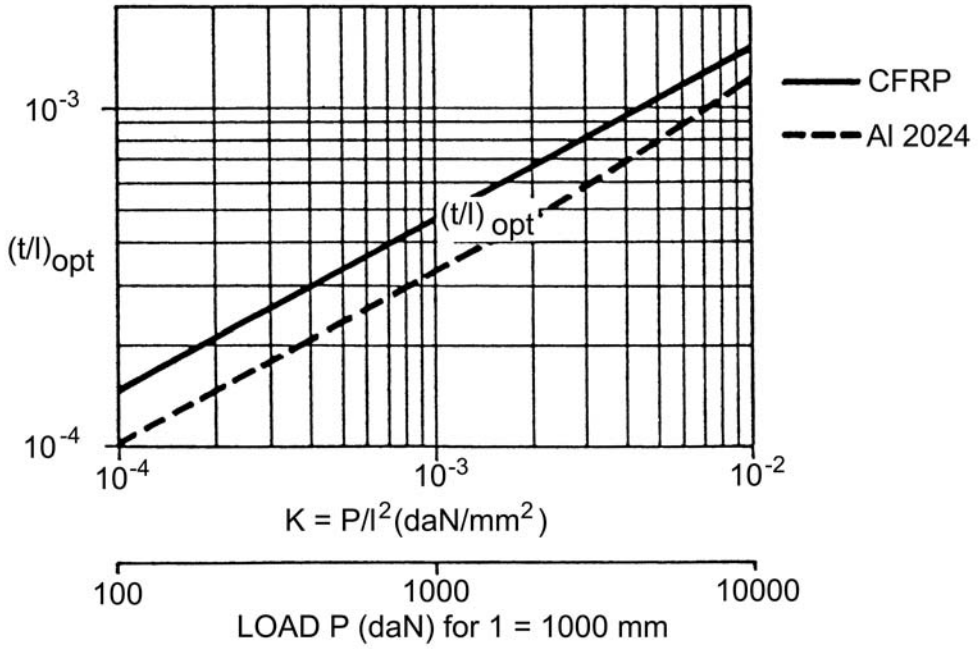

Figure 25.3-5 - Strut optimisation: Optimum thickness

25.4 Optimisation of compression tubes

25.4.1 General

A method is described for sizing tubular members subject to either:

- Axial load only (column), or
- Axial load plus bending moment (beam column).

The material is assumed to be homogeneous orthotropic. The equations have been derived from Ref. [25-4], [25-5], [25-6], [25-7], [25-8], [25-9].

Shear deflection is included. Both ends of the tube are assumed to be simply supported. The configuration and loading condition is shown in Figure 25.4.1. For a simplified method for initial sizing of tubular columns under axial compressive load only, [See: 25.3].

[See also: 27.4 for a procedure for detailed analysis of thin walled orthotropic cylindrical shells, including columns]

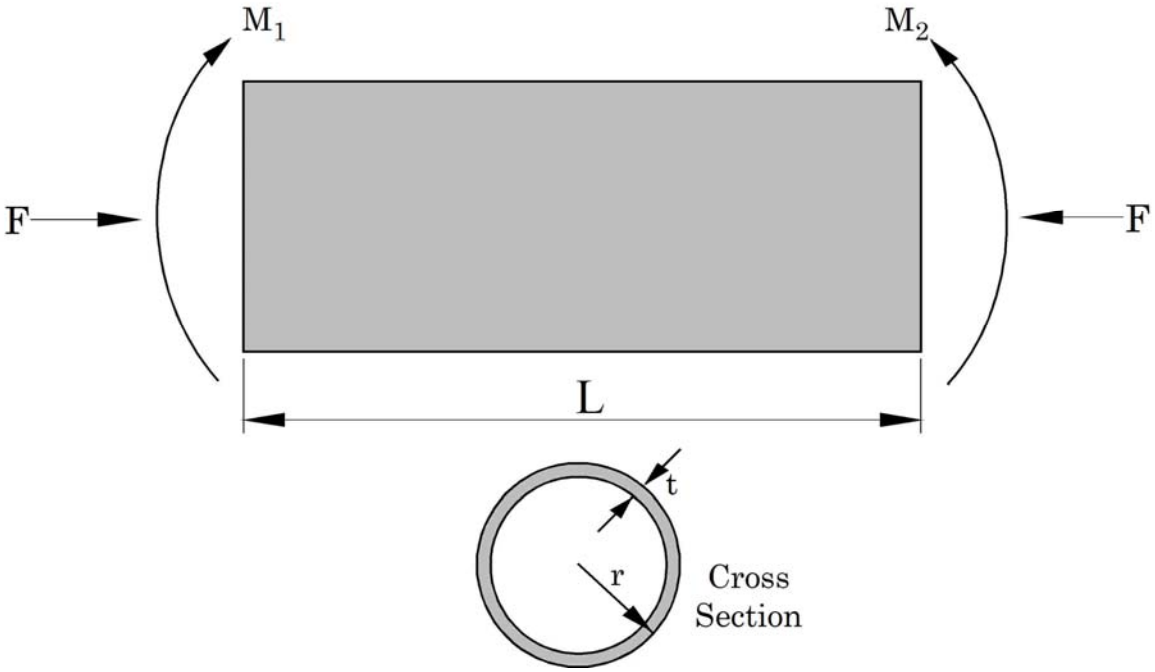

Figure 25.4-1 - Notation: Beam column configuration and loading conditions

25.4.2 Critical column buckling load

F_c is determined by:

$$F_c = \frac{F_e}{1 + \frac{nF_e}{AG_{LT}}} \qquad [25.4\text{-}1]$$

where:

Euler buckling load: $F_e = \frac{\pi^2 E_L I}{L^2}$

Approximation of moment of inertia: $I = \pi t R^3$

E_L = Young's modulus in longitudinal direction of the tube

G_{LT} = in-plane shear modulus

A = 2_πtR, cross section area

n = "shear coefficient", defined by:

$\frac{nQ}{AG_{LT}}$ = change in slope of the deflection curve, produced by a shearing force Q,

Deflection of a tube due to shearing force Q is:

$$w_s = \frac{QL}{\pi R t G_{LT}}$$

$$\text{Slope} = \frac{w_s}{L} = \frac{2Q}{AG_{LT}} = \frac{nQ}{AG_{LT}}$$

Thus: $n = 2$ for tubes

The critical column buckling stress is given by:

$$\sigma_c = \frac{\sigma_e}{1 + \frac{2}{G_{LT}}\sigma_e} = \frac{1}{\frac{1}{\sigma_e} + \frac{2}{G_{LT}}} \qquad [25.4\text{-}2]$$

With:

$$\sigma_e = \frac{E_L}{2}\left(\frac{\pi R}{L}\right)^2 \qquad [25.4\text{-}3]$$

25.4.3 Local buckling stress for circular cylinders

$$\sigma_{cr} = \sqrt{\frac{E_L E_T}{3(1-\nu_{TL}\nu_{LT})}}\frac{t}{R}K\gamma \qquad [25.4\text{-}4]$$

E_T Young's modulus in circumferential direction of the tube

$K = \sqrt{\frac{2G_{LT}}{\sqrt{E_L E_T}}\left(1+\sqrt{\nu_{TL}\nu_{LT}}\right)}$ for unsymmetric buckling:

or:

$K = 1$ for axi-symmetric buckling, whichever is less

ν_{LT}, ν_{TL} Poisson's ratio of a composite associated with normal stresses in longitudinal and circumferential direction, respectively

γ Correlation factor, to account for disparity between theory and experiments

$\gamma = 1 - 0.901(1 - e^{-\phi})$ For axial compression

$\gamma = 1 - 0.731(1 - e^{-\phi})$ For bending

$\phi = \frac{1}{29.8}\sqrt{\frac{R}{\rho}}$

$p = \sqrt[4]{\frac{D_L D_T}{\overline{E}_L \overline{E}_T}}$ geometric mean of the radii of gyration axial and circumferential directions of cylinder wall.

D_L, D_T bending stiffnesses in axial and circumferential direction of cylinder wall

E_L, E_T extensional stiffnesses in axial and circumferential direction of cylinder wall

The important restrictive assumptions are:

- end conditions are neglected.
- large buckle wave numbers are assumed.

25.4.4 Applied stress

25.4.4.1 General

Maximum compressive stress of a hinged beam-column under compressive load F and bending moments, [See: Figure 25.3.2].

$$\sigma_{max} = \sigma_F \left(1 + \frac{2M_{max}}{FR} \right) \qquad [25.4\text{-}5]$$

with:

$$\sigma_F = \frac{F}{A} \qquad [25.4\text{-}6]$$

$$M_{\max} = \sqrt{\left(\frac{M_2 - M_1 \cos \frac{L}{j}}{\sin \frac{L}{j}} \right)^2 + M_1^{\,2}} \qquad [25.4\text{-}7]$$

where:

$$j = \frac{L}{\pi} \sqrt{\frac{F_c}{F}} \text{, i.e. } \frac{L}{j} = \pi \sqrt{\frac{\sigma_F}{\sigma_c}} \qquad [25.4\text{-}8]$$

25.4.4.2 Formulation of the optimisation

Combination of the equations by the substitution of the applied stress $\sigma_F = \frac{F}{A}$ (Equation [25.4-6]) into Equation [25.4-3] gives:

$$\sigma_e = \frac{\pi E_L}{4L^2} \frac{F}{\sigma_F} \frac{R}{t}, \quad \text{Euler buckling stress} \qquad [25.4\text{-}9]$$

From Equation 25.04.4:

$$\frac{R}{t} = \sqrt{\frac{E_L E_T}{3\left(1 - \nu_{TL}\nu_{LT}\right)}} K\gamma \frac{1}{\sigma_{cr}} \qquad [25.4\text{-}10]$$

Combining Equation [25.4-9] and Equation [25.4-10] gives:

$$\sigma_e = \frac{\pi E_L \gamma K \sqrt{\frac{E_L E_T}{3(1-\nu_{TL}\nu_{LT})}}}{4L^2} \frac{F}{\sigma_F \sigma_{cr}} \qquad [25.4\text{-}11]$$

Rearranging Equation [25.4-2] gives:

$$\frac{1}{\sigma_c} = \frac{1}{\sigma_e} + \frac{2}{G_{LT}}$$

And by substituting Equation [25.4-11] into it:

$$\frac{1}{\sigma_c} = \frac{4\sigma_F \sigma_{cr}}{\pi E_L \gamma K \sqrt{\frac{E_L E_T}{3(1-\nu_{TL}\nu_{LT})}} \frac{F}{L^2}} + \frac{2}{G_{LT}} \qquad [25.4\text{-}12]$$

Where: σ_c = column buckling stress

Up to this point the nominal stress, the column buckling and local stresses are included. The bending stresses are incorporated next. Substituting Equation [25.4-12] into Equation [25.4-8] gives:

$$\frac{L}{j} = \pi \sqrt{\sigma_F \frac{4\sigma_F \sigma_{cr}}{\pi E_L \gamma K \sqrt{\frac{E_L E_T}{3(1-\nu_{TL}\nu_{LT})}} \frac{F}{L^2}} + \frac{2}{G_{LT}}} \qquad [25.4\text{-}13]$$

The mean radius, *R*, is derived from Equation [25.4-4] and by replacing t from the nominal stress relationship:

$$\sigma_F = \frac{F}{2\pi R t}$$

Hence:

$$R = \sqrt{K\gamma\sqrt{\frac{E_L E_T}{3(1-\nu_{TL}\nu_{LT})}}\frac{F}{2\pi\sigma_F\sigma_{cr}}} \qquad [25.4\text{-}14]$$

With this definition, Equation [25.4-5] can be rearranged:

$$\sigma_{max} = \sigma_F\left[1+\sqrt{\frac{8\pi\sigma_F\sigma_{cr}}{F^3 K\gamma\sqrt{\frac{E_L E_T}{3(1-\nu_{LT}\nu_{TL})}}}\left(\frac{M_2 - M_1 cos\,{}^{L}\!/_{j}}{sin\,{}^{L}\!/_{j}}\right)^2 + M_1{}^2}\right] \qquad [25.4\text{-}15]$$

Where L/j is given by Equation [25.4-13].

Minimum beam column mass is obtained by setting $\sigma max = \sigma_{cr}$ (local buckling). Hence, Equation [25.4-15] can be used to search for the maximum nominal stress σ_F as a function of σ_{cr}, which is varied between the bounds:

max $\sigma_{cr} = \sigma_{cu}$, σ_{cu} = compressive ultimate stress of the laminate

min $\sigma_{cr} = \sigma_{cr,0}$

With $\sigma_{cr,0}$ being the optimum local buckling stress of the ideal column (loaded only by an axial compressive force, i.e. $M_1 = M_2 = 0$).

$\sigma_{cr,0}$ is determined from the condition:

$$\boldsymbol{\sigma_F = \sigma_c = \sigma_{cr} = \sigma_{cr,0}}$$

i.e. by equating the nominal stress to the column buckling stress and the local buckling stress.

Equation [25.4-12] is used to determine $\sigma_{cr,0}$ giving:

$$\frac{4\sigma_{cr,0}^{3}}{\pi E_L \gamma K \sqrt{\frac{E_L E_T}{3(1-\nu_{TL}\nu_{LT})}}\frac{F}{L^2}} + \frac{2\sigma_{cr,0}}{G_{LT}} = 1 \qquad [25.4\text{-}16]$$

Equation [25.4-15] needs insertion of the correlation factor γ which depends on the tube geometry. Since R and t are still to be determined, a preliminary estimation is made for them to get an initial γ. This initial γ is checked after having completed the first analysis loop, and replaced by an improved second estimation.

Having determined the maximum nominal stress σ_F and the related local buckling stress σ_{cr} (Equation [25.4-15]), the mean tube radius R is calculated from Equation [25.4-14]) and the wall thickness from:

$$A = 2\pi Rt = \frac{F}{\sigma_F} \qquad [25.4\text{-}17]$$

25.5 References

25.5.1 General

[25-1] W. Hertel
'Optimaldimensionierung von Druckstäben aus faserverstärkten Kunststoffen mit integrierten Anschlußaugen'
Dissertation TU Berlin 1974

[25-2] F.R. Shanley
'Weight-strength analysis of aircraft structures'
McGraw-Hill Book Co., New York

[25-3] J. Wiedemann
'Optimaldimensionierung von Bauweisen'
3. Lehrgang für Raumfahrttechnik, Aachen 1964

[25-4] S.P. Timoshenko & J.M. Gere
'Theory of elastic stability'

[25-5] Bruhn
'Analysis and design of flight vehicles structures'

[25-6] NASA: SP-8007
'Buckling of thin walled circular cylinders'

[25-7] N. Corvelli and R. Carri
'Evaluation of boron epoxy reinforced titanium tubular truss for application to a Space Shuttle booster thrust structure'
App. C, NASA TN D 6778, 1972

[25-8] J.R. Lager
'Composite Space Shuttle support structure'

[25-9] J.G. Davis
'Compressive instability and strength of uniaxial filament reinforced epoxy tubes'
NASA, TN D 5697

25.5.2 ECSS documents

[See: ECSS website]

ECSS-Q-70-71	Data for selection of space materials and processes, previously ESA PSS-01-701.
ECSS-E-HB-32-21	Adhesive bonding handbook for advanced structural materials, previously ESA PSS-03-210.

26
Design of sandwich structures

26.1 Notation

a	Plate length in x-direction
a_i, i=0, 1	Coefficients in shell analysis
A_{ij}, i,j=4, 5	Sandwich plate/shell transverse stiffness coefficients in contracted notation (classical lamination theory)
b	Plate length in y-direction
B_x, B_y, B_{xy}	Sandwich shell in-plane/extensional stiffness coeffecients
d	Distance between facing mid-/reference surfaces of sandwich panel
D	Sandwich panel bending stiffness
D_{ij}, ij=1, 2, 6	Sandwich plate/shell bending stiffnesses in contracted notation (classical lamination theory)
D_x, D_y, D_{xy}	Sandwich plate/shell bending stiffnesses in xy-plane
E	Young´s modulus (isotropic)
E^*	Equivalent or quasi-isotropic Young´s modulus
E_f	Young´s modulus of faces (isotropic)
E_{fxi}, E_{fyi}, i=t, b	Young´s moduli of faces – top face i = t, bottom face i = b
F	Strength
G	Shear modulus (isotropic)
G_{cxz}, G_{cyz}	Transverse shear moduli of core material in xz and yz planes, respectively (orthotropic)
G_{fxyi},i=t, b	In-plane shear modulus of faces – top face i = t, bottom face i = b (orthotropic)
k_n	Knock-down factor
k_x	Non-dimensional buckling coefficient (NASA approach SP 8007)
K	Non-dimensional buckling coefficient

K	Structural efficiency
K_d	Non-domensional dimpling (intra-cell buckling) coefficient
L	“Length” direction of honeycomb core
L	Length of circular cylindrical shell
M	Mass
N_i, i=x, y	Normal stress resultant
P_i, i=x, y	Applied compressive loading per unit width
Q	Wrinkling factor
R	Radius of circular cylindrical shell
S	Sandwich panel shearing stiffness
S	Honeycomb cell size (diameter of inscribed circle)
S_i, i=x, y	Sandwich plate/shell transverse stiffnesses
t	Thickness (total thickness of sandwich assembly)
t_c	Core thickness
t_f	Face thickness
t_{fi}, i=t, b	Face thickness – top face $i = t$, bottom face $i = b$
T	“Transverse” direction of honeycomb core
u	Displacement in x-direction
v	Displacement in y-direction
w	Lateral or transverse deflection in z-direction
W	“Width” direction of honeycomb core
x	In-plane coordinate direction
y	In-plane coordinate direction
z	Transverse or out-of-plane coordinate direction
z	Curvature parameter
α_i, i=1-5	Coefficients in shell analysis
β_i, i=1-3	Stiffness coefficients in shell analysis
η, i=1-4	Proportionality factor
θ	Shear factor
θ_i, i=x, y	Shear factors, x- and y-directions, respectively
ν	Poisson´s ratio
ν_f	Poisson´s ratio of face (isotropic)
ν_{ij}, i,j=x, y	Poisson Poisson´s ratio of face (orthotropic)
ρ_i, i=f, c	Density – face $i = f$, core $i = c$
σ	Normal stress
τ	Shear stress
ψ	Rotation of normal to beam/plate/shell reference surface

Subscripts:

b	Bending (deformation/displacement)
b	Bottom (face)
c	Core
c	Compression (strength)
cr	Critical
d	Dimpling (intra-cell buckling)
f	Face of facing
m	Wave number, *x*-direction
n	Wave number, *y*-direction
s	Shear (deformation/displacement or strength
t	Top (face)
t	Tension (strength)
wr	Wrinkling
x	In-plane direction
y	In-plane direction
xy	in-plane for faces
xz, yz	Transverse core planes
z	Transverse or out-of-plane direction
0	Reference or mid-surface property
1, 2, 6	Notation corresponding to so-called “contracted” notation commonly used in classical lamination theory (as opposed to “tensor notation”).

26.2 Introduction

26.2.1 The structural sandwich concept

The ASTM (American Society for Testing and Materials) defines a sandwich structure as follows:

"A structural sandwich is a special form of a laminated composite comprising of a combination of different materials that are bonded to each to so as to utilise the properties of each separate component to the structural advantage of the whole assembly."

In practice a sandwich structure (beam, panel, plate or shell) can be considered as a special type of composite laminate where a thick, lightweight and compliant core material separates two thin, stiff, strong and relatively dense faces (or facings); as shown schematically in Figure 26.2.1 and Figure 26.2.2. Such sandwich structures have gained widespread acceptance as an excellent way to obtain extremely lightweight structural components with very high bending stiffness, high strength and high buckling resistance.

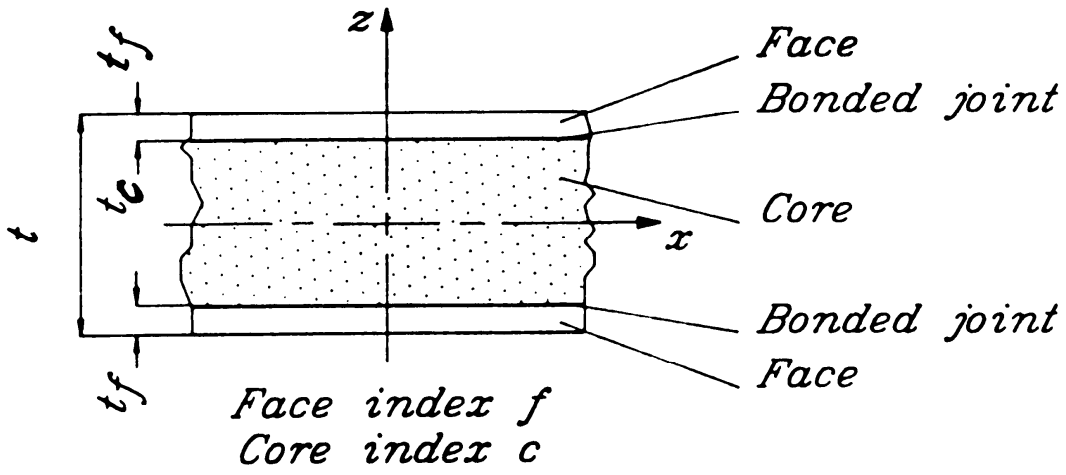

Figure 26.2-1 – Schematic illustration of sandwich panel

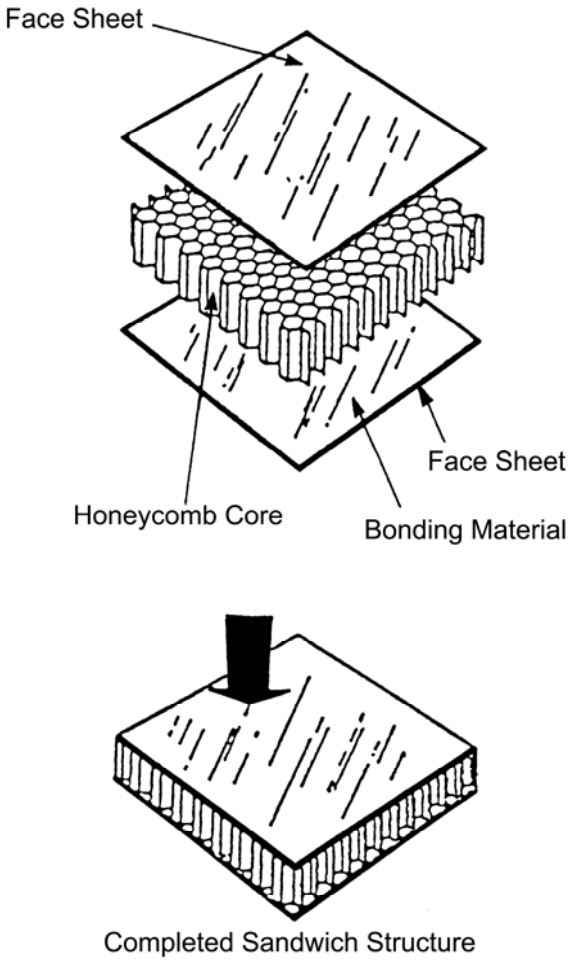

Figure 26.2-2 - The components of a honeycomb-cored sandwich panel

A simple "thought experiment" highlights the mass effectiveness of sandwich structures:

A beam of a material with a given Young´s modulus, *E*, and a given strength is considered. The beam is subject to a bending moment, and the mass, bending stiffness and strength are set to unity. Suppose now that the beam is cut in two halves and the parts separated by a lightweight core material. Given those parameters, the relative mass, stiffness and strength properties of sandwich beams can be found; as given in Figure 26.2.3, Ref. [26-1].

Consequently, by using the sandwich concept, the bending stiffness and strength can be substantially increased in comparison with a single skin (homogeneous) structure without adding much mass.

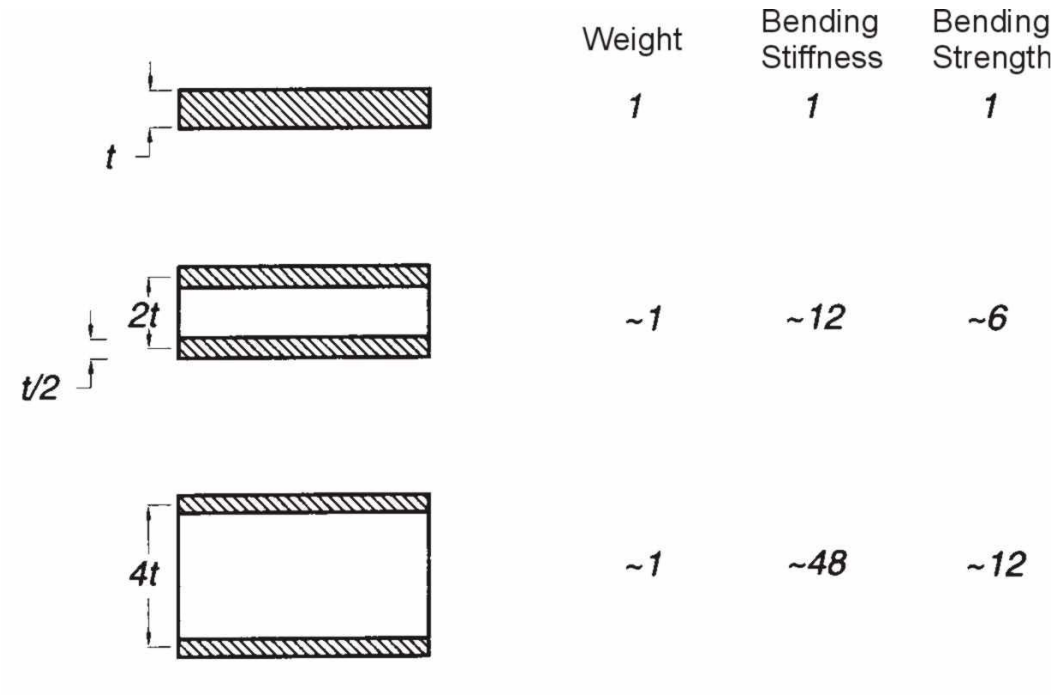

Figure 26.2-3 – Comparison between beams with monolithic and sandwich cross sections

26.2.2 Historical background and overview

The history of sandwich structures dates back to the first half of the 19th century, where the concept of using two faces separated by a distance so as to utilise the composite action of the two faces was discussed by a Frenchman, Duleau, in 1820, and later by the Englishman, Fairbairn in 1840, Ref. [26-1].

However, the sandwich concept was not used to any great extent until almost 100 years later in the famous Second World War de Havilland "Mosquito" fighter-bomber aircraft; shown in Figure 26.2.4. In this aircraft, sandwich panels with wood veneer faces and balsa core were used for control surfaces.

Figure 26.2-4 – World War II, De Havilland "Mosquito" fighter-bomber aircraft

The first theoretical works on the analysis and design of sandwich structures were published towards the end of World War II, where pioneering contributions among others were given by Gough, Elam and Bruyne, Ref. [26-2] and Hoff, Ref. [26-3] (collection of selected papers).

Since then, the science and technology of sandwich structures has progressed tremendously, and today far more comprehensive and advanced uses of sandwich structures are being made.

Figure 26.2.5 shows an example of a 'state of the art' antenna-reflector, which uses an ultra lightweight sandwich construction, [See also: 30.13].

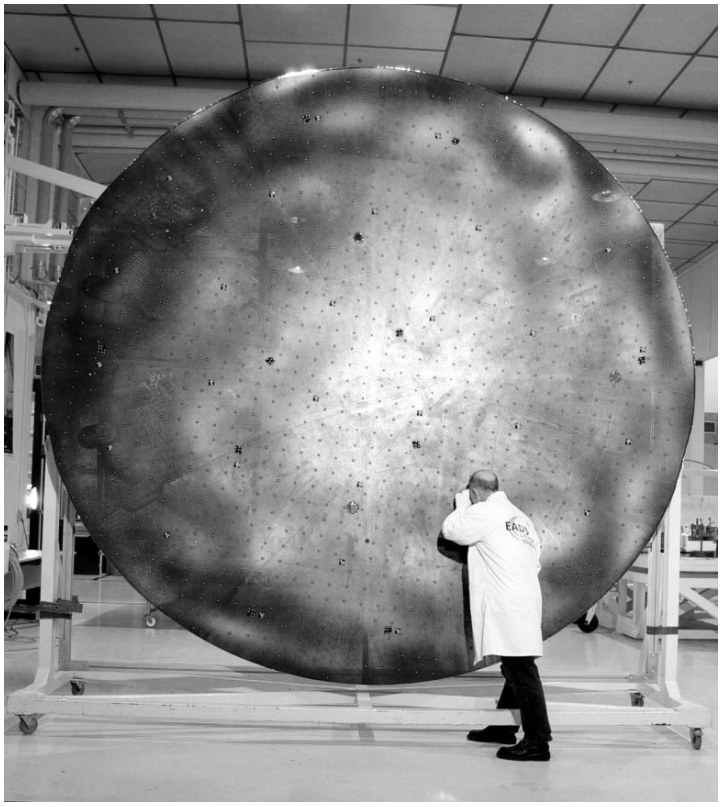

Figure 26.2-5 – ASAS reflector: Example of lightweight sandwich structure

26.2.3 Applications

26.2.3.1 General

Sandwich structures are being used successfully for a variety of applications covering the range from hulls and superstructures for ships and boats, wind turbine blades, automotive and train structures and finally aircraft and spacecraft structures. The main spacecraft applications of honeycomb sandwich structures include:

- Tanks,
- Shipping containers,
- Structural shells,
- Heat shields,
- Inter-tank structures,
- Antenna reflectors,
- Radomes,
- Electronic packaging.

26.2.3.2 Advantages

Some of the most important advantages of sandwich structures in comparison with homogeneous, monolithic structures include:

- Very high stiffness to weight ratio (bending stiffness, buckling resistance),
- High strength to weight ratio.
- Excellent fatigue properties in general, especially in comparison with mechanically fastened structural material systems.
- Smooth and flat surfaces: The manufacturing techniques used to cut core materials produce extremely flat surfaces, and the resulting surfaces can also be extremely smooth and flat.
- Thermal and acoustic properties can be tailored: The availability of both metallic and non-metallic facings and cores provide the designer with the capability to design for a minimum or maximum heat transfer rate. For extremely low rates, the honeycomb core can be filled with foam prior to bonding.
- High energy absorption and impact resistance can be achieved.
- "Multifunctional" capabilities, where it is possible to combine many functions, such as structural, thermal and acoustic performance characteristics, into a sandwich structure by proper design and choice of core and face materials.
- Value in production quantities: The simplicity of bonded structures reduces the manpower costs associated with mechanically fastening and constructing hardware. Whilst initial tooling costs can be high for complex bonded systems, this one-off cost is quickly absorbed in production run unit costs.

26.2.3.3 Disadvantages

Some of the most important disadvantages of sandwich structures in comparison with homogeneous, monolithic structures include:

- Sensitivity to localised effects due to concentrated loads, restrictive boundary conditions, joints and geometric and material discontinuities [See: 26.5 and 26.7].
- Reliable non-destructive testing or evaluation can be difficult to achieve.
- Damage tolerance can be problematic and damage tolerance assessment is difficult.
- Quality assurance of bonding between face sheets and core is difficult.
- Difficulty of draping onto curved surfaces.

26.2.3.4 Design approach

The successful implemenation of a sandwich structure needs evaluation of:

- Design considerations associated with sandwich structures, including the characteristics and properties of the individual elements making up a sandwich structure, [See: 26.6; 26.7], and the considerations necessary to integrate them into a sandwich design, [See: 26.8]. Suitable design procedures, [See: 26.9].
- Analytical and numerical methods for structural analysis, [See: 26.5], including failure modes, [See: 26.4].
- Manufacturing aspects, along with means of attaching to sandwich panels, e.g. use of insert systems for fixings,[See: 26.8].

[See also: Chapter 23 for inserts; ECSS-E-HB-32-22 - insert design handbook]

26.2.3.5 Theoretical approach

With respect to the design of sandwich structures, a number of theoretical approaches have evolved over the years. Within this Chapter, the most widely known of these are presented and discussed with respect to their application to the types of sandwich structures found in space applications. The overall aim is to provide the designer with a basic understanding of the use of such theories and the restrictive assumptions applied.

In all cases, the theories and approaches presented can be used for preliminary design purposes only.

[See also: ECSS-E-HB-32-22; ECSS-E-HB-32-21; ECSS-E-HB-32-34]

26.3 Constituent materials and manufacturing

26.3.1 General

A sandwich structure consists of several constituents; the faces, the core material and the adhesive joints, [See: 26.2; Figure 26.2.1 and Figure 26.2.2].

The faces can be made of different materials, joints can be made of different adhesives and the core material can change over the in-plane as well as the out-of-plane sandwich panel directions. All of these depend on the functional and structural demands and on the manufacturing process. The possible choice of materials is vast, and the design of sandwich structures is just as much a materials selection problem as a sizing problem.

26.3.2 Face materials and their properties

The primary function of the faces (also known as facings, face sheets or face skins) is to provide the necessary extensional and in plane shear stiffness to carry the in-plane extensional and shear loading applied directly or transferred through the sandwich core material (bending, transverse shear and torsion). The properties of primary importance for the faces are:

- High stiffness giving high bending stiffness of the sandwich structure,
- High tensile and compressive strength,
- High in-plane shear strength,
- Impact resistance,
- Environmental resistance, e.g. thermal, radiation, UV.
- Dimensional stability,
- Surface finish.

The commonly used materials for facings can be divided into two main groups:

- Metallic
- Non-metallic.

For aerospace applications the metallic group comprises aluminium and titanium alloys, whereas the most important of the non-metallic face materials are fibre-reinforced polymer resin materials.

In the aerospace industry, the facings most commonly chosen are resin impregnated fibreglass cloth (usually prepreg) and carbon fibre prepreg, either as unidirectional tape or woven fabric.

[See: Chapter 3 for the mechanical properties of commonly used facing materials]

26.3.3 Core materials and their properties

26.3.3.1 General

The properties of primary interest for core materials used in sandwich structures are:

- Low density,
- High through-thickness shear modulus,
- High through-thickness shear strength,

- High through-thickness stiffness,
- Thermal properties,
- Acoustic properties.

For spacecraft applications, the most commonly used sandwich core materials can be divided into the main groups, Ref. [26-68]:

- Honeycombs.
- Foams:
  - polymer,
  - SiC silicon carbide lightweight cores, [See also: Chapter 43]
  - metallic.

26.3.4 Cores: Honeycomb materials

26.3.4.1 Cell shape

Honeycomb materials can be manufactured in a variety of cell shapes such as square, rectangular, triangular or corrugated, but the most commonly used shape is hexagonal.

Figure 26.3.1 illustrates several shapes of honeycomb core cells, Ref. [26-1] [26-4].

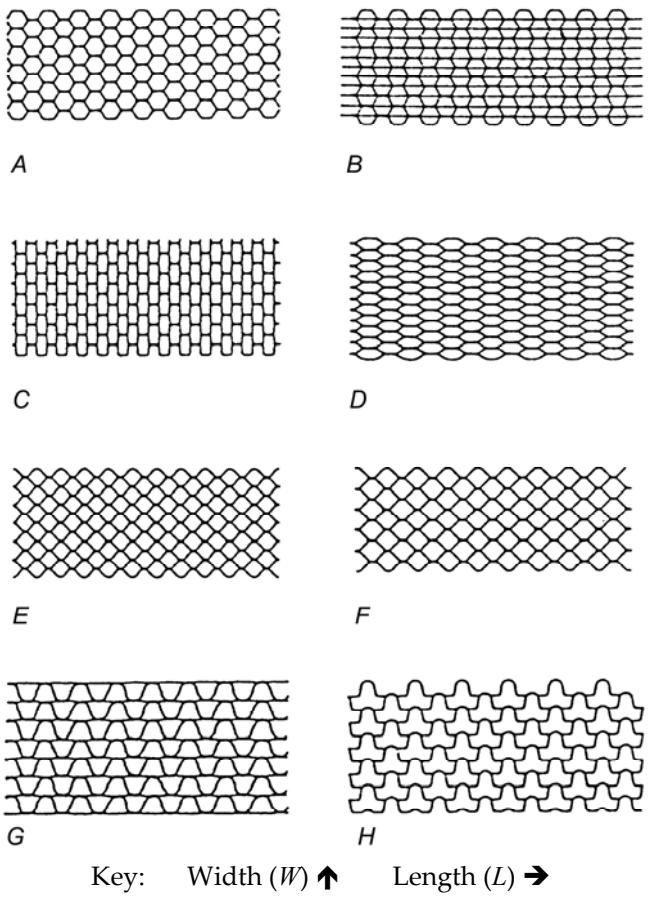

Figure 26.3-1 – Honeycomb cores: Common cell configurations

Metallic honeycombs are manufactured in two different ways, Ref. [26-1] [26-32]:

- The corrugating process, where pre-corrugated metal sheets are bonded together and stacked into blocks. When the adhesive has cured, blocks with the necessary thickness can be cut from the stack. This process is often used for the manufacture of high-density metallic honeycombs.
- The expansion process, which begins with the stacking of thin planar sheets of the web material on which adhesive nodes have been printed. By stacking many thin layers in this way a block is made. Each block is then cut into the desired thickness (T-direction or through-thickness direction). When the adhesive has cured it can be expanded by pulling in the *W*-direction; shown in Figure 26.3.1, until the desired cell shape is achieved.

Non-metallic, fibre-reinforced plastic honeycombs are manufactured by impregnating a prefabricated cell-shaped fabric in a resin bath.

Owing to the manufacturing methods involved, honeycomb cores are orthotropic. This is easily seen as both the corrugation and the expansion processes produce double cell-walls in one direction and single in the other. Over-expanded cells also create additional orthotropy. There are three principal directions to which the material properties of honeycombs are referred; shown in Figure 26.3.1:

- width (*W*),
- length (*L*)
- through-thickness (*T*),

The resulting directional properties are adapted to the anticipated loads.

Under- or over-expansion of the core changes its cell shape and density. The over-expanded hexagonal core [Figure 26.3.1C] changes directional properties, such that the *L*-direction becomes slightly the weaker, or more compliant of the two major axes. Since the reduction in the *L*-direction strength can amount to 30%, any processing that changes cell shape has to be avoided.

Over-expanded cores [Figure 26.3.1C] and so-called "flex cores" [Figure 26.3.1H] are primarily used when the core material needs to be curved in the manufacturing of the sandwich structural element. Over-expanded hexagonal and flex-core shapes reduce anticlastic bending and cell wall buckling when curved.

Many other cell shapes exist including: reinforced hexagonal [Figure 26.3.1B], square [Figure 26.3.1CE] and corrugated [Figure 26.3.1G].

26.3.4.2 Cell size

Although the cell size tends to be a secondary variable for most mechanical properties of core materials, it is primary in determining the:

- strength level of the core-to-face attachment, or, conversely;
- lower limit on core-to-panel adhesive weight, and;
- stress levels at which intra-cell buckling or face dimpling of face occur, [See: 26.7].

26.3.4.3 Thickness

The shear and compressive properties for a specific core type can only be obtained when test methods are carefully specified and controlled, and the correct thickness of core tested.

26.3.4.4 Specimen geometry and test method

Like the thickness, specimen geometry and test method should be stipulated and carefully controlled in order to obtain comparability with the values obtained by others.

26.3.5 Cores: Honeycomb properties

26.3.5.1 General

The physical and mechanical properties of honeycomb core materials are strongly influenced by the characteristics of the materials from which they are manufactured as well as the honeycomb geometry. For instance, the honeycomb shear strength varies significantly with core thickness depending upon the test method, skin thickness and many other factors. Generally, the apparent (measured) honeycomb shear strength decreases significantly with increasing core thickness due to the above factors as well as an increased tendency for cell wall buckling.

26.3.5.2 Density

All mechanical properties increase with higher density. This is illustrated in Figure 26.3.2 for the stabilised compression strength, and in Figure 26.3.3 and Figure 26.3.4 for the shear strengths, Ref. [26-4] [26-5].

A stabilised compressive strength, also called flatwise compressive strength, represents the ultimate compressive strength of the honeycomb when loaded in the *T*-direction. Normally for this test, the facings are adhesively bonded to the honeycomb material (stabilised compressive).

Alternatively, the bare compressive strength is the ultimate compressive strength of the core when loaded in the T-direction without stabilisation of the cell edges. This value is normally used for an acceptance criteria, since this test is easier and faster to perform. The bare compressive strength is lower than the stabilised compressive strength.

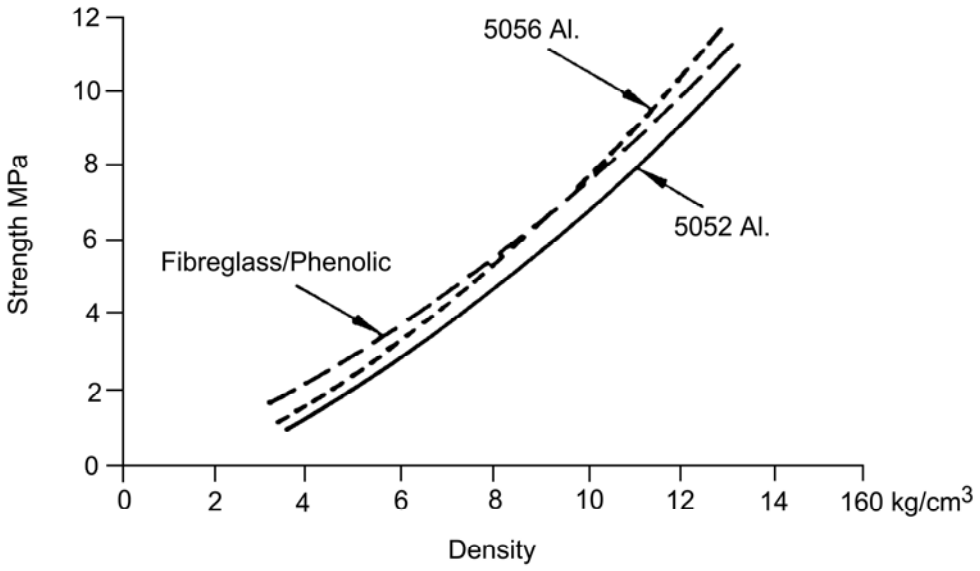

Figure 26.3-2 – Honeycomb cores: Typical stabilised compression strength (*T*-direction)

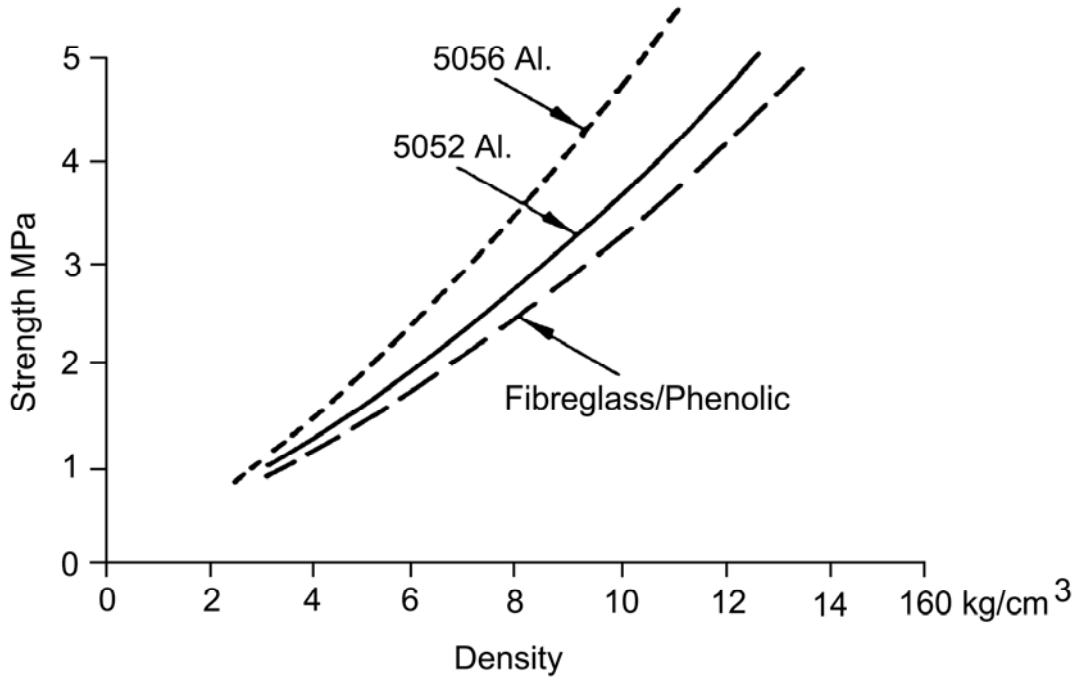

Figure 26.3-3 - Honeycomb cores: Typical 'L' shear strength

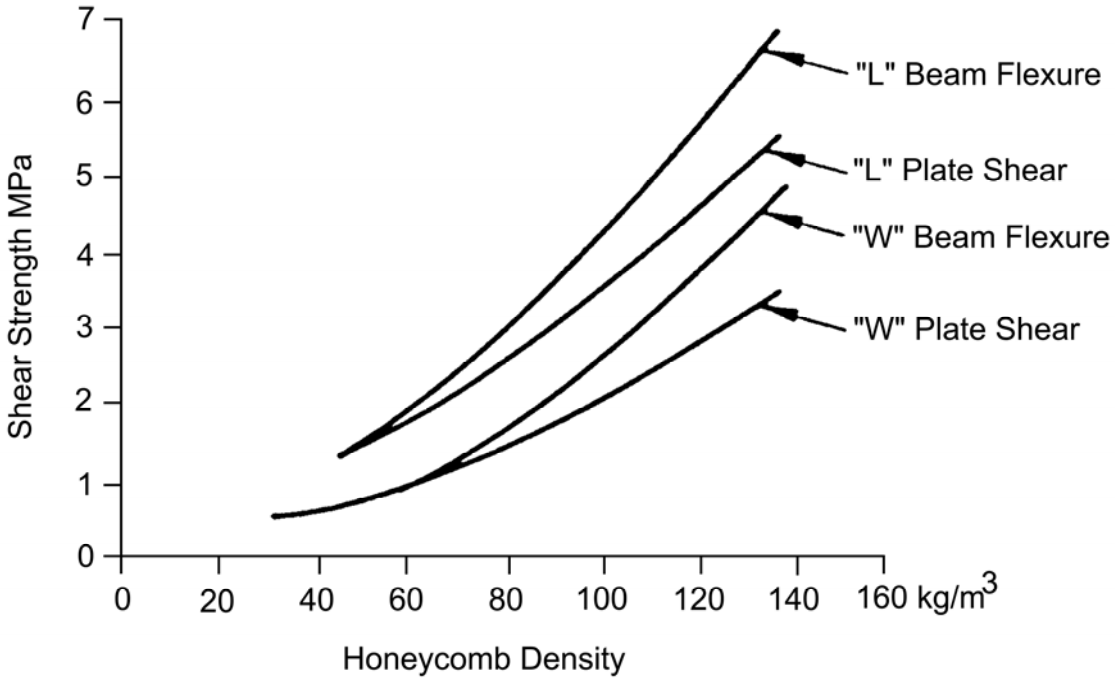

Figure 26.3-4 - Honeycomb cores: Typical plate shear v density for 5052 aluminium core

26.3.6 Cores: Metallic honeycomb

26.3.6.1 Aluminium alloys

Aluminium honeycombs have been used extensively for aerospace applications. They are commonly made of aluminium alloys 5052, 5056 and 2024, Ref. [26-4] [26-5]:

- 5052 is a general purpose alloy, and is the most often used aircraft grade. 5052 can be delivered with a corrosion resistant surface treatment.
- 5056 is a high strength version of 5052 (the strongest of the aircraft grades), and is available with a corrosion resistant surface treatment.
- 2024 is a heat treated aluminium alloy with good properties at elevated temperatures.

The 5052 and 5056 aluminium alloy honeycombs can be used in environments up to 180°C and 2024 up to about 210°C, Ref. [26-4] [26-5].

The cell wall foil of the honeycombs can be perforated with small holes to enable venting during cure of the adhesive, Ref. [26-4] [26-5].

Aluminium honeycomb cores remain the most widely used, as well as the most versatile of the various core materials obtainable. They are very often found to possess the most favourable performance-to-cost ratio. The densities of commercially available expanded aluminium cores typically vary from 32 kg/m³ to 192 kg/m³. A summary of commercially available aluminium cores is given in Table 26.3.1, Ref. [26-4]. Reference is also made to the honeycomb material data sheets provided by Hexcel Corporation, Ref. [26-5].

Table 26.3-1 – Honeycomb cores: Properties of 5056, 2024 and 5052 hexagonal aluminium cores

HEXCEL Honeycomb Designation	ρ*	Compressive					σ**	Plate shear					
		Bare		Stabilised				L direction			W direction		
		Strength kPa		Strength kPa		Modulus MPa		Strength kPa		Modulus MPa	Strength kPa		Modulus MPa
Cell - Material - Gauge		typical	minimum	typical	minimum	typical	typical	typical	minimum	typical	typical	minimum	typical
5056 Hexagonal Aluminium Honeycomb													
1/16 - 5056 - 0.0007	101	6894x		7584x		2275x		4447x		655x	2551x		262x
1/16 - 5056 - 0.001	144	11721p		12410p		3447p		6756p		758p	4136p		344p
1/8 - 5056 - 0.0007 †	50	2344	1723	2482	1792	668	1172	1723	1378	310	1068	758	137
1/8 -5056-0.001 †	72	4343	3275	4619	3447	1275	2206	2930	2413	482	1758	1413	262
1/8 - 5056 - 0.0015	98	6895	5240	7584	5688	2034	3689	4413	3620	703	2551	2103	262
1/8 - 5056 - 0.002	130	10480	8274	11721	8963	2999	5585	6205	5102	986	3585	3034	352
5/32 - 5056 - 0.0007	42	1758	1241	1793	1276	483	827	1379	1048	248	827	552	117
5/32 - 5056 - 0.001	61	3275	2482	3447	2586	965	1620	2310	1875	393	1413	1069	165
5/32 - 5056 - 0.0015	85	5654	4240	5964	4482	1655	2896	3654	2999	586	2137	1724	228
5/32 - 5056 - 0.002	111	8412	6343	9239	6895	2413	4482	5240	4206	814	2965	2482	296
3/16 - 5056 - 0.0007	32	1069	758	1103	827	310	517	965	724	186	586	345	90
3/16 - 5056 - 0.001 †	50	2344	1724	2482	1793	669	1172	1758	1379	310	1069	758	138
3/16 - 5056 - 0.0015	70	4137	3172	4482	3378	1241	2137	2827	2344	469	1689	1365	190
3/16 - 5056 - 0.002	91	6274	4723	6757	5068	1862	3309	4033	3309	648	2344	1931	248
1/4 - 5056 - 0.0007	26	689	517	758	552	207	345	621	538	138	414	262	83
1/4 - 5056 - 0.001 †	37	1413	1000	1448	1069	400	689	1172	896	221	724	427	103
1/4 - 5056 - 0.0015	54	2723	2068	2896	2172	793	1379	1999	1586	345	1207	896	152
1/4 - 5056 - 0.002	69	3999	3034	4275	3206	1186	2068	2758	2241	462	1655	1310	186
1/4 - 5056 - 0.0025	83	5447	4137	5654	4447	1586	2827	3447	2930	579	2068	1689	221
3/8 - 5056 - 0.0007	16	241	172	345	241	103	241	414	310	103	241	172	62
3/8 - 5056 - 0.001	26	689	517	758	552	207	345	621	538	138	414	262	83
3/8 - 5056 - 0.0015	37	1413	1069	1448	1069	400	689	1172	896	221	724	427	103
3/8 - 5056 - 0.002	48	2206	1655	2344	1793	634	1103	1689	1310	296	l000	689	131
2024 Hexagonal Aluminium Honeycomb													
1/8 - 2024 - 0.0015	80	4826	3620	5378	4275	1379	2930	3447	2758	565	2172	1724	228
1/8 - 2024 - 0.002	107	7584	5688	8446	6757	2068	4413	5240	4137	814	3241	2586	310
1/8 - 2024 - 0.0025	128	10204	7584	11376	9101	2620	5792	6619	5309	1020	4068	3241	372
1/8 - 2024 - 0.003	152	13583	10170	15858	11893	3309	7722	7929	6550	1172	4482	4033	441
3/16 - 2024 - 0.0015	56	2275	1724	2551	1999	593	1379	1999	1586	379	1241	986	159
1/4 - 2024 - 0.0015	45	1517	1138	1724	1207	276	758	1379	965	290	827	607	131

5052 Hexagonal Aluminium Honeycomb													
1/16 - 5052 - 0.0007	101	5998p		6274p		1896p		3516p		621p	2206p		276p
1/16 - 5052 - 0.001	144	10204x		10342x		2896x		5343x		724x	3585x		365x
1/8 - 5052 - 0.0007 †	50	1862	1379	1999	1482	517	896	1448	1069	310	896	621	152
1/8 - 5052 - 0.001 †	72	3585	2586	3758	2792	1034	1793	2344	1965	483	1517	1158	214
1/8 - 5052 - 0.0015 †	98	5998	4482	6274	4688	1655	3103	3482	3137	676	2206	1875	283
1/8 - 5052 - 0.002 †	130	9653	6895	10135	7584	2413	5171	4999	4619	931	3137	2758	372
1/8 - 5052 - 0.003	192	15168p		16030p		6205p		7584p			4309p		
5/32 - 5052 - 0.0007	42	1379	1034	1482	1103	379	621	1138	827	255	689	483	131
5/32 - 5052 - 0.001	61	2723	1965	2827	2068	758	1276	1862	1482	386	1207	862	182
5/32 - 5052 - 0.0015	85	4757	3378	4964	3689	1344	2344	2896	2551	579	1862	1482	248
5/32 - 5052 - 0.002	111	7446	5309	7791	5516	1965	3964	4068	3723	786	2586	2261	320
5/32 - 5052 - 0.0025 ‡	135	10549	7377	11032	8136	2551	5516	5240	4757	965	3275	2896	386
3/16 - 5052 - 0.0007	32	896	621	931	689	234	414	827	552	186	483	317	99
3/16 - 5052 - 0.001 †	50	1862	1379	1999	1482	517	896	1448	1069	310	896	621	152
3/16 - 5052 - 0.0015 †	70	3447	2482	3620	2654	1000	1724	2275	1931	469	1482	1103	207
3/16 - 5052 - 0.002 †	91	5309	3861	5585	4137	1517	2689	3172	2827	621	2068	1682	265
3/16 - 5052 - 0.0025	111	7446	5309	7791	5516	1965	3964	4068	3723	786	2586	2261	320
3/16 - 5052 - 0.003	130	9653	6895	10135	7584	2413	5171	4999	4619	931	3137	2758	372
1/4 - 5052 - 0.0007	26	586	414	655	483	138	276	586	414	145	345	221	76
1/4 - 5052 - 0.001	37	1138	827	1207	896	310	517	965	689	221	586	393	112
1/4 - 5052,- 0.0015	54	2206	1655	2344	1724	621	1034	1620	1241	345	1034	724	165
1/4 - 5052 - 0.002	69	3309	2413	3482	2551	965	1586	2206	1827	455	1448	1069	205
1/4 - 5052 - 0.0025	83	4619	3447	4757	3516	1310	2310	2827	2482	565	1827	1379	244
1/4 - 5052 - 0.003	96	5861	4344	6067	4551	1620	2965	3413	3068	662	2172	1827	279
1/4 - 5052 - 0.004 †	127	9377	6688	9791	7239	2344	4999	4826	4482	896	3034	2689	364
3/8 - 5052 - 0.0007	16	207	138	310	138	69	172	310	221	83	207	138	48
3/8 - 5052 - 0.001	26	586	414	655	483	138	276	586	414	145	345	221	76
3/8 - 5052 - 0.0015	37	1138	827	1207	896	310	517	965	689	221	586	393	112
3/8 - 5052 - 0.002	48	1793	1310	1862	1379	483	827	1379	1000	296	862	586	146
3/8 - 5052 - 0.0025 ‡	59	2551	1862	2689	1965	724	1241	1793	1379	379	1172	793	179
3/8 - 5052 - 0.003	67	3172	2310	3344	2448	931	1517	2137	1758	448	1379	1034	200
3/8 - 5052 - 0.004	86	4964	3447	5137	3689	1379	2482	2965	2620	593	1931	1572	254
3/8 - 5052 - 0.005 ‡	104	6688	4826	7033	5171	1827	3482	3758	3447	724	2413	2068	300

ρ* - Nominal Density, kg/m^3 σ** - Crush strength values shown are average or typical; actual values may vary because of density, tolerances, etc.

x = Predicted values. p = Preliminary properties. † Core types most readily available. ‡ Minimum order may be required.

26.3.7 Cores: Non-metallic honeycomb

26.3.7.1 General

Non-metallic honeycombs are available with glass, aramid or even carbon fibre-reinforcement. The resins in which the fibres are embedded include phenolics, heat-resistant phenolics and polyimide. The phenolic impregnated types have a maximum working temperature up to about 180°C and the polyimide impregnated cores can be used up to about 250°C, Ref. [26-1].

A brief survey of the properties and applications of glass fibre and aramid reinforced honeycomb types is described.

26.3.7.2 Glass fibre-reinforced honeycomb

Glass fibre-reinforced plastic honeycomb is most commonly used in electrically sensitive parts, such as radomes and antennas, or where a heat-resistant resin and low thermal conductivity make it a natural choice. It has also seen distinguished service as a matrix for retaining non-structural ablative materials, such as soft silicone rubbers or syntactic rigid epoxy foams, which otherwise could not have been used effectively as ablative heat shields on the Gemini and Apollo re entry vehicles, [See also: 71.3].

Glass fibre honeycombs are available in a range of cell sizes (5mm, 6mm, 3mm and 10mm) with a 3 mm cell available in a bias weave glass reinforcement. Typically, the densities range from 32 kg/m^3 to 192 kg/m^3.

Data are presented in Table 26.3.2 for some commonly used glass-based honeycombs and Table 26.3.3 for some special purpose products, Ref. [26-4].

Reference is also made to the honeycomb material data sheets provided by Hexcel Corporation, Ref. [26-5].

Table 26.3-2 - Properties of commonly used glass reinforced plastic honeycombs

HEXCEL Honeycomb Designation	Compressive					Plate shear					
	Bare		Stabilised			L direction			W direction		
	Strength kPa		Strength kPa		Modulus MPa	Strength kPa		Modulus MPa	Strength kPa	Modulus MPa	
Material - Cell - Density	typical	minimum	typical	minimum	typical	typical	minimum	typical	typical	minimum	typical
Hexagonal											
HRP - 3/16 - 4.0	3447	2413	4137	3309	393	1793	1448	79	965	758	34
HRP - 3/16 - 5.5	5516	4137	6481	5171	655	2930	2551	134	1517	1310	59
HRP - 3/16 - 7.0	7929	6205	8481	6895	938	3447		193	1999		86
HRP - 3/16 - 8.0	9653	7584	11032	8825	1131	4551	4137	234	2758	2551	103
HRP - 3/16 - 12.0	15720	11032	15858	12411	1793p	6481p	5619p	379p	3930p	3447p	172p
HPR - 1/4 - 3.5	2413	1793	3447	2758	317	1586	1172	62	827	689	24
HPR - 1/4 - 4.5	4344	3103	4826	3861	483	2068	1724	97	1172	965	41
HPR - 1/4 - 5.0	4826	3516	5654	4551	579	2344		117	1379		52
HPR - 1/4 - 6.5	7067	5861	8136	6205	827	3103		172	1793		76
HPR - 3/8 - 2.2	1034	724	1379	1000	90	724	517	34	414	310	14
HPR - 3/8 - 3.2	2206	1689	3034	2413	262	1379	1103	55	724	586	21
HPR - 3/8 - 4.5	4206	3103	4757	3792	448	2068	1793	97	1172	1034	41
HPR - 3/8 - 6.0	6205	5171	6895	5171	689	2758	2344	155	1793	1448	69
HPR - 3/8 - 8.0	7308	6343	8274		1034p	3585		214p	2206		90p
Ox-Core											
HRP / OX - 1/4 - 4.5	3585	2413	4309p		296p	1448		55	1724		105
HPR / OX - 1/4 - 5.5	5585	4137	6550p		448p	1862p		72	2275		124
HRP / OX - 1/4 - 7.0	7929		8481p		579p	2723p		97p	3103p		138p
HRP / OX - 3/8 - 3.2	2344	1793	2930p		221p	965		31p	1034p		62p
HRP / OX - 3/8 - 5.5	4826	3999	5654p		414p	1655		69p	2068p		117p
Flex-Core											
HRP / F35 - 2.5	1241		1655		172	862p		86p	483p		48p
HRP / F35 - 3.5	2206		2758	2068	255	1379	965	103	724	517	69
HRP / F35 - 4.5	3034		4137		338	1931		152	965		83
HRP / F50 - 3.5	2068		2930	2068	255	1344	965	138	689	517	69
HRP / F50 - 4.5	2758		4137	3447	338	1827	1379	172	965	689	90
HRP / F50 - 5.5	4137p		6067p		421p	2689p		217p	1413p		110p

Test data obtained at 12.70mm thickness. p = preliminary properties.

Table 26.3-3 - Properties of special purpose glass reinforced plastic honeycombs

HEXCEL Honeycomb Designation	Compressive				Plate shear					
	Bare	Stabilised			L direction			W direction		
	Strength kPa	Strength kPa		Modulus MPa	Strength kPa		Modulus MPa	Strength kPa		Modulus MPa
Material - Cell - Density	typical	typical	minimum	typical	typical	minimum	typical	typical	minimum	typical
Glass Reinforced Polyimide Honeycomb										
HRH 327 - 3/16 - 4.0		3033		344	1930		199	896		68
HRH 327 - 3/16 - 4.5		3585	2757	399	2206	1516	227	1034	758	75
HRH 327 - 3/16 - 5.0		4136		468	2551		255	1241		86
HRH 327 - 3/16 - 6.0		5377	4309	599	3171	2378	310	1585	1172	103
HRH 327 - 3/16 - 8.0		8963	6894	868	4481	3447	427	2826	2275	151
HRH 327 - 3/8 - 4.0		3033	2240	344	1930	1344	199	1034	689	82
HRH 327 - 3/8 - 5.5		4688	3723	537	2895	2068	282	1447	1103	93
HRH 327 - 3/8 - 7.0		6894p		730p	3792p		365p	2137p		127p
Glass Reinforced Phenolic Honeycomb (Bias Weave Reinforcement)										
HFT - 1/8 - 3.0	2068p	2413p		151p	1275p		117p	655p		48p
HFT - 1/8 - 4.0	2688p	3964p		310p	2068p		220p	1034p		82p
HFT - 1/8 - 5.5	3619p	6618p		461p	2930p		289p	1551p		117p
HFT - I/8 - 8.0	9997p	11203p		689p	3964p		331p	2344p		172p
HFT - 3/16 - 1.8	517p	827p		97p	724p		89p	344p		27p
HFT - 3/16 - 2.0	689p	1172p		117p	792p		103p	413p		34p
HFT - 3/16 - 3.0	1896p	2585p		220p	1378p		165p	689p		62p
HFT - 3/16 - 4.0	2999p	3792p		310p	1896p		206p	965p		82p
HFT / OX - 3/16 - 6.0	6894p	7584p		461p	1999p		89p	2309p		206p

Test data obtained at 12.70 mm thickness. Honeycomb is not normally tested for bare compressive strength. p = preliminary properties

26.3.7.3 Aramid

Another well-known type of fibre-impregnated honeycomb is made of Nomex® paper, which is an aramid fibre based fabric expanded in in much the same way as aluminium and glass fabric honeycomb.

Aramid or Nomex® honeycomb is an especially tough and damage-resistant product. The mechanical properties, particularly the stiffnesses, of the material are somewhat lower than aluminium, but it possesses a unique ability to survive overloads in local areas without permanent damage.

Data are presented in Table 26.3.4 for a range of Nomex®-based honeycomb cores, Ref. [26-4].

Table 26.3-4 – Properties of Nomex honeycombs

HEXCEL Honeycomb Designation Material - Cell - Density (Gauge)	Compressive					Plate Shear					
	Bare		Stabilised			L direction			W direction		
	Strength kPa		Strength kPa		Modulus MPa	Strength kPa		Modulus MPa	Strength kPa		Modulus MPa
	typical	minimum	typical	minimum	typical	typical	minimum	typical	typical	minimum	typical
Nomex Paper Honeycomb											
Hexagonal											
HRH 10 - 1/8 - 1.8 (1.5)	758	482	896	586		620	448	25	344	248	13..
HRH 10 - 1/8 - 3.0 (2)	2068	1241	2275	1861	137	1241	1116	48	655	586	24
HRH 10 - 1/8 - 4.0 (2)	34473	2275	3861	3240	193	1689	1551	63	965	758	32
HRH 10 - 1/8 - 5.0 (3)	6205	4136	6377	4550		2240	1620		1206	827	
HRH 10 - 1/8 - 6.0 (3)	7411	5515	7756	5688	413	2551	1792	89	1378	930	41
HRH 10 - 1/8 - 8.0 (3)	10859	7584	11721	8618	537	3378	2447	110	1723	1310	53
HRH 10 - 1/8 - 9.0 (3)	11721	9652	12410	11031	620	3585	2551	117	1861	1654	62
HRH 10 - 5/32 - 5.0 (4)	5515p		6205p			2482p		72	1241p		34
HRH 10 - 5/32 - 9.0 (4)	12238p		14134p			3619p		124	1965p		65
HRH 10 - 3/16 - 2.0 (2)	1034	620	1172	723	75	758	496	28	379	275	15
HRH 10 - 3/16 - 3.0 (2)	2068	1241	2275	1861	137	1034	896	34	655	461	24
HRH 10 - 3/16 - 4.0 (2)	3447	2206	3861	3240	193	1689	1482	53	965	758	32
HRH 10 - 3/16 - 4.5 (5)	2930	2206	3275	2757		1999	1551	65	999	758	27
HRH 10 - 3/16 - 6.0 (5)	4481	3998	4826	4481		2688	2275	99	1275	1034	41
HRH 10 - 1/4 - 1.5 (2)	620	310	655	379	41	517	310	20	241	158	10
HRH 10 - 1/4 - 2.0 (2)	1034	551	1172	723	75	758	496	28	379	248	19
HRH 10 - 1/4 - 3.1 (5)	1896	1241	1965	1654		1172	930	48	586	413	20
HRH 10 - 1/4 - 4.0 (5)	2551	2137	2757	2482		1654	1378	51	861	655	24
HRH 10 - 3/8 - 1.5 (2)	620	310	655	379	41	517	310	20	241	158	10
HRH 10 - 3/8 - 2.0 (2)	1034	551	1172	723	75	758	496	28	379	248	15
HRH 10 - 3/8 - 3.0 (5)	1965p		2068p		117p	1172p		38p	655p		20p
OX-Core											
HRH 10/OX - 3/16 - 1.8 (2)	758	482	896			413	310	13	413	241	20
HRH 10/OX - 3/16 - 3.0 (2)	2516	1723	2757	1861	11	792	655	20	861	655	41
HRH 10/OX - 1/4 - 3.0 (2)	2413	1447	2654	1723	117	758	620	20	792	620	41
continued											

Flex-Core											
HRH 10/ F35 - 2.5 (3)	1034	723	1172	820	82p	482	337	27p	275	193	13p
HRH 10/ F35 - 3.5 (5)	2068p		2413p		16p	1034p		39p	551p		19p
HRH 10/ F35 - 4.5 (5)	3102p		3378p		227p	1861p		59p	1034p		25p
HRH 10/ F50 - 3.5 (3)	2068	1303	2413p	1496	16	1034	6929	39p	551	386	19p
HRH 10/ F50 - 4.5 (5)	3102p		3378p		227p	1861p		50p	1034p		25p
HRH 10/ F50 - 5.0 (5)	3792		4309	3619	255	2275	2068	55	1310	1103	28
HRH 10/ F50 - 5.5 (5)	4481p		4826p		289p	2688		60p	1620		31p

Test data obtained at 12.70 mm thickness. Nomex is a registered trademark of Du Pont. p = preliminary properties.

26.3.7.4 Carbon (C) honeycomb core

Carbon (C) honeycombs are used for specialised applications, usually when dimensional-stability is a major factor. The characteristic features of carbon honeycombs include low density, low CTE and CME and high thermal conductivity. Typical mechanical properties of Ultracor carbon honeycombs are given in Table 26.3.5, Ref. [26-6].

Table 26.3-5 – Selected properties of Ultracor carbon honeycombs

		Compression		Plate shear			
Product		Stabilized		L Direction		W Direction	
material-cell-density[1]	Construction	Strength [MPa]	Modulus [MPa]	Strength [MPa]	Modulus [MPa]	Strength [MPa]	Modulus [MPa]]
UCF-145-3/8-0.8[2]	±30° YSH70A	0.26	64	0.17	131		
UCF-126-3/8-2.0	±45° YSH50A	1.19	117	1.04	276	0.59	165
UCF-356-3/8-3.5	±45° T300	4.21	303	3.86	407	1.83	192
UCF-172-3/16-3.5	±45° M46J	3.53	372	2.21	626	1.37	337
UCF-121-1/4-3.0	Triax T300	2.7	324	2.07	186		
UCF-78-3/8-4.0	0/60/120 Triax	1.96		1.48	145	0.841	66

[1]density in lb/ft^3
[2]thermal conductivity of cell wall 84 W/mK

26.3.8 Cores: Foams

26.3.8.1 General

The relatively recent development of high density and high quality foams of various material compositions, has had a major impact on sandwich concepts. Cellular foams often do not offer the same high stiffness to weight ratios as honeycomb cores, but they have other important features that can be advantageous in many applications, including:

- Cellular foams are solid on the macroscopic level (i.e. they appear as continua), which makes the machining and manufacturing of sandwich elements much easier,
- The cellular foam surfaces are easy to bond to, and surface preparation and shaping is easy
- Polymeric cellular foams offer high thermal insulation and acoustic damping
- Higher damping properties than honeycomb cores

Among the cellular materials used for spacecraft applications are acrylimide foam, polyvinylchloride foam and more recently special silicon carbide (SiC) foams. In addition, metallic foams also offer some interesting new opportunities.

Cellular core materials (foams) are often considered as isotropic, even if this for some foam types, such as PVC, is not strictly true because of the manufacturing process.

26.3.8.2 Polymethacrylimide foams (PMI)

Acrylimide foams are made from expanded imide-modified polyacrylates. The mechanical properties are very good, probably the best of all commercially-available polymer cellular foams, but the price is also the highest. PMI is fairly brittle with an ultimate elongation to failure of about 3% in tension. PMI foams also exhibit high-temperature resistance, which makes it possible to use PMI foams in conjunction with epoxy prepregs in autoclave manufacturing processes up to about 180°C.

The cell structure of PMI foams is very fine with closed cells and densities ranging from 30 kg/m^3 to 300 kg/m^3. PMI foams are traded under the name Rohacell®. The mechanical properties of Rohacell PMI core materials are given in Table 26.3.6.

For other material properties or properties of other Rohacell© foams reference is made to the Rohacell material data sheets provided by Business Degussa AG, Ref. [26-7].

Table 26.3-6 – Mechanical properties of Rohacell© PMI foam cores

Properties	ROHACELL® 51 WF	ROHACELL® 71 WF	ROHACELL® 110 WF	ROHACELL® 200 WF
ρ [kg/m^3]	52	75	110	205
F_c [MPa]	0.8	1.7	3.6	9.0
F_t [MPa]	1.6	2.2	3.7	6.8
F_s [MPa]	0.8	1.3	2.4	5.0
E [MPa]	75	105	180	350
G [MPa]	24	42	70	150

26.3.8.3 PVC - polyvinylchloride foam

PVC foams exist in two different forms; one purely thermoplastic also called linear PVS, and one cross-linked iso-cyanate modified type. The linear PVC foam type exhibits high ductility, reasonably good mechanical properties (stiffness and strength) but softens at elevated temperatures. The cross-linked PVC foam type is more rigid, has higher stiffness and strength, is less heat sensitive, but also more brittle. PVC foams are available in densities from 30 kg/m^3 to 400 kg/m^3. PVC foams are used in numerous sandwich applications ranging from pure insulation applications to aerospace structures, and is the most widely used of all foam core materials. The cost is lower than PMI foams, but the temperature resistance of PVC foams is usually restricted to below 100°C, which means that PVC cannot be used in autoclave manufacturing processes. The cell structure of PVC foams is about 95% closed cells for the lower densities and almost entirely closed cells for the higher densities.

For material properties reference is made to the material data sheets provided by DIAB International for cross-linked PVC foams, Ref. [26-8], and to data sheets provided by Alcan Airex for linear PVC foam types, Ref. [26-9].

26.3.8.4 SiC silicon carbide foams

Silicon carbide foams are porous, open-celled structures made from interconnected lattices of ceramic ligaments. The pattern of cells and ligaments repeats regularly through the foam, providing uniform material characteristics throughout.

The foam structure has a high void volume, large surface area, and low flow resistance. It is also lightweight, strong, fracture and thermal shock resistant, and both electrically and thermally conductive. This contrasts strongly with other ceramic foams which are usually relatively brittle, hence fragile, and non-conductive.

SiC foams are suitable for a number of applications, including high temperature applications, since they enable effective operational temperatures as high as 2200°C. Thus SiC can endure the extreme conditions that are usually expected from solid ceramic materials, but at a fraction of the weight.

Potential applications include heat exchangers, filters, composite and sandwich panels and heat shielding. For space applications, SiC-based foams have been considered for mirrors. Here, the excellent intrinsic thermo-mechanical properties of the silicon carbide with a structural design based on a sandwich structure composed of two SiC face sheets deposited on a foam core of the same material, makes is possible to manufacture very light and stiff space mirrors, Ref. [26-10]. An example of selected properties of a particular SiC foam (Duocel) is given in Table 26.3.7, Ref. [26-11].

Table 26.3-7 – Selected properties Duocel SiC foam (8% nominal density)

DUOCEL silicon carbide foam	Value
Nominal density (%)	8%
Compression strength (MPa)	1.38
Flexural strength (MPa)	2.76
Shear strength (MPa)	0.69
Young's modulus (GPa)	2.76
Poisson's ratio	0.22
Thermal conductivity: (W/m°C) 250°C 1000°C 1450°C	 5.28 1.85 1.34
Thermal expansion coefficient: ($\times 10^{-6}$ /°C) Room temperature 200°C 500°C 700°C	 2.2 3.7 4.6 4.9
Sublimation point (°C)	2700
Maximum temperature (°C) Continuous use in inert atmosphere)	2200
Oxidation resistance (°C)	1650

26.3.8.5 Metallic foams

Metal foams have low densities with good shear and fracture strength and are ideal for sandwich construction. The resulting structure can be used for energy absorption and for lightweight structural applications. Applications in impact-absorbing systems probably offer the greatest potential for metallic foams due to their ability to absorb large amounts of energy at almost constant pressure. Open cell foams have large accessible surface areas and high cell-wall conduction giving excellent heat transfer ability. The acoustic properties of metallic foams mean that they can be used in many places where sound absorption is essential.

Figure 26.3-5 – Metal foam: Example of aluminium foam

Table 26.3.8 provides a summary of data from several metal foam manufacturers, Ref. [26-73].

Table 26.3-8 – Example of properties of various metallic foams

Manufacturer/tradename	Alporas	Alulight	Cymat	ERG	Inco
Material	Al	Al	Al-SiC	Al	Ni
Structure	Closed	Closed	Closed	Open	Open
Density (Mg/m^3)	0.2-0.25	0.3-1.0	0.07-0.56	0.16-0.25	0.26-0.37
Relative density	0.08-0.1	0.1-0.35	0.02-0.2	0.05-0.1	0.03-0.04
Young's modulus (GPa)	0.4-1.0	1.7-12	0.02-2.0	0.06-0.3	0.4-1.0
Shear modulus (GPa)	0.3-0.35	0.6-5.2	0.001-1.0	0.02-0.1	0.17-0.37
Poissons ratio	0.31-0.34	0.31-0.34	0.31-0.34	0.31-0.34	0.31-0.34
Compressive strength (MPa)	1.3-1.7	1.9-14.0	0.04-7.0	0.9-3.0	0.6-1.1
Tensile strength (MPa)	1.6-1.9	2.2-30	0.05-8.5	1.9-3.5	1.0-2.4
Melting point (K)	910-920	840-850	830-910	830-920	1700-1720
Max service temperature (K)	400-420	400-430	500-530	380-420	550-650
Min service tempertaure (K)	1-2	1-2	1-2	1-2	1-2
Specific heat (J/kgK)	830-870	910-920	830-870	850-950	450-460
Thermal conductivity (W/mK)	3.5-4.5	3.0-35	0.3-10	6.0-11	0.2-0.3
Resistivity (ohm.m $\times 10^{-8}$)	210-250	20-200	90-3000	180-450	300-500

A summary of potential applications for metallic foams in spacecraft include:

- Impact energy absorption parts
- Non-flammable ceiling and wall panels with improved thermal and sound insulation
- Compressor casings
- Heat exchangers, filters, catalysts
- Instrument housing
- Acoustic transducers
- Structural parts for spacecraft
- Housings for electronic devices providing electromagnetic and heat shielding
- Sound absorbers for difficult conditions, e.g. high temperature, flowing gas, vibrations, sterile environment.

26.3.9 Adhesives: Characteristics

26.3.9.1 General

Film or paste adhesives are usually used for face sheet to core bonding and foaming adhesives for core junctions. The type of adhesive used depends on the manufacturing process (e.g. co-cured or secondary bonded face sheets) and the application requirements. For example, for cryogenic applications adhesives that remain ductile at low temperatures are available; for applications requiring high thermal conductivity such as radiator panels, silver doped adhesives are applied. All major adhesive suppliers have some space-qualified adhesives and potting compounds in their product range. A more detailed discussion is given in ECSS-E-HB-32-21 - Adhesive bonding handbook, Ref. [26-12].

Adhesives, as they apply to sandwich structures, constitute a somewhat different family of materials from those used to bond an open cellular core to a stiff, continuous facing.

Although such differences are less important with some of the 'modified' epoxy materials, they remain a basic consideration for designers and fabricators in order to avoid otherwise inevitable problems. Some of the factors that need consideration are presented.

[See: Chapter 21 for more information on adhesive joints and adhesives]

26.3.9.2 Adhesive types

Some examples of the adhesives used in sandwich panel manufacture are listed in Table 26.3.8.

As part of the selection process, establish with the supplier the availability of a product or equivalent.

26.3.9.3 Products given off during cure

Some adhesive types, such as phenolics, give off a vapour as a product of the cure reaction, and the evolution of these secondary materials can lead to several problems, including:

- Internal pressure, resulting in a little or no bond in some areas, or 'blisters'.
- Core splitting, as the gas forces its way to a lower pressure area.
- Core movement, sometimes several centimetres, resulting in an unusable cured part.
- Subsequent corrosion of core or skins by the chemical action of the vapour or its condensate.

Table 26.3-9 – Adhesive material systems for sandwich structures

Trade Name [Supplier]	Description
Aerobond 2143 [Loctite]	Paste
FM53 [Cytec]	Film epoxy modified
FM73 [Cytec]	Nitrile epoxy modified film unsupported
FM400 [Cytec]	Epoxy modified
FM410 [Cytec]	Epoxy. Foaming film adhesive for core-to-core junctions
Amicon A-452 [Emerson & Cuming]	Paste
C7/W [Armstrong]	Paste
Plastilock 717A [BF Goodrich]	Film
Araldite AV100 [Huntsman]	Epoxy 2-part liquid
Araldite AV138 [Huntsman]	Epoxy 2-part paste
Redux 312 [Hexcel]	Epoxy modified film unsupported
Redux 319 [Hexcel]	Epoxy film adhesive for core to skin bonding
Redux 340 [Hexcel]	Epoxy film adhesive for core to skin bonding
Hysol EA9309NA [Loctite]	2-part paste
Hysol 9601 [Loctite]	Film
Epibond 123/945 [Huntsman]	
Epibond 123/931 [Huntsman]	Paste
RTV 566 [General Electric]	Silicone 2-part
RTV-S691 [Wacker-Chemie]	Silicone 2-part RTV vulcanising
AF 126 [3M]	Epoxy modified
AF 143 [3M]	Epoxy modified film
AF 163-2M [3M]	Film
AF 163-K [3M]	Film
EC 2214 [3M]	Paste
EC 2216 [3M]	Epoxy modified 2-part paste
Metlbond 329 [Cytec]	Epoxy-novolac modified supported film
Metlbond 1133 [Cytec]	Modified epoxy film
EA9351 [Loctite]	Bismaleimide one-part paste
XEZ9369 [Loctite]	Bismaleimide modified. One-part paste
EA9655 [Loctite]	Bismaleimide modified. Film supported

26.3.9.4 Bonding pressure

Adhesives such as the phenolics and some others need curing pressures higher than atmospheric in order to prevent excessive porosity.

Most core materials cannot withstand compressive bonding loads exceeding a few atmospheres. Consequently high-pressure curing adhesive systems cannot be used.

26.3.9.5 Fillet forming

In order to achieve a good attachment to an open cell core, such as honeycomb, the adhesive should exhibit a unique combination of surface wetting and controlled flow during the early stages of cure.

Controlled flow prevents the adhesive from flowing down the cell wall and leaving a low strength top skin attachment and an overweight bottom skin attachment.

26.3.9.6 Adaptability

The vapour, pressure and fillet forming characteristics of adhesives also apply to skin-to-skin or skin-to-doubler attachment. In the case of contoured parts, the adhesive also should be a good gap filler without appreciable strength penalty, since tolerance control of details is much more difficult to achieve on contoured than on flat panels. A greater degree of latitude for misfit is usually necessary.

26.3.9.7 Bondline control

Bondline control is the capability of the adhesive to resist being squeezed out from between faying surfaces when excessive pressure is applied to a local area of the part during cure. Many adhesives are formulated to achieve good core filleting and are subsequently given controlled flow by adding an open weave cloth or fibrous web, contained within a thicker film of adhesive. This scrim cloth then prevents the faying surfaces from squeezing out all the adhesive, preventing areas of low bond strength.

Bondline control is necessary due to mis-fitting details, and is generally the opposite of adaptability.

26.3.9.8 Toughness

Toughness has many meanings with regard to adhesives. Usually it refers to the resistance shown by the adhesive to bondline crack growth under impact loading.

For sandwich core-to-facing bonds, it refers to the resistance shown by the adhesive to loads which act to separate the facings from the core under either static or dynamic conditions. It is found from experience that greater toughness in the bondline usually equates to greater durability, and thus to longer service life.

26.3.9.9 Peel tests for sandwich adhesives

Many types of test have been devised to measure toughness, but the most common one used for sandwich structure is the “climbing drum” peel test. This has the virtue of being easily duplicated, as well as possessing an obvious relationship to the toughness value sought, [See: Chapter 7 for test methods and standards].

Values of peel strength vary considerably, depending upon the:

- Toughness of the adhesive,
- Amount of adhesive used,
- Density of the core,
- Cell size of the core,
- Direction of peel (with or across the ribbon direction),
- Adequacy of the surface preparation,
- Degradation of the adherend surface subsequent to bonding.

Because such variables can give widely differing peel strengths for the same adhesive, all of them should be properly understood and controlled if the test is to be used and its value compared to other results.

The peel test is adaptable for use with nearly any skin material, although it becomes impractical for very thick or very stiff skins.

26.3.10 Manufacturing of sandwich panels

The process of manufacturing sandwich structures comprises of the:

- Application of pressure,
- Application of temperature (both pressure and temperature in the precise amounts needed for adhesive cure),
- Provision for tooling and fixtures to hold the assembly in the desired shape and retain all the details in their proper positions during cure.

Many different ways of providing these conditions are used, from vacuum bags or simple presses to autoclaves and unit tools, where volume and complexity can justify them.

Most of the equipment is similar to that used to produce bonded structures or fibre-reinforced plastic parts where no sandwich structure is involved. However, bonding of sandwich structures is nearly always performed at lower pressures than the bonding of low density core structures, and tooling is sometimes lower in cost as a result. Apart from the need for a lower maximum pressure, there is little noticeable difference between a sandwich bonding facility and one for non sandwich bonding.

26.3.11 Bonding sandwich elements

Some general advice that can be offered to alleviate problems with sandwich bonding includes:

- Ensure that the core is properly dimensioned to fit the space it is intended to occupy. If it has been stretched to cover from one edge member to the other, any shrinkage during cure can cause voids next to an edge member. If it is under-thickness at an edge, the adjoining edge member or fitting can hold the facing away from the core and result in an un-bonded area.
- If a honeycomb core is being used, the adhesive between the core and the faces become much thinner than the same adhesive between the edges of solid inserts and the facings. For this reason, it is usual that the core is as much as 0.25 mm thicker than adjoining solid parts in the same assembly.
- The elevated temperatures that most core to facing adhesives are cured at are often inaccurately measured. The cure temperature can only be measured accurately in the adhesive being cured, which obviously poses access problems. Some workshops insert thermocouples directly into the bondline to determine tempera-ture and leave the thermocouple permanently in the part after cure.
- Most adhesives flow at an early point in the cure cycle. At this time, the bondline changes in thickness by substantial amounts. The tooling employed to establish the shape of the part and hold details in place has also to enable the details to move into the final cured position. For example: A hot platen press, in which the platens close on the sandwich as the bondlines grow thinner. An autoclave, in which a flexible bag follows the details as the adhesive flows, continuously transmitting the autoclave pressure to the shrinking assembly. Most adhesives are very weak and prone to cracking as they pass through the gel point.
- Inserts or heavy members being cured as a part of a very light assembly heat up much more slowly, giving rise to warping problems on cool-down. Warping on very light parts can also be caused by one side cooling too fast as a result of being removed from half of the still hot tooling

while the other side remains at the tool temperature, or by one side heating faster or to a higher temperature than the opposite face. Caution is also necessary with composite cores. Slower heat-up rates or better heat distribution in the tool design prevents these problems.

- Ensure that an escape route is provided for trapped air and gases from a totally enclosed part during cure. This is particularly important in parts which are vacuum bagged to a female tool and cured in an autoclave. A coarse bleeder cloth enclosed inside the bag is useful in preventing the bag from sealing off portions of the assembly as pressure is being applied. Critical or expensive assemblies have several vacuum lines attached at different points of the bag, each monitored separately by a pressure recorder.
- Caul plates are carefully matched to the job they are expected to perform. These tooling aids are often used to cover the top of an assembly containing several different pieces of core, inserts and edges, so that a thin skin does not push each detail to the minimum bondline thickness and result in an uneven outer surface. When the caul plate is moderately stiffer than the top skin, the bonding pressure is transmitted more to the thicker inserts and less to the undersized inserts, enabling all of the details to 'float' in the adhesive before cure, resulting in optimum relative placement of all the internal details in the sandwich. If the caul plate is extremely thick or stiff, it can simply bridge between oversized details, and the probability of producing voids or un-bonded areas over the thinner details is substantially increased. Generally, the caul plate is not more than two or three times the thickness of the sandwich facing material. Where thicker caul plates are used, the dimensional control over the size of detail parts in the assembly have to be correspondingly better. The advantage of using such a thick caul plate comes from the ability to give both sides of a sandwich part the smooth appearance usually obtained only on the 'tool side'.
- Ensure that core, pre-cured or rigid edges, inserts skins, or other relatively stiff parts comprising the lay-up, have close dimensional control to enable adhesives or resins to achieve the target strengths. In simple bonded assemblies, a figure of ± 0.1 mm is necessary, while assemblies having multiple layers of prepreg or many layers of thin metal doublers can sometimes be successfully produced with much less demanding dimensional tolerances.
- Many special purpose tools are available when core materials are cut, trimmed, carved or shaped. Sawing is the most common machining method, using either conventional blade tooth patterns, or, for some trimming operations, a special 'honeycomb band', in which the blade appears to be running backward, with the teeth sharpened on the back side so that each tooth acts as a slicing knife blade. A different type of saw is also used as a mandrel-mounted router bit. Router speeds vary from between 1,200 rpm to 30,000 rpm for blade diameters of 18mm to 100mm. Roll forming can be accomplished on metal cores, while non metal cores usually are heat formed. In either case, forming can be much easier if an inherently formable cell configuration is selected.

26.4 Failure modes and failure criteria

26.4.1 Survey of general 'sandwich failure modes'

26.4.1.1 General

Sandwich structures are intrinsically layered composite structures, where the variation of the material properties from layer to layer can be very large. Thus, sandwich structures can fail in several ways, each one giving a constraint on the load-carrying capability of the layered sandwich assembly.

The most commonly occurring failure modes are shown schematically in Figure 26.4.1, Ref. [26-1], [26-13].

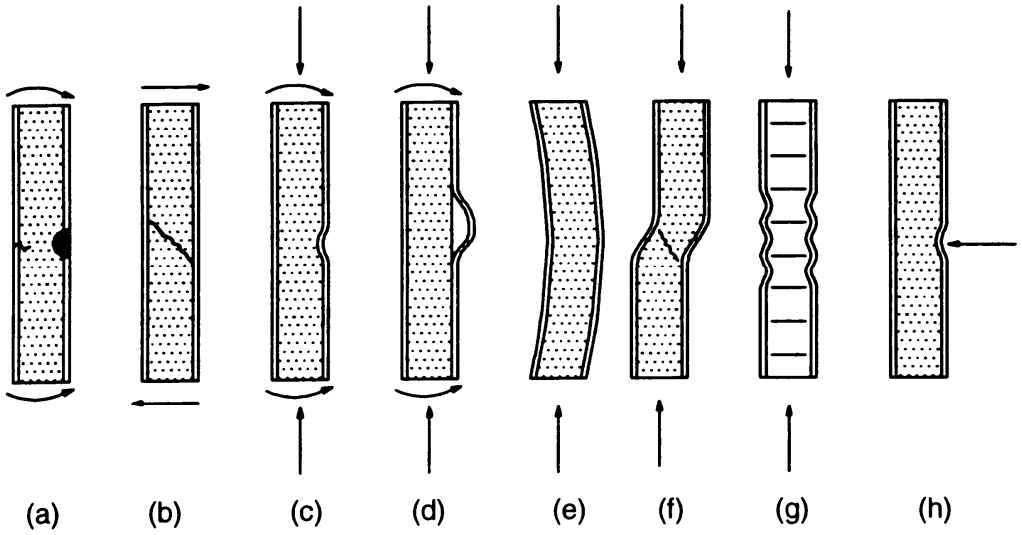

(a) Face fracture or yield
(b) Core shear
(c) and (d) Face wrinkling
(e) Global buckling
(f) Shear crimping
(g) Intracell buckling or dimpling
(h) Local indentation

Figure 26.4-1 – Sandwich panels: Common failure modes

26.4.1.2 Global modes

A number of failure modes are due to the 'global' loading of the sandwich structure, i.e. they appear together with deformation patterns that are directly related to the 'global' or 'overall' load response. These global failure modes include:

- Face fracture or yield failure – Figure 26.4.1a, where initial failure can occur in either the compression or tension face. It is caused by insufficient panel thickness, facing thickness or facing strength.
- Core shear failure – Figure 26.4.1b; which is caused by insufficient core strength or panel thickness.
- Global or general buckling – Figure 26.4.1e, which is caused by insufficient panel thickness or insufficient core shear rigidity, [See: 26.6].
- Shear crimping – Figure 26.4.1f, which sometimes occurs after, and as a consequence of, global buckling. It is caused by low core shear modulus, or low adhesive shear strength, [See: 26.6].

26.4.1.3 modes

In addition to the global modes of failure, a number of failure modes are determined by effects at a sub-structural or local level. These local failure modes include:

- Face wrinkling – Figure 26.4.1c and d, where the sandwich facing buckles with a short-wave local buckling pattern as a "plate on an elastic foundation". It can buckle inwards or outwards, depending on the relative strengths of the core in compression and the adhesive in flatwise tension, [See: 26.7].

- Intra-cell buckling or "dimpling" – Figure 26.4.1g, a local failure mode that only occurs in sandwich structures with cellular honeycomb type of cores. In addition, it only occurs with very thin facings and large core cells. This effect can cause failure by propagating across adjacent cells, thus inducing face wrinkling, [See: 26.7].
- Local indentation – Figure 26.4.1h, which is caused by insufficient bending stiffness of the facing or insufficient transverse core stiffness. It can lead to face fracture (or failure) or core crushing in cores with low compression strength, [See: 26.5].

[See: 26.6 and 26.7 for further discussion of the most important global and local instability and buckling failure modes]

26.4.2 Face failure

The face failure modes include:

- Brittle or yielding failure, depending on the properties and constitution of the facings.
- Failure in the fibre-reinforced composite facings, [See: Chapter 11] .
- Failure of the face loaded in compression. This failure mode can occur under the action of direct stresses, but is usually associated with buckling failure, which in turn can be either 'global' or 'local'; as shown in Figure 26.4.1.

26.4.3 Core failure

The core failure modes include:

- Shear failure; Figure 26.4.1b.
- Compression. This mode of failure is most often seen as core crushing under the action of local indentation loading; Figure 26.4.1h.
- Tension failure. This mode of failure is most often seen for polymeric foam materials in association with wrinkling failure; Figure 26.4.1d.
- Interface failure (adhesive). This mode of failure is most often seen in association with wrinkling or intracell buckling failure, where the adhesive interfaces can experience severe tensile and shear stresses; Figure 26.4.1d and g.

26.5 Modelling of sandwich structures

26.5.1 General

Sandwich panels are inherently layered structures containing at least five separate layers, i.e. two faces, a core and two adhesive layers. In many cases there are more layers, e.g. when laminated composite facings are used.

The modelling and analysis of sandwich structures can be carried out using a variety of different approaches, and the choice of model depends on the information and results needed. Thus, when analysing a sandwich assembly for design purposes, it is first necessary to decide which type of results are neeeded to enable decision-making in the design process.

A brief discussion is provided of the most common models and methods of analysis, together with some of the problems and issues that these can be used to assess.

26.5.2 Simple theories and ESL equivalent single layer models

26.5.2.1 General

From an analytical point of view, the simplest models are the so-called ESL (equivalent single layer) models or theories. There are several models belonging to this category. The common feature is that they treat the sandwich assembly as a single layer, in which a set of assumed kinematic relationships determine the variation of the displacement field through-the-thickness of the sandwich assembly under consideration.

The features of the two simplest first-order shear deformation and ESL theories are discussed briefly, i.e.:

- Love-Kirchhoff theory
- ESL and simple multi-layer theories

26.5.2.2 Classical and first-order shear deformation theories

The analyses corresponding to this class of theory assume that the transverse core stiffness is infinite, thus keeping the distances between the mid-surfaces of the faces constant, this is also known as an anti-plane core.

26.5.3 Love-Kirchhoff theory

The simplest way to model a sandwich structure is to adopt the classical beam, plate or shell theories, i.e. to adopt the basic small-deformation Bernoulli-Euler beam theory, or plate and shell theories based on the Love-Kirchhoff assumptions for:

- isotropic linear-elastic plates, Ref. [26-14].
- orthotropic composite plates, Ref. [26-15].

The baseline physical assumption in these theories is that plane cross sections (of beam, plate or shell elements) remain straight, strain-free and perpendicular to the reference axis or plane after deformation. With reference to Figure 26.5.1, the corresponding kinematic relations for a plate are:

$$u = u_0 - z\frac{dw}{dx}, \quad v = v_0 - z\frac{dw}{dy}, \quad w = w_0 \qquad [26.5\text{-}1]$$

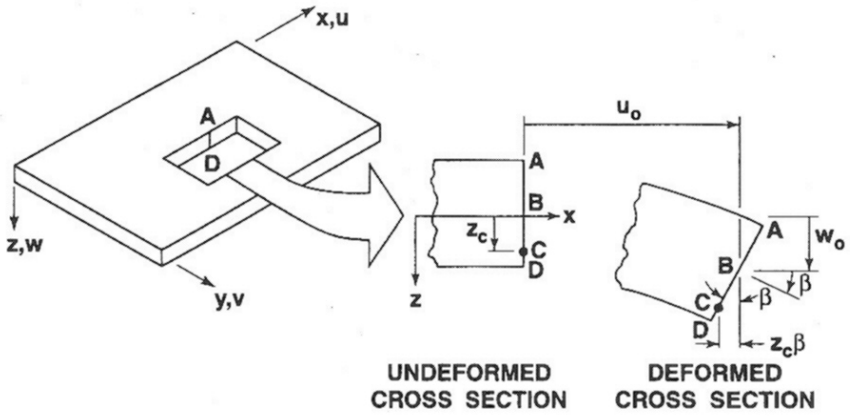

where subscript "0" refers to the middle plane. The displacements in the *x*, *y* and *z*-directions are denoted by *u*, *v* and *w*, respectively.

Figure 26.5-1 – Geometry of deformation for sandwich plate in *x*-*z* plane

The implication of Equation [26.5-1] is that the shear deformations are assumed to be nil, or that the transverse shearing angle γ is zero, thus implying that the deformations are solely caused by the action of the internal bending resultants.

This assumption is poor for the case of sandwich structures, which are characterised by having a relatively thick and compliant core material that is deformable in shear. Consequently, the results obtained are usually quite inaccurate, especially with respect to the predicted deformations. More specifically, the plate stiffness is over-predicted because the finite transverse shear stiffness is ignored.

With respect to the determination of the stress state, the model provides reasonably accurate estimates of the bending stresses, whereas the transverse shear stresses are much less accurately determined and the transverse normal stresses are not predicted at all.

Consequently, it is not advisable to analyse sandwich structures using classical beam, plate, shell models or theories based on the Love-Kirchhoff assumptions.

26.5.4 ESL and simple multi-layer theories

A more accurate and physically consistent model is obtained if the transverse shear deformations are included in analysis. The simplest way of doing this is to adopt the partial deflections approach. This refers to the baseline assumption that the total deflection for any type of sandwich structure, e.g. beams, plates or shells, consist of two parts (bending and shear) that can be superimposed:

$$w = w_b + w_s \qquad [26.5\text{-}2]$$

where:

w_b: *deflections due to internal bending resultants*

w_s: *deflections due to transverse shear resultants*

It is further assumed that the two different deformation parts w_b and w_s are independent.

In the classical first-order shear deformation theory, it is assumed that the shearing angle is constant over the cross-section, so that the kinematic relations corresponding to the Reissner-Mindlin plate theory can be used, Ref. [26-16], [26-17]:

$$u = u_0 + z\psi_x, \quad v = v_0 + z\psi_y, \quad w = w_0 \qquad [26.5\text{-}3]$$

where:

ψ_x: cross section rotations in the x-direction.

ψ_y : the cross section rotations in the y-direction

Reissner-Mindlin type plate theories are widely-used for the analysis and modelling of structures made of laminated composite materials. However, the inherent assumption that all layers behave in the same manner (an ESL theory) is less meaningful for structural sandwich plates, where two stiff face sheets (often composite laminates in their own right) are separated by a thick and compliant core material.

For sandwich plates, special variants of the first-order shear deformation theory were developed where a different behaviour is assumed for the faces and the core, Ref. [26-1], [26-18], [26-32], [26-55]. These models provide a more consistent physical interpretation of the behaviour of sandwich structures, while at the same time, they are mathematically as simple as the classical Reissner-Mindlin plate theory.

The partial deflections approach, in Equation [26.5-2], can also form the basis for the simplest multi-layer theory, where it is assumed that:

- faces obey the Love-Kirchhoff assumptions,
- shearing angle is assumed constant and non-zero across the core thickness.

This has proven reasonable for sandwich structures with so-called ‘weak’, ‘anti-plane’ or ‘compliant’ cores. These are equivalent concepts that are used to describe an idealised core in which the stretching and shearing stiffnesses in planes parallel with the face sheets are zero, but the shear modulus perpendicular to the face sheets is finite.

The kinematics corresponding to this type of structural sandwich plate model are shown in Figure 26.5.2, Ref. [26-1]. It forms the basis of the theories presented, Ref. [26-1], [26-18], [26-32], [26-55], and still assumes that the sandwich beam or plate thickness remains unchanged during deformation, i.e. transverse normal strains assumed to be zero.

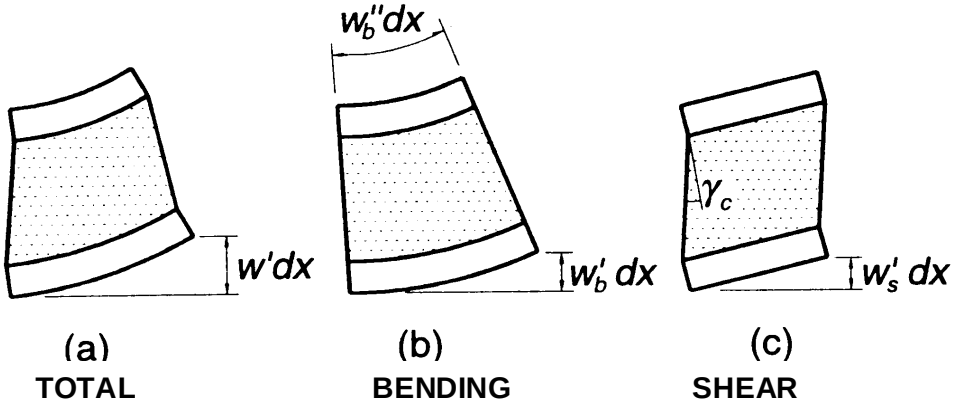

Figure 26.5-2 – Deformed sandwich element

Given the fundamental assumptions regarding the kinematics, a complete set of governing equations can be derived for the sandwich plate problem according to the simple multi-layer sandwich model. These equations and their solution for various problems are not reproduced here, Ref. [26-1], [26-18], [26-32], [26-55].

With respect to the deformations, the overall (global) displacements are predicted reasonably accurately using the Mindlin-Reissner model (ESL) or the simple multi-layer formulation. In fact, the two different model types provide predictions that are almost identical with respect to the overall (or global) deformation behaviour and stiffness.

Concerning the stress state, the two models provide accurate estimates of the bending stresses, whereas the shear and transverse normal stresses are not predicted directly. However, these stresses can be estimated by integration of the equilibrium equations through the sandwich laminate thickness.

Figure 26.5.3 shows the distribution of direct (bending) and shear stresses (obtained by integration of equilibrium equations throught the sandwich thickness) in a sandwich beam element for different levels of approximation, Ref. [26-1].

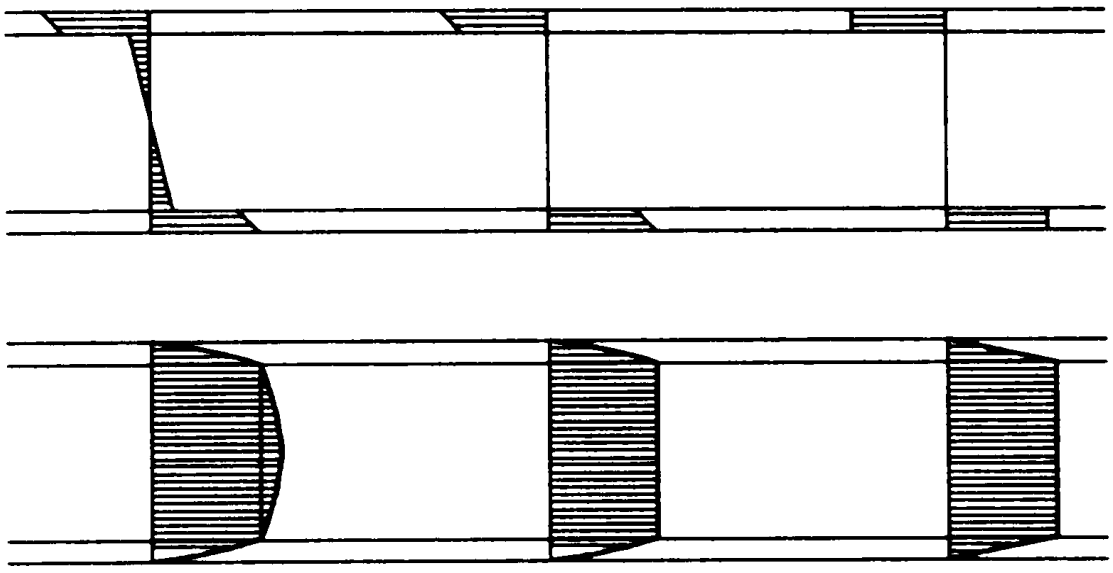

No approximations $E_c << E_f$ $E_c <<$ **E**$_f$ **and** $t_f << t_c$

Figure 26.5-3 – Bending and shear stresses in sandwich element for different levels of approximations

It is seen from Figure 26.5.3 that ideally the faces are loaded in a membrane state of stress, whereas the core is loaded in a state of uniform shear. Thus, the role of the faces is to carry the bending moment loading, and the role of the core is to carry the shear load.

The models described comply with the so-called C_z^0-compatibility requirements, which includes single-layer (with C_z^1-compatibility) as well as multi-layer models.

26.5.4.1 ESL and simple multi-layer models: Advantages and disadvantages

ESL and simple multi-layer models other than the classical and first-order shear deformation theories also exist, Ref. [26-19].

The advantages and disadvantages associated with the use of ESL and simple multi-layer formulations can be summarised as:

- Advantages:
  - Simple to use.
  - Computationally cost effective.
  - Good prediction of global deformation behaviour if transverse shear effects are included, i.e. first-order shear deformation theory or higher).
  - Good prediction of global or overall bending and shear stresses.

- Disadvantages:
  - Do not account accurately for the inherent layered nature of sandwich structures.
  - Based on the assumption of an anti-plane core, i.e. they do not account for the transverse flexibility of the sandwich core (sandwich panel thickness assumed to be constant). Thus, inherently, the transverse normal strain is assumed zero.
  - Do not provide a physically consistent description and interpretation of the boundary conditions imposed on a sandwich structure; as shown in Figure 26.5.4.
  - The shear and transverse normal stresses cannot be derived directly due to the limitations imposed through the assumed kinematic behaviour. However, these stresses can be estimated by direct integration of the equilibrium equations through the sandwich laminate thickness.
  - Do not accurately account for the inducement of local effects, e.g. the stress concentrations occurring under the action of localised loading, in the vicinity of restrictive boundary conditions or near joints.

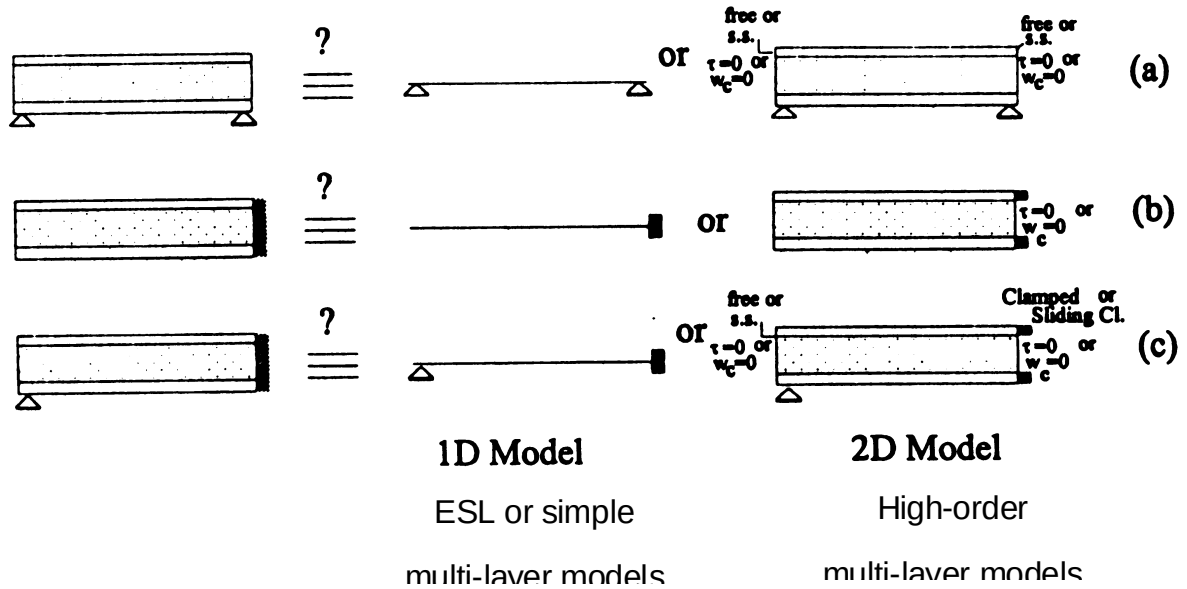

Figure 26.5-4 – Boundary conditions imposed on a sandwich panel

26.5.5 High-order and advanced multi-layer models

26.5.5.1 General

Various high-order theories exist for the modelling of multi-layered structures, both as laminates and sandwiches, Ref. [26-20], [26-21], [26-22], [26-23]. In the literature, high-order through-the-thickness displacement fields in the form of polynomials of varying order or trigonometric series are assumed *a priori* for each layer. The governing equations and the appropriate boundary conditions are derived using integration through-the-thickness along with a variational principle.

26.5.5.2 Special high-order formulation

A special high-order formulation for the analysis of symmetric *3*-layer sandwich plates, Ref. [26-19], includes the presence of transverse normal stresses in the core material. The transverse flexibility is, however, not included in the formulation, thus ignoring the effects associated with changes of the plate thickness, i.e. $\varepsilon_z = 0$.

26.5.5.3 Shear and transverse normal stresses

More recently, two cost-effective finite-element formulations for the rapid estimation of the shear and transverse normal stresses in sandwich structures were proposed and evaluated, Ref. [26-72].

With simple and more advanced multi-layer models, it is possible to estimate the shear and transverse normal stresses by direct integration of the equilibrium equations in the through-the-thickness direction. This additional procedure, in that it is additional relative to the restrictive assumptions specified, is based entirely on equilibrium considerations. It has proven to be efficient and reasonably accurate for both monolithic and composite layered beam and plate structures in which the individual layers are of comparable constitution in terms of stiffness properties. However, in some cases it fails to describe accurately the load redistribution due to the interaction between the 'deformation' (stiffness) and 'stress' problems that are inherently coupled for any statically indeterminate problem. Bending of beams, plates and shells are inherently statically indeterminate problems. These are especially important for sandwich-type structures with stiff faces and compliant or soft cores.

26.5.5.4 Transverse flexibility of the core

The importance of including the transverse flexibility of the core, i.e. to account for core thickness changes during deformation of the sandwich panel, becomes especially important when addressing problems associated with load-introduction or support and those involving material and geometric discontinuities in sandwich structures with soft or compliant cores.

To address these concerns, a special high-order theory was developed that was specially adapted for the analysis of sandwich structure panels with soft or compliant cores, i.e. two face sheets separated by a compliant core material, Ref. [26-24], [26-25], [26-26], [26-27], [26-28].

In this particular formulation, no restrictions on the through-the-thickness displacement distributions are initially imposed, and the high-order effects predicted by the theory are direct results of the formulation.

The formulation includes the transverse flexibility of the core material; thus enabling the description of localised bending effects associated with local changes in the sandwich panel thickness.

The assumptions in this formulation are:

- The faces are modelled as laminated beams or plates obeying the Love-Kirchhoff assumptions.
- The core is modelled as an elastic continuum only possessing transverse normal and shear stiffnesses, i.e. the in-plane Young´s modulus parallel with the faces is assumed to be nil. This again implies that the in-plane core normal stresses are zero. In other words, the core type considered is a transversely isotropic 'weak' core where the plane of isotropy is parallel to the core middle plane.

Considering, for simplicity, a sandwich beam, the assumptions made, together with the enforcement of compatibility of displacements across the core-to-face interfaces, leads to the closed-form solution for the stress and displacement field in the core material:

$$\tau_c(x,z) = \tau_c(x)$$

$$\sigma_{cz}(x,z) = \frac{E_c}{t_c}\left(w_b - w_t\right) + \tau_{c,x}\left(\frac{t_c}{2} - z\right)$$

$$w_c(x,z) = w_t + \left(w_b - w_t\right)\frac{z}{t_c} - \frac{\tau_{c,x} z\left(z - t_c\right)}{2E_c} \qquad \text{[26.5-4]}$$

$$u_c(x,z) = \frac{\tau_c z}{G_c} - \frac{\tau_{c,xx}}{2E_c}\left(\frac{z^2 t_c}{2} - \frac{z^3}{3}\right) - w_{b,x}\frac{z^2}{2t_c} - w_{t,x}\left(-\frac{z^2}{2t_c} + z + \frac{t_{ft}}{2}\right) + u_{0t}$$

Where:

τ_c : *core shear stress;*

σ_{cz} : *core transverse normal stress;*

w_b : *out-of-plane displacements of the bottom face sheet;*

w_t : *out-of-plane displacements of the top face sheet;*

u_{0t} : *longitudinal displacement of the mid-line of the top face;*

u_c : *longidudinal displacements of the core;*

t_c : *core thickness,*

t_{ft} : *thickness of the top face*

$(),_x$: *the first-order derivatives (gradients) of the variables stated.*

$(),_{xx}$: *the second-order derivatives (gradients) of the variables stated.*

Figure 26.5.5, Ref. [26-24], [26-25], [26-26], shows the non-linear variation of the core displacement components through-the-thickness of the core for the sandwich beam case; predicted by Equation [26.5-4]. It shows that cross sections that are plane prior to deformation do not remain plane after deformation; compare this with Equation [26.5-1] and Equation [26.5-3]).

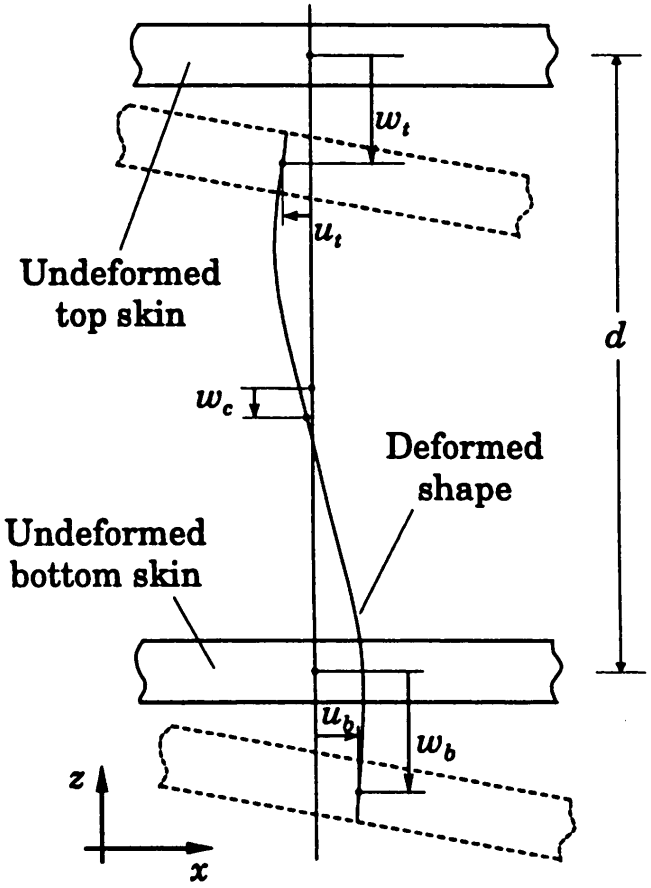

Figure 26.5-5 – Non-linear displacements through sandwich cross-section

In addition, Equation [26.5-4] predicts the presence of transverse normal stresses in the core that vary linearly across the core thickness. The core shear stresses are also predicted to be constant through-the-thickness of the core. The results can be generalised to sandwich plates and shells.

The high-order sandwich theory, as applied for the analysis of 3-layer sandwich panels with soft or compliant cores, was validated experimentally, Ref. [26-29], [26-30], and validated through a comprehensive comparative study with other models, including finite-element and exact theory of elasticity solutions, Ref. [26-31].

Such high-order sandwich theory formulations have been used for the study and analysis of a multitude of sandwich panel problems involving localised effects, such as sandwich panels with inserts under general loading conditions, Ref. [26-65], [26-66], [26-67].

[See also: 26.6, 26.8]

26.5.5.5 High-order sandwich theory: Advantages and disadvantages

The advantages and disadvantages associated with the use of the high-order sandwich theory can be summarised as:

- Advantages:
  - Physically consistent modelling of the inherent layered nature of sandwich structures
  - Physically consistent modelling and interpretation of boundary conditions: boundary conditions are imposed on each layer of the assembly, i.e. top face, core and bottom face.
  - Includes 'global' as well as local bending and shearing effects, i.e. it captures the overall deformations and load response, along with the local deformations and stress concentrations occurring under the action of localised loading in the vicinity of restrictive boundary conditions, e.g. near joints.
- Disadvantages:
  - High mathematical complexity.
  - Closed-form solutions difficult to obtain.
  - Can be computationally expensive.

26.5.6 Localised effects

26.5.6.1 General

Sandwich structures are notoriously sensitive to failure by the application of concentrated external loads, due to localised effects in the vicinity of restrictive boundary conditions or due to abrupt geometric and material changes.

26.5.6.2 Local bending

Figure 26.5.6 illustrates the load response corresponding to the very simple case of a sandwich beam subjected to 3-point bending load (concentrated line loading).

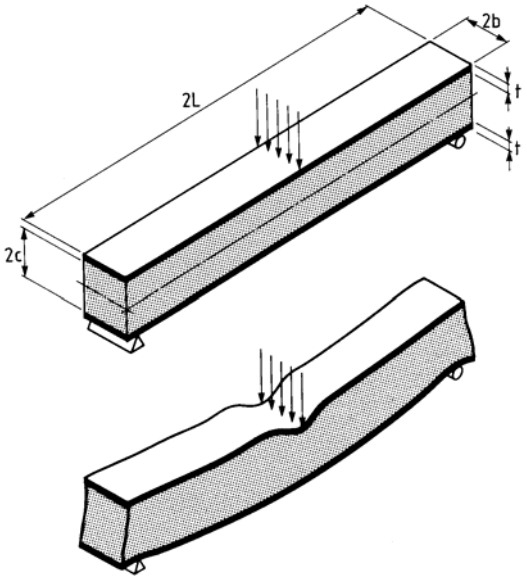

Figure 26.5-6 – Sandwich panel: Local bending effects

The problem of localised bending is inherently associated with transverse core flexibility, i.e. the thickness of the sandwich can change during deformation. Whilst this can be analysed using the high-order sandwich theory, it is also possible to obtain a simple approximate solution (estimate) by adopting the analogy of considering the loaded facing as a beam or plate supported by an elastic foundation; as shown schematically in Figure 26.5.7.

Further details concerning the treatment of localised effects and use of the elastic foundation analogy are given in Ref. [26-32].

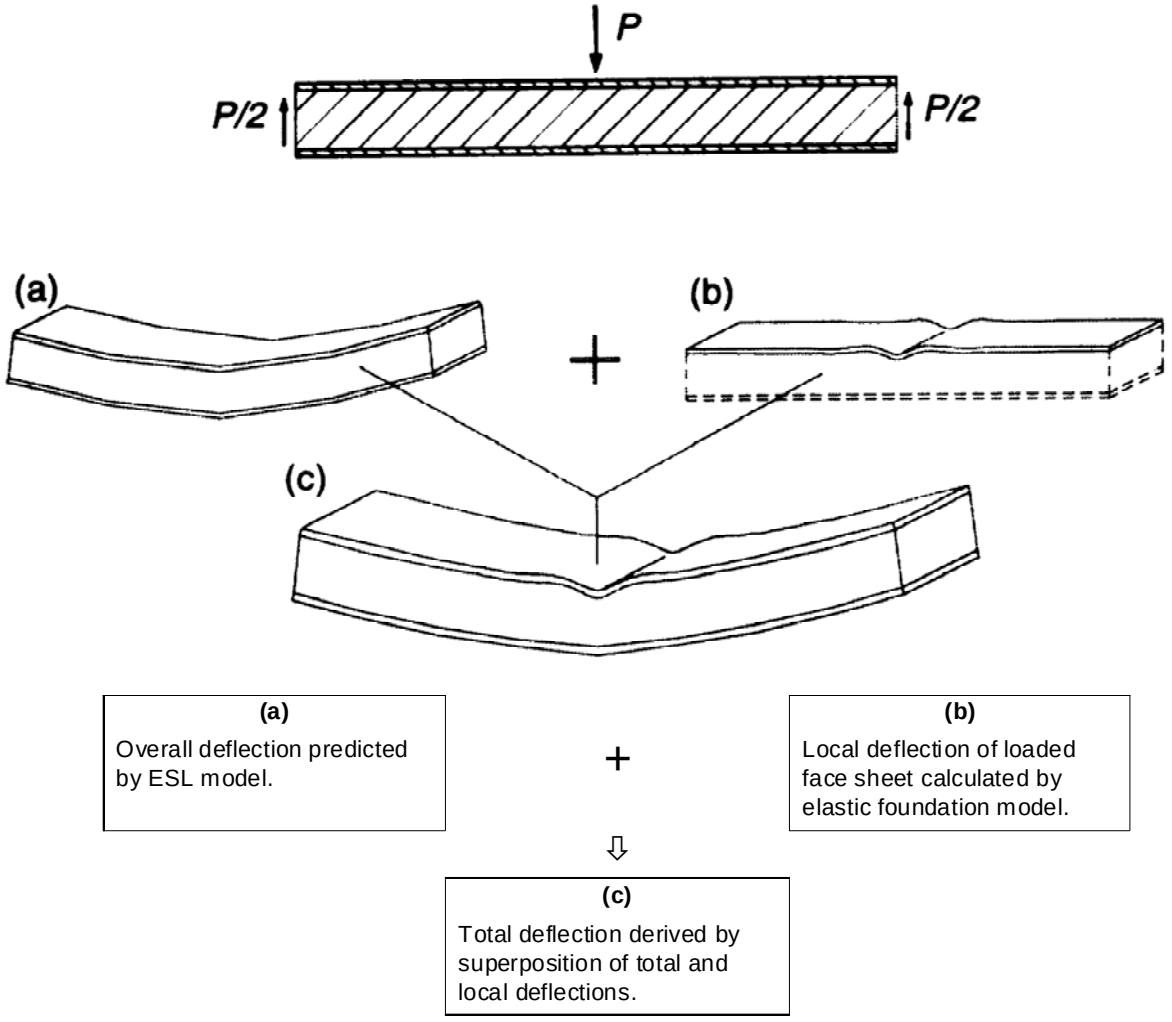

Figure 26.5-7 – Approximate modelling of local bending effects in sandwich panel loaded in 3-point bending

26.5.7 FEA finite element analysis

26.5.7.1 General

Detailed analysis and design studies of sandwich structures are usually carried out using finite element analysis (FEA).

26.5.7.2 Stiffness and strength analysis

For stiffness and strength analyses sandwich structures are usually modelled with 2D shell elements with equivalent membrane, bending and transverse shear properties or with 2D layered shell elements in which equivalent homogeneous orthotropic properties are used for the core layer.

Most finite element codes do not directly provide margin of safety (MOS) for sandwich failure modes. Hence, general element forces are extracted from the strength analysis and used in laminate analysis programs or special post-processing routines to calculate MOS.

Equations to calculate the MOS against typical sandwich failure modes such as face sheet failure, wrinkling, dimpling or face sheet buckling are given. For global structural buckling analyses of sandwich structures, knock-down factors that account for imperfections in the structure and loads need to be applied, [See: 26.6].

An additional issue of special concern when conducting stiffness and strength analysis of sandwich structures using 2D shell elements is the effect referred to as 'shear locking', Ref. [26-33]. Shear locking represents an artificial and non-physical stiffening effect, which is inherently induced in many 2D shell finite elements. Different FEA formulations attempt to circumvent this problem, Ref. [26-33], but so far no generally applicable methods to avoid this exists. Thus, for each particular case where FEA analysis is conducted on sandwich structures care is needed to eliminate shear locking effects by careful convergence studies and by proper choice of finite element formulation.

26.5.7.3 Thermal and thermo-elastic analyses

For thermal and thermo-elastic analysis of dimensionally-stable structures, a more accurate representation of sandwich structures is needed. The through-thickness thermal expansion of the sandwich core can have a significant influence on thermo-elastic distortions, particularly for curved or doubly-curved structures such as reflectors. In addition, when the core is bonded between face sheets it has some influence on the in-plane stiffness, which is usually neglected in the simple sandwich models.

Under space environmental conditions, significant temperature gradients can develop in the plane of the structure as well as through the thickness of the sandwich assembly. The through-thickness temperature gradient strongly depends on an equivalent thermal conductivity that includes material thermal conductivity and radiative heat exchange.

To account for these effects, a common approach is to model the core with 3D solid elements having homogenised core material properties and the face sheets with shell or layered shell elements. The homogenised core properties can in the simplest case be defined using handbook-type equations or analytical models as implemented in composite analysis software such as ESAComp. However, detailed finite element models of representative unit cells of the sandwich in which each cell of the core, the adhesive between core and skin and the skins are modelled, often need to be used to derive homogenised properties. The use of such detailed models for larger structures such as an entire reflector are usually time, cost and resource prohibitive. Instead, different homogenisation methods are discussed in Ref. [26-34], [26-35], [26-36].

26.5.7.4 Localised effects

Owing to the low stiffness and strength in the thickness direction of sandwich structures, the design of local load introductions, corners and joints needs to be validated through 2D or 3D analyses to a much larger extent than is usually the case for monolithic metallic and composite structures.

For the same reason, curved sandwich shells with small radii of curvature (rule of thumb: less than 10 times the sandwich shell thickness) also need to be analysed in 3D to account for the transverse normal stresses not included in 2D shell elements.

26.6 Global buckling instability of sandwich structures

26.6.1 General

Overall or global buckling is one of the failure modes of concern in the design of sandwich structures, [See: Figure 26.4.1, e and f]. A few criteria for such instability phenomena are discussed briefly.

The global buckling instability modes that occur in sandwich structures, [See: 26.4], are presented in some detail along with their modelling, within the theoretical framework known as ESL, equivalent single layer, models, [See: 26.5].

Whilst these theories are available in a wide number of published sources, the aim here is to provide the designer with a basic understanding of the use of such theories and the restrictive assumptions applied.

Over the past 30 to 40 years, a number of theories and approaches have evolved for the analysis of sandwich shells. Buckling of sandwich cylinders is a particularly complex matter that cannot be accomplished accurately by simple closed-form, hand calculations.

A review of a number of common theories is included to enable designers to make an informed selection as to which is appropriate for their particular application, [See: 26.6.4].

In all cases, the theories and approaches presented can be used for preliminary design purposes only.

[See also: 26.7 for local buckling instability of sandwich structures]

26.6.2 Buckling of sandwich panels

26.6.2.1 General

Buckling of itself sometimes does not damage a sandwich structure, but it still should be avoided since a structure that has buckled can have lost its capacity of fulfilling its purpose.

The actual buckling load can also be the ultimate load-bearing capacity of the sandwich structure or component, since its buckled shape cannot sustain any further loading. Whether initial buckling leads to loss of stability, or the sandwich structure can in fact sustain further loading into the post-buckled regime depends on the actual structural configuration.

Post-buckling behaviour is not treated any further herein, but a few important results regarding buckling of simply-supported sandwich plates, core shear instability and circular cylindrical sandwich shells are discussed.

[See: Chapter 27 for the design of thin-walled structures including plate analysis and buckling analysis]

26.6.2.2 Isotropic sandwich plate with thin faces

The governing stability equation for buckling of isotropic sandwich plates with thin faces can be derived from a first-order shear deformation theory applicable to sandwich plates [See: Equation [26.5-3]. Such a theory can be developed easily using basic assumptions; described in 26.5, [See: Figure 26.5.2], i.e. by assuming an anti-plane core and adopting the partial deflections approach; [See: Equation [26.5-2]].

Assume that a rectangular sandwich plate of side lengths a and b, respectively, is subjected to in-plane forces N_x and N_y, equal to $-P_x$ and $-P_y$ in the x and y direction respectively; as shown in Figure 26.6.1.

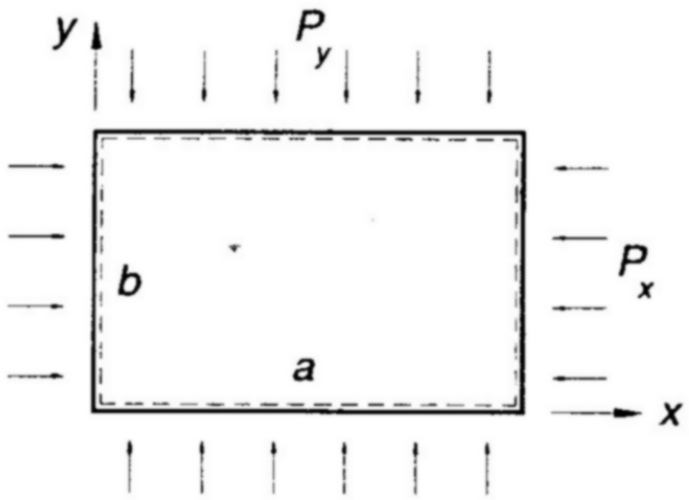

Figure 26.6-1 – Sandwich plate subjected to biaxial compression

For simply supported edges along all four sides of the plate, the assumed lateral displacement satisfying the boundary conditions along the edges $x = 0,a$ and $y = 0,b$ is represented by:

$$w = \hat{w} \sin \frac{m\pi x}{a} \sin \frac{m\pi y}{b} \qquad [26.6\text{-}1]$$

Where:

m : number of half waves in the x-direction

n : the number of half waves in the y-direction

ŵ : the amplitude of the buckling pattern.

Inserting Equation [26.6-1] in the governing plate equations, Ref. [26-1], [26-32], [26-37], yields the governing stability equation for which the minimum (with respect to the wave numbers m and n) is sought for given in-plane loads P_x and P_y:

$$\frac{D}{(1-\nu^2)}\left[\left(\frac{m\pi}{a}\right)^2+\left(\frac{n\pi}{b}\right)^2\right]=\left[P_x\left(\frac{m\pi}{a}\right)^2+P_y\left(\frac{n\pi}{b}\right)^2\right]\left[1+\frac{D}{S(1-\nu^2)}\left\{\left(\frac{m\pi}{a}\right)^2+\left(\frac{n\pi}{b}\right)^2\right\}\right] \qquad [26.6\text{-}2]$$

Where:

D : the bending rigidity,

S : the transverse shear stiffness

ν : the Poisson´s ratio of the sandwich plate.

The sandwich plate stiffness parameters, given in Equation [26.6-2] can be evaluated approximately by Equation [26.6-3], which is valid for isotropic faces and core, Ref. [26-1]:

$$D = \int z^2 E dz \approx \frac{E_{ft} t_{ft} E_{fb} t_{fb} d^2}{(E_{ft} t_{ft} + E_{fb} t_{fb})},$$

$$S \approx \frac{G_c d^2}{t_c}, \quad d = \frac{(t_{ft} + t_{fb})}{2} + t_c$$

[26.6-3]

Where:

t_{ft}, *: the thicknesses of the top face.*

t_{fb} *: bottom face and core,*

t_c *: the thicknesses of the core.*

E_{ft} *: the Young´s moduli of the top faces.*

E_{fb} *: the Young´s moduli of the bottom faces.*

As a simple example, assume now that the compression loading is uniaxial with $N_x = -P_x = -P$ and $N_y = -P_y = 0$.

The minimum value of Equation [26.6-2] always corresponds to n = 1 for this load case, and after insertion and simplification the non-dimensional buckling coefficient K can be expressed as, Ref. [26-1]:

$$K = \frac{(1-\nu^2)b^2}{\pi^2 D} P = \frac{\left(\frac{mb}{a} + \frac{a}{mb}\right)^2}{1 + \pi^2 \theta \left[\left(\frac{mb}{a}\right)^2 + 1\right]}$$

[26.6-4]

Where:

θ = $D/(1\text{-}\nu 2)b2S$ is the shear factor.

The expression given by Equation [26.6-4] can be found also in many other references including Ref. [26-37].

Leissa, Ref. [26-37], presents a survey of the most important works on the buckling analysis of plates and shells including sandwich plates, but with slightly different notation. The actual buckling load is found from Equation [26.6-4] for the value of *m* giving the minimum load *P*.

Figure 26.6.2 shows a plot of the values determined by Equation [26.6-4], Ref. [26-1], [26-37].

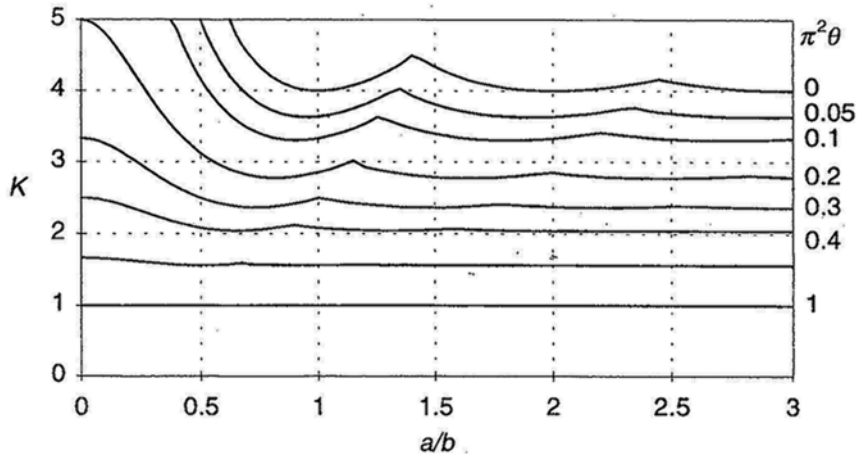

Key: Lines correspond to $\pi^2\theta$ = 0, 0.05, 0.1, 0.2, 0.3, 0.4, 0.6 and 1.0, Ref. [1].

Figure 26.6-2 – Buckling coefficients for a simply supported isotropic sandwich plate subjected to uniaxial compression

Figure 26.6.2 shows that the effect of finite shear stiffness is that for a given aspect ratio *a*/*b*, the buckling coefficient *K* is lowered compared with classical isotropic plates (shear factor $\theta = 0$), and that the buckling mode is shifted towards an increased number of buckles.

For the case of the shear stiffness, *S*, approaching infinity (i.e. shear factor $\theta = 0$), i.e. corresponding to a plate with infinite shear stiffness (classical thin plate theory), Equation [26.6-4] becomes, Ref. [26-1]:

$$K = \frac{(1-\nu^2)b^2}{\pi^2 D} P_b = \left(\frac{mb}{a} + \frac{a}{mb}\right)^2 \qquad [26.6\text{-}5]$$

This is the buckling coefficient of an ordinary isotropic plate (pure bending buckling).

At the other limit, the bending stiffness, *D*, equals infinity, Equations. [26.6-4] becomes, Ref. [26-1]:

$$K = \frac{(1-\nu^2)b^2}{\pi^2 D} P_s = \frac{\left(1+\left(\frac{a}{mb}\right)^2\right)}{\pi^2 \theta}$$

or [26.6-6]

$$P_s = S\left(1+\left(\frac{a}{mb}\right)^2\right)$$

This corresponds to pure shear buckling.

26.6.2.3 Orthothropic sandwich plate with thin faces

For the case of sandwich plates with orthotropic laminated dissimilar faces, the procedure for deriving the governing stability equation, assuming simply-supported conditions along all four plate edges, is the same as for the anti-plane core, first-order shear deformation theory based on partial deflections approach.

Accordingly, the lateral displacements of the sandwich plate can again be described using Equation [26.6-1].

Assuming now that the sandwich plate is loaded in uniaxial compression loading N_x ; shown in Figure 26.6.1

By using the notation, Ref. [26-1]:

$$\theta_x = \frac{D_x}{a^2 S_x (1-\nu_{xy}\nu_{yx})},$$

[26.6-7]

$$\theta_y = \frac{D_y}{b^2 S_y (1-\nu_{xy}\nu_{yx})}$$

For the shear factors (isotropic sandwich case):

$\theta_x = \theta_y = \theta = D/(1\text{-}\nu 2)b2S)$

and, by identifying that the minimum buckling load corresponds to n=1, i.e. one wave only in the direction perpendicular to the load, then the governing stability equation for which the minimum with respect to the wave number m is sought for a given in-plane load Px is expressed as, Ref. [26-1]:

$$\frac{b^2(1-\nu_{xy}\nu_{yx})}{\pi^2 D_y}\left(\frac{mb}{a}\right)^2\left[\frac{\pi^4\theta_y^2 S_y}{S_x}\left(1-\frac{\nu_{xy}^2 D_y}{D_x}\right)\left\{\frac{D_x D_{xy}}{2D_y^2}\left(\frac{mb}{a}\right)^4+\frac{D_x-\nu_{xy}D_{xy}}{D_y}\left(\frac{mb}{a}\right)^2+\frac{D_{xy}}{2D_y}\right\}\right.$$

$$\left.+\pi^2\theta_y\left\{\left(\frac{mb}{a}\right)^2\left(\frac{D_x S_y}{D_y S_x}+\frac{D_{xy}}{2D_x}\left(\frac{D_x}{D_y}-\nu_{xy}^2\right)\right)+\left(1+\frac{D_{xy}}{2D_x}\left(\frac{D_x}{D_y}-\nu_{xy}^2\right)\frac{S_x}{S_y}\right)\right\}+1\right] \qquad \text{[26.6-8]}$$

$$=\pi^2\theta_y\left(1-\frac{\nu_{xy}^2 D_y}{D_x}\right)\left[\frac{D_x D_{xy}}{2D_y^2}\left(\frac{mb}{a}\right)^4+\frac{D_x-\nu_{xy}D_{xy}}{D_y}\left(\frac{mb}{a}\right)^2+\frac{D_{xy}}{2D_y}\right]\left[\left(\frac{mb}{a}\right)^2+\frac{S_x}{S_y}\right]$$

$$+\frac{D_x}{D_y}\left(\frac{mb}{a}\right)^4+2\left(\frac{D_{xy}}{D_y}-\frac{\nu_{xy}^2 D_{xy}}{D_x}+\nu_{xy}\right)\left(\frac{mb}{a}\right)^2+1$$

Where:

D_x, D_y and D_{xy} are the sandwich plate bending stiffnesses

S_x and S_y, and the sandwich plate shear stiffnesses

All these values are given by the expressions, Ref. [26-1]:

$$D_x = \int z^2 E_{fx} dz \approx \frac{E_{fxt} t_{ft} E_{fxb} t_{fb} d^2}{E_{fxt} t_{ft} + E_{fxb} t_{fb}},$$

$$D_y = \int z^2 E_{fy} dz \approx \frac{E_{fyt} t_{ft} E_{fyb} t_{fb} d^2}{E_{fy1} t_{f1} + E_{fy2} t_{f2}}$$

$$D_{xy} = \int 2z^2 G_{fxy} dz \approx \frac{G_{fxyt} t_{ft} G_{fxyb} t_{fb} d^2}{G_{fxyt} t_{ft} + G_{fxyb} t_{fb}}$$

[26.6-9]

$$S_x = \frac{G_{cxz} d^2}{t_c},$$

$$S_y = \frac{G_{cyz} d^2}{t_c},$$

$$d = \frac{\left(t_{ft} + t_{fb}\right)}{2} + t_c$$

Where:

t_{ft}, : *thickness of the top face*

t_{fb} : *thickness of the bottom face*

t_c : *thickness of the core*

E_{fit} : *Young's modulus of the top face in the x-and y-directions,*

E_{fib} : *the Young's modulus of the bottom face in the x-and y-directions,*

$_i=_{x,y}$: *x-and y-directions,*

G_{fxyt} : *in-plane shear moduli of the top face*

G_{fxyb} : *the in-plane shear moduli of the bottom face.*

G_{cxz} *and* G_{cyz} : *the core shear moduli.*

The expressions in Equation [26.6-9] are derived by following a straightforward strength of materials approach, and the resulting "physical" sandwich plate stiffness coefficients, can be related to the bending stiffnesses D_{ij}, (i,j=1,2,6) and the transverse shear stiffnesses A_{ij} (i,j=4,5) in so-called

"contracted notation" defined from classical lamination theory, [See: Chapter 10 and Chapter 27; Ref. [26-15] as given in Equation [26.6-10], Ref. [26-1]:

$$D_{11} = \frac{D_x}{1-\nu_{xy}\nu_{yx}}, \quad D_{22} = \frac{D_y}{1-\nu_{xy}\nu_{yx}}, \quad D_{12} = \frac{\nu_{yx}D_x}{1-\nu_{xy}\nu_{yx}} = \frac{\nu_{xy}D_y}{1-\nu_{xy}\nu_{yx}}, \quad 2D_{66} = D_{xy}$$
$$A_{44} = t_c G_{cyz} \approx S_y, \quad A_{45} = 0, \quad A_{55} = t_c G_{cxz} \approx S_x \qquad [26.6\text{-}10]$$

Equation [26.6-8] appears somewhat complex, but by plotting the in-plane compressive load P_x against the aspect ratio a/b for various integral values of the wave number m, the same kind of buckling curves, as shown in Figure 26.6.2, for isotropic sandwich plates can be developed. The non-dimensional buckling coefficient K can be defined as:

$$K = \frac{b^2(1-\nu_{xy}\nu_{yx})}{\pi^2 D_x} \qquad [26.6\text{-}11]$$

Figure 26.6.3 shows the influence of varying the transverse properties on the buckling of a simply-supported sandwich plate subjected to uniaxial compression loading P_x, Ref. [26-1].

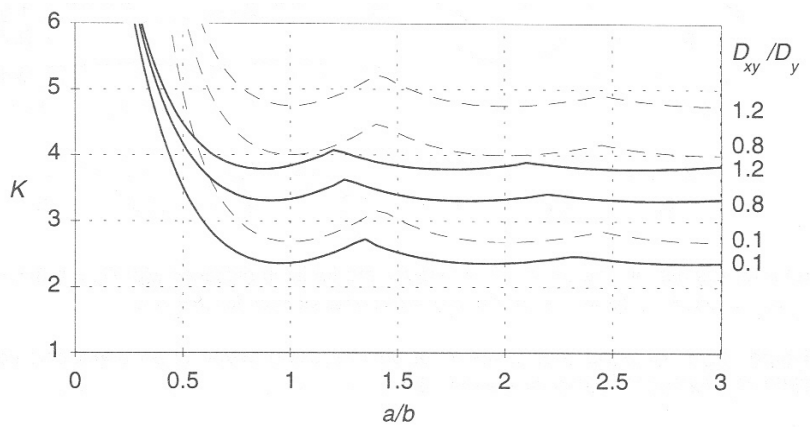

(a) *K* versus *a/b* for different D_{xy}. All curves are for $D_x=D_y$, $\nu_{xy}=\nu_{yx}=0.25$ and isotropic core. Solid lines are for $\pi^2\theta_x=\pi^2\theta_y=0.1$ and dashed lines for $\pi^2\theta=0$ (i.e. classical thin plate).

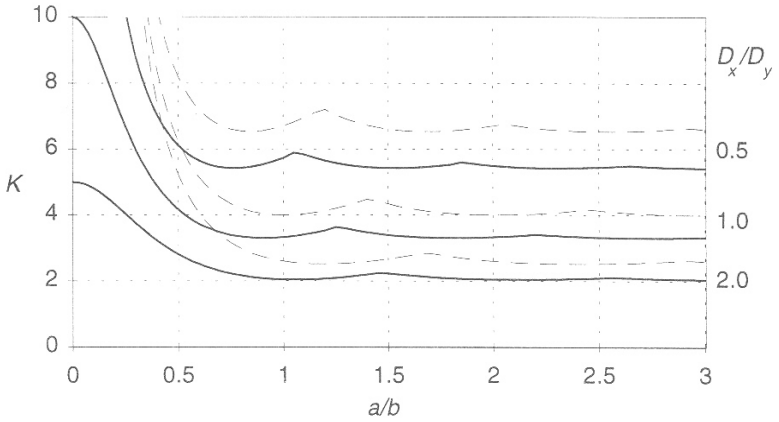

(b) *K* versus *a/b* for different D_y. All curves are for $D_{xy}=0.8D_x$, $\nu_{xy}=\nu_{yx}=0.25\sqrt{D_x/D_y}$ and isotropic core. Solid lines are for $\pi^2\theta_y=0.1$ and dashed lines for $\pi^2\theta_y=0$.

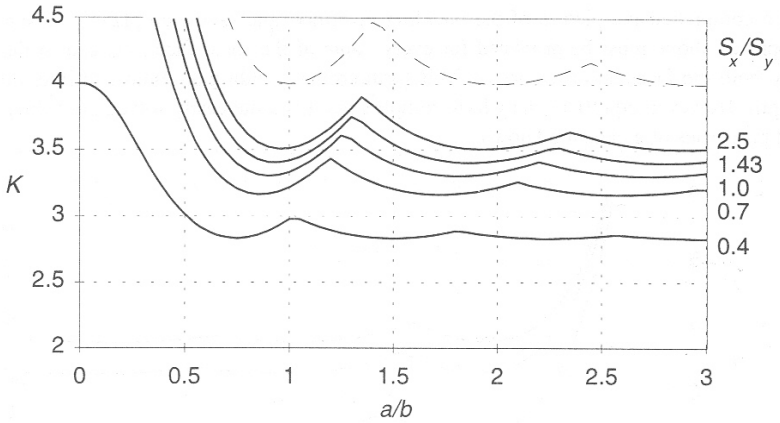

(c) *K* versus *a/b* for different S_x/S_y. All curves are for isotropic faces with $D_{xy}=0.8D_x=0.8\,D_y$ $\nu_{xy}=\nu_{yx}=0.25$. Solid lines are for $\pi^2\theta_y=0.1$ and dashed lines for $\pi^2\theta_y=0$.

Figure 26.6-3 – Buckling coefficients K versus a/b orthotropic sandwich plates loaded in uniaxial compression

From Figure 26.6.3 it is seen that the critical buckling load decreases with decreasing torsional stiffness D_{xy}, and it also decreases if the bending stiffness D_y or the shear stiffness S_y in the direction perpendicular to the load, respectively, decreases.

For a more comprehensive set of buckling curves for laminated composite and sandwich plates subjected to various loading conditions and assuming a multitude of different boundary conditions, reference is given by Leissa, Ref. [26-37]. In addition, the software package ESAComp can evaluate the buckling loads for composite laminated and sandwich plates.

26.6.3 Shear "crimping"

The shear crimping failure mode, [See: Figure 26.4.1 f], is actually the same as the limit of the general buckling mode considering thin faces, i.e. when the critical load equals P_s=S; Equation [26.6-6].

The failure is due to pure shear instability, and is most often caused as a result of large out-of-plane deformations in a post-buckled state, when the transverse shear resultants build up due to the excessive deformation.

26.6.4 Buckling of cylindrical sandwich shells subjected to axisymmetric compression loading

26.6.4.1 General

Solutions for the critical buckling strength of sandwich cylindrical shells with orthotropic facing material for the face sheets and orthotropic core are given in Ref. [26-38], [26-39], [26-40], [26-41], [26-42].

Most of these methods are variations of solutions being established for orthotropic cylinders and neglect the transverse shear deformation or the in-plane shear and torsional rigidity.

Table 26.6.1 summarises the features of these various methods. A comprehensive and perhaps the most complete analysis is given by Bert, Crisman and Nordby; Ref. [26-38]. This considers both the orthotropic properties of the face sheets and the transverse shear stiffnesses, G_{cxy} and G_{cyz}, of the core.

A comparison of failure loads, calculated by the different methods is also summarised in Table 26.6.1, Ref. [26-43]. This shows that the results can vary by about 30%.

Table 26.6-1 - Comparison of sandwich shell failure load predictions

Method [Reference]	Normalised critical buckling load n_{xc}		K.D.F (2)	N^*_{xc} (3)	Transverse shear deformation included
	without in-plane shear and torsional rigidity	with in-plane shear and torsional rigidity			
BOSOR 4 Ref. [26-44]	0.81 - 0.93 (1)	1.05	1.0	1.05	N
Bert, Crisman, Nordby Ref. [26-38]	-	1.0 (5)	1.0 (5)	1.0 (5)	Y
NASA SP 8007 Ref. [26-39]	-	1.4	0.91 (4)	1.27	Y
Dickson Ref. [26-45]	0.77	-	1.0	-	N
van der Neut Ref. [26-46]	0.79	1.12	1.0	1.12	N
Tennyson Ref. [26-47]	-	1.09	1.0	1.09	N
Fulton Ref. [26-40], [26-41]	-	1.26	1.0	1.26	N
Reese, Bert Ref. [26-42]	-	1.01	1.0	1.01	Y

Key:
(1) with in-plane shear rigidity
(2) K.D.F. - knock-down factor acc. to Equation [26.6-25]
(3) N^*_{xc} - N_{xc} , (K.D.F)
(4) K.D.F from diagram Ref. [26-48], normalised with K.D.F. as given by Equation [26.6-25]
(5) Comparison baseline values (1.0), with respect to Bert, Ref. [26-36]

The summary of equations, Ref. [26-43], based on the solution of Bert, Crisman and Nordby, Ref. [26-38], presented here can be used as the basis for calculating the minimum weight of a sandwich cylinder subjected to a given compressive load. A simple variation of facing and core parameters (computer program) results in an optimum sandwich cylinder with minimum weight, [See: 26.9].

General instability is only one failure mode which can be responsible for the loss of a sandwich structure, [See also: Figure 26.4.1]. Possible failure modes, other than overall or global instability, include:

- Local instability:
  - Face sheet wrinkling, [See: 26.7]
  - Dimpling (intracell buckling), [See: 26.7]
  - Material failure, [See: Chapter 11].
  - Insufficient compression strength of face sheets caused by use of inappropriate material (UD properties)

— Insufficient compression strength of face sheets caused by inappropriate lay-up (fibre orientation) of the laminate

26.6.4.2 Method of Bert

The critical compression stress of a sandwich cylinder with identical orthotropic faces and an orthotropic core are given, based on the solution of Bert, Crisman and Nordby, Ref. [26-38].

Figure 26.6.4 shows a schematic view of the dimensions and stresses used in the calculations, Ref. [26-38].

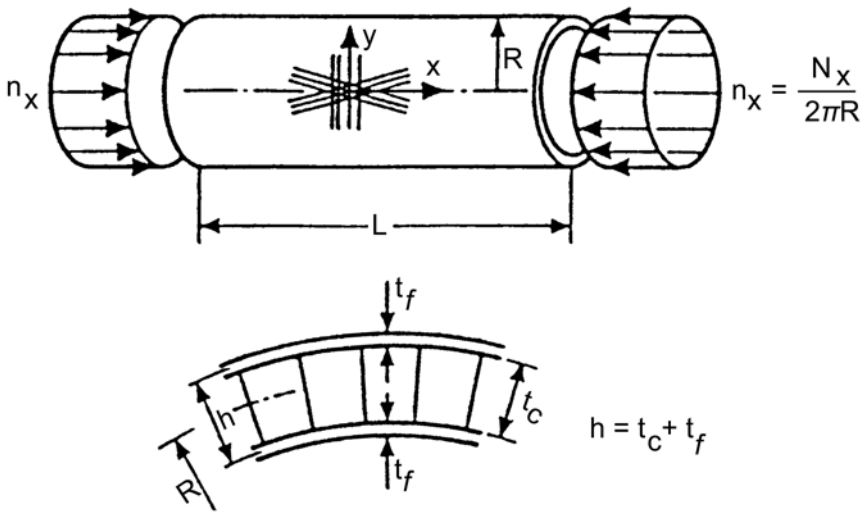

$$N_x = \frac{P}{2\pi R}$$

where P is the total axial

Figure 26.6-4 - Sandwich cylinder: Loads and dimensions for calculations

In general, the critical compression stress of a sandwich cylinder can be determined by:

$$\sigma_{cr} = \frac{N_{x,cr}}{2t_f} \qquad [26.6\text{-}12]$$

From Ref. [26-41], n_{xc} is defined as:

$$N_{x,cr} = a_0 + a_1 \qquad [26.6\text{-}13]$$

Where:

$$a_0 = \left(\alpha_1^2\alpha_5 + \alpha_2^2\alpha_4 - 2\alpha_1\alpha_2\alpha_3\right)\left(\alpha_3^2 - \alpha_4\alpha_5\right)^{-1} m^{*-2} \qquad [26.6\text{-}14]$$

And:

$$a_1 = m^{*-2}\left\{D_x m^{*4} + 2\beta_1 m^{*2} n^{*2} + D_y n^{*4} + \beta_2\left[B_x m^{*4} + \beta_3 m^{*2} n^{*2} + B_y n^{*4}\right]^{-1}\right\} \quad [26.6\text{-}15]$$

Where the terms in Equation [26.6-14] and Equation [26.6-15] are defined by

$$\beta_1 = \nu_{yx} D_x + D_{xy}$$

$$\beta_2 = \frac{B_x B_y m^{*4}}{R^2}$$

$$\beta_3 = \frac{B_x B_y}{B_{xy}} - 2\nu_{xy} B_y$$

$$\alpha_1 = D_x m^{*3} + \left(\nu_{yx} D_x + D_{xy}\right) m^* n^{*2}$$

$$\alpha_2 = D_y n^{*3} + \left(\nu_{xy} D_y + D_{xy}\right) m^{*2} n^*$$

$$\alpha_3 = \left[\left(\nu_{xy} D_y\right) + \left(D_{xy}/2\right)\right] m^* n^*$$

$$\alpha_4 = S_x + D_x m^{*2} + \left(D_{xy}/2\right) n^{*2}$$

$$\alpha_5 = S_y + D_y n^{*2} + \left(D_{xy}/2\right) m^{*2}$$

The stiffness, sandwich shell bending and transverse shear stiffness coefficients are defined according to Ref. [26-38], and are consistent with Equation [26.6-10] (i.e. with classical lamination theory), even though the "x,y"-notation system is used rather than the "1,2,6" notation.

The stiffness coefficients are defined here by (d=(t_f+t_c), identical faces):

$$B_x = 2t_f E_x \quad [26.6\text{-}16]$$

$$B_y = 2t_f E_y \quad [26.6\text{-}17]$$

$$B_{xy} = 2t_f G_{xy} \quad [26.6\text{-}18]$$

$$D_x = \frac{d^2 B_x}{4\left(1 - \nu_{xy}\nu_{yx}\right)} \quad [26.6\text{-}19]$$

$$D_y = \frac{d^2 B_y}{4\left(1 - \nu_{xy}\nu_{yx}\right)} \quad [26.6\text{-}20]$$

$$D_{xy} = \frac{d^2 B_{xy}}{2} \quad [26.6\text{-}21]$$

$$S_x = \frac{G_{cx} d^2}{t_c}, \quad [26.6\text{-}22]$$

$$S_y = \frac{G_{cy} d^2}{t_c} \quad [26.6\text{-}23]$$

The specific axial and circumferential wave numbers are defined by:

$$m^* = \frac{m\pi}{L} \; ; \quad n^* = \frac{n}{2R}$$

26.6.4.3 Knock down factor

To consider initial imperfections of the sandwich cylinder, a "knock-down factor" from Ref. [26-48] can be used

$$\left(R/s\right)_e = 0.428 \; R \sqrt{\frac{B_x}{D_x + D_y}} \quad [26.6\text{-}24]$$

where the stiffness parameters B_x, D_x and D_y are defined in Equation [26.6-16], Equation [26.6-19] and Equation [26.6-20].

The knock-down factor, k_n, corresponding to 99% probability becomes

$$k_n = \rho_{99} = 6.48\left(R/s\right)_e^{-0.54} \quad [26.6\text{-}25]$$

[See also: Equation [27.4-15] and Equation [27.4-16] for knock-down factors of 50% and 90% probability]

Thus, the critical buckling stress reduces to

$$\sigma_{cr}^{*} = \sigma_{cr} k_n \quad [26.6\text{-}26]$$

or

$$N_{x,cr}^{*} = N_{x,cr} k_n \quad [26.6\text{-}27]$$

26.6.4.4 Total mass of a sandwich cylinder

The total mass is given by:

$$M = L2\pi R(2t_f\rho_f + t_c\rho_c) \quad [26.6\text{-}28]$$

Adhesive layers are not considered because the amount of adhesive is generally determined by optimisation.

26.6.4.5 Minimum mass design

An optimum sandwich cylinder (L, R, n_x are given) yields a minimum mass if the variables t_f, t_c, ρ_f, ρ_c and the modulus ratio E_x/E_y are chosen correctly.

A pre design calculation is given for optimum sandwich cylinders, where general instability and wrinkling are restricted, [See: 26.9].

26.6.4.6 Method of NASA SP 8007

The solution for the critical buckling load of a sandwich cylinder is taken from Ref. [26-39], with a modification to consider orthotropic face sheets. Transverse shear deformation is also included.

According to NASA SP 8007, Ref. [26-39], the critical load for general instability failure is:

$$N_{x,cr} = k_x \frac{\pi^2 D_x}{L^2} \quad [26.6\text{-}29]$$

The bending stiffness D_x can be calculated by:

$$D_x = \frac{E^* t_f d^2}{2\left(1-\nu^{*2}\right)} \qquad [26.6\text{-}30]$$

where: E^* is the quasi isotropic modulus and ν^* is Poisson's ratio.

$$E^* = \sqrt{E_x E_y} \qquad [26.6\text{-}31]$$

$$\nu^* = \sqrt{\nu_{xy}\nu_{yx}} \qquad [26.6\text{-}32]$$

The buckling coefficient k_x for moderately long cylinders can be determined by Figure 26.6.5 in conjunction with Figure 26.6.6, Ref. [26-39].

Figure 26.6.5 shows the relation of the buckling coefficient to the curvature parameter, z, for different R^*, the ratio of bending stiffness of facings to shear stiffness of the core.

The curvature parameter z is given by:

$$z = 2\frac{L^2}{Rh}\sqrt{1-\nu^{*2}} \qquad [26.6\text{-}33]$$

while

$$R^* = \frac{\pi^2 D_x}{L^2 D_{qx}} \qquad [26.6\text{-}34]$$

The shear stiffness of the core is:

$$D_{qx} = \frac{G_{xz} d^2}{t_c} \qquad [26.6\text{-}35]$$

Together with the knock-down factor k_n, which is given in Figure 26.6.6, Ref. [26-39], for different ratios of R/h, k_x can be taken from Figure 26.6.5, Ref. [26-39].

A comparison of the results with those calculated by Bert can result in significant differences of up to 40%, [See also: Table 26.6.1].

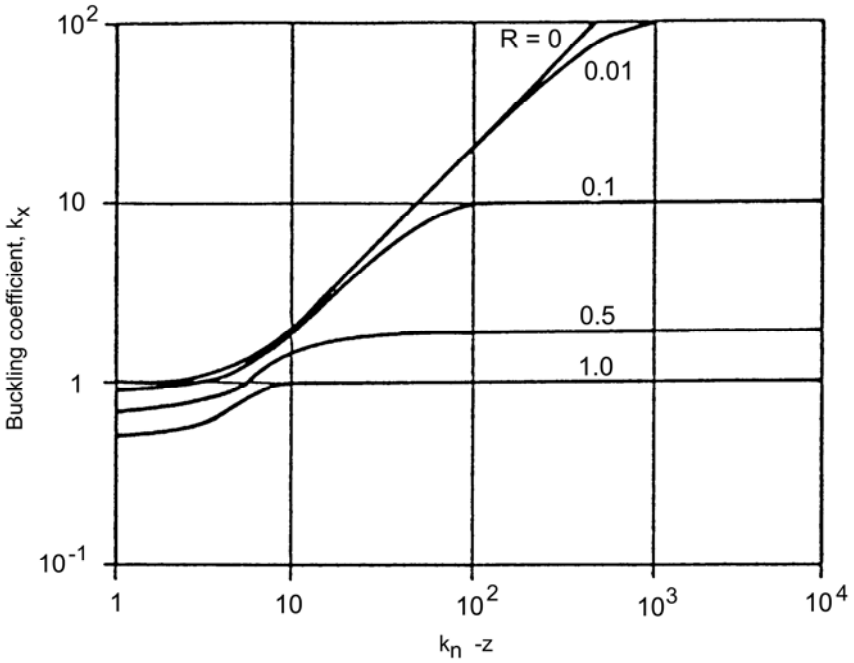

Figure 26.6-5 - Buckling coefficient

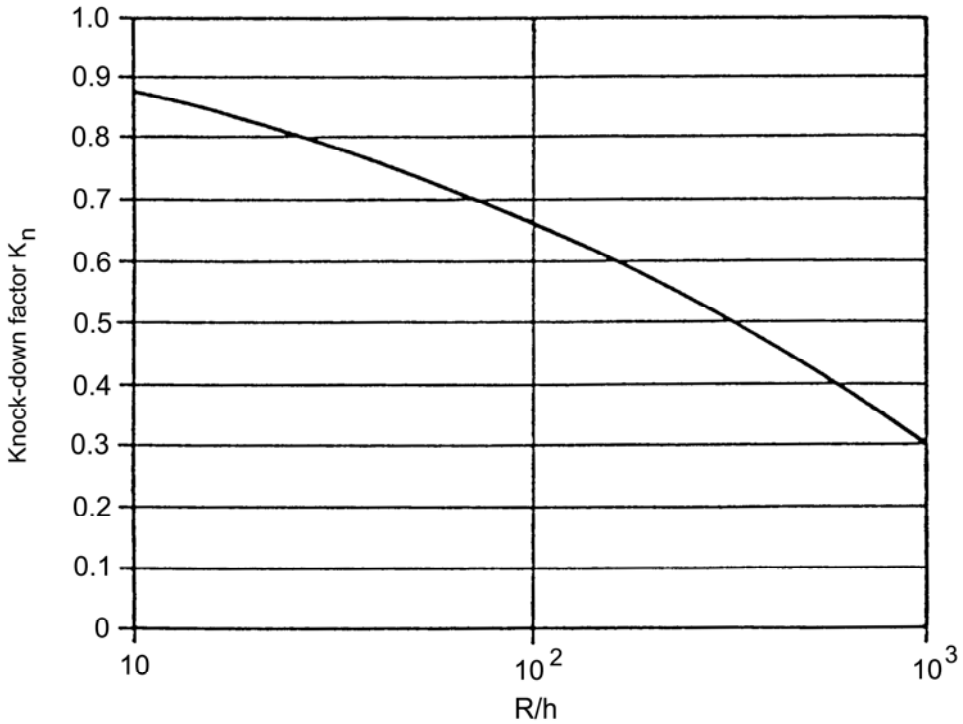

Figure 26.6-6 - Knock down factor

26.7 Local buckling instability of sandwich structures

26.7.1 General

The two local buckling instability modes of sandwich structures, [See: 26.4], are presented along with details of their modelling. Both modes are strongly influenced by the properties of the core. Whereas guidelines on the theoretical approach for the analysis of wrinkling are fairly well established, [See: 26.7.2], prediction of intra-cell buckling poses more problems.

For intra-cell buckling, also commonly known as dimpling, a number of theories have evolved over time, [See: 26.7.3]. All of these 'classical' models have some shortcomings in that they cannot predict dimpling accurately. This is particularly the case for sandwich structures with very thin and strongly orthotropic facings (strongly directional stiffness properties) as are commonly used in space structures.

To address this problem further, a more recent model is presented from an ESA-funded study. This model, which more realistically takes into account the boundary conditions observed experimentally, shows a reasonable, but still conservative, correlation between predicted values and those obtained from testing.

In all cases, the theories and approaches presented can be used for preliminary design purposes only.

The the transverse core stiffness usually exerts negligible influence on the bending behaviour of sandwich structures, except for cases of highly-localised loading, [See: Figure 26.4.1 h], or when localised effects occur due to abrupt changes of geometry or material properties. This is also valid for global or overall buckling of sandwich structures.

However, local buckling instability phenomena like wrinkling and intra-cell buckling ("dimpling"), [See: Figure 26.4.1 c, d and g], are strongly dependent on the transverse core stiffness. Both types of instability appear as local, short-wavelength face buckling.

[See also: 26.6 for global buckling instability of sandwich structures]

26.7.2 Wrinkling instability

26.7.2.1 General

Wrinkling can simply be considered as buckling of a thin face elastically supported by an elastic medium, i.e. the core.

Information with respect to the wrinkling of sandwich plates subjected to unidirectional axial compression loading is presented.

The combined loading case can be found in e.g. NASA CR-1457, Ref. [26-50].

26.7.2.2 Wrinkling modes

Figure 26.7.1 shows the different wrinkling modes that can occur.

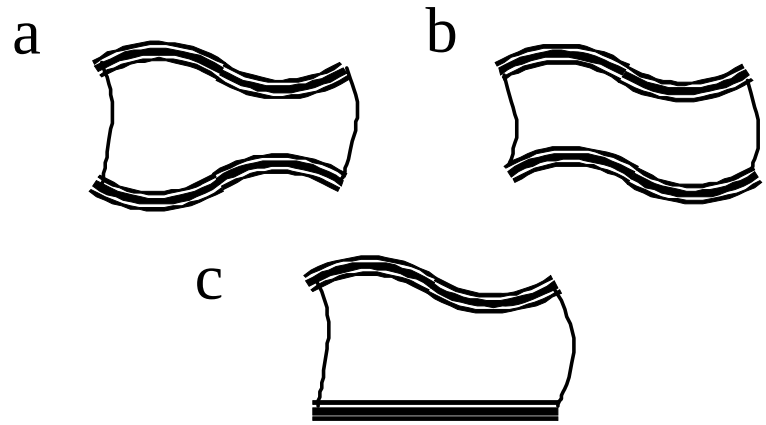

(a) **Symmetric** ("hourglass mode") b) **Anti-symmetric** ("snake mode")

(c) **Asymmetric** ("single-sided mode")

Figure 26.7-1 – Wrinkling modes

In general, the three different modes of wrinkling can be decsribed as:

- Symmetric wrinkling mode, also known as 'hourglass' mode, is related to higher wrinkling loads than "anti-symmetric" and "asymmetric" modes for realistic sandwich configurations, Ref. [26-49]. Thus, "symmetric" wrinkling is of little relevance for engineering applications.
- Anti-symmetric wrinkling mode, also known as 'in-phase' or 'snake' mode, is common for orthotropic core materials, where the shear stiffness is considerably lower than the through-thickness Young´s modulus, for example honeycombs, and for sandwiches with thin core.
- Asymmetric wrinkling, also known as 'single-sided' mode can appear in sandwich structures loaded in bending where only one face is subjected to compression loading, or if the sandwich has unsymmetric faces, one with lower buckling load than the other.

The wrinkling load can be derived in many different ways, either based on formulating and solving the governing equations directly or based on energy methods, Ref. [26-53], [26-54], [26-55].

The methods vary from each other with respect to the assumptions made regarding the decay of the core stresses in the elastic foundation formulation, but the different approaches yield approximately the same result for the buckling stress, Ref. [26-1], [26-52].

In the discussion here, the relevant face modulus E_f is defined as the modulus in the principal compression stress direction, while $\nu_f = \sqrt{\nu_x \nu_y}$.

For this case, the tensile loads can be ignored with respect to the possible elevating influence. Figure 26.7.2 shows the loads and dimensions of a sandwich plate.

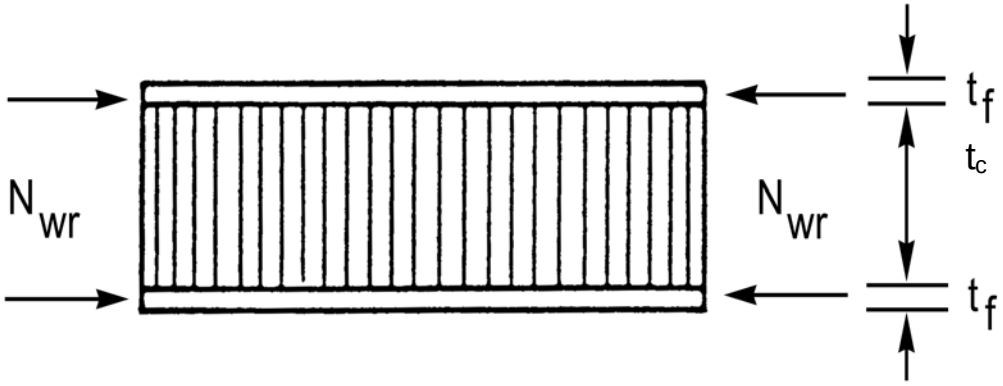

Figure 26.7-2 - Sandwich plate with load and dimensions

26.7.2.3 Ultimate face wrinkling stress of sandwich plates with an isotropic core

The theory of plates on an elastic foundation leads to the expression:

$$\sigma_{wr} = Q\sqrt[3]{\frac{E_c E_f G_c}{\left(1-\nu_f^2\right)}} \qquad [26.7\text{-}1]$$

Where

E_c: *Young's modulus of the core in the through-thickness direction,*

Q = *0.825, where the value corresponds to the ideal condition of a plate without initial imperfections, Ref.* [26-49].

The results of experiments, Ref. [26-50], showed that Q had to be reduced to Q = 0.5 for a safe design value.

26.7.2.4 Ultimate wrinkling stress of sandwich plates with an orthotropic core (honey-combs)

Using the theory of a plate on an elastic foundation, the ultimate wrinkling stress can be calculated by:

$$\sigma_{wr} = Q\sqrt{\frac{E_c E_f t_f}{\left(1-\nu_f^2\right)t_c}} \qquad [26.7\text{-}2]$$

Where:

E_c: *Young's modulus of the core in the through-thickness direction.*

From Ref. [26-49], [26-50], the factor $Q = 0.816$ for this case does not consider the initial imperfections, e.g. the initial waviness of the facings. Thus a more conservative value of $Q = 0.33$ is suggested in Ref. [26-49].

26.7.2.5 Verification of factor *Q* by tests

To verify Q especially for thin facings, several tests were performed. The types of samples tested are given in Table 26.7-1 Ref. [26-49], [26-50].

Table 26.7-1 – Sandwich plates: Wrinkling test samples

	Facings	**Core**
1	Carbon fibre (CFRP) t_f = 0.145 mm, 0°/90° lay-up	Aluminium honeycomb t_c = 18 mm; s = 9.525 mm
2	Carbon fibre t_f = 0.435 mm, 0°/90°/±45° lay-up	Aluminium honeycomb t_c = 18 mm; s = 9.525 mm
3	Carbon fibre t_f = 0.435 mm, 0°/90° lay-up	Aluminium honeycomb t_c = 18 mm; s = 9.525 mm
4	Carbon fibre t_f = 0.145 mm, 0°/90° lay-up	Aluminium honeycomb t_c = 18 mm; s = 4.7625 mm
5	Carbon fibre t_f = 0.145 mm, 0°/90° lay-up	Aluminium honeycomb t_c = 18 mm; s = 9.525 mm
6	Carbon fibre t_f = 0.2 mm, 0°/90° lay-up	Aluminium honeycomb t_c = 18 mm; s = 3.175 mm
7	Carbon fibre t_f = 0.8712 mm	Nylon fibre/Phenolic resin t_c = 13 mm; s = 4.76 mm
8	Carbon fibre t_f = 0.145 mm	Aluminium honeycomb t_c = 20 mm; s = 9.525 mm

Key: t_f : thickness of facing; t_c : thickness of core; s : size of a honeycomb cell

Experimental compression test results are shown in Figure 26.7.3, Ref. [26-49], where the ultimate stress measured in MPa (N/mm²) is plotted against the wrinkling stress σ_{wr}; as defined by Equation [26.7-3].

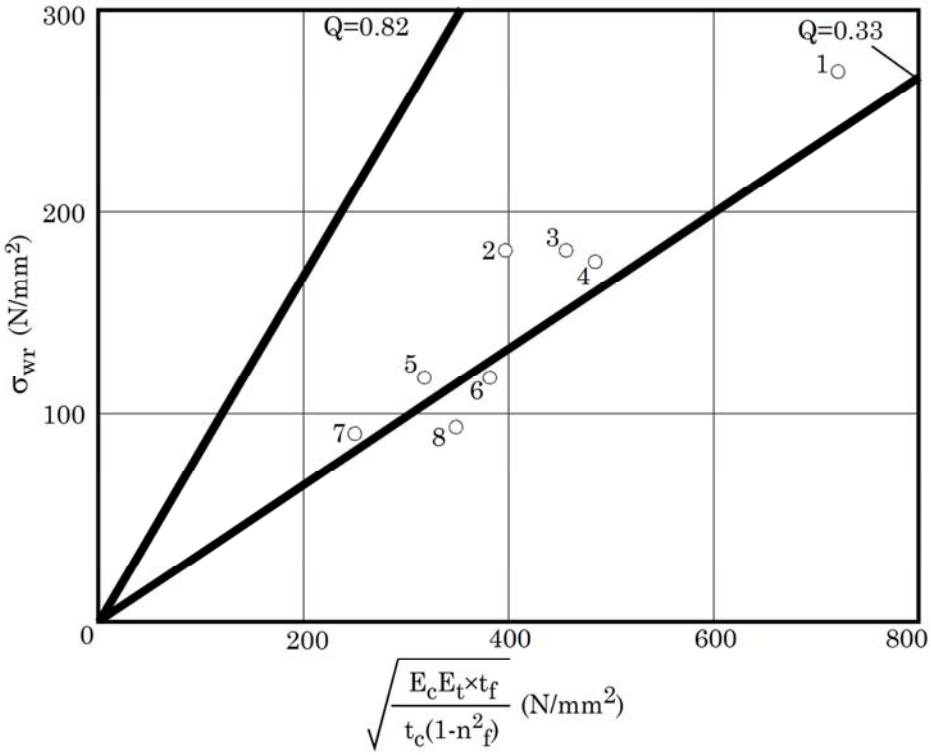

Figure 26.7-3 - Sandwich plates: Wrinkling test results

From Figure 26.7.3, it is seen that Q = 0.33 represents a reasonable value for the design of sandwich panels loaded in compression. Although most of the samples show a higher ultimate strength than predicted for Q = 0.33, it is advisable to perform tests in the early design stages, especially in the presence of combined loadings.

26.7.3 Intra-cell buckling or 'dimpling'

26.7.3.1 General

Intra-cell buckling or 'dimpling' can occur for sandwich panels where the core does not provide continuous support of the faces, i.e. in sandwiches with corrugated core, web-core or honeycomb core, and where the wave-length of the buckling pattern is determined by the core cell size.

26.7.3.2 Classical dimpling formulae

The classical approach behind the prediction of intra-cell buckling is largely empirically based. The underlying assumption is that each intra-cell plate, i.e. the parts of the sandwich faces that are supported along the honeycomb core cell edges, can be approximated by a rectangular plate simply-supported along all edges, and with side lengths equal to the diameter S of the circle that can be inscribed in the honeycomb cells. This leads to the expression (the "Norris" formula) for the critical buckling stress for homogeneous and isotropic faces loaded in unidirectional compression, Ref. [26-1], [26-54], [26-55], [26-56]:

$$\left(\sigma_{cr}\right)^{CLASSICAL} = \frac{K_d E_f}{(1-\nu_f^2)}\left[\frac{t_f}{S}\right]^2 \qquad [26.7\text{-}3]$$

Where:

E_f : *Young's modulus of the face material,*

t_f : *thickness of the face material,*

ν_f : *Poisson's ratio of the face material,*

K_d : *an empirical factor.*

The factor K_d in Equation [26.7-4] is used for "calibration" purposes to account for more or less restrictive boundary conditions imposed along the plate (cell) edges.

Usually, K_d is specified to be $K_d = 2$, which according to Ref. [26-43] represents a good estimation; as shown in Figure 26.7.4.

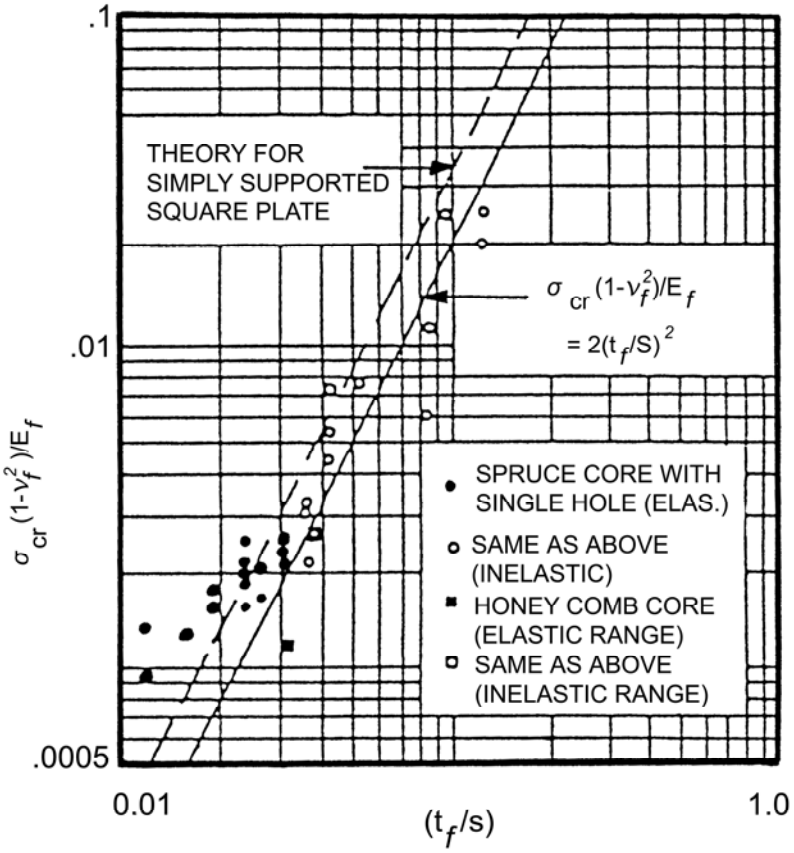

Figure 26.7-4 - Dimpling stress under uniaxial compression

Figure 26.7.5 shows the measurement of cell size, where S gives the diameter of the largest circle that can be inscribed in a core cell.

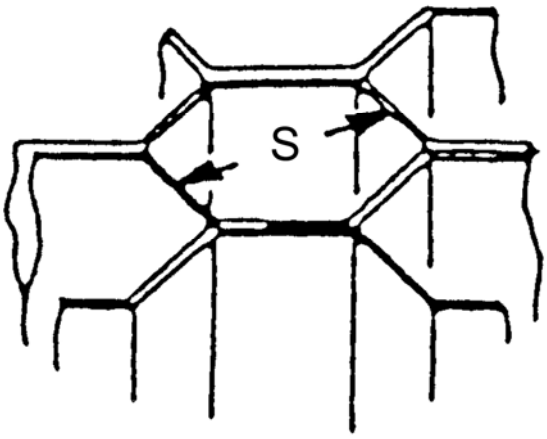

Figure 26.7-5 - Measurement of sandwich core cell size

An attempt to justify the semi empirical coefficient of $K_d = 2$ was made in Ref. [26-57]. By means of the finite difference method, the coefficient was found to be slightly higher, and the critical dimpling stress can be estimated as:

$$\sigma_{cr} = 2.25 \frac{E_f}{(1-\nu_f^2)} \left[\frac{t_f}{S}\right]^2 \qquad [26.7\text{-}4]$$

To account for the orthotropic properties of composite facings, Ref. [26-58] substitutes the modulus E_f of the isotropic facing by Ex which is the longitudinal modulus of a laminate, and the Poisson's ratio ν_f of the isotropic facing by a quasi-isotropic or equivalent Poisson's ratio $\nu_f = \sqrt{\nu_{xy}\nu_{yx}}$.

With this, Equation [26.7-5] can be rewritten as

$$\sigma_{cr} = 2.25 \frac{E_x}{(1-\nu_{xy}\nu_{yx})} \left[\frac{t_f}{S}\right]^2 \qquad [26.7\text{-}5]$$

26.7.3.3 Improved prediction of dimpling for strongly orthotropic facings

A technology demonstration programme regarding the use of lightweight composite sandwich structures for spacecraft, known as the 'CSE Composite Structural Element Study', was conducted by Fokker Aircraft BV for the European Space Agency, Ref. [26-58], [26-59].

In the CSE study, it was found that Equation [26.7-4] and Equation [26.7-6] are inadequate for the prediction of the dimpling load for honeycomb-cored sandwich panels with strongly orthotropic faces.

Some earlier work on intra-cell buckling of sandwich panels with orthotropic faces was conducted Ref. [26-60], [26-61], but the test results presented did not include faces with strongly orthotropic (unidirectional) characteristics.

However, a systematic experimental investigation of the intra-cell buckling behaviour of several different sandwich plate configurations with strongly orthotropic very thin facings and honeycomb cores, Ref. [26-63], demonstrated that Equation [26.7-4] to Equation [26.7-6] provide overly conservative predictions, i.e. by a factor of 2 to 3 for the cases tested.

The reason for the conservative predictions obtained from the classical Norris formula was revealed by a close inspection of the data in Ref. [26-63]. The dimpling patterns in all cases appeared as illustrated schematically in Figure 26.7.6, Ref. [26-64]. This is clearly seen in Figure 26.7.7, Ref. [26-63], [26-64], which shows the development of dimpling for a particular sandwich plate configuration having CFRP facings on an aluminium honeycomb core.

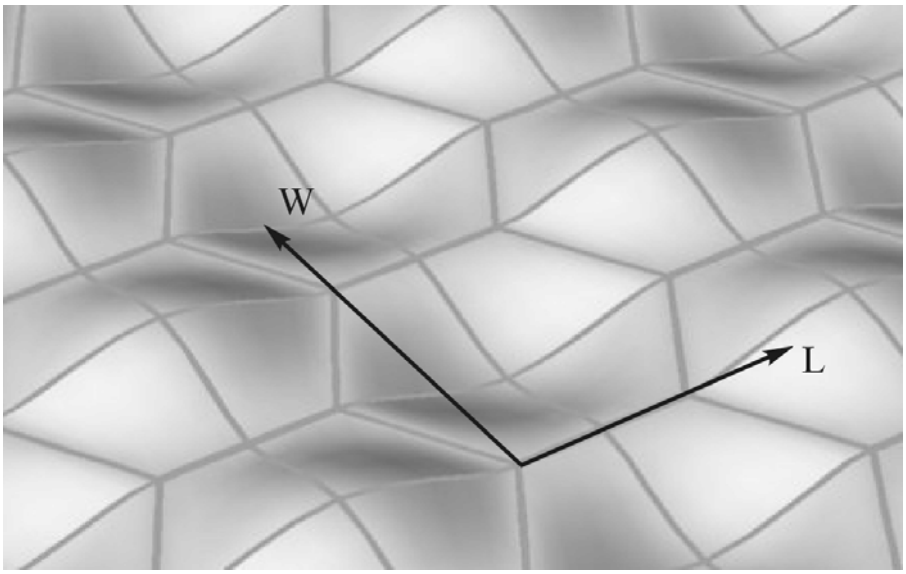

Figure 26.7-6 - Characteristic intra-cell buckling pattern observed experimentally

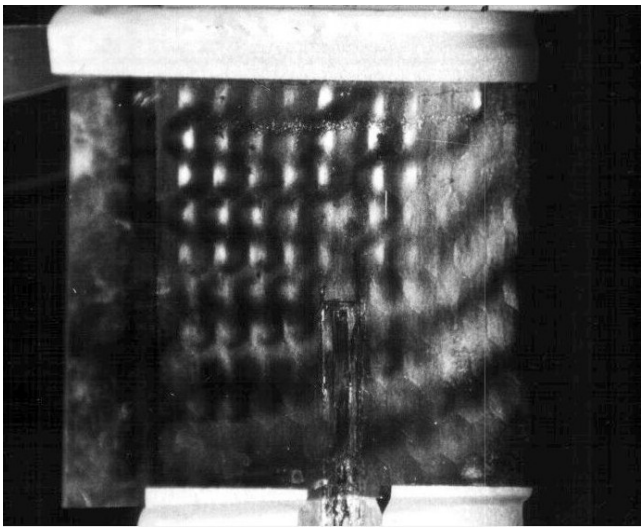

N = 102.4 N/mm

Figure 26.7-7 - Development of intra-cell buckling for sandwich test specimen (CFRP/Al-honeycomb core)

The significance of the observation is important in relation to the classical intra-cell buckling models; Equation [26.7-4] to Equation [26.7-6]. Thus, from Figure 26.7.6 and Figure 26.7.7, it is seen that the boundary conditions in the *L*-direction (also the loading direction) along the edges of each intra-cell plate of the honeycomb core resemble clamped conditions. The angled plate edges at each end of the honeycomb cells display a deformation behaviour that closely resembles that encountered at simple supports. This means that the basic assumptions behind Equations [26.7-3] to [26.7-5], i.e. the assumed simple support boundary conditions along the edges of the idealised "inscribed" rectangular plate (often referred to as SSSS boundary conditions), do not resemble the "real" boundary conditions observed. SSSS means 'simple support conditions' along all 4 sides of the plate.

Based on the experimental evidence, an idealised model for the intra-cell buckling problem was proposed in Ref. [26-64], which resembles the observed behaviour more realistically for strongly orthotropic thin faces. Essentially the model assumes that the intra-cell face-plates to behave as symmetric rectangular specially orthotropic plates with the two edges that are parallel to the honeycomb *L*-direction (and parallel to the loading direction) clamped, and the two remaining opposite edges simply supported (often referred to as SCSC boundary conditions); as shown in Figure 26.7.8. SCSC means 'simple support - clamped - simple support – clamped' conditions alonge the 4 plate edges.

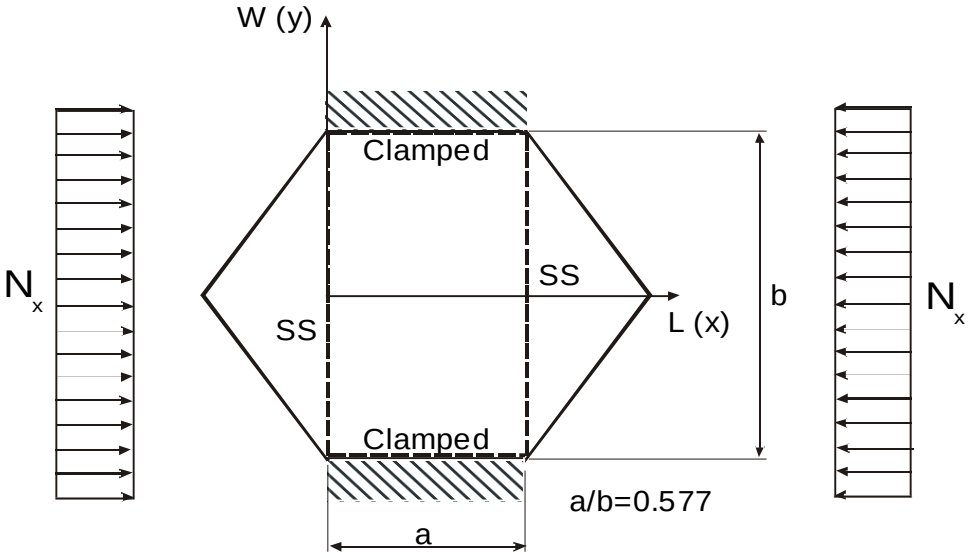

Improved model showing geometry, SCSC boundary conditions and external loading,

Figure 26.7-8 – Improved intra-cell face plate model

An approximate solution for this model was developed in Ref. [26-64], and the expression for the critical normal stress resultant is (units: N/mm):

$$\left(N_{cr}\right)^{improved} = \frac{K_d D_{22}}{b^2} \quad where \quad K_d = \pi^2 \left[\frac{D_{11}}{D_{22}} \left(\frac{b}{a}\right)^2 + \frac{8}{3} \frac{\left(D_{12} + 2\,D_{66}\right)}{D_{22}} + \frac{16}{3} \left(\frac{a}{b}\right)^2 \right] \qquad [26.7\text{-}6]$$

where the D_{ij}, i,j=1,2,6 are the face laminate bending stiffness coefficients according to classical lamination theory (contracted notation), [See: Chapters 10; Chapters 11; Ref. [26-15].

The critical normal stress resultant N_{cr} is related to the average critical dimpling stress ⊚cr by the expression $N_{cr} = \sigma_{cr}\, t_f$.

The predictions of Equation [26.6-7] were shown to be within 15% of the experimental mean values reported in Ref. [26-63], and the predicted values were lower than the measured dimpling loads in all cases, which indicates that the predictions are conservative.

26.8 Design considerations associated with sandwich structures

26.8.1 General

The sandwich concept is very advantageous from a structural point of view, because the stiff outer faces are extremely effective in withstanding bending loads applied to the panel or shell, whilst the compliant core offers a high resistance to shear loads.

Possessing very high stiffness-to-weight and strength-to-weight ratios, sandwich panels are superior load-carrying structural elements for many industrial applications.

Despite the many advantages, sandwich panels are basically unsuited for carrying localised loads because the core does not have the necessary stiffness to distribute the forces effectively, [See: 26.5]. Localised effects, however, are unavoidable in practical sandwich structures, because they occur at locations such as:

- Edge closures and joints
- Mechanical fasteners, e.g. inserts, bolts and rivets, to enable joining to other sandwich sub-structures.
- Geometrical and material discontinuities, e.g. change of core or face properties, core splices and face doublers.

All the local design features cause localised bending effects, which lead to local stress concentration that can lead to a premature structural failure. Therefore these pose particular problems in the design of sandwich structures. Some brief practical considerations and 'good practice' design solutions are presented.

26.8.2 Edge closures and joints

It is generally good practice to close off the edges in a sandwich panel construction. The edge closure protects the core from accidental damage, serves as a seal against moisture ingress and provides edge reinforcement to enable transfer and distribution of edge attachment loads. Normally several alternatives exist, so the best approach should be chosen.

For example, both of the edge close out details shown in Figure 26.8.1 perform essentially the same function at the same weight, but placing the legs of the channel facing outward instead of inward saves costs.

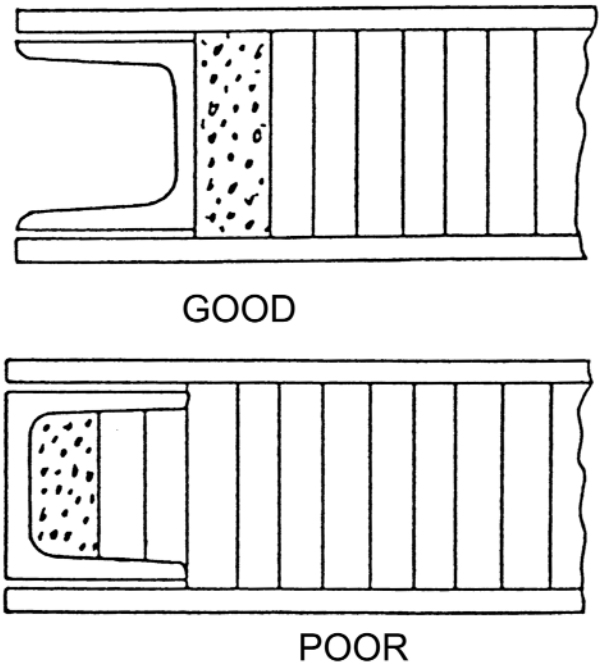

Figure 26.8-1 - Sandwich panel edge closure

Examples of joints, additional edge treatments and corners are shown in Figure 26.8.2.

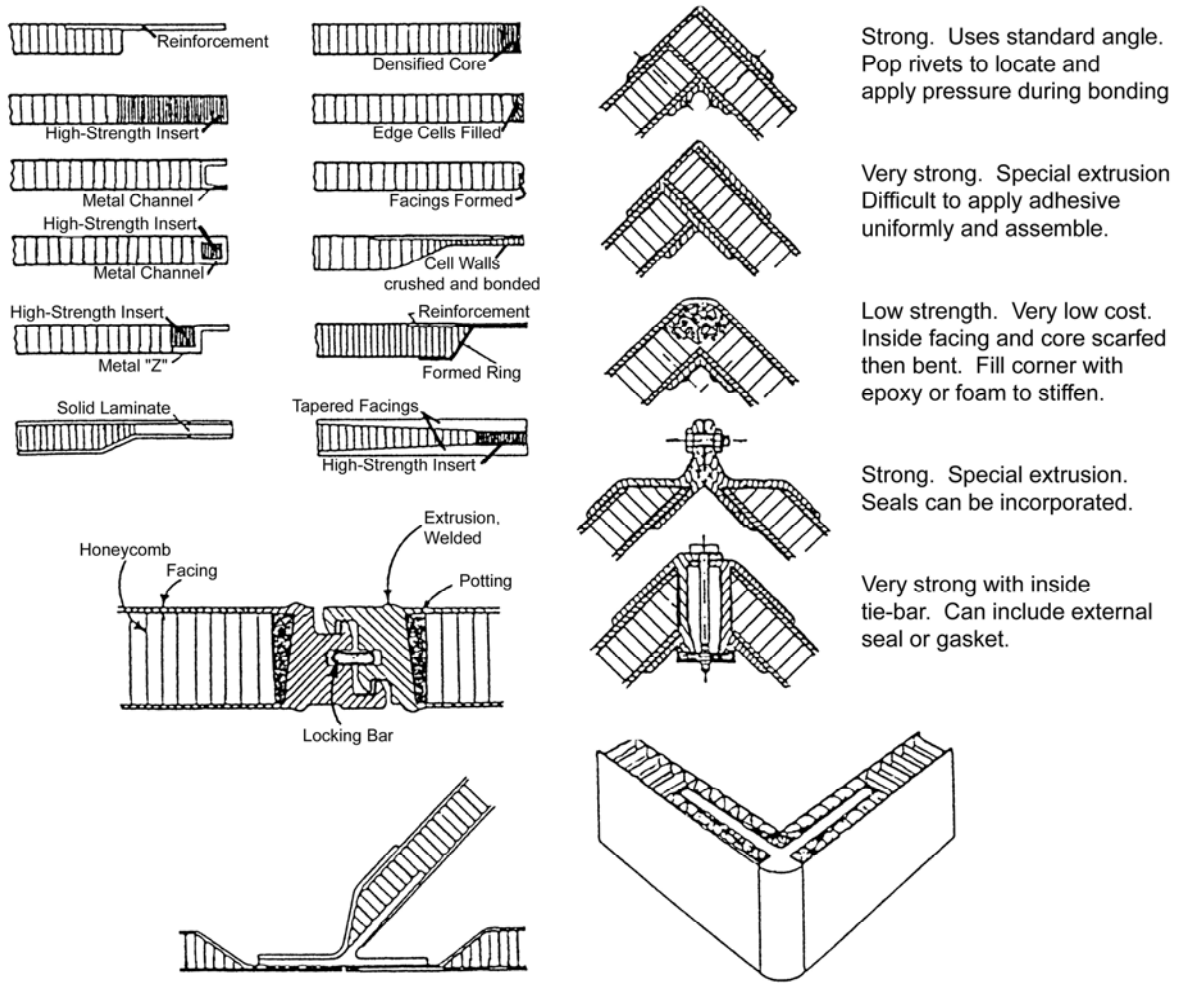

Figure 26.8-2 – Design details in sandwich structures: Examples of edges, joints and corners

26.8.3 Mechanical fasteners

26.8.3.1 General

Care is needed in the selection of a joining solution involving mechanical fasteners because of the localised loading effects created in sandwich panels. This applies to fastener systems such as:

- inserts, either the conventional metal potted types or novel inserts, involving composite materials.
- bolts and rivets.

26.8.3.2 Potted inserts

An insert is a local change in stiffness and strength of a sandwich panel, the purpose of which is to distribute a localised load in an appropriate manner into the sandwich panel.

Sandwich structures are basically unsuited for carrying localised loads, [See: 26.5], so, ideally, the use of inserts is to be avoided. This is clearly impractical, so it is very important to choose an appropriate type of insert, Ref. [26-32].

Insert systems in sandwich structures for equipment mounting usually comprise three main components, i.e. insert, sandwich structure and potting (polymer material), Ref. [26-65].

Figure 26.8.3 shows the basic types of conventional potted inserts used in spacecraft applications, Ref. [26-65]. Their load-carrying capability can be ranked as:

- Through-the-thickness insert highest
- Fully potted insert ↓
- Partially potted insert lowest

There are a wide range of commercially-available potted inserts available and used in space applications.

[See: Chapter 23; ECSS-E-HB-32-22 – Insert design handbook]

Further details concerning the analysis and structural design of sandwich panels with inserts can be found in Ref. [26-30], [26-66], [26-67].

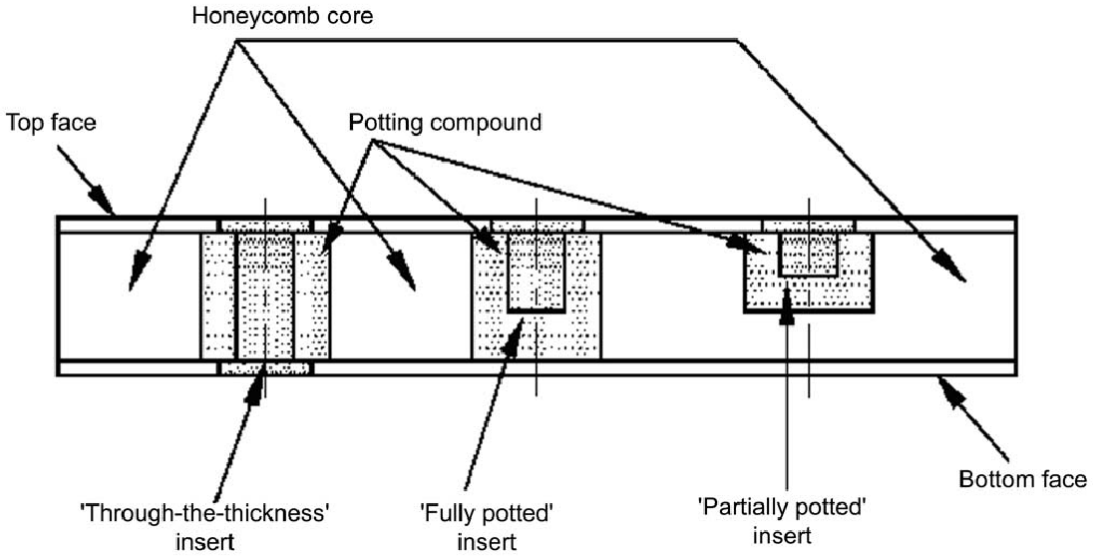

Figure 26.8-3 – Types of potted inserts for sandwich structures (ECSS-E-HB-32-22)

26.8.3.3 Novel inserts

Recent developments in insert technology can be summarised as:

- Carbon-fibre tube inserts, which have a carbon-fibre tube bonded in the core; as shown in Figure 26.8.4a. The test results show that these inserts can save mass and provide excellent performance, Ref. [26-68]. Initially developed by DLR and qualified for the Rosetta project, [See: 30.11], carbon-fibre tube inserts are now considered suitable for use in other space structure designs where mass-efficiency is an important design driver, [See: ECSS-E-HB-32-22].
- CFRP inserts; as shown in Figure 26.8.4b, which are made of carbon-fibre reinforced thermoplastic and moulded to form an insert system. Available from isotech (CH), they are under evaluation for sandwich panels, Ref. [26-68].

(a) Carbon-fibre tube insert
Reproduced courtesy of DLR

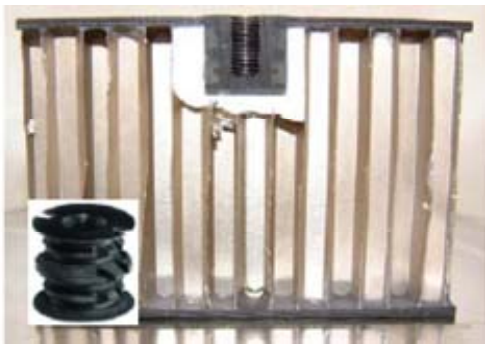

(b) CFRP insert
Reproduced courtesy of icotec AG

Figure 26.8-4 – Novel insert designs

26.8.3.4 Bolts and rivets

Where there is not enough space available for progressive doublers or wide-area bonded overlaps to carry high loads, the addition of rivets or bolts is sometimes the only solution. Their use, however, often results in a lower fatigue life for the structure, in addition to the increased mass.

26.8.4 Geometrical and material discontinuities

26.8.4.1 General

Sandwich panel designs can include local features in the core or to the facings, e.g. to accommodate changes in geomtery or to improve the panel characteristics locally.

26.8.4.2 Change of core densities

Several densities of core can be used in a single panel, each appropriate to the load carried in its area. As shown in Figure 26.8.5, the mating edges of the different types of core are adhesively bonded together; known as a 'core splice'.

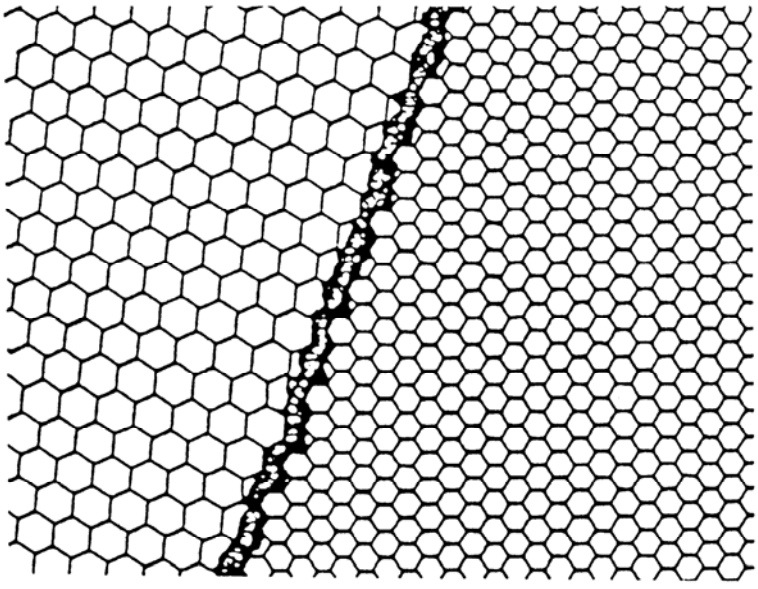

Figure 26.8-5 – Sandwich panels: Bonding different densities of core

26.8.4.3 Thickness transitions and core splices

The type of core thickness transition, shown in Figure 26.8.6, is common for either straight line or irregularly shaped transitions. The skin is shaped and trimmed to give the best possible match between core and facing during cure.

Core splicing is accomplished by bonding the edges of the core together during cure of the sandwich panel.

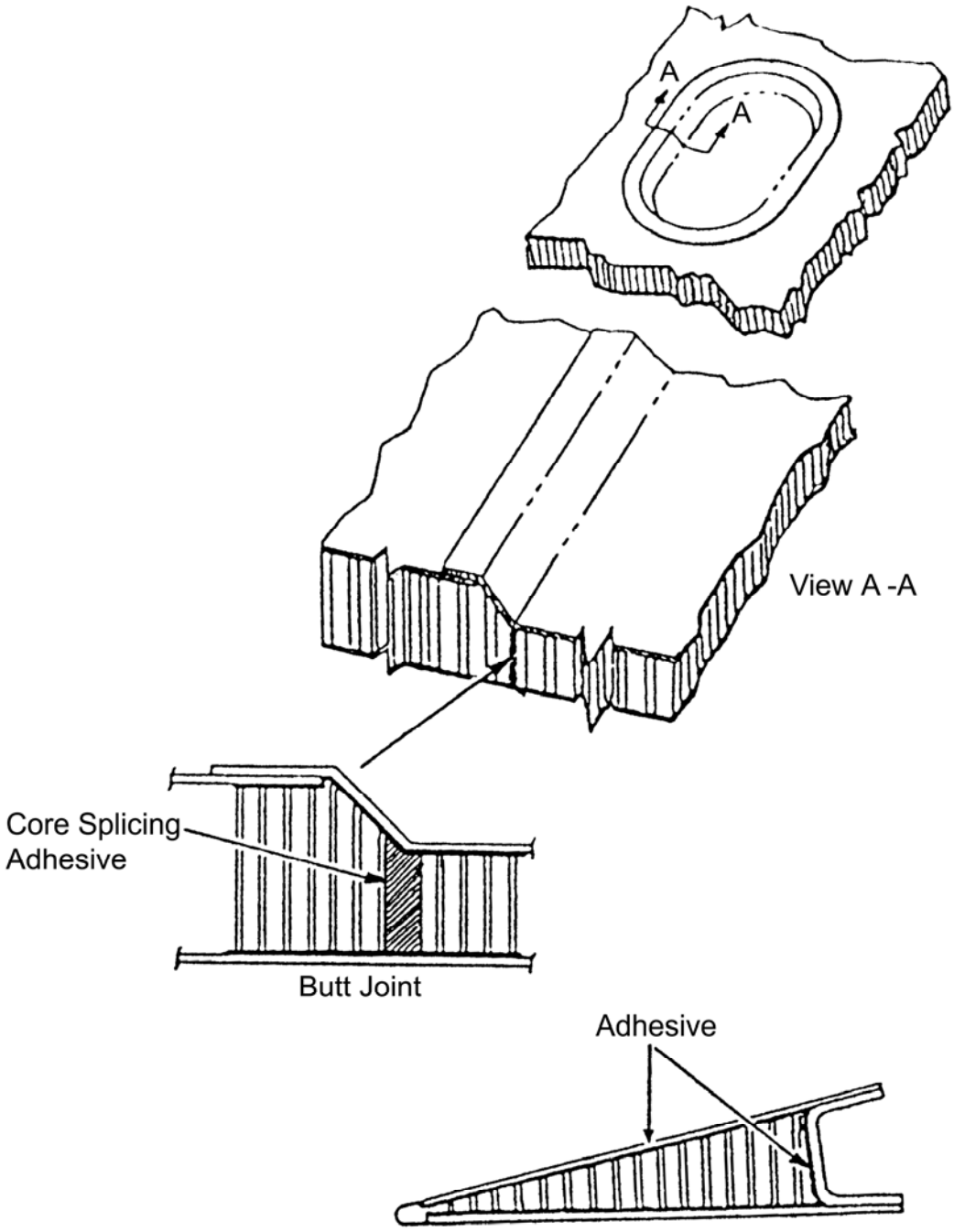

Figure 26.8-6 - Sandwich panels: Core thickness transition

26.8.4.4 Face doublers

Instead of heavier facings over the entire part, local doublers can be used for facings made of composites. The solution is simple because extra plies can be added to carry the higher loads exactly where they are needed.

External doublers rather than internal doublers tend to be used wherever possible. The use of internal doublers usually means that a relief cut or crushing is needed in the core to prevent bridging and a consequent unbonded area where the doubler ends; as shown in Figure 26.8.7. The joggle splice is usually used for prepregs.

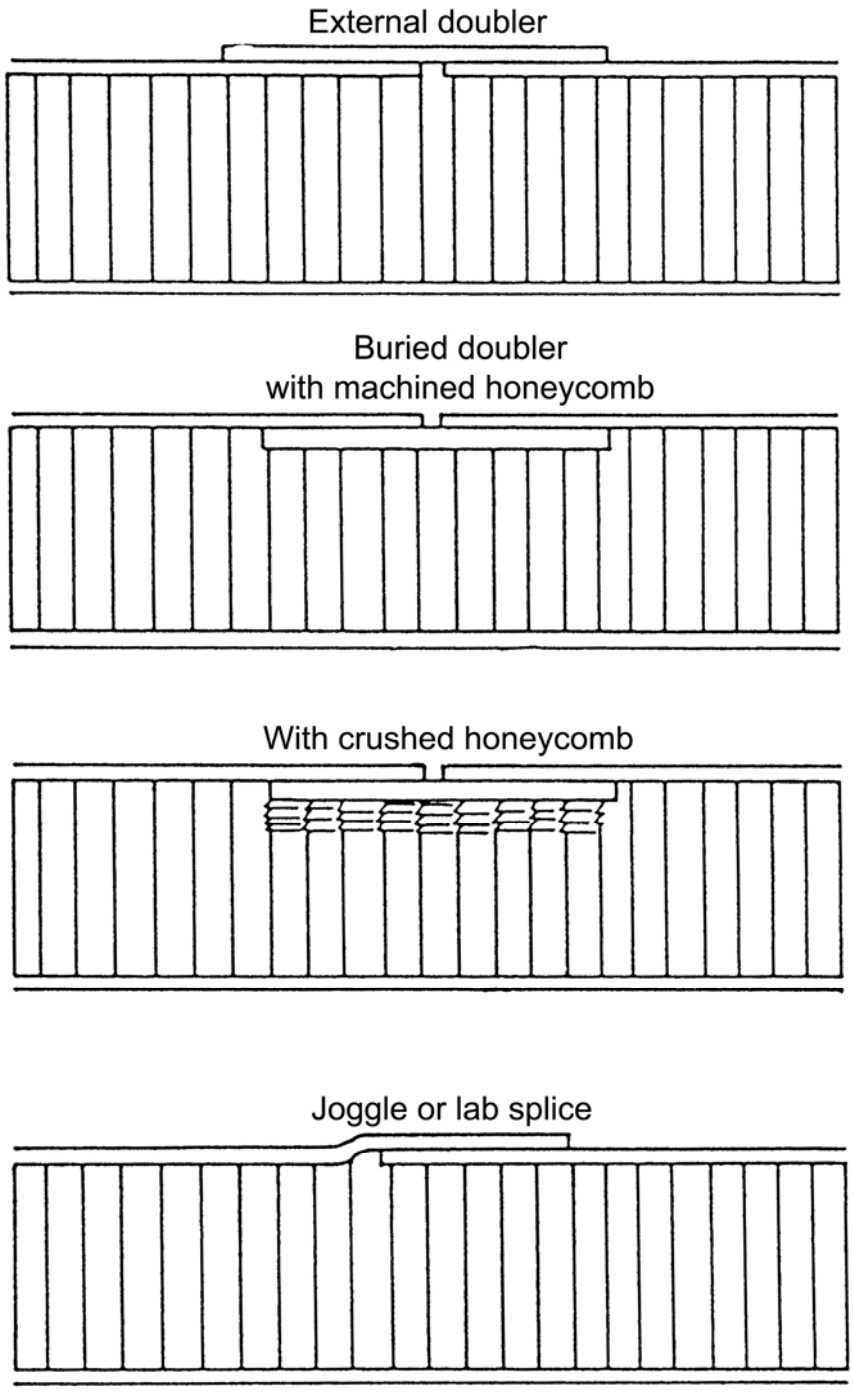

Figure 26.8-7 – Sandwich panels: External and internal doublers

26.9 Design procedures

26.9.1 General design of sandwich structures

The design of a sandwich structure is often an integrated process of sizing and materials selection in order to get not only a feasible design, but also, in some sense, an optimum design with respect to one or more objectives.

The general objectives in the design of sandwich structures include:

- Reduce the mass
- Increase the stiffness
- Increase the strength
- Use less expensive facing or skin materials
- Combination of the objectives.

Depending on the application, other objectives are sometimes involved. These can be reduced tooling or other costs, achieving aerodynamic smoothness, reducing reflected noise or increasing the durability under exposure to acoustic energy.

26.9.2 Design approach for sandwich structures

26.9.2.1 Design criteria

Sandwich structures are designed to meet a number of basic structural criteria, which include:

- The facings need to be thick enough to withstand the tensile, compressive and in plane shear stresses induced by the design loads.
- The core needs to possess sufficient strength to withstand the transverse shear stresses induced by the design loads.
- The sandwich structure needs to possess sufficient bending and shear stiffness to avoid excessive deflections.
- The core needs to be thick enough and have a sufficient shear modulus to prevent overall buckling of the sandwich under load.
- The compressive modulus of the core and compressive strength of the facings need to be sufficient to prevent wrinkling of the faces under the design load.
- The core cells need to be small enough to prevent intra-cell buckling (dimpling) of the facings under design loads.
- The core needs to possess sufficient compressive strength to resist crushing (indentation) by design loads acting normal to the panel facings or by compressive stresses induced through flexure.
- The sandwich panel close-outs and attachment points need to have sufficient strength and tie in with the core and facings to transmit the loads to the rest of the structure.

26.9.2.2 Design optimisation

Methods can be described for the optimum design of sandwich structures, which in this context means the stipulation of sizes and materials to provide minimum mass, maximum stiffness or strength or minimum cost subject to one or several constraints. The constraints can be the list of design criteria, but are often combined.

Such simple methods are extremely useful because they serve as a good starting point for the design process. Since there are generally many different constraints on a sandwich structure, an optimum solution can be very difficult to identify without use of general mathematical programming techniques. These are often both complex and costly, but have improved considerably over the last decade with respect to computational efficiency and ability to treat realistic design problems having many design variables and multiple constraints, Ref. [26-69], [26-70], [26-71].

26.9.2.3 'Intelligent sizing'

Focusing on the simpler design methodologies, where only the most important constraints are considered and using a simple optimisation technique, it is possible to obtain 'intelligent sizing' rather than optimisation.

Intelligent sizing can also be carried out at the initial design level using ESAComp; a composites analysis and design software package available from Componeering Inc.

As an illustration of 'intelligent sizing', a case study concerning the pre-design of a circular cylindrical sandwich shell is presented, [See: 26.9.3].

26.9.3 Case study: Pre design calculation of an optimised circular sandwich shell

26.9.3.1 General

The equations provided were determined using the approach of Bert, Crisman and Nordby, Ref. [26-38], for general global instability, [See: 26.6]. They also consider the wrinkling of the face sheets, Ref. [26-1]. [26-49], as a limiting factor for the allowable buckling load, [See: 26.7].

Material failure (facing failure) is determined by laminated plate theory and intracell buckling, dimpling, is checked separately, [See: Chapter 11, 26.4, 26.6, 26.7].

26.9.3.2 Approach

An evaluation of various sandwich cylinders with orthotropic facings and orthotropic core has led to a set of semi-empirical solutions for the determination of:

- Minimum mass.
- Optimum core thickness.
- Optimum facing thickness.
- Optimum core density.

The basis for all the equations is a fixed outer geometry (length L, radius R), face sheet material (longitudinal and transverse modulus E_x, E_y) and a defined ultimate running load n_x.

All dependent parameters are expressed as functions of the structural efficiency, $K = N_x / R$, and a quasi isotropic or equivalent Young´s modulus, $E^* = \sqrt{E_x E_y}$.

26.9.3.3 Minimum mass

If *R*, *L*, *E** and N_x are known, Figure 26.9.1, Ref. [26-38], can be used to calculate the approximate minimum mass of an optimised sandwich cylinder (optimised parameter: t_f/t_c, ρ_c/ρ_f).

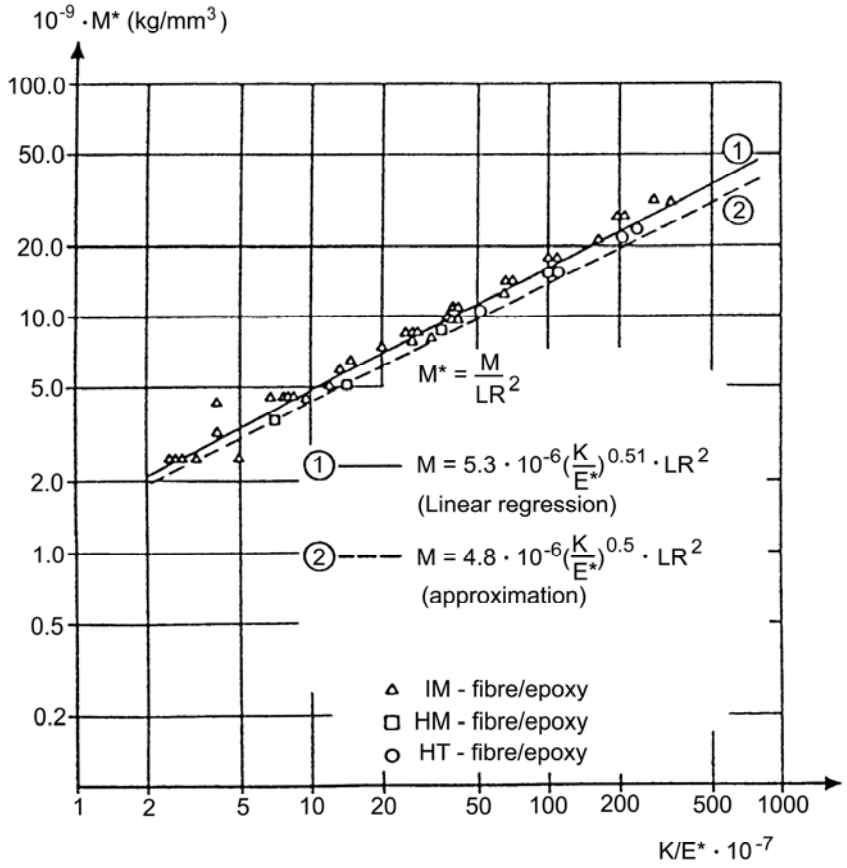

Figure 26.9-1 - Determination of minimum mass of an optimised sandwich

As can be seen in Figure 26.9.1, the minimum mass is defined by:

$$m^* = \frac{M}{LR^2} \approx f\left(\frac{K}{E^*}\right)^{1/2} \qquad [26.9\text{-}1]$$

or

$$M \approx \eta_1 LR^2\left(\frac{K}{E^*}\right)^{1/2} \qquad [26.9\text{-}2]$$

where η_1 contains the optimised parameters t_f/t_c and ρ_c/ρ_f.

η_1 can be set to:

$$\eta_1 \approx 4.8\times10^{-6} \quad [26.9\text{-}3]$$

Equation [26.9-2] then becomes:

$$M \approx 4.8\times10^{-6} LR^2\left(\frac{K}{E^*}\right)^{1/2} \quad [26.9\text{-}4]$$

26.9.3.4 Optimum core thickness

For a known structural efficiency K, a defined material E^* and a given radius, the optimum core thickness t_c can be taken from Figure 26.9.2, Ref. [26-38]:

$$t_c / R \approx f\left(\frac{K}{E^*}\right)^{1/3} \quad [26.9\text{-}5]$$

or

$$t_c \approx \eta_2 R\left(\frac{K}{E^*}\right)^{1/3} \quad [26.9\text{-}6]$$

The proportional factor η_2 can be taken as $\eta_2 = 0.6$, thus Equation [26.9-6] becomes:

$$t_c \approx 0.6R\left(\frac{K}{E^*}\right)^{1/3} \quad [26.9\text{-}7]$$

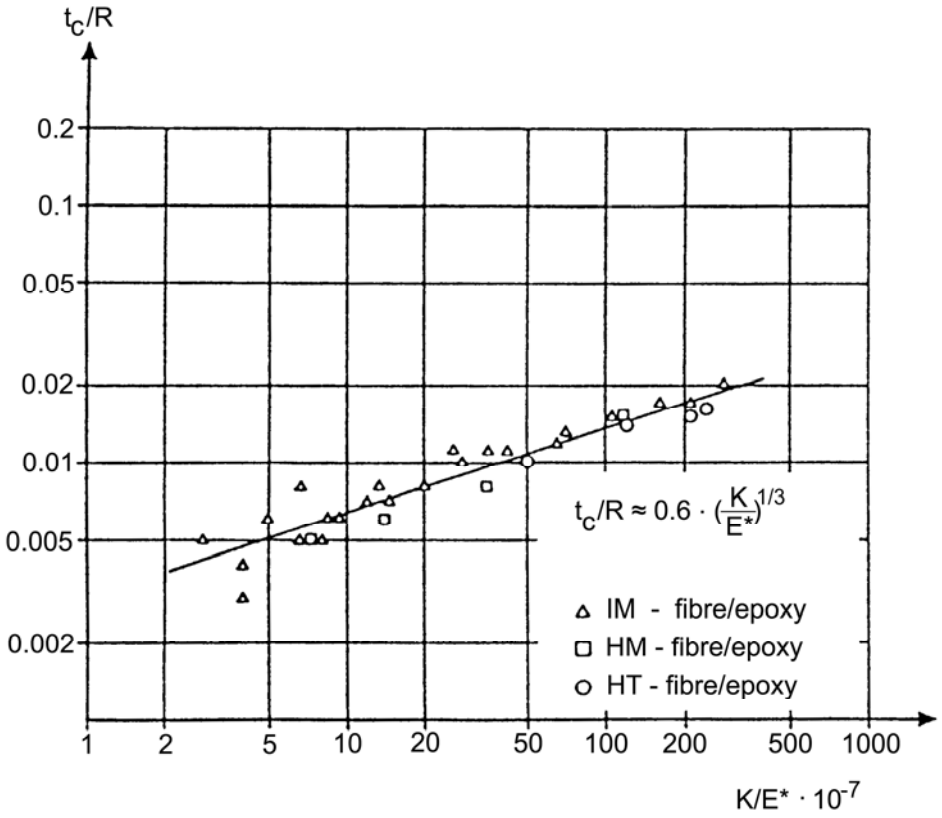

Figure 26.9-2 - Optimum sandwich core thickness

26.9.3.5 Optimum facing thickness

In Figure 26.9.3, Ref. [26-38], the thickness ratio t_f/t_c is shown as a function of structural efficiency, as given by the relationship:

$$t_f / t_c \approx f\left(\frac{K}{E^*}\right)^{0.17} \qquad [26.9\text{-}8]$$

Within the range of:

$$10\times10^{-7} \leq \frac{K}{E^*} \leq 200\times10^{-7}$$

The ratio of t_f/t_c is assumed to be constant, such that:

$$t_f / t_c = 0.035 = \text{constant} \qquad [26.9\text{-}9]$$

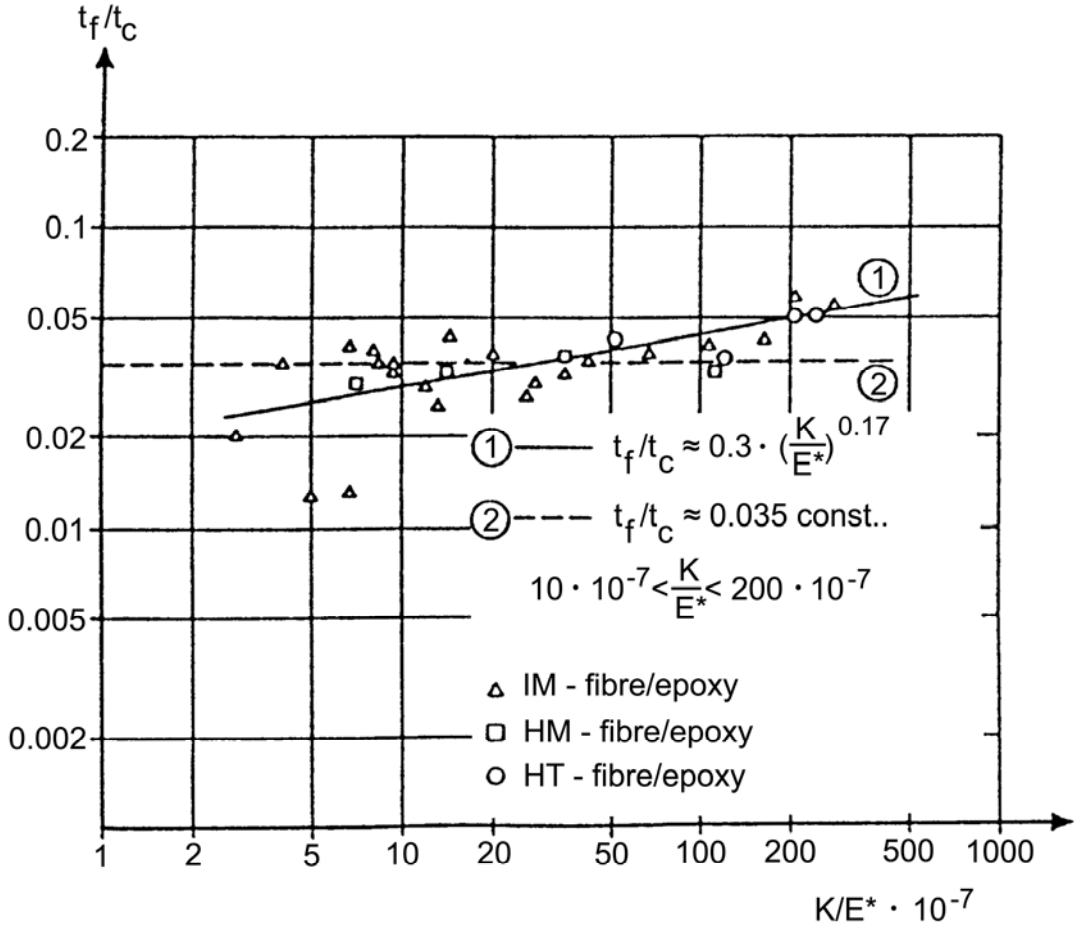

Figure 26.9-3 - Optimum sandwich facing thickness

Introducing a proportional factor $\eta_3 = 0.3$, Equation [26.9-8] becomes:

$$t_f / t_c \approx \eta_3 \left(\frac{K}{E^*} \right)^{0.17} \approx 0.3 \left(\frac{K}{E^*} \right)^{0.17} \qquad [26.9\text{-}10]$$

or:

$$t_f \approx 0.3 t_c \left(\frac{K}{E^*} \right)^{0.17} \qquad [26.9\text{-}11]$$

26.9.3.6 Optimum core density

The optimum core density can be determined by using Figure 26.9.4, Ref. [26-38].

Although the results show a large scatter, it seems to be possible to predict the optimum core density by:

$$\rho_c / \rho_f \approx f\left(\frac{K}{E^*}\right)^{1/3} \qquad [26.9\text{-}12]$$

for values of $K/E^* > 10 \times 10^{-7}$.

Values of $K/E^* < 10 \times 10^{-7}$, for practical reasons, result in:

$\rho_c/\rho_f \approx 0.01$ (lowest density available for cores: 16×10^{-7} kg/mm³).

Equation [26.9-12], together with a proportional factor $\eta_4 = 1.4$ gives:

$$\rho_c \approx \eta_4 \rho_f \left(\frac{K}{E^*}\right)^{1/3} \approx 1.4 \rho_f \left(\frac{K}{E^*}\right)^{1/3} \qquad [26.9\text{-}13]$$

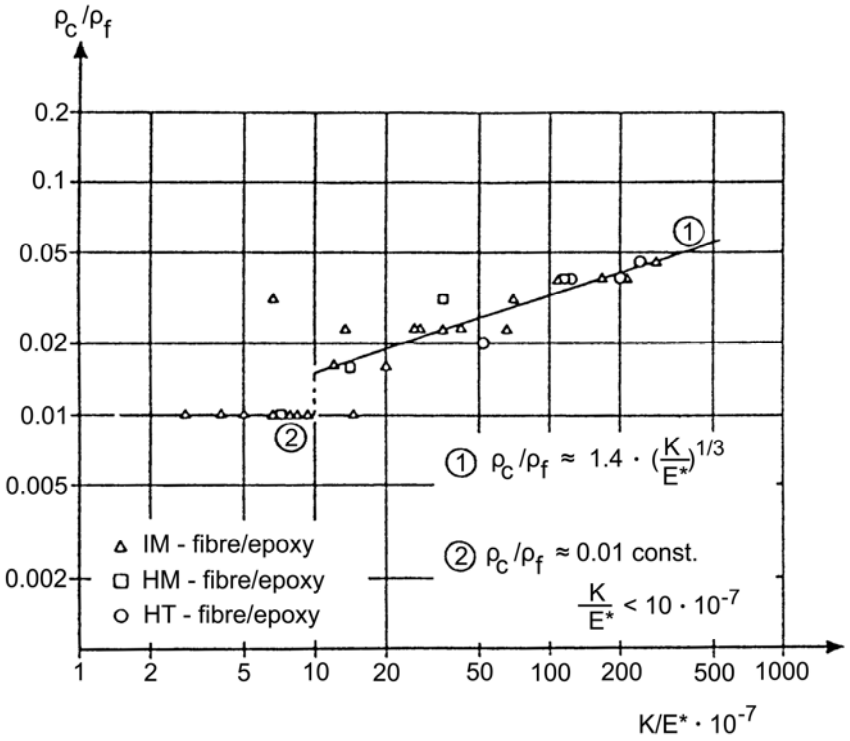

Figure 26.9-4 - Optimum sandwich core density

26.9.3.7 Summary

The evaluation of the design of cylindrical sandwich shells loaded in compression shows that in addition to a minimum mass, a minimum buckling stress can also be desirable. This prevents an overstressing of the facing material and avoids facing failure due to compression stress restrictions.

A modulus ratio of $E_x/E_y \approx 2.0$ appears to be a reasonable choice.

26.10 References

26.10.1 General

[26-1] D. Zenkert
"An Introduction to sandwich construction"
Chameleon Press Ltd., UK, 1995

[26-2] G.S. Gough, C.F. Elam, N.D. Bruyne
"The stabilization of a thin sheet by a continuous supporting medium"
J. Royal. Aero. Soc., Vol. 44, 1940, pp. 12-43.

[26-3] N.J. Hoff
"Monocoque, sandwich and composite aerospace structures – selected papers"
Technomic Publishing, 1985

[26-4] A. Marshall
"Sandwich Construction" in "Handbook of Composites"
Ed. G. Lubin, Van Nostrand Reinhold Company, New York 1982, pp. 557-601

[26-5] HexWeb® Honeycomb Data Sheets
Hexcel Corporation, www.hexcel.com/Products/Core+Materials

[26-6] Ultracor Data Sheets
Ultracor Inc. www.ultracorinc.com

[26-7] PMI (Rohacell®) foam core data sheets
Business Unit Plexiglass of Degussa AG www.rohacell.com

[26-8] Data sheets for cross-linked PVC foams
DIAB www.diabgroup.com

[26-9] Data sheets for linear PVC foams
Alcan Airex www.alcanairex.com

[26-10] A. Novi et al.
"Lightweight SiC foamed mirrors for space applications"
Optomechanical Design and Engineering 2001
(Ed. A. E. Hatheway), Proceedings of SPIE Vol. 4444, 2001

[26-11] Duocel Silicium Carbide Foam Data sheets
ERG Materials and Aerospace Corporation, CA, USA
www.ergaerospace.com/duocel/sic.htm

[26-12] ECSS-E-HB-32-21 Adhesive bonding handbook

[26-13] MIL-HDBK-23-A
"Structural Sandwich Composites"
U.S. Government Printing Office, 1974

[26-14] S.P. Timoshenko & Woinowsky-Krieger
"Theory of plates and shells"

McGraw-Hill, 2nd Edition, 1970

[26-15] R.M. Jones
"Mechanics of Composite Materials"
2nd Edition, Taylor & Francis, 1999

[26-16] E. Reissner
"The effect of transverse shear deformation on the bending of elastic plates"
Journal of Applied Mechanics, Transactions of the ASME, Vol. 12, 1945, pp. A69-A77

[26-17] R.D. Mindlin
"The influence of rotatory inertia and shear on flexural motionas of isotropic, elastic plates"
Journal of Applied Mechanics, Transactions of the ASME, Vol. 18, 1951, pp. 31-38

[26-18] C. Libove & S.B. Batdorf
"A general small-deflection theory for flat sandwich plates"
NACA TN 1526, 1948

[26-19] L. Librescu
"Elastostatics and Kinetics of Anisotropic and Heterogeneous Shell-Type Structures"
Noordhoff International Publishing, Leyden, 1975

[26-20] K.H. Lo, R.M. Christensen & E.M. Wu
"A High-Order Theory of Plate Deformation"
Transactions of the ASME, Journal of Applied Mechanics, Vol. 44, 1977, pp.669-676

[26-21] M. Stein
"Nonlinear Theory for Plates and Shells Including the Effects of transverse Shearing"
AIAA Journal, Vol. 24 (9), 1986, pp. 1537-1544

[26-22] J.N. Reddy
"A Simple Higher-Order Theory for Laminated Composite Shells"
Transactions of the ASME, Journal of Applied Mechanics, Vol. 51, 1984, pp. 745-752

[26-23] J.N. Reddy
"Exact Solution of Moderately Thick Laminated Shells"
Transactions of the ASCE, Journal of Engineering Mechanics, Vol. 10 (5), 1984, pp. 794-809

[26-24] Y. Frostig & M. Baruch
"Bending of Sandwich Beams with Transversely Flexible Core"
AIAA Journal, Vol.28 (11), 1990, pp. 523-531

[26-25] Y. Frostig, M. Baruch, O. Vilnai, I. Sheinman
"High-order Theory for Sandwich Beam Bending with Transversely Flexible Core"
Journal of ASCE, EM Division, Vol. 118, 1992, pp. 1026 1043

[26-26] Y. Frostig
"On Stress Concentration in the Bending of Sandwich Beams with Transversely Flexible Core"
Composite Structures, Vol. 24, 1993, 161-169

[26-27] Y. Frostig & Y. Shenhar
"High-order Bending of Sandwich Beams with a Transversely Flexible Core and Unsymmetrical Laminated Composite Skins"
Composites Engineering, Vol. 5, 1995, 405-414

[26-28] Y. Frostig & M. Baruch
"Localized Load Effects in High-Order Bending of Sandwich Panels with Transversely Flexible Core"
Journal of ASCE, EM Division, Vol. 122 (11), 1996

[26-29] O.T. Thomsen & Y. Frostig
"Localized Bending Effects in Sandwich Panels: Photoelastic Investigation versus High-Order Sandwich Theory Results"
Composite Structures, Vol. 37 (1), 1997, pp. 97-108

[26-30] V.S. Sokolinsky, H. Shen, L. Vaikhanski, S.R. Nutt
"Experimental and analytical study of nonlinear bending response of sandwich beams"
Composite Structures, Vol.60 (2), 2003, pp. 219–229

[26-31] S.R. Swanson
"An examination of a high-order theory for sandwich beams"
Composite Structures 44 (2–3), 1999, pp.169–177

[26-32] D. Zenkert (Ed.)
"The handbook of sandwich construction"
EMAS Publishing, Chameleon Press Ltd., London, 1997

[26-33] R.D. Cook, D.S. Malkus, M.E. Plesha & R.J. Witt
"Concepts and applications of finite element analysis"
4th Edition, John Wiley & Sons, 2002

[26-34] W.S. Burton and A.K. Noor
"Assessment of continuum models for sandwich panel honeycomb cores"
Computer methods in applied mechanics and engineering, Vol. 145, 1997, pp. 341-360

[26-35] D.B. Goetschel and D.W. Radford
"Analytical Development of Through-Thickness Properties of Composite Laminates"
Journal of Advanced Materials, Vol. 28 (4) 1997, pp. 37-46

[26-36] J. Hohe and W. Becker
"Effective stress-strain relations for two-dimensional cellular sandwich cores: Homogenization, material models and properties"
Applied Mechanics Reviews, Vol. 55 (1) 2002, pp. 61-87

[26-37] A. W. Leissa
"Buckling of laminated composite and shell panels"

AFWAL-TR-85-3069, 1985

[26-38] C.W. Bert et al.
"Buckling of cylindrical and conical sandwich shells with orthotropic facings"
AIAA Journal, Vol. 7, No. 2, pp. 250 - 257 (Feb. 1969)
Erratum, AIAA Journal, Vol. 7, No. 9, p. 1824 (Sept. 1969)

[26-39] NASA SP 8007
"Space vehicle design criteria, buckling of thin-walled circular cylinders"

[26-40] R.E. Fulton
"Effect of face sheet stiffness on buckling of curved plates and cylindrical shells of sandwich construction in axial compression"
NASA TN D 2783, April 1965

[26-41] R.E. Fulton & N.P. Sykes
"Effect of face sheet stiffness on buckling of cylindrical shells of sandwich construction"
NASA TN D 3454, June 1966

[26-42] C.D. Reese & C.W. Bert
"Simplified design equations for buckling of axially compressed sandwich cylinders with orthotropic facing and core"
J. Aircraft, Vol. 6, No. 6, pp. 515 - 519, Nov. - Dec., 1969

[26-43] "Handbook of structural stability"
Corona Publishing Company, Ltd, Tokyo, 1971

[26-44] D. Bushnell
"BOSOR 4 - Program for stress, buckling and vibration of complex shells of revolution"

[26-45] J.N. Dickson & R.H. Brolliar
"The general instability of ring stiffened corrugated cylinders under axial compression"
NASA TN D 3098, January 1966

[26-46] A. Van der Neut
"General instability of stiffened cylindrical shells under axial compression"
National Luchtvaart laboratorium, Holland
Vol. 13, 1947 pp. 57 – 84

[26-47] R.C. Tennyson et al.
"The effect of axisymmetric shape imperfections on the buckling of laminated anisotropic circular cylinders"
Trans. Canadian Aeronautics Space Inst.
Vol. 4, No. 2 Sept. 1971

[26-48] B.O. Almroth et al.
"Design criteria for axially loaded cylindrical shells"
J. Spacecraft and Rockets, Vol. 7 (1970), June, pp. 714 – 720

[26-49] H. Bansemir
"Gesamtstabilität von Sandwichplattenstreifen mit orthotroper Zwischenschicht und isotropen Deckschichten"
BB, TN D124 13/73, 1973

[26-50] R.T. Sullins et al.
"Manual for structural stability analysis of sandwich plates and shells"
NASA CR 1457, Dec. 1969

[26-51] V. Skvortsov & O.T.Thomsen
"Local instability of shallow sandwich shells for the general case of orthotropy, curvature and loading"
Composite Structures, Volume 70, Issue 3, September 2005, Pages 343-355

[26-52] L. Fagerberg
"Wrinkling of sandwich panels for marine applications"
PhD.Thesis, Royal Institute of Technology
Dept. of Aeronautical and Vehicle Engineering, 2003

[26-53] N.J. Hoff & S.E.Mautner
"Buckling of sandwich type panels"
Journal of the Aeronautical Sciences
Vol.12, No.3, July 1945, pp. 285-297

[26-54] F.J.Plantema
"Sandwich construction"
John Wiley & Sons, New York, 1966

[26-55] H.G. Allen
"Analysis and design of structural sandwich panels"
Pergamon Press, Oxford, 1969

[26-56] C.B. Norris & W.J. Kommers
"Short column compressive strength of sandwich constructions as affected by the size of cells of honeycomb materials"
Forest Products Laboratory (FPL) Report 1817, 1950

[26-57] R. M. Hussein
"Composite panels/plates - Analysis and design"
Technomic Publishing Co., Inc., 1986

[26-58] Fokker BV
TR R 86 080, Final report of composite structural element study (CSE), 1986

[26-59] C. Blaas et al.
"Local instability for sandwich panels"
Fokker report TR-N-84-CSE-061, 1984

[26-60] T.R.A. Pearce, & J.P.H. Webber.
"Buckling of sandwich panels with laminated face plates"
Aeronautical Quarterly, May 1972

[26-61] T.R.A. Pearce & J.P.H. Webber
"Experimental buckling loads of sandwich panels with carbon fibre face plates"
Aeronautical Quarterly, November 1973

[26-62] H. Bansemir & K. Pfeifer
"Local instability of sandwich structures with thin fibre reinforced face skins for space applications"
SAMPE European Chapter, Third Technology Conference, London, March 1983

[26-63] W.M. Banks & G.B. Chai
"The behaviour of CFRP Sandwich Panels under in-plane compressive loading"
University of Strathclyde, ESA Contract - Purchase Order No. 52853, January 1988

[26-64] O.T. Thomsen & W.M. Banks
"An improved model for the prediction of intra-cell buckling in CFRP sandwich panels under in-plane compressive loading"
Composite Structures, Vol. 65, No.3, 2004, pp. 259-268

[26-65] ECSS-E-HB-32-22 Insert design handbook

[26-66] O.T. Thomsen & W. Rits
"Analysis and design of sandwich plates with inserts: A high-order sandwich plate theory approach"
Composites Part B, Vol. 29B, 1998, pp. 795-807

[26-67] O.T. Thomsen
"Sandwich plates with through-the-thickness and fully potted inserts: evaluation of differences in structural behaviour"
Composite Structures, Vol. 40, No. 2, 1998, pp. 159-174, 1998

[26-68] A. Obst
"Design of sandwich structures for space applications"
Chapter 18 in "Theory and applications of sandwich structures"
Ed. R.A. Shenoi et al., University of Southampton, UK, 2005

[26-69] R.T. Haftka & Z. Gürdal
"Elements of structural optimization"
3rd Edition, Kluwer, Dordrecht, ISBN-0-7923-1504-9, 1992

[26-70] Z. Gürdal, R. T. Haftka, P. Hajela
"Design and optimization of laminated composite materials"
John Wiley & Sons, New York, ISBN 0-471-25276-X, 1999

[26-71] G.N. Vanderplats
"Numerical optimisation techniques for engineering design"
Vanderplats Research and Development Inc., Colorado Springs, 2001

[26-72] A. Wetzel, L. Kärger, R. Rolfes, K. Rohwer
"Evaluation of two finite element formulations for a rapid 3D stress analysis of sandwich structures". Computers and Structures, Vol. 83, 2005, pp. 1537–1545

[26-73] "Metal Foams Homepage"
National Physical Laboratory, UK,
www.npl.co.uk/materials/metal_foams/index.html

26.10.2 ECSS documents

[See: ECSS website]

ECSS-E-HB-32-24	Buckling of structures
ECSS-E-HB-32-21	Adhesive bonding handbook for advanced structural materials; previously ESA PSS-03-210
ECSS-E-HB-32-22	Insert design handbook; previously ESA PSS-03-1202.

27
Design of thin-walled structures

27.1 Introduction

27.1.1 General

Stiff thin-walled structural components are commonly-used in space hardware because they offer mass-efficiency.

Some examples of thin-walled structures include:

- Plates, [See: 21.2].
- Profiles, [See: 21.3].
- Cylindrical shells:
  - stiffened, [See: 21.4; 21.5 - examples].
  - unstiffened, [See: 21.6].

As part of the increasing interest in deployable structures, a variety of new concepts have evolved using thin-walled structures, e.g.:

- Rigid components, usually in the form of conventional tubes or truss structures, [See also: Chapter 25].
- Flexible components, which are stowed in a folded configuration for launch, deployed in space and then rigidised, [See: 27.2- inflatable structures].

27.1.2 Design aspects

Thin-walled unstiffened and stiffened structures are most susceptible to instability and failures due to localised loading.

The anisotropic nature of composites makes these phenomena more complicated than in conventional materials.

Complex materials configurations are used in deployable structures, such as combinations of very thin polymer films, metal foils with or without a fibre-reinforced composite layer. In general, rigidised inflatable structures are prone to the same types of instability and local failure as those made of composites. For further information on the subject see ECSS-E-HB-32-24A - Buckling of Structures.

27.2 Inflatable structures

27.2.1 Introduction

Any deployable structure is essentially an assembly of prefabricated components that can be transformed from a closed, compact form or folded configuration to a predetermined, expanded, complete and stable structure capable of supporting loads, Ref. [27-18].

Although first considered in the 1950's, Ref. [27-19], current initiatives on inflatable structures are part of a group of technologies associated with the development of often large, extremely lightweight structures destined to be deployed in space. Recent and on-going work builds on an existing technology base along with results from earlier ground and in-orbit demonstration programmes. In some of these, inflatable deployable structures up to about 30m were constructed and flown.

The advantages of inflatable deployable structures are the perceived performance enhancements over mechanically deployable structures. The ability to be packaged into small volumes of varying shape is seen as a means of reducing launch cost by more efficient use of launcher volume or by use of smaller launchers. Efficient use of lightweight materials can provide significant mass reductions. Additionally, the apparent simplicity of inflatables is viewed as a means of increasing reliability.

A disadvantage of any deployable structure is that, whatever the means of deployment and rigidisation used, it has to be completely reliable. Failure to deploy fully or rigidise correctly can result in reduced performance, e.g. antenna-reflectors and solar arrays, so compromising the mission.

[See also: 28.11 for antenna-reflector development]

Since Contraves' inflatable structures in the 1980s, [See: 28.12], various organisations worldwide have been committed to developing inflatable technologies for space, e.g. NASA, ESA, Ref. [27-21], [27-22], [27-28].

A European perspective for inflatable technologies is summarised in Figure 27.7.1, Ref. [27-31].

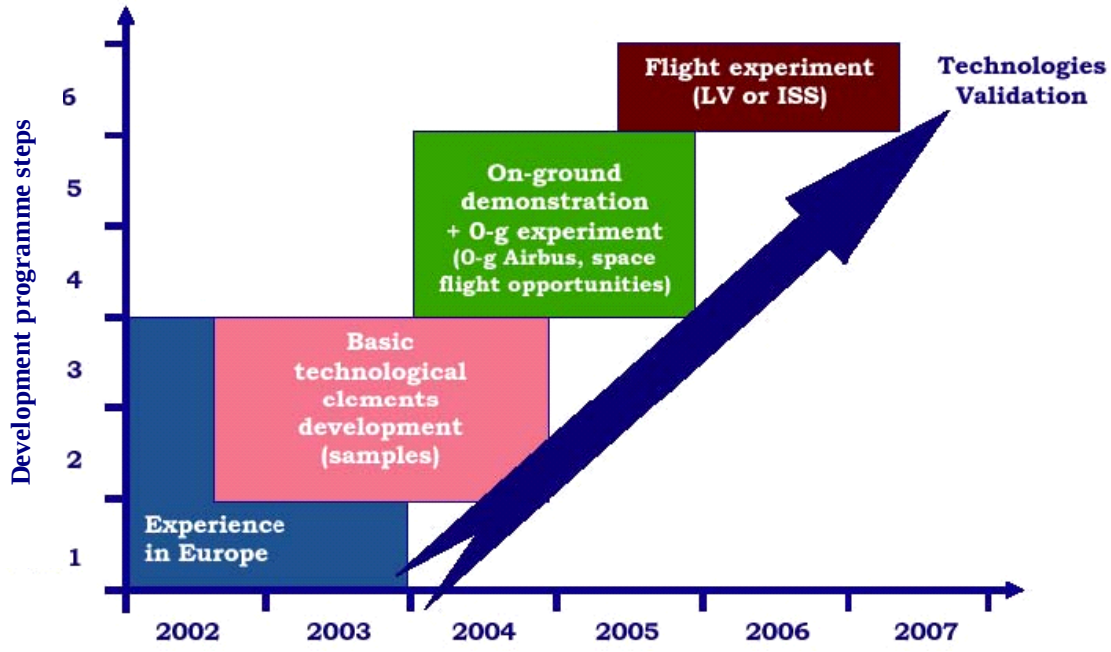

Figure 27.2-1 – Inflatable technologies: European perspective

27.2.2 Applications

27.2.2.1 Deployable structures

Within the space industry, conventional means of deploying rigid structures are well-established and proven, e.g. using mechanisms, such as latches made of shape memory alloys; pyro-devices; unfurlable antenna concepts, [See: 28.12].

More recent concepts for deployable structures include:

- Antennas, Ref. [27-26]
- Solar arrays, Ref. [27-31], [27-41]
- Solar sails, Ref. [27-26]
- Sunshields, Ref. [27-44]
- Gossamer structures, Ref. [27-21], [27-22], [27-24], [27-26]
- Entry and landing systems, Ref. [27-32]
- Space and planetary habitats, Ref. [27-33]

27.2.2.2 Inflatable structures

Some of the deployable concepts proposed make use of inflatable technologies. These can be broadly grouped as:

- Inflation by gas to obtain the shape and then the shape maintained by gas pressure; often known as membrane structures, e.g.
  - ESA QUASAT antenna, Ref. [27-42].
  - NASA IAE inflatable antenna experiment, Ref. [27-32].
  - Payload landing, e.g. inflatable parachutes; Mars Pathfinder 'gas-bags', Ref. [27-32].
- Deployment of a flexible, packed structure by some form of mechanism, inflation by gas to obtain the final shape. The shape is then maintained by gas pressure.
- Inflation of a flexible material, by gas, to achieve the shape followed by a material rigidisation process, e.g. UV- or radiation-curing of a composite matrix phase, e.g. ESA advanced solar array, Ref. [27-31]; ARISS telescope, Ref. [27-32].

27.2.3 Overall configuration

Depending on the application, many concepts for large deployable structures envisage the use of very thin materials, such as:

- antenna-reflectors, made of transparent and metallised polymer films, often only a few microns thick.
- solar arrays, thin silicon or other semiconductor materials bonded to a flexible or hinged support.

These are attached to a supporting structure, which is also made of thin flexible materials that are rigidised after deployment; usually to create long, extremely thin-walled tubes.

27.2.4 Materials

27.2.4.1 Membranes

The types of thin polymer films proposed often have proven stability in the space environment, because they are commonly-used for thermal control purposes.

Some examples include, Ref. [27-20], [27-23]:

- Kapton® from DuPont (bare or metallised).
- Mylar® from DuPont Teijin(bare or metallised).
- FEP Teflon® from DuPont or Norton FEP from St. Gobain -Performance Plastics Div. (Ireland).
- LaRC® grades, from NASA.
- Triton COR® grades, from Triton Systems (USA).

Other concepts use layered constructions of one or more thin films, e.g. aluminium film laminates, which are also considered for structural members, Ref. [27-36].

27.2.4.2 Structural members

Depending on the application, concepts for supporting structures tend to be either a series of tubes, known as masts or booms, Ref. [27-26], [27-31], or truss-type configurations, Ref. [27-19], [27-40]. Masts or booms can be parallel-sided or tapered. Several tubes can also be used in a bundle.

All of the tubes are very thin-walled and often of a layered construction of different materials. Each layer is usually a few microns thick. The individual layers can be bonded together (laminated) or not. Thin tube walls need to be flexible enough for folding, packing and inflation.

The inside layer, known as a membrane or bladder, acts as an impermeable barrier to prevent gas escaping and deflating the structure. Its other function is to provide a consolidation pressure for rigidisation processes involving curing of a composite layer.

The middle layer effectively is the load-carrying material, e.g. a fibre-reinforced composite or metal foil, which acts together with the inner and outer layers to support all of the design and environmental loads.

The external layer both restrains and protects the structure in its packed configuration. As some constructions contain resin phases in an uncured state, they are tacky and likely to stick together and disrupt deployment. Once deployed and rigidised, the external layer provides protection from the space environment.

Some examples of material combinations include:

- Aluminium film laminates, containing 1100-alloy aluminium foil (<100μm thick) placed between Mylar® or Kapton® polymer films, Ref. [27-36]. This technology was first used in early balloon-type concepts launched by NASA, e.g. ECHO, EXPLORER IX and XIX, but more recently as tubular struts, Ref. [27-35], [27-36].
- Composite and polymer films, e.g.:

  - Carbon fibre braid with ASPMI thermoset resin between layers of polyimide film, Ref. [27-38].
  - Glass-fibres in a photo curable resin matrix between two layers of polyimide film, Ref. [27-31].
  - Glass fibre braid with UV-curable resin over a polyester-based bladder, UV-transparent restraint layer (polyester or quartz textile), Ref. [27-39].
- Textiles and polymer films.
- Textiles coated with polymers, e.g.:
  - Neoprene-coated Kevlar® textile, Ref. [27-19].
  - Silicone-coated Vectran® woven textile, Ref. [27-33], [27-37].

Within biomimetic studies, some smart materials are being targeted for deployable structures, e.g. an evolution of a Canadian concept first developed in the 1970s, STEMS 'storable tubular extendable members' have shape-memory wires embedded in fibre-reinforced thermoplastic matrix composites, Ref. [27-34]

27.2.5 Rigidisation

Over the years, many different rigidisation processes for deployable structures have been proposed and evaluated to some extent. Some of the most common types are summarised with respect to inflatable structures, Ref. [27-35], [27-36]:

- Composites with thermosetting matrix phases, where heat is necessary to initiate and complete curing. This tends to demand high power. Developments with heater wires embedded in the composite are seen as a means of reducing power demands, e.g. 15W/m^2 for carbon-epoxy composites.
- Foams, where either the internal cavity of the structure or an internal surface layer is coated with a material that expands and becomes rigid after deployment. The foam can also be seen as contributing to the load-bearing capacity of the structure.
- High-pressure inflation to plastically deform a metal foil, e.g. aluminium film laminates.
- Hydrogel or water-soluble materials, in which the water evaporates under the vacuum of space to harden the material. The outgassing can be problematical in some applications.
- Inflation gas reaction, where the gas used to inflate the structure contains a chemical that provokes a reaction in the composite matrix phase. This type of rigidisation process was investigated by Contraves in collaboration with Ciba-Geigy.
- Plasticiser or solvent boil-off, in which one or more of the constituents of a composite matrix phase evaporates under the vacuum of space. As with hydrogel processes, the effects of outgassing are concern.
- Shape memory materials, either embedded in composites (smart materials) or enclosed within the structure that, when activated, take on a predetermined shape.
- SOTC second-order transition change, where materials are warmed to above their glass transition point to become flexible for deployment and then cool below the Tg to become rigid.

- Sublimating powders, where the structure is filled with a suitable powder that sublimes in space to provide the gas inflation pressure. This method was used in early balloon-type experiments, e.g. NASA ECHO programme.
- Sub-Tg, where the temperature of the composite polymer matrix phase is reduced below its' glass transition temperature. Such polymers are flexible prior to deployment and gradually harden in the low temperatures in space. A means of uniformly decreasing the temperature is needed to avoid distortion, e.g. progressive cooling through insulation.
- UV-curing composite matrix phases, also known as 'photocure' where cure occurs after exposure to UV in space or from lamps. These materials tend to have lower power demands than heat-cured systems, but need careful optimisation, e.g. UV-dose, temperature range and deployment time, Ref. [27-39].

27.2.6 Evaluation and testing

Depending on the concept and the intended applications, factors to be considered in test and evaluation include, Ref. [27-24]:

- Atomic oxygen effects, Ref. [27-20].
- Solar UV and radiation effects (materials and models), Ref. [27-20].
- Electromagnetic characteristics.
- Optical characteristics.
- Multidisciplinary testing aspects .
- Rigidisation materials testing .
- Inflation systems testing and modelling, e.g. by finite element, Ref. [27-29].
- Modelling of materials, Ref. [27-30].
- Modelling of rigidisation mechanisms, Ref. [27-29].
- Packing.
- Testing and simulation of deployment.
- Simulation of environments (long-term exposure), Ref. [27-33].

As with all space structures, the long-term durability of thin materials needs evaluation with respect to exposure to the space environment. Results of tensile tests and solar absorption after 5-years exposure to simulated GEO or LEO environment suggested that fluorinated polymers showed least degradation, Ref. [27-20], [27-23], [27-40]. In some concepts, extreme lightweight structures cannot withstand gravity, so cannot be fully tested prior to launch. Therefore adequate means of simulation and modelling of materials and structures is necessary in such cases. Where rigidisation processes rely on the space environment, this too has to be simulated correctly on Earth.

27.2.7 Design aspects

27.2.7.1 General

The perceived uses, hence design factors, for inflatable structures are both wide-ranging and very mission dependent. In addition to mass and cost, which are design-drivers for all space hardware, the key points related to the design of inflatables are grouped as, Ref. [27-36]:

- Materials selection and manufacturing processes,
- Deployment, mechanisms, processes and reliability.
- Rigidisation, processes and reliability.

Each subject has a number of factors to be fully-addressed, concurrently during the overall design process.

27.2.7.2 Materials selection

Factors to be considered during materials and process selection include, Ref. [27-36], [27-40]:

- High-specific stiffness and strength to optimise both structural performance and mass.
- Trade-off between mechanical properties to meet stiffness demands and ability to be folded and packed, e.g. severe creases in carbon or glass fibres can result in breakage.
- Compatibility between materials in their packed, deployed and rigidised state, e.g. bonding between layers, galvanic effects, chemical compatibility between components of uncured resins and adjacent materials (corrosion),
- Low CTE to reduce thermal distortion and optimise mass of thermal control materials
- No adverse effects from packing, deployment and rigidisation that could reduce material performance, e.g. folds, creases, wrinkles, flexing, shrinkage, creep, uneven cure, or system level problems, e.g. final shape and dimensional tolerances for antennas.
- No degradation occurs whilst stored, e.g. 2 years or more, under given storage conditions (temperature, humidity).
- Low outgassing under combined thermal and vacuum conditions, both prior to and after rigidisation.
- Performance retention when exposed to the space environment in either a packed or deployed state, e.g. effects of thermal ageing, thermal cycling, radiation exposure.
- Use of established and proven manufacturing processes and means of validation and control, e.g. large areas of bonded layers; seams; joints.
- Ease of manufacturing and handling. This can be especially difficult for large areas of thin materials.
- Ability to model the materials accurately, e.g. stiffness, strength, buckling, bending or thermal behaviour.

The support structures are usually made of hollow, extremely thin-walled, long tubes. Therefore, the design of such structures needs consideration of, Ref. [27-35], [27-38]:

- Compressive buckling (global and local),
- Beam stiffness and natural frequency,
- Beam bending and buckling
- Geometry-related parameters, i.e. diameter, thickness, length
- Material parameters, i.e. modulus, strength, density.

27.2.7.3 Deployment

Factors to be considered during the design of mechanisms and deployment processes include, Ref. [27-36]:

- Minimise energy demands from the spacecraft to deploy and rigidise, e.g. mechanisms to unpack structures; gas delivery systems to inflate structures; materials that need heat to cure during rigidisation.
- Simplification of systems to improve reliability compared with more complex options.
- Ensure that deployment system achieves the as-designed shape, e.g. capable of removing creases and wrinkles.
- Ability to simulate or model the deployment process accurately.

27.2.7.4 Rigidisation

Factors to be considered for the rigidisation process are closely linked to the materials selected, Ref. [27-36]:

- Rapid, predictable and reliable rigidisation processes, e.g.
  - Solely inflatable structures that are rigidised by gas alone need to take their shape and intended orientation quickly after deployment to avoid incurring damage, e.g. creases, twists or tears from contact with other structures.
  - Inflated then rigidised systems are flexible when first deployed and need to attain their as-designed stiffness quickly, e.g. before UV-curing, an inflated structure is susceptible to damage of the gas-retaining bladder causing leaks. This could produce distortion in the intended final shape or incomplete consolidation of the composite.
- Ability to simulate or model the rigidisation process accurately, Ref. [27-29].
- Known and controlled process to avoid rigidisation whilst in a packed configuration or during deployment, e.g. composite out-life.
- Flexibility of process to enable full rigidisation under various thermal environments and conditions encountered on Earth and in space.
- Capability to produce the as-designed shape without degradation of performance or damaging the materials.
- Monitoring of rigidisation process and verification of when rigidisation is complete.
- Reversible and reliable process to enable ground testing and acceptance of the integrated flight system. Many of the rigidisation processes for composites are ‘one shot’ and not reversible whereas inflation by gas alone is reversible.
- Ease of ground testing with adequate quality control procedures for large scale structures.

27.2.8 Inflatable structures: Examples

27.2.8.1 ECHO balloons

Developed by NASA and flown in the 1960s, the ECHO I balloon was made of a large number of 12μm thick, aluminised Mylar® gores bonded together to form a 30.5 m sphere, Ref. [27-19]. This is essentially conventional balloon construction technology, but using very thin modern materials.

The balloon weighed about 62 kg and was stowed in a 0.6m diameter cylinder for launch. Deployment and rigidisation used about 14kg of sublimating powder contained within the balloon structure.

ECHO I was launched in 1960 attained an initial orbit of 1000 miles which changed over time due to solar pressure. It remained operational for several months and provided a sufficiently large reflective profile, Ref. [27-19].

27.2.8.2 ITSAT inflatable solar array

ITSAT inflatable torus solar array was part of the US ASTP advanced space technology programme conducted in the 1990s. It considered means of providing power to small satellites with power demands exceeding 100W.

The design-development programme produced a solar array wing in the 200W to 1000W class, with a projected power density (200W class) of 93W/kg including structure and deployment mechanisms, Ref. [27-41].

The main features can be summarised as, Ref. [27-41]:

- Silicon cells (50μm thick) on a Kapton® film substrate, folded accordion-style for stowage.
- Support structure consisting of:
  - rectangular frame made up of two cylinders or booms which are stored flat and folded for launch. These are then inflated and rigidised. The boom cylinders were made of aluminium film laminates.
  - array stowage box and cover made of a CFRP sandwich.
- Deployment: Inflation of the booms by dry nitrogen gas
- Rigidisation: By controlled straining of the aluminium film laminate beyond its elastic limit.

Demonstrator solar arrays were constructed and evaluated with qualification tests, i.e. random vibration, deployment under vacuum, natural frequency and thermal cycling. The protoflight model achieved 36% less power than anticipated, which was attributed to problems with material availability. The simplicity of the deployment system was considered to save as much as half the cost of competing, conventional designs, Ref. [27-41].

27.2.8.3 Contraves inflatable structures

Conducted under ESA-ESTEC QUASAT and FIRST programmes, Contraves designed and developed a number of inflatable structures in the 1980s, including, Ref. [27-19], [27-42], [27-43], [27-44]:

- Axi-symmetric reflector antennas for VLBI very large baseline interferometry. A 1/3-scale VLBI demonstrator, 6m diameter, was constructed and evaluated, [See also: 28.12]
- Offset reflectors for land mobile communications: A 10m × 12m L-band reflector antenna was constructed and tested for surface precision and mechanical performance.
- Sunshade support structures for telescopes and large sensors: A functional scale model of a truss structure to support MLI flexible insulation panels.

The antenna inflatable structures were basically two parabolic membranes supported on a peripheral toroidal structure. The membranes each consisted of multiple 'pie-shaped' gores. One membrane was RF transparent, the other metallised to ensure RF reflectivity.

Kevlar® fibres, combined with a matrix phase which cured by solar heating after deployment-rigidisation in-orbit, provided the load-carrying capability of the gores.

The same materials technology was applied for the truss structure development.

27.2.8.4 IN-STEP IAE inflatable antenna experiment

The NASA IAE flew in 1996 with the aim of evaluating inflatable technology with respect to, Ref. [27-19]:

- Cost of building large inflatable structures.
- Mechanical packing efficiency.
- Reliability of deployment.
- Surface precision, verified by measurements in-orbit.

The IAE consisted of a 14m off-axis parabolic inflatable reflector with its torus and strut support structure. The reflector was made of 6μm thick aluminised Mylar® film with the canopy of transparent film of the same thickness. The reflector was stressed by inflation to about 8MPa (1200psi) in order to achieve the correct shape and surface accuracy, e.g. a few mm rms. The torus-strut support structure was made of 0.3mm thick neoprene-coated Kevlar® textile, Ref. [27-19].

27.2.8.5 ESA Advanced Solar Array

Under the ESA's technology and research programme, started in 2004, an EADS-ST collaboration study produced a breadboard model for a 3.2 m long inflatable solar array; as shown in Figure 27.07.2, Ref. [27-31].

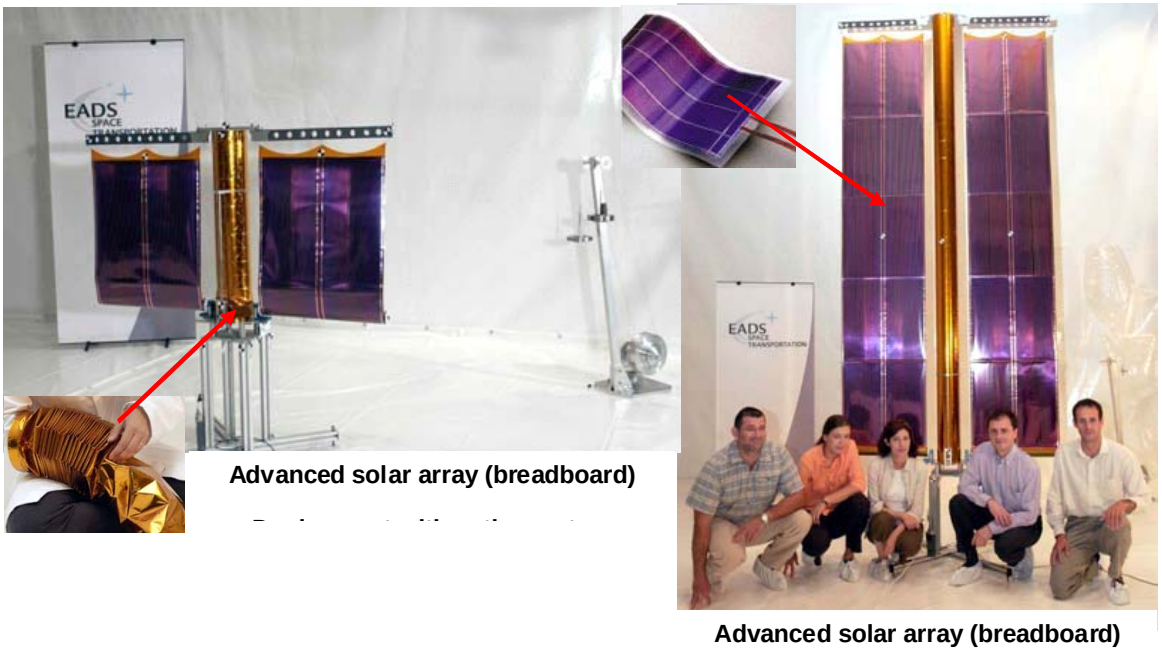

Figure 27.2-2 – Inflatable technologies: ESA advanced solar array (breadboard)

The main features can be summarised as, Ref. [27-31]:

- Thin film solar cells, consisting of amorphous silicon deposited on a flexible polymer support.
- Boom: Glass-fibre composite (photo curing) between two thin polyimide films.
- Deployment, by the proprietary TADEC system incorporated in the boom.
- Rigidisation, by gas inflation and photo curing.
- Size: 0.123 m3 (folded volume); 3.2 m × 1.6 m (deployed).
- Mass (overall): 7.2 kg

Glass fibres are necessary to accomplish proper photo curing of the composite layer.

27.3 References

27.3.1 General

[27-1] W. Hertel
'Faserverstärkte Kunststoffe, Theorie und Anwendung'
Vortrag an der Fachhochschule Trier

[27-2] W. Hertel
'Entwicklung einer Kegelschale in CFK Wellstruktur-Bauweise'
DGLR 78-156

[27-3] R. Jones
'Mechanics of composite materials'
N.Y. 1975

[27-4] H. Öry
'Krafteinleitung in glasfaserverstärkte Kunstofstoffbauelemente'
WGL Bericht Nr. 4, Braunschweig 1962

[27-5] R.M. Jones
'Buckling and vibration of unsymmetrically laminated cross ply rectangular plates'
AIAA 73 368

[27-6] E.E. Spier
'Stability of graphite epoxy structures with arbitrary symmetrical laminates'
Exp. Mechanics

[27-7] B.O. Almroth and D.O. Brush
'Buckling of bars, plates and shells'
McGraw Hill, 1975

[27-8] W.T. Koiter
'On the stability of elastic equilibrium'
NASA TTF 10, 1967

[27-9] A. Van der Neut
'General instability of stiffened cylindrical shells under axial compression'
National Luchtvaartlaboratorium, Holland, Vol. 13
Rept. S. 314 (1947)

[27-10] R.C. Tennyson et al
'The effect of axisymmetric shape imperfections on the buckling of laminated anisotropic circular cylinders'
Trans. Canadian Aeronautics Space Institute, Vo. 4, No. 2, Sept 1971

[27-11] N.S. Khot & V.B. Venkayya
'Effect of fibre orientation on initial postbuckling behaviour and imperfection sensitivity of composite cylindrical shells'
AFFDL Report TR 70 125, 1970

[27-12] B.O. Almroth et al
'Design of criteria for axially loaded cylindrical shells'

[27-13] NASA: SP-8007
'Buckling of thin walled circular cylinders'

[27-14] E.F. Bruhn
'Analysis and design of flight vehicle structures'
Tri State Offset Company, 1965

[27-15] R. Zimmermann
'Optimisation of axially compressed CFRP cylinders'
ESA SP-238: Proc. of Conference: 'Spacecraft Structures'

CNES, Toulouse, 3 6 Dec. 1985

[27-16] R.C. Tennyson & J.S. Hansen: University of Toronto
Institute for Aerospace Studies
'Buckling analysis of composite cylinders'
EUROMECH Conference 'Flexible Shells - Theory and Applications', Munich, 1983

[27-17] F.R. Shanley
'Simplified analysis of general instability of stiffened shells in pure bending'
Journal of Aero. Sciences, 16, Oct. 1949

[27-18] C.J. Gante
'Deployable structures, analysis and design'
Journal of Structural Engineering, Vol. 128, No. 7, July 2002, p962
WIT Press ISBN 1-85312-606-8

[27-19] R. E. Freeland et al. :JPL/L'Garde Inc (USA)
'Inflatable Deployable Space Structures Technology - Summary'
http://www.lgarde.com/people/papers/spacestructs.html

[27-20] W. K. Stuckey et al: Aerospace Corp (USA)
'Space Environment Test of Materials for Inflatable Structures'
Report Number: A572943 (April 1998)

[27-21] 2nd European Workshop on Inflatable Space Structures,
ESA Conference, 21-23 June 2004 , Tivoli, Italy.

[27-22] 5th European Workshop on Inflatable Space Structures,
ESA/ESTEC Conference, October 2006, Noordwijk, NL

[27-23] J. Dever et al: NASA Glenn Research Centre (USA)
'Exposure of Polymer film Thermal Control Materials on the Materials International Space Station Experminet (MISSE)'
NASA TN-2002- 211363 (February 2002)
from: http://misse2.larc.nasa.gov/TM-2002-211363.pdf

[27-24] C.H.M. Jenkins: Montana State University (USA)
'Gossamer Spacecraft: Membrane and Inflatable Structures Technology for Space Applications'
ISBN 1-56347-403-42001, AIAA (Hardback) 2001

[27-25] C.H.M. Jenkins: Montana State University (USA)
'Recent Advances in Gossamer Spacecraft
ISBN: 1-56347-777-7 AIAA (Hardback) 2006

[27-26] C. Sickenger: DLR Brauscheweig (D)
'Ultra lightweight deployable structures'
4th International Conference on Thin-walled structures, Loughborough, UK June 2004

[27-27] TU Delft (NL)
'Projects: Inflatable aerospace structures
http://www.sml.lr.tudelft.nl/

[27-28] Session 7: Deployable structures
Proceedings of European Conference on Spacecraft structures, Materials and Mechanical Testing ESA-ESTEC Noordwijk (NL) 10-12 May, 2005. ESA-SP-581 (August 2005)

[27-29] M. Bruyneel et al: SAMTEC (B)
'First results of the PASTISS project'
Proceedings of European Conference on Spacecraft structures, Materials and Mechanical Testing ESA-ESTEC Noordwijk (NL) 10-12 May, 2005. ESA-SP-581 (August 2005)

[27-30] A. Obst et al: ESA-ESTEC
'Modelling of triaxial woven fabrics for antenna reflectors'
Proceedings of European Conference on Spacecraft structures, Materials and Mechanical Testing ESA-ESTEC Noordwijk (NL) 10-12 May, 2005. ESA-SP-581 (August 2005)

[27-31] V. Peypoudat et al: EADS-ST (Bordeaux)/IDEAMECH (CH)/VHF Technologies (CH)
'Development of 3.2 m long inflatable and rigidised solar array breadboard'
Proceedings of European Conference on Spacecraft structures, Materials and Mechanical Testing ESA-ESTEC Noordwijk (NL) 10-12 May, 2005. ESA-SP-581 (August 2005)

[27-32] A. Lennon & S. Pellegrino: Consultant/Cambridge Uni. (UK)
'Structural mechanics of lobed inflatable structures'
Proceedings of European Conference on Spacecraft structures, Materials and Mechanical Testing ESA-ESTEC Noordwijk (NL) 10-12 May, 2005. ESA-SP-581 (August 2005)

[27-33] S. Mileti: University of La Sapeinza, Rome (I)
'Reliable numerical approach for a design of an inflatable Moon/Mars habitat based on material tests in the SAS simulator'
Proceedings of European Conference on Spacecraft structures, Materials and Mechanical Testing ESA-ESTEC Noordwijk (NL) 10-12 May, 2005. ESA-SP-581 (August 2005)

[27-34] M. Ayre: ESA-ESTEC Advanced Concept Team (NL) /D'Appolonia (I)/Uni. of Bath (UK)
'Novel concepts of space deployable systems based on energy storage textile based structures'
Proceedings of European Conference on Spacecraft structures, Materials and Mechanical Testing ESA-ESTEC Noordwijk (NL) 10-12 May, 2005. ESA-SP-581 (August 2005)

[27-35] B Derbes: L'Garde (USA)
'Case studies in inflatable rigidisable structural concepts for space power'
AIAA-99-1089

[27-36] D.P. Gadogan & S.E. Scarborough: ILC Dover Inc. (USA)
'Rigidisable materials for use in Gossamer space inflatable structures'
AIAA-2001-1417: AIAA Gossamer Spacecraft Forum, April 16-19, Seattle (USA)

[27-37] Vectran® fibre: Product data and applications
http://www.vectranfiber.com/index.asp

[27-38] V. Barbet et al: Alcatel Space (F)/Ideamech (F)/ESTEC (NL)
'Mechanical testing of inflatable space structure beams'
Proceedings of European Conference on Spacecraft structures, Materials and Mechanical Testing ESA-ESTEC Noordwijk (NL) 10-12 May, 2005. ESA-SP-581 (August 2005)

[27-39] Y.M Lefevre et al: Astrium Space (F)/Ideamech (F)/Zodiac (F)/ESTEC (NL)
'Materials and wall concepts for UV-curable inflatable space structures'
Proceedings of European Conference on Spacecraft structures, Materials and Mechanical Testing ESA-ESTEC Noordwijk (NL) 10-12 May, 2005. ESA-SP-581 (August 2005)

[27-40] K. Seifart et al: Hoch Tecnologie System (D)/ESTEC (NL)
'Deployable structure for flexible solar generator'
Proceedings of European Conference on Spacecraft structures, Materials and Mechanical Testing ESA-ESTEC Noordwijk (NL) 10-12 May, 2005. ESA-SP-581 (August 2005)

[27-41] P.K. Malone & G.T. Williams: L'Garde (USA)
'Lightweight inflatable solar array'
Journal of Proulsion & Power, Vol. 12, No. 5, Sept.-Oct. 1996

[27-42] G.G. Ribaldi & M.C. Bermasconi: Contraves (CH)
'QUASAT programme: The ESA reflector'
IAF-84-400: 36th International Astronautical Congress, Stockholm (1985)

[27-43] M.C. Bermasconi et al: Contraves (CH)
'Large inflatable, space-rigidised antenna reflectors: Land mobile services development'
IAF-87-315: 38th International Astronautical Congress, Brighton, UK (1987)

[27-44] M.C. Bermasconi et al: Contraves (CH)
'Space-rigidised thermal shield for ESA FIRST 'far infrared space telescope'
3rd European Symposium on Space Thermal Control and Life Systems, ESA-ESTEC, Noorwijk, NL. SP-288 (1988)

28
Design of dimensionally stable structures

28.1 Introduction

28.1.1 General

For space applications demanding high dimensional stability, the thermal expansion characteristics of structures has to be taken into account. This is the case where structural components need to maintain their relative position or shape, or where precise dimensions (close tolerances) are guaranteed over a long time period, e.g. reflectors, antennas, mirrors, optical equipment or other sensor systems, Ref. [28-1]. The basic categories of dimensional stability are short term or long term, [See also: 28.2].

28.1.2 Short term

Dimensional stability that is controlled during the time of measurement and calibration on Earth prior to launch, i.e. little or no distortion due to moisture, thermal or other effects. This is closely linked to the as-made state of polymer composites.

28.1.3 Long term

Dimensional stability that is maintained over the operational life of the assembled structure. This includes integration, launch and operation in space.

Some of the typical applications for thermally-stable structural elements described are:

- Radio-frequency (RF) antennas and reflectors [See: 28.11, 28.12]:
  - MBB double-hinged rib reflector,
  - SELENIA hinged-tip reflector,
  - DORNIER daisy,
  - CASA 11/14 GHz reflector,
  - MBB polarisation sensitive reflector,
  - ERA dichroic sub-reflector,
  - CSELT/SELENIA dichroic sub-reflector,
  - CASA radiometer,
  - BAe shaped gridded reflectors,

  - DORNIER CFRP SAR antenna,
  - ARTEMIS LLM and SKDR reflectors,
  - Frequency selective surface (FSS) sub-reflector.
- Infrared and optical telescopes [See: 28.13]:
  - Far infrared and submillimetre space telescope (FIRST),
  - Soft X-ray telescope (SXT),
  - X-ray multi-mirror telescope (XMM).
- Optical structures [See: 28.14, 28.15]:
  - Mars observer camera (MOC),
  - High stability telescope structures (HSTS),
  - Radiometers.

A general overview of the main demands for dimensional stability under various environmental conditions is given. The effects of environment-related parameters on the design of dimensionally stable structures are also considered.

Dimensionally stable structures are those which need to retain their physical shape and dimensions under the cyclic thermal conditions experienced in orbit, typically -150°C to +100°C. Maintaining the dimensional tolerances is becoming more exacting because:

- Structures are becoming larger,
- Signal frequencies are increasing, e.g. applications now span RF, UV, X-ray and visual wavelength spectra,
- Optical devices demand very tight control on tolerances,
- Mission life is increasing, e.g. 30 years in orbit.

No single material can meet the demands of every structure and mission. The available material options are discussed with respect to possible applications.

The measurement and calibration of dimensionally stable structures usually need laser interferometer techniques, Ref. [28-2].

28.1.4 Basic properties of materials

All of the materials discussed have a structural, load-bearing function at some point during the mission. The desirable material characteristics are:

- High stiffness to weight ratio,
- Low, stable CTE,
- Inert to space environments.

Further application-specific needs can include:

- High thermal conductivity,

- Electrical nonconductance, e.g. signal transparent dielectrics, fulfilled by materials such as Kevlar™, Nomex™, quartz and glass fibre.

For the majority of applications, materials are chosen from commercially available carbon fibre-reinforced CFRP epoxies, particularly those with ultra-high modulus, UHM fibres. In recent years, the established position of UHM carbon fibre-reinforced epoxies has been challenged as the demand for the retention of dimensional tolerances has become more exacting. This has resulted in greater interest in:

- Low moisture absorbent thermosetting resins, e.g. cyanate esters,
- Improved PAN and pitch-based UHM carbon fibres,
- Thermoplastic matrices,
- Metal and ceramic matrix composites.
-

The majority of future projects are likely to use thermoset CFRP materials, because the technology base is widely established. This is particularly true of RF antennas and reflectors. Other low, stable CTE materials are likely to be considered for applications, such as optical devices.

28.2 Characteristics for dimensional stability

28.2.1 Characteristics

28.2.1.1 General

The characteristic attributes for dimensionally stable structures are generally defined by the:

- Operational tasks,
- Environmental conditions and applied loads during:
  - ascent
  - orbit

Orbit conditions have traditionally been in LEO or GEO. There are now increasing uses of composites for deep space missions to other planets, which have their own orbit environments.

It is possible to differentiate between short term and long term dimensional stability, [See: 28.1].

28.2.1.2 Short-term dimensional stability

The main charachteristics for structures or structural elements, which have to maintain their geometry during a measurement, are determined by the 'overall allowable distortion'.

For structures in orbit, it is most important to avoid thermally-induced distortion. These distortions can be tolerable within a certain range because of active controlling of the elements, but where close tolerances are needed one has to design with very low (near-zero) coefficients of thermal expansion. Furthermore, high-stiffness structural elements are also needed.

Examples of tolerable distortions are:

- Thermally-stable structures: approximately 1µm,
- RF antenna structures: a surface accuracy of 1mm RMS, typically.

28.2.1.3 Long-term dimensional stability

This imposes several important factors on the structure. A long period between manufacture and operational task in orbit gives the risk of perturbations from a variety of effects. The allowable tolerances for the distortion are not as high as for short-term stability. To minimise effects resulting from the environmental conditions during manufacture, the assembly and transportation of the dimensionally stable structure should be controlled to avoid additional mechanical loads, which can result in permanent distortions.

The main mechanical loads on the structure during launch result from:

- Static accelerations,
- Dynamic accelerations due to vibration,
- High acoustic levels.

To avoid excessive load increases resulting from resonant vibrations, it is usually stated that the first natural frequency of the structure does not fall below a given value. From this, the structural stiffness can then be calculated.

After launch, both the space environment and also the acting loads cause further perturbation to the dimensional stability of the structure. The environment comprises:

- High vacuum,
- High-intensity ultraviolet radiation,
- Wide temperature fluctuations.

[See: 28.7, 28.8, 28.9 and Chapter 20]

The environment can change the dimensions of the structure, as well as the basic material properties, or have secondary effects such as contamination of structural elements by outgassing of condensable matter, [See: 28.7 and Chapter 20].

28.2.1.4 Design considerations

Good design practice of a dimensionally stable structure takes into account all of the effects by defining items that consider:

- Allowable expansion or contraction due to temperature changes,
- Moisture,
- Definition of allowable outgassing, and
- Mechanical loads.

Mechanical loads occur in space during:

- Transfer from a lower to a geostationary orbit, or
- Translational and rotational movement as the structure is placed into final position for its planned tasks.

These mechanical loads are relatively low compared with the loads resulting from acceleration during ascent.

28.3 Design critical areas

28.3.1 General

The dimensional stability of certain space structures, e.g. antennas and telescopes, is a critical design consideration.

The ability to 'tailor' the coefficient of thermal expansion to be close to zero is an important reason for selecting CFRP.

It is necessary to evaluate the controlling parameters to ensure that the intended CTE is actually achieved.

The important causes of perturbation of dimensional stability are:

- Wide temperature variations, [See: Chapter 12 for temperature effects].
- Moisture absorption and desorption in thermosetting composites such as carbon/epoxy.

Evaluation of the effects of moisture CME is crucial because the range of expansion and contraction possible is much wider than that resulting from temperature changes, i.e. CTE. This leads to greater deformations than are generally expected.

[See: 28.8 and Chapter 13]

Other parameters influencing dimensional stability are factors associated with, Ref. [28-3], [28-4]:

- Materials and lay-up, including defects, e.g. delaminations, voids and fibre misalignment.
- Thickness and geometry effects.
- Microcracking, both thermally- and moisture-induced.
- Micro-yield strength.
- Micro-creep, including relaxation.
- Long term environmental effects, including radiation, atomic oxygen, thermal cycling, [See also: Chapter 20].

Materials selection is not the only route to achieving a dimensionally stable design. Active and passive thermal control play an important role in reducing the effects of temperature cycling. Smart actuator technologies, applied as shape compensation and micro-vibration suppression, can have a significant role in control of dimensional stability whilst in orbit, [See: 28.16].

28.3.2 CTE control by design

CTE control, particularly for optical devices, involves the implementation of good design practices, Ref. [28-5]. These include:

- Maintain material, as well as geometric, symmetry wherever possible, i.e. balanced, symmetric laminates and sandwich constructions, bond joints, material splices and egg-crating configurations.
- Maintain control of adhesive bondline thickness.
- Eliminate the through-thickness CTE effects of CFRP, whenever appropriate.
- Avoid the use of angle clips and bend radii with small radius-to-thickness ratios (for thermal considerations).

- Minimise CTE differences between adjacent materials.
- Isolate any sensitive parts structurally from unavoidable thermal deflections (in the critical direction).

28.4 Material options

28.4.1 General

A low CTE is a primary parameter for materials selection. In this respect, carbon fibres, and to a lesser extent aramids, are the most attractive reinforcing phases for composites. These are used in laminate form, either by themselves, or as the face sheets in sandwich panel constructions. The fibres are generally used with epoxy thermosetting resins, but other thermosets and thermoplastics can also be used; given commercial considerations. Carbon fibres can also be used to give a low CTE in metal and ceramic matrix composites.

Whilst a zero CTE value is desirable in many applications, it is not usually feasible to produce a practical laminate with this characteristic. It is more important to have consistent and stable CTE behaviour for theoretical design prediction and manufacturing.

28.4.2 Polymer composite constructions

The principal constituents from which composite constructions can be made are:

- Thermoset resins, e.g.:
  - Toughened epoxies, Ref. [28-6], [28-7], [28-8], [28-9], [28-10].
  - Cyanate esters, Ref. [28-11], [28-12], [28-13], [28-14], [28-15], [28-16].
- Thermoplastics: Ref. [28-17], [28-18].
  - PEEK (APC2).
  - PEI.
- UHM carbon fibres, e.g.:
  - Toray M55J/M60J.
  - Mitsubishi Dialed K135/K137/K139.
  - Nippon Granoc XN-50/XN-70.
- Aramid fibres, e.g.:
  - Kevlar 49.
  - Twaron HM.
- Sandwich core materials, e.g.:
  - Aluminium.
  - CFRP.
  - ARP.
  - Nomex.
  - possibly some foams

As the space industry uses low volumes of materials, the continued commercial availability of materials and process technologies is of keen concern.

A number of first generation CFRP epoxies, widely used in space, are no longer commercially available, e.g. GY-70 fibres and Amoco prepreg systems.

28.4.3 MMC and CMC materials

28.4.3.1 General

Metal and ceramic matrix composites have not yet been applied in significant quantities in space programmes. Originally these materials were developed for structural functions, often at high temperatures. Their use in dimensionally stable applications is now proposed as a means of avoiding the instabilities associated with polymer composites, Ref. [28-19]. MMC and CMC technology is characterised currently by:

- High cost.
- Limited manufacturing expertise.
- Difficulty in machining and fabrication.
- Complex microstructures and failure mechanisms.
- Lack of mechanical and physical property data.

The most likely future space applications are for optical devices, such as mirrors and mirror substrates. MMC materials have high thermal conductivities. Both materials are being considered for electrical and electronic substrates with selected CTE characteristics.

[See also: Chapter 86]

28.4.3.2 Metal matrix composites

For dimensionally stable applications, MMC materials have:

- carbon fibre reinforcement (essential), and
- either a magnesium or aluminium alloy matrix.

The use of a metal matrix avoids CTE changes caused by outgassing, moisture absorption and radiation damage. For carbon fibre MMC material, consistent, low CTE behaviour is achieved by enhancing the fibre/matrix interface strength and reducing residual stresses caused by high process temperatures. The anisotropy of the composite means that the CTE in the transverse and through-thickness directions are matrix dominated. There are also problems associated with matrix creep and microcracking at fibre/matrix interfaces, [See also: 84.6].

Aerospatiale (France) have expertise in carbon reinforced magnesium for use in dimensionally stable applications, Ref. [28-20], [28-21].

Where very low CTE is not essential, particulate reinforced aluminium alloys can be appropriate. The particles suppress the high CTE of aluminium whilst the composite retains good thermal conductivity.

28.4.3.3 Ceramic and inorganic matrix composites

This group of materials includes:

- Glass and glass-ceramic matrix composites (GMC and GCMC).
- Ceramic matrix composites, e.g. C/SiC.

The attraction of these stiff materials is the relatively low, positive CTE of the matrices, e.g. typically between 3×10^{-6} /°C and 10×10^{-6} /°C, coupled with their environmental stability under most space orbital conditions. Again, carbon fibres are essential for zero CTE material constructions, [See also: 84.7].

The current, realistic, options for commercial development are composites having glass (borosilicate), silicon carbide or carbon matrix; largely because of the limited availability of commercial materials.

28.5 Effect of composite lay-up

28.5.1 Composite anisotropy

Carbon fibres possess zero, or slightly negative, CTE in the axial (0°) direction. In the transverse (90°) direction, the CTE is positive and large. All matrices, of whatever type, have positive CTEs to some extent.

Composites exhibit CTE anisotropy because, in practical laminates, fibres cannot be placed in all orientations. The CTE can therefore be controlled in preferred directions, but not in others. The through-thickness CTE of cross-ply laminates is highly positive.

For antennas and reflectors, minimum gauge sections are normally necessary, often demanding the use of thin CFRP UD unidirectional or fabric prepregs. Laminates with 0°/90°, 4-ply UD are popular, with an overall thickness of 250μm, or equivalent thickness in fabric. For thicker laminates, ±45° and ±60° plies can be included to assist in producing quasi-isostatic constructions.

To control through-thickness CTE, the use of 3-D fibre preforms for MMC and CMC is feasible if the application demands it and can tolerate sufficient depth of section, e.g. mirrors.

28.5.2 UHM CFRP prepregs

28.5.2.1 General

For satellites, the need for high stiffness and low mass drives material selection towards ultra-high modulus, UHM, carbon fibre composites.

28.5.2.2 New generation prepregs

Commercial availability can be a problem because the space industry is a low-volume consumer. In 1993, an industry accepted and standard fibre, Celanese GY70, was withdrawn from the market. GY70 had modest strength and low strain to failure which was improved by the newer generation Japanese fibres. This promoted a search for replacements, coupled with a wish to improve on the first generation epoxy prepregs by identifying resins with lower moisture absorption and reduced susceptibility to microcracking.

In an ESTEC supported study (1993/94) on microcracking behaviour, Ref. [28-22], the participating European companies showed a preference for the certain prepreg materials, i.e.:

- Ciba Geigy/Brochier Vicotex M18/Toray M55J,
- Cyanamid Cycom 950-1/M55J,
- Fiberite 934/M55J, and
- YLA RS3 (cyanate ester)/XN-50A or M55J.

The exercise confirmed a slight preference amongst many to retain epoxy-based prepregs for their immediate requirements. However, the cyanate ester systems, including Fiberite 954-3, continue to be developed, Ref. [28-11]. European space hardware is already being constructed using cyanate ester composites. The study revealed that microcracking behaviour was very dependent on how individual contractors processed the respective prepregs. The effect of the processing techniques was so strong as to camouflage any individual material differences as to microcracking resistance.

The pitch-based UHM fibres, e.g. XN-50/XN-70 and K137/K139, have very high thermal conductivities, which can be considered essential for some applications. Toray M55J, a PAN-based fibre, has a much lower thermal conductivity but superior strength and wide commercial availability, making it suitable for structural configurations.

28.5.3 Fibre and ply misalignment

Where precise thermal expansion characteristics are needed, even a small amount of fibre misalignment can be crucial, Ref. [28-23]. Mathematical models are available to quantify the variations caused by misalignment in lay-up and processing, and compare these with predictions from the idealised design, Ref. [28-24].

28.5.4 Material selection

28.5.4.1 General

The criteria for the selection of appropriate material are generally the same as for other composite structures and can be classified as:

- Mechanical and physical properties of fibre/matrix systems,
- Susceptibility to environmental effects,
- Ease of processing and manufacturing.

The mechanical, physical and environmental resistance includes parameters directly affecting design for dimensional stability, these are:

- Stiffness.
- Operational temperature range.
- Coefficient of thermal expansion, CTE.
- Coefficient of moisture expansion, CME.
- Moisture absorption and desorption behaviour.
- Thermal conductivity.

- Radiation damage.
- Electromagnetic wave reflectance for antenna applications.

These properties are mainly related to the choice of appropriate fibres and resins as well as to the choice of an optimum lay-up. Sandwich structures have some special features which also are taken into account.

General guidelines on the selection of materials are given in Ref. [28-25].

28.5.4.2 Fibre type

The factors to consider are:

- High modulus fibres: To minimise dimensional changes caused by internally and externally applied stresses, a fibre with as high a modulus as possible are used. In general, the higher the modulus the higher the cost and the lower the strength. Consequently, depending on the overall requirements, it is not always practical to use the highest-modulus fibres.
- CTE: Thermal expansion and other properties tend to be less dependent on the fibre type than mechanical properties. The longitudinal CTE of the fibre is usually slightly negative and not linear with temperature. Even after prepregging, the expansion coefficient remains negative or only slightly positive, although the resin itself has a large positive expansion coefficient. Figure 28.05.1 shows this effect and depicts the variation of the CTE with fibre angle.
- Hybrid laminates: In the quest for a particular CTE behaviour from a structure, more than one grade (or type) of fibre can be used. HT and UHM carbon fibres have been used together in order to optimise the physical and mechanical properties, Ref. [28-26]. Combined carbon/aramid composites are also included as hybrids. The resulting laminate always has to have a balanced construction.

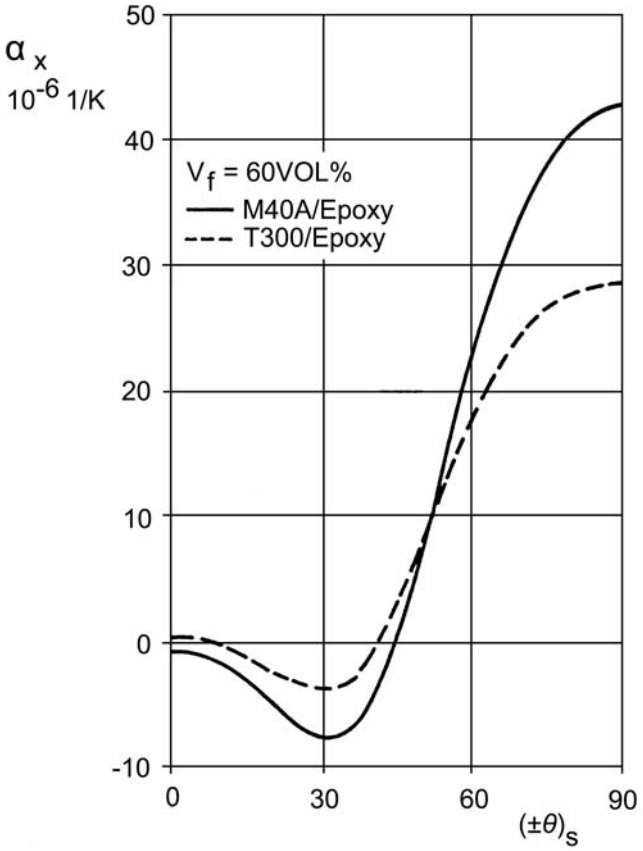

Figure 28.5-1 - Coefficient of thermal expansion α_x for $[\pm\theta]_s$ angle ply laminate

28.5.4.3 Type of matrix

The factors to consider include:

- Moisture resistance: To reduce the moisture absorption and hence the distortion caused by swelling, a moisture-insensitive resin is needed. The differences in coefficient of swelling are significant, as shown in Figure 28.05.2.
- Resin chemistry: The molecular structure of the resin influences the moisture absorption and hence the swelling capacity.

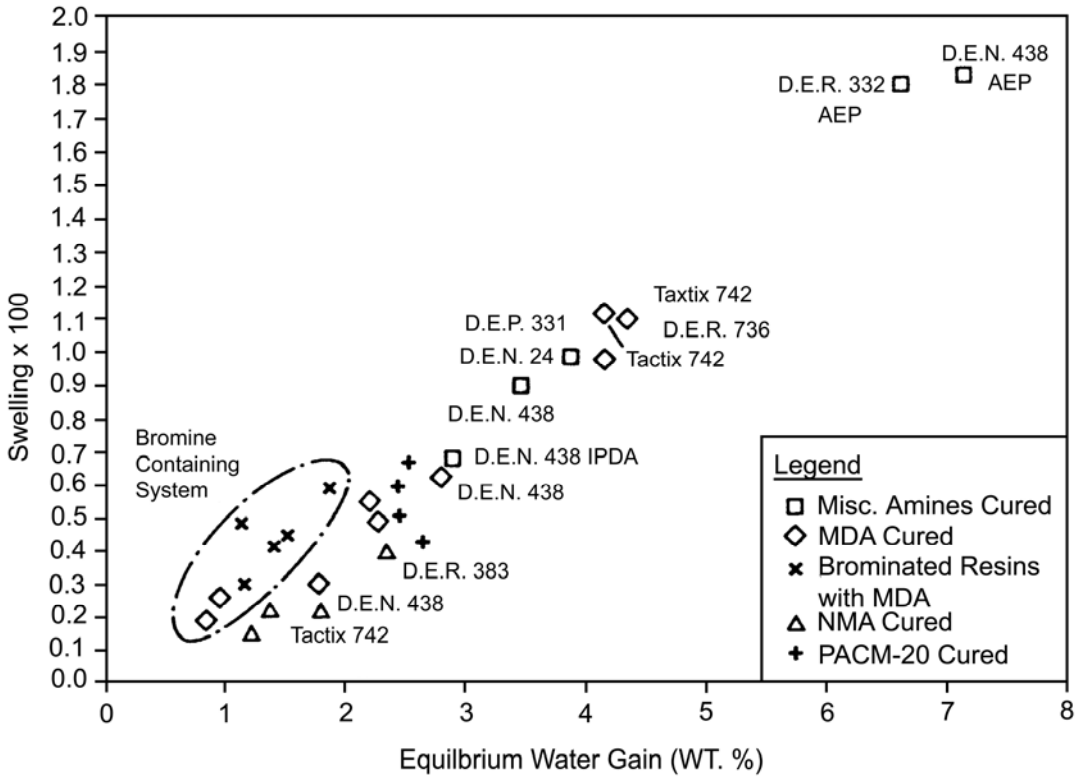

Figure 28.5-2 - Moisture: Typical swelling of several different cured resins

Figure 28.05.3 shows the differences in the moisture content of some different fibre/resin systems exposed to 100% RH at 66°C.

The thermoplastic composite absorbs only about 0.1% moisture; the related deformation is also small.

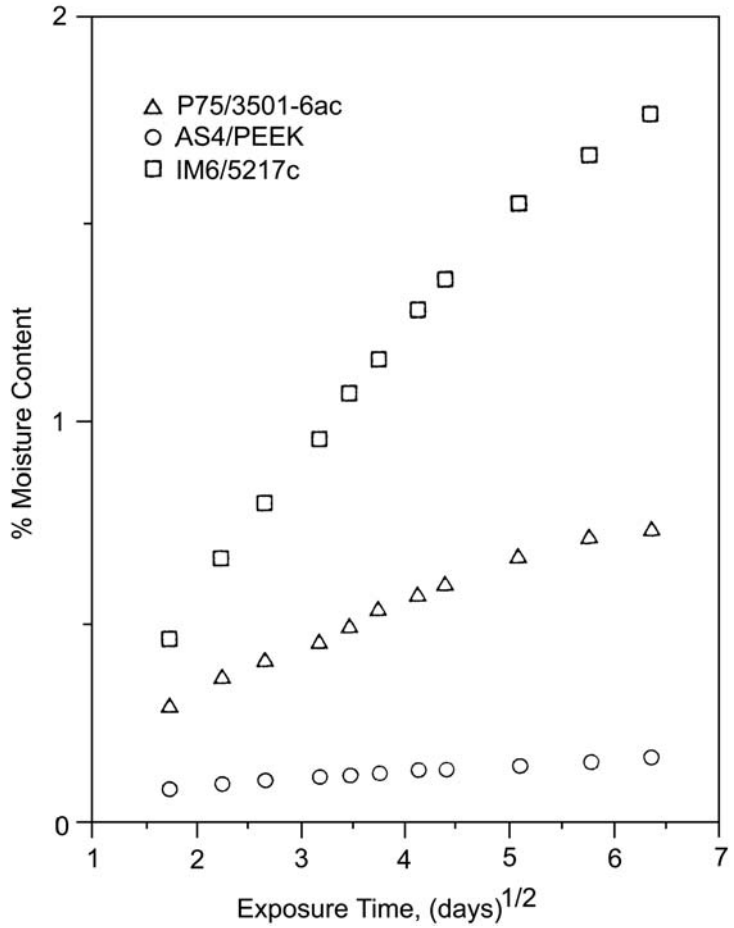

Figure 28.5-3 - Typical moisture absorption of different composites at 66°C and 100% RH

[See: Chapter 6 for further information on thermoplastic composites]

28.5.4.4 Lay up configuration

The main factor to consider is related to the composite lay-up. Owing to the highly anisotropic nature of unidirectional prepreg, a multi-directional lay-up can provide a coefficient of thermal expansion, CTE, close to zero.

The optimum lay up for a GY 70/Code 69 composite can be [± 45°]s. Figure 28.05.4 shows the calculated CTE for various lay-ups. The slope of the curve shows that any misalignment of the fibres has a strong influence on the designed CTE. It is therefore advisable to add some 0° plies to the lay-up, giving a dramatic drop in the slope. A lay-up containing 40% of 0° plies and 60% ±θ plies, with angle θ ranging from 60° to 80°, is suggested. This lay-up has good longitudinal and transverse properties because it is quasi isotropic [0°/± 60°].

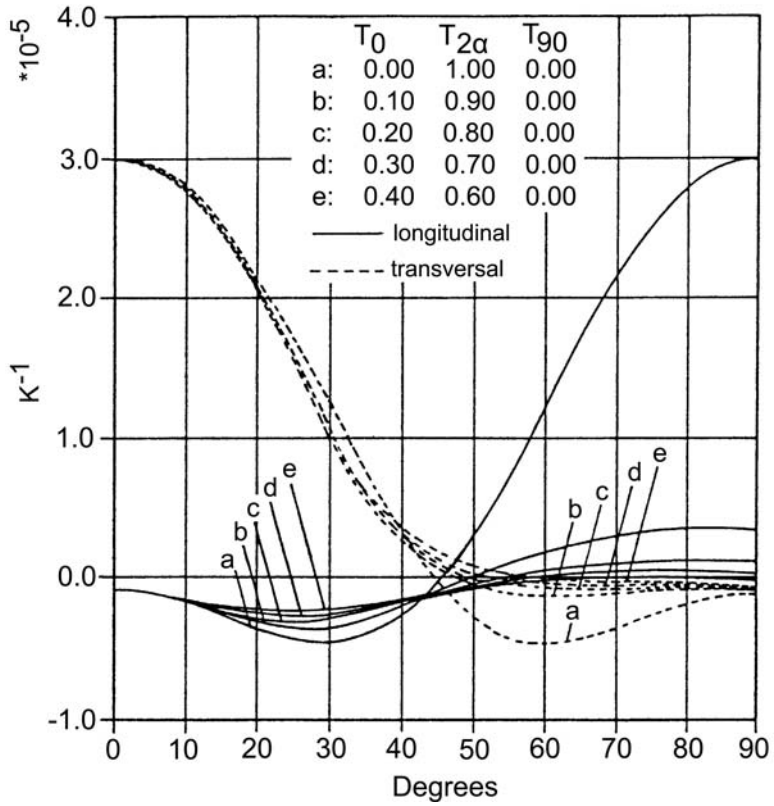

Figure 28.5-4 - Calculated Thermal expansion coefficient for various lay ups of carbon/epoxy: GY 70/Code 69

28.5.4.5 Residual stresses

The factors to consider include:

- Fibre and matrix CTE differences: Owing to the nature of the material, significant stresses exist within each ply. The residual stresses, which arise inside the structure, are mainly dependent upon the different CTEs of the materials. The effects of the differences in CTE between the fibres and matrix of a composite material cannot be compensated for, and lead to an internal tension state when the temperature decreases below the plasticisation point of the matrix during the curing cycle.
- With ageing or thermal cycling, the in-built stresses can cause cracking of the resin matrix. The cracks can propagate though the resin and, if two adjacent plies are closely oriented, the crack can also propagate from one to the other.

The overall consequence of residual stress is a CTE which changes with time and so influences the overall dimensional stability of the structure, [See: 28.9].

28.5.4.6 Balanced lay ups

The factors to consider are:

- Face skins: For CFRP face skins on sandwich structures, it is very important that any dimensional changes occurring in the face skins are equal, as any unbalanced stresses act at a significant distance from the neutral plane of the construction. It is therefore necessary to ensure that any changes due to thermal, hygroscopic or other influences do not result in out of plane displacements. The mechanical and thermal properties of the face skins can be equalised if the same lay-up configurations are used. If unbalanced face skins are used, it is essential that each face skin stacking sequence is a mirror image of the other. This ensures that any out of plane forces are balanced by the other skin. The use of wholly balanced face skins simplifies the fabrication of the sandwich structure as each skin remains flat during lay-up. However, balanced face skins demand an increased number of plies in the laminate. In some structures this can provide unnecessary strength and stiffness with an accompanying weight penalty.
- Laminates: The factors discussed for face skins are equally applicable to the design of simple laminated composites.

28.6 Sandwich structures

28.6.1 General

Sandwich constructions offer the ability to produce very rigid structures with minimal mass, [See: Chapter 26].

Very thin face sheets are feasible, typically of the 0°/90° construction, [See also: 28.5 – Balanced lay-ups].

The choice of available core materials has increased over the years. Sandwich constructions can be co-cured or bonded using an adhesive film.

28.6.2 Core material

28.6.2.1 General

There are a number of core materials available for sandwich structures, but for space applications honeycomb is generally used. The commonly used honeycomb materials are:

- aluminium alloy,
- carbon fibre-reinforced plastic (CFRP),
- aramid reinforced-plastic (ARP).

Glass reinforced-plastic and polymer foams are also used sometimes.

[See also: 26.4 - Sandwich core materials]

28.6.2.2 Aluminium honeycomb

This is the most popular type, largely because it is readily available in many sizes (cell shape, cell size and thickness) and offers good shear and compressive properties. Aluminium has good thermal conductivity, which assists in equalising temperature differences between the sandwich faces.

One significant disadvantage with aluminium is its high, positive CTE, which determines the expansion of a sandwich panel in the through-thickness direction.

28.6.2.3 CFRP honeycomb

This is more frequently used when the through-thickness CTE of the sandwich panel is low and controlled. However, it is costly and available in few standard forms; often it is specifically produced. It is less robust than aluminium and difficult to machine.

28.6.2.4 ARP honeycomb

Aramid fibre composite cores are occasionally used were electrical insulation demands (signal transparency) preclude the use of aluminium or CFRP. Kevlar™ has a low CTE, whereas the CTEs of the cheaper Nomex™ versions are high.

The compressive and shear strength of Kevlar honeycomb is poor. It is prone to moisture absorption. It is difficult to machine, has limited availability and is also costly.

28.6.3 Core thermal conductivity

This property needs thorough evaluation during the design of a sandwich structure. If the structure is likely to be heated on one face only, e.g. an antenna in sunlight, good core conductivity helps to maintain both faces at similar temperatures, hence reducing thermal gradients.

Aluminium has good thermal conductivity, as do CFRP honeycombs made from UHM pitch fibres.

28.6.4 Sandwich constructions

28.6.4.1 Discontinuities

Within any sandwich structure, there are many discontinuities arising from the necessity for the structure to perform its function. These include:

- Holes,
- Inserts,
- Joints,
- Edge Members.

Tests have shown that these do not affect the dimensional stability where there is no external load.

- Edge members: Other than the purely cosmetic ones, edge members are tailored to the sandwich panel to which they are attached. Wherever possible, the CTE is matched and the edge member provided with some shear strength. This can be achieved by the use of ± 45° plies.
- Doublers and stiffeners: When added in positions of high stress, doublers and stiffeners can unbalance a lay-up configuration unless a similar doubler is placed on the other face. If the doublers are small, this is not always necessary, except where extreme dimensional stability is needed.

[See also: Chapter 26]

28.7 Space environments

28.7.1 General

The missions for dimensionally stable structures vary depending on whether they orbit the Earth or are interplanetary (deep space). There are several common Earth orbits, each with its own environment, [See also: Chapter 20].

The main environmental factors can be summarised as:

- Low Earth orbit (LEO), [See also: 20.3]:
  - Altitude ~500 km, i.e. Space shuttle and space station regime,
  - Thermal cycling (acute),
  - Atomic oxygen (ATOX) erosion,
  - Vacuum ultra-violet (VUV),
  - Micrometeoroid and debris impact.
- Geostationary Earth orbit (GEO), [See also: 20.4]:
  - Altitude ~36,000 km,
  - High vacuum,
  - Temperature (wide spectrum),
  - Thermal cycles (reduced number compared with LEO),
  - Radiation degradation possible.

The main concerns with regard to composites used in dimensionally stable structures are:

- Outgassing,
- Thermal Cycling,
- Radiation Damage.

28.7.2 Outgassing

28.7.2.1 General

Materials used in European spacecraft conform to ECSS-Q-ST-70-02 for minimum outgassing requirements with respect to total mass loss, TML, and collectable condensable volatile material, CVCM. The materials mentioned within this chapter achieve this basic requirement, [See: 28.12].

For highly dimensionally stable structures constructed from polymer composites, outgassing is limited beyond that stated in the requirement.

Metal and ceramic-based composites do not contain constituents which outgas.

28.7.2.2 Moisture absorption

The moisture content of epoxy CFRP materials is fairly low; from about 0.5% to 1% fully saturated. Satellites are manufactured and stored under controlled humidity conditions to ensure that the moisture absorption is as low as possible. However, problems can arise when antennas and reflectors are calibrated in these stored conditions prior to being launched. In orbit, the absorbed moisture, although low, is outgassed and small changes in the dimensions of the structure occur.

Whereas in the past such dimensional changes were often ignored, it is unlikely to be the case in future projects. There is therefore an increased motivation to specify CFRP and ARP materials with a matrix phase which is less prone to moisture absorption.

28.7.2.3 Coefficient of moisture expansion (CME)

The CME is increasingly considered to be an important parameter in defining the acceptance of a composite material. Newer generation epoxies and cyanate esters offer lower CME values.

28.7.3 Thermal cycling

28.7.3.1 Microcracking

Severe and repetitive thermal cycling is an important mechanism in the microscopic cracking of polymer composites. Microcracking results when residual stresses in the matrix exceed the strength of the matrix or matrix/fibre interface. It occurs mainly during the cooling part of the cure cycle and is caused by the differential contraction between the high positive CTE of the matrix and the low, negative axial fibre CTE.

28.7.3.2 Matrix selection factors

The choice of matrix is strongly influenced by the maximum anticipated operating temperature. This defines the minimum acceptable matrix glass transition temperature, Tg and, in turn, the cure temperature. The temperature at which residual stresses are retained in the matrix is directly linked to the cured resin Tg.

The residual stresses continue to increase with decreasing temperature, so the minimum temperature during thermal cycling gives the highest microcracking stress. Therefore high cure temperatures and extreme low temperatures in service represent the conditions most conducive to microcracking.

It has been established that the level of microcracking can be reduced by careful selection of:

- Cure temperature, where 130°C curing is preferable to 170°C.
- Matrix: Use toughened, high strain matrices, e.g. cyanate esters.
- Lay-up: Where possible, ±30° and ±60° are preferable to acute angle fibre crossovers, e.g. 0°/90°, ±45°.

It is not always possible to optimise these factors for microcracking performance because of other design criteria.

28.7.3.3 Fibre/matrix interface

The fibre/matrix interface has an important role in determining the susceptibility of a composite to microcracking.

Some fibre/matrix combinations have better interfacial adhesion than others and this translates itself into higher transverse (90°) ply strengths.

28.7.3.4 Microcrack location and density

Microcracking is progressive. The location and extent of cracks determines their seriousness with respect to the composite properties:

- Initially, the majority are intralaminar, i.e. within a single UD ply.
- When the crack density (population) becomes high or when cracks join up, microcracking is considered to be more serious.
- Interlaminar cracking (between plies) and cracks which traverse two plies are more serious.

A commonly used criterion for comparing materials is the number of 'cracks per unit length' of conditioned composites, i.e. post thermal cycling. Materials with between 0 cracks/cm and 5 cracks/cm are considered to be more desirable than those with higher crack populations, e.g. from 15 cracks/cm to more than 20 cracks/cm.

28.7.3.5 Pre-calibration thermal cycling

For some applications, the entire structure is thermally cycled prior to launch to deliberately induce microcracking prior to calibration. This is based on the assumption that the majority of microcracks occur within the first few (up to 10) thermal cycles encountered by a structure, and that after this the microcrack population stabilises.

Whilst valid for some applications, structures experiencing 30,000, or even 150,000+ cycles, do not always reach an equilibrium condition. For very highly dimensionally stable structures, a non-equilibrium state can be very significant. Microcracking behaviour is very dependent on laminate lay-up and thickness.

28.7.4 Radiation damage

28.7.4.1 General

Orbiting composite structures experience radiation dosages from a variety of sources, [See: 20.11].

28.7.4.2 Embrittlement

Unreinforced polymers are modified by radiation, resulting in embrittlement after prolonged exposure. Composites experience some immediate sub-surface degradation of the matrix phase. However, the surface reinforcing fibres screen the majority of the matrix from the radiation, inhibiting bulk degradation of the composite. Consequently, modifications to the overall mechanical properties of CFRP are very small (~5%), and often difficult to discern.

28.7.4.3 Property changes

CTE measurements also show little change due to radiation. Some evidence suggests that very high dosages (>1000 Mrad) of penetrative radiation can significantly change mechanical properties and CTE. This has not been extensively studied, but can become of significance when the duration of a mission approaches 30 years.

Metal and ceramic-based composites do not have constituents that are significantly degraded by radiation.

28.7.5 Low Earth orbit

28.7.5.1 Atomic oxygen (ATOX)

Examination of composite specimens flown on the LDEF 'long duration exposure facility' from 1985 to 1990 revealed that CFRP erodes significantly under the ATOX flux in LEO, [See also: 20.8 for LDEF; 20.13 for ATOX].

It is therefore accepted that CFRP needs protective coatings on those surfaces experiencing the highest flux. The erosion and removal of surface material has a direct effect on both mechanical properties and CTE.

28.7.5.2 Debris

The accumulated damage from debris and micrometeoroid impacts cannot be underestimated. Selective protective shielding against impacts is usually needed for certain areas of a structure.

Metal and ceramic-based composites have matrix phases that are more capable of resisting long-term LEO exposure.

28.7.6 Surface coatings

The application of coatings to polymer composites is undertaken only as a last resort because of the difficulties in obtaining reliable adhesion. Some circumstances which can dictate the need to apply protective, or surface modifying, coatings are :

- Inhibit moisture absorption, e.g. metallic barriers.
- Inhibit ATOX erosion, e.g. silicon-containing polymer coatings.
- Provide thermal control, e.g. paints.
- Provide a reflective coating, e.g. sputtered metals.
- Provide continuity of electrical conductivity.

Such coatings can modify the CTE behaviour of composites to some extent.

[See also: 20.14 for siloxanes and silicon-based polymers; 20.15 for protective coatings]

28.8 Effect of moisture

28.8.1 General

It is known that during storage or service, polymer composite materials, in particular carbon/epoxy, absorb moisture directly from the atmosphere. This moisture begins to be released once the material is exposed to the space environment.

For complete moisture desorption, several weeks are necessary during which the moisture can change the geometry of manufactured composite hardware by acting as a:

- swelling agent, and
- plasticiser.

An example of a typical moisture exposure schedule is given in Table 28.08.1, Ref. [28-27].

The coefficient of moisture expansion (CME) is an important material selection parameter for composites used in dimensionally stable structures.

[See also: Chapter 13 and 20.7 for moisture effects on composites]

Table 28.8-1 - Typical moisture exposure schedule

Activity	Time (days)	Relative Humidity	Comments
Structure fabrication	110	50	-
Bakeout	5	0	Vacuum bake at 75°C
Telescope assembly and test	340	12 -30	12 hours exposure each level
Vibration tests	24	50-5	Exposed 12 hours, bagged and purged 12 hours
Thermal vacuum test	14	0	-
Preparation for shipment	10	50	Exposed
Shipping containers	30	5	-
Spacecraft integration	120	60	-
Pre-launch	30	50 20	16 hours 8 hours
Orbit	730	0	2 years in orbit

28.8.2 Swelling agent

A given concentration of evenly distributed, absorbed moisture causes the volume of the epoxy matrix to expand in a manner completely analogous to that caused by an increase in temperature. Although moisture-induced swelling is a reversible phenomenon, debonding caused by tensile interface stresses can contribute to a permanent dimensional change and alteration of thermo mechanical properties.

Furthermore, the moisture desorption in orbit results in shrinkage which should be taken into account when designing for dimensional stability. Figure 28.8.1 illustrates the shrinkage due to moisture desorption.

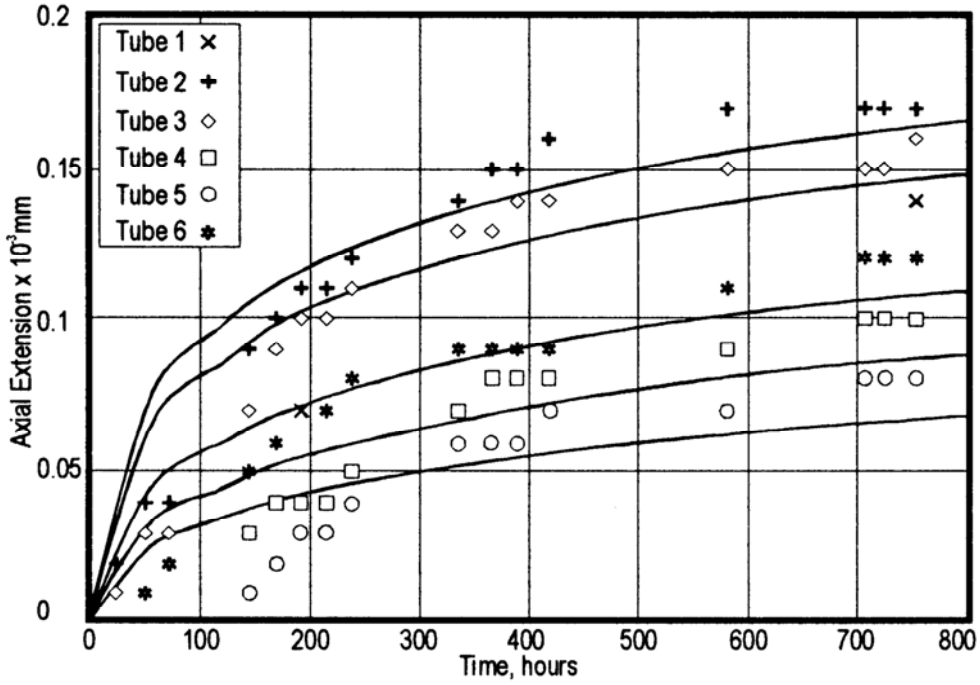

Figure 28.8-1 - Moisture: Shrinkage during desorption

28.8.3 Plasticiser

Moisture acts as a plasticiser in the epoxy resin, which lowers the glass transition temperature, Tg. This produces a change in the matrix dependent mechanical properties of the composite, particularly at elevated temperature, including:

- CTE
- Interlaminar shear strength.

To minimise the problem, because it is not possible to fully avoid moisture-induced distortion, the basic approaches are:

- Use of impermeable matrix materials, e.g. thermoplastics, [See: Figure 28.5.2 and Figure 28.5.3].
- Use of isolating barriers, although these can cause distortion because of their own large CTE.
- Store the structure in a controlled atmosphere, which is often difficult to achieve throughout the time preceding launch.
-

[See also: Chapter 13 for further information about moisture effects on composites and the analysis of related effects]

28.8.4 Coefficient of moisture expansion (CME)

Comparison of composite CME data is often difficult because materials are rarely tested under the same conditions or have the same fibre.

The data provided in Table 28.8.2 compare a new generation, low absorbency cyanate ester resin with that of a well established older generation epoxy.

Table 28.8-2 - Basic comparison of moisture absorbing properties of a cyanate ester and epoxy matrix resin

Resin	Moisture Diffusivity K^H (m²/s)		Maximum Moisture Content *Cm* (%)		Coefficient of Moisture Expansion β (m/m)	
	RT	93°C	RT	93°C	RT	93°C
RS-3†	$8.94x10^{-13}$	$1.34x10^{-11}$	1.2	1.5	0.149	0.156
F934‡	$8.31x10^{-14}$	$2.69x10^{-12}$	6	7	0.261	0.267

Key: † : Cyanate ester ‡ : Epoxy

28.9 Effect of thermal cycling

28.9.1 Material properties

28.9.1.1 General

For composite structures, it is necessary to understand how temperature affects the basic properties of the materials.

For orbiting space structures, the exposure to cold space, coupled with radiant solar heating, can lead to a wide range of operating temperatures which affect the strength and stiffness of the materials.

[See also: Chapter 4 for more detailed information]

28.9.1.2 Coefficient of thermal expansion

The elevated cure temperature of carbon/epoxy composites and the ambient cold of space mean that the coefficient of thermal expansion is also important, especially for the large components.

Distortion arising from variations in CTE can strongly influence the dimensional stability. Microcracking is a primary cause of CTE variations, although some other environmental effects are also important, [See also: 20.9].

Tests show that microcracking can result from thermal cycling. In general, the CTE tends to decrease with increasing numbers of thermal cycles and the majority of this decrease is concentrated in the first few cycles. The cause of this phenomenon is linked to the consequent increase of microcracks, which weaken the bonding between fibre and matrix, as shown in Figure 28.9.1, Ref. [28-27].

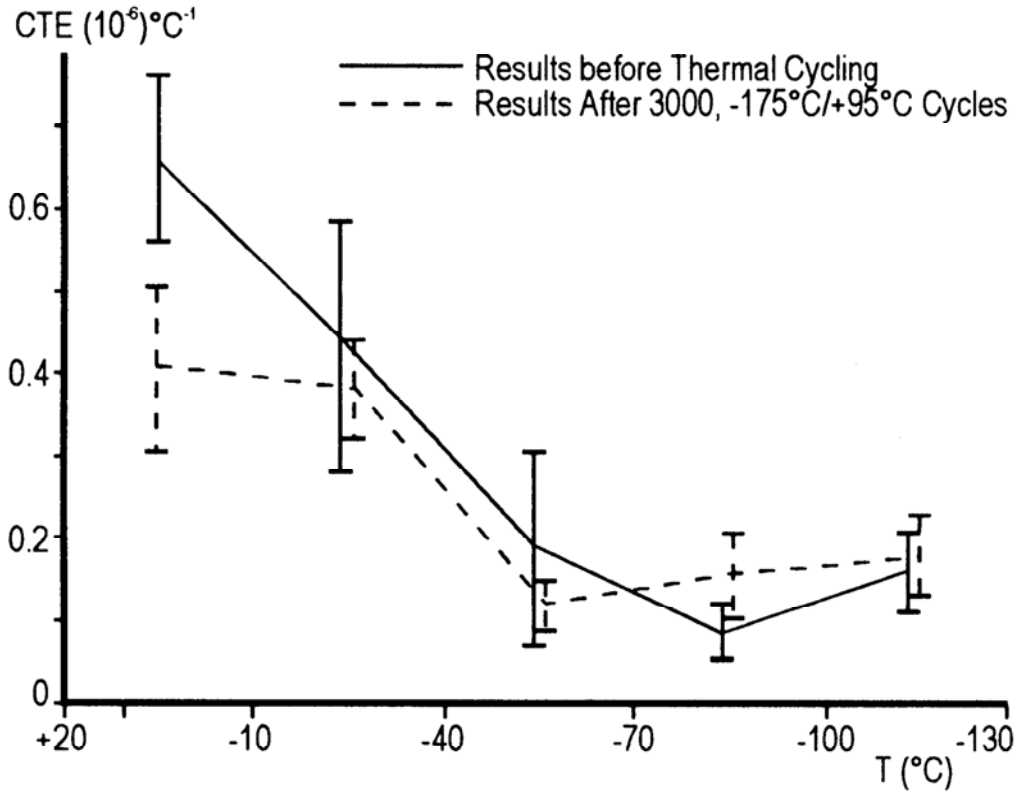

Figure 28.9-1 - Influence of thermal cycling on the CTE

28.10 Joints

28.10.1 General

The chosen joining technique for a dimensionally stable structure is particularly important, because the joint can be a significant source of expansion.

28.10.2 Adhesive bonding

Adhesive bonding has an important role in the assembly of satellite and spacecraft structures, especially where composites are used, [See: Chapter 21].

Adhesively-bonded metallic end fittings are attractive for connecting tubular structures, because joints can be both very strong and mass efficient. However, metals, such as aluminium and titanium alloys, have high CTE values. Where this cannot be tolerated, a connection can be made using, for example, CFRP clam-shell designs, Ref. [28-28].

For structures such as telescopes, all of the components are often made from a low CTE material, usually CFRP.

The selection of an acceptable adhesive is driven by the:

- mechanical performance specified for the joint, and
- compatibility with space environments.

[See also: ECSS-E-HB-32-21 - Adhesive bonding handbook]

28.10.3 Fasteners and inserts

Where adhesive bonding is inappropriate, the mechanical systems are used are:

- threaded fasteners, [See: Chapter 22].
- insert systems, [See: Chapter 23].

There is often an incentive to use metals having a low CTE for connections within dimensionally stable structures. Consequently, titanium and Invar can be preferred to aluminium, despite the mass penalty, [See: ECSS-Q-ST-70-46 for general requirements for the procurement of threaded fasteners].

[See also: ECSS-E-HB-32-22 - Insert design handbook; ECSS-E-HB-32-23 - Guidelines on the design of bolted joints]

28.11 RF antenna structures

28.11.1 Basic Characteristics

The characteristics demanded of antenna and reflector structures include:

- Low mass,
- Storable for launch,
- Resistant to launch loadings and the acoustic environment,
- Deployable in space to their full dimensions, and
- Resistant to the orbit environment for the intended operational life.
-

[See also: 28.12 for examples of antenna structures]

28.11.2 Performance

The performance of antenna reflectors is dependent upon their dimensional stability. Small dimensional variations of the reflecting surface cause an important loss in efficiency. These variations become a critical design parameter for large, high-stability antennas manufactured from high-modulus carbon/epoxy composites, as shown in Figure 28.11.1, Ref. [28-3].

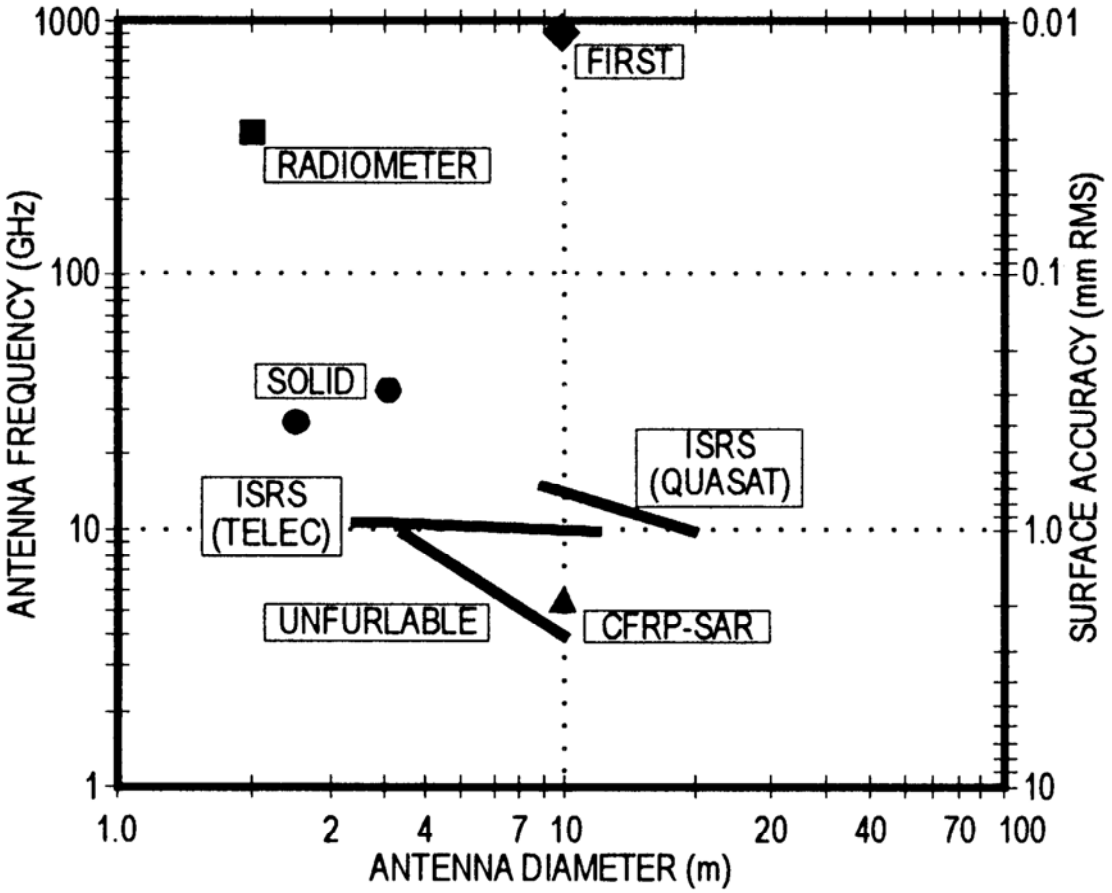

Figure 28.11-1 - Antenna surface precision and usable frequency versus size

The factors that can influence the dimensional stability, hence the performance, of antenna structures are:

- Space environment, [See: 28.7] including the length of exposure, [See: 28.2].
- Coefficient of thermal expansion, [See: 28.3].
- Material options, [See: 28.4], including the effect of composite lay-up, [See: 28.5] and sandwich panel components, [See: 28.6].
- Effects of moisture, [See: 28.8].
- Effects of thermal cycling, [See: 28.9].
- Joints, [See: 28.10].

[See also: 28.12 for a survey of developed RF antenna structures with a description of their main characteristics and special features]

28.11.3 Selection of type of construction

28.11.3.1 General

In antenna design, composites for lightweight constructions can be differentiated as:

- Sandwich structure,
- Monolithic structure,
- Framework construction.

The type of construction chosen depends upon the:

- Antenna system used: rigid, inflatable, unfurlable,
- Dimensions: space required, accuracy requirements,
- Loads: static and dynamic,
- Strength criteria,
- Natural frequency requirements,
- Frequency range.
- Ventilation,

28.11.3.2 Sandwich structures

The advantages and limitations of sandwich structures are summarised in Table 28.11.1.

Table 28.11-1 - Antenna structures: Advantages and limitations of sandwich structures

Advantages	Disadvantages
High accuracy requirements can be met.	If the part to be constructed is very small, these advantages cannot be fully realised, since the calculated required thickness of the skin cannot be manufactured.
High natural frequencies are possible even with large-scale antenna reflectors.	Load introductions for axial and transverse loads need to be constructed carefully.
Support of the skins by cores avoids local instability.	Expensive manufacturing (several bonding and cure cycles are necessary).
Shells with low weight per unit area can be realised.	Ventilation needs to be taken into account. (Skin as open net or perforated honeycomb).
Can be used for foldable antenna structures.	
Suited for 'large-scale reflectors' with a limited number of load introductions that are not too near to each other.	

28.11.3.3 Monolithic structures

Monolithic structures are suitable for highly-loaded and compact parts. The walls of the structure are of such a thickness that a separate support system is not necessary.

28.11.3.4 Framework construction

Framework constructions are suitable for open structures where high stiffness and light weight are needed over a large volume.

Special attention needs to be paid to the cross-links and load introduction areas of the framework. The construction criteria are:

- Thermal properties and expansion compatibility if the load introduction mountings are made of metal.
- Assembly and means of adjustment.

The framework members are frequently manufactured as tubes. Filament winding is an ideal process for the manufacturing of such items, [See also: 29.13 for filament-wound optical structures; 38.5 for manufacturing by filament winding].

Although the members are almost always subjected to uniaxial loads, it is advisable that they are not made using unidirectional laminates only. A small proportion of laminates with 90° and ±45° fibre orientation is necessary to ensure handling stability and to avoid failures due to local instability.

For the same reasons, it can be useful to design the walls of large-diameter tubes as sandwich structures, [See: Chapter 26].

[See also: Chapter 25 - Struts]

28.12 RF Antenna structures: Examples

28.12.1 General

The examples of developed antennas provide an overview as to the:

- Different types of antenna structure used,
- Configurations,
- Applications, and
- Precision achieved.

Where possible, approximate dates for the design to launch period are given to assist in differentiating the ages of the technologies.

28.12.2 Deployable reflectors

28.12.2.1 MBB double-hinged rib reflector

Also known as MBB unfurlable mesh antenna reflector (UMA), Figure 28.12.1 shows the stowed and deployed configuration, Ref. [28-29].

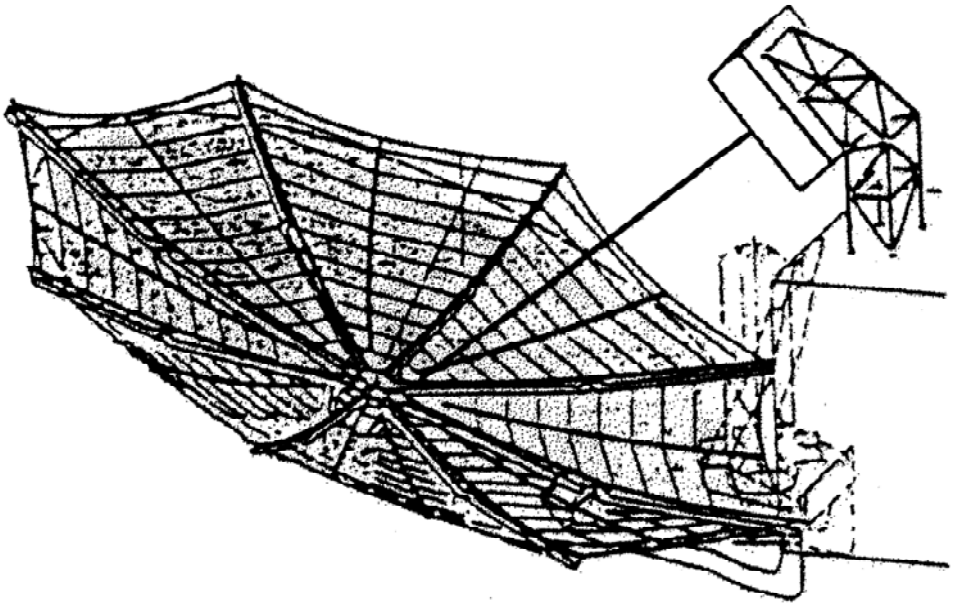

Figure 28.12-1 - Antenna examples: MBB double-hinged rib reflector

The reflector was developed in the late 1980s by MBB to meet the Canadian M-SAT requirements, Ref. [28-30]. It was designed for high stiffness with eigenfrequencies of 4 Hz deployed and >35 Hz stowed for launch. The aperture diameter was 5 m, with a focal length of 3.125 m.

Characteristics include:

- Construction: Described as a 'double-hinged umbrella':
  - Reflector surface: knitted gold-plated Mo-wire mesh tensioned by 8 foldable CFRP main ribs and 8 intermediate ribs.
  - Main ribs: Hinged to a central hub made of CFRP sandwich, which carried a deployment and retraction actuator in its centre.
  - Deployed position: The straight main ribs were locked and inner and outer ribs adjusted to each other at certain angles. Mesh adjustment to the parabolic surface was then achieved by stand-offs along the rib parts.
  - Parabolic contour between the main ribs was obtained by intermediate ribs (CFRP ribbons); tensioned during deployment by means of cables leading to the main ribs.
- Application: 3.6 m to 8 m diameter and 12 GHz to 1.6 GHz frequency.
- Precision: From 0.2 mm to 0.7 mm RMS.
- Reflector density: 2 kg/m2.

28.12.2.2 Contraves inflatable space rigidised reflector

Figure 28.12.2 shows the deployment scheme, Ref. [29-29]. The characteristics include:

- Concept: Inflatable, space rigidised.
- Construction: Thermally-cured resin with Kevlar fibre material and metallised Kapton.
- Application: From 5 m to 20 m diameter, and from 20 GHz to 800 MHz frequency.
- Precision: 1 mm RMS.
- Reflector density: 0.4 kg/m2.

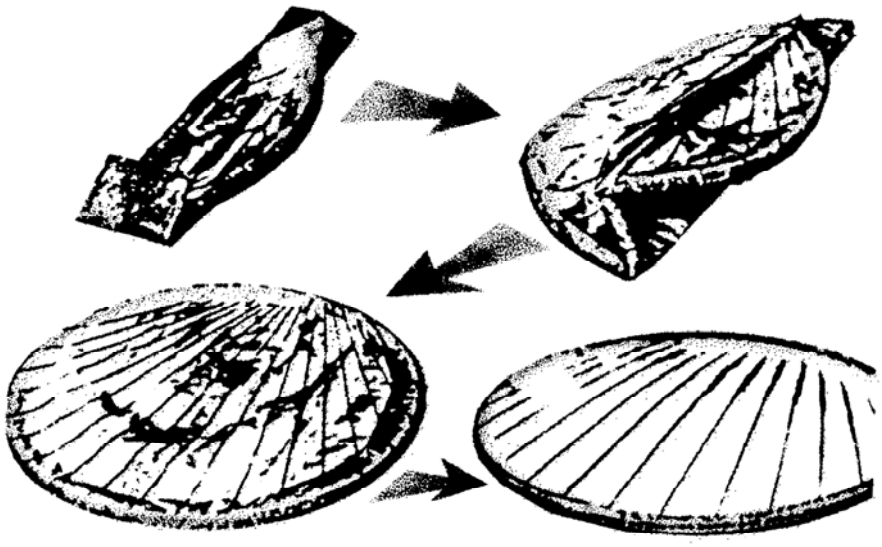

Figure 28.12-2 - Antenna examples: Deployment scheme for CONTRAVES inflatable space rigidised reflector

28.12.3 Solid deployable reflectors

28.12.3.1 SELENIA hinged tip reflector (Ka-band 20/30 GHz)

This ESA-funded ASTP development construction was completed in 1988 and the deployed configuration is shown in Figure 28.12.3, Ref. [28-29]. The characteristics are:

- Concept: Three-piece reflector, including two hinged tips, to fit inside Ariane 4 shroud, Ref. [28-31].
- Construction: Sandwich rib stiffened structure with UHM CFRP skin and aluminium honeycomb core of 6.35 mm.
- Materials: 4 ply (0°/90°/90°/0°) 934/P75S face skins co-cured with FM-300M film adhesive. Stiffeners of sandwich construction with 6-layer (0, ±60)s skins. All used 60μm prepreg.
- Application: 3.7 m aperture diameter at 20 GHz from a 4.0 m diameter reflector.
- Precision: 0.3 mm RMS.
- Operating temperature range: from -180°C to +100°C.
- Reflector density: 3.4 kg/m2, with a total mass of reflector 42 kg.

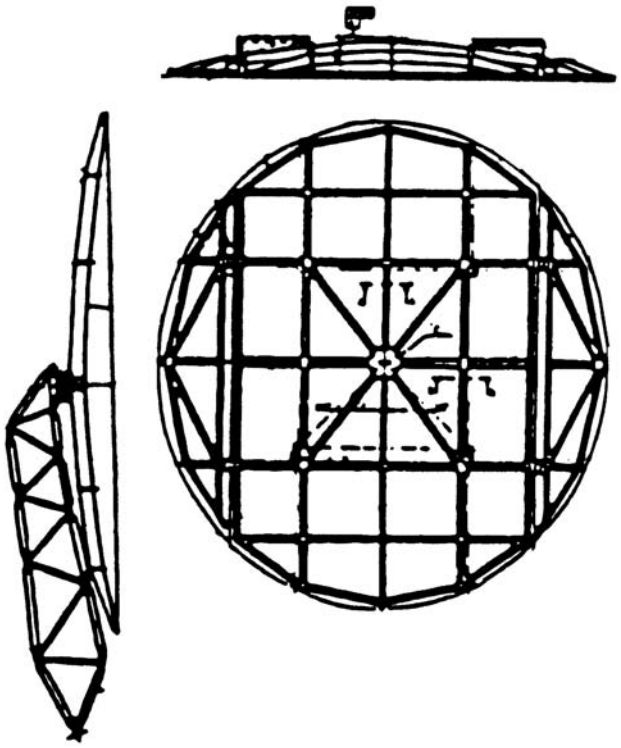

Figure 28.12-3 - Antenna examples: SELENIA 20/30 GHz reflector

28.12.3.2 Dornier DAISY

DAISY stands for deployable antenna integral system. The reflector is shown in Figure 28.12.4, Ref. [28-29]. The characteristics include:

- Concept: Deployable, rigid-panel reflector.
- Construction: Sandwich panels with CFRP skin and 40 mm Kevlar core.
- Application: 8 m diameter at 3000 GHz.
- Precision: 8μm RMS.
- Reflector density: 6 kg/m^2.

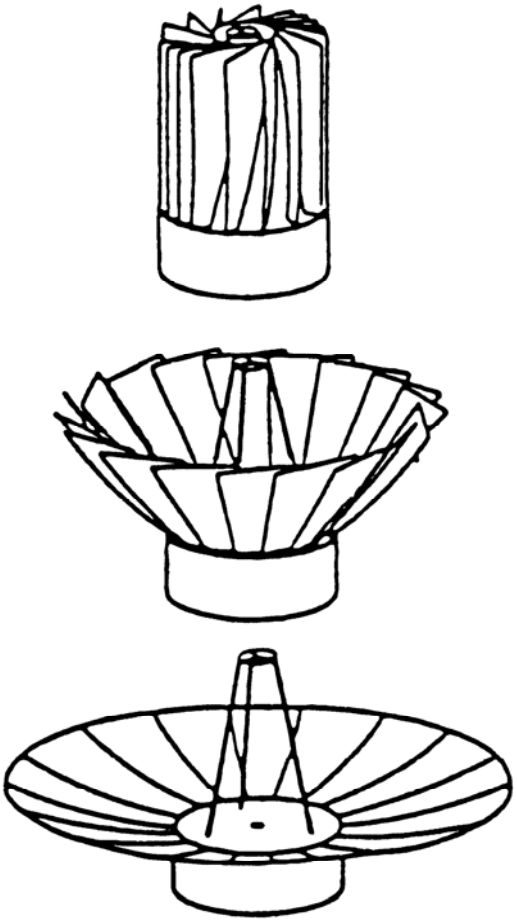

Figure 28.12-4 - Antenna examples: Dornier DAISY

28.12.4 Solid reflectors

28.12.4.1 CASA 11/14 GHz reflector

The mathematical model of the reflector is shown in Figure 28.12.5, Ref. [28-29]. The characteristics include:

- Concept: Biggest one-piece reflector within Ariane 4 shroud.
- Construction: Sandwich rib-stiffened structure with CFRP skin and 8 mm aluminium honeycomb.
- Application: 3.1 m x 2.3 m dimension and 11/14 GHz frequency.
- Precision: 0.4 mm RMS.
- Reflector density: 2.8 kg/m2.

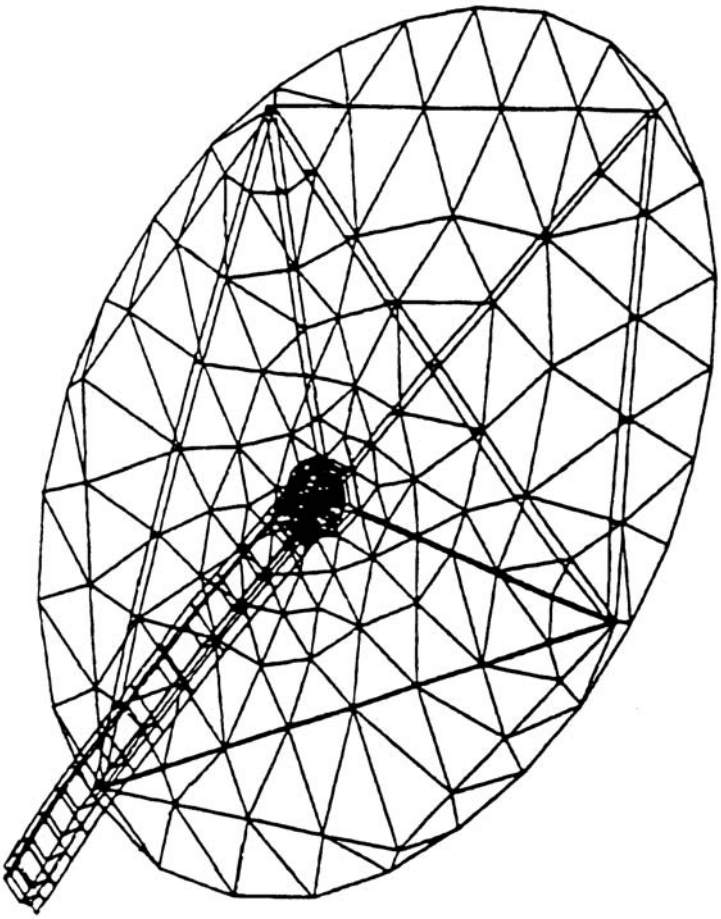

Figure 28.12-5 - Antenna examples: Mathematical model of CASA 11/14 GHz reflector

28.12.4.2 MBB polarisation sensitive reflector

The characteristics of the reflector, shown in Figure 28.12.6 Ref. [28-29], are.

- Concept: Two reflectors tilted and off-axis for horizontal and vertical polarisation.
- Construction: Conductive wire bound onto a Kevlar skin and 6.2mm Nomex core.
- Application: From 1.1 m to 1.8 m diameter and 4/6 GHz.
- Precision: ±2 mm displacement.
- Reflector density: 3.7 kg/m^2.

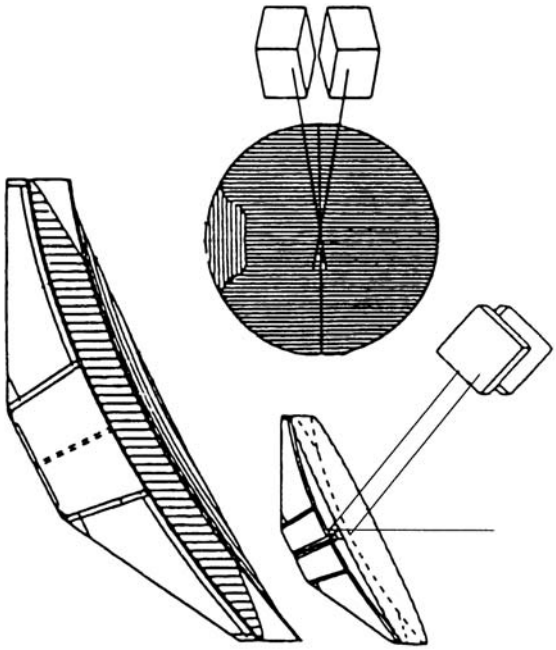

Figure 28.12-6 - Antenna examples: MBB polarisation sensitive reflector

28.12.4.3 ERA dichroic sub-reflector

The sub-reflector is shown in Figure 28.12.7, Ref. [28-29].

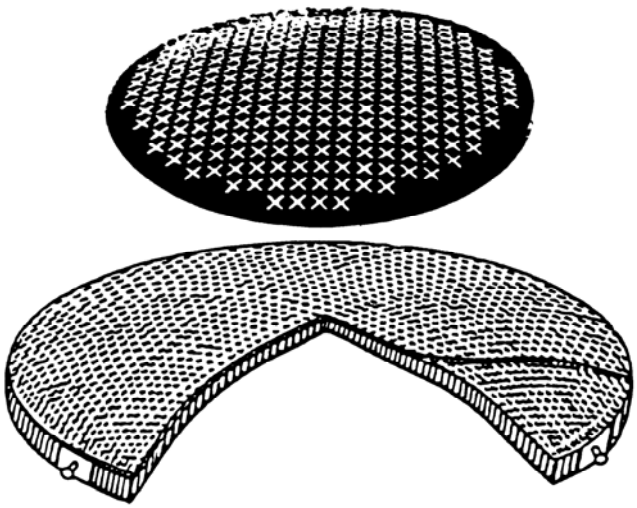

Figure 28.12-7 - Antenna examples: ERA dichroic sub-reflector

The characteristics include:

- Features: Sub-reflector transparent to 11/14 GHz frequency and reflecting at 20 GHz.
- Construction: Conductive crosses bonded on a Kevlar skin and 20mm Nomex core.
- Application: 1.1 m diameter at 11/14 GHz.
- Precision: 0.3 mm RMS.
- Sub-reflector density: 4.5 kg/m2.

28.12.4.4 CSELT/SELENIA dichroic sub-reflector

The characteristics include:

- Features: Sub-reflector transparent to 11/14 GHz frequency and reflecting at 20 GHz.
- Construction: Dichroic surfaces (conductive crosses) embedded in the 5 mm Kevlar core each side, as shown in Figure 28.12.8, Ref. [28-29].
- Application: 1.1 m diameter at 20/30 GHz and 11/14 GHz.
- Precision: 0.2 mm RMS.
- Sub-reflector density: 4 kg/m^2.

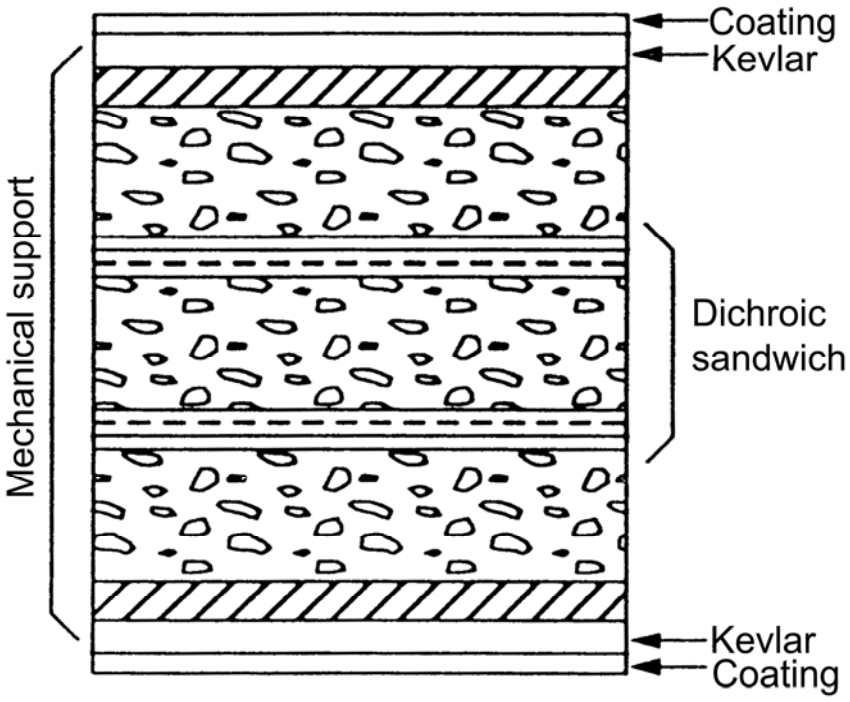

Figure 28.12-8 - Antenna examples: CSELT/SELENIA dichroic sub-reflector

28.12.4.5 CASA radiometer

The basic reflector configuration is shown in Figure 28.12.9, Ref. [28-29]. The characteristics include:

- Concept: High-precision reflector.
- Construction: Thermo-stable sandwich, metallised, 20 mm thick.
- Application: 2 m diameter at 180 GHz.
- Precision: 15 µm to 30 µm RMS.
- Reflector density: 4.5 kg/m^2.

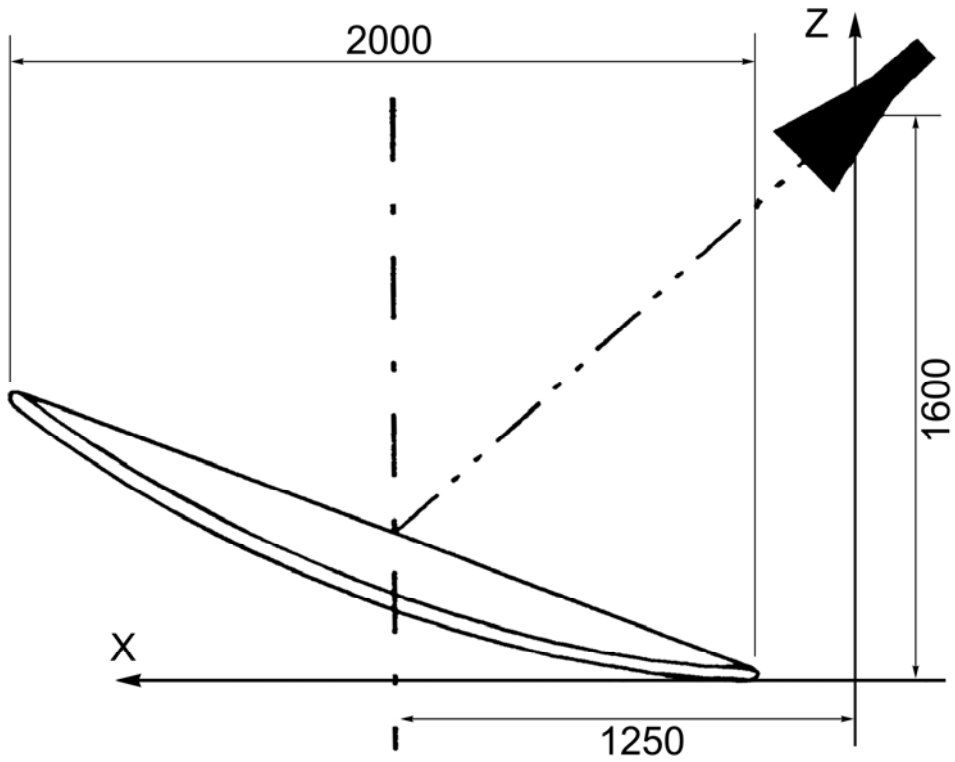

Figure 28.12-9 - Antenna examples: CASA radiometer geometry

28.12.4.6 BAe shaped gridded reflectors

The characteristics include:

- Construction:
  - All-Kevlar composite-sandwich construction, Ref. [28-32].
  - Two solid reflectors are stowed against the main body of the satellite. A single reflector configuration is shown in Figure 28.12.10, Ref. [28-32].
  - Deployment is by a combination of pyrotechnic release nuts and spring driven eddy current damper units.
  - Alignment of the reflectors is assisted by the use of active and passive trunnions.
- Performance:
  - Reflector diameter: 2300 mm.
  - Nominal focal length: 1900 mm.
  - Nominal shell rotation: 8°.
  - Reflector beam pointing : < ± 0.02°.
- Other features:
  - Reflector gridding is achieved by the vapour deposition of aluminium (0.3 μm) over the smooth reflective surface. This is subsequently laser etched to give the gridded pattern.
  - To control thermal distortion, the reflector has a sunshield. The construction of this is illustrated in Figure 28.12.11, Ref. [28-32]. The blanket thickness can be varied to optimise both thermal performance and the mass budget of each mission.

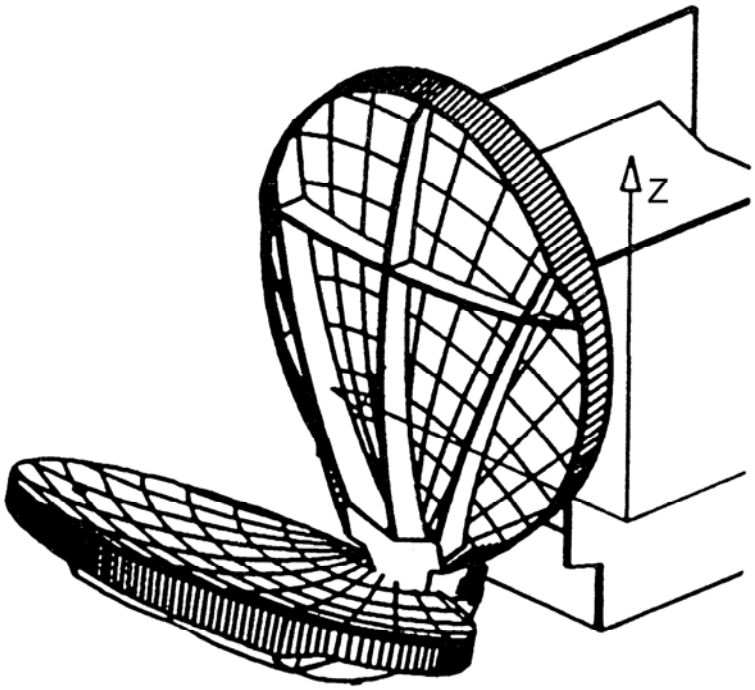

Figure 28.12-10 - Antenna examples: BAe gridded reflector (stowed and deployed configuration)

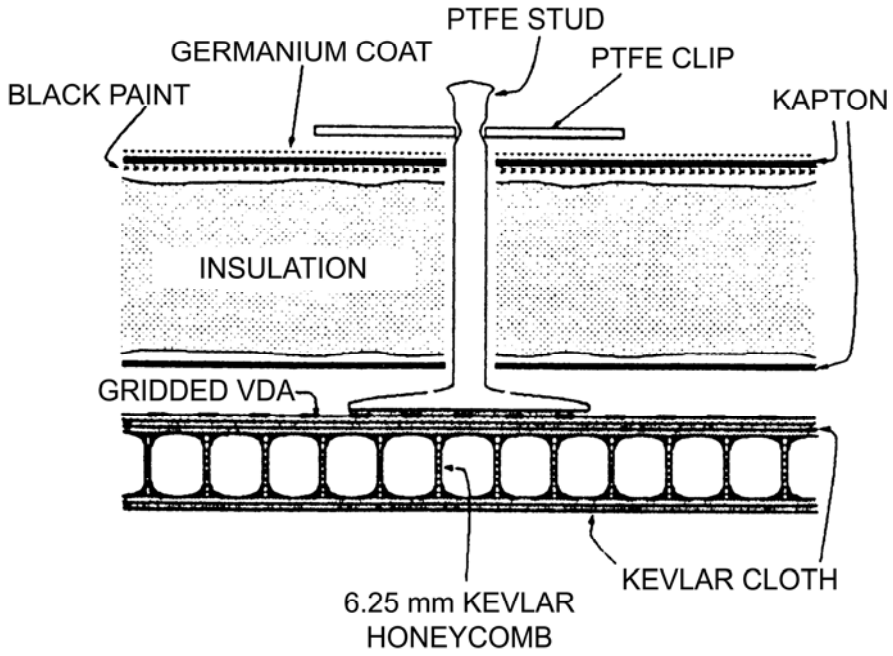

Figure 28.12-11 - Antenna examples: BAe gridded reflector - general sunshield construction

28.12.4.7 ARTEMIS LLM and SKDR antenna reflectors

Artemis uses satellite-to-satellite communications between its SILEX laser data-relay payload and lower orbiting craft. Artemis is a dual-purpose craft operating in geostationary orbit at 36000 km altitude. It also advances satellite telecommunications for cellular mobile telephones. It carries two payloads:

- LLM (L-band land mobile), and
- SKDR (S/Ka-band data relay): Radio data-relay payload.

Each payload needs a parabolic reflector, which, as of 1995, was under development and testing by CASA.

- Concept: 3.3 m x 2.8 m parabolic reflectors.
- Construction: To meet the precision requirements, the design uses a combination of newer materials, all with low CTE and CME, with good resistance to microcracking:
- Dish skin material: Cyanate ester prepregs RS3/XN50A and RS3/Kevlar 49.
- Core material: Kevlar HRH 49-1/4-2.1.
- Backing structure ribs: RS3/XN50A and RS3/T300 combined with HRH 49-1/4-2.1 core.
- Application: Artemis payloads.
- Precision: <100 μm RMS.
- Reflector density: Not stated.

28.12.5 Planer arrays

28.12.5.1 Dornier CFRP SAR Antenna

The deployed configuration is shown in Figure 28.12.12, Ref. [28-29]. The characteristics include:

- Concept: Deployable panel/truss.
- Construction: CFRP metallised waveguide panels.
- Application: 10 m x 1 m array at 5.3 GHz frequency.
- Precision: 2 mm RMS.
- Array density: 4 kg/m2.

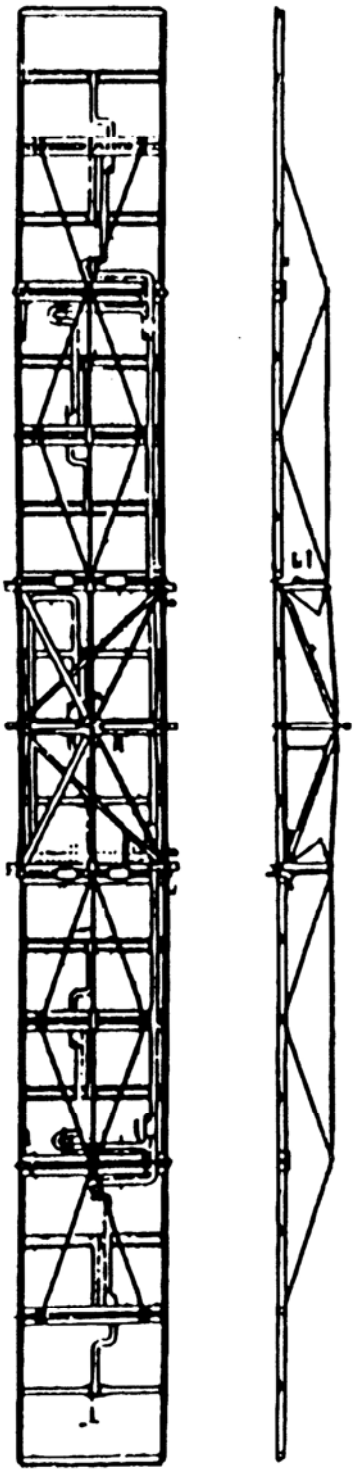

Figure 28.12-12 - Antenna examples: DORNIER CFRP SAR antenna

28.12.6 Frequency selective reflectors

28.12.6.1 Frequency selective surface (FSS) sub-reflector

Intended for launch in 1996, NASA JPL commissioned a four-frequency telecommunication system for:

- CRAF (comet rendezvous and flyby), and
- Cassini (Saturn orbit).

The development of a frequency-selective-surface, FSS, sub-reflector was needed to be integrated into the high-gain antenna subsystem, Ref. [28-33]. The FSS multiplexes S, X, Ku and Ka frequency band wavelengths. As of late 1991, the project can be summarised as:

- Basic performance:
  - 10 year to 12 year mission duration,
  - Multiple RF frequencies at S (2.3 GHz), X (7.2 and 8.4 GHz), Ku (13.8 GHz) and Ka (32 and 34 GHz),
  - A single high gain antenna (HGA) incorporating an FSS sub-reflector for cassegrain configuration at X and Ka bands, and a prime focus configuration at S and Ku bands,
  - Temperature range (for design purposes): -200°C to +125°C,
  - Full scale antenna diameter of 685 mm.
- Concepts: Two possible designs were investigated; as shown in Figure 28.12.13 and Figure 28.12.14, Ref. [28-33]:
  - 'Add-on approach': Using two screens, with the front FSS screen (Ka surface) reflecting Ka band, but passing S, X and Ku. The back screen (3 frequency surface) reflects X band, but passes S and Ku,
  - 'Integrated approach': Using a single FSS screen to reflect X and Ka wavelengths, but pass S and Ku wavelengths.
- Construction: Both screens were supported by a dielectric composite structure consisting of a sandwich construction made of:
  - 3-ply Kevlar 49 fabric face skins using Style 120/F-161 (100μm thick) Hexcel prepreg, with 55% fibre volume fraction and 170°C cure.
  - Kevlar-epoxy honeycomb core (Hexcel HRH-49, 19.05 mm thick) was selected after comparison with Rohacell 51-WF polymethacrylimide foam core.
  - FM 123-2 film adhesive was used for bonding all sandwich constructions with the honeycomb core.
  - 'Add-on design': Copper grid elements were fabricated on 25μm or 50μm Kapton film by thick film contact photolithography; as shown in Figure 28.12.15, Ref. [28-33].
  - 'Integrated design': FSS grid elements were supported and etched on a high dielectric constant material; Duroid 6010.5 from Rogers Corp.

At the end of the development work, the add-on screen approach was preferred on the grounds of ease of manufacturing and better mechanical properties, despite having inferior RF performance to the integrated approach.

The HGA flight hardware was to be fabricated by ASI/Alenia in 1992.

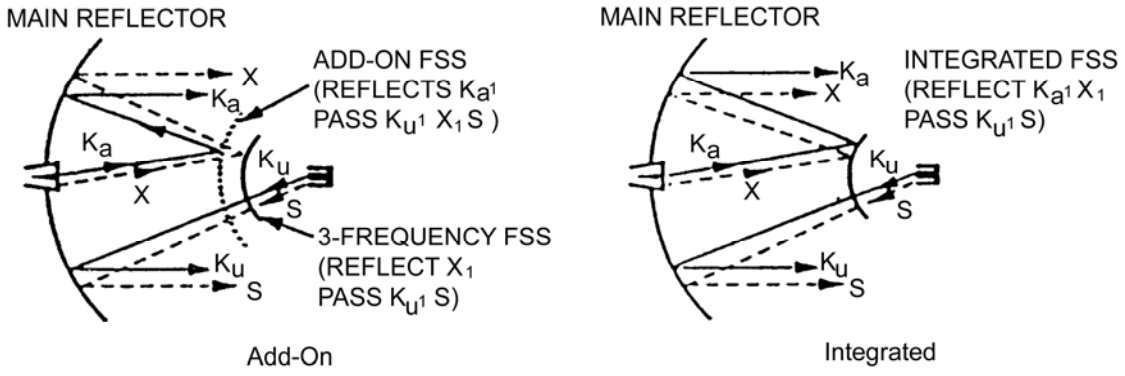

Figure 28.12-13 - Antenna examples: Design approaches for frequency selective surface (FSS) sub-reflector

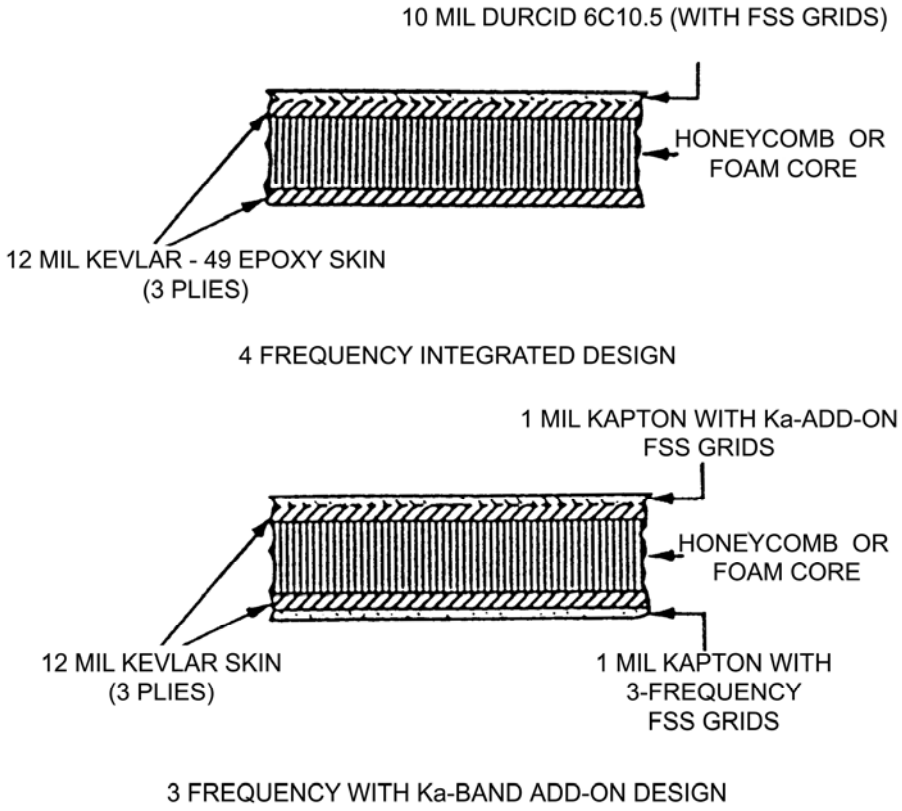

Figure 28.12-14 - Antenna examples: Design approaches for frequency selective surface (FSS) sub-reflector: Flat panel design cross-sections

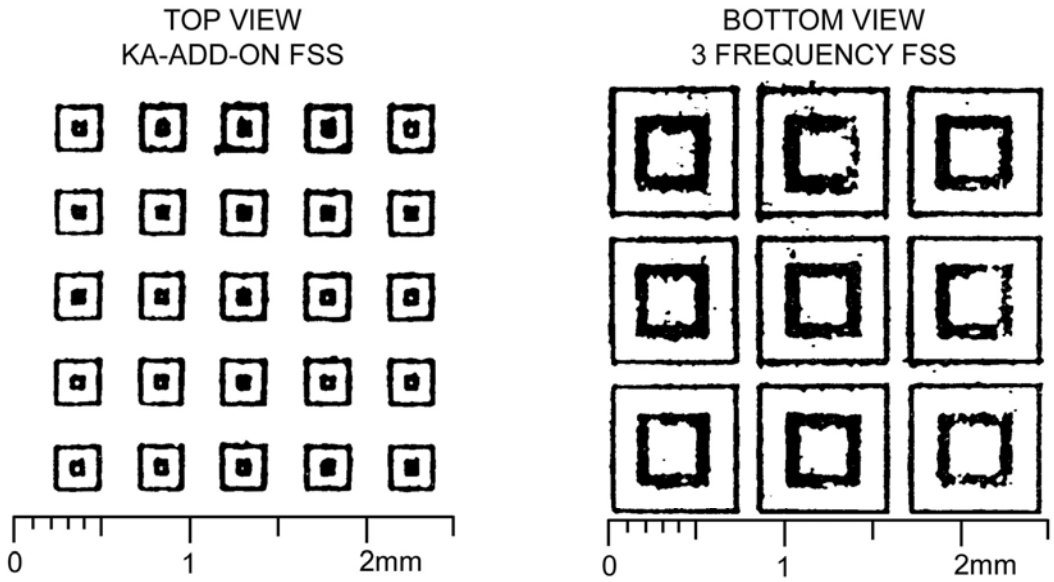

Figure 28.12-15 - Antenna examples: Design approaches for frequency selective surface (FSS) sub-reflector: Add-on design on Kevlar/epoxy face sheet: Representative double square loop FSS periodic array

28.13 IR and X-ray telescopes

28.13.1 General

To produce images in the ultra-violet (UV) and X-ray wavelengths, telescope devices are designed to collect and focus this radiation. Such telescopes use reflectors or mirrors for this purpose. The designs for these collectors have largely evolved from the principles established for RF reflectors, although dimensional stability under all operating conditions is more exacting. This has led to emphasis on producing very low and controlled CTE constructions through materials selection and design.

28.13.2 Technology demonstrators

28.13.2.1 NASA precision segmented reflector program

The 'precision segmented reflector program' (~1990), sponsored by NASA, is an example of developments toward very high precision reflectors for astrophysics missions.

28.13.2.2 Large deployable reflector (LDR)

The LDR 'large deployable reflector' is shown in Figure 28.13.1, Ref. [28-6]. This large telescope is intended to explore the far infrared through the sub-millimetre spectrum with 20 m reflectors having a surface accuracy of better than 3 μm RMS, Ref. [28-6].

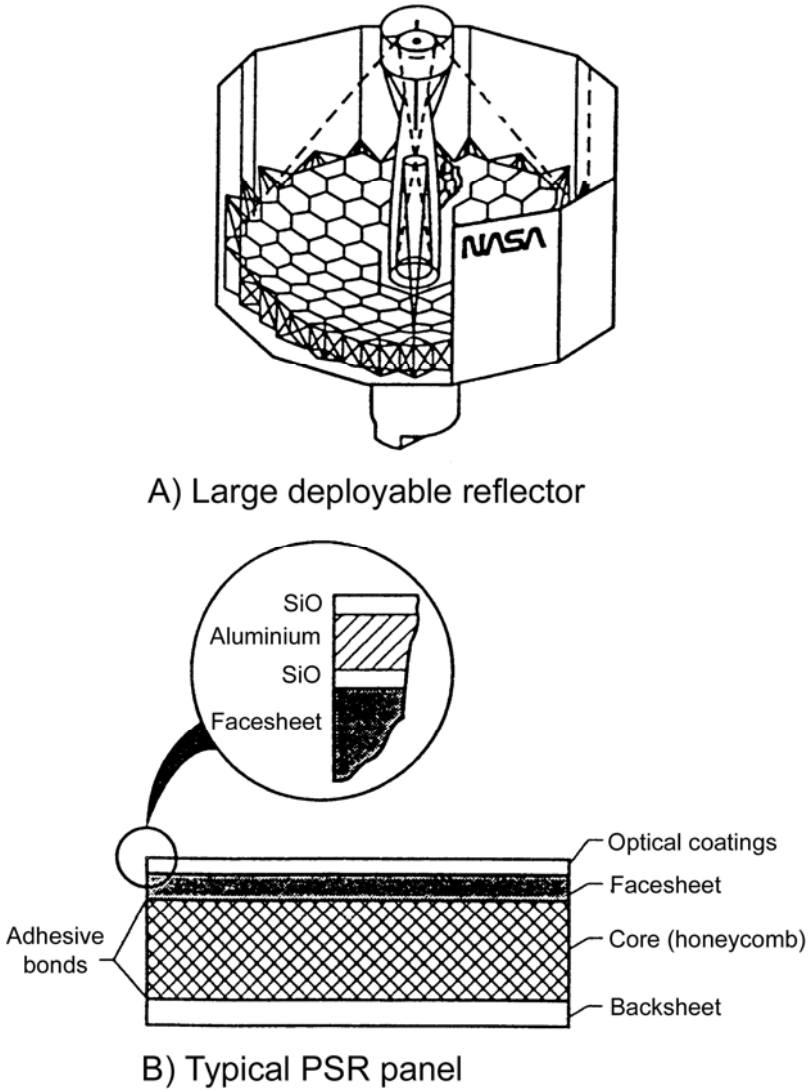

Figure 28.13-1 - IR and X-ray telescopes: Schematics of LDR and typical PSR panel

A major part of the program centres on structural materials for the reflector panels capable of operating in LEO (or possibly GEO). Some comments on the materials considered are given in Table 28.13.1, Ref. [28-6].

Table 28.13-1 - IR and X-ray telescopes: Candidate CFRP materials for PSR

Material	Process Temp.	Supplier	Comments
C6000/F155†	121°C	Hexcel	Toughened epoxy
T50/ERL 1962	176°C	Amoco	Toughened epoxy, formulated for microcracking resistance
P75/PEEK	390°C	ICI Fiberite	Thermoplastic
UHM/F584	176°C	Hexcel	Rubber toughened epoxy
P75/930	135°C	ICI Fiberite	Low cure temperature epoxy
P75/934	121°C ‡	ICI Fiberite	Conventional CFRP, low temperature cure
UHM/HX1571	71°C	Hexcel	Experimental toughened polyether
Key: † : baseline ‡ : modified			

The features of the program include:

- Material and operational performance:
  - Low in-plane and through-thickness CTE sandwich panels of 5 kg/m² to 10 kg/m² areal weight and a parabolic surface with 2.4 m focal length.
  - Quasi-isotropic face sheets, [0°,+45°, 90°,-45°]s, with tensile modulus >69 GPa.
  - Face sheet CTE: < 1.0 x10^{-6} /°C.
  - Resistant to 1000 Mrad electron radiation.
  - Resistant to thermal cycling (100 cycles) and microcracking in the range of -100°C to +65°C in LEO.
  - Capable of sustaining -173°C ±20°C for operation GEO.
  - Low CTE core (graphite phenolic honeycomb evaluated).
- Material evaluation: This centred on IM and UHM CFRP composites for the face sheets. The selected materials, of USA origin, were the most promising candidates for microcracking resistance and radiation stability:
  - Only T50/ERL 1962 showed no microcracking after testing. The P75/PEEK had 20 cracks/cm in the as-made condition.
  - All materials were subsequently concluded to be susceptible to microcracking at the low temperatures experienced in GEO.
  - It was concluded that the fibre/matrix interface characteristics largely determined the microcracking behaviour and the use of low curing temperatures offered only slight improvement.

This work confirmed the inability of most epoxy UHM CFRP materials to sustain severe thermal cycling without microcracking. Most of these materials are no longer commercially available. Emphasis has moved to cyanate esters with other fibres.

28.13.2.3 Far infrared and submillimetre space telescope (FIRST)

Intended for launch in 2007, both CASA, Ref. [28-34] and Dornier, Ref.[28-23], [28-26], [28-35] have participated in establishing technologies for the FIRST telescope between 1989 and 1994. These can be summarised as:

- Application: Exploration of space in the submillimetre and far-infrared range (85 μm to 900 μm) by means of photometry and spectroscopy. Hence the precision required.
- Construction: Various concepts using CFRP honeycombs with CFRP face-sheets as the basis for a large reflector. Initial development studies centred on smaller versions of the antenna, with 1.1 m and 3.0 m reflectors, before going on to the full size model, as shown in Figure 28.13.2, Ref. [28-35].
- Precision: 7 μm overall RMS.
- Core concepts: The CFRP core study produced different cell shapes. These were:
  - a rigid core of slotted CFRP sheets,
  - a flexible core (similar to conventional honeycomb but with different cell shapes),
  - 60° CFRP segments (triangles with rounded corners bonded together).

All concepts had to be manufactured specifically for the project.

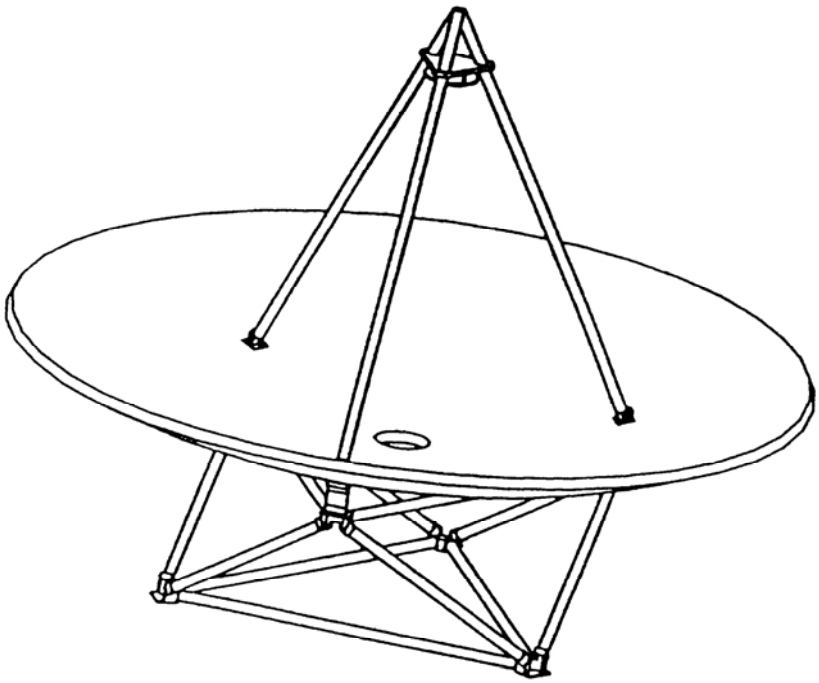

Figure 28.13-2 - IR and X-ray telescopes: 4.5m FIRST reflector

- Core specifications:
  - CTE: ± 0.2 x 10-6 /°C.
  - Core shear modulus: 500 MPa.
  - Bulk density: 50 kg/m^3.
- Initial reflector constructed:
  - 1.1 m diameter.
  - Used low temperature curing M60J/L20-SL UHM CFRP which has low moisture absorption characteristics, Ref. [28-35]. This material replaced P75/SG 12 (Amoco), used in earlier studies, which was found to be brittle and did not offer such favourable CTE characteristics.
- 60° segments (used by Dornier) became the preferred option. The sequential manufacturing stages are:
  - individually made by wrapping around mandrels,
  - placed on a mould cavity and co-cured,
  - mandrels released,
  - core machined,
  - core bonded to pre-manufactured CFRP face-skins, as shown in Figure 28.13.3, Ref. [28-35].

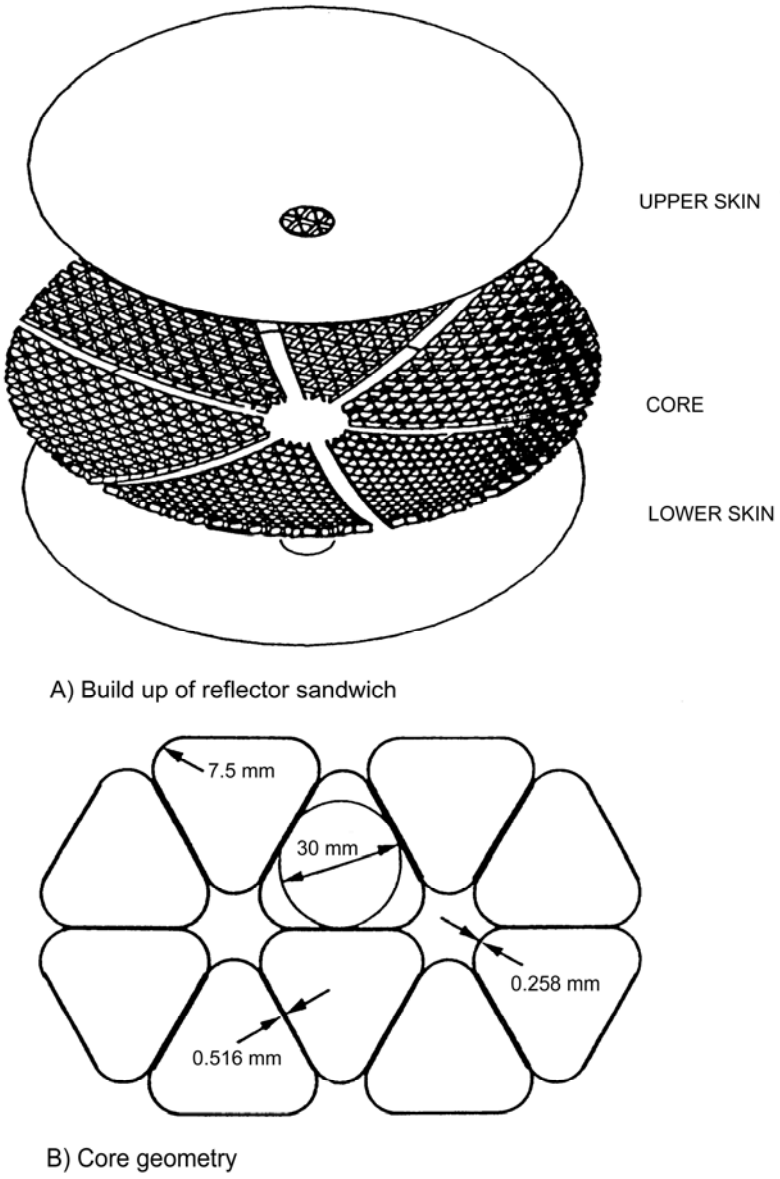

Figure 28.13-3 - IR and X-ray telescopes: FIRST reflector -construction of core and sandwich reflector

- Sensitivity of surface accuracy (7 μm specified): Evaluated and the necessary design tools established with respect to:
  - fibre volume fraction and alignment,
  - core CTE, and
  - core thickness.
- Reflector profile, characterised for, Ref. [28-23]:
  - vacuum, and
  - low temperatures.

With a full understanding of the design parameters, the combination of manufacturing variations and thermally induced changes to surface accuracy are such that the 7μm figure can be realised.

28.13.3 Soft X-ray telescope (SXT)

28.13.3.1 General

The SXT is part of the Solar-A (solar flares study project). It is a joint mission between the 'Japanese Institute of Space and Astronautical Science' (ISAS) and NASA; launched in 1991, Ref. [28-36].

The SXT telescope assembly is shown in Figure 28.13.4, Ref. [28-36]. The performance specification can be defined as:

- Grazing incidence telescope of 1.55 m effective focal length.
- Focus maintained to ±25 μm.
- Total telescope mass of less than 20 kg (actual 13 kg).
- Fundamental resonant frequency >100 Hz; actual first mode 155 Hz.
- Operating temperature range from -10°C to +25°C (survival range for design purposes from -30°C to + 60°C).
- Longitudinal thermal expansion of metering tube to be slightly negative, to compensate for positive expansion of titanium mounting fixtures.

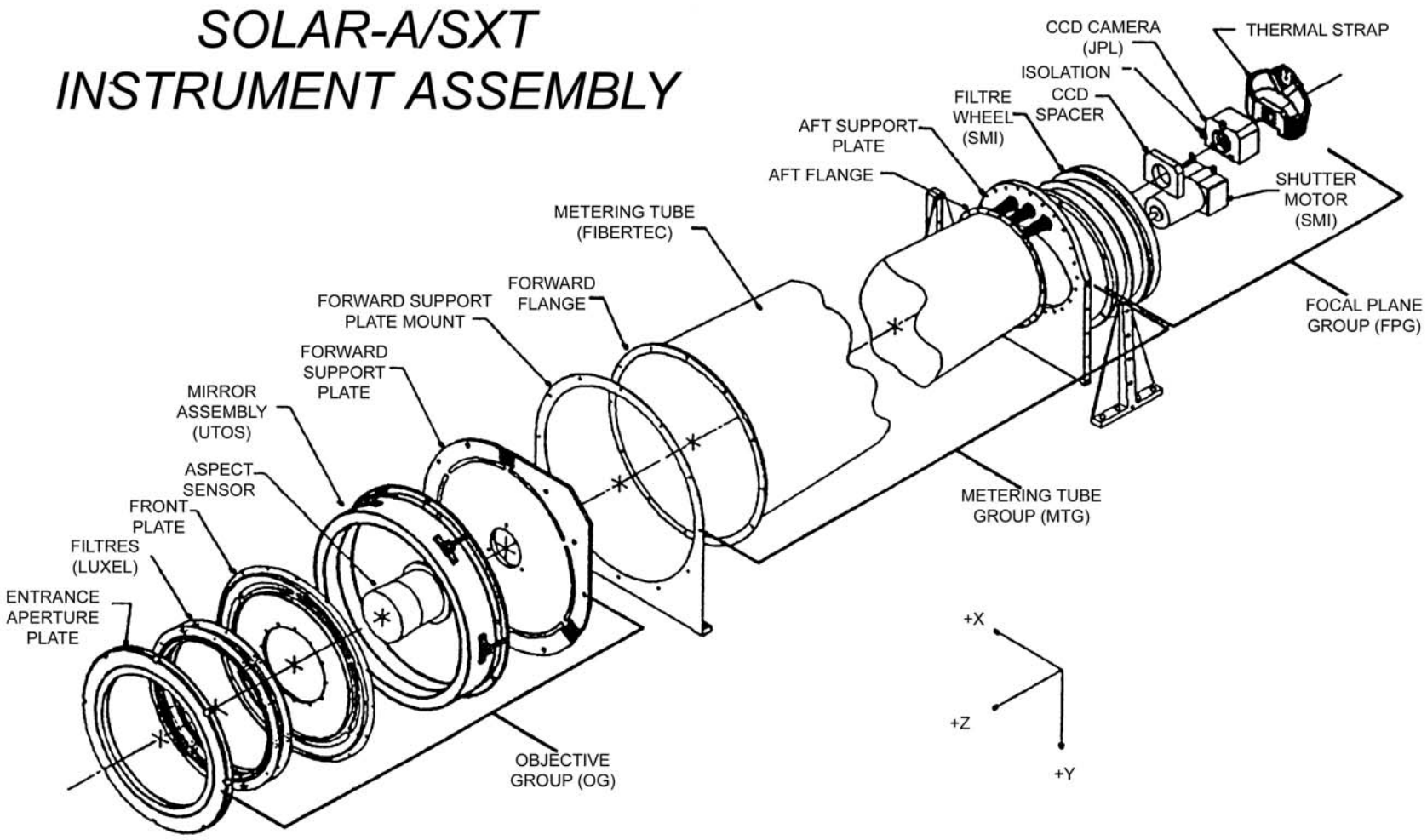

Figure 28.13-4 - IR and X-ray telescopes: SXT telescope assembly

28.13.3.2 Metering tube

One of the primary structural members of the telescope is an epoxy CFRP metering tube manufactured by Lockheed Palo Alto Research Laboratory, LPARL. The role of the metering tube is to maintain the:

- structural stability of the telescope during launch, and
- focal length through various environmental conditions.

A schematic view of the metering tube is shown in Figure 28.13.5, Ref. [28-36]. The construction, as defined by the performance specification, was:

- Symmetrical 13-ply hybrid CFRP construction, as shown in Figure 28.13.5, Ref. [28-36].
- UHM P75/3501 in longitudinal direction for negative CTE.
- Standard modulus AS4/3501 in 45° plies to minimise the risk of microcracking.
- Calculated longitudinal CTE: -0.22×10^{-6} /°C.
- Radial CTE designed to match that of titanium.
- All flanges bonded in place with Hysol EA934 adhesive.
-

As the operating temperature range is very small, the risk of microcracking is low. It enables established materials to be used despite the brittleness of 3501 resin.

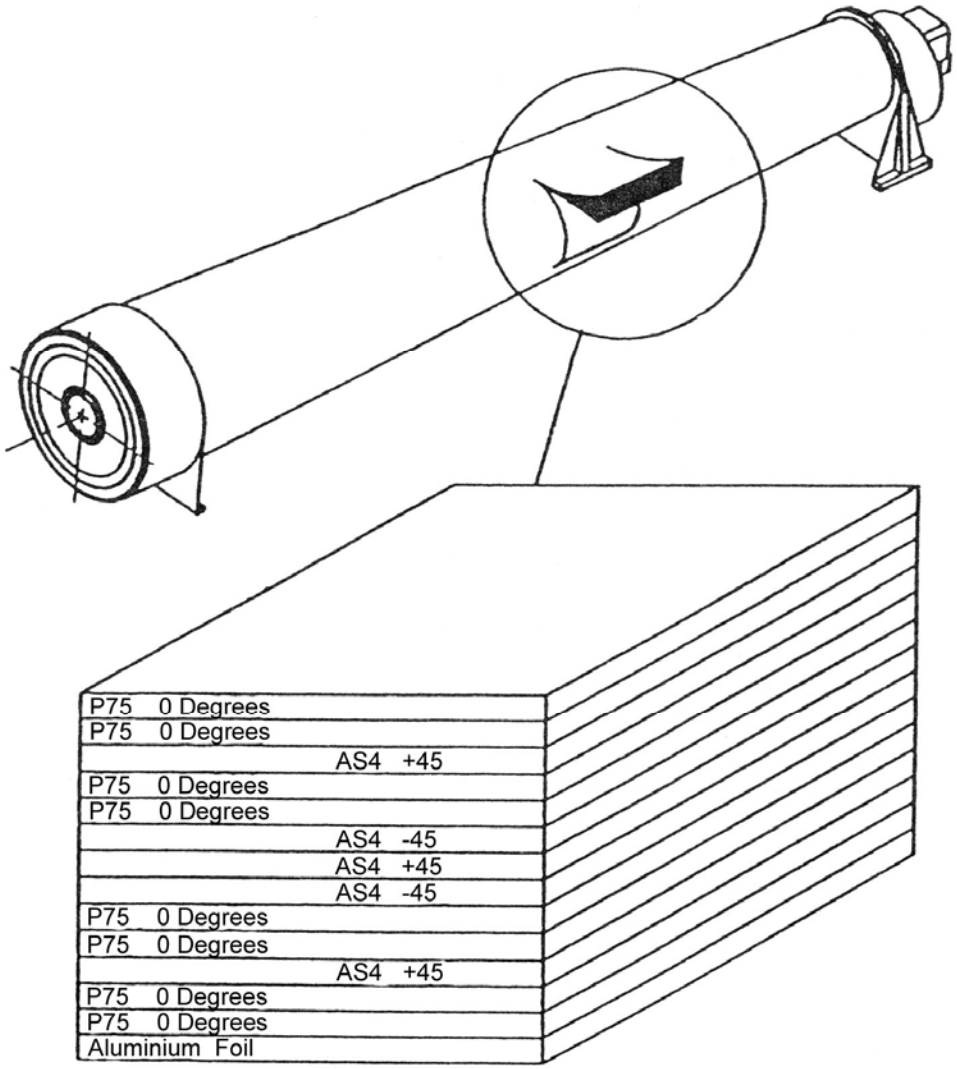

Figure 28.13-5 - IR and X-ray telescopes: Schematic of SXT telescope metering tube

The precautions taken to stabilise the structure were:

- A 25 μm aluminium foil moisture barrier was co-cured on the inside of the metering tube. The outside was not covered to enable outgassing.
- The design compensated for outgassing by defocusing the telescope prior to launch. Shrinkage, occurring in orbit, then restored the proper focus position.
- The telescope was stored in 'dry conditions' during testing and integration.

28.13.4 X-ray multi-mirror telescope (XMM)

Launched in December 1999, XMM was an ESA-funded development programme for an X-ray telescope. The main features can be summarised as:

- Concept:
  - Three mirror modules, each consisting of 58 highly nested, thin walled (~1mm) mirror shells, Ref. [28-26].
  - The parabolic and hyperbolic mirror shells range from 300mm to 700 mm in diameter and 600 mm in length. These are arranged within each other as nested tubes.
- Mirror shell:
  - Absolute radius < 5 μm.
  - Circumferential slope < 1 arcmin.
  - Surface microroughness < 1 nm RMS.
- Construction: To meet the accuracy, it uses:
  - high precision, filament wound CFRP carriers.
  - Carriers are replicated from high-precision, gold-coated glass mandrels. The gold/epoxy transfers to the carrier to make the mirror surface.

28.14 Optical structures and devices

28.14.1 General

Optical structures and devices encompass those operating within visible wavelengths or using lasers for signal transmission. The total assembly normally consists of the:

- Optics, and
- Surrounding support structure and enclosure.

A significant problem is to combat the usual, uneven heating of the assembly in orbit. This creates uneven thermal expansion within individual components. Predicting and controlling their response determines the success of the design.

28.14.2 Mirrors and optics

28.14.2.1 Materials

Mirrors, by necessity, are very stiff with reflective surfaces.

Traditionally, monolithic materials such as low expansion glasses have been used, e.g. Zerodur™. These materials have modest specific stiffnesses resulting in heavy designs.

CFRP constructions are also feasible, often with 'egg-crate' substructures. The CFRP face is ground and a metallic coating applied. This is then polished to provide the light-reflective surface, Ref. [28-37], [28-38].

Some metal matrix composites, MMC, and ceramic matrix composite, CMC, materials can improve on glasses by providing lightweight constructions, Ref. [28-39], [28-40], [28-41]. The materials studied include:

- Particulate-reinforced MMCs, such as:
  - Mg/C, [See also: Chapter 44].
  - Al/C, [See also: Chapter 46].
- Borosilicate/C, [See also: Chapter 53]
- C/SiC, [See also: Chapter 52]

28.14.3 Cameras and telescopes

28.14.3.1 General

These contain the mirrors and optics arranged in the desired configuration. Around these items there is a support structure and enclosure. As with antennas, the support structure has to survive launch and provide the necessary thermal and dimensional control in orbit. Some examples of launched structures include:

- Hubble space telescope.
- Mars observer camera, [See: 28.15].

28.14.3.2 Materials

The support structure and enclosure is normally CFRP. Sometimes a mixture of UHM and HS fibres is used to balance the structural and CTE requirements. CFRP optical structures are also used for terrestrial applications, Ref. [28-42], [28-43].

28.14.4 Radiometers

28.14.4.1 General

Radiometers scan in the visible and UV wavelengths, typically to collect data for global and local weather predictions, Ref. [28-44]. These can operate in either LEO or GEO.

The construction usually consists of:

- central tube, which houses the instrumentation, and
- surrounding panels, which act as the:
  - interface with the spacecraft,
  - load-introduction points,
  - thermal radiators or coolers to control the temperature within a narrow range, e.g. 20°C.

28.14.4.2 Materials

An assembly is usually made of CFRP with a central CFRP tube structure onto which are mounted functional sandwich panels.

[See: 28.15 for examples of optical structures]

28.15 Optical structures: Examples

28.15.1 Mars observer camera (MOC)

28.15.1.1 General

The MOC is one of several instruments aboard the Mars observer spacecraft. It is intended to record visual images of the surface of the planet Mars. Composite Optics Inc. was responsible for producing the composite containment structure for engineering and flight models between 1987 and 1991. This application has particularly severe thermal variations caused by the Martian orbit, whilst demanding predictable and controllable dimensional stability for the correct functioning of the optics and cameras, Ref. [28-5]. Lessons learnt from developing and testing the engineering model are incorporated as changes for the flight model.

Figure 28.15.1 shows the basic construction of the MOC, Ref. [28-5]. The major structural assemblies reviewed are the:

- Main body structural assembly (MBSA),
- Secondary mirror support assembly (SMSA),
- Wide-angle support assembly (WASA).

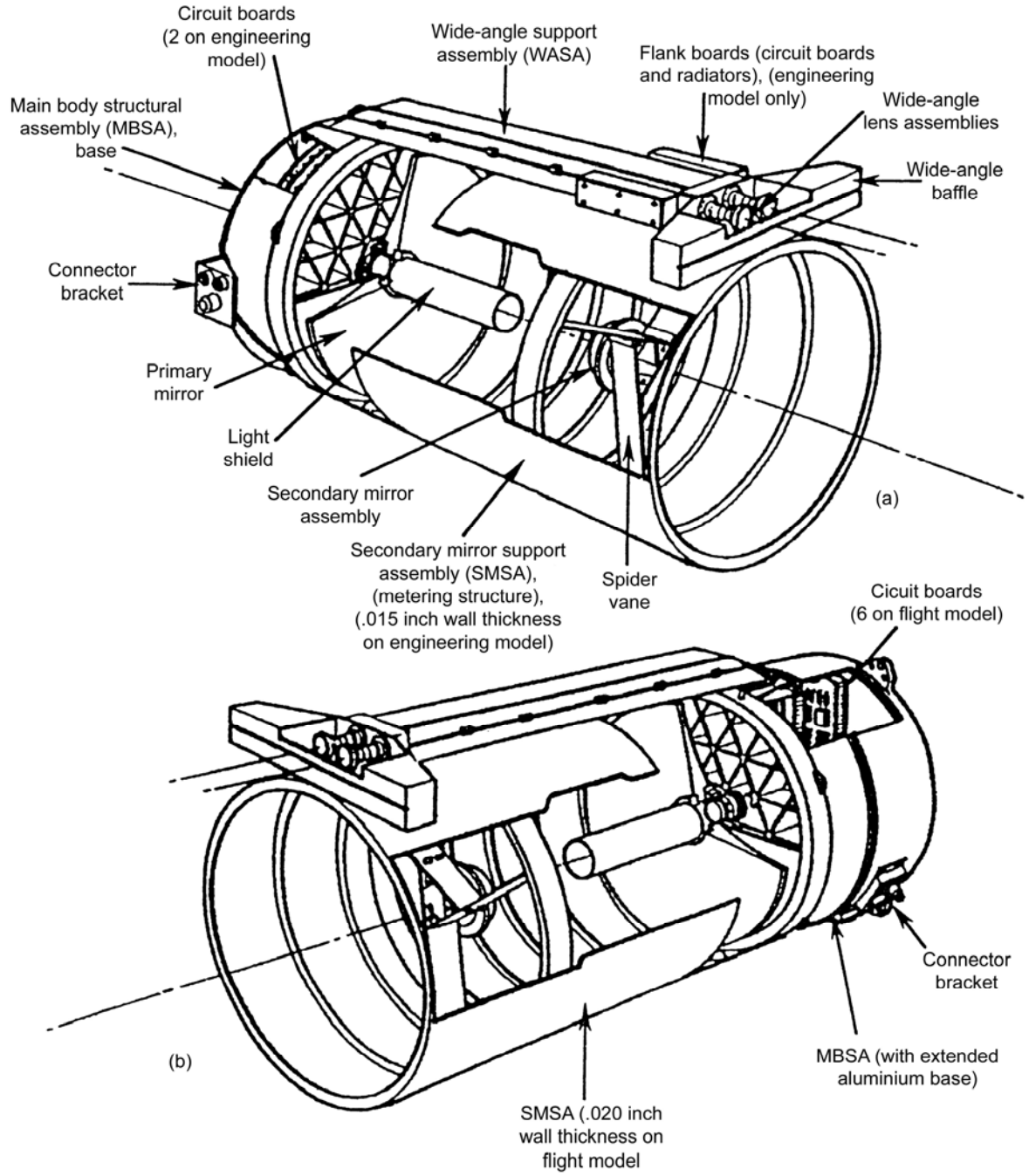

Figure 28.15-1 - Optical structures examples: Basic construction of Mars observer camera - engineering model and flight model

28.15.1.2 Basic performance specification

The basic specification can be summarised as:

- Launcher: Designed for Titan III or Space Shuttle.
- External interplanetary transit temperature: -270°C, which needs electric heaters to warm parts of MOC.
- Anticipated cruise temperature range: from -18°C within the MOC to -105°C on external surface.

- On-orbit temperatures vary in or out of the planet's shadow, and as Mars orbits the Sun.
- Optical systems:
  - one narrow-angle camera, and
  - two wide-angle cameras.
- Mass allocation:
  - 8.4 kg in total for the engineering model, of which
  - 4.6 kg allocated to the structure.
  - Necessary modifications to the flight model later raised the total mass to 11.5 kg.

28.15.1.3 Main body structural assembly (MBSA)

The MBSA is a CFRP construction which acts as the base for the narrow-angle telescope and houses the electronics. It consists of:

- A cylindrical assembly consisting of 'egg-crate' lattice structure constructed from pre-cured laminates (ribs), onto which a top and bottom face sheet are bonded. This provides a mount for the primary mirror assembly.
- A continuous titanium base ring (aluminium in the flight model) for part of the attachment assembly to the host spacecraft (aluminium nadir panel).
- An invar mounting ring between MBSA and the primary mirror.
- Six invar fittings to connect with SMSA.
- T300/934 composite cone section for thermal flexure transition between MOC (titanium ring) and aluminium nadir panel.

28.15.1.4 Secondary mirror support assembly (SMSA)

This is the metering structure which accurately separates the secondary and primary mirrors, and provides an outer baffle for the narrow-angle telescope. It consists of:

- Tube (principle component):
  - UHM CFRP.
  - 650 mm long and 390 mm in diameter.
  - 11 stiffening rings along the length.
  - Wall thickness: 508 μm on the flight model (381 μm on engineering model).
- Attachment (tube to secondary mirror assembly) using 9 Invar fittings.
- Light shield (for the primary mirror):
  - tube of T300/934 composite, with an
  - Invar flange base.

28.15.1.5 Wide-angle support assembly (WASA)

This supports the wide-angle lens assemblies and the wide-angle baffle and consists of:

- Tube (main component):
  - UHM CFRP.

— 50 mm square tube.

- Wide-angle lens assemblies:
  - — Attached to the titanium 'transition bracket' at the upper end of the WASA.
  - — The transition bracket accommodates the transition of the relatively high-CTE titanium lens housings to the low-CTE CFRP WASA tube.
- Wide-angle baffle made of UHM CFRP which attaches to the transition bracket.

28.15.1.6 Materials

The UHM CFRP material selection was dominated by the usual concerns of:

- CTE,
- microcracking resistance (over -140°C to +65°C range),
- low moisture absorption

Additionally, the CFRP had to be amenable to a COI-proprietary moisture barrier system.

Of the prepreg systems evaluated, P75S/ERL1962 was preferred to P75S/930, P75S/934 or GY70/ERL1962. The characteristics were:

- 63.5 μm UD prepregs,
- [0°,±60°]s or [0°,45°,90°,135°]s laminates,
- Near-zero in-plane CTE ($0 \pm 0.18 \times 10^{-6}$ /°C).

28.15.1.7 Design features

To compensate for the thermal cycling experienced in orbit during image recording the different expansion of structural components had to be balanced to retain focusing. This included:

- Compensation for changes in the length of the metering tube:
  - — A passive system was adopted using a 6061 aluminium spacer.
  - — The spacer was located behind the secondary mirror mount. As the primary moved with the contracting metering tube, the secondary did likewise, thereby 'athermalising' the system.
  - — The optimum spacer thickness for the engineering model was 250 μm, giving a calculated focus shift of only 48 μm.
  - — The structure proved to be thermally self-compensating; the largest contributions to thermal defocusing came from primary mirror curvature and primary mirror mounting base displacement.
- Moisture absorption in CFRP sections compounded the problems associated with thermally-induced dimensional changes. To resolve this, the structure was assembled in a fully dry state to set the correct focal lengths. The procedure adopted was:

a. Assemble the telescope and align with moisture saturated CFRP components.

b. Vacuum bake the aligned telescope at 65°C for 7 days.

c. Back-fill the oven with nitrogen and cool.

d. Bag the telescope and purge with further nitrogen.

e. Move the telescope to a dehumidified room (30% RH at 32°C) for manual realignment within 2 hours. Further localised purging of the telescope can enable working for up to 9 hours.

f. Repeat steps 2) to 5) to re-check the alignment.

g. Expose the telescope to ambient and launch conditions to enable moisture reabsorption.

h. After launch: The MOC is baked-out on the way to Mars using 90 Watt heaters to warm the metering structure to 42°C for 74 days to remove absorbed moisture.

- Moisture absorption barrier:
  - The original specification called for a proprietary 3-layer eutectic coating to be applied to the UHM CFRP metering structure to inhibit moisture absorption.
  - The intended 18 μm thick coating was of nickel + gold + indium-tin or indium-bismuth; adding 160 g to the structure.
  - Whilst effective in reducing the level of moisture absorption, the moisture barrier was rejected because it increased the effective CTE of the metering tube beyond an acceptable limit.

28.15.2 High-stability telescope structures (HSTS)

28.15.2.1 General

A feasibility study, which addressed the requirements for telescope support structures, was completed by CASA in 1992, Ref. [28-45]. These structures are characterised by:

- very accurate pointing,
- large physical dimensions,
- attached telescope and components are of greater mass than the supporting structure itself.

Previous structures such as the 'large space telescope' (LST) and 'grazing incidence solar telescope' (GRIST) were evaluated. This resulted in a basic specification for the study of:

- Geometry: 3 m diameter, 6 m high truss-structure, built up of a 4 m high cylinder section and a 2 m high conical section and upper diameter of 1.5 m; as shown in Figure 28.15.2, Ref. [28-45].
- Loads: The structure had to be capable of sustaining:
  - 200 kg at the top, and
  - 200 kg distributed around the cylinder/cone interface.
- Stiffness: Minimum frequencies:
  - 35 Hz (axial), and
  - 15 Hz (lateral).
- Temperature range from -100°C to +123°C.
- Global CTE: 0.2 x 10^{-6} /°C; zero CTE structure (<10^{-8} /°C), ideally.
- Materials which exhibit:
  - high micro-yield strength, and

— low micro-creep.

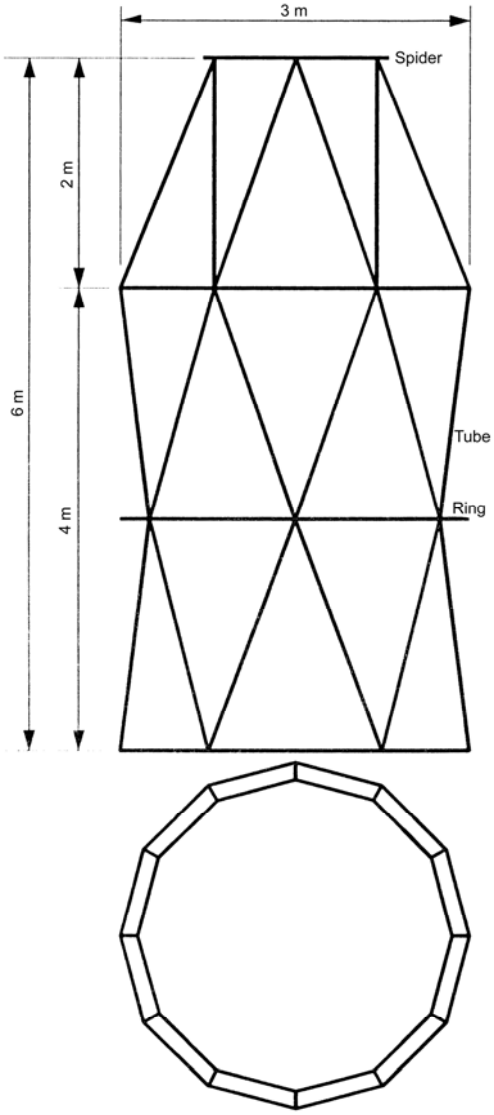

Figure 28.15-2 - Optical structures examples: HSTS demonstrator

28.15.2.2 Materials

The specification dictated that the structure was made of CFRP. GY70/Code 87 was chosen as the baseline material, with the addition of Grafil XAS carbon fibre to modify the CTE and reduce costs.

A truss-structure configuration was developed with CFRP material tailored for each component, including:

- Rings,
- Tubes,
- Panels, and
- Joints:
  - slotted tubes,
  - rigid connecting plates (gusset), or

— bonded clips (tube and ring clips).

FM24 was the baseline adhesive system.

The effect of thermal cycling and moisture absorption on composite behaviour was investigated. No unexpected adverse change in composite behaviour was recorded.

28.15.2.3 Joints

Although the programme called for a 1/3 scale model structure to be tested, a test section representative of part of the total structure was assembled. This consisted of tube and ring elements with examples of all the joint connections. Two typical joint configurations are shown in Figure 28.15.3 and Figure 28.15.4, Ref. [28-45]. All components were made of CFRP.

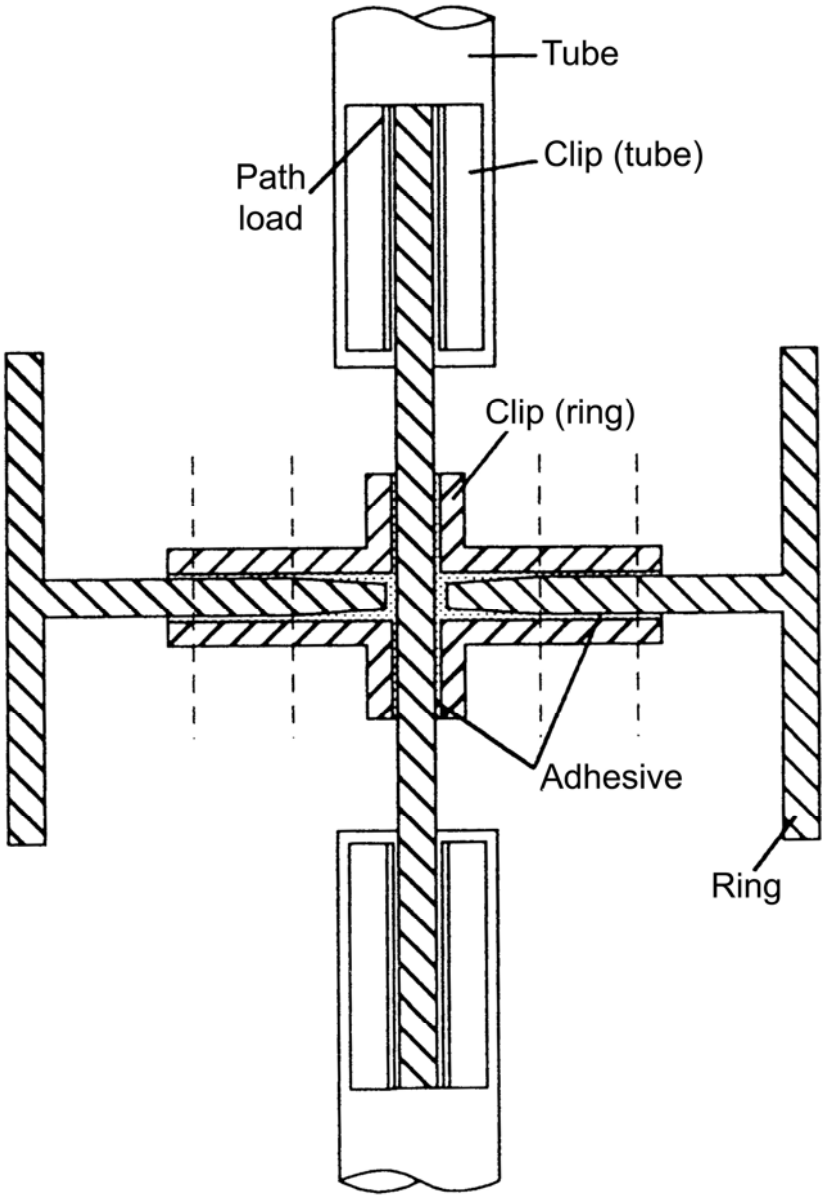

Figure 28.15-3 - Optical structures examples: HSTS ring-to-tube joint

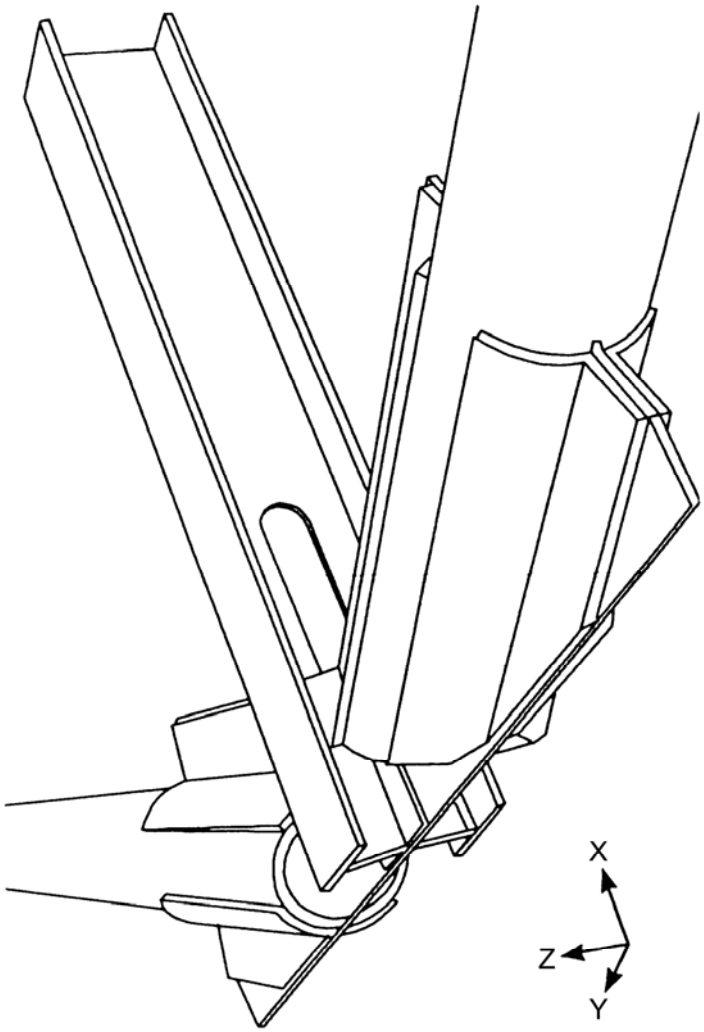

Figure 28.15-4 - Optical structures examples: HSTS test specimen joint

28.15.3 Semiconductor laser inter-satellite link experiment (SILEX)

28.15.3.1 General

SILEX is a revolutionary laser data-relay payload, Ref. [28-46], [28-47]. It was part of a technology demonstrator for commercial satellite phone networks. The laser systems consist of optics for transmissions between satellites, hence very stable structures, assemblies and platforms are needed. Two payloads were flown on:

- Spot 4 in LEO, and
- Artemis in GEO, [See also: 28.12 for reflectors].

The first communication between Spot 4 and Artemis was made in November 2001.

28.15.3.2 Structural configuration

SILEX consists of a telescope transmitting and receiving data from an optical head bench (OHB). These items are the optical assembly (OA) and are isostatically mounted on a closed box: the mobile part carrier structure (MPCS). The overall SILEX configuration is shown in Figure 28.15.5, Ref. [28-46].

The MPCS is pointed towards Artemis using a two-axis coarse pointing mechanism arm (CPM). This arm is fixed onto Spot 4 through the coarse pointing support bracket which is mounted on the aerial spacecraft interface structure (ASIFS/CPASB).

In addition, the titanium launch locking devices (LLD) maintain the MPCS during launch before being released in orbit. The optical head thermal hood (OHTH) performs the fine thermal control of the OHB.

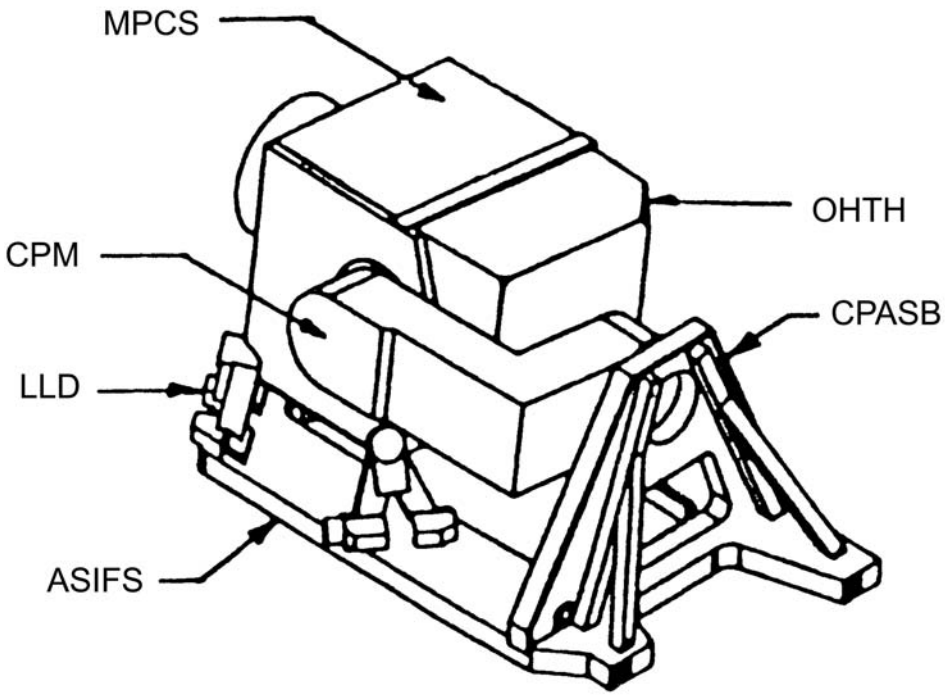

Key:

MPCS :	Mobile Part Carrier Structure	ASIFS:	Areal Spacecraft Interface Structure
CPM:	Coarse Pointing Mechanism	OHTH:	Optical Head Thermal Hood
LLD:	Launch Locking Devices	CPASB:	Coarse Pointing Areal Support Bracket

Figure 28.15-5 - Optical structures examples: SILEX architecture

The main features can be summarised as:

- MPCS design requirements (made by MAN Technologie AG):
  - demountability,
  - stiffness and structural stability; containing the telescope and electronic equipment.
- MPCS construction:
  - box with three demountable panels made of UHM CFRP/alloy honeycomb core sandwich.

— M55J/914 was used for the skins (0.6 mm to 1.5 mm) and AG5 aluminium honeycomb; densities from 32 kg/m³ to 130 kg/m³. This combination provides the necessary thermal conductivity characteristics compatible with precise thermal control for the OHB.

— An unusual [0°/+36°/+72°/-72°2/-36°/0°]s lay-up was used in some locations, in addition to more conventional configurations.

— Titanium fittings are specified for their low CTE compared with other metals.

- MPCS additional features:

— CFRP corners for joining panels, and

— CFRP ring for carrying loads from the OA.

To obtain the desired CTE characteristics, the sandwich panels were conditioned with 10 thermal cycles (from -40°C to +70°C) under vacuum.

A change to low moisture absorbent composites, e.g. cyanate ester RS-3 or Fiberite 954-3, was considered in order to enhance the stability.

28.15.3.3 Isostatic mounts

Between 1990 and 1992 a study by CASA defined the construction of a demonstrator SILEX isostatic mounting platform for the optical head bench (OHB). The OHB engineering qualification model was complete by 1994 and the flight model preparation followed for launch in 1997. The general OHB lay-out is shown in Figure 28.15.6, Ref. [28-48].

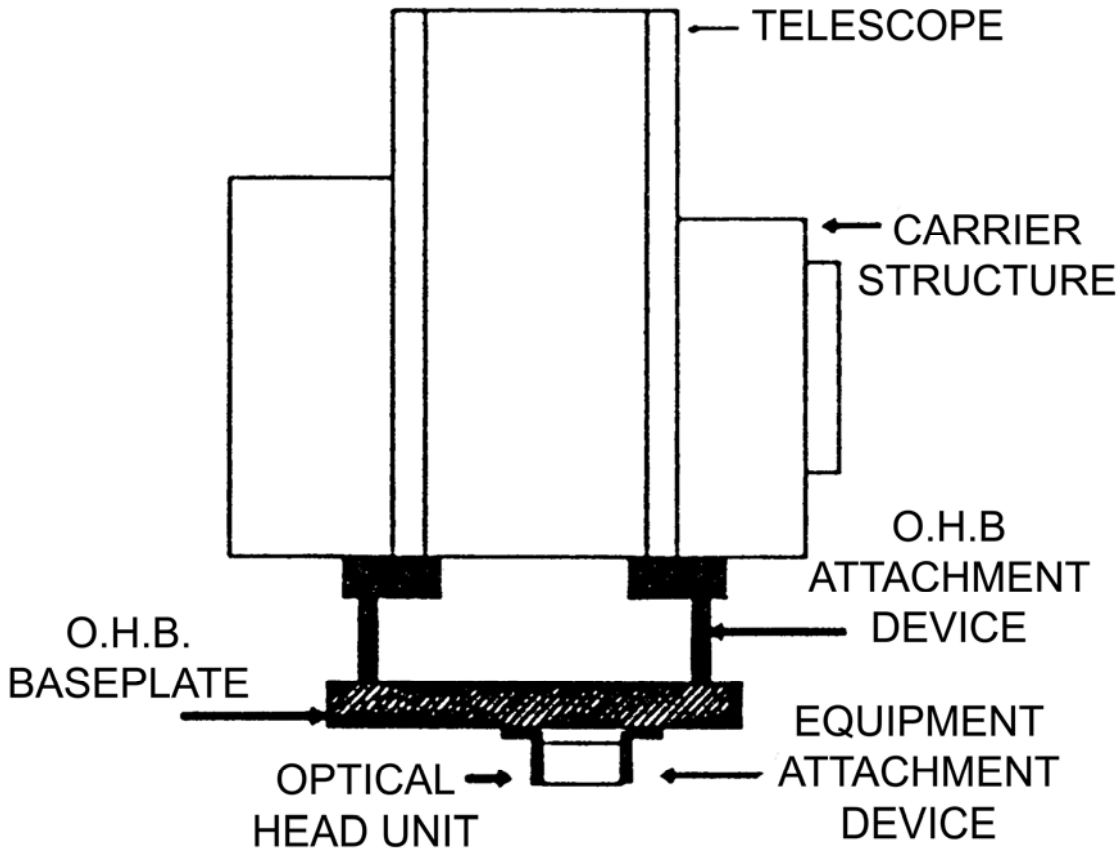

Figure 28.15-6 - Optical structures examples: SILEX OHB lay-out

The main features can be summarised as:

- OHB attachment design absorbs distortions caused in the carrier structure by thermal cycling.
- OHB attachment construction: The structural and dimensional stability were only met by using a sandwich concept with CFRP skins and a CFRP core; as shown in Figure 28.15.7, Ref. [28-48]. A compromise was reached to find the optimum skin thickness and core depth.
- OHB construction: bench plate and isostatic attachment device. The basic constituents are:
  - Baseplate: Skins and core of GY70/Code 87 in (0°,±60°)s construction, bonded with Hysol EA 9394 adhesive.
  - Inserts: Invar.
  - Attachment devices (baseplate to carrier structure): Ti 6Al 4V.
  - Optical unit isostatic attachment devices (optical units to optical bench): GY70/Code 87 (0°, ±60°,±45°)s plates.

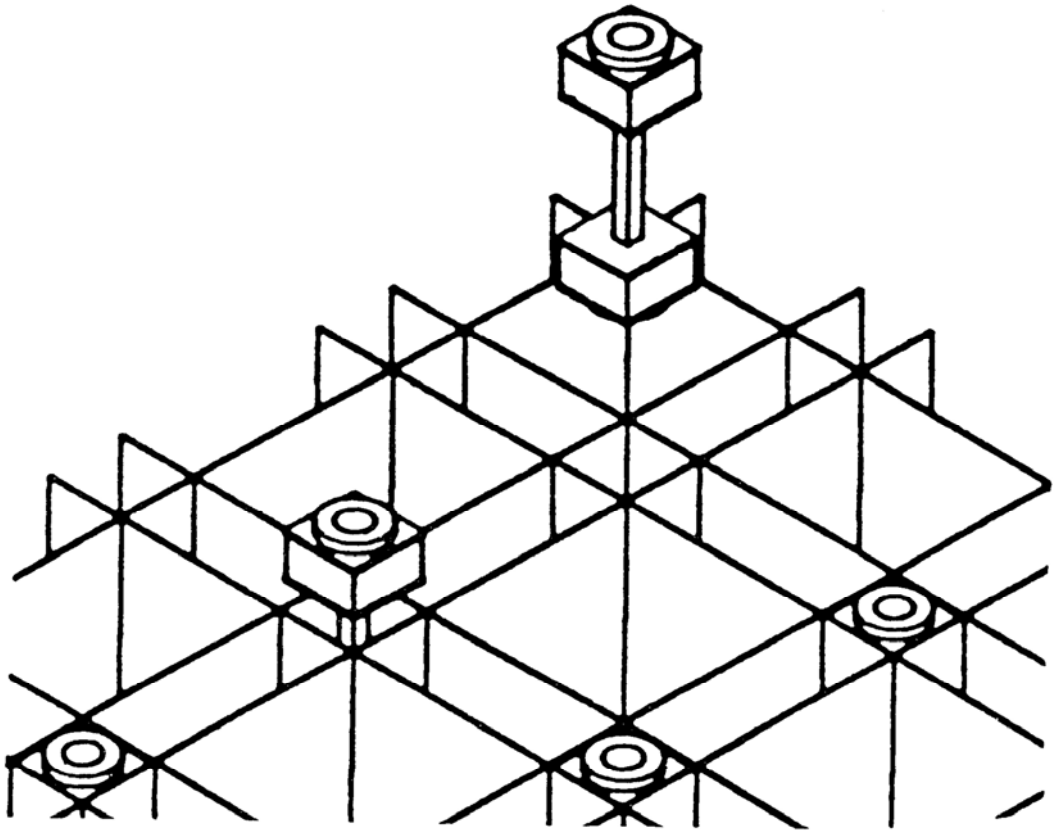

Figure 28.15-7 - Optical structures examples: SILEX OHB core assembly in CFRP

28.15.4 Scan mirror

28.15.4.1 General

The development of an ultra-lightweight scan mirror substrate was supported by ESTEC with participation from DASA-Ottobrunn, SGL Carbon and IABG, Ref. [28-49]. The application is a

spinning enhanced visible and IR imager instrument, known as SEVIRI, to be carried on MSG; the second generation Meteosat satellites. MSG-1, renamed Meteosat-8, was launched in August 2002.

Within an ultra-lightweight scanning mirror (ULSM) are:

- a ribbed substrate, as shown in Figure 28.15.8, Ref. [28-49].
- a CFRP support frame, and
- isostatic mounts.

In operation, the mirror rotates at 100 rpm, with mirror tip loadings of 3.2 G. Rib thicknesses are typically 1.25 mm, with 2 mm for the face sheet.

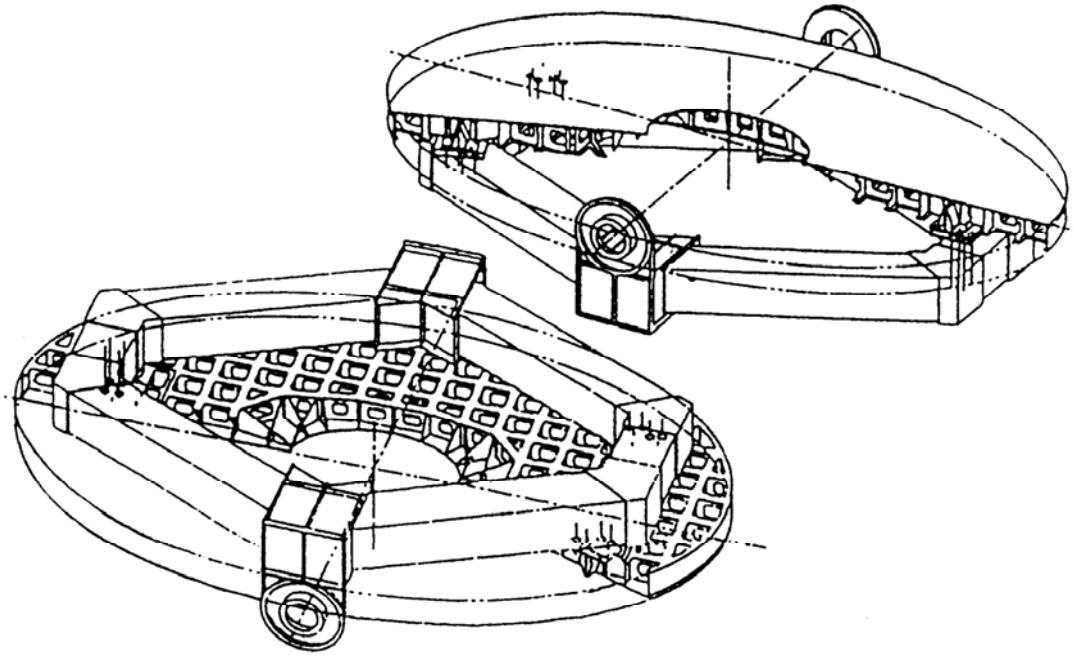

Figure 28.15-8 - Optical structures examples: Ultra-lightweight scanning mirror (ULSM)

28.15.4.2 Demonstrator substrates

The main features are:

- Construction, as of 1993:
  - Dimensions: 800 mm x 600 mm.
  - Mass: 5.45 kg.
- Materials: C-SiC, a chopped carbon fibre felt reinforced silicon carbide, which is expected to be extremely stable in the working environment, so fully retaining the dimensions, [See also: 52.3]. The attractions of C-SiC for this application are:
  - high stiffness (238 GPa),
  - low CTE (+2.2 x10^{-6} /°C), and
  - good thermal conductivity (125 W/m/°C^{-1}).

[See also: 52.3 for C-SiC composites; 57.2 for potential applications of CMCs in high-precision optical structures]

28.16 Smart technologies

28.16.1 General

Dimensionally stable materials are unlikely to meet all of the demands of future space projects. Consequently, ESA/ESTEC has a policy to invest in active smart techniques to control the stability of structures that cannot be achieved by materials selection or by thermal control, [See also: Chapter 90].

For dimensionally stable designs, the broad categories of appropriate 'smart technologies' are:

- Active compensation, and
- Microvibration damping.

[See also: Chapter 92 for potential space applications of smart technologies]

28.16.2 Active compensation

Where in-orbit conditions induce distortions in a structure, e.g. reflectors, actuators can be used to restore the shape, Ref. [28-50], [28-51], [28-52]. Such systems are only viable if the additional mass and power consumption can be tolerated to produce acceptable structural stability. Piezoelectric ceramic transducers showed promise in early demonstrator configurations of simple beams, struts and sandwich panels, [See also: 92.6].

28.16.3 Microvibration damping

Undesirable microvibrations were induced in orbit in both the:

- Hubble space telescope owing to 'thermal ratcheting', and
- Olympus satellite owing to misalignment of the inertia wheel.

Active systems, based on piezoelectric actuators, are considered to reduce the amplitude of vibrations by introducing anti-phase vibration energy, [See also: 92.5].

The analysis of structural response is particularly important in optimising the positioning of actuators in order to minimise the total active system mass and power consumption.

28.17 References

28.17.1 General

[28-1] D.P. Bashford & D.C.G. Eaton: ERA (UK)/ ESTEC
'The use of high stiffness material and dimensionally stable materials in spacecraft applications'
Proceedings of the International Workshop on Advanced Materials for High Precision Detectors, CERN-Archamps,
28-30 September 1994, p9-19, CERN 94-07, ISSN 0007-8328/ISBN 92-9083-066-2

[28-2] I. Cabeza
'A high dimensional stability structures verification facility'
Proceedings of the International Workshop on Advanced Materials for High Precision Detectors, CERN-Archamps,
28-30 September 1994, CERN 94-07, ISSN 0007-8328/ISBN 92-9083-066-2

[28-3] E.G. Wolff
'Dimensional stability of carbon fiber reinforced plastic tubes'
29th National SAMPE Symposium, April 3 - 5, 1984

[28-4] S. Yalvac et al
'Transverse ply cracking in toughened and untoughened graphite/epoxy and graphite/polycyanate crossply laminates'
Journal of Composite Materials, Vol.25, Dec. 1991, p1653-1667

[28-5] A.R. Telkamp & E.A. Derby
'Design considerations for composite materials used in the Mars observer camera'
SPIE Proceedings: Advances in Optical Structure Systems, 16-19 April 1990, Volume 1303, ISBN 08194-0354-7, p416-436

[28-6] S.S. Tompkins et al
'The development of composite materials for spacecraft precision reflector panels'
SPIE Proceedings: Advances in Optical Structure Systems, 16-19 April 1990, Volume 1303, ISBN 08194-0354-7, p512-523

[28-7] C. Blair & J. Zakrzewski
'Evaluation of mechanical and thermophysical properties for dimensionally stable high modulus graphite/epoxy composites'
22nd International SAMPE Technical Conference
6-8 November 1990, p918-931

[28-8] R. Jones et al
'Extended thermal cycle testing of graphite/epoxy composite struts for space station applications'
34th International SAMPE Symposium
8-11 May 1989, p1207-1213

[28-9] P.W. Manders & D.R. Maas
'Thin carbon fiber prepregs for dimensionally critical structures'
SPIE Proceedings: Advances in Optical Structure Systems
16-19 April 1990, Volume 1303, ISBN 08194-0354-7, p536-545

[28-10] C. Blair & J. Zakrzewski
Coefficient of thermal and moisture expansion and moisture absorption for dimensionally stable quasi-isotropic high modulus graphite fibre/epoxy composites'
SPIE Proceedings: Advances in Optical Structure Systems
16-19 April 1990, Volume 1303, ISBN 08194-0354-7, p524-535

[28-11] T. Matsumoto et al
'On the performance of high modulus pitch-based carbon fiber/toughened polycyanate ester resin composite'

37th International SAMPE Symposium
9-12 March 1992, p137-146

[28-12] P.C. Yang et al
'Rubber-toughened cyanate composites - properties & toughening mechanism'
36th International SAMPE Symposium
15-18 April 1991, p437-448

[28-13] P. Lefebvre et al
'Moisture resistant & toughened cyanate systems for aerospace applications in Europe'
Society of Manufacturing Engineers Paper EM91-104

[28-14] G. Almen et al
'Toughened cyanates for aerospace applications'
35th International SAMPE Symposium, 2-5 April 1990, p408-418

[28-15] F.W. Lee et al
'High service temperature, damage tolerant prepreg systems based on cyanate chemistry'
35th International SAMPE Symposium, 2-5 April 1990, p162-174

[28-16] D.A. Shimp & S.J. Ising
'New cyanate ester resin with low temperature (125-200°C) cure capability'
35th International SAMPE Symposium
2-5 April 1990, p1044-1056

[28-17] E.M. Silverman et al
'Design of high stiffness & low CTE thermoplastic composite spacecraft structures'
SAMPE Journal, Vol. 25, No.5, Sept./Oct. 1989, p39-46

[28-18] E.M. Silverman et al
'Graphite & Kevlar thermoplastic composites for spacecraft applications'
34th International SAMPE Symposium, 8-11 May 1989, p770-779

[28-19] M. Lane et al
'Potential applications of MMC & aluminium lithium alloys in cameras for CRAF Spacecraft'
34th International SAMPE Symposium, 8-11 May 1989, p798-809

[28-20] L. Cornec & J. Clariou
'Carbon-magnesium metal matrix composites material & processes for light weight aerospace structures'
Proceedings of the International Symposium on Advanced Materials for Lightweight Structures '94, ESTEC , Noordwijk
March 1994, ESA WPP-070, p563-568

[28-21] J. Pernon
'High dimensional stability structure: metal matrix composites'
Proceedings of the International Workshop on Advanced Materials for High Precision Detectors, CERN-Archamps
28-30 September 1994

[28-22] D.P. Bashford
'Microcracking behaviour of epoxy & cyanate ester UHM CFRP composites'
ERA Technology Report 76-0362, Work Order No. 34
ESTEC Contract 7090/87/NL/PP, April 1994

[28-23] D. Ehmann & G. Helwig
'Material tailoring & design optimisation for the FIRST reflector'
Proceedings of the International Symposium on Advanced Materials for Lightweight Structures '94, ESTEC , Noordwijk
March 1994, ESA WPP-070, p49-56

[28-24] C.M. Hinckley
'Statistical evaluation of the variation in laminated composite properties resulting from ply misalignment'
SPIE Proceedings: Advances in Optical Structure Systems
16-19 April 1990, Volume 1303, ISBN 08194-0354-7, p497-511

[28-25] British Aerospace Dynamic Group (Space)
'Design guide for dimensionally stable CFRP structures'
ESA Contract 4252/80/NL/AK

[28-26] G. Helwig
'Highly dimensional stable composite structures.'
Proceedings of the International Workshop on Advanced Materials for High Precision Detectors, CERN-Archamps
28-30 September 1994, CERN 94-07
ISSN 0007-8328/ISBN 92-9083-066-2

[28-27] M. Marchetti & F. Morganti
'The dimensional stability of advanced composite antenna reflectors: Analytical & test evaluation'
Workshop on Mechanical Technology for Antennas
ESA/ESTEC, Noordwijk, The Netherlands 1984

[28-28] R. Schütze
'Lightweight structures based on CFRP sandwich struts & CFRP connections'
Proceedings of the International Symposium on Advanced Materials for Lightweight Structures '94, ESTEC , Noordwijk
March 1994, ESA WPP-070, p615-620

[28-29] 'Mechanical technology for antennas'
ESA SP-261

[28-30] H. Kellermeier et al
'Surface contour measurement and performance analysis and verification of the MBB unfurlable mesh reflector'
MBB Publication

[28-31] F. Grimaldi et al
Development of a large deployable carbon fiber composite antenna structure for future advanced communications satellites'
Materials & Processing - Move into the 90's - European SAMPE symposium 1989. p197-210
Published by Elsevier Science Publishers B.V.

[28-32] R.J. Wimmer
'Mechanical design of advanced shaped gridded reflectors structures for space applications'
Proceedings of the International Symposium on Advanced Materials for Lightweight Structures '94, ESTEC , Noordwijk
March 1994, ESA WPP-070, p45-48

[28-33] G.S. Hickey & T. Wu
'Development of a four-frequency selective surface prototype spacecraft antenna'
37th International SAMPE Symposium, 9-12 March 1992, p50-62

[28-34] A. Alonso et al
'An approach to high precision antenna structures by a CFRP Core sandwich concept'
An International Symposium on Advanced Materials for Lightweight Structures, ESTEC, Noordwijk, March 1992
ESA SP-336, p39-44

[28-35] G. Helwig et al
'Low cost & thermally stable sandwich design for FIRST'
An International Symposium on Advanced Materials for Lightweight Structures, ESTEC, Noordwijk, March 1992
ESA SP-336, p45-50

[28-36] B.K. Jurcevich & M.E. Bruner
'Use of graphite epoxy composites in the Solar-A soft X-ray telescope'
SPIE Proceedings: Advances in Optical Structure Systems
16-19 April 1990, Volume 1303, ISBN 08194-0354-7, p406-415

[28-37] J.A. Sultana & S.E. Forman
'A graphite/epoxy composite mirror for beam steering applications'
SPIE Proceedings: Advances in Optical Structure Systems
16-19 April 1990, Volume 1303, ISBN 08194-0354-7, p477-487

[28-38] R.A. Brand & J.E. Marks
'Composite structures for optical mirror applications'
SPIE Proceedings: Advances in Optical Structure Systems
16-19 April 1990, Volume 1303, ISBN 08194-0354-7, p488-496

[28-39] A.L. Geiger
'Metal matrix composite foam: A new material for sandwich-construction mirrors'
SPIE Proceedings: Advances in Optical Structure Systems
16-19 April 1990, Volume 1303, ISBN 08194-0354-7, p546-553

[28-40] R. Wendt & M. Misra
'Fabrication of near-net shape graphite/magnesium composites for large mirrors'
SPIE Proceedings: Advances in Optical Structure Systems
16-19 April 1990, Volume 1303, ISBN 08194-0354-7, p554-561

[28-41] E. Estrada et al
'Silicon carbide for highly stable structures, thermomechanical properties & adhesive bonding characteristics'
Proceedings of the International Symposium on Advanced Materials for Lightweight Structures '94, ESTEC , Noordwijk
March 1994, ESA WPP-070, p69-74

[28-42] C.R. Olds et al
'Composite structures for a large optical test bed'
SPIE Proceedings: Advances in Optical Structure Systems
16-19 April 1990, Volume 1303, ISBN 08194-0354-7, p448-457

[28-43] P. Richardson
'Athermalisation of electro-optic (EO) test equipment optical structures using low-expansion graphite\epoxy composites'
SPIE Proceedings: Advances in Optical Structure Systems
16-19 April 1990, Volume 1303, ISBN 08194-0354-7, p458-464

[28-44] R.A. Hookman & G.E. Zurmehly
'The application of composite materials to spaceborne radiometer instrument design'
SPIE Proceedings: Advances in Optical Structure Systems
16-19 April 1990, Volume 1303, ISBN 08194-0354-7, p465-474

[28-45] 'High stability telescope structures'
Final Report, CASA Space Division
ESA Contract No. 56/83/NL/PB (SC), November 1992

[28-46] B. Gergonne et al
'SILEX optimal terminal structure overview of the design & stability performances'
Proceedings of the International Symposium on Advanced Materials for Lightweight Structures '94, ESTEC , Noordwijk
March 1994, ESA WPP-070, p57-62

[28-47] F. Arévalo
'High stability supporting platforms for optical communications'
Proceedings of the International Workshop on Advanced Materials for High Precision Detectors, CERN-Archamps
28-30 September 1994, CERN 94-07
ISSN 0007-8328/ISBN 92-9083-066-2

[28-48] E. Ozores et al
'Development tests for a high-stability optical bench'
An International Symposium on Advanced Materials for Lightweight Structures, ESTEC, Noordwijk
March 1992, ESA SP-336, p271-276

[28-49] M. Deyerler et al
'C/SiC - An ultra-lightweight structural material for optical components & further space applications'
Proceedings of the International Symposium on Advanced Materials for Lightweight Structures '94, ESTEC, Noordwijk
March 1994, ESA WPP-070, p63-68

[28-50] R. Lammering & J. Melcher
'Smart structures research at DLR'
Proceedings of the International Symposium on Advanced Materials for Lightweight Structures '94, ESTEC , Noordwijk
March 1994, ESA WPP-070, p475-480

[28-51] D. Scheulen & H. Baier
'Smart materials for active vibration damping & shape control'
Proceedings of the International Symposium on Advanced Materials for Lightweight Structures '94, ESTEC , Noordwijk
March 1994, ESA WPP-070, p485-490

[28-52] E. Olmo & A. Jiménez
'Structural shape control of CFRP beams using embedded piezoelectrics'
Proceedings of the International Symposium on Advanced Materials for Lightweight Structures '94, ESTEC , Noordwijk
March 1994, ESA WPP-070, p519-525

28.17.2 ECSS documents

[See: ECSS website]

ECSS-Q-ST-70-02	Thermal vacuum outgassing test for the screening of space materials; previously ESA PSS-01-702
ECSS-Q-ST-70-04	Thermal testing for the evaluation of space materials, processes, mechanical parts and assemblies; previously ESA PSS-01-704.
ECSS-Q-ST-70-46	Requirements for manufacturing and procurement of threaded fasteners
ECSS-E-HB-32-21	Adhesive bonding handbook; previously ESA PSS-03-210.
ECSS-E-HB-32-22	Insert design handbook; previously ESA PSS-03-1202
ECSS-E-HB-32-23	Threaded fasteners handbook; previously ESA PSS-03-208.

29
Filament wound pressure vessels, tanks and structures

29.1 Introduction

29.1.1 General

The proven uses of composite filament winding technology are described, particularly for pressure vessels. Also discussed are some of the anticipated future applications. Examples are provided of filament wound tanks and structures.

29.1.2 Uses of filament winding

Filament winding is an appropriate processing technique for space programme applications and structural configurations such as:

- Cryogenic fuel tanks, [See: 29.11].
- Launcher structures, tanks and pressure vessels, [See: 29.10].
- Optical structures, [See: 29.13].
- Pressurant and propellant tanks, [See: 29.3].
- Pressure vessels, [See: 29.6 for design concepts].
- Satellite central cylinders, [See: 29.12].
- Solid propellant motor cases, [See: 29.9; 29.10].
- Struts and booms, e.g. SPAS strut configurations for Eureca.
- Water tanks.

29.1.3 Pressure vessels

Filament winding is widely accepted as the preferred means of producing lightweight pressure vessels. Pressure vessels are used in many different satellite applications, including:

- Pressurant tanks, [See: 29.3].
- Liquid propellant tanks, [See: 29.3].
- Tanks for operating gases, [See: 29.3].
- Solid-propellant motor cases, [See: 29.9].

From the experience of developing European solid rocket motors, information is provided for the different pressure vessel design concepts, with regard to:

- Requirements, [See: 29.4].
- Safety factors, [See: 29.5].
- Design concepts, [See: 29.6].
- Material selection, [See: 29.7].
- Dimensioning theories, [See: 29.8].

29.1.4 Options with filament winding

The attributes of filament winding that differentiate this processing route from autoclave-based manufacturing techniques, include:

- ideally suited to cylindrical and spherical designs,
- large diameter windings up to 4 m,
- automated and rapid fibre placement,
- optimum fibre placement,
- short processing cycles,
- single part constructions.

These points indicate that filament winding offers possible attractions for controlling costs on large cylindrical designs and repeat manufacturing, as can be found within launchers. Any cost savings through filament winding are dependent on the number of unit produced.

[See also: 38.4 for autoclave moulding; 38.5 for filament winding]

29.2 Developments in filament winding

29.2.1 Introduction

Filament winding has been established for many years as a processing technique for composites, notably for pressure vessels.

A number of further developments have enhanced this processing route which in turn has influenced design and manufacturing of other structures. These include:

- Manufacturing capabilities, e.g. machines and mandrels.
- Materials.
- Pressure vessel liner technology.

29.2.2 Manufacturing capabilities

29.2.2.1 Multi-axis CNC filament winding machines

Developments in machinery now enable very large structures to be wound with high degrees of freedom for fibre wind patterns and orientations.

29.2.2.2 Mandrel technology

This can encompass a range of options including:

- Steel, which offers high thermal expansion for consolidation pressure during curing, Ref. [29-1].
- Temperature-controlled multiple-section aluminium mandrels, Ref. [29-2].
- Low melting point alloys for small components.
- Wash-out mandrels of hard materials, such as plasters, moulded sand with PVA or silicate binders, and moulded or machined salt. These are principally used for small components, but gypsum with glass microspheres is used for the MAGE motors.
- Reusable inflatable mandrels for large rocket motor cases; including continuous fibre-reinforced reusable inflatables (collapsible composite mandrel). Up to 3 bar pressure is used for inflation with a fibre-reinforced rubber design, Ref. [29-3]. Features of these are:
  - Compaction pressure can be adjusted in relation to inflation pressure.
  - Delivery times for mandrels are short and the life-cycle cost lower than traditional metal constructions.
  - Co-cured ablative insulators are feasible where uncured insulation material, e.g. EPDM - ethylene propylene elastomer, is applied to the mandrel before winding and is then cured at the same time as the epoxy composite.
- Low cost composite tooling for large structures, Ref. [28-4].

29.2.2.3 Capabilities

These include:

- Unidirectional (UD) prepreg procured specifically for winding.
- Wet resin impregnation at the point of winding with direct multiple tow, e.g. 12k fibres per tow.
- Fibre volume fractions of 60% are achievable for greater mass efficiency by avoiding resin-rich components.
- Thermoplastic prepreg, e.g. PEEK APC2,

29.2.3 Materials

29.2.3.1 High-strength fibres

For pressure vessels, the main criterion for obtaining mass-efficient designs is that reinforcing fibres possess high specific tensile strength. There has been an evolution in the preferred fibres to meet this need. Initially these were high-strength glass (R- and S-glass), before the advent of aramid fibres, notably Kevlar™ 49. Glass fibres are still extensively used in a wide range of industrial applications, not least because a large database exists on their performance characteristics.

The most mass efficient designs are achieved using the newer generation of high-strength carbon fibres; available since 1985, Ref. [29-48], [29-51]. These have become the preferred fibres for many space programmes. They typically include fibre grades T-40, HT-46-9A, T700, T800 and T1000.

Table 29.2.1 provides the basic mechanical performance data for the newer generation high-strength carbon fibres.

Table 29.2-1 - High strength carbon fibres for potentially mass efficient pressure vessels

Carbon Fibre	Tensile Modulus, E (GPa)	Ultimate Tensile Strength, UTS (MPa)	Strain to Failure (%)	Fibre Density
IM7	303	5300	1.8	1.8
T40	290	5650	1.8	1.81
HT-46-9A	317	5690	1.8	1.81
T800	294	5490	1.9	1.81
T1000H	294	6370	2.1	1.8
T1000	294	7060	2.4	1.82

Key: These are manufacturer's declared fibre property values.

The stress rupture behaviour of glass fibres is a limiting factor on service life, more so than with Kevlar or carbon fibre constructions. This is illustrated in Figure 29.2.1, Ref. [29-6]. Graphite is carbon fibre.

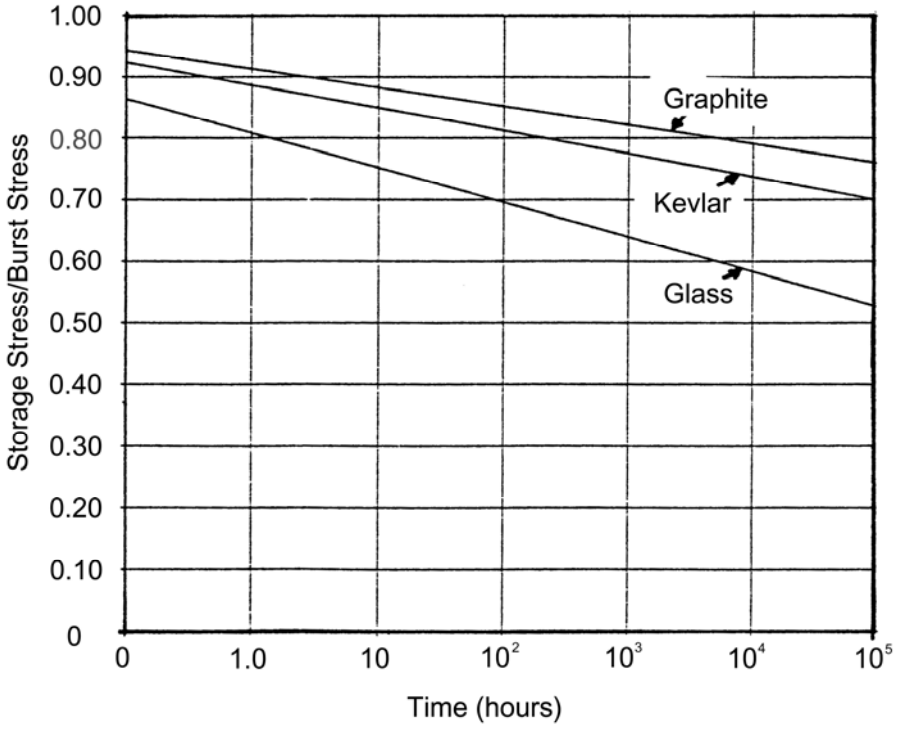

Figure 29.2-1 - 50 percentile fibre life

29.2.3.2 Resins

Optimised thermosetting resin formulations for filament winding can achieve:

- Fibre volume fractions of 60%, approaching that of prepregs.
- Controlled viscosity.
- Long pot-lives (long gel times) to assist with processing.
- Post curing capabilities; to enable low temperature processing, with increased resin glass transition temperature achieved by additional elevated temperature post curing.
- Compatibility with fibre mechanical characteristics.

29.2.3.3 Thermoplastics

The option to wind thermoplastic prepregs, e.g. PEEK APC2, is possible, with potential use for future cryogenic tank constructions, Ref. [29-5]. The thermoplastics offer improved toughness and possible reductions in manufacturing costs, when the technology is optimised. The main constraint is a lack of space-approved materials and proven capabilities.

29.2.4 Pressure vessel liner technology

The evolution of composite pressure vessel development has been influenced by:

- The preference for leak-before-burst as the acceptable mode of failure at ultimate pressure.
- The use of different liner materials, e.g.
  - aluminium and titanium alloys for lightweight designs.
  - stainless steel, Inconel and Monel also applied for techniques with welded liners.
- Thinner wall liners, down to 500 μm from 2.5 mm for smaller tanks, with heat treatment and prestressing.
- Seamless liners which are stretch-formed rather than welded.

This has resulted in a transition from filament reinforced metal vessels to metal lined filament wound pressure vessels. This produces more mass efficient designs.

29.3 Pressurant and propellant tanks

29.3.1 Introduction

29.3.1.1 General

For orbiting structures and conventional launchers, pressure vessels are used for:

- Pressurant tanks for containing helium gas, typically operating between 20,000 kPa and 67,000 kPa.
- Propulsion tanks containing fuels, i.e.
  - hydrazine as a monopropellant in one tank,

— MMH (or hydrazine) and N_2O_4 as an oxidiser (bipropellants) in two tanks; typically between 2,000 kPa and 3,500 Kpa, but in some cases up to 13,500 kPa.

Table 29.3.1 gives typical space-system pressure-vessel specification, Ref. [29-7], [29-8].

Table 29.3-1 - Typical space system pressure vessel specification

Length:	75 to 3000 mm
Diameter:	25 to 1150 mm
Volume:	0.2 to 820 litres
Operating Pressure:	20,000 to 67,000 kPa
Burst Safety Factor:	1.5 to 3
Helium Leak Rate:	1×10^{-4} to 1×10^{-8} cm^3/s
Cycle Life:	5 to 10000 MEOP cycles
Service Life:	1 to 30 years under load
Outgassing:	to ESA PSS-01-702 or NHB-8060.1B
Operating Temperature:	-70 to + 120°C
Humidity:	0 to 100%
Internal Cleanliness:	level 40 to MIL-STD-1246
Ambient Pressure:	sea level to space vacuum
Shape:	cylindrical, near spherical, spherical
Mountings:	straps, skirts, lugs, tabs, cradles, bosses

29.3.1.2 Space Shuttle MMU- manned manoeuvring unit

The MMU 'manned manoeuvring unit' for Space Shuttle astronauts uses a pair of 250 mm diameter, 790 mm long Kevlar 49™/seamless 6061-T62 aluminium cylinders to store nitrogen at 20,000 kPa for the MMU propulsion system, Ref. [29-8], [29-9]. This is an example of older Kevlar-based technology.

29.3.2 All-metal tanks

29.3.2.1 General

Tanks made of metal alloy only still have an important role in the containment of liquid propellants, e.g. monomethylhydrazine (MMH) as fuel and nitrogen tetroxide (N_2O_4) as oxidiser, Ref. [29-10], [29-11], [29-12]; especially for lower operating pressures, typically from 2,000 to 3,000 kPa. So, it is not sensible to change to composites for all designs, when thin-walled metal constructions offer optimum mass solutions.

29.3.2.2 Examples

Each Cluster satellite had six propellant tanks, Ref. [29-12]. These were TIG welded Ti-6Al-4V spheres, each 540 mm in diameter with a capacity of 98 litres. A 2,300 kPa MEOP over 120 pressure cycles applied on each tank, which weighed 6 kg empty.

All-metal tanks are used on Ariane 5 upper stages for placement of payloads in transfer orbits.

29.3.2.3 Material compatibility

The important effects considered in the selection of materials for fuel tanks are the compatibility between:

- Tankage material and the propellant, e.g. contamination with oxides leading to injector blockage or flow reduction.
- Propellant and the tank material, e.g. corrosion.

Any interaction between propellant and tank material is more important for long-duration missions, such as 15 years, than for launchers where storage and flight duration usually do not exceed one month.

Good compatibility has been demonstrated with titanium alloys and AISI 301/304 L stainless steels. Pickling and electropolishing is often used as a means of passivating the alloys. These considerations also apply to metallic liner materials for composite tanks.

29.3.3 Leak-before-burst concept

For composite pressure vessel designs with low safety factors, as used in space programmes, the concept of leak-before-burst is implemented; formalised by MIL-STD-1522A in 1984, Ref. [29-13].

Accumulated data suggests that the leak-before-burst (LBB) criterion can be established by the relationship of the ratio of liner to total membrane load and the overshoot of the load-transfer mechanism on the supporting overwrap, as the result of a suddenly applied load.

Since the dynamic overshoot can conservatively be assumed to equal the load being transferred, the load that the wrap can achieve is equal to the overwrap load prior to the crack plus twice the load in the liner.

This calculated load can be compared with the virgin burst load to define the threshold of burst. Figure 29.3.1 shows this relationship, Ref. [29-6].

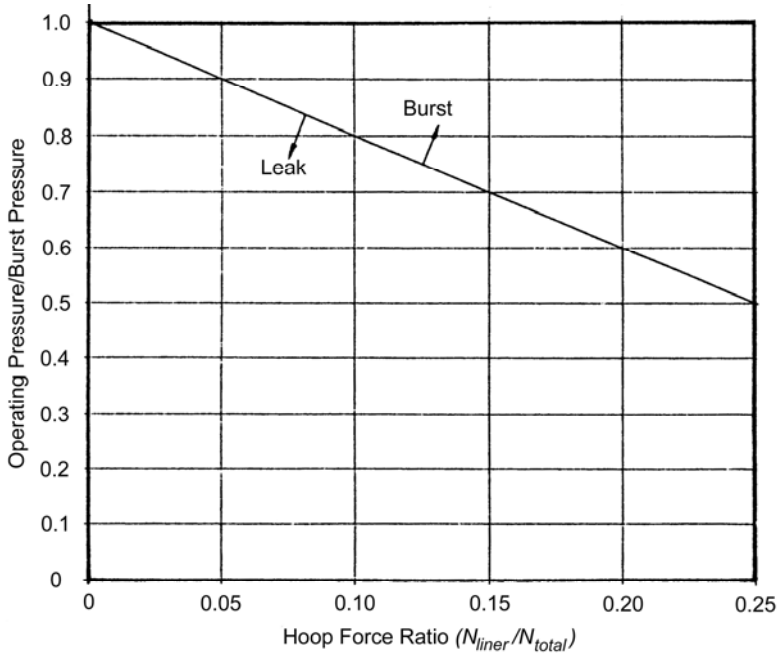

Figure 29.3-1 - Leak/burst threshold

There have been other suggestions about more complex relationships, including energy stored, gas impingement with the composite, and the rate of load reduction of gas versus liquid, Ref. [29-6]. However, evidence suggests that the threshold shown in Figure 29.3.1 is valid.

29.3.4 Seamless metal liners

29.3.4.1 General

The functions fulfilled by metal liners include:

- Prevent leakage and are impermeable to gaseous and liquid contents.
- Act as a mandrel for the overwrap.
- Provide the boss for a valve or fluid connection fittings.
- Share the pressure load during service.

The desired physical properties for liner assemblies, i.e. parent metal, weldments (if applicable), polar fittings (boss) and transition areas, include:

- High yield and ultimate strength-to-weight ratio for low tank mass.
- Adequate biaxial ductility (strain compatibility) up the fracture stress (strain) of the composite for controlled and repeatable failure level and mode.
- Resistance to fatigue for adequate life, when subjected to repetitive loading over the high compression-to-tension stress range associated with composite tanks.
- Constrictive liner buckling strength when compressed by overwrap.
- A liner material with a fracture toughness and thickness that, if failure occurs at the operating pressure, the mode is leakage without rupture.

Seamless aluminium liners are made by using dies of various sizes that progressively shape and draw a circular plate, as shown in Figure 29.3.2, Ref. [29-9].

A computer-controlled, spinning process closes the resulting open-ended shell to form the liner's neck and shoulder.

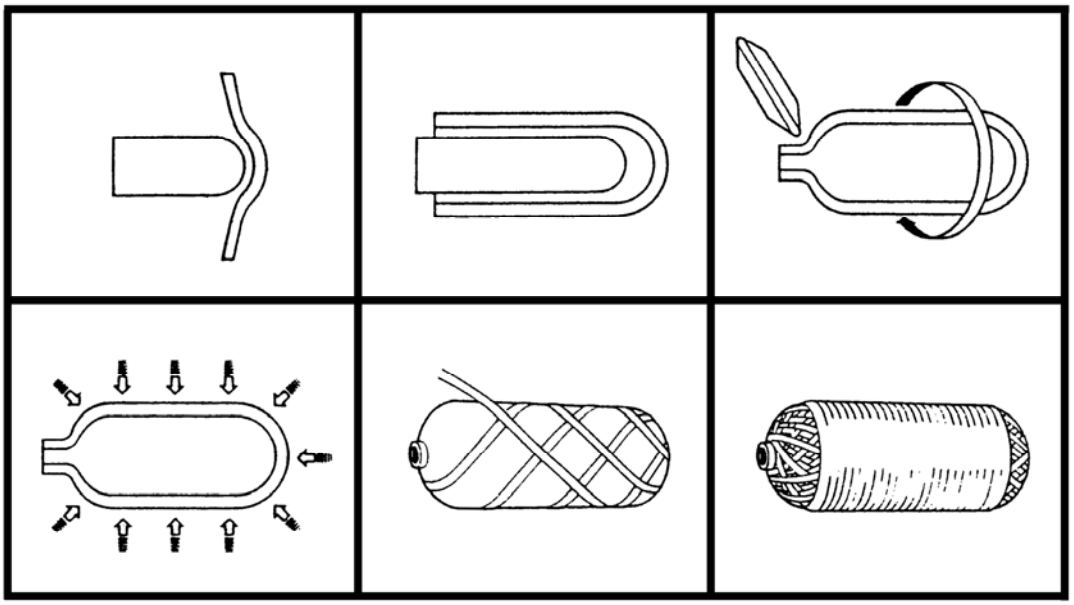

Figure 29.3-2 - Manufacture of seamless aluminium liners

Double-ported liners are fabricated by spin closing the two ends of extruded metal tubing. After heat treating, each liner is machined to trim the boss and to provide threads for a valve or fluid line connection.

Design of the inlet and outlet port area uses standard metal pressure vessel analyses because the composite does not reinforce this area. The port can also perform other load-bearing functions which are taken into account during the design. For example, the port is often used as the support structure for securing the vessel to the main body of a satellite. It is therefore subject to dynamic loads induced by the system, Ref. [29-8].

Liners often contribute very little toward carrying the pressure load, i.e. 10% to 15%. Increasing the capability of the overwrap is the most efficient means of increasing the pressure capacity for a specific tank volume. This can be achieved in a number of ways, including:

- Fibre selection,
- Increasing fibre volume fractions,
- Thickening the overwrap.

Aluminium alloy 6061-T62 is a preferred material for liners of pressure vessels in the USA. Chemical milling of seamless aluminium liners can be used to optimise wall thickness, typically in the 0.35 mm to 0.46 mm range, Ref. [29-9]. When winding onto very thin-walled liners, it can be necessary to pressurise the vessel during winding to avoid it collapsing; typically by 1 bar to 6 bar. The pressure can also be increased as winding progresses, Ref. [29-7].

The cyclic life of a tank is a function of the fatigue behaviour of the aluminium liner due to the growth of an initial crack or flaw, Ref. [29-6]. The rate of flaw growth is a function of the operating strain range. The number of cycles to produce a through crack is a function of the thickness of the liner for a given initial flaw depth.

Figure 29.3.3 shows typical curves describing these relationships, Ref. [29-6]. For space designs, qualification of a design typically requires that four times the defined operating cycles be demonstrated.

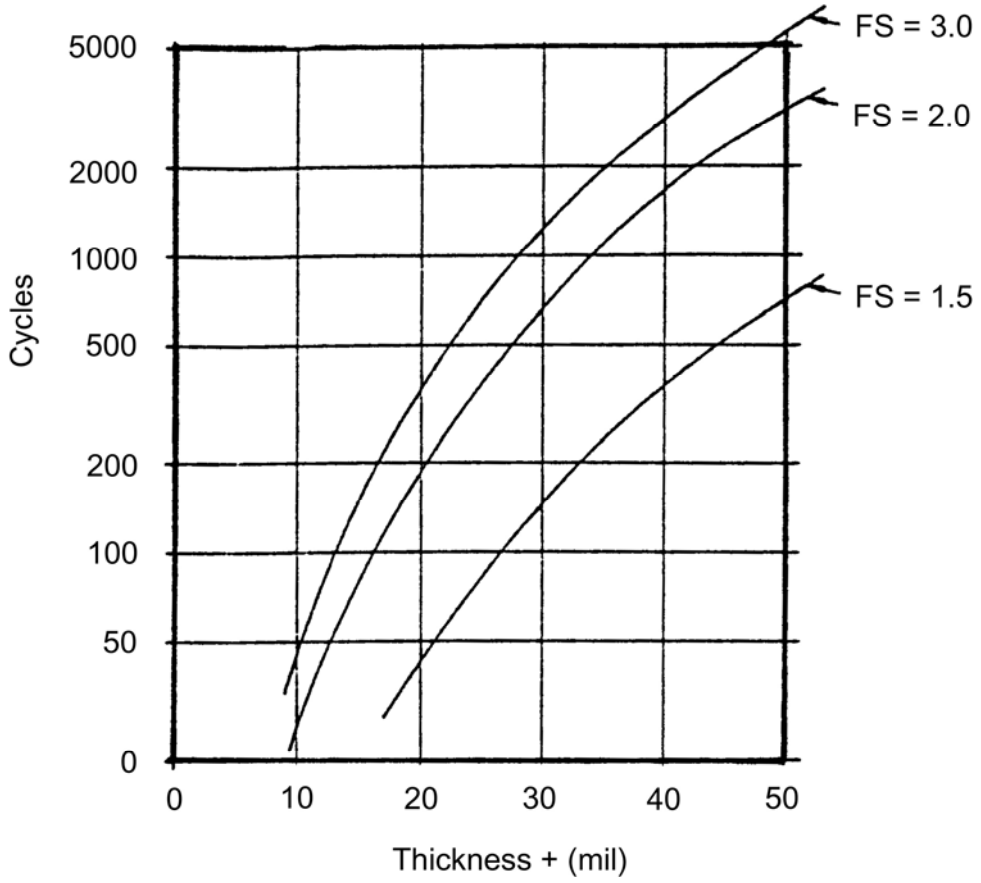

FS = factor of safety.

Figure 29.3-3 - Typical cyclic life of aluminium liners

29.3.4.2 Metal liner materials

The various liner materials that have been used in European space programmes include, Ref. [29-14]:

- Maraging steel (X2 NiCoMo 18 8 5): Used for large cylindrical vessels because of good cold formability and spin rolling characteristics. Vessel domes can be made by hydromechanical deep drawing followed by TIG welding.
- Stainless steel (X12 CrNi 177, AISI 301/X2 CrNi 1911, AISI 304L): Cryoforming (at -196°C) of this austenitic steel is a process for achieving high strength and fracture toughness.
- Titanium alloys (Ti-15V-3Cr-3Al-3Sn [β-alloy], Ti-6Al-4V): The β-alloy has attractions over the conventional TI-6Al-4V in that it has excellent formability enabling deep drawn tank shells to be made. Cost savings can be made over the traditional machined forging route and the β-alloy offers high strengths.
- Aluminium alloy 2219: Forgings are machined and flow-turned, followed by electron-beam welding.

[See also: Chapter 46 for aluminium alloys; Chapter 47 for titanium alloys]

Table 29.3.2 shows characteristics of some possible liner materials, Ref. [29-14].

Table 29.3-2 - Data on liner materials (material state in prestressed vessel)

	Yield Strength (MPa)	Tensile Strength (MPa)	Density (kg/m^3)	Tensile Modulus (GPa)	K_{IC} ($N/mm^{3/2}$)
X2NiCoMo 18 5 5	1750	1800	8000	190	3500
X12CrNi 17 7	1550	1640	7900	185	3500
Ti-Al6-4V	1000	1100	4430	108	2100
Al2219-T87	370	440	2820	72	1146
Ti-15V-3Cr-3Sn-Al	1100	1200	4730	101	3300

6061-T62, widely used in the USA, has a nominal yield stress of 276 MPa and ultimate tensile strength of 310 MPa.

29.3.5 Design considerations

Design and analysis procedures for filament-wound tanks with internal liners include consideration of, Ref. [29-9], [29-15]:

- Load and strain compatibility of the overwrapped filament-wound composite and internal liner. This is achieved by prestressing the two components which results in an extension of the elastic operating range of the liner, Ref. [29-14], as shown in Figure 29.3.4, Ref. [29-22].
- Effects of prestress into the plastic region of the metal shell.
- Prestress set-up between the liner and overwrapped composite shell during fabrication and proof testing.
- Compressive loads on the internal liner and possible need for bonding to keep the liner from buckling.
- Thermal contraction and expansion characteristics of the construction materials.
- Effects of cyclic and sustained loading on fatigue life and residual strength.

Special attention should be given in order to ensure that:

- Liner compressive stress at zero pressure after proof test does not exceed the bond strength of a thin metallic liner, or the constrictive overwrap buckling strength of a load-sharing liner.
- Design allowables are not exceeded by operational stresses in the liner or overwrap at operating pressure and temperature.
- The required burst factor of safety is provided prior to exceeding liner biaxial tension ductility capability.
- Operating stress in the liner is chosen to enable the required number of pressure cycles (safe life).
- Fibre tensile prestress and operating stress are selected according to fatigue life and sustained loading (stress rupture) requirements.
- Fibre failure or a surpassing of the liner's biaxial tension ductility capability is avoided until the required burst factor of safety has been achieved.

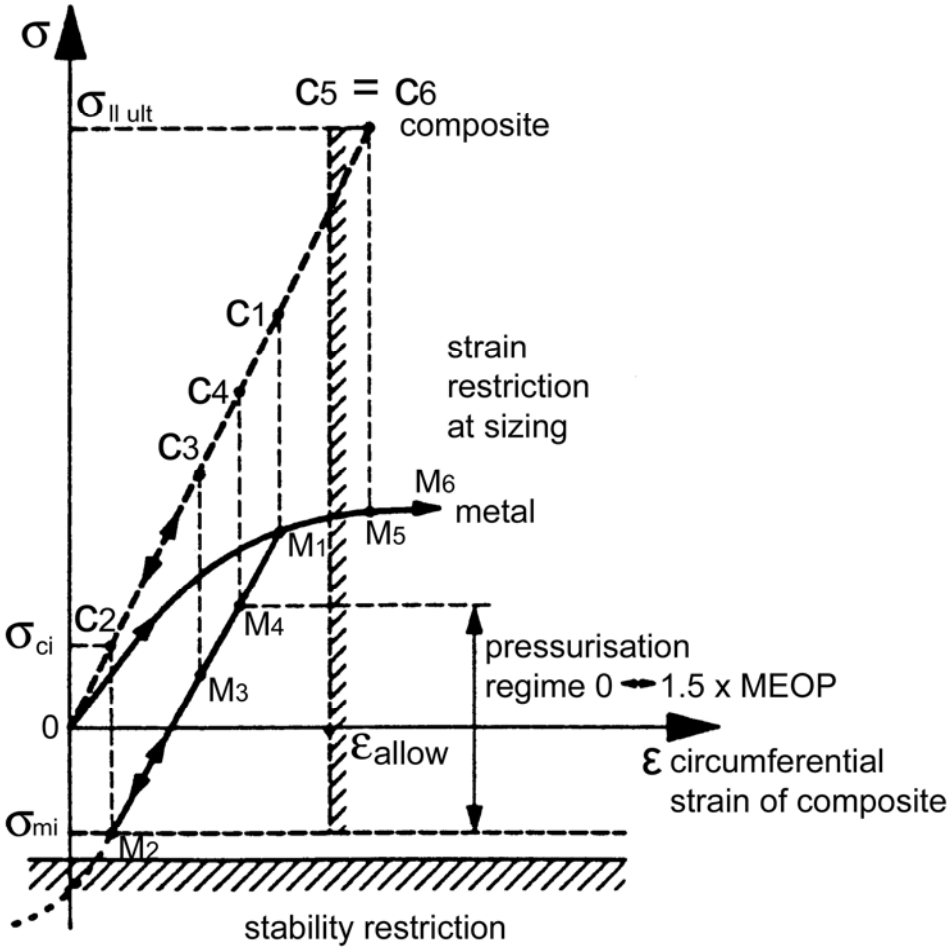

Key:		
	0 - M1 - M2	sizing cycle
	0 - C1 - C2	sizing cycle
	C2, M2	equilibrium state after sizing
	C3, M3	state at MEOP
	C4, M4	state at proof pressure
	C5, M5	state at design burst pressure
	C6, M6	ultimate stress/strain values

Figure 29.3-4 - Stress-strain curve for prestressed composite vessel

The very high-strength carbon fibres have higher modulus of elasticity than glass or Kevlar™ 49 fibres. This enables better matching of stress-strain relationships between the composite and the metal liner, either aluminium or titanium, to the point where thinner liners can be used.

A barrier cloth, typically a glass-fibre cloth, scrim or mat, is used to separate the carbon fibres and aluminium because contact between them poses a galvanic corrosion potential. Barrier layers are combined with film adhesives to provide a bond between liner and composite. This bond is critical for distributing uniformly the plastic strains in the liner when small variations in liner thickness occur.

29.3.6 Pressure vessel performance factor

29.3.6.1 General

The performance factor used to determine pressure vessel design efficiency is:

$$P_b V / W \qquad [29.3\text{-}1]$$

Where:

P_b = *burst pressure,*

V = *internal vessel volume*

W = *mass of vessel.*

The shape of the pressure vessel influences the performance factor.

Longer and smaller-diameter composite vessels are lighter than spherical vessels for a given burst pressure and volume. The reasons for this are, Ref. [29-8]:

- The filament wrap carries pressure load more efficiently in the hoop direction (circumferentially around the cylinder) than in the helical direction (end-to-end around the domed ends of the pressure vessel). Consequently, increasing the cylinder surface area relative to the dome surface area results in a lighter vessel. The highest performance factors can be achieved for vessels with *L*/*D* ratios greater than 2.0.
- The thinnest part of the liner is the cylindrical portion of the pressure vessel. The liner thickness gradually increases from the dome-to-cylinder junction until it reaches maximum thickness at the port boss. Increasing length, rather than diameter, to achieve the desired volume results in lower mass because the inefficient domes become a smaller proportion of the vessel.

These factors also assist in explaining why wholly metal spherical vessels are still manufactured for lower pressure applications to fit in a defined space, and are unlikely to be superseded by composite constructions as little or no mass reduction can occur.

Table 29.3.3 provides examples of tanks made for space applications by one manufacturer where comparisons can be made between dimensions, performance and mass, Ref. [29-7], [29-8].

Table 29.3-3 - Performance of pressure vessels made by SCI, (USA), for satellite use

Length (mm)	Diameter (mm)	Volume, V (litres)	Operating Pressure (bar)	Ave. Burst Pressure, P_b (bar)	Operating Cycles	Mass, W (kg)	P_bV/W (km)	Composite
317.5	33	0.23	667	1075	>50	0.1	25.2	T1000/Epoxy
208	114	1.21	667	1045	>50	0.5	25.8	T1000/Epoxy
467	168	6.88	453	727	>100	2.7	18.9	T1000/Epoxy
566	168	8.21	387	737	>100	2.7	22.9	T1000/Epoxy
353	360	20.1	400	823	>100	8.2	20.6	HT46-9A/Ep
635	335	43.43	287	453	>50	6.8	29.5	T1000/Epoxy
673	419	67.27	300	460	>100	10.5	30.1	T1000/Epoxy
607	500	77.18	30.9	107	>100	9.5	8.9	T1000/Epoxy

Liner material: 6061-T62

The analysis of pressure vessel performance with respect to stresses in the laminate is not yet fully clarified. A netting analysis can be applied to obtain the stresses in individual plies. It has been shown that either fibre stress or strain can be used as a failure criterion with no correction needed for transverse effects, Ref. [29-16].

29.3.6.2 Stress-rupture lifetimes

As the design life of pressure vessels is extended, e.g. to 30 years in the case of space stations, the issue of stress rupture needs to be addressed when the applied safety factor is 2.0.

[See also: Figure 29.2.1 for the stress rupture behaviour of different fibres]

Initial Weibull analysis, Ref. [29-17], suggests that at 50% of design ultimate loading of carbon/epoxy CFRP has a 99.99% probability of surviving stress rupture over 30 years, compared with 99.8% for Kevlar/epoxy and 22% for glass/epoxy.

Other probabilities that have been calculated are shown in Table 29.3.4., Ref. [29-17].

Table 29.3-4 - Stress-rupture lifetime probabilities for various fibres

Ultimate Burst Strength (%)	Probability (life > 30 years)		
	Glass, %	Kevlar, %	Carbon, %
90	~0	~0	24
80	~0	~0	90
70	~0	~0	99.2
60	~0	91	99.9
50	22	99.8	99.99
40	97	99.998	99.999

29.3.7 Intelsat VII pressurant tanks

The INTELSAT VII satellite has an integrated bipropellant propulsion subsystem. Pressurisation for the fuel and oxidiser tanks is provided by helium contained in two spherical pressurant tanks, each 457 mm in diameter, Ref. [29-18].

In 1990, a metal-lined composite version was produced by Brunswick Corporation to meet the specification given in Table 29.3.5, Ref. [29-18].

Table 29.3-5 - Performance requirements for INTELSAT VII pressurant tank

Minimum Volume	49.1 litres
Maximum Mass (unfilled)	9.07 kg
Operating Pressure	267 bar
Proof Pressure	347 bar
Burst Pressure	400 bar
Pressurised Life	1 year
Cycle Life	88
Storage Life	5 years
Helium Leak Rate (sccs)	$<1.0 \times 10^{-6}$

The features of the tank constructed were:

- Liner:
  - Two 1.11 mm thick hemispherical shells joined by an equatorial girth weld; by gas tungsten arc welding.
  - 6061-T6 alloy.
- Composite:
  - 6.1 mm thick in the equatorial region,
  - Amoco T-40 carbon fibre roving,
- Resin:
  - Brunswick Lincoln Resin Formulation LRF 0205, a high performance amine-cured epoxy resin, cured at 150°C.

The mass contributions are given in Table 29.3.6, Ref. [29-18].

Table 29.3-6 - Tank mass summary

Composite:	Fibre Resin Total Composite	3.68 1.83 5.51 kg
Liner:	Membrane Weld Build-up Bosses (domes) Tube (cylindical part) Total Liner	1.99 0.18 1.07 0.03 3.27 kg
Other:	Scrim Cloth Barrier Coat Total Other	0.19 0.11 0.30 kg
Total Maximum Mass Budgeted **Average of six flight tanks**		9.08 kg 8.66 kg

Figure 29.3.5 provides an insight into the strain behaviour of constituents of the tank during pressurisation, Ref. [29-18].

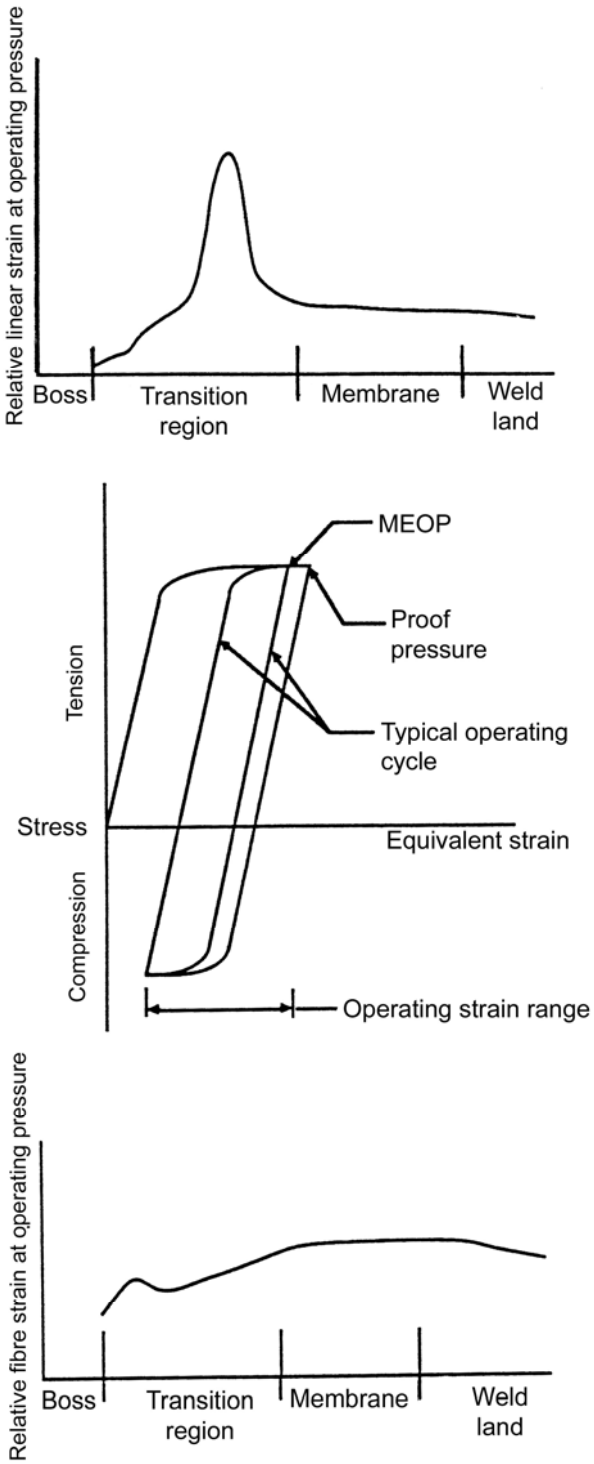

Figure 29.3-5 - Strain distributions within INTELSAT VII pressurant tanks

29.3.8 Aerospatiale pressurant tanks

Aerospatiale developed a CFRP overwrapped titanium liner construction to replace a previous design using Kevlar reinforcement, Ref. [29-19].

The baseline performance of K49/Ti vessels came from TVSAT/TDF1 and EUROSTAR. The technology was demonstrated on two spherical tanks of differing capacities. The characteristics of the two tanks are given in Table 29.3.7, Ref. [29-19].

Table 29.3-7 - Characteristics of Aerospatiale CFRP/Ti spherical pressurant vessels

	35 Litre Tank	51 Litre Tank
Operating Pressure:	276 bar (extended to 300 bar)	276 bar
Safety Factors:	1.5 on proof (414 bar) 2.0 on minimum burst (552 bar)	1.3 on proof (359 bar) 1.5 on minimum burst (414 bar)
Maximum Burst:	640 bar	453 bar
Mass:	7.2 kg	7.8 kg
Life (SF = 4):	250 cycles at operating pressure	250 cycles at operating pressure
Liner - Ti-6Al-4V	0.9 mm equatorial	0.9 mm equatorial
Composite - Epoxy	IM6 / B4-13 9 layers - 5.2 mm	IM6 / B4-13 7 layers - 4.0 mm
Mass of Equivalent K49/Ti Constructions	7.9 kg for operation at 250 bar	11.2 kg for operation at 276 bar

Features of the development of the tanks include:

- A 100°C cure B4-13 epoxy resin was developed by Aerospatiale for the application.
- A test and qualification programme with cyclic pressures and temperatures, Ref. [29-19], confirmed the anticipated performance of these designs.
- The maximum achieved burst pressures exceeded the initial burst requirements by 10% to 15%, so enabling the operating pressure to be increased from 276 bar to 300 bar for the 35 litre tank with the higher safety factors applied.
- Aerospatiale concluded that CFRP/Ti tanks can operate over a wider temperature range than Kevlar 49/Ti equivalents, i.e. 60°C to +70°C compared with -30°C to +50°C.

The 35 litre design achieved a performance factor (PbV/W) of 32.2 km and the 51 litre design a value of 30.2 km.

29.4 Pressure vessels - Characteristics

29.4.1 General

Information is presented from the development of the MAGE series of solid rocket motors and includes:

- Requirements, [See: 29.4].
- Safety factors, [See: 29.5].
- Design concept, [See: 29.6].
- Material selection, [See: 29.7].
- Dimensioning theories, [See: 29.8].
- Solid propellant motor cases, [See: 29.9].

It is provided as an overview to designing pressure vessels in general.

29.4.2 Dimension restrictions

To achieve high efficiency, the weight of the pressure vessel and additional structural parts should be kept to a minimum. Restrictions for the layout are also the:

- Given maximum possible dimensions,
- Desired inner volume, and
- Interfaces to other structures.

For the first layout of the pressure vessel, all these requirements can often be reduced to the major points:

- MEOP: maximum expected operational pressure,
- Weight,
- Eigenfrequencies,
- Maximum and minimum temperature,
- Dimensions.

29.4.3 Specified load cases

The specification of the load cases for the in-service time of the structure includes:

- MEOP: maximum expected operational pressure,
- Number of expected load pressure cycles,
- Dynamic load cases:
  - required minimum eigenfrequencies,

  - accelerations,
  - sinusoidal vibrations,
  - random vibrations,
  - spin-up.
- Thermal load cases,
- Static load cases:
  - steady state accelerations,
  - steady spin rates.

29.4.4 Loads during manufacture

Important factors for the layout are the loads during manufacture, such as:

- Curing cycle temperature,
- Post-manufacture machining of interfaces, if necessary.

29.4.5 Environmental conditions

The environmental conditions to be considered in the layout are determined by the intended use of the pressure vessel. These influence the general design concept. Conditions are:

- Temperature,
- Humidity,
- Contents of the vessel, which determines the type of liner.

Other items to be considered are:

- Impact of particles in space, and
- Effect of tools during manufacturing.

29.5 Pressure vessels - Safety factors

29.5.1 General

When requirements, [See: 29.4] are transformed into design loads, safety factors are always considered. These factors are often:

- Specified, or
- Taken from experience, or
- From standards, e.g. MIL 1522A.

29.5.2 Proposed safety factors

Some proposed values are given in Table 29.5.1 for a case with MEOP = 60 bar. These values can be:

- Lower for low-pressure applications, and
- Higher for high-pressure application and manned flights.

Table 29.5-1 - Pressure vessels: Proposed safety factors for space applications

Safety Factors	Unmanned	HP/Manned
For vessels, based on MEOP:		
Proof pressure level	1.05	1.5
Burst pressure level	1.30	2.0
For joint structure, metallic parts based on service loads:		
Yield strength (metals)	1.20	-
Ultimate strength	1.50	-
Stability limit	1.30	-
Additional factors for junctions	1.50	-

29.5.3 Composite material failure mode

Composite materials have two different failure modes, matrix failure and fibre failure. The permissible type of failure is defined for each structural part.

29.5.4 Service life

The total structure has to be designed in such a way that its behaviour does not change under any load conditions encountered during its service life.

29.5.5 Damage tolerance

Damage tolerances should be considered in the design, especially in the case of manned flight applications.

29.5.6 Reliability

The reliability of the structure is proved by calculation and supported by a series of tests.

29.6 Pressure vessels - Design concepts

29.6.1 Basic concepts

29.6.1.1 Vessel type and application

The vessels can be grouped as:

- Spherical vessels: These are chosen for high-pressure applications when relatively small dimensions are needed. The nature of the stored gas or fluid normally dictates that vessels have a liner.
- Isotensoid-shaped vessels: For most pressure vessels of larger dimensions, a configuration comprising two isotensoid domes and a cylindrical part is chosen. They are used for:
  - Low-pressures, e.g. Ariane 4 water tank for first stage, one isotensoid, piggy-backed to propulsion tank.
  - Medium-pressure, e.g. solid-propellant rocket motors, such as for MAGE, IRIS and EBM family.
  - High-pressure, e.g. oxygen bottles.

29.6.1.2 Fixing and interfaces

Pressure vessels are always joined to the surrounding structures. Polar openings, either single or multiple, are used for the inlet and outlet of the stored matter or, in the case of motor cases, for the igniter. Consequently, fittings need to be designed to provide the interface between the vessel and, say, piping or a nozzle.

29.6.1.3 Use of composite materials

Composite materials can never be pressure-tight, so every vessel for high-pressure gases constructed from composite materials need a liner.

29.6.1.4 Liners

Liners can consist of various materials, for example:

- Low-pressure vessels: It is sufficient to protect the inner surface by varnishing.
- High-pressure vessels: The liner has additional functions. It has to protect the composite material against the possibly aggressive contents and can provide a load-carrying function.

The liner is often designed to ensure a 'leak-before-burst' behaviour, with gaseous or liquid contents, but not for solid rocket motors. Where high-velocity debris is present, such as for orbiting structures, this has considerable significance.

For medium-pressure applications, such as solid rocket motors, the liner has a number of functions:

- Leak tightness,
- Protection against high temperatures,
- Mechanical interface between case material and propellant, assuring adhesion between case and propellant
- Compensation of differing thermal expansions between case and propellant,

- Provision of a ballistic function in certain areas, to restrict the effects of burning propellant.

These aspects restrict the choice of liner materials.

29.6.2 Isotensoid-shaped pressure vessels

A solution for the design of a pressure vessel is a configuration having:

- two geodesically (or planar) wound domes, and
- a cylindrical part, for which net theory is used.

Net theory means that the single fibres are treated for load-carrying only in the fibre direction. There are no stresses normal to the fibre direction.

This type of construction is typified by the MAGE series of solid rocket motors, [See also: 29.9]. In addition to the composite vessel, structural parts for the load-transfer to the main structure and two fittings are also necessary; as shown in Figure 29.6.1, Ref. [29-54].

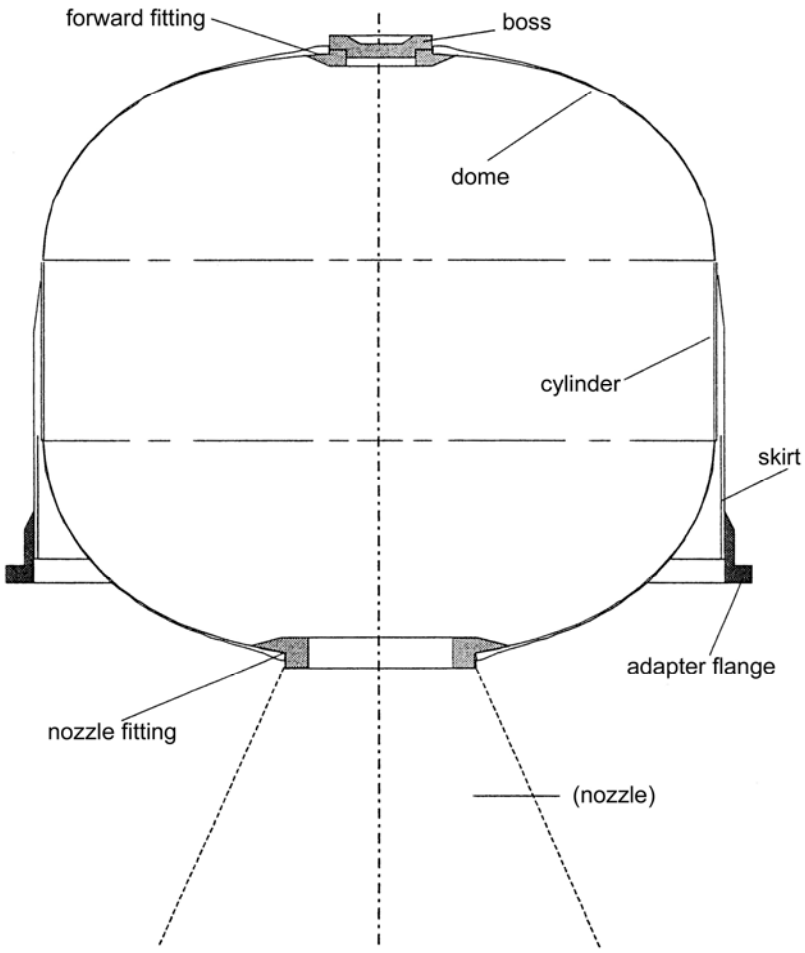

Figure 29.6-1 - Pressure vessels: Typical components of a solid propellant motor case as represented by MAGE

For an optimum solution, each dome is dimensioned in such a way that at the specified burst-pressure level the strength of the fibre material is reached simultaneously in all single fibres at all locations. This kind of membrane shell is called isotensoid.

The vessel is 'wet-wound' using either rovings or unidirectional prepregs. Consequently, it is necessary to design the inner contour to prevent a possible slippage of the material on the mandrel during winding.

In spite of low friction, this can be achieved if the fibres represent the shortest distance between two points on the membrane shell. The path of the fibres from the equator to the polar opening is a geodesic line, as shown in Figure 29.6.2. The equation for this line is Clairaut's Law:

$$r \sin \alpha = e \qquad [29.6\text{-}1]$$

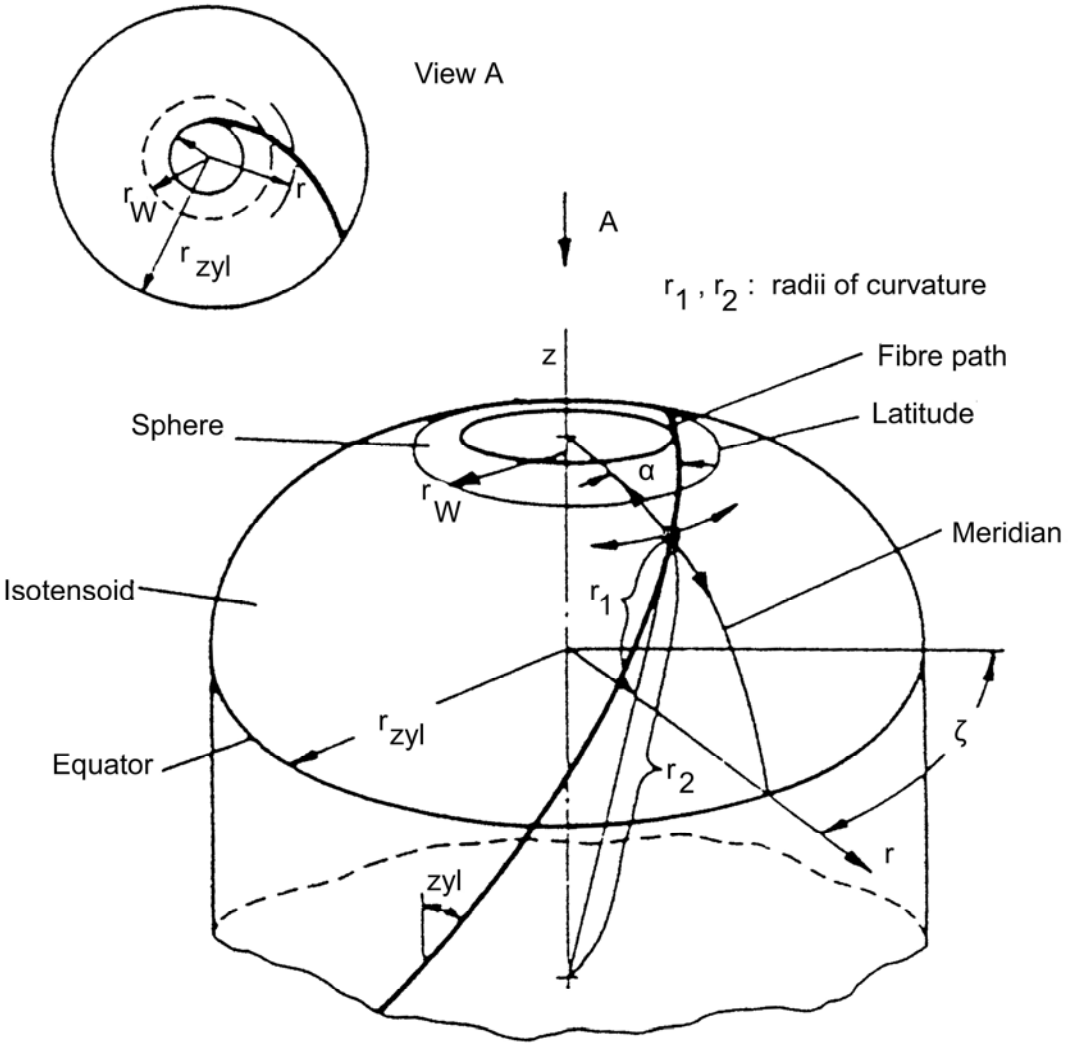

Figure 29.6-2 - Pressure vessels: Geodetic winding

These theoretical assumptions are not always applicable when:

- At the equator of the vessel, the components dome, cylindrical part and joint structure are connected. These parts have different stiffnesses in all directions. Strain compatibility has to be guaranteed in this area. The consequence for the dome is that the membrane theory is no longer valid. Bending moments and transverse shear effects have to be carried by the isotensoid dome.
- Normally the two polar openings have different diameters. Consequently, the theoretically calculated functions of the winding angle and the wall thickness over the radius cannot be obtained during manufacture. The difference between theory and practice is dependent on the axial length of the cylindrical part. Pressure vessels with a cylinder that is relatively long with respect to the diameter enable the fibres to be shifted during the winding process in order to reduce this effect.

The options for coping with the deviations from theory in the layout phase are:

- The contour of the dome and consequently the functions of the winding angle and the thickness can be adapted. Additional calculation work is necessary to obtain a transition contour between the equator and the undisturbed isotensoid membrane dome.
- The additional loads can be covered by layout factors based on experience. Although easier, such a design does not provide the minimum weight solution. Layout factors used need to be justified and, if necessary, corrected after the first prototype tests.

It is difficult to give general advice on how to choose layout factors. They are dependent on the case parameters:

- inner radius, r_i
- polar openings, e_1, e_2
- cylindrical length, l_{cyl}
- MEOP requested, p_i

To give an idea of the factors, K_D, for the dimensioning of the domes and K_C for the dimensioning of the hoop layers in the cylindrical part, examples, both for MEOP p = 55 bar, are given in Table 29.6.1. These values have been proven by tests.

Table 29.6-1 - Isotensoid pressure vessels: Example layout factors

Example	r_i	e_1/ e_2	l_{cyl}	K_{Dome}	K_{Cyl}
1	370	0.35	350	1.2	1.1
2	640	0.28	170	1.25	1.2

[See: Figure 29.6.2 and Figure 29.8.1 for definition of these parameters]

29.6.3 Joint structures

The concept and the type of the material selected for the skirt structure is dependent on the overall configuration, as shown in Figure 29.6.3.

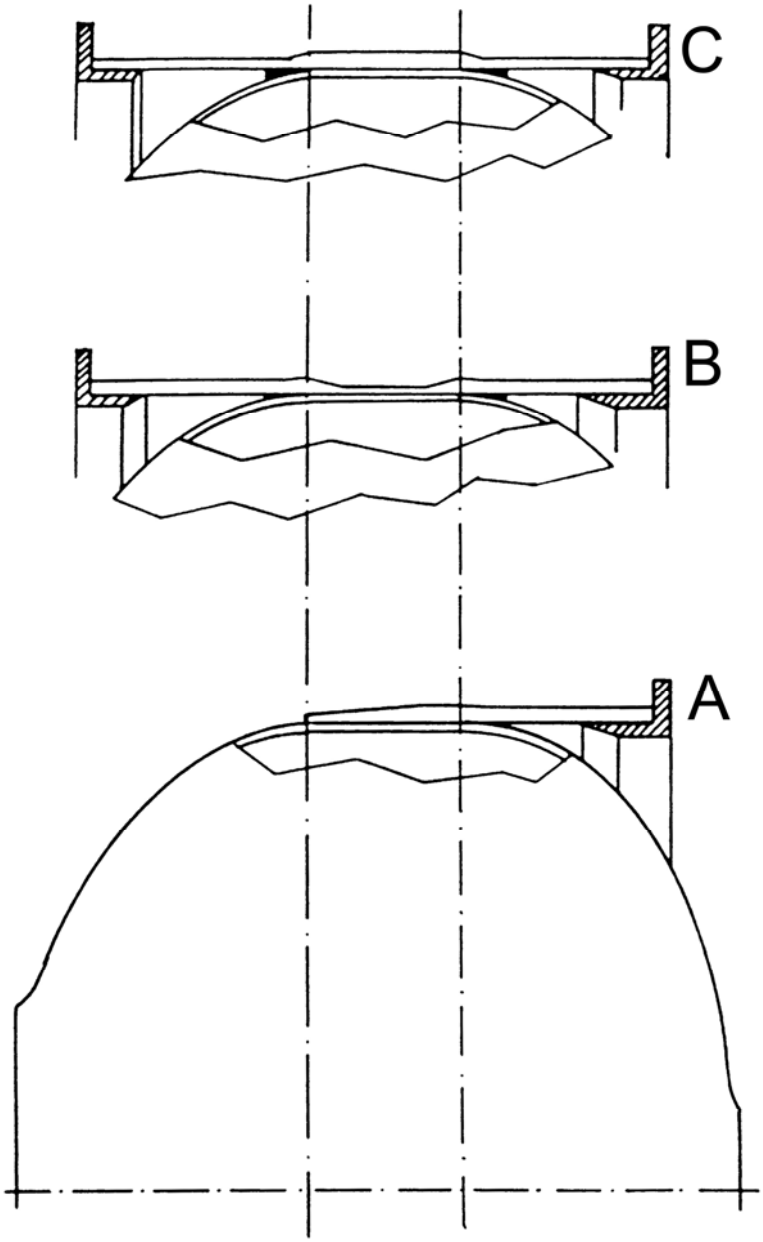

Key:

a. Skirt on one side.
b. Skirt on two sides, without load transfer from flange to flange.
c. Skirt on two sides, with load transfer from flange to flange.

Figure 29.6-3 - Pressure vessels: Configurations of skirt structures

For vessels having:

- One skirt: All layers except the necessary hoop layers are manufactured using cloth material with lay-up angles, as shown in Figure 29.6.4 and in Table 29.6.2.
- Two separated skirts: cloth layers also have to be chosen.

- Two skirts (load transfer): Transmit loads from flange to flange. The layers carrying the axial and lateral loads can be wound rovings. Because of the higher fibre volume content, this reduces the weight. In this case, the 0° and ±45° layers can be replaced by ±α layers.

To reduce peak stresses in the area of the equator, an elastomer interlayer can be considered, [See: Figure 29.6.4]. In cases where connections to the main structure are at the fittings via brackets, mainly carbon cloth layers are used.

Table 29.6-2 - Pressure vessels: Function of the different layers, as on MAGE construction

Material	Type	Winding Angle	Function of the Layer
Aramid	Roving	±α	Inner pressure
Aramid	Roving	90°	Inner pressure circumferential stiffness
Aramid	Cloth	±45°	Shear stiffness and loading
Carbon	Cloth	0°	Axial stiffness and loading
Glass	Cloth	0°/90°	Protection, load transfer
Glass	Mat	0°/90°	Bonding agent for elastomer
Adiprene	Elastomer	-	Peak stress reduction

[See: Figure 29.6.4]

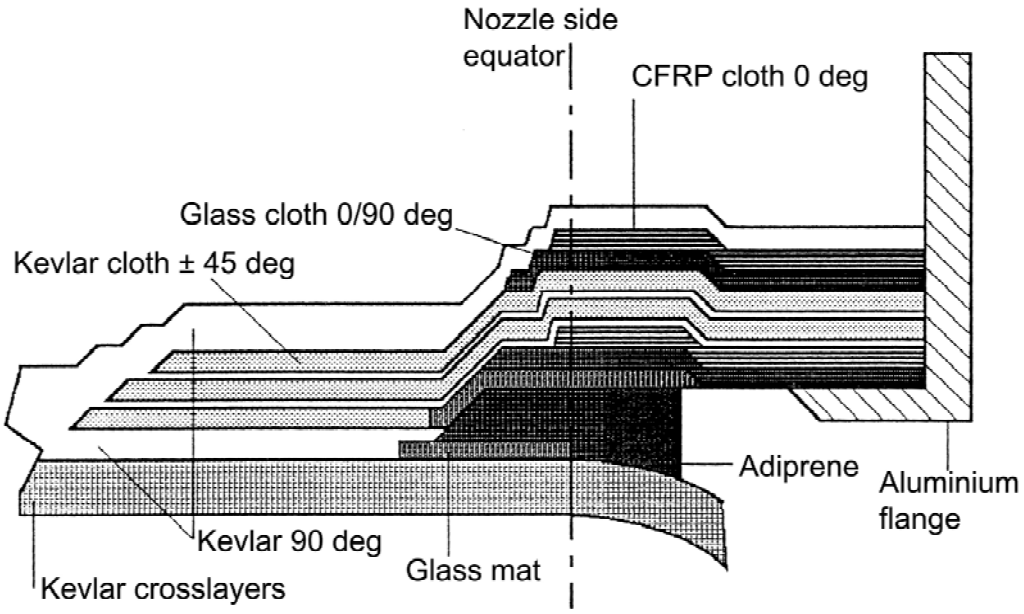

Figure 29.6-4 - Pressure vessels: Typical lay-up of a skirt, as represented by MAGE

29.7 Pressure vessels - Material selection

29.7.1 Basic rules

The important considerations are:

- Material quality: The evaluation of all materials selected for the complete vessel structure needs to be restricted to approved materials for aerospace applications which are produced according to production standards with quality controlled and guaranteed material data, [See: ECSS-Q-ST-70; ECSS-Q-70-71].
- Material data: For the layout, it is necessary to take realistic material data by using:
  - guaranteed values from the suppliers (guaranteed only for incoming).
  - Design allowable 'A-values' obtained from proper material tests.

Owing to different scatter in competing pressure vessel materials, the allowable values can be considerably different from typical values.

For the comparison of test results with stress analysis, material data values are taken from the batches of the material used.

29.7.2 Composite materials for pressure vessels

29.7.2.1 General

To select the case material, criteria to be considered are:

- Minimum specific weight,
- High elongation,
- High strength,
- Good workability,
- Damage control.

29.7.2.2 Selection

The material selection represents a compromise between theoretical data and the results achieved during material, component and structure tests. Factors to be considered include:

- For isotensoid-shaped pressure vessels with different polar openings, aramid fibres in an epoxy matrix have shown satisfactory behaviour.
- For mainly cylindrical vessels, very high-strength, intermediate modulus carbon fibres (IM-VHS) are now preferred to high-tensile (HT) carbon fibres, Kevlar™ 49 or glass fibres. This is because they give higher structural efficiency in this relatively simple design and lead to higher confidence in the design allowables.

29.7.2.3 Properties

Figure 29.7.1 shows typical material data for the selected fibres.

These data are typical values and not design allowables.

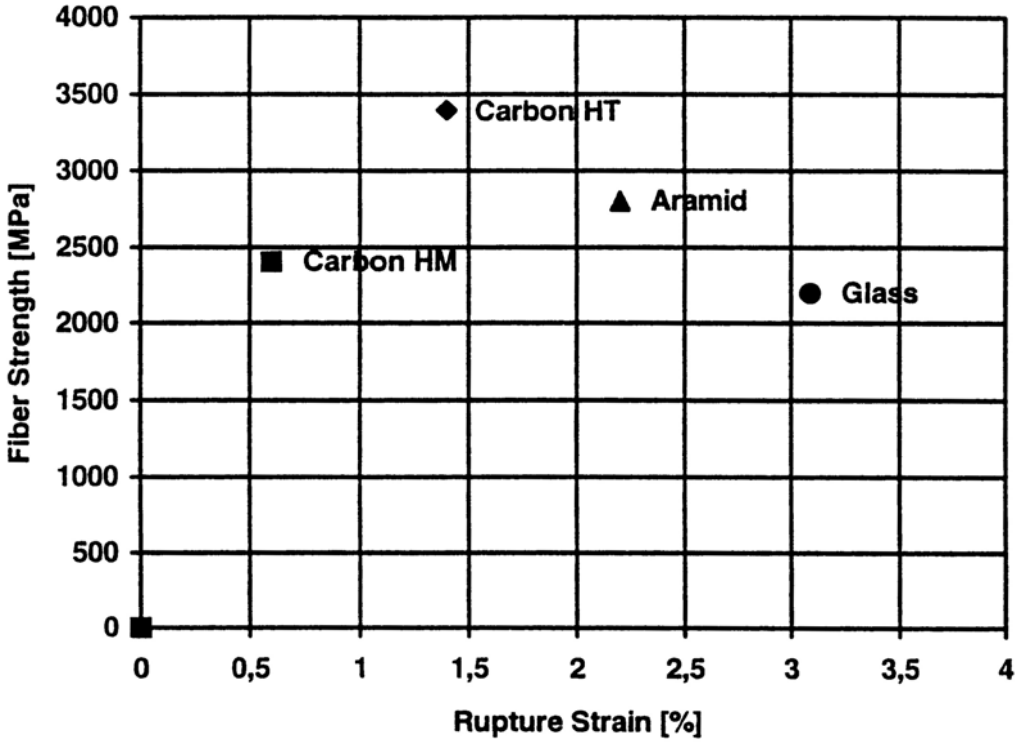

Material	Fibre Tensile Modulus (GPa)	Fibre Tensile Strength (MPa)	Fibre Tensile Strain to Failure (%)	Specific Modulus (10^5 m^2 s^{-2})
Carbon (IM-VHS)	294	5490	1.9	162.4
Carbon (HT)	230	3400	1.4	135
Carbon (HM)	390	2400	0.6	200
Aramid	128	2800	2.2	90
E-glass	70	2200	3.1	28

These are not Allowables

Figure 29.7-1 - Pressure vessels: Some typical values for fibres

29.7.2.4 Testing for allowable

The strength allowables cannot be taken from strand fibre tests due to roving crossings and bending. Experience shows that these values are never reached in the burst tests of pressure vessels.

It is therefore more appropriate to use a filament wound ring, machined from a cylinder, as providing a more accurate measure of the composite strength in relation to the method of manufacture and the adverse effects of strand tests.

For aramid fibres, the National Ordnance Laboratory (NOL) ring tests gave strength values which are about 30% lower than the values achieved in strand fibre tests, Ref. [29-1]. These values are realistic for pressure vessel layout. The NOL rings can be tested according to the ASTM D 2290 standard.

[See also: Chapter 3 for materials data; Chapter 7 for test methods]

29.7.2.5 Manufacturing

A general statement on the workability, e.g. problems during handling and processing, cannot be made. This is more or less determined by company expertise and experience.

29.7.3 Materials for the joint structure

29.7.3.1 Composite materials

Connection between the pressure vessel and other structures can be achieved by a cylindrical structure, often called the 'skirt', [See: Figure 29.6.3]. The skirt is also made from composite materials.

The criteria for dimensioning the skirt are:

- Minimum weight,
- Stiffness to achieve the stated eigenfrequencies,
- Strength to transmit the nozzle thrust and the dynamic load,
- Elongation compatibility with the pressure vessel, and
- Good workability.

The main criteria are the necessary axial and lateral stiffness and minimum weight. Therefore, mainly carbon fibre materials are used for this application. To ensure elongation compatibility, all hoop layers are of the same material as that of the pressure vessel.

Depending on the configuration of the skirt, either wound rovings or cloth materials are used; preferably wound rovings because efficiency (weight, possible stacking sequence) is better than for cloth materials.

29.7.3.2 Metallic materials

Metallic fittings (bosses) are needed to connect the pressure vessel to other structures at the polar openings. The joint structure is also connected to other structures by a metallic flange. For these applications, high-strength aluminium alloy or steel is used.

In making a selection, it is important to consider the:

- Loads acting on these parts,
- Mass, and
- Availability of the raw material.

29.7.3.3 Elastomers

Elastomer materials are used:

- to reduce shear stress peaks in the area of load-transfer between the pressure vessel and the joint structure, and
- for the connection of the fittings to the composite vessel.

Some typical elastomer property data, at room temperature, are shown in Table 29.7.1.

[See: 75.3 for elastomer materials]

Table 29.7-1 - Pressure vessels: Typical elastomer property data, at RT

Property	Typical Value
Shear modulus, G	15 N/mm^2
Tensile strength, σ_B	35 N/mm^2
Strain to failure, ε_B	400 %
Poisson's ratio, ν	0.48
Shear strength, τ_B	16 N/mm^2

29.8 Pressure vessels - Dimensioning theories

29.8.1 General

The theories presented are those used for the development of the MAGE series of solid rocket motors led by MAN Technologie AG.

Algorithms are given for the layout of the structure. These are established and proven by actual vessel projects, such as the MAGE motor case. Theoretical background is also given, including that taken from literature.

For the initial design phase, approximations are proposed.

At the end of this initial design phase, the layout is frozen and subsequent analysis uses finite element methods.

29.8.2 Analytical notation

A_F	cross section of all fibres at the equator
A_R	single roving cross section
C_A	axial stiffness
C_S	lateral stiffness
e	polar opening
f	eigenfrequency
h	height
K_D, K_Z	layout factors for dome and composite parts
l	length
m	mass
n_{SPF}	quantity of simultaneously processed fibres
n_{min}	minimum quantity of windings
p	inner pressure
r	radius, radial co-ordinate axis
R	radius of spherical segment
t	wall thickness
t_f	wall thickness of fibres: $t_f = t\phi$
V	volume
z	axial co-ordinate axis
z_K	axial co-ordinate of spherical shell
α	winding angle of pressure vessel cross layers
ϕ	fibre volume content
σ_{FB}	fibre strength
( )'	d/dz

Subscripts:

a	outer contour
F	fitting
Fl	flange
i	inner contour
cyl	cylindrical part
w	inflection point
TOT	total
s	joint structure, skirt
α	cross-layers
0	equator
90	hoop-layers

29.8.3 Isotensoid-shaped pressure vessels

29.8.3.1 General

Figure 29.8.1 defines the variables used, Ref. [29-54].

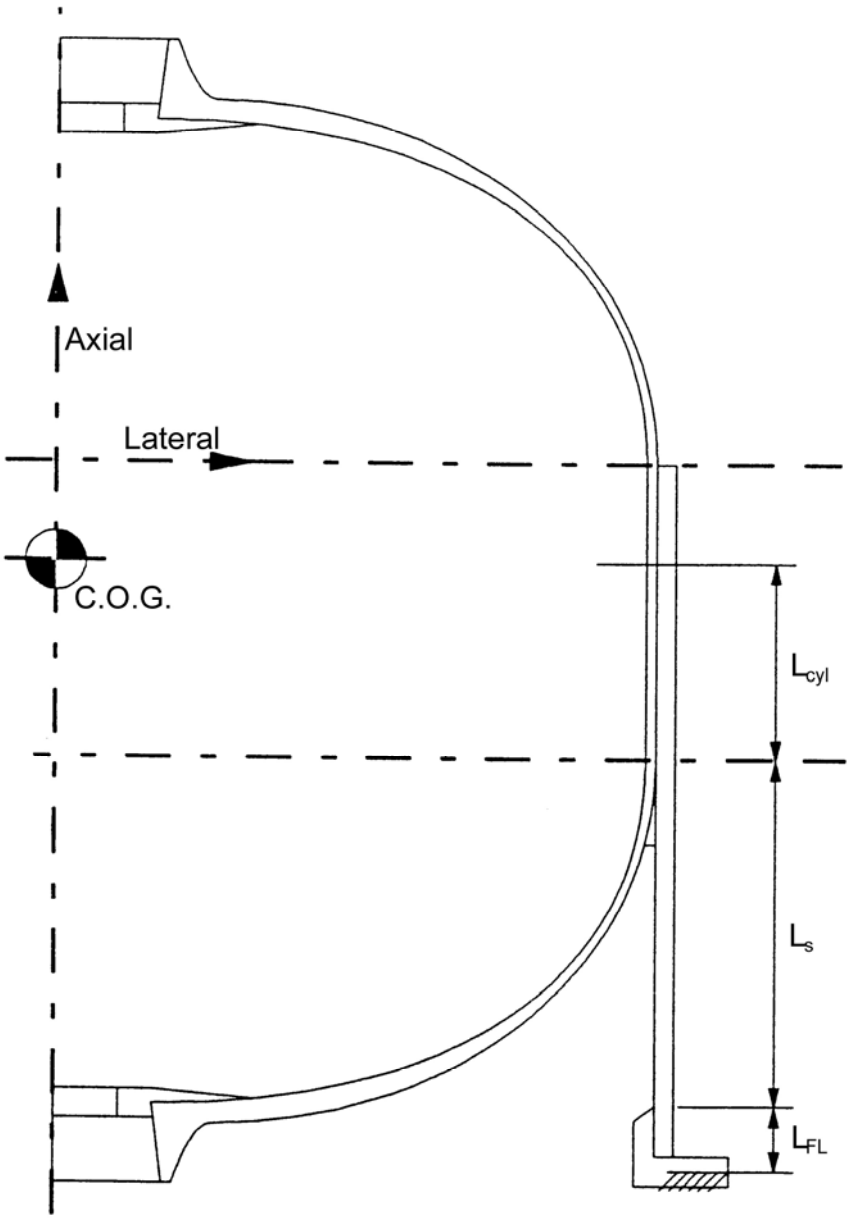

Figure 29.8-1 - Pressure vessel dimensioning, from MAGE: Definition of design variables

29.8.3.2 Dimensioning of case bottom

Winding angle is given by:

$$\alpha_o = arcsin\,\bar{e} = arcsin\frac{e}{r} \qquad [29.8\text{-}1]$$

Wall thickness is given by:

$$t_{\alpha o} = K_D \frac{p_i r_i}{2\sigma_{FB}\left(1-\bar{e}^2\right)} \qquad [29.8\text{-}2]$$

NOTE Including layout factor K_D (ca. 1.2 to 1.3), to cover bending influences in the dome.

$$t_\alpha = \frac{t_{F\alpha o}}{\phi}$$

Quantity of windings needed:

$$A_F = t_{F\alpha o}\, cos\,\alpha_o\, 2\pi r_i \qquad [29.8\text{-}3]$$

$$n_{min} = \frac{A_F}{2 n_{SPF} A_R} \qquad [29.8\text{-}4]$$

For cases with different polar openings, this calculation is performed for both domes. In this case, the larger value of the two calculated wall thicknesses dimensions the quantity of windings necessary.

29.8.3.3 Dimensioning of the hoop layer wall thickness in the cylindrical part

For identical polar openings:

$$\bar{e}_m = \frac{e}{r_i} \qquad [29.8\text{-}5]$$

For different polar openings:

$$\bar{e}_m = \frac{e_1 + e_2}{2r_i} \qquad [29.8\text{-}6]$$

$$t_{F90} = K_Z \frac{p_i r_i}{2\sigma_{FB}} \qquad [29.8\text{-}7]$$

$$t_{90} = \frac{t_{F90}}{\phi} \qquad [29.8\text{-}8]$$

NOTE Including layout factor K_Z (ca. 1.2).

Total wall thickness in the cylindrical part to absorb the inner pressure:

$$t_{cyl} = t_{\alpha o} + t_{90} \qquad [29.8\text{-}9]$$

29.8.3.4 Inner contour of the dome

Differential equation:

$$r'' + \frac{1 + r'^2}{2}\left(2 - tan^2\,\alpha\right) = 0 \qquad [29.8\text{-}10]$$

This equation is valid only up to the point of inflection. The location of this point is given by:

$$r_w = \sqrt{\frac{3}{2}}\,e \qquad [29.8\text{-}11]$$

Starting from the point of inflection up to the polar opening, a spherical shell can be attached. This shell is determined by:

$$\phi_w = 90° + arctan\, r'_w \qquad [29.8\text{-}12]$$

where:

r'_w is the gradient of the isotensoid contour at the point of inflection.

The locations of the inflection points are given by:

$$R = \frac{r_w}{sin\,\phi_w} \qquad [29.8\text{-}13]$$

$$Z_K = Z_w - \frac{r_w}{sin\,\phi_w} \qquad [29.8\text{-}14]$$

29.8.3.5 Winding angle in the dome

Clairault's Law:

$$\alpha(r) = arcsin\frac{e}{r} \qquad [29.8\text{-}15]$$

29.8.3.6 Wall thickness in the dome

Wall thickness is determined by:

$$t(r) = t_{\alpha o}\frac{tan\,\alpha(r)}{tan\,\alpha_o} \qquad [29.8\text{-}16]$$

For $\alpha = 90°$ the result of this equation is theoretically $t = \infty$.

To consider the manufactured bulge near the pole, it can be stated that in the range of (empirical) $e < r < (e + 10\text{mm})$ the wall thickness is:

$$t(r) < t(e + 10\text{mm}) = \text{constant}$$

29.8.3.7 Determination of the outer contour

Determination of the outer contour

The outer contour can be calculated from the inner contour and the wall thickness, considering that the wall thickness is determined normal to the inner contour. Therefore, the equation to be solved is:

$$t(r) = \sqrt{(r_a - r)^2 + (z_a - z)^2} \qquad [29.8\text{-}17]$$

29.8.3.8 Determination of volume, mass, moment of inertia and position of the centre of gravity

These values can be obtained by idealising the dome into a series of cylindrical sub-elements, using the known contour. For the volume, this approach gives:

$$V = \sum^{n} \pi(z_{i+1} - z_i)\left(\frac{r_i + r_{i+1}}{2}\right)^2 \qquad [29.8\text{-}18]$$

Where

n = number of sub-elements

The location of the centre of gravity is then given by:

$$z_s = \frac{1}{m}\sum^{n} z_{si} m_i \qquad [29.8\text{-}19]$$

29.8.3.9 Dimensioning of the cylindrical part

For this area, the composite lay-up is already defined. Missing is the required length. To determine this, the possibilities are:

The total length of the case is given by:

$$h_{cyl} = l_{tot} - h_1 - h_2 \qquad [29.8\text{-}20]$$

The volume required is determined by:

$$h_{cyl} = \frac{1}{\pi r_i^{\,2}}\left(V_{tot} - V_1 - V_2\right) \qquad [29.8\text{-}21]$$

From experience, it can be stated that the volume is required and the total length of the case is often restricted.

29.8.3.10 Fittings

A possible configuration of the fittings is given in Figure 29.8.2.

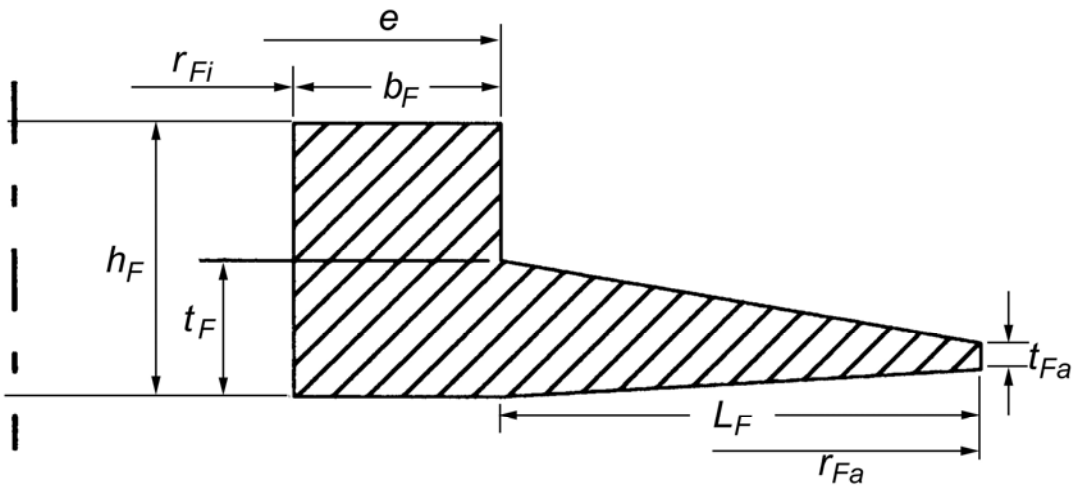

Figure 29.8-2 - Pressure vessel dimensioning: Definition of fitting variables

The values to be defined are those depending on the:

- Inner pressure and material data:
  - thickness of fitting flange, t_F
  - length of fitting flange, l_F
- Interfaces to other structural parts:
  - width of fitting, b_F, or
  - inner radius of the fitting, r_{Fi}
  - height of the fitting, h_F

The critical value is the thickness, t_F , at the base of the flange. No general algorithm exists to determine this value. In literature, it is treated partly as loaded only by bending, partly treated as loaded only in shear.

For the connection of the fitting to the composite case, again no general solution exists. It can be achieved by:

- Applying an elastomer interlayer, which is capable of taking the existing shear force and deformation.
- Bonding the fitting directly to the composite using the matrix as a bonding agent.

In either case the fitting uses a form lock for fixation.

The geometrical shape of the contact area between fitting and composite case is dependent on the overall dimensions, i.e.:

- Large case inner diameter, small polar opening leads to a flat or conical contact surface.
- Small case inner diameter, large polar opening leads to a contact surface that is shaped to correspond to the inner surface of the vessel.

29.8.4 Joint structures

29.8.4.1 Fittings

All types of pressure vessel have metallic or ceramic fittings as interfaces to, e.g.

- Nozzles,
- Piping, or
- Vessel closure.

Where these fittings are loaded by inner pressure, the layout is as described for the layout of the different vessel concepts.

Fittings are also designed to enable threaded fastenings to other parts. The dimensioning of the fastening is performed using the existing standards.

For smaller pressure vessels, the connection to the surrounding structures is also performed by the fittings. This means that these parts also have to take into account the transmission of all loads and be dimensioned correctly..

29.8.4.2 Skirts

Larger pressure vessels are normally fixed to the surrounding main structures by a skirt, which is a cylindrical part made of composite material. The skirt is attached to the cylindrical part. It is manufactured in a second step, after pre-curing of the vessel. Figure 29.8.3 shows a general configuration.

For the layout of the skirt, all load cases should be considered and evaluated to meet:

- Strength and stiffness requirements.
- Elongation compatible to the pressure vessel.
- Minimum weight requirement.

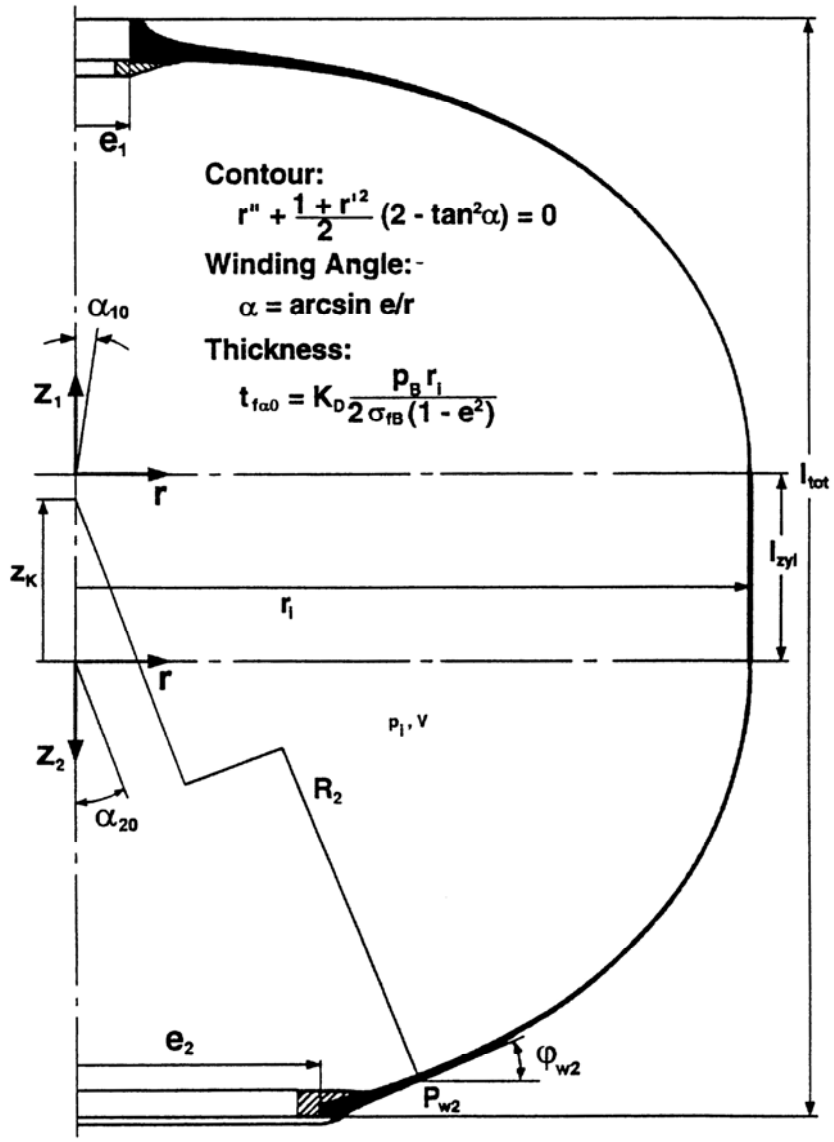

Figure 29.8-3 - Pressure vessels: Definition of joint structure variables

Defining the stacking sequence is generally performed by means of the well known laminate theory. For the vibration load cases, quasi static loads have to be established.

To check the stiffnesses and eigenfrequencies, it is sufficient as a first approach, to idealise the structure as a one-mass system, [See: Figure 29.8.3].

The eigenfrequencies are gained from:

$$f_{ax} = \frac{1}{2\pi}\sqrt{\frac{C_A}{m}} \qquad [29.8\text{-}22]$$

$$f_{lat} = \frac{1}{2\pi}\sqrt{\frac{C_s}{m}} \qquad [29.8\text{-}23]$$

The stiffnesses are calculated by separating the skirt structure from the centre of gravity to the flange in sections with constant lay-up. For example:

$$\frac{1}{C_A} = \frac{1}{C_{A_{cyl}}} + \frac{1}{C_{AS}} + \frac{1}{C_{AFl}} \qquad [29.8\text{-}24]$$

$$\frac{1}{C_S} = \frac{1}{C_{S_{cyl}}} + \frac{1}{C_{SS}} + \frac{1}{C_{SFl}} \qquad [29.8\text{-}25]$$

The stiffnesses of these sections are calculated by:

$$C_A = \frac{2\pi r_{mi} t_i}{\left(s_{11_i} - \frac{s_{12_i}^{\ 2}}{s_{11_i}}\right) L_i} \qquad [29.8\text{-}26]$$

$$C_S = \frac{\pi G_i \, r_{mi} \, t_i}{L_i} \qquad [29.8\text{-}27]$$

With: s_{11_i}, s_{12_i} : coefficients of the composite compliance matrix

G_i : composite shear modulus

The layout is an iteration process between stiffness and strength requirements.

To verify the design before detailed stress analysis, it is advisable to make a preliminary analysis using a program such as NASTRAN, [See also: Chapter 16 for composite analysis software].

29.8.4.3 Flanges

The principal concepts are:

- Separated flange, made of high-strength aluminium alloy or from composite materials connected to the skirt by:
  - bonding (with a possible formlock), or
  - riveting.
- Integrated composite flange, produced by adding layers and so avoiding bonding or riveting.

The layout of the flange (flange area) is mainly dictated by the stiffness requirements.

Another possible concept is to fix the pressure vessel to the main structure by a flange, which is attached in the cylindrical part of the vessel. This can reduce the weight of the whole case significantly.

29.8.5 Manufacturing

29.8.5.1 General

The possible manufacturing methods are strictly limited by the dimensioning, e.g.:

- Contour,
- Wall thicknesses,
- Winding angles.

The vessel is wet-wound.

29.8.5.2 Mandrel

The mandrel is designed to meet the thermal behaviour of the vessel. The main types are:

- Lost mandrel: A mixture of gypsum and glass bubbles is a proven solution.
- Reusable mandrel: Used for a series of cases with an identical configuration.

[See also: 29.2 for developments in mandrel technology]

29.8.5.3 Fittings

The fittings are coated with the elastomer interlayer and attached to the mandrel. The mandrel is be covered by a foil in order to prevent contamination of the inner surface of the case.

29.8.5.4 Fabrication

Owing to the restricted pot-life of the matrix system, the case is normally manufactured in two major steps. These are:

- Winding of the vessel. In order to obtain a homogeneous winding lay-up, a multi-star pattern is be used. The number of rovings wound simultaneously is fixed also by the lifetime of the matrix system. After the cross layers of the vessel have been wound, a curing process is performed before the elastomer parts at the equator are applied.
- Re-work of the cylindrical part and the attachment of the mandrel to create the joint structure. Depending on the concept, the skirt is built up from cloth or rovings - also wet in wet. The case is cured again.

After removal of the skirt mandrel, the adapter ring is connected to the case.

Finally, the interfaces are machined, after which the case is ready for acceptance tests.

29.9 Solid propellant motor cases

29.9.1 General

Various designs of solid propellant motor cases are presented. These are grouped as:

- proven technology:
  - satellite solid propellant motors, or solid rocket motors, for orbit injection or orbit transfer, e.g. MAGE (Moteur d'Apogée Géostationaire Europeéne) and IRIS (Italian Research Interim Stage) motors.
  - solid propellant motors for ballistic missiles, e.g. Trident and MX systems.
- developing technology for recent or future operational space programmes, such as cylindrical composite boosters for launchers.

Table 29.9.1 provides a résumé of the composite motor cases manufactured for various programmes worldwide, Ref [29-54].

Table 29.9-1 - Worldwide list of solid propellant motors with composite cases

Case	Case Material	Company [Country]	Purpose	First Flight/ Launcher	Max Dimensions, length/diameter (mm)	MEOP (bar)	Nozzle Material	Insulation Material
MAGE 1	K49/Ep	SEP/BPD/MAN [Europe]	Apogee booster	1981 Ariane	1125/766	-	Sepcarbonix C-C	EPDM
MAGE 1s	K49/Ep	SEP/BPD/MAN [Europe]	Apogee booster	1985 Ariane	1288/766	-	Sepcarbonix C-C	EPDM
MAGE 2	K49/Ep	SEP/BPD/MAN [Europe]	Apogee booster	1983 Ariane	1525/766	48.0	Sepcarbonix C-C	EPDM
EBM	K49/Ep	BPD/MAN [Europe]	Apogee booster	Fired 1994	1748/1351	55.0	C-phenolic SiO_2 phenolic	improved EPDM
IRIS	K49/Ep	Alenia/BPD/ MAN [Europe]	Apogee booster	1992 Ariane/STS	1748/1351	55.0	C-phenolic	EPDM
ASLV stage 4	K49/Ep	ISRO [India]	SLV booster	1983 SLV-3	1390/655	29.0	graphite C-phenolic	-
PSLV stage 3	K49/Ep	ISRO [India]	booster	~1993 planned	3541/1988	62.9 max	graphite C-phenolic	EPDM
IUS SRM-1/Orbus 21	K49/Ep	CSD [USA]	GTO	1992 STS, Titan	3520/2340	57.9 max	C-C	EPDM
IUS SRM-2/Orbus 6	K49/Ep	CSD [USA]	GEO	1992 STS, Titan	2080/1610	57.1 max	C-C	EPDM
Star 31/TE-M-762	K49/Ep	Thiokol [USA]	Stage 3	- Scout G-1	2873/762	-	C-C C-phenolic	-
PAM-D2, Star 63 D	K49/Ep	Thiokol [USA]	Upper stage, perigee	1985 STS, Titan	1830/1600	-	C-C C-phenolic	EPDM
PAM-A	-	Thiokol, CSD [USA]	Upper stage	1978/9 Minuteman	-/-	-	-	-
TU-903	K49/Ep	Thiokol [USA]	Stage 0	- Taurus	8480/2337	-	-	-
KM-M	epoxy CFRP	Nissan [Japan]	Kick stage	1990 M-3Sll	1307/840	59.0 max	Carbon cloth phenolic	-
Orion 50S	IM7/epoxy	Hercules	Stage 1	1990	9390/1271	-	Carbon	EPDM

Case	Case Material	Company [Country]	Purpose	First Flight/ Launcher	Max Dimensions, length/diameter (mm)	MEOP (bar)	Nozzle Material	Insulation Material
	CFRP	[USA]		Pegasus, Taurus			phenolic	
Orion 50	IM7/epoxy CFRP	Hercules [USA]	Stage 2	1990 Pegasus, Taurus	3837/1271	-	Carbon phenolic	EPDM
Orion 38	IM7/epoxy CFRP	Hercules [USA]	Stage 3	1990 Pegasus, Taurus	2080/965	-	Carbon phenolic	EPDM
Castor 4A(B)	CFRP	Thiokol [USA]	Booster	1989 Delta	8087/1016	49.9 max	Carbon-phenolic	-
Castor 25GT	CFRP	Thiokol [USA]	Stage 1	- ICBM	7570/1169	-	-	-
GEM	epoxy CFRP	Hercules [USA]	Booster	1990 Delta 7925	1296/1016	-	-	-
Castor 120	epoxy CFRP	Thiokol [USA]	Booster	1995 -	8801/2363	98.6 max	C-C	EPDM
Orbus 1	T-40/ep CFRP	UT [USA]	Stage, motor	1990 -	1249/692	66.7 max	C-C C-phenolic	EPDM
Orbus 7S	S-901/ep GFRP	UT [USA]	Perigee	1984 -	2273/1320	43.5 max	tungsten throat C-phenolic	Buna-N
ASLV stage 3	GFRP	ISRO [India]	Stage	1979 ASLV	2437/815	43.5 max	-	-
Star 20/TE-M-640	GFRP	Thiokol [USA]	Stage	- Scout	1485/500	-	graphite, plastics and steel	-
Orion 1/2	G-12 composite	SST [USA]	Single Stage 1	- Orion	3500 or 4500/230 or 250	-	SiO_2 phenolic graphite	-
M-34	-	Nissan [Japan]	Stage 3 of M5	- -	-/2200	-	-	-

29.9.2 Solid rocket motors - Mage and IRIS series

Since 1975, the MAGE and IRIS designs have been developed and produced by MAN Technologie, in conjunction with BPD Difesa e Spazio, now FIAT AVIO, and SEP (for MAGE only). The characteristics of these motors are given in Table 29.9.2, Ref [29-11], [29-26], [29-54].

Table 29.9-2 - Characteristics of MAGE and IRIS rocket motors

Characteristics	MAGE 1	MAGE 1S	MAGE 2	IRIS/EBM
Total Length (mm)	1125	1298	1525	1864/-
SRM case length (mm)	628	728	845	1020
Max Diameter (mm)	766			1310
Volume [l]	212	260	309	985
Mass (kg) : Composite Case Empty Motor Propellant	 9.0 33.8 355	 11.4 39.0 410	 13.7 38.0 490	 50.0/45.0 141/127 1615
Satellites	Meteosat P1, OP1, OP2, P2, OP3	Giotto, Lageous II	Marecs, ECS 1 to 5, Hipparcos, Telecom 1A-C	Lageous II for IRIS. None for EBM.

The basic MAGE motor design is shown in Figure 29.9.1, Ref [29-54], and consists of:

- Pressure vessel, with two isotensoid geodetically wound domes and a cylindrical portion.
- Kevlar 49/epoxy in a multi-star winding pattern for the cross layers of the domes.
- Interface fittings to fix the nozzle and igniter.
- Adapter skirt and flange for connecting the pressure vessel with the structure.
- Elastomer interlayer at the transition zone of the cylindrical part to the adapter skirt.

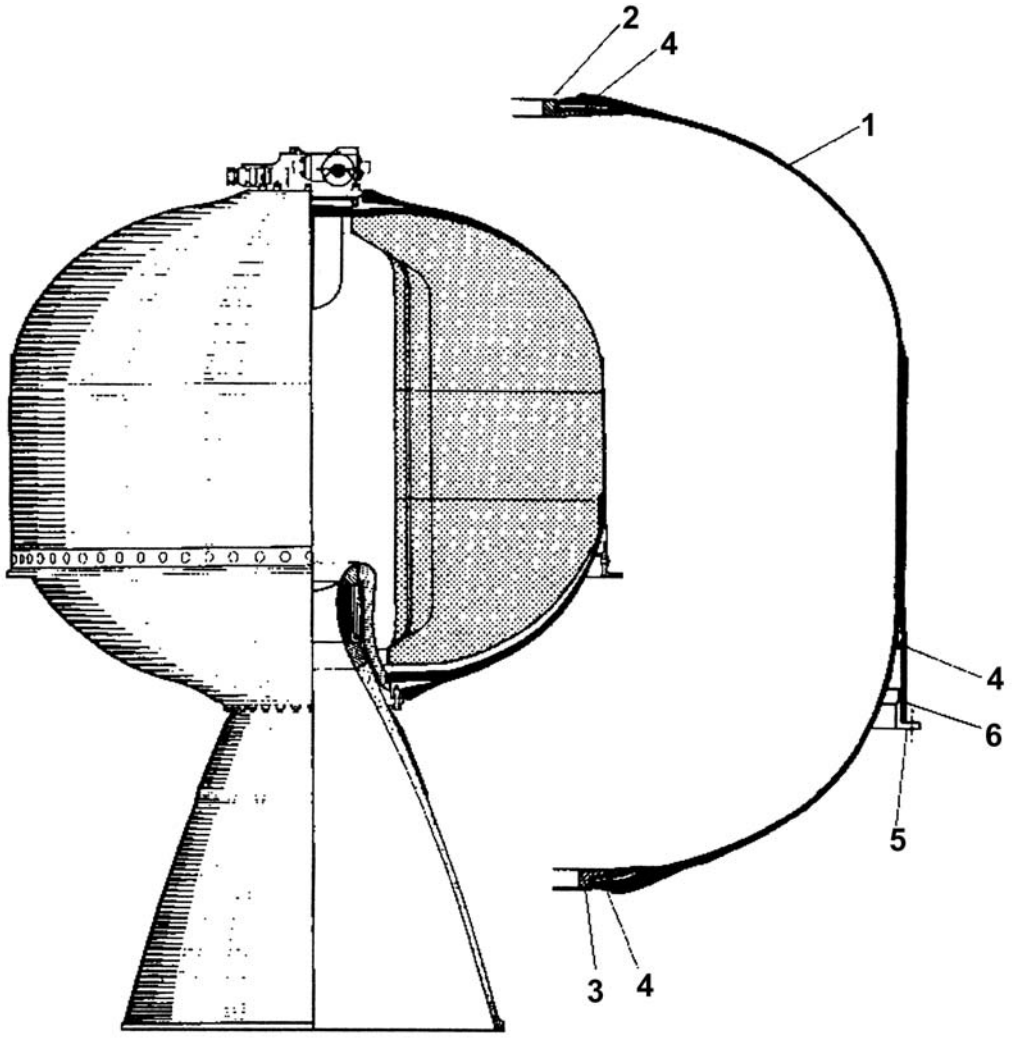

Key:

1	Pressure vessel	4	Elastomer interlayer
2	Polar fitting (igniter side)	5	Adapter flange
3	Polar fitting (nozzle side)	6	Adapter skirt

Figure 29.9-1 - MAGE 1 configuration

Several improvements have been instigated in the MAGE series, in relation to the skirt-case connection.

The IRIS motor is a kick-stage, perigee motor to launch satellites up to a mass of 900 kg from the US Space Shuttle. The design of IRIS has an interface to the spacecraft and another to the satellite adapter, to accommodate the application as a perigee motor.

Based on the vessel dimensions of IRIS, MAN developed a case with a single skirt and an integrated CFRP flange for use in the EBM program.

The results of the design evolution throughout the MAGE-IRIS series are described.

29.9.3 Design characteristics of IRIS/EBM

29.9.3.1 Safety Factors

The safety factors which were applied to IRIS/EBM cases for unmanned operation are shown in Table 29.9.3.

Table 29.9-3 - Safety factors applied to IRIS/EBM cases for unmanned operation

Safety Factor	Value
For vessels, based on MEOP:	
Proof Pressure Level	1.05
Minimum Burst Pressure Level	1.3
For joint structure (skirt), metallic parts based on service loads:	
Yield Strength (metals)	1.2
Ultimate Strength	1.5
Stability Limit (General and Local Buckling)	1.3
Fitting Factor	1.25

An additional fitting factor covers the mechanical connections, i.e.:

- bolting of the SRM to the surrounding structure (satellite) at the interface of the adapter flange, and
- riveting of the metallic adapter flanges to the composite skirt.

29.9.3.2 Design values for the EBM

Design values for the EBM case are shown in Table 29.9.4.

Table 29.9-4 - Design values for the EBM case

MEOP	55 bar		
Thrust at MEOP	80 kN		
Quasi-static loads:			
Acceleration in z-axis	±12g		
Acceleration in x,y-axis	±5g		
Sinusoidal Vibration Levels:		Freq. [Hz]	Amplification Factor
z-direction	10g	15 ÷ 16	1
	4g	60 ÷ 100	4
x-, y-direction	7g	12.6÷ 30	1
	3g	30 ÷ 100	6
Random Vibration Levels:	Power Spectral Density		Amplification Factor
z-direction	0.130 g^2/Hz		4
x-, y-direction	0.042 g^2/Hz		6
Minimum Eigenfrequencies:			
z-direction	80 Hz		
x-, y-direction	60 Hz		
Vessel volume	985 litres		
Dimensions:			
Maximum length	1020 mm		
Maximum diameter	1310 mm		

29.9.3.3 Skirt structure

The skirt fulfils the criteria of:

- Minmum mass,
- Sufficient stiffness to achieve stated eigenfrequencies,
- Sufficient strength to transmit loads from vessel to the satellite,
- Elongation compatibility with the pressure vessel,
- Suitable manufacturing route to shape the skirt to the vessel.

CFRP has the preferred stiffness characteristics. Wet lamination is necessary to lay the material, either by winding of roving or hand lay-up of cloth.

The MAGE and EBM cases have only one skirt. This is best layed-up with carbon or aramid cloth. IRIS has two skirts, which can be wound using T300 carbon fibre rovings.

Glass cloth is also incorporated in areas where holes are drilled for riveting the adapter flange. The presence of glass fibres also improves the through-laminate strength and reduces the occurrence of delaminations.

The skirt lay-up for MAGE, [See: Figure 29.6.4], can be compared with the EBM case skirt lay-up with an integrated flange in Figure 29.9.2, Ref [29-54].

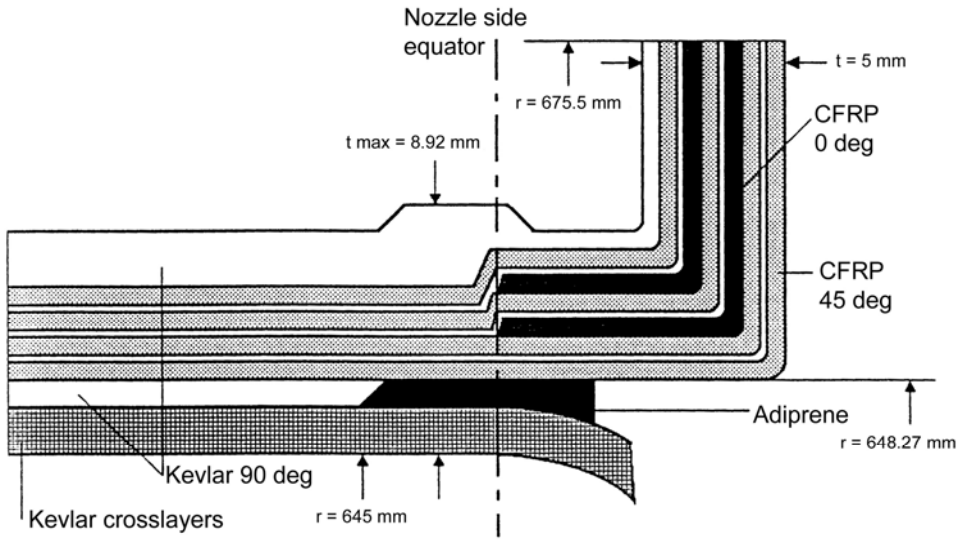

Figure 29.9-2 - Skirt lay-up with integrated flange for the EBM case

29.9.3.4 Pressure vessel design

The domes are designed separately taking into account the polar openings e_1 and e_2 and the radius at the equator r_i. With these parameters each dome is defined by, [See: Figure 29.8.3]:

- The contour is determined using the differential equation, [See: 29.8 - Eq [29.8-10].
- The local winding angle is dependent on the local inner radius, using 'Clairaut's Law', [See: 29.8 - Eq [29.8-15].

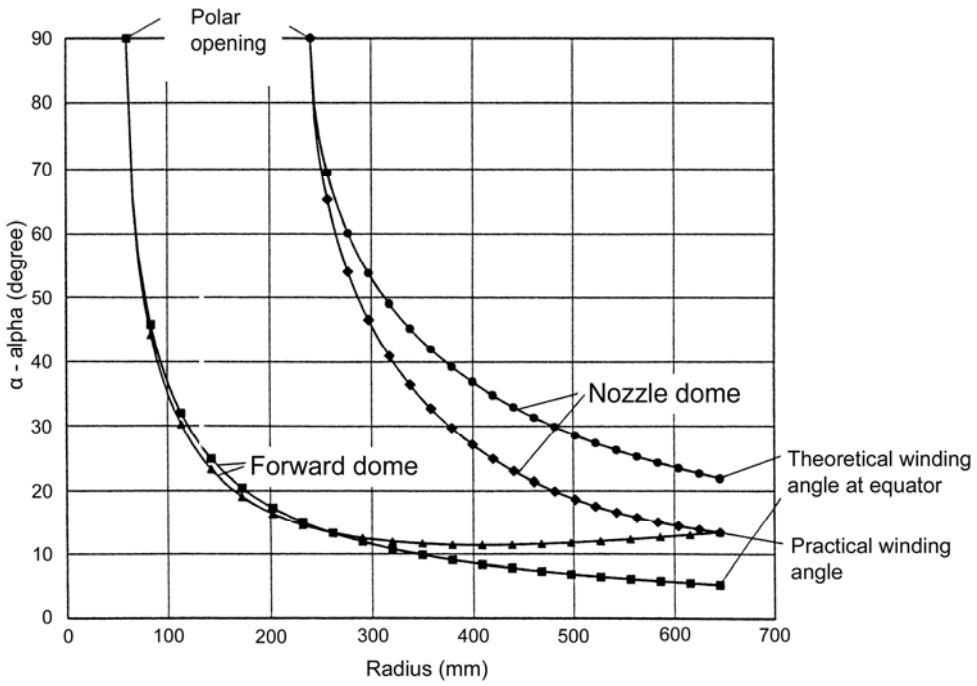

Figure 29.9-3 - Theoretical and practical winding angles over radius for the two IRIS/EBM domes

The aim is to achieve equal stress at each point in the fibres, without the presence of shear stresses. The necessary thickness of the fibres at the equator is determined by the equation given in Figure 29.8.3. The theory of the isotensoid is not valid in the equatorial areas. Here the membrane status is disturbed due to stiffness differences between the dome and cylindrical part. Design factors are used to cover these effects. For IRIS and EBM cases the factors are:

For the dome	$K_D = 1.2$
For the cylindrical part:	$K_C = 1.2$

Taking account of the two different polar openings, the actual local winding angles differ from the theoretically determined local winding angles. For the IRIS/EBM case the values of winding angle are shown in Table 29.9.5.

Table 29.9-5 - IRIS/EBM winding angles

IRIS and EBM	Nozzle Dome	Forward Dome
Theoretical Winding Angle	20.99°	5.34°
Practical Winding Angle	13.1°	

The theoretical angles cannot be achieved in the winding process, because the short cylindrical length does not enable a shifting of the roving from one equator to the other. This effect causes a deviation of the local windings for the whole vessel, [See: Figure 29.9.3].

The dome profile can be optimised to increase pressure vessel performance, not least by increasing the volume of propellant, with shallow, flattened domes, Ref. [29-52], [29-53], [29-56]. The use of high-stiffness CFRP enables compressive buckling to be contained, making flattened domes feasible.

29.9.3.5 Numerical analysis

Whilst analytical methods and laminate theory can configure the case structure, verification is necessary by geometrical non-linear FE analysis techniques, such as NASTRAN, Ref [29-55].

The aim is to idealise the change in winding angle and dome thickness. The FE approach can then correlate the deformation behaviour of the vessel during pressure testing with those predicted by theory. This is important as manufacturing parameters, e.g. fibre tensioning and matrix curing, have the effect of modifying the predicted response.

29.9.3.6 Manufacturing

Wet winding on a lost mandrel of gypsum containing glass microspheres is used to manufacture the pressure vessel. The mandrel material has similar thermal expansion characteristics to the composite used for the vessel. A reusable mandrel was deemed too expensive for the limited production run of these cases. The skirt structure uses a reusable steel mandrel.

The manufacturing sequence for the vessel is:

- Application of FEP release foil to mandrel.
- Surface prepared fittings mounted on mandrel.
- Elastomeric interlayer applied.
- Vessel winding with high-precision CNC winding machine, with time restrictions imposed by the epoxy resin pot-life:
  - 6 rovings for MAGE
  - 12 rovings for IRIS/EBM
  - applied in multi-star pattern, with cross-layers followed by hoop windings.
- After post curing, the cylinder is CNC machined to remove surplus layers of material and the elastomer layer added. The skirt mandrel is fixed in position.
- After intermediate cure, the skirt is applied.
- After final curing, mandrels are removed and the skirt machined to the final dimensions.

29.9.3.7 Quality control

To ensure the necessary product assurance, QA included:

- Material properties checked against procurement specification,
- Process and production parameters recorded and compared with previous versions, including NOL-ring tests on windings and DTA assessment of resin characteristics,
- All vessels proof tested to 1.05 times MEOP, with X-ray inspection before and after pressurisation.

29.9.4 Inertial upper stage (IUS)

Both SRM-1 (Orbus 21) and SRM-2 (Orbus 6) are used in the 'inertial upper stage' (IUS), which is part of the STS.

The IUS can be used on TITAN launchers to provide the propulsion necessary to move satellites in LEO to higher orbits or embark on interplanetary missions. The SRM-1 case is also used for the 'transfer orbit stage' (TOS). Thus different combinations between the SRMs enable different missions to be considered; as shown in Figure 29.9.4.

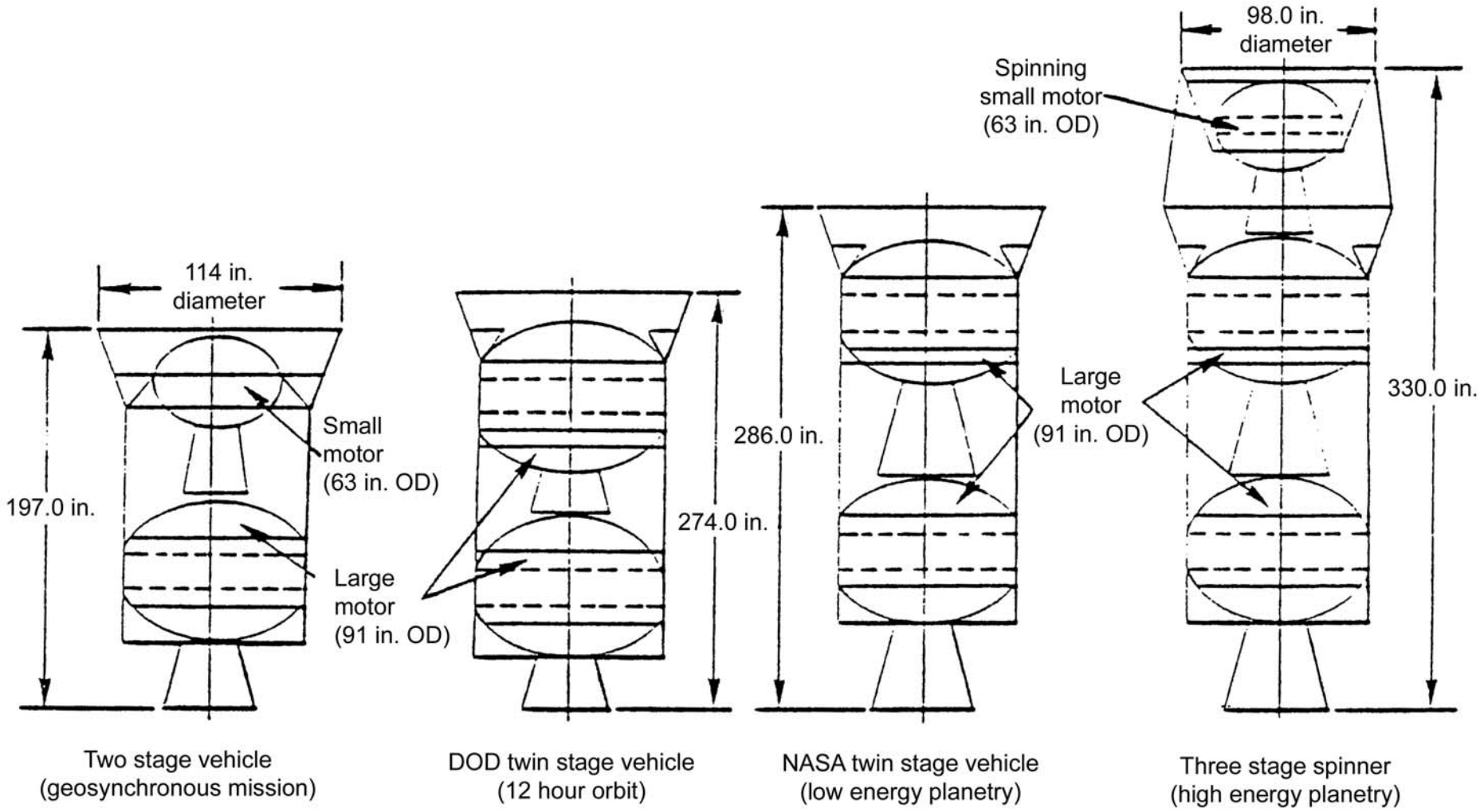

Figure 29.9-4 - Stage configuration for IUS

The skirt of the larger motor case forms part of the primary structure of the IUS. Like the MAGE motor, these use Kevlar 49/epoxy material for the pressure vessel, but with variations to the design.

For SRM-1, the skirt structure is integrally wound, where the lay-up consists of aramid fibre layers, stacked in axial, ±45° and hoop layers. Elastomer is applied to reduce peak stresses between the vessel and skirt. The stage is designed such that the flanges connecting the motors are not part of the case structure.

The SRM-2 is similarly designed, but unlike the SRM-1, the skirt is only designed to withstand the acceleration and vibration levels, and is not part of the primary structure.

29.9.5 CFRP motor case designs

As with propellant and pressurant vessels, there is an incentive to use high-performance carbon fibres for motor cases instead of aramid fibres, e.g. Kevlar 49. Carbon fibres such as IM-7 and Toray T-800 offer opportunities for mass efficient designs.

Developments are increasing worldwide for such constructions and flights began in 1990, [See: Table 29.9.1]. Some of the notable developments include, Ref. [29-27], [29-28], [29-54]:

- BPD Difesa & Spazio (Italy): A hybrid titanium-CFRP design with T800/Fiberite 977-2 epoxy resin, Ref [29-28].
- Institute of Space and Astronautical Science (Japan): All-CFRP motor casings for the new-generation M-V satellite launcher, Ref [29-27]. Three variants vary in volume from 6000 litres to 50000 litres and from 2 m to 11 m. in length.
- Lockheed launch vehicle (LLV) family: The CFRP SRM cases offer a range of modular configurations for payloads from 800 kg to 3600 kg. The propulsion components are based on Castor 120 CFRP boosters and Orbus 21 D Kevlar 49/epoxy solid rocket motor, with Castor IVA strap-on boosters, Ref [29-54].
- KM-M case (Japan): A sophisticated case with a CFRP vessel (800 mm diameter, 788 mm in length) and CFRP skirt. The adapter rings for this kick stage are integrally manufactured from CFRP. It also has CFRP fittings.

29.9.6 Booster motor cases

29.9.6.1 Large metal booster motor cases

Large booster motor cases for launchers are traditionally made of steel. Their cylindrical shape lends them to formed metal constructions with sections welded together. Steel is also a low cost material suitable for a single-shot launches. The total mass of steel booster cases is dependent on the launcher configuration but can be more than 20 tonnes each.

Details of those for Ariane 4 and 5 are shown in Table 29.9.6, Ref [29-24].

Table 29.9-6 - Booster motor case details for Ariane 4 and 5

	PAP Ariane 4	CPN Ariane 5
Diameter (mm)	1070	3050
Case Mass (kg)	1966	19600
Wall thickness (mm)	5	8
Material	AISI 4130 (or 30 CD4S)	48 CDN4 10 (or D6AC)
Fabrication route	Roulé-soudé + Soudage TIG + Assemblage par FE	Viroles fluotournées
Key: PAP: Propulseurs d'Appoint à Poudre CPN: Corps de Propulseurs à Poudre.		

[See also: 46.9 for details of mass savings on the Space Shuttle external tank]

29.9.6.2 Large composite booster motor cases

Reducing the mass of the booster case can be a means of upgrading the lift-capacity of a launcher without the need to development a new launcher.

The implementation of filament-wound composite cylinders has been examined as a means of achieving reduced mass at a lower cost than developing a new launcher.

Up to 1990, Morton Thiokol in conjunction with Hercules produced filament-wound cases (FWC) for the booster motors of the Space Shuttle, Ref [29-50].

The characteristics included:

- Four FWCs made up a motor.
- FWCs were 3.66 m in diameter and joined together with steel pins.
- The forward and centre FWCs were 7.6 m in length, and the aft FWCs were somewhat shorter.
- The thickness of the membrane region away from the ends was approximately 36 mm. The ends were thicker to withstand the concentrated pin loads.
- Construction material: Hercules AS4W-12K / HBRF-55A epoxy.
- Fibre orientations: 0° and ±56.5°

The design was mainly constrained by the need to sustain internal pressurisation and resist longitudinal growth and bending moments on launch. The impact and damage tolerance of this design was also extensively studied, Ref. [29-10], [29-29].

The conclusion was that the construction was susceptible to non-visible impact damage that could be significant for a structure with a factor of safety of 1.4. If the kinetic energy of an impact exceeded 123J with an appropriate indentor, then the damage could be considered critical.

The study recommended protecting the FWC from the possibility of impact loadings during handling: important not least because of the mass of the structure.

29.10 Launchers

29.10.1 General

Pressure vessels for launchers are larger than those found on satellites and therefore of greater mass. Potential mass savings can be very significant when efficient filament-wound designs are pursued.

The Ariane series of launcher highlights the advances made with time in the manufacturing of helium pressurant tanks.

[See also: 29.11 for launcher cryo-tanks]

29.10.2 Ariane 4 tanks

In 1988, Aerospatiale developed an upgraded spherical helium pressurant tank, CHA HP L33, for the second-stage of Ariane 4, Ref. [29-20], [29-21]. This tank conformed to the specifications A4 SG 1 10 and MIL STD 1522A.

The previous tank was an all-metal construction.

The constraints imposed were:

- maximum individual mass of 32 kg; each launcher has 3 units,
- safety and reliability at least equivalent to all-metal tanks,
- compatibility with existing mountings used for metal tanks,
- capacity of 123 litre, with a MEOP of 326 bars,
- safety factor of 2.0.

A mass saving of 26 kg was proposed for each tank; giving a total mass saving of 78 kg for the launcher, i.e. 3 units × 26 kg mass-saving each.

The new design used:

- Kevlar™ 49 fibres with S14 epoxy resin; a total mass 21 kg.
- 27 layers of composite.
- Titanium alloy Ti-6Al-4V liner; a total mass 10.2 kg.
- Liners were made by machining forged blanks and electron beam welding.

The design achieved a performance factor, $P_b V/W$ = 28.7 km, [See also: 29.3 for pressure vessel performance factor].

The K49/Ti construction was the predecessor of the CFRP/Ti designs that appeared a few years later, [See also: 29.3 and Table 29.3.7].

29.10.3 Ariane 5 pressure vessels

29.10.3.1 General

Ariane 5 has three large composite high-pressure vessels, Ref. [29-11], [29-14], [29-22], [29-23], [29-24], [29-25]. The technology for the L33 tank in Ariane 4 has been extended to a 300 litre CFRP/Ti spherical tank of 400 bar MEOP and diameter of 800 mm, Ref. [29-24].

In addition there are the GAT and GAM vessels manufactured by MAN Technologie.

29.10.3.2 High-pressure vessels GAT and GAM

The GAM HPV is intended for the storage of hydraulic fluid pressurised by gaseous helium needed by the servo-actuators of the Groupe d'Activation Moteur (GAM), Ref. [29-22].

The Groupe d'Activation Tuyère (GAT) activates the nozzle of the solid booster stage and includes two very similar HPVs. The pneumatic tank (PHPV) is intended for the storage of gaseous helium needed for pressurising the hydraulic fluid in the hydraulic tank (HHPV). The tanks are cylindrical; as imposed by the constraints of the space envelope available.

The performance factor, P_bV/W, values are lower than expected due to the additional mass of heavy metal attachments.

The design characteristics for the final tank are given in Table 29.10.1, Ref. [29-22].

Table 29.10-1 - Technical characteristics for HPV GAT and GAM

	GAT	GAM
Design characteristics:		
Volume (litres)	520	183
Maximum Mass (kg)	191	56
MEOP (bar)	450	230
Proof Pressure (bar)	675	345
Minimum Burst Pressure (bar)	900	460
Storage Life (years)	6	6
Operating Fluids	Hydraulic fluid and gaseous He	
Cycling Life	116 x MEOP + 4 x proof pressure + 4 X MEOP with 10^5 cycles dynamic load	
Leakage Rate ($Ncm^3.sec$)	$< 2 \times 10^{-3}$	$< 2 \times 10^{-3}$
Performance Factor P_bV/W (km)	25	15.5
Tank Characteristics:		
Tank Length (mm)	4661	1839
Outer Diameter (mm)	434	420
Liner Thickness (mm)	1.6	1.6
Composite Wall Thickness (mm)	13.1	6.4

The GAT and GAM design and subsequent manufacturing is done by MAN Technologie AG, Ref. [29-14], [29-22], [29-23], [29-25].

The features of the designs include, Ref. [29-22], [29-23]:

- Maraging steel X2NiCoMo 1885 liner:
  - high specific elastic limit,
  - high uniform elongation capability, no necking during prestressing,
  - high specific elastic modulus , no buckling after prestressing,
  - sufficient fracture toughness to reach leakage before burst,
  - reduced hydrogen embrittlement,
  - good manufacturing properties.
- Toray T800H 12000 40B carbon fibre:
  - high specific strength for minimum mass design,
  - high specific modulus for low liner strain during operation,
  - good winding properties,
  - availability.
- Ciba Geigy XW-1202 / HY932W epoxy resin system:
  - compatibility with fibre,
  - good curing characteristics for thick laminates, no excessive exotherm,
  - long pot-life.

The liners are welded constructions consisting of cylinder, domes and bosses, having the characteristics of:

- Die-forged domes.
- Seamless cylinders made by ring-roll forging, with spin-forming down to 1.6 mm thickness.
- Two-pass TIG welding on square butt configuration without the addition of filler metal.
- Heat treatment:
  - solution heat-treatment at 830°C ± 10°C for 1 hour,
  - precipitation hardening at 550°C ± 5°C for 3 hours.

For winding process used comprised of:

- Cleaning with Shellsol™,
- Application of a chromate-free, epoxy anti-corrosion primer,
- Application of a hydrocarbon wax polish,
- Lay-up of glass fibres,
- Two-stage winding with intermediate curing,

This process produced a fibre volume fraction of 63%.

A 'sizing cycle' is performed on the tanks to prestress the construction. The tank is inflated to reach the defined plastic deformation of the metallic liner, i.e.

- GAT stress of 70 MPa,
- GAM HPV stress of 40 MPa.

After release of the pressure, the mismatch in size of the plastically deformed liner and the elastically behaving overwrap results in an equilibrium state between the compression stresses in the liner and the tension stresses in the overwrap, [See also: Figure 29.3.4 for a schematic representation for the circumferential stress].

At burst pressure, the liner is contributing 15% to load sharing. The design is such as to avoid liner buckling or exceeding the compressive limit of the steel when the completed tank is unpressurised.

29.10.3.3 Liquid propellant tanks for Ariane 5

All-metal tanks are used for storage of propellants MMH and N_2O_4 within the Ariane 5 upper stage, Ref. [29-14].

All-metal tanks have to be compatible with fuels, and vice-versa, therefore AISI 301/304 L stainless steel and titanium alloys are preferred.

29.10.3.4 Ariane 5 cryogenic tanks

[See: 29.11]

29.11 Cryogenic tanks

29.11.1 General

The main applications for cryogenic tanks are found in:

- Conventional single-shot launchers, e.g. Ariane 5.
- Reusable launcher concepts for both SSTO and TSTO configurations, e.g.:
  - X-programme demonstrator vehicles, X-33 and X-34.
  - FESTIP development technologies.

Both conventional and reusable vehicles have tanks to contain liquid hydrogen, LH, at -253°C (20K) and liquid oxygen, LOX, at -183°C (90K).

An incentive to consider filament-wound tanks is the mass-saving possible, so enabling the payload capacity to be maximised, especially where the payload margin is small, Ref. [29-30] to [29-35].

29.11.2 Factors to be considered

These can be broadly defined as:

- Mechanical and fracture properties of polymer composites at cryogenic temperatures.
- Whether a polymer composite construction can withstand the thermal-cycling induced by repetitive loading of cryogenic fuel.
- Selection of the most suitable polymer composites available.
- Compatible of polymer composites with LH and LOX.
- Susceptibility of composite constructions to damage by thermal shock during refuelling.
- Use of liners to control gas permeation through polymer composites.
- Whether adhesive joints for tank assembly can be used and whether they can sustain the operating conditions.
- The implications for load-introduction points on composite tanks
- The optimum structural configuration for a cryogenic tank in a reusable space plane.
- Whether the tank design can be made cost-effectively by filament winding.

29.11.3 Single-mission conventional launchers

The H10 3rd stage of Ariane 4 has two tanks of total mass 700 kg that carry 11800 kg of LOX and LH. These are made of aluminium alloy 7020 (AZ5G), Ref. [29-24].

In Ariane 5, the main LH and LOX tanks for the H150 1st stage are made of aluminium alloy 2219 (AU6MT), Ref. [29-24]. The combined tank mass is 5050 kg containing 156200 kg (156.2 tonnes) of fuel.

29.11.4 Multiple-mission spaceplanes

29.11.4.1 General

The concepts for spaceplanes are numerous and cryogenic tanks form a major proportion of their structural volume and mass. There is a strong incentive to use the tank not only for containing fuel but also to provide a primary structural load-carrying function, i.e. normally associated with the airframe. Such tanks need to provide load introduction points for associated structural elements.

In addition, the thermal management of cryogenic fuels and the surface heating experienced by operational spaceplanes is undertaken within a mass-efficient design. The implications of tank insulation have therefore to be evaluated.

With these broad needs in mind, the various tank configurations proposed are, Ref. [29-30], [29-36]:

- Hot structure, non-integral tank.
- Cold structure, integral tank.
- Hot structure, integral tank.

29.11.4.2 Classification of cryogenic tank designs

The basic criteria used to classify possible tank designs are, Ref. [29-32]:

- Mechanical function:
  - integral tank, which acts as the airframe,
  - 'hybrid tank', an aeroshell concept of a tank-thrust structure within an airframe structure or aeroshell,
  - non-integral tank, a heavy concept where the tank is suspended within the airframe.
- Thermal function, where the tank has a hot thermal protection system, HTP, or a cold system, CTP. These can be coupled or not with the tank wall structure, e.g.:
  - Hot structure, a simple sandwich-type construction with very high thermal stresses between the cold and hot surfaces.
  - Partially-insulated structure, having permutations of HTP-to-structure, CTP-to-structure and structure-to-CTP.
  - Totally-insulated structure, which is segregated into distinct functions for each layer, i.e. HTP-to-CTP-to-stiffened structure.

Within the many possible variations, filament-wound tanks can be considered along with some form of external thermal protection and insulation.

29.11.4.3 Polymer composites for cryogenic tanks

Work on establishing the suitability of polymer composites for cryogenic tanks is progressing. In many cases, the materials considered most suitable have only been commercially available for a few years. Data needs to be acquired before there is sufficient confidence to proceed with tank development.

McDonnell Douglas has gained experience in assessing the behaviour of polymer composites and testing tank configurations representative of those proposed for NASP, Ref. [29-30], [29-35], [29-37], [29-38], [29-39].

The polymer-based CFRP composites evaluated are:

- Thermoset systems: AS4/8551-7, IM6/18271-E, IM6/1827, and T40/9405.
- Thermoplastic system: IM6/APC-2.

The broad conclusions drawn from the study, include Ref. [29-35]:

- Unlined composite tanks can be used for LH without excessive permeation.
- A permissible permeation rate of 10^{-4} to 10^{-3} scc/s in^2 was stated; where: scc/s in^2 stands for 'standard cubic centimetre per second per square inch of surface area'.
- All the composites examined as quasi-isotropic laminates achieved less than 2.0×10^{-6} scc/s in^2 under the conditions of:
  - Uncycled at 4K, and after 150 thermal cycles from RT to 4K

— Thermomechanical cycling from 0 MPa to 297 MPa in tension at 4K with 150 thermal cycles from RT to 4K.

- Mechanical strength retention of composites at cryogenic temperatures was excellent with virtually no loss in performance.
- With IM6/PEEK and titanium alloy as the baseline substrates, the efficiency of adhesive bonds was evaluated, Ref. [29-40]. From the 8 adhesives tested, two showed acceptable performance; FM300 (film) and EA9394 (paste). These retained approximately 60% to 70% of ambient shear strength at 4K and fulfilled the minimum shear strength criteria of 10 MPa at cryogenic temperatures and 8 MPa at 120°C. Some of the adhesives examined were very unsuccessful and retained little or no strength at cryogenic temperatures.
- Trials with bonded joints showed that the presence of adhesively bonded overlaps did not noticeably affect hydrogen permeation rates.
- Trial 250 mm diameter unlined Hercules IM7/8551-7 pressure vessels were evaluated under cyclic pressure (up to 20 bar) and temperature conditions. The vessel integrity was retained and hydrogen permeation rates were below the maximum permissible value.
- A 4050 litre unlined tank representative of a NASP configuration was tested.
- LOX compatibility was partially addressed, with permeation and oxidation not deemed a problem.
- Explosion hazards: the ignitability of polymer composites is said to vary widely, with some showing good resistance.
- Minimising potential ignition sources is under consideration rather than any fundamental concerns over LOX compatibility.

The technical and practical aspects of uninsulated, filament-wound composite LOX tank designs, for pressure-fed rocket boosters, have been examined, Ref. [29-31]. Typical operating conditions are 23 bar at 90 K.

The design features identified as most promising were:

- An uninsulated, bonded interface between liner and composite.
- Design burst pressure of 1.5 times maximum expected operating pressure of 23 bar.
- A toughened epoxy resin system specifically formulated for cryogenic service.
- A 300-series stainless steel metallic liner (~ 0.15 mm thick) for fuel compatibility.
- Use of inflatable mandrels.
- Moderate fibre prestressing with internal pressure during peak cure pressure.
- Low temperature epoxy cure cycle, i.e. below 80°C.
- Autofretage-proof test of 120% maximum operating pressure.

The cost of producing large wound composite structures indicates that composite structures can be cost-effective, not least because the part count is lower compared with a metallic fabrication, Ref. [29-38], [29-39]. However, it is recognised that the structure is designed with composite manufacturing techniques in mind, e.g. by filament winding.

For comparison, some automated processes for prepreg placement for subsequent autoclaving are not necessarily the most cost-effective means of achieving the composite configurations, Ref. [29-38], [29-39].

From 1996 onwards, the USA reusable launch vehicle, RLV, technology program is building the SSTO X-33 and X-34 flight demonstrators based on experience of the DC-X Clipper Graham. This includes the development of full-scale CFRP tanks for LH and LOX containment; typically made from IM7/Fiberite 977 epoxy.

[See also: 92.3 for condition monitoring of cryogenic tanks in reusable vehicles]

29.11.4.4 FESTIP concepts

Between 1995 and 1997, the FESTIP future European space transportation investigation programme, conducted preliminary studies on polymer composite cryogenic tanks, Ref. [29-58].

The composite evaluated was an autoclave-cured cyanate ester resin Fiberite 954-2A with IM7 carbon fibres.

Figure 29.11.1 shows a CFRP design for LH containment integrated with ceramic-based thermal protection systems, Ref. [29-58].

In parallel, an aluminium-lithium alloy construction was studied for LOX containment. These studies are evaluating the behaviour of CFRP in conjunction with liquid cryogenic fuels. The option for filament-winding a CFRP tank was to be reviewed a later in the programme.

29.11.5 Possible materials

In view of the relative immaturity of cryogenic tank constructions, other than existing steel configurations for launchers, no attempt is made to indicate preferred materials.

The materials that have been proposed for tank constructions, along with comments on their suitability include:

- Metallic designs, e.g. use of conventional titanium or aluminium alloys are generally too heavy.
- Welded aluminium-lithium alloy designs are more mass-efficient, but material procurement can be difficult, coupled with the need to develop expertise in welding Al-Li alloys. The Space Shuttle 'super lightweight tank' made of aluminium-lithium alloy first flew in June 1998 on mission STS-91, [See: 46.9 for Space Shuttle External Tank; Table 46.9.1 for associated mass-savings].
- Toughened epoxy or thermoplastic composites can provide lightweight designs, but there is insufficient performance data to provide acceptable confidence levels.
- Filament winding of large tanks is preferred to bonded designs based on assembled panels. This provides a lower cost and avoids uncertainties of jointing.
- Metal matrix composite designs use expensive materials of uncertain continued commercial availability along with insufficient performance data and associated manufacturing technologies.

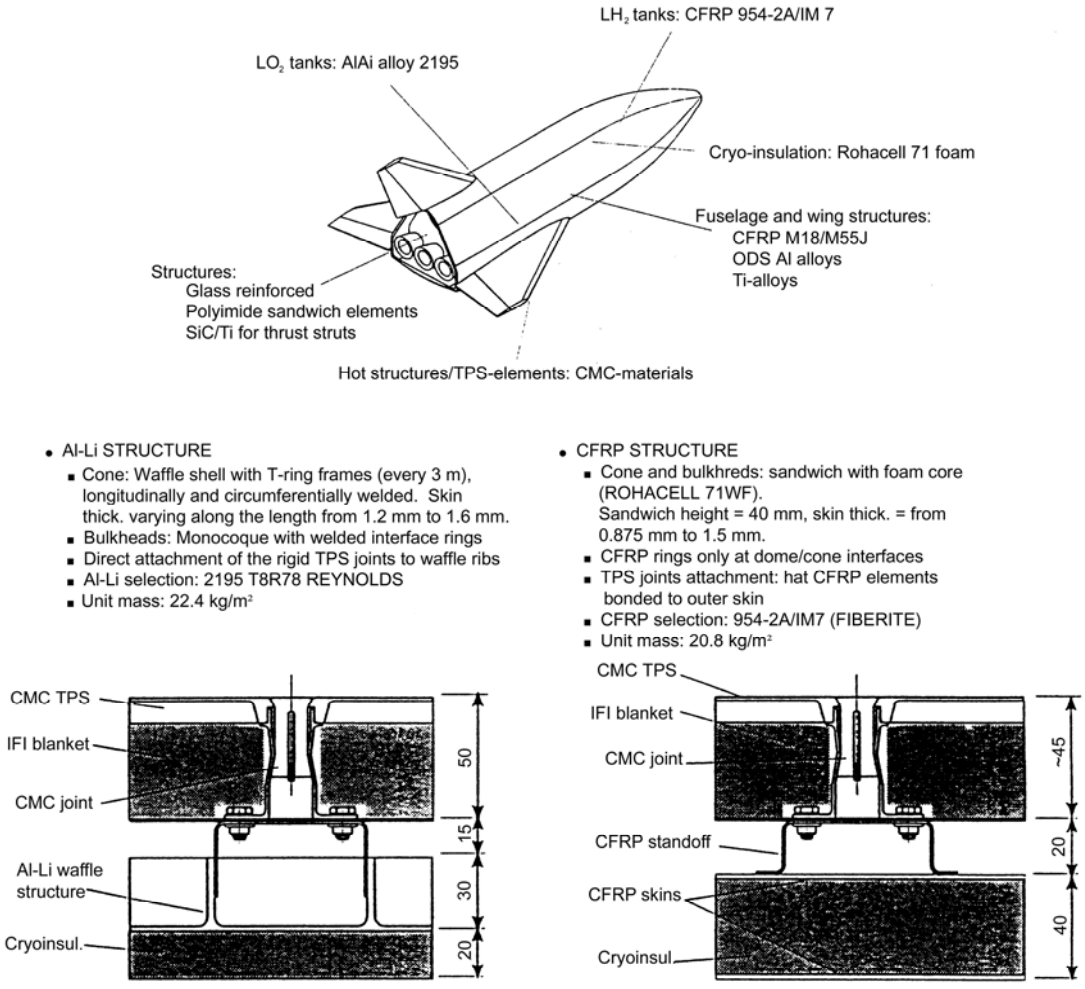

Figure 29.11-1 - Cryogenic tank concepts from the FESTIP programme

29.12 Satellite central cylinders – Filament wound

29.12.1 General

Traditionally, the central cylinders of satellites are aluminium alloy constructions. Developments since 1985 have shown an increasing preference to use CFRP sandwich constructions for central cylinders, principally as a means of saving mass, Ref. [29-1], [29-2], [29-41], [29-42], [29-43], [29-44].Mass savings are typically in the order of 30% to 40% compared with aluminium.

The initial composite constructions used a number of moulded sandwich panel segments to make up the cylinder, Ref. [29-41], [29-42], [29-43]. Latterly, the use of filament winding to produce a single piece construction has been proposed, Ref. [29-1], [29-2].

Sandwich constructions have been extensively used for the central structures of SKYNET and EUROSTAR. Other examples include SPELDA, SYLDA and SPELTRA.

The factors of particular interest when producing central cylinder designs are:

- Mass,
- Joining techniques, and
- Costs.

Several technical solutions are feasible to produce cylindrical constructions, including:

- Corrugated aluminium design with ring stiffeners.
- Blade-stiffened CFRP panel.
- Corrugated CFRP panel, [See: 30.3], Ref. [29-45],
- Bonded CFRP sandwich panel construction, [See: 30.4]:
  - classical bonded designs.
  - cocured designs, Ref. [29-43], [29-44].
- Filament-wound CFRP sandwich cylinder,
- Filament-wound monocoque CFRP cylinder.

29.12.2 CFRP central cylinder constructions

29.12.2.1 General

The details of some designs for satellite central cylinders are presented as examples, [See also: 30.3 DFS Kopernikus central cylinder; 30.4 Olympus C.S.E. cylinder].

29.12.2.2 Fokker Olympus satellite derivative: 1984-88

The original lower part of the propulsion module of the Olympus central cylinder was a corrugated aluminium construction. The characteristics of this are shown in Table 29.12.1.

Table 29.12-1 - Olympus central cylinder characteristics

Diameter	1200 mm
Length	1265 mm
Aluminium sheet thickness	0.5 mm
5 intermediate ringframes	
End ring connections	
Total Mass	23.5 kg
Ultimate Load Levels: Horizontal : Vertical:	89.8 kN 65.6 kN
Running Loads:	- 135 N/mm compressive at lower interface + 100 N/mm tension + 50 N/mm shear
Lateral frequency	10 to 20 Hz
Axial frequency	35 to 50 Hz

Blade stiffened and corrugated CFRP designs were considered but rejected because the, Ref. [29-41], [29-42]:

- Blade stiffened design was too heavy when taking into account the load-introduction demands.
- Corrugated design was mass-efficient, from 17.4 kg to 18.5 kg in total, but had high recurring and non-recurring manufacturing costs.

The sandwich designs weighed:

- 14.8 kg for a bonded design, and
- 16.8 kg for a bolted design.

The bonded design needed two aluminium end-rings with a simple bonded channel groove joint, which was cheaper to implement than the bolted configuration.

A reduced-scale demonstrator cylinder was produced; 1170 mm diameter by 1265 mm in height. The characteristic of this can be summarised as, [See also: 30.4]:

- Two shell segments with a T-profile at the shear web connection.
- Sandwich with symmetrical faces of 5 layers (±25°, 0°, ±25°) with ply thickness of 0.05 mm.
- T300/Code 92 CFRP with 60% fibre volume fraction.
- Aluminium honeycomb core 5056-0.0007" 3/16" with Redux 312L adhesive.
- The CFRP skins were made separately and subsequently bonded with the honeycomb.
- Localised CFRP reinforcements near end-rings.

The study demonstrated that a 42% mass saving was possible over the previous metallic design.

The part count for a sandwich construction was reduced by a factor 10, which resulted in the total cost being only marginally higher (6%) than the aluminium predecessor.

29.12.2.3 Aerospatiale cocured CFRP honeycomb central cylinder: 1985

Aerospatiale produced a cocured construction for the ARABSAT programme, Ref. [29-43]. The cylinder was slightly conical; the diameter varied from 906 mm to 958 mm over the height of 2144 mm.

The programme concluded that design simplifications were achievable by changing from a classical separate skin manufacturing route to a cocured construction. Reduced timescales and cost-savings were possible because of the lower number of parts, coupled with the need for fewer moulds.

29.12.2.4 CASA cocured central cylinder for Artemis: 1991-96

A cocured CFRP sandwich cylinder was developed to an Artemis configuration, Ref. [29-44], [29-57]. The demonstrator cylinder was 1629 mm in length and 1202 mm in diameter. The features that can be highlighted include:

- CFRP face skins of M55J fibre supplied as Vicotex 914/G-967 prepreg; with M40J/G-829 as the back-up prepreg.
- Fibre lay-up using a prepreg ply thickness of 0.18 mm. Depending on position, either:
  - 2 layers of ±25°, or
  - 3 layers of [+25°, 0°, -25°].

- Two thicknesses of aluminium honeycomb, 3/16″ and 1/8″:
  - Core-to-core bonds made using Redux 208/5-NA adhesive.
  - Skin-to-core bonds made using Redux 319L adhesive, with Redux 119 primer.
- Total demonstrator cylinder mass of 29.8 kg, including ring, inserts and cleats.

The cocured design was chosen as being more cost-effective than a reinforced monocoque CFRP or corrugated CFRP designs. The final Artemis central cylinder was made using the same technology, but with an increased length of 2529 mm; a total of 3 units were made.

29.12.2.5 British Aerospace EUROSTAR central cylinder: 1990

The application of sandwich panel designs by can be traced to the SKYNET IV and EUROSTAR series satellites; also the SPELDA launch structure.

The accepted technique of bonding pre-moulded face skins onto honeycomb core was applied. This was considered a time-consuming route to produce a series of satellites. Filament winding was pursued in order to reduce time scales, Ref. [29-1].

The original design used 10 mm thick aluminium honeycomb core, bonded with 0.8 mm Courtaulds HM-S 10K/Code 69 face skins, where 4 segments made a complete cylinder.

To filament-wind a cylindrical structure sandwich structure, the important issues addressed were:

- producing a balanced configuration,
- direct winding onto the honeycomb core,
- achieving a high fibre volume fraction for a low mass design with wet winding,
- control of winding patterns to optimise lay-up thickness,
- avoidance of porosity with low angle windings, where consolidation forces are low.

The characteristics of the cylinder produced by filament winding are given in Table 29.12.2.

Table 29.12-2 - British Aerospace EUROSTAR central cylinder

Internal Diameter (mm):	485
External Diameter (mm):	509
Length (mm):	880
Face skin thickness (mm):	1.0
Fibre volume fraction:	60±5%
Voidage:	<2.0%
Fibre orientations (w.r.t. cylinder axis):	[±10°, ±45°, ±45°, ±10°]

A steel mandrel was chosen, onto which was wound 6000 filament tow Celion G50-300 HM carbon fibres (E = 350 GPa) with Shell 9000 series epoxy resin. This produced a band 3.3 mm wide.

Initial problems with excessive faceskin thickness were overcome, by lowering average thicknesses from 1.16 mm to 0.95 mm to attain an acceptable fibre volume fraction.

A qualification cylinder configured for Telecom II gave acceptable results and so confirmed the validity of the technology. A comparison of the mass between the traditional segmented, autoclave construction and the filament wound design, of 10.2 kg, showed that the filament-wound version to be slightly lighter; approximately 7%.

Whilst the composite faceskins were marginally thicker on the wound version, the elimination of additional material, such as bonded doublers, used in the conventional construction more than compensated for this.

The filament-wound construction was consequently adopted for EUROSTAR structures, including LOCSTAR and HISPASAT.

29.12.2.6 Stork/UCN DRS derivative: 1992

A demonstrator model, tested in 1992, was used to confirm the validity of a filament-wound thrust-cylinder design for ITALSAT 2, Ref. [29-2]. The design had aluminium end-rings, a lower-tank interface and provisions for an upper-tank interface.

The demonstrator was characterised by the use of:

- A 3-ply [±22.5°, 90°] lay-up of 53% fibre volume fraction.
- M46JB carbon fibre with EPON 9400/9450 epoxy resin system.
- Incorporation of local reinforcement in the form of prepreg braid tape [0°, 90°] or [±45°, 90°] at load introduction points, e.g. inserts.
- Different aluminium cores depending on location; 1/4”- 5052-0.0007P or 1/8” -5052-0.0010P.

The manufacturing procedure was:

a. Laying of the inner reinforcement located at the lower tank interface and lower end ring.

a. Winding of the inner skin.

b. Oven-gelling of the inner skin and inner reinforcement, with bleeder fabric and aramid fibre overwrap during the consolidation period only.

c. Applying adhesive film (FM300) and positioning of honeycomb segments on inner skin; with FM 410 adhesive foam in gaps between honeycomb segments.

d. Bonding of honeycomb core segments onto inner skin; with aramid fibre overwrap.

e. Winding of outer skin over honeycomb and FM 300 adhesive film, followed by compaction with overwrap.

f. Laying of outer reinforcements located at the lower tank interface-to-lower end ring and the upper tank interface.

g. Gelling of outer skin and outer reinforcements, again with bleeder fabric and aramid overwrap.

h. Cylinder removed from mandrel.

i. Oven curing of free-standing wound assembly.

j. Cylinder replaced on mandrel and cut to length.

k. Bonding, using EC 2216 A/B adhesive, of upper and lower tank aluminium (2024-T3) interface strips.

l. Drilling of holes at upper and lower tank-interface.

m. Bonding of tank-interface inserts.

n. Bonding of upper and lower aluminium (2024-T3) end-rings.

The final mass of the cylinder was 18.78 kg compared with an initial target of 20 kg for a diameter of 1110 mm.

29.12.3 Attributes of filament-wound sandwich central cylinders

Compared with other means of manufacturing composite central cylinders, the benefits that can be gained include:

- Lower recurring costs.
- Shorter production times.
- High-accuracy on shape and dimensional tolerances.
- Mass equal to, or marginally less than, sandwich designs made by conventional autoclaved techniques.
- Lower part count compared with other designs, either metallic or composite,
- Suitable manufacturing route for long production runs, Ref. [29-39].

There are also suggestions that a filament-wound monocoque design can be a more cost-effective means of manufacturing a cylinder, albeit it with a mass penalty compared with a sandwich construction. This is the object of further investigation that could result in another route for producing cylindrical constructions.

In conclusion, there are various possible routes for designing and manufacturing CFRP composite cylinders. They each have subtle disadvantages and attributes when compared with each other.

Selection is strongly influenced by the experience and processing capabilities of each contractor. Mass differences between CFRP designs are likely to be small, e.g. within 10% of each other.

Filament winding has cost benefits, providing that a sufficiently long production run is possible where the design of units remains unchanged.

29.13 Optical structures

29.13.1 General

Optical structures demand very high dimensional stability. CFRP has become the preferred construction material, [See: 28.14].

Cylinders are convenient shapes for telescope constructions. The production of a filament wound tube as opposed to an assembled autoclave moulded panel construction is a natural evolution, as described for central cylinder designs, [See: 29.12].

ORFEUS, the ‘orbiting and retrievable far and extreme ultraviolet spectrometer’, is given as an example.

29.13.2 ORFEUS telescope

ORFEUS is a 1.1 m diameter by 4 m long telescope integrated into the ASTRO-SPAS satellite, Ref. [29-46].

The design constraints led to a filament-wound tube stiffened on the outer side with autoclave-cured CFRP profiles. Flanges and other interfaces were mainly made of Invar, a low CTE nickel-iron alloy. An Invar foil covered the inner surface of the tube to limit outgassing. ASTRO-SPAS, with ORFEUS integrated, is shown in Figure 29.13.1, Ref. [29-46].

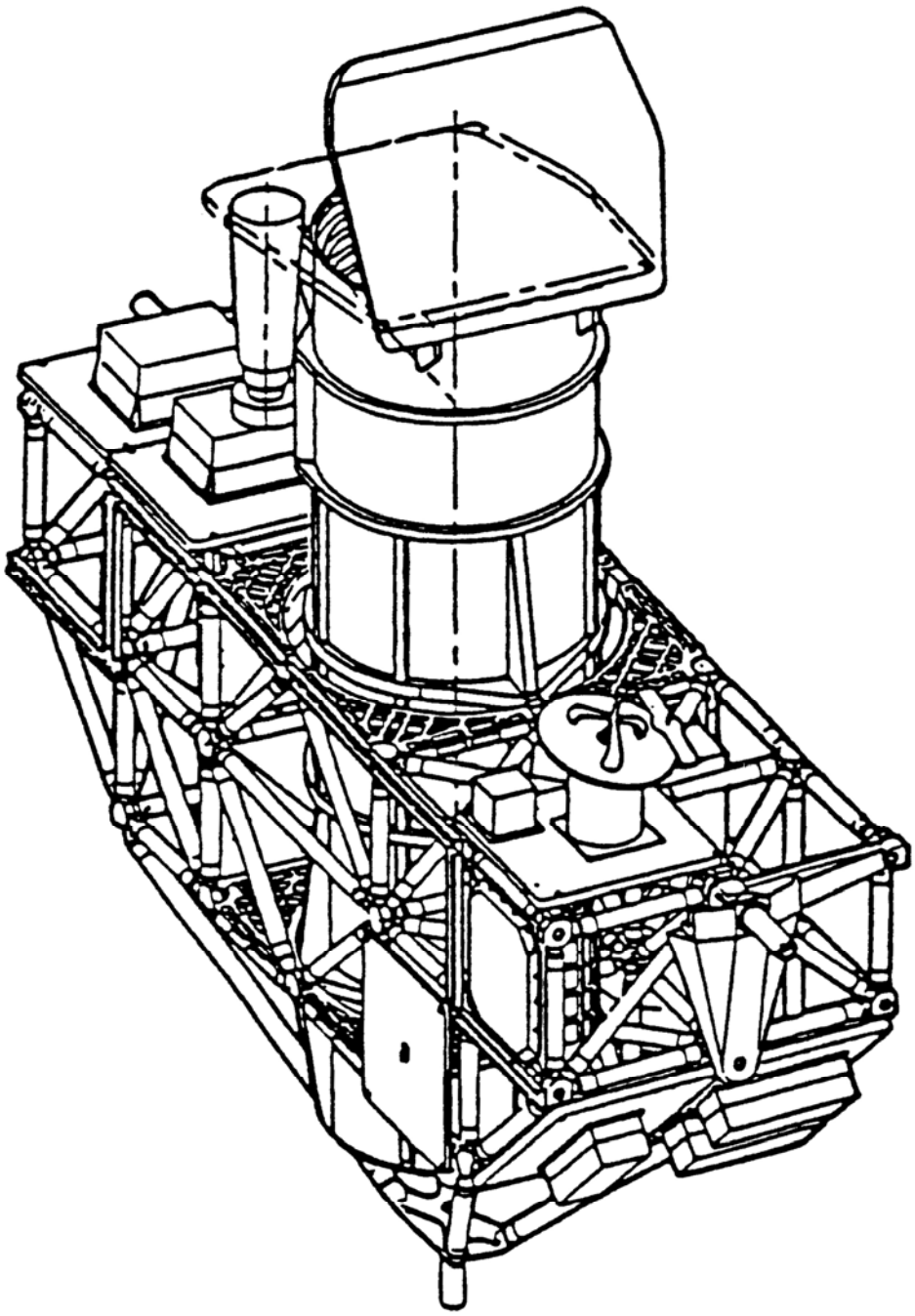

Figure 29.13-1 - ASTRO-SPAS with integrated ORFEUS

The main instrumentation of ORFEUS comprised of a 1 m diameter parabolic mirror and two spectrometers. The design had to meet several constraints, including:

- Ouside dimensions were limited by ASTRO-SPAS and Space Shuttle.
- Interfaces for ASTRO-SPAS fittings, mirror carrier plate, echelle spectrometer, Rowland spectrometer, Star Sensor, MLI, ground support equipment and harness fasteners.
- A global CTE of 0.8 x 10^{-6} /°C.
- Length, parallelism and angle tolerances of flanges and interfaces of the range 0.1 mm, in order to enable precise adjustment.
- A minimum eigenfrequency of 35 Hz.
- The final monolithic CFRP cylinder features included:
- Ciba M10 epoxy Toray M40 UD tape and woven CFRP, fibre volume fraction of 55%.
- 7 layer laminate construction of [90°, ±25°, 90°, ±25°, 90°].
- Titanium riveted assembly instead of adhesive bonding in order to control the amount of high CTE material included in the construction.

The integrated mass of the ORFEUS structure was about 250 kg.

29.13.3 Cylindrical and conical structures

In 1995, Alenia Spazio reported developments in filament winding technology for cylindrical and conical sandwich structures, Ref. [29-47].

Development conical configurations were produced that were representative of an X-ray satellite optical bench.

Prepreg tow having high-modulus carbon fibres (Toray M40J) was used for the windings and Ciba Geigy 914 resin system. Steel tooling was used.

Conventional sandwich core materials of aluminium and Nomex™, and co-curing procedures with conventional adhesives are reported. A 1/4- scale seamless cylinder and cones were prepared, 1150 mm long and 510 mm diameter. Some problems concerning fibre waviness were deemed solvable.

29.14 References

29.14.1 General

[29-1] G.M. Teare
'Filament winding of satellite structures'
Proceedings of ESA Symposium: Space Applications of Advanced Structural Materials. ESTEC, 21-23 March 1990
ESA SP-303, p257-260

[29-2] C.A.L. Kemper et al
'Design and manufacturing of filament wound thrust cylinder'
Proceedings of International Symposium on Advanced Materials for Lightweight Structures, ESTEC, 25-27 March 1992, ESA SP-336, p51-56

[29-3] D.J. Moser
'Inflatable mandrel fabrication technology: Advantages for the containment of rocket propellants'
AIAA Paper 92-3058, Proceedings of the Joint Propulsion Conference and Exhibition, Nashville, 6-8 July 1992

[29-4] T.S. Miller & C.J. Fortin
'Fabrication of low cost composite tooling for filament winding large structures'
37th International SAMPE Symposium, March 9-12, 1992
p1160-1169

[29-5] M.L. Enders
'Developments in thermoplastic filament winding'
22nd International SAMPE Technical Conference, Nov 6-8 1990, p88-97

[29-6] F.J. Darms
'Space age pressure vessels'
36th International SAMPE Symposium, April 15-18, 1991
p818-826

[29-7] C. Braun et al
'Advanced composite fiber/metal pressure vessels for space systems applications'
AIAA Paper 91-1976, Proceedings of the 27th Joint Propulsion Conference, June 1991

[29-8] R.C. Haddock & F.J. Darms
'Space system applications of advanced composite fiber/metal pressure vessels'
AIAA Paper 90-2227, Proceedings of the 26th Joint Propulsion Conference and Exhibition, Orlando, 16-18 June 1990

[29-9] E.E. Morris
'High-pressure, high-performance filament-wound carbon/epoxy pressurant tanks with seamless aluminium liners for expendable launch vehicles and spacecraft'
34th International SAMPE Symposium, May 8-11, 1989
p1545-1555

[29-10] C.C. Poe
'Impact damage and residual tension strength of a thick graphite/epoxy rocket motor case'
Journal of Spacecraft and Rockets, Vol. 29, No. 3
May-June 1992, p394-404

[29-11] R. Forster
'Application of advanced structural materials in propellant tanks and pressure vessels'
Proceedings of ESA Symposium on Space Applications of Advanced Structural Materials, ESTEC, 21-23 March 1990
ESA SP-303, p261-266

[29-12] I. Ballinger
'Design and qualification of the cluster satellite propellant tankage'
AIAA Paper 93-2096, Proceedings of the 29th Joint Propulsion Conference

[29-13] MIL-STD-1522A (USAF)
'Standard general requirements for safe design and operation of pressurized missile and space systems.' 28 May 1984

[29-14] R. Forster
'Application of advanced structural materials in pressure vessels for Ariane 5 and Hermes'
AIAA Paper 90-2249, Proceedings of the 26th Joint Propulsion Conference and Exhibition, Orlando, 16-18 June 1990

[29-15] R.C. Haddock et al
'Safety of filament wrapped graphite/epoxy composite pressure vessels for aerospace applications'
AIAA 91-2409, AIAA/ASME/SAE/ASEE 27th Joint Propulsion Conference, 24-26 June 1991

[29-16] S.R. Swanson
'Strength design criteria for carbon/epoxy pressure vessels'
J. Spacecraft, Vol. 27, No. 5, p522-526

[29-17] D.A. Thomas
'Long-life assessment of graphite/epoxy materials for Space Station Freedom pressure vessels'
J.Propulsion, Vol. 8, No. 1, Jan-Feb 1992, p87-92

[29-18] D. Tiller et al
'Design and qualification of a carbon overwrapped, aluminium-lined pressurant tank for Intelsat VII satellite'
AIAA Paper 91-2092, Proceedings of the 27th Joint Propulsion Conference, June 1991

[29-19] P. Charpentier & D. Zorzetto
'High performance titanium/carbon composite gas storage pressure vessel for space use'
AIAA Paper 90-2223, Proceedings of the 26th Joint Propulsion Conference and Exhibition, Orlando, 16-18 June 1990

[29-20] Y. Valy & P. Coquet
'Wound helium pressurant tank development for 2nd stage of Ariane 4 Launcher'
AIAA Paper 90-2347, Proceedings of the 26th Joint Propulsion Conference and Exhibition, Orlando, 16-18 June 1990

[29-21] Y. Valy & P. Coquet
'Wound helium pressurant tank development for second Stage of Ariane 4 launcher'
Advanced Structural Materials. ESTEC, 21-23 March 1990
ESA SP-303, p267-272

[29-22] P. Wächter
'Design and verification of the high pressure vessels GAT and GAM'
In "Ariane 5 Structures and Technologies", Proceedings of Symposium at Arcachon, May 1993, published by Cépaduès-Editions for CNES, ISBN: 2-85428-347-3, p119-126

[29-23] W. Radtke
'GAT and GAM high pressure vessels - materials and manufacturing'
In "Ariane 5 Structures and Technologies", Proceedings of Symposium at Arcachon, May 1993, published by Cépaduès-Editions for CNES, ISBN: 2-85428-347-3, p739-750

[29-24] D. Lestrat & Y. Prel
'Evolution et choix des technologies pour les réservoirs des lanceurs Ariane'
International Symposium on Advanced Materials for Lightweight Structures '94. ESTEC, 22-25 March 1995
ESA WPP-070, p441-454

[29-25] W. Radtke
'Effective propellant and high pressure tankage'
International Symposium on Advanced Materials for Lightweight Structures '94. ESTEC, 22-25 March 1995
ESA WPP-070, p467-472

[29-26] H. Krings & J. Scharringhausen
'Fibre reinforced plastic cases for solid propellant motors'
ESA SP-243, Proceedings of Workshop - Composites Design for Space Applications, 15-18 October 1985, p295-299

[29-27] J. Onoda et al
'Development status of M-V rocket structures and mechanisms'
International Symposium on Space Technology and Science
Japan, 17-22 May 1992, p503-507

[29-28] V. Giavotto et al
'Fabrication and testing of a hybrid titanium-composite integral filament wound solid rocket motor case'
38th International SAMPE Symposium, 10-13 May 1993
p623-633

[29-29] C.C. Poe
'Summary of a study to determine low-velocity impact damage and residual tension strength for a thick graphite/epoxy motor case'
Proceedings of ICAS 17th Congress, Stockholm, Sweden, 9-14 Sept 1990, p1005-1016

[29-30] M.T. Callaghan
'Use of resin composites for cryogenic tankage'
Cryogenics, April 1991, Vol. 31, p282-286

[29-31] D.J. Moser
'Prospects for composite LOX tankage'

AIAA Paper 93-2249, Proceedings of the 29th Joint Propulsion Conference and Exhibition, California, 28-30 June 1993

[29-32] P.Millanvois & P.Berthomet
'Designs and materials for future cryogenic tanks'
Advanced Materials: Design for Space Applications. A Workshop ESTEC, 23-25 March 1988, ESA WPP-004, p97-104

[29-33] H.S.Greenberg
'Trade study plan for graphite composite primary structure (GCPS)'
NASA-CR-196868, 29 July, 1994 & NASA-CR-196866
2 September, 1994

[29-34] H.S. Greenburg
'Selection process for trade study - reusable hydrogen composite tank system (RHCTS)'
NASA-CR-196874, 2 September 1994

[29-35] M.J. Robinson
'Composite cryogenic propellant tank development'
AIAA-94-1375-CP

[29-36] K. Dayton
'National Aerospace Plane integrated fuselage/cryotank risk reduction program'
AIAA 93-2564, AIAA/SAE/ASME/ASEE 29th Joint Propulsion Conference and Exhibition, 28-30 June 1993

[29-37] M.J. Robinson et al
'Advanced composite structures for launch vehicles'
Proceedings of the 22nd International SAMPE Technical Conference, 6-8 November 1990

[29-38] M.J. Robinson
'A qualitative analysis of some of the issues affecting the cost of composite structures'
23rd International SAMPE Technical Conference
22-24 October 1991, p1-14

[29-39] M.J. Robinson et al
'Advanced composite structures for launch vehicles'
SAMPE Quarterly, January 1991, p26-37

[29-40] D.C. Goeders & J.L. Perry
'Adhesive bonding PEEK/IM6 composite for cryogenic applications'
Proceedings of 36th International SAMPE Symposium
15-18 April 1991, p348-361

[29-41] 'Composite structural element (CSE) study'
Fokker B.V. Final Report TR-R-86-CSE-080, 1986
ESA Contract No. 5928/84/NL/PB (ESA CR(X) 3306)

[29-42] C. Blaas et al
'Study of a CFRP replacement for the Olympus central cylinder'
Advanced Materials: Design for Space Applications. A Workshop

ESTEC, 23-25 March 1988, ESA WPP-004, p219-225

[29-43] J.L. Pettex
'Comparison of classical and cocuring manufacturing techniques for a CFRP honeycomb central tube'
ESA SP-243, Proceedings of Workshop - Composites Design for Space Applications, 15-18 October 1985, p291-294

[29-44] A. Jimenez et al
'Design and development of a CFRP central cylinder for satellites'
Proceedings of International Symposium; 'Advanced Materials for Lightweight Structures', ESTEC, 25-27 March 1992, ESA SP-336, p33-38

[29-45] D. Brosda
'On the development of a corrugated CFRP central cylinder'
ESA SP-243, Proceedings of Workshop - Composites Design for Space Applications, 15-18 October 1985, p285-290

[29-46] T. Schaeffler
'Orfeus CFRP structure. A high stiffness - low thermal strain space telescope structure'
Proceedings of the International Conference on Spacecraft Structures and Mechanical Testing, Noordwijk, The Netherlands, April 1991, ESA SP-321, p893-899

[29-47] B. Fornari et al
'Manufacture of cylindrical and conical CFRP/sandwich structure for spacecraft applications'
40th International SAMPE Symposium, May 8-11, 1995
p1603-1615

[29-48] C.H. Parr
'Composites for propulsion applications - An overview'
AIAA Paper 88-3127, AIAA/ASME/SAE/ASEE 24th Joint Propulsion Conference, 11-13 July 1988

[29-49] J.A. Bailie
'Application of composites to missile structures - A review'
SAMPE Quarterly, January 1981, p1-8

[29-50] M.J. Messick et al
'Space Shuttle filament wound case compressive strength study: Part II - Analysis"
AIAA Paper 86-1417

[29-51] A.K. Munjal
'Use of fiber-reinforced composites in rocket motor industry'
SAMPE Quarterly, January 1986, p1-11

[29-52] E.W. Tackett et al
'Carbon pressure vessel performance with changing dome profiles'
AIAA Paper 84-1351, AIAA/ASME/SAE/ASEE 20th Joint Propulsion Conference, 11-13 June 1984

[29-53] M. Maheshwari and R.L. Grover
'Development of an advanced composite rocket motor case for internal and external load environments'
AIAA Paper 84-1352, AIAA/ASME/SAE/ASEE 20th Joint Propulsion Conference, 11-13 June 1984

[29-54] 'Solid rocket motor case improvement program - State of the art report'
MAN Technologie Document A211 618 - RA 006, November 1995

[29-55] J. Scharringhausen & R.G. Cuntze
'FEM-calculations on the domes of fibre reinforced plastic cases for solid propellant motors'
Advanced Structural Materials: Design for Space Applications - A Workshop. March 1988, ESTEC, ESA WPP-004, p257-263

[29-56] 'Solid rocket motor case improvement program - Executive summary'
MAN Technologie Document A211 618 - RA 008, Issue 1
November 1995

[29-57] 'Carbon fibre technology for space applications - Executive summary'
CASA Report CAS-CFT-RPT-0002
ESTEC Contract No.9231/90/NL/PP

[29-58] FESTIP year workshop, 17-18 October 1996. ESA/ESTEC Summary handout

29.14.2 ECSS documents

[See: ECSS website]

ECSS-Q-ST-70-02	Thermal vacuum outgassing test for the screening of space materials; previously ESA PSS-01-702
ECSS-Q-70-71	Data for selection of space materials and processes; previously ESA PSS-01-701
ECSS-Q-ST-70	Materials, mechanical parts and processes; previously ESA PSS-01-70

29.14.3 NASA standards

NASA STD 6001	Flammability, odor, offgassing and compatibility requirements and test procedures for materials in environments that support combustion; previously NASA NHB 6080.1

30
Examples of developed structures

30.1 Introduction

Some examples of composite structural elements developed for space applications are described. These include applications for:

- Launchers, [See: 30.2; 30.5; 30.6; 30.8].
- Satellites, [See: 30.3; 30.4].
- Payload support structures, [See: 30.7].

Where possible, each application includes information related to:

- The main requirements (design driver),
- The solutions related to structural design, and
- Details on the design features.

30.2 Ariane 4: Interstage 2/3

30.2.1 Contractor

Developed by: Fokker BV Space Division, (NL), Ref. [30-1], [30-3].

30.2.2 Characteristics

30.2.2.1 Function

A blade-stiffened CFRP cylindrical structure that connects the 2nd and 3rd stage of the Ariane 4 launcher, as shown schematically in Figure 30.2.1.

The composite interstage was developed as an alternative for the classical aluminium alloy configuration.

30.2.2.2 Mass reduction

The total mass reduction in comparison with the aluminium structure was about 20% for the same costs.

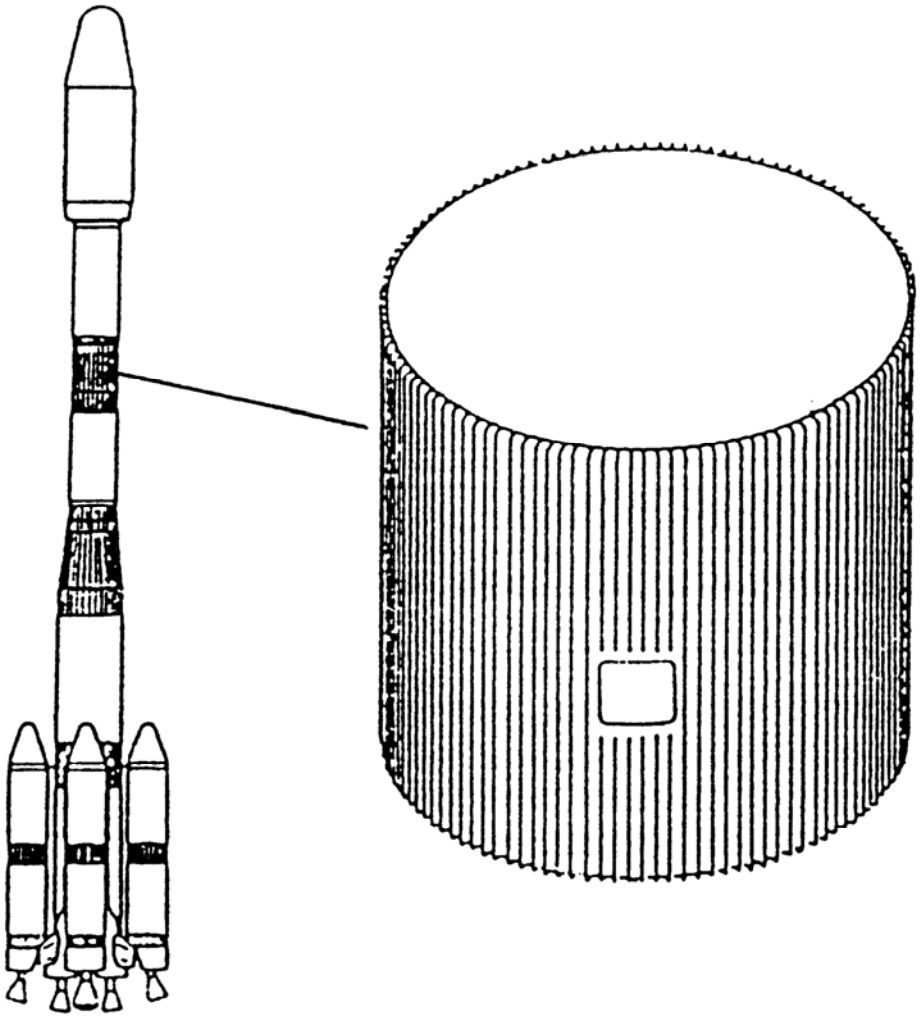

Figure 30.2-1 - Ariane 4: Interstage 2/3

30.2.2.3 Advantages

The blade-stiffened configuration was preferred because:

- The process for production was ready for application.
- Mass difference compared with a sandwich shell is less than 10% (considering also the additional weight for the end connections).
- Connections can simply be made by bolts and lap joints.
- Good inspectability of the solid laminate.
- Low vulnerability because of the thick laminate.

Figure 30.2.2 shows the dimensions of a blade-stiffened section.

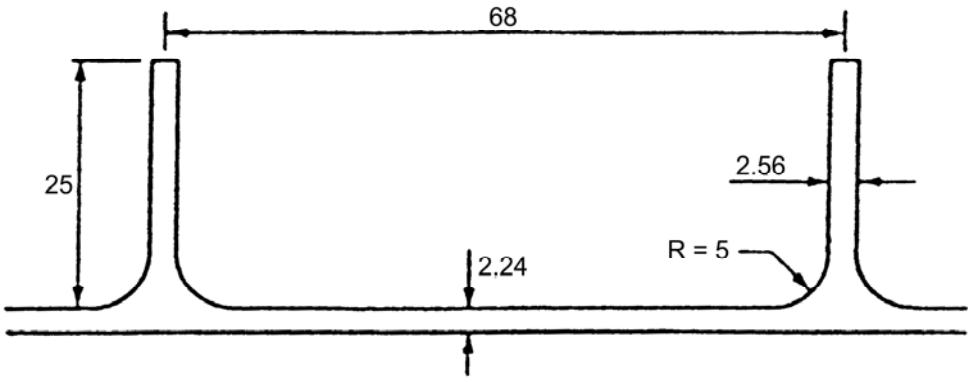

Figure 30.2-2 - Ariane 4 Interstage 2/3: Blade stiffened dimensions

30.2.3 Structural configuration

30.2.3.1 General

The structure is assembled from several component parts:

- Two aluminium end rings, with flanges and 240 bolt holes.
- Five aluminium intermediate ring frames.
- Eight curved blade-stiffened CFRP panels (2.7 m²).

30.2.3.2 Geometry

Radius:	1300 mm.
Height:	2730 mm.

30.2.3.3 Thicknesses

Skin:	2.24 mm.
Stiffener:	2.56 mm.
Stiffener pitch:	68 mm.
Stiffener height:	25 mm.

30.2.3.4 Material

CFRP prepreg T300/976.

30.2.3.5 Lay-up

Skin:	±45° / 0°4 / ±45° / 0°4 / ±45°.
Stiffener:	±45° / 0°5 / ±45° / 0°5 / ±45°.

Radius between stiffener and skin is filled with 0° fibres.

30.2.3.6 Limit loads

Limit loads (compression): 389 N/mm.

30.2.3.7 Weight of structure

Final weight of structure: 212 kg.

30.2.3.8 Special features

The stringer was specially shaped to reduce stress concentrations at the end, as shown in Figure 30.2.3.

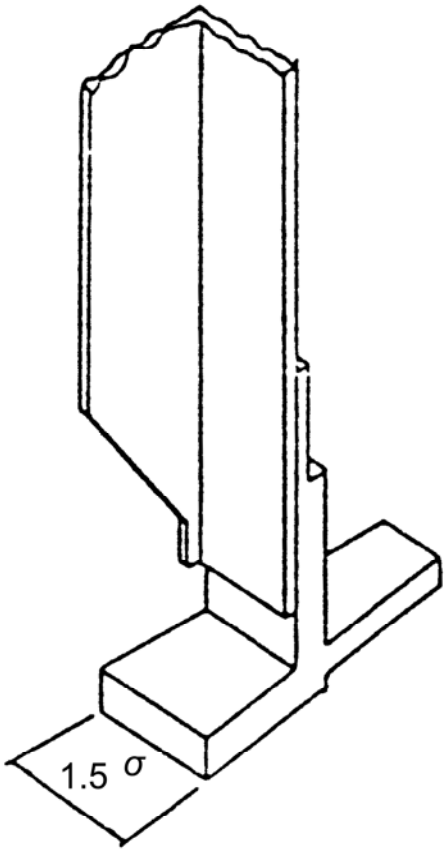

Figure 30.2-3 - Ariane 4 Interstage 2/3: Special feature

30.3 DFS Kopernikus: Central cylinder

30.3.1 Contractor

Developed by MBB/ERNO Raumfahrttechnik GmbH, Bremen, (D), Ref. [30-1], [30-3].

30.3.2 Characteristics

30.3.2.1 Function

A corrugated CFRP structure for the central cylinder of the German communication satellite DFS 'Kopernikus'. The layout is shown in Figure 30.3.1.

30.3.2.2 Mass

A corrugated cylindrical shell structure with internal and external frame belts was chosen because of the high structural efficiency and low mass.

30.3.2.3 Advantages

The design concept promised advantages, including:

- High reliability because it is easy to inspect.
- Simple interconnection of the individual structural parts of the central tube by light rivets.
- Simple attachment of additional structural components, e.g. supports, by rivets.
- Availability of 'hard points' for concentrated radial load introduction at the discrete frames.
- Simple repair method, i.e. bending of doubler to damaged corrugation zone and securing by rivets to prevent peeling.

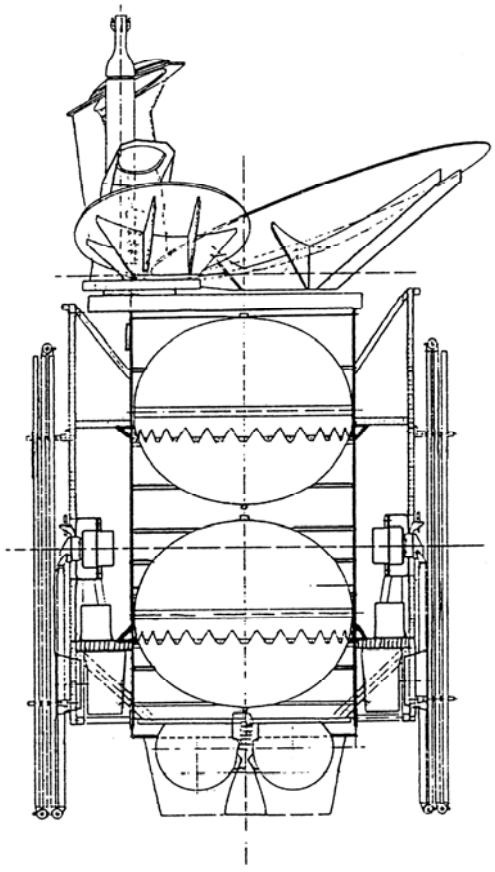

Figure 30.3-1 - DFS: Central cylinder

30.3.3 Structural configuration

30.3.3.1 Geometry

Figure 30.3.2 shows the overall geometry of the central cyclinder.

Radius:	469 mm
Height:	1780 mm
Corrugation angle:	60°
Corrugation height:	10 mm
Number of corrugations:	84
Thickness:	0.4 to 0.7 mm

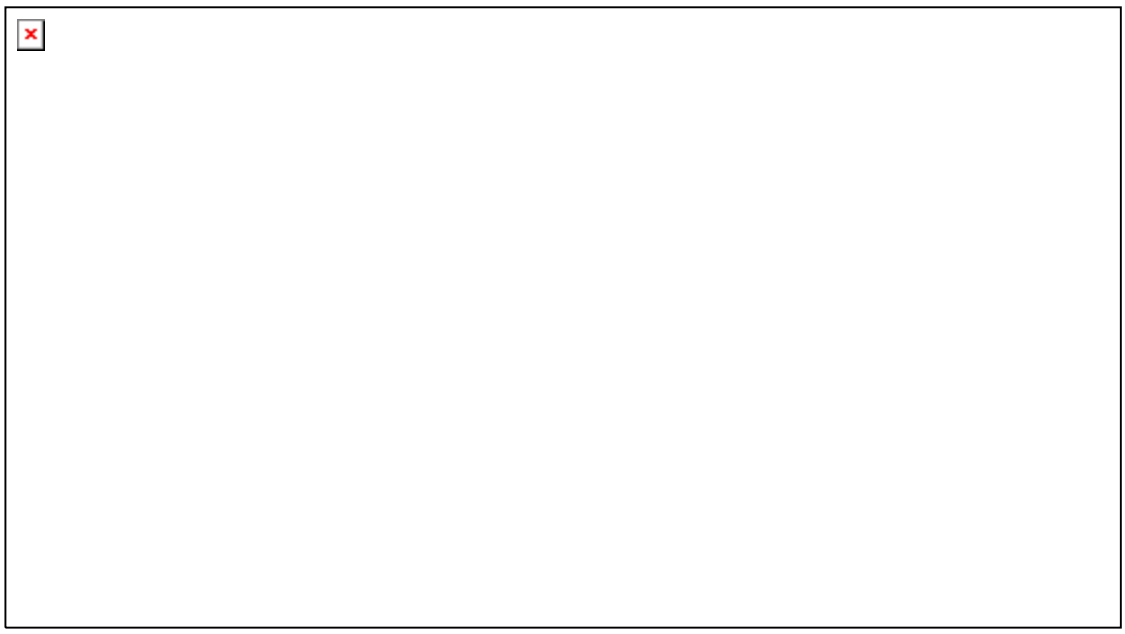

Figure 30.3-2 - DFS Kopernikus central cylinder: Geometry

30.3.3.2 Material

CFRP prepreg T300/914.

The material selection was affected by the frequency constraints. The logical initial choice of high-modulus carbon fibres was changed to high-strength fibres for improved damage tolerance.

30.3.3.3 Lay-up

Corrugation: [±32.5 / $0°_i$]s.

With i = 0, 1, 3 varying over the length.

30.3.3.4 Loads

Loads used: Ultimate load (compression): 250 N/mm.

Ultimate load (shear): 80 N/mm.

30.3.3.5 Frequencies

Frequencies used: Axial: $f_a \geq 35$ Hz.

Lateral: $f_l \geq 15$ Hz.

30.3.3.6 Weight of structure

Final weight of assembled central cylinder, including frames, platform rings and belts: 10.7 kg.

30.3.3.7 Special features

The platform rings are shaped as open triangles made of HM 4 harness satin prepreg (4 layers; thickness: 0.9 mm). One U shaped ring (antenna platform ring) also made of HM-4 harness satin prepreg (5 layers; thickness: 1.2 mm). Figure 30.3.3 shows this feature.

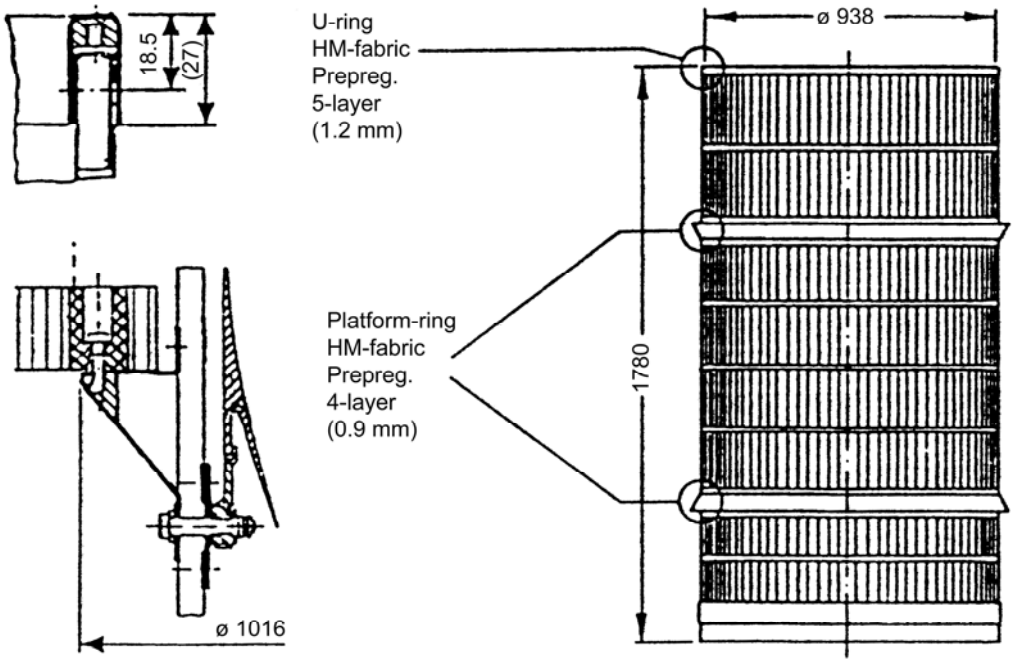

Figure 30.3-3 - DFS Kopernikus central cylinder: Special features

30.4 Olympus C.S.E. cylinder

30.4.1 Contractor

Developed by Fokker BV, Amsterdam, (NL), Ref. [30-2], [30-3].

30.4.2 Characteristics

30.4.2.1 Function

Performed a feasibility study of a composite structure, used as the lower part of the propulsion module of the central cylinder, on the Olympus satellite. The position of cylinder is shown in Figure 30.4.1.

The C.S.E. is designed as a sandwich structure.

30.4.2.2 Mass reduction

By replacing the original aluminium structure with a CFRP structure, a mass saving of 40% is feasible.

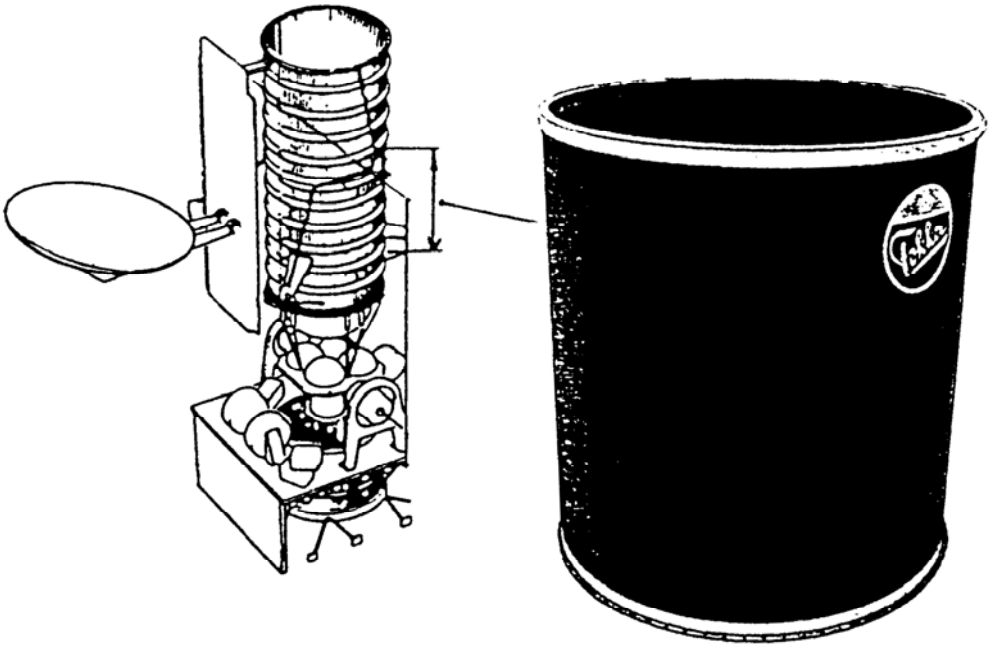

Figure 30.4-1 - Olympus: C.S.E cylinder

30.4.2.3 Advantages

The production method used for the C.S.E. cylinder is such that the number of components, compared with the aluminium version, is reduced by a factor 10. Only one mould is needed for the production of two semicylindrical sandwich shells.

30.4.2.4 Geometry

Figure 30.4.2 shows the cylinder geometry, along with the materials used at various positions.

Radius:	585 mm.
Height:	1265 mm.

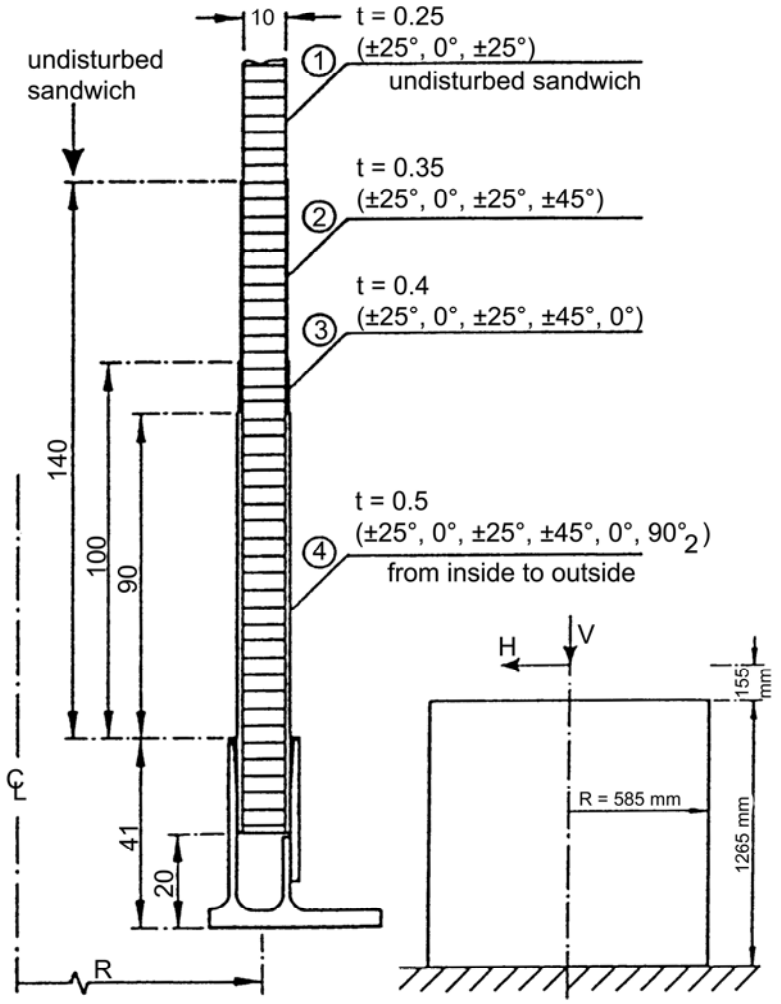

Figure 30.4-2 - Olympus C.S.E. cylinder: Geometry and materials

30.4.2.5 Thicknesses

Skin:	0.25 to 0.5 mm.
Core:	10 mm.

30.4.2.6 Material

CFRP prepreg:	T300/ Code 92.
Core:	Aluminium 5056.
Core cell size:	3/16", 0.0007".

30.4.2.7 Lay-up

[See: Figure 30.4.2]:

①	[±25°/0°/±25°].
②	[±45°/±25°/0°/±25°].
③	[0°/±45°/±25°/0°/±25°].
④	[90°2/0°/±45°/±25°/0°/±25°].

30.4.2.8 Loads

Loads used:

Limit load (compression): 96.4 N/mm.

Ultimate load (compression): 135 N/mm.

30.4.2.9 Frequencies

Frequencies used:

Axial: 35 Hz < fa < 50 Hz.

Lateral: 10 Hz < fl < 20 Hz.

30.4.2.10 Weight of structure

Weight of assembled cylinder, with reinforcements, CFRP connection strips, repair stickers and cold bonding adhesive-foam: 7.88 kg.

30.4.2.11 Special features

The connection of the end rings is shown in Figure 30.4.3.

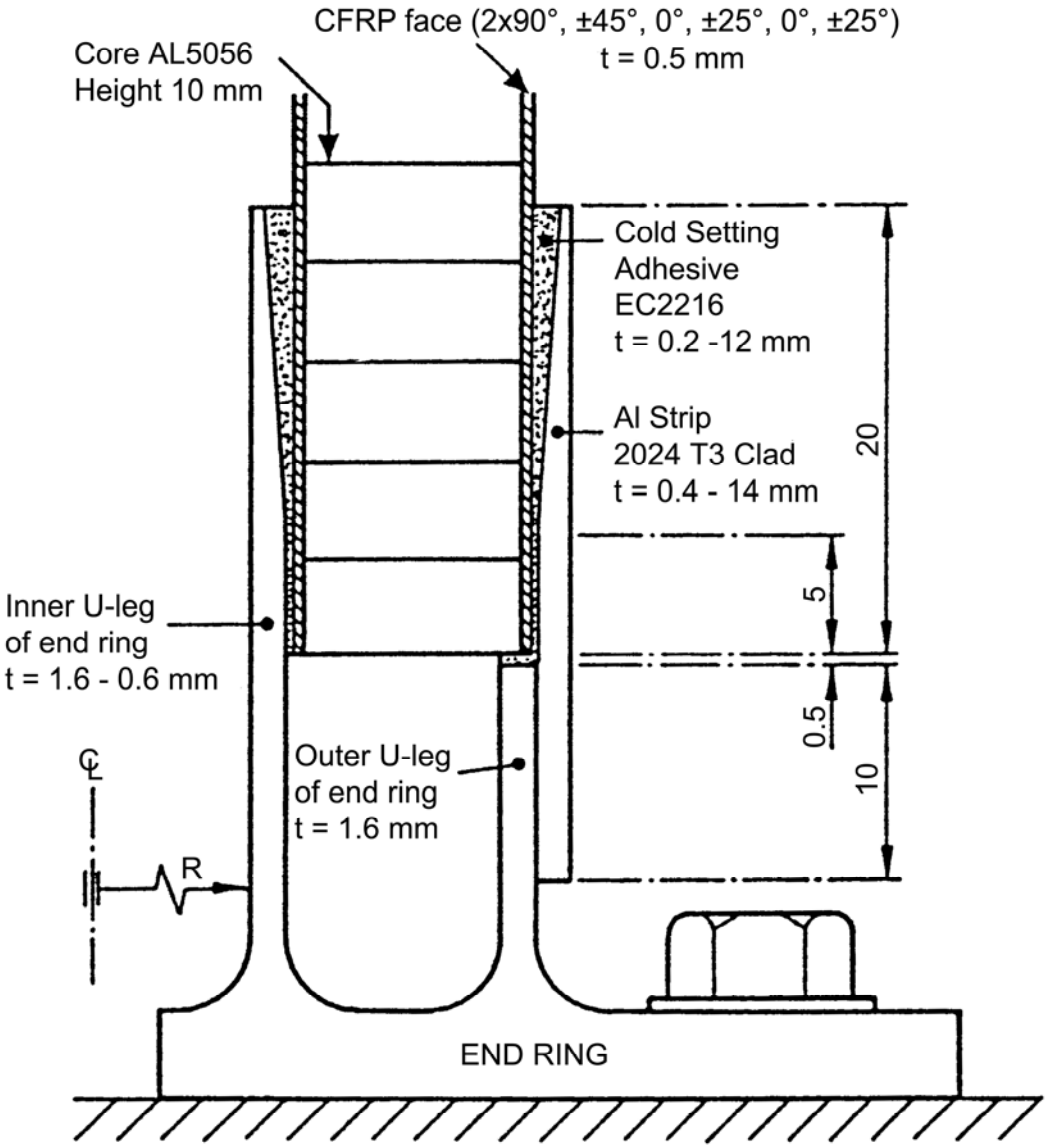

Figure 30.4-3 - Olympus C.S.E. cylinder: Special feature

30.5 Ariane 4: Adapter 937-B

30.5.1 Contractor

Developed by CASA Space Division, Madrid (E), Ref. [30-4].

30.5.2 Characteristics

30.5.2.1 Function

CFRP sandwich truncated conical structure that connects the satellite with the inner cone of the vehicle equipment bay or with the upper zone of the SPELDA of Ariane 4. The position of the adapter is shown in Figure 30.5.1.

Maximum satellite mass: 2300 kg.

30.5.3 Structural configuration

30.5.3.1 Geometry

Bottom diameter: 1920 mm.

Top diameter: 945 mm.

Height: 1079 mm.

Core:

- Central zone: Skin thickness: 1.08 mm.
  - Lay-up: [+45° / 0°4 / -45°].
  - Core: 12 mm.
- End zone: Skin thickness: 1.92 mm.
  - Lay-up: [45°]3.
  - Core: 12 mm.

30.5.3.2 Materials

Skins: Vicotex 914/G829 (M 40 fibre).

Reinforcements: Vicotex 914/G803 (T 300 fibre).

Core: Aluminium honeycomb type NIDA 4.20p and type NIDA 3.58p.

End rings: Aluminium alloy 7075-T7351.

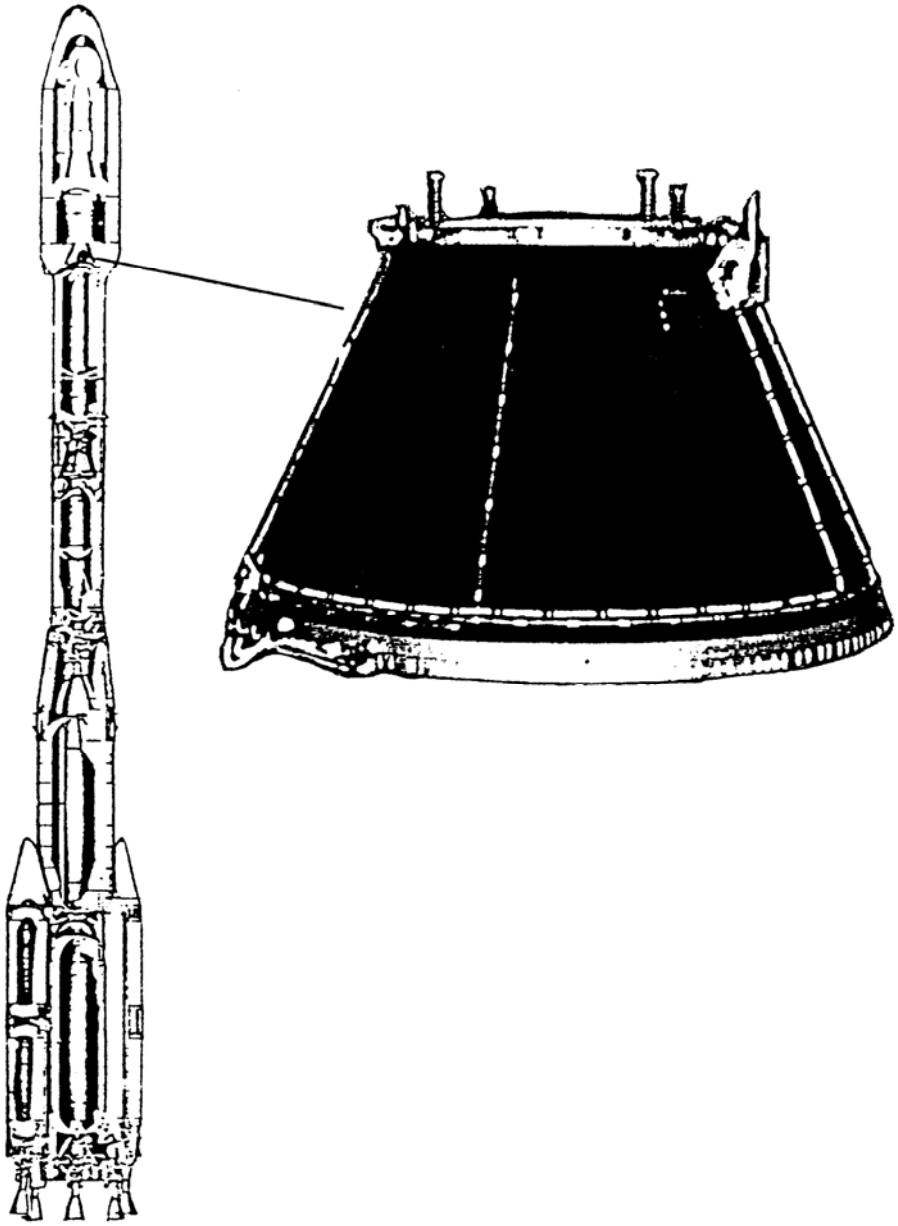

Figure 30.5-1 - Ariane 4: Adapter 937-B

30.5.3.3 Loads

Loads used:

Compressive flux:	95 N/mm.
Mass:	46.5 kg.

30.5.3.4 Special features

Sandwich shell manufactured in one piece by co-curing technology; Figure 30.5.2 shows the overall shape.

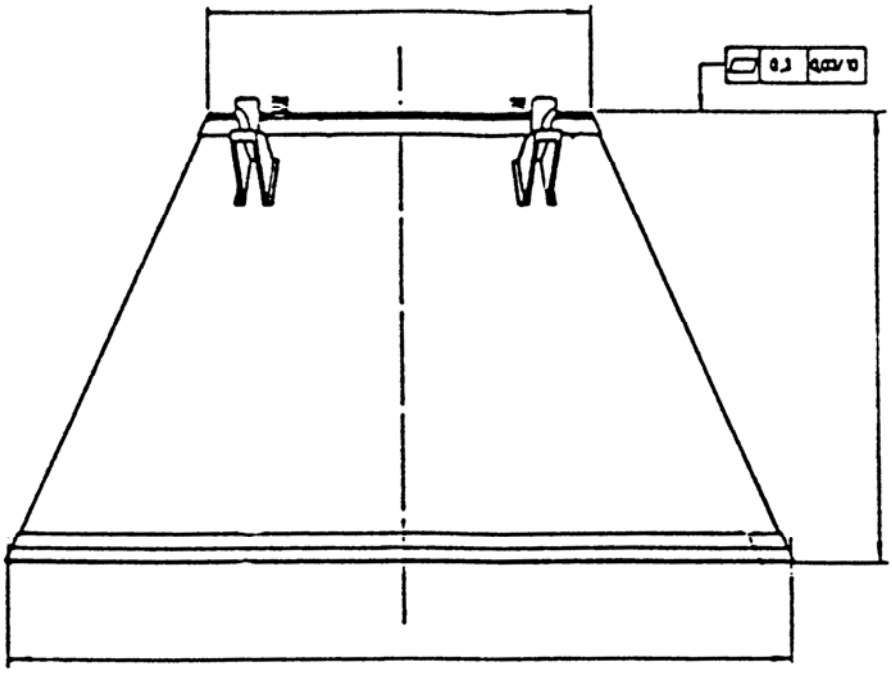

Figure 30.5-2 - Ariane 4 937-B adapter: Special features

30.6 Ariane 4: Vehicle equipment bay

30.6.1 Contractors

This was developed by main contractor Matra Espace, (F), along with CASA Space Division (E), as subcontractor for the inner cone study and structure manufacturing, Ref. [30-4].

30.6.2 Characteristics

Figure 30.6.1 shows the position of the vehicle equipment bay. The structural detail is shown in Figure 30.6.2.

The structure is composed of:

- Outer cone: CFRP sandwich conical structure connecting the SPELDA or the 'Coiffe' with the equipment platform ring. It is manufactured in six sectors.
- Inner cone: CFRP sandwich conical structure connecting the payload adapter with the outer cone. It is manufactured in six sectors.
- Outer fairing: CFRP sandwich conical structure, protecting the equipment situated on the equipment platform. It is manufactured in twelve sectors.
- Equipment platform: Aluminium sandwich manufactured in six sectors, where equipment is fixed.

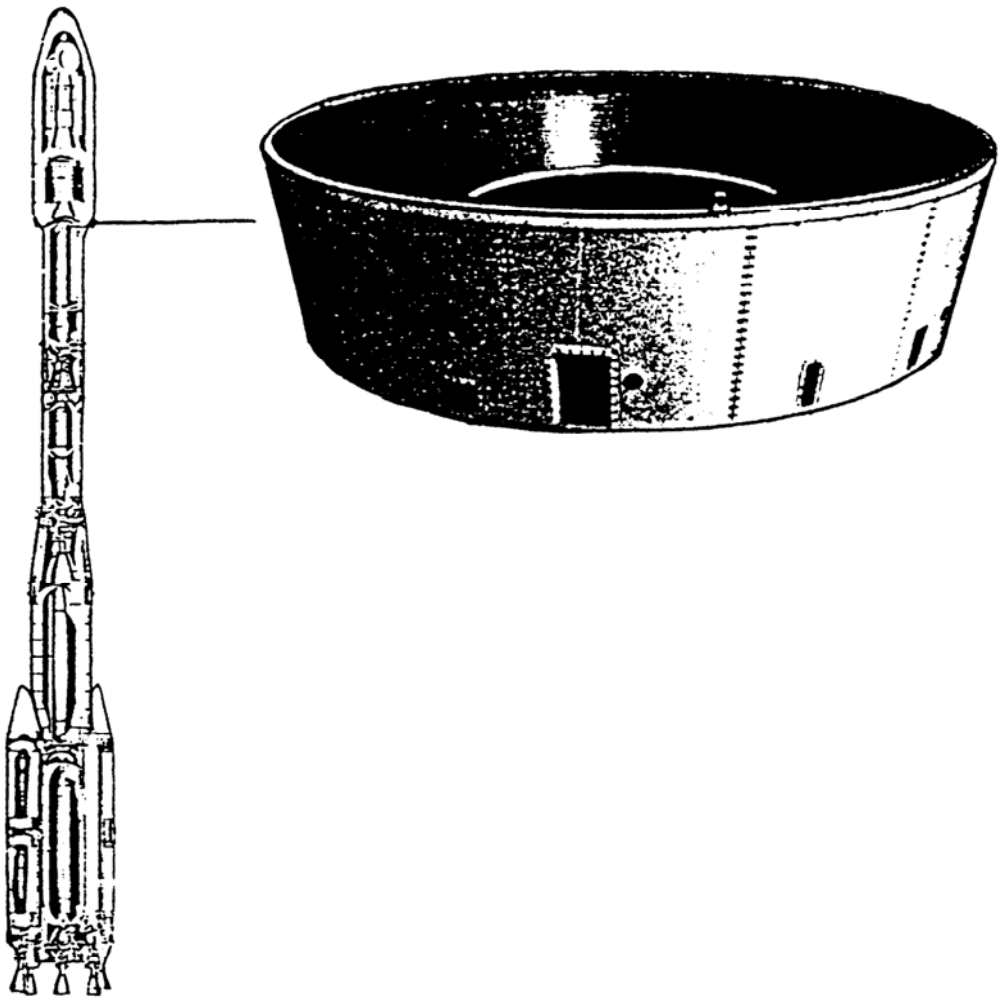

Figure 30.6-1 - Ariane 4: Vehicle equipment bay

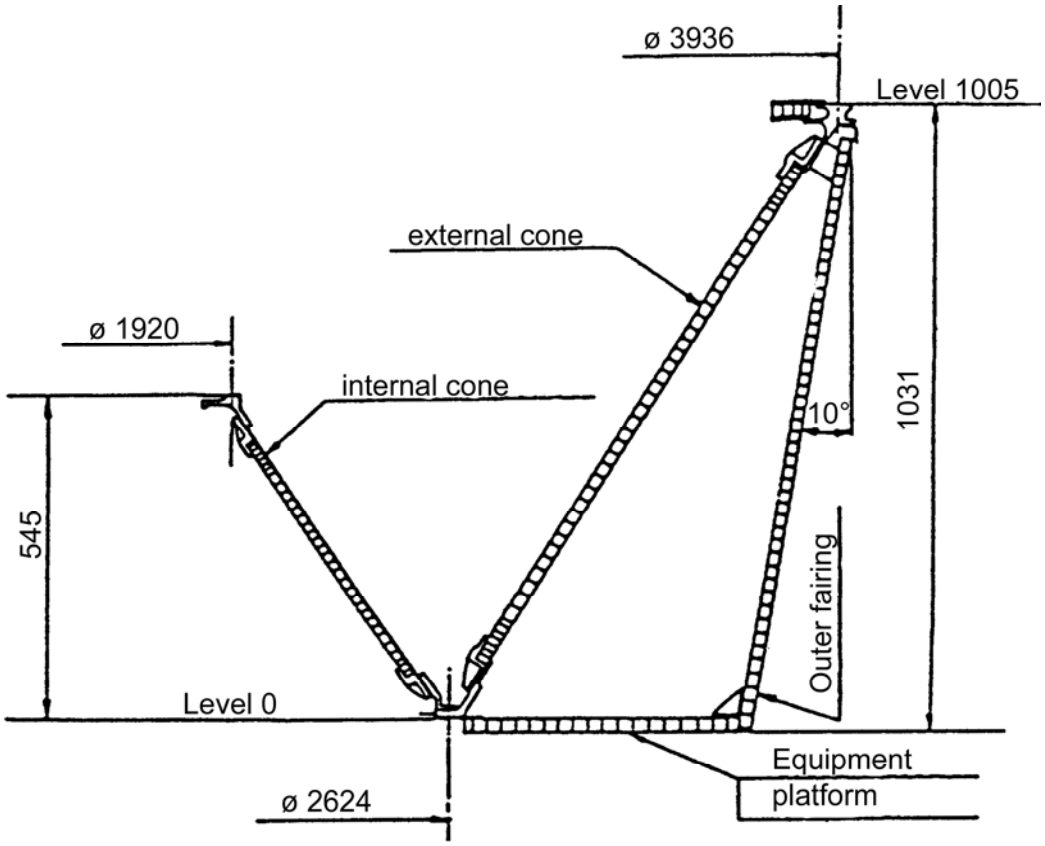

Figure 30.6-2 - Ariane 4: Vehicle equipment bay: Structural detail

30.6.3 Structural configuration

Table 30.6.1 combines details of the geometry, materials and mass for the major components, excluding the equipment platform.

Table 30.6-1 - Ariane 4 vehicle equipment bay: Geometry, materials and mass of major component parts

Item	Major Component Parts		
	Outer Cone	Inner Cone	Outer Fairing
Geometry			
Bottom dia.:	2624 mm	2624 mm	-
Top dia.:	3936 mm	1920 mm	-
Height:	1031 mm	531 mm	-
Skin thickness:	1.72 to 3.44 mm	0.43 to 0.86 mm	0.36 mm
Skin lay-up:	[45°/04°/±45°]	$[0°/\pm45°/0°]_n$	[0°/90°]
Core thickness:	20 mm	15 mm	23 mm
Materials			
Skins:	Vicotex 108/T300 tape Victotex 108/G814 fabric	Vicotex 108/T300 tape Victotex 108/G814 fabric	Victotex 108/G814 fabric
Core:	Aluminium honeycomb	Aluminium honeycomb	Aluminium honeycomb
Core Spec.:	Types NIDA 4-20 and 4-40	Types NIDA 4-20 and 4-40	Types NIDA 4-20p and 3-50p
Mass			
	170 kg	46.6 kg	36 kg

30.7 SPAS: Strut elements

30.7.1 Contractor

Developed by MBB Space Division, Ottobrunn, (D), Ref. [30-1].

30.7.2 Characteristics

30.7.2.1 General

The strut elements for SPAS-type structures consist of a carbon fibre tube and two titanium mounting elements. The mountings are fitted by tapered, double-shear adhesively bonded joints. The overall construction can be seen in Figure 30.7.1

30.7.2.2 Function

The standardised struts are used to build a modular square box framework structure. Applications for this kind of structure are:

- Shuttle pallet satellite (SPAS).
- Unique support structure (USS on Spacelab D1 mission).
- European retrievable carrier (EURECA).

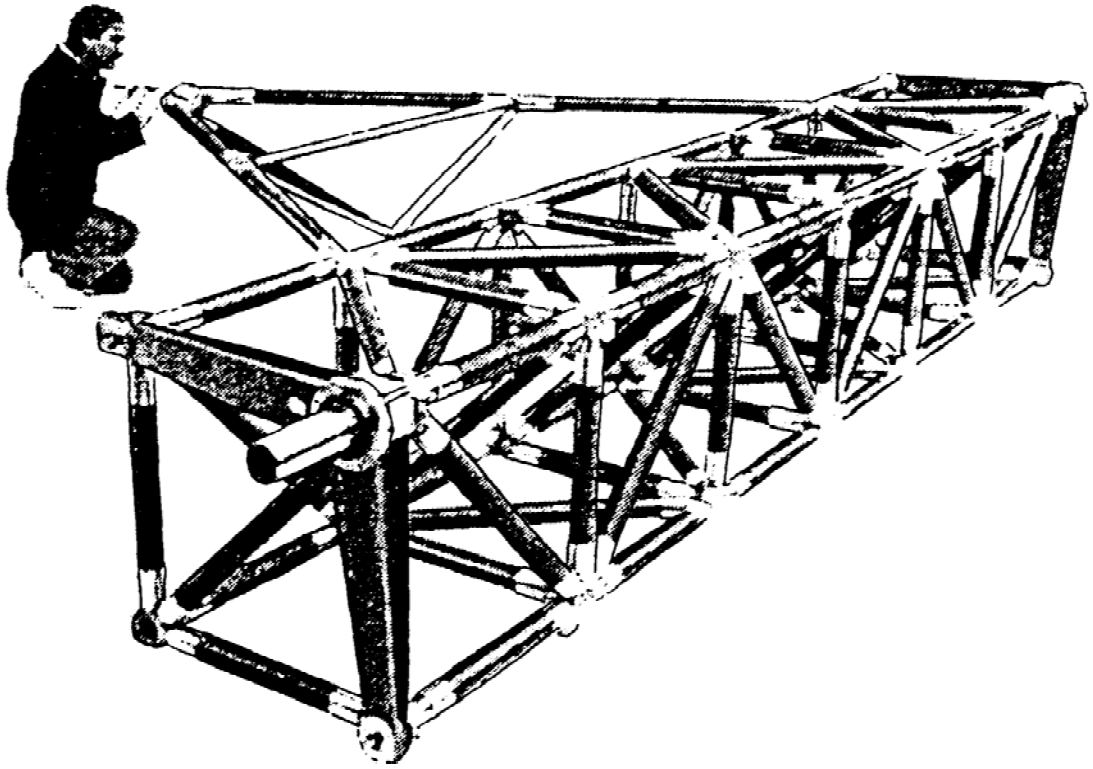

Figure 30.7-1 - SPAS: Strut elements

30.7.3 Structural configuration

30.7.3.1 Geometry

Diameter of struts:	65 mm
Wall thickness:	2.5 mm
Standard length of straight strut/node assembly:	700 mm.
Standard length of diagonal strut/node assembly:	990 mm.

30.7.3.2 Materials

High modulus carbon fibre Toray M40 / Ciba Geigy 209/HT 972.

30.7.3.3 Lay-up

0° with protective outer layer of 90° T300.

30.7.3.4 Load capability

Ultimate load (P99.95 %): 167 kN.

30.7.3.5 Weight

Strut/node assembly (700 mm): 1.5 kg.

30.7.3.6 Manufacturing and assembly

A titanium end-fitting is adhesively bonded to each end of the strut. The bond configuration is double scarf. The adhesive is a cold-curing type. The struts have longitudinal fibre layers for bonding.

The struts and the titanium nodes are fastened together via conical transition elements and stretch bolts, such that each strut element of the framework can be individually mounted or exchanged.

Figure 30.7.2 shows the conical transition and stretch bolt and the assembly detail is shown in Figure 30.7.3.

The stretch bolts are pre-stressed so that no gapping between the conical transition and the node element can occur under maximum expected tension load of strut.

30.7.3.7 Special features

Optimised carbon fibre composite-to titanium bonded section, as shown in Figure 30.7.4, in order to achieve:

- Uniform stress distribution along the bonded section and suppression of stress peaks in the case of external and thermally induced loads.
- Extremely close manufacturing tolerances for carbon fibre tubes and titanium fittings.

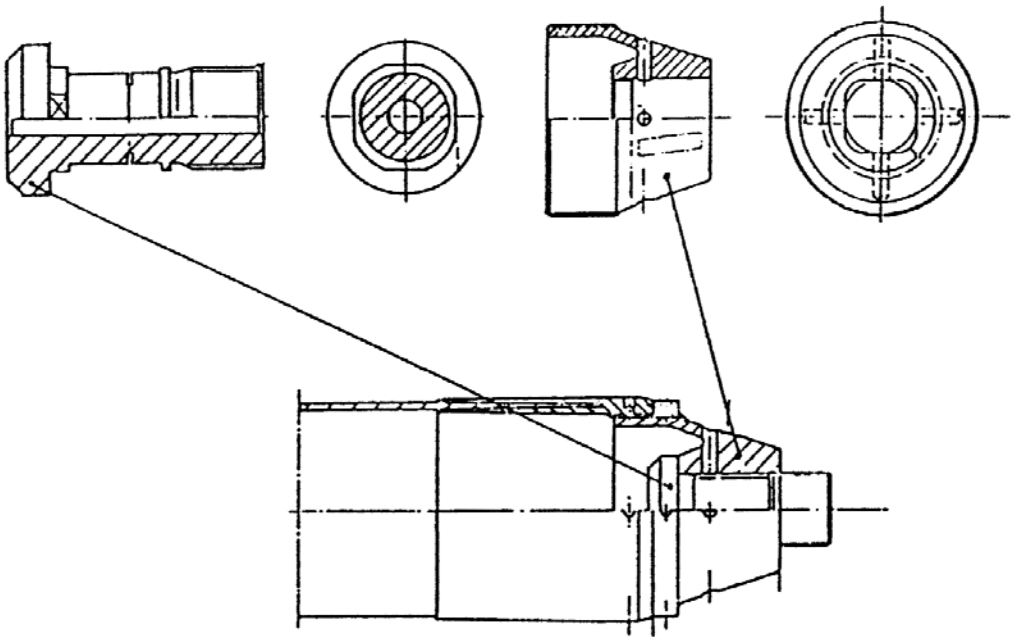

Figure 30.7-2 - SPAS strut element: Conical transition and stretch bolt

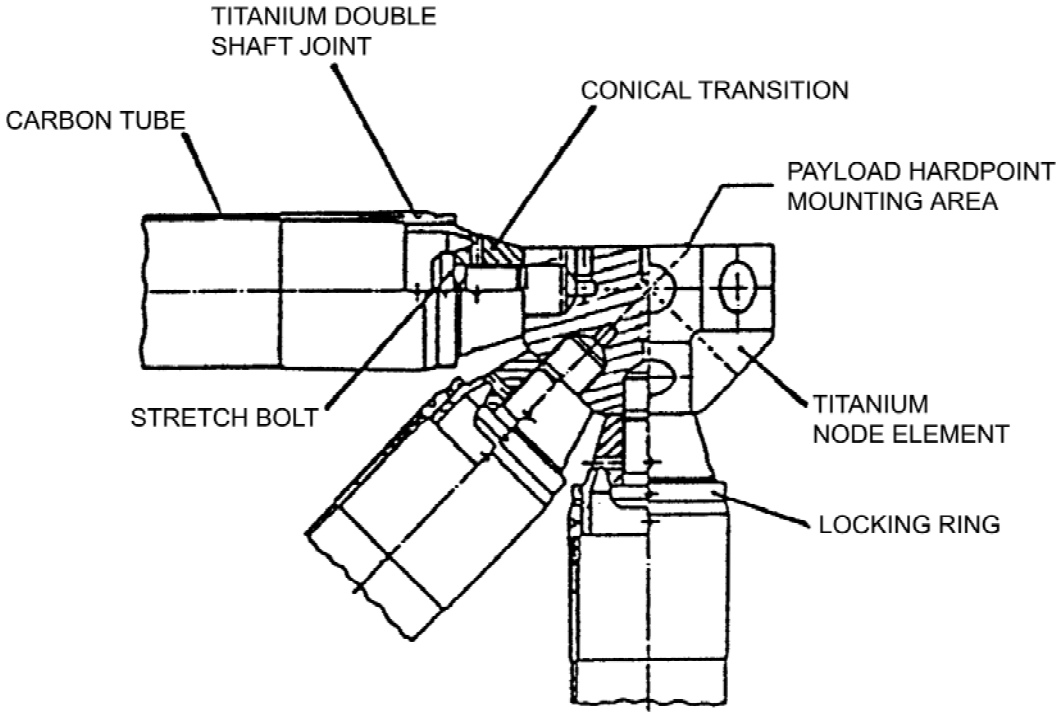

Figure 30.7-3 - SPAS strut element: Assembly detail

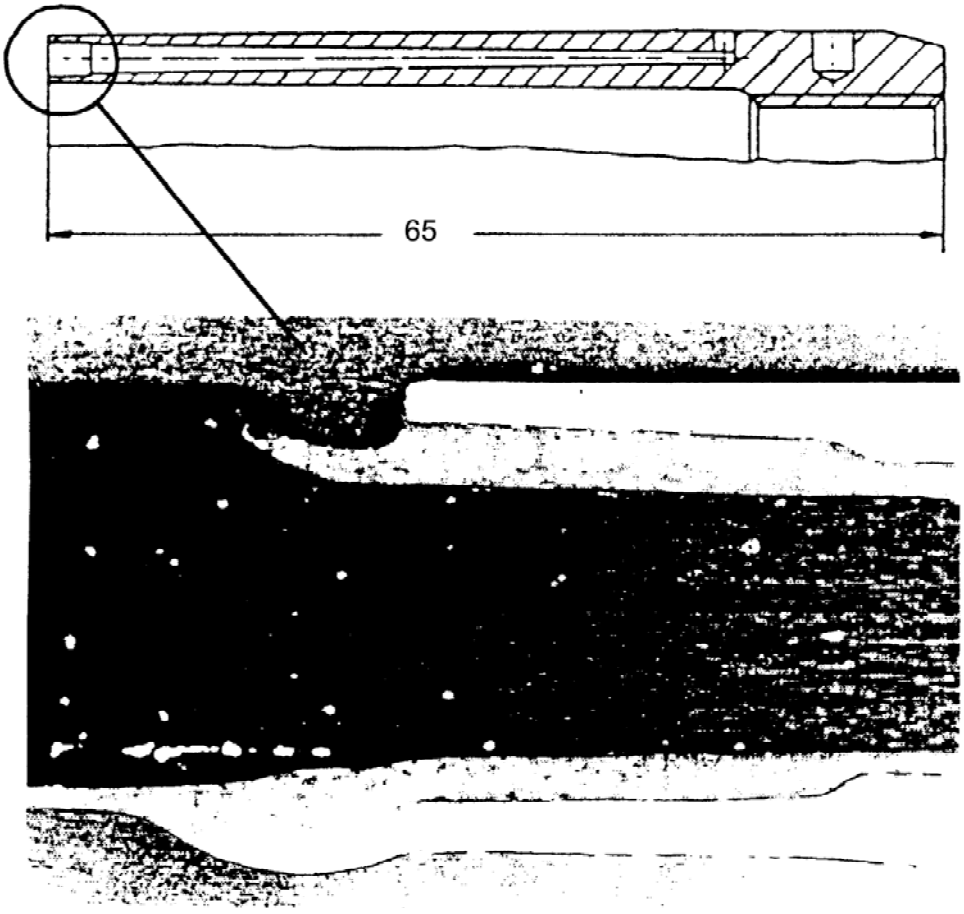

Figure 30.7-4 - SPAS strut elements: Optimised bonded section

30.8 Ariane 4: SPELDA

30.8.1 Contractor

Developed by British Aerospace - BAe Space Division, Stevenage, (UK), Ref. [30-1].

30.8.2 Characteristics

30.8.2.1 Function

SPELDA, the'structure porteuse externe de lancement double Ariane' is for launching two satellites, whilst fulfilling the functions of the external structure of the ARIANE 4 vehicle. Figure 30.8.1 shows the position on the launcher. The assembly is shown in Figure 30.8.2. At the time, it was one of the largest CFRP structures built within the European space industry.

30.8.3 Structural configuration

30.8.3.1 General

The SPELDA structure consists of:

- A cylindrical, carbon-fibre faced honeycomb sandwich shell supporting the fairing and enclosing the inner spacecraft, and
- An upper truncated conical CFRP faced honeycomb sandwich shell supporting the upper spacecraft.

The cylindrical and conical shell structures are designed as 1/3 panels bonded to each other by the use of CFRP butt straps.

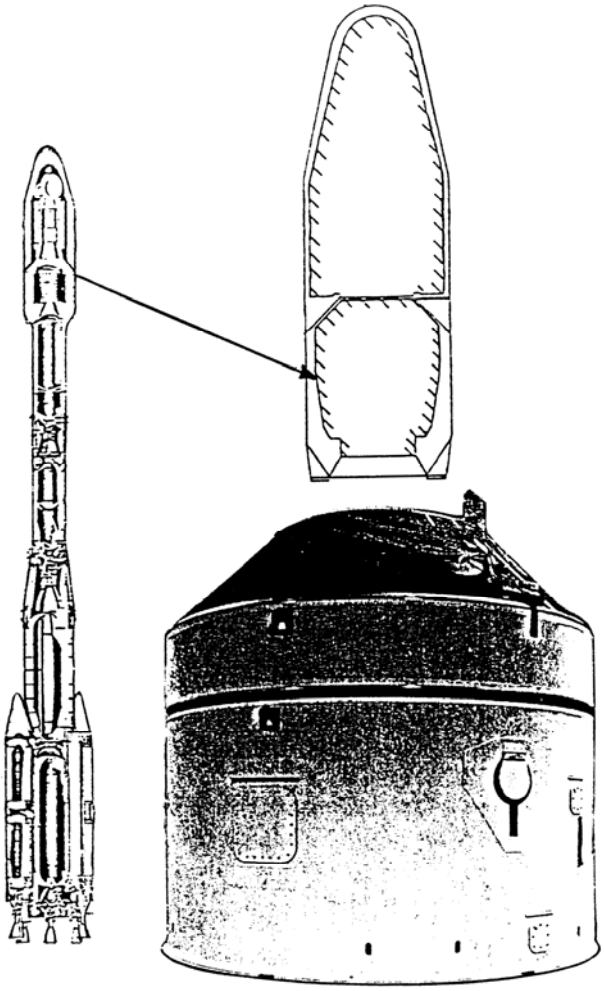

Figure 30.8-1 - Ariane 4: SPELDA

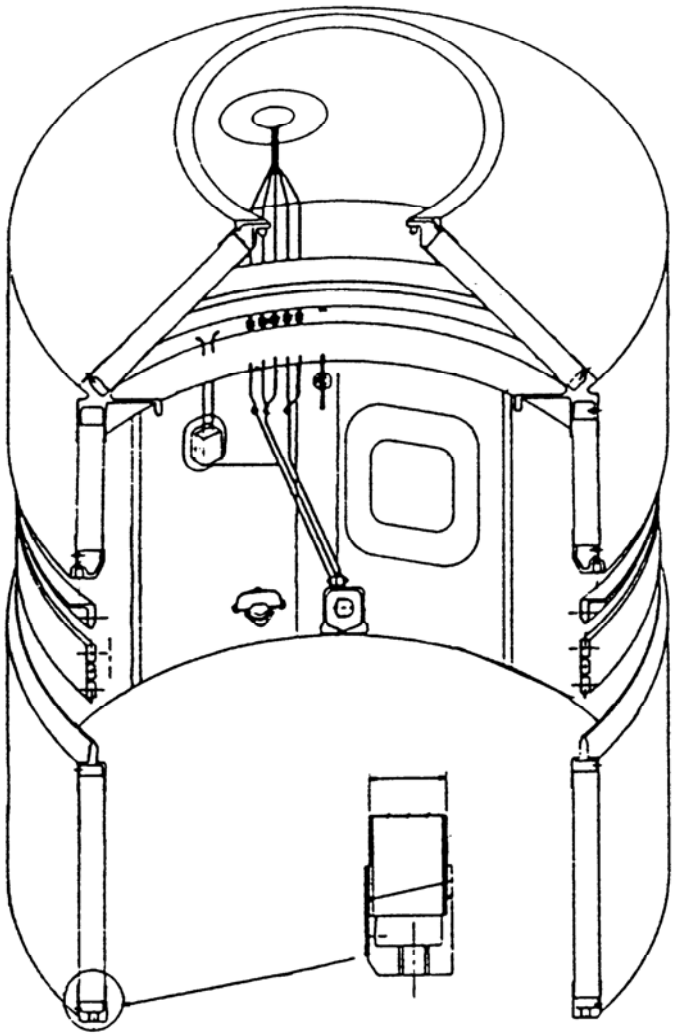

Figure 30.8-2 - Ariane 4 SPELDA: Assembly

30.8.3.2 Separation

The separation of the SPELDA structure is achieved by means of a LCCD 'linear charge cord device' which cuts the SPELDA along a horizontal plane. Springs impart a vertical impulse to jettison the SPELDA top. The separation plane is between the upper and lower cylindrical shells.

SPELDA are available in long, short and mini sizes. The major difference between each type of SPELDA is the height of the upper cylinder. The mini SPELDA does not have a lower cylinder structure.

30.8.3.3 Geometry

Table 30.8.1 gives the dimensions and a summary of the materials for the types of SPELDA.

Table 30.8-1 - Ariane 4 SPELDA: Geometry

	Type of SPELDA		
	Long	Short	Mini
Geometry			
Diameter (mm):	3982	3982	3982
Height of Cone (mm):	966	966	966
Upper Cylinder (mm):	1647	647	1784
Lower Cylinder (mm):	2137	2137	-
Total Height (mm):	4780	3780	2780
Thickness of one CFRP Face Sheet			
Cone (mm):	0.55	0.55	0.75
Upper cylinder (mm):	0.75	0.75	0.75
Lower cylinder (mm):	0.55	0.55	-
Thickness of Honeycomb Core			
Core (mm):	27.5	27.5	27.5

30.8.3.4 Materials

Face sheets: TENAX J HMA/Fiberite 934.

Core: 5056 aluminium honeycomb 3/16" - 0.0007".

30.8.3.5 Lay-up

Cone (mini SPELDA only): [0°/0°/60°/90°/-60°/0°/0°]

Lower cylinder and cone: [0°/60°/90°/-60°/0°]

Upper cylinder: [0°/60°/ 60°/90°/-60°/60°/0°]

Butt straps: [60°/60°/-60°/60°]

30.8.3.6 Loads

Table 30.8.2 gives the strength and stiffness charachteristics.

Table 30.8-2 - Ariane 4 SPELDA: Strength and stiffness charachteristics

Charachteristics **for Stiffness** (Displacement of Upper Payload x 10^{-8} m/N)			
	Compression	Tension	Lateral
Short SPELDA	0.95	0.95	5.64
Mini SPELDA	0.69	0.69	5.64
Charachteristics **for Strength for Short SPELDA** (N/m Peak Running Load)			
	Compression	Tension	Lateral
Top of Cone	66829	44282	14854
Top of Cylinder	70263	37115	17616
Base of Cylinder	96941	62694	18910

30.8.3.7 Final mass

Table 30.8.3 compares the target mass with that measured for the short SPELDA.

Table 30.8-3 - Ariane 4 SPELDA: Final mass

Type of SPELDA	Required (kg)	Measured (kg)
Long	< 462.43	-
Short	< 411.61	401 - 404
Mini	< 322	-

30.8.3.8 Special features

The SPELDA panels are assembled by the use of CFRP butt straps which provide a continuous load path for the shell structure in the hoop and shear directions, with adequate strength and without introducing excessive axial overflux. The joint detail is shown in Figure 30.8.3.

Joining is accomplished by the application of heater mats to cure the high-temperature film adhesive used, whilst at the same time expanding the foaming adhesive of the core joint. The joint is made, as is the within-panel joint, by localised vacuum bagging.

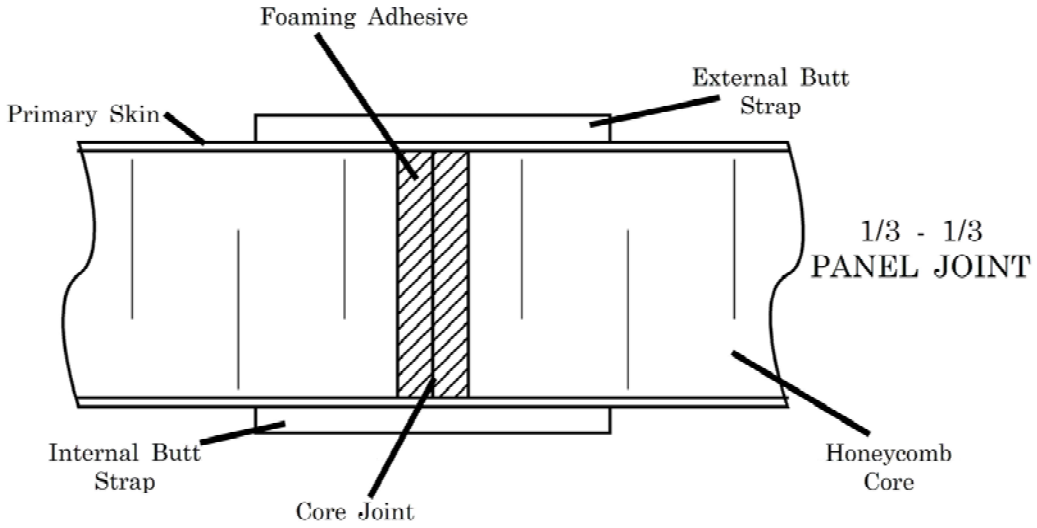

Figure 30.8-3 - Ariane 4 SPELDA: Joint detail

30.9 Ariane 5: SYLDA 5

30.9.1 Contractor

Developed by EADS Space Transportation, Les Mureaux, France, (previously Friedrichshafen, Germany).

30.9.2 Characteristics

30.9.2.1 General

SYLDA 5, shown in Figure 30.9.1, is an acronym for **S**ystème de **L**anceur **D**ouble **A**riane **5** (Ariane 5 double launch system). The main components are sandwich panels made of CFRP/aluminium honeycomb material forming two conical sections separated by a central cylinder. These components are joined together by aluminium alloy connecting rings.

Figure 30.9-1 - Ariane 5: SYLDA

30.9.2.2 Concept

SYLDA consists of an extremely light sandwich structure whose height depends on the mission requirements (size of the satellites). Heights vary from 4.9 m to 6.4 m for different payload combinations. The total mass of the 4.9 m variant is 428 kg.

30.9.2.3 Function

SYLDA's main purpose is to carry a second, upper payload during launch and flight into orbit. In the Ariane 5 double-launch configuration one satellite is carried inside the SYLDA structure and the other on top of it, as shown in Figure 30.9.2.

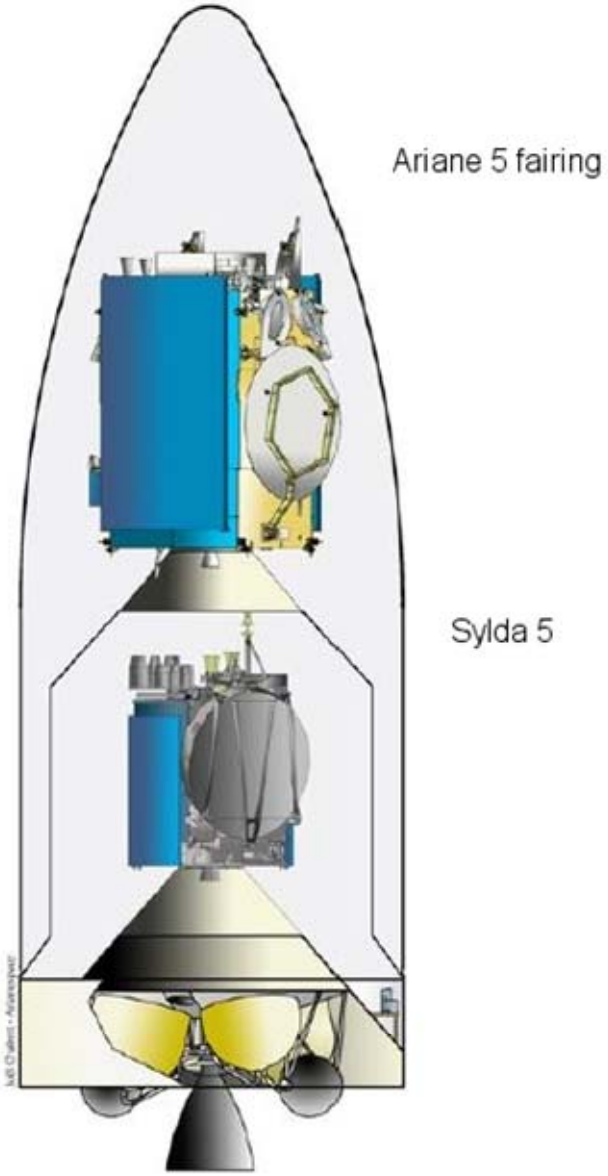

Figure 30.9-2 – Ariane 5: SYLDA launch configuration

30.9.3 Structural configuration

As shown in Figure 30.9.3, the SYLDA structure comprises:

- A lower truncated conical CFRP-faced aluminium honeycomb sandwich shell interfacing with the Ariane 5 launcher:
  - external aluminium ring E (diameter 5.4 m)
  - bottom cone, consisting of 4 panels with brackets for electrical connectors and jettison system consisting of eight spring cartridges to separate the cone from the central cylinder
- A cylindrical, carbon-fibre faced aluminium honeycomb sandwich shell enclosing the lower spacecraft:
  - internal aluminium ring D2 reinforced with IM type carbon fibre and equipped with an integrated pyrotechnic separation system

— cylinder made of 4 panels, with access holes

— internal aluminium ring C reinforced with UHM carbon fibre

- An upper truncated conical CFRP-faced aluminium honeycomb sandwich shell interfacing with the upper spacecraft:

— top cone structure made of 4 panels, with venting holes and brackets for electrical connectors

— external aluminium ring B (diameter 2.6 m)

Hand lay-up is used for sandwich panel manufacture. The cylindrical and conical shell 1/4 panels are bonded to each other using RT-curing CFRP straps, known as lashings.

30.9.4 Materials

30.9.4.1 Main components

Sandwich panels:	180 °C-curing epoxy reinforced with high modulus carbon fibre; 180 °C-curing epoxy adhesive; Aluminium honeycomb core.
Straps:	180 °C-curing epoxy reinforced with high strength carbon fibre.
Strap bonding (lashing):	RT-curing epoxy (with bondline control and accurate tooling and substrate dimensions).
Aluminium rings:	Not stated (local carbon fibre reinforcement, See: Special features).

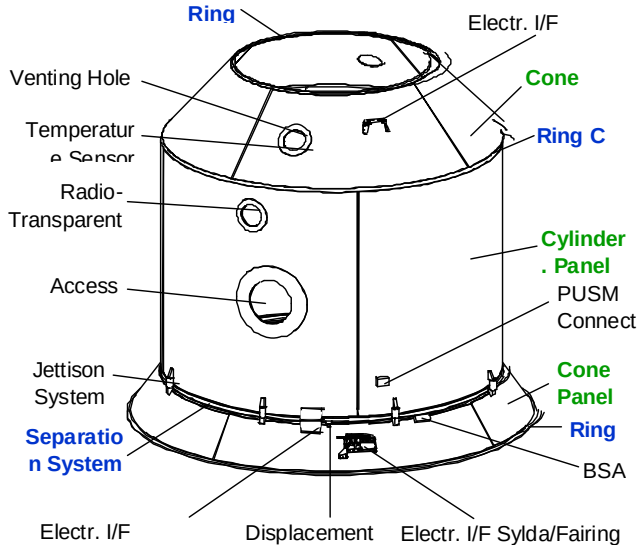

Figure 30.9-3 – Ariane 5: SYLDA structural configuration

30.9.4.2 Special features

Ring C and D2 are reinforced by carbon fibre winding in order to increase stiffness, as shown in Figure 30.9.4.

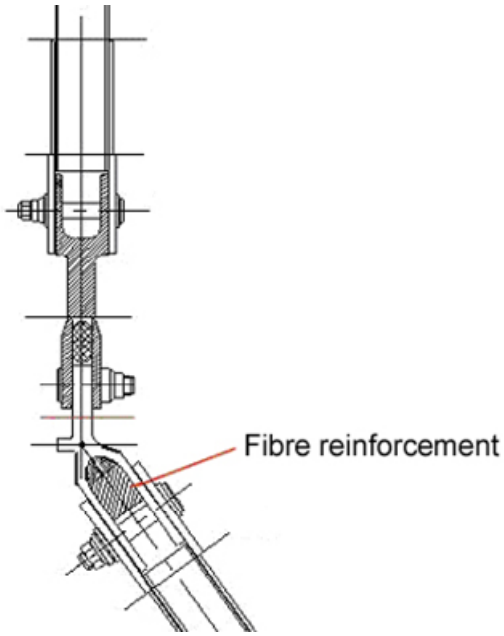

Figure 30.9-4 – Ariane 5: SYLDA joint detail

30.9.5 Analysis

Various analyses were performed to establish performance, i.e.:

- Structural analysis:
  - buckling,
  - stiffness,
  - static loads.
- Dynamic analysis:
  - assessment of equipment behaviour.
- Thermal analysis:
  - response of structure and equipment to thermal environment.
- Jettison analysis:
  - design of springs,
  - impact on structure,
  - calculations of mass, centre of gravity and inertia.

30.9.6 Testing

Various tests were performed for qualification, i.e.:

- Static load to failure.
- Dynamic to establish modal behaviour and determination of transfer function.
- Jettison to demonstrate correct operation of ring and springs.

30.9.7 Inspection

Inspection was used to establish:

- Thickness-per-ply measurement check of CFRP skins.
- Sandwich panel quality, using a water-jet-coupled ultrasonic technique.

30.9.8 Conclusions

The challenges faced by EADS ST during the development and manufacturing phases included:

- Technical:
  - Mass.
  - Effects on the behaviour of the Ariane 5 environment (including the newer, higher-capacity, ECA version).
  - Jettison characteristics.
- Industrial:
  - Manufacturing rate for such structures,
  - Quality assurance, e.g. tools, procurement.

30.10 ALADIN structure

30.10.1 Contractor

Kayser-Threde GmbH (KTH), Germany. Prime contractor for the Phase C/D contract from July 2003 to December 2005.

Customer: EADS Astrium Toulouse (ASF).

Subcontractors for CFRP manufacturing:

- Brühlmeier Modellbau AG, Switzerland,
- Invent GmbH, Germany.

30.10.2 Application

ALADIN structure is the CFRP primary and secondary structure for the spaceborne Lidar instrument. It is part of ESA's Earth-explorer mission, ADM-AEOLUS, to analyse atmospheric dynamics using an

active optical system. To acheive this, a laser beam is directed into Earth's atmosphere, reflecting back weak signals that can be analysed using the Doppler effect.

30.10.3 Objective of project

The contract with ASF comprised:

- Design,
- Development,
- Verification,
- Parts, materials and processes (PMP) qualification,
- Manufacturing, assembly, integration and testing (MAIT), including qualification using a structural thermal model (STM),
- Final MAIT of the PFM proto-flight model.

30.10.4 Concept

30.10.4.1 Primary structure

As shown in Figure 30.10.1, the PST primary structure has three basic sub-units:

- MS - main structure.
- SIS - satellite interface structure, which provides the interface to the bus platform by means of four stainless steel SIM satellite interface mounts.
- STS - star tracker support structure; shown in Figure 30.10.2.

All of these structures are made from sandwich panels with CFRP facesheets and aluminium-honeycomb cores.

30.10.4.2 Secondary structure

As shown in Figure 30.10.1, the STS secondary structure comprises:

- IEB - instrument external baffle.
- THS - three thermal heat shields, along with a thermal hood for the OBAT optical bench assembly.

The IEB consists of a lower conical, and two cylindrical, frameworks constructed of CFRP struts with metallic ring segments and nodes.

THS1, 2 and 3 and OBAT are used for thermal control purposes and all are made from single aluminium sheets with attached thermal hardware.

30.10.4.3 Dimensions

The ALADIN structure has an overall height of 2.6 m, an IEB diameter of 1.6 m and a satellite interface to telescope interface distance on main structure, top-side of 1 m.

The main structure and satellite interface structure are octagonal in shape with overall dimensions of 1.1 m × 1.5 m.

30.10.4.4 Proto-flight model

Figure 30.10.3 and Figure 30.10.4 show views of the ALADIN structure PFM proto-flight model.

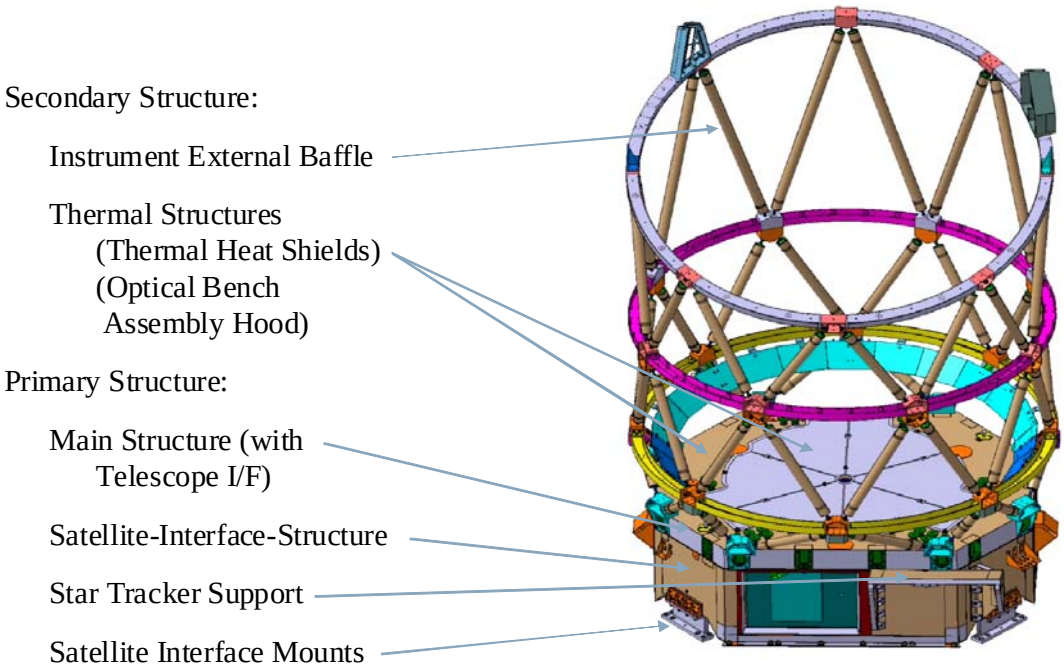

Figure 30.10-1 - ALADIN: Design concept

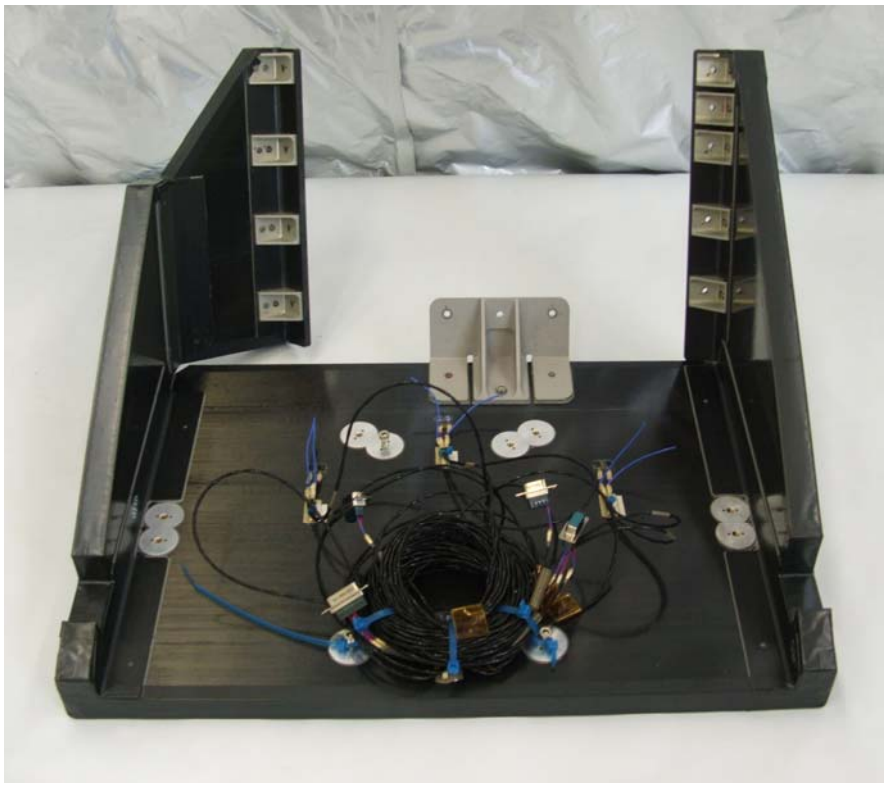

Figure 30.10-2 – ALADIN: Star tracker support

Figure 30.10-3 - ALADIN: Structure, proto-flight model (PFM)

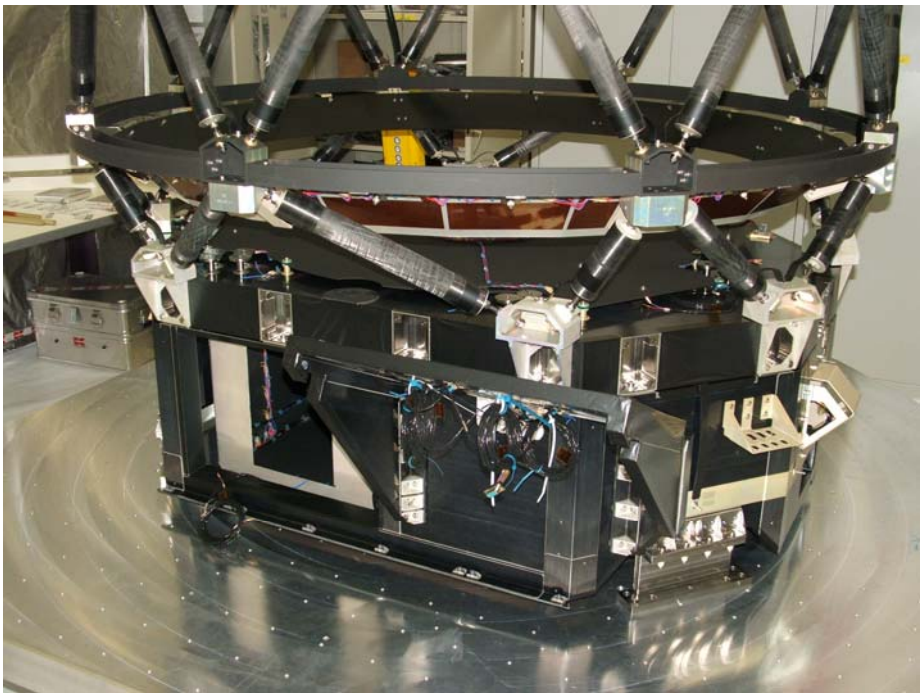

Figure 30.10-4 – ALADIN: Primary structure, proto-flight model (PFM)

30.10.5 Design parameters

For the PST, three main design parameters were taken into account:

- To withstand the high loads caused by the attached instruments and telescope on the MS and other infrastructure equipment on the SIS, e.g. harness, connector brackets, star tracker. This amounts to 250kg of attached hardware. The high loads arise in the IEB because of the the high dynamic input levels (22.5g axial and 10g lateral) at the bus I/F.
- To provide maximum stiffness such that ALADIN is dynamically fully de-coupled from the platform.
- To provide a structure with very high stability, primarily between the star tracker and the telescope axis (of the order of 10μm) to ensure the instrument's full operation in the short, medium and long term, taking into account the thermal variations across the structure.

All SST parts were designed in such a way as to withstand the loads caused by dynamic excitation of their own masses. This was critical for the large IEB, where small 1 kg antennas on the top rim have a maximum acceleration of 80g RMS leading to strange local, and global, IEB dynamic behaviour.

In addition to resisting high loads and providing adequate stiffness and stability, the overall ALADIN structural configuration had a stringent mass budget of 140 kg, with very close mass margins, and had to meet all the interface functions

To fulfil all of the challenging demands, all PST facesheets used a prepreg system with very low CTE and CME properties. The MS is 100 mm thick and has about 100 aluminium inserts of various types to provide all the necessary interfacing.

To mount the telescope 30 mm above the top of the MS, special titanium inserts were used, which passed through the MS and connected the upper and lower facesheets; also providing advantages in thermal conductivity.

The 18 load transfer points between MS and SIS consisted of titanium brackets bonded into the honeycomb edges. The STS is repositionable on close tolerance pins because several mounting and dismounting activities were necessary during manufacture. This method retained the tight dimensional tolerances needed between the star tracker interface plane and the telescope axis.

The IEB framework configuration, mainly the lower conical strut arrangement, was optimised for maximum stiffness. The single ring elements and framework nodes are made from aluminium alloy. To cope with the high temperature gradient acting on the IEB, a special end-fitting was designed with bonding between CFRP parts only.

THS1, 2 and 3 are all made from single aluminium sheets with thermal hardware bonded on the back side and a high reflectivity paint on the top side. The OBAT is similar, but both thermal hardware and the paint are on the inner side.

30.10.6 Analysis

Extensive verification analyses were conducted, particularly for strength and stability. For the structural analysis, a full CLA coupled-load analysis was performed. This was because the interface loads are higher for the dynamic than for the quasistatic load case under the given boundary conditions. For the SST, the dimensioning load cases were taken from the CLA results.

For strength justification of critical CFRP parts, failure analysis used the Puck failure criterion. This showed marked differences from the results obtained using the Tsai-Wu criterion which demonstrates the need for more physically-based failure criteria for critical load cases, identifying margins in the structural design.

30.10.7 Materials

For the PST facesheets a prepreg-system M55J/LTM123 from ACG (UK) was used. This matrix system is a Cyanate Ester which gives low CTE and CME properties for the laminate.

The CFRP struts also used M55J fibres, but in this case in with an epoxy matrix system LY556/HY906/DY from Vantico. The CTE and CME constraints in the struts are somewhat less severe than for the PST facesheets.

AA6082-T6 aluminium alloy was used for the thermal heat shield and OBAT hood.. Machined parts were made from AA7075-T7351.

Two different adhesive systems were used:

- Araldite AV138/HV998 for bonding of inserts and strut fittings,
- Hysol EA9394 for facesheet-to-core and bracket-into-sandwich-panel bonding.

30.10.8 Special features

A special strut fitting has been designed to cope with the large temperature variations of the IEB and to minimize stresses in the bonds, as shown in Figure 30.10.5.

Figure 30.10-5 – ALADIN: IEB middle cylinder (left), CFRP IEB strut end fitting (centre) and typical IEB node (right)

30.10.9 Manufacture

The facesheets were manufactured using an autoclave moulding technique. All subsequent bonding (core-to-facesheet, bracket and insert integration) was carried out at room temperature.

The CFRP struts were made by filament winding.

30.10.10 Test

30.10.10.1 Materials and processes

PMP qualification tests demonstrated the performance of the materials and bonding used in the structure. Particular attention was paid to the new strut end-fitting design. This led to a full strut qualification program which demonstrated a load capability of up to 30 kN.

A complete witness-test-sample program was used for workmanship quality control. Similarly for all inserts, which were tested to limit load.

30.10.10.2 Structure

The ALADIN structure underwent a complete qualification test program for the STM (thermal cycling and vibration) and acceptance test program for the PFM (thermal cycling, vibration, depressurisation and outgassing).

30.10.11 Inspection

All CFRP parts were inspected before and after testing using ultrasonic inspection.

A 3D measurement device was used to verify structural tolerances. For dimensional envelope control of the baffle before and after testing, a 3D camera system was used, with a resolution of better than 0.1 mm.

30.10.12 Conclusions

A high-performance CFRP structure was successfully produced for the advanced ADM AEOLUS program. It demonstrated the ability to withstand very high loads with the necessary stiffness and stability for in-orbit operation. The design was based on standard principles, but with a new strut end-fitting.

The materials met the stringent PMP demands, such as outgassing. Proven material systems and combinations were used, since these were well known from previous hardware projects.

30.11 ROSETTA lander structure

30.11.1 Contractor

Developed and built by the DLR Institute of Structural Mechanics, Braunschweig (D), Ref. [30-5].

30.11.2 Function

A multi-functional CFRP structure for the lander 'Philae' of the ESA cornerstone mission Rosetta, which was launched on 2nd March 2004 from CSG Kourou. It is due to land on the comet Churyumov-Gerasimenko in 2014. The structure supports a variety of mechanical loads during launch, cruise, and landing, and needs to ensure very good thermal isolation of its inner and outer parts. The basic configuration is shown in Figure 30.11.1.

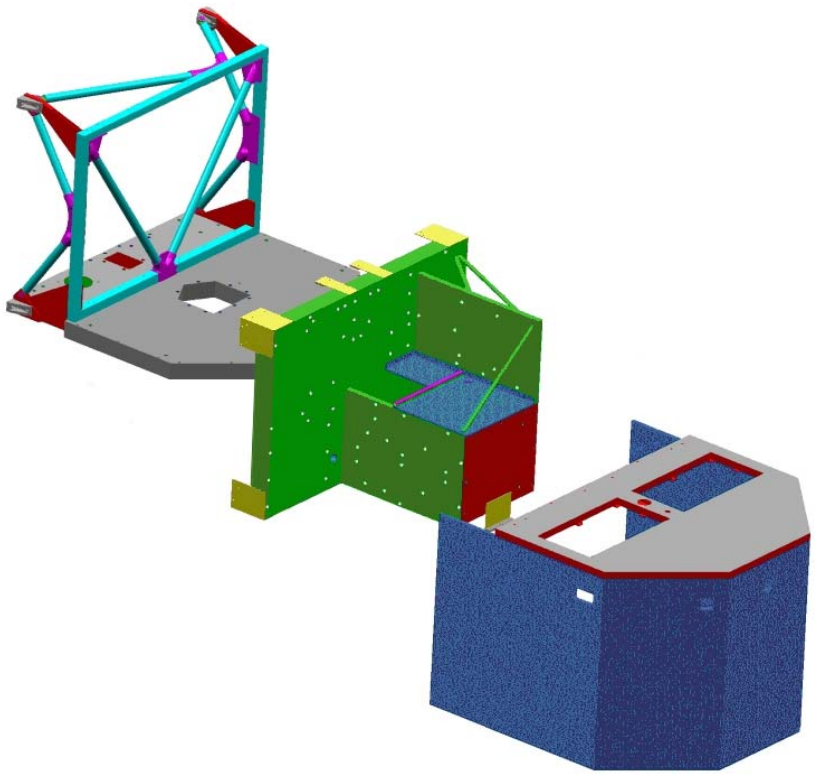

Figure 30.11-1 – Rosetta: Basic configuration of the lander structure (without the landing gear)

30.11.3 Mass

A structure consisting of light-weight carbon-fibre sandwich plates and carbon-fibre frames and rods was chosen in order to achieve high stiffness and strength within the mass budget. The overall mass of the primary structure is 18.2 kg.

30.11.4 Structural configuration

30.11.4.1 General

The primary structure consists of three basic assembly units:

- Instrument carrier.
- Base plate and support truss.
- Solar hood.

30.11.4.2 Instrument carrier

The instrument carrier is the central unit of the lander structure; as shown in Figure 30.11.2. It consists of:

- A rectangular instrument platform,
- Two auxiliary plates standing perpendicular to the instrument platform,
- A front plate
- A top plate
- Two auxiliary plates situated between the front and top plates,
- Stiffening struts,
- A stiffening triangle,
- Eight Kevlar webs,
- A Kevlar angle.

The asymmetric configuration of this unit is necessary to accommodate the scientific payload.

All sub-system and payload units needing thermal protection against the cometary environment (−160 °C during the night) are mounted on the instrument carrier which is then completely enclosed with MLI multi-layer insulation.

The only rigid connections between this ‘warm compartment’ and the outer parts of the structure are the eight webs, an angle, and two tubes inserted in the base plate. All of these items are made of Kevlar®.

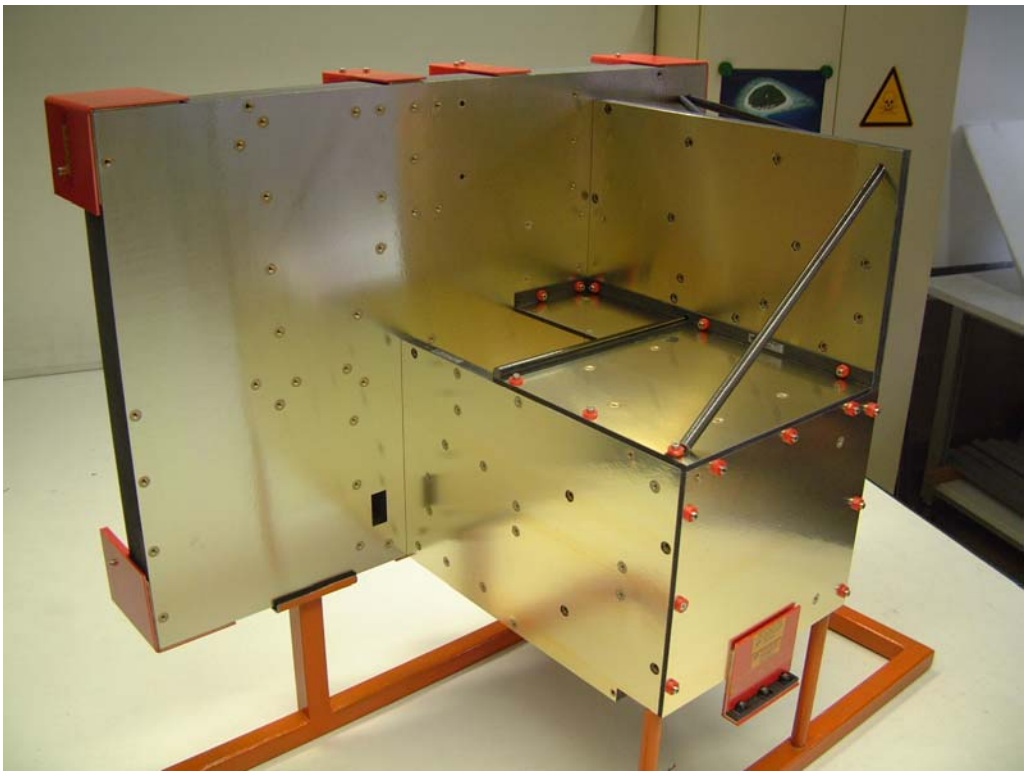

NOTE The red plastic covers and washers are only protective and were removed during the integration.

Figure 30.11-2 – Rosetta: View of the instrument carrier

30.11.4.3 Base plate and support truss

The base plate and support truss were manufactured separately but assembled before delivery. Together they form the second assembly unit; as shown in Figure 30.11.3.

The base plate carries the landing gear and, on its free part (the so-called 'balcony'), houses the tools and instruments which operate outside the warm compartment. It serves as an operating platform for the whole lander throughout the mission. i.e.:

- Cruise flight,
- Ejection from the Rosetta orbiter,
- Descent to the surface,
- All operations on the comet.

During launch, all the forces between the Lander and the Orbiter are transferred through the four corners of the support truss, where the MSS adapters, made of titanium alloy, are attached.

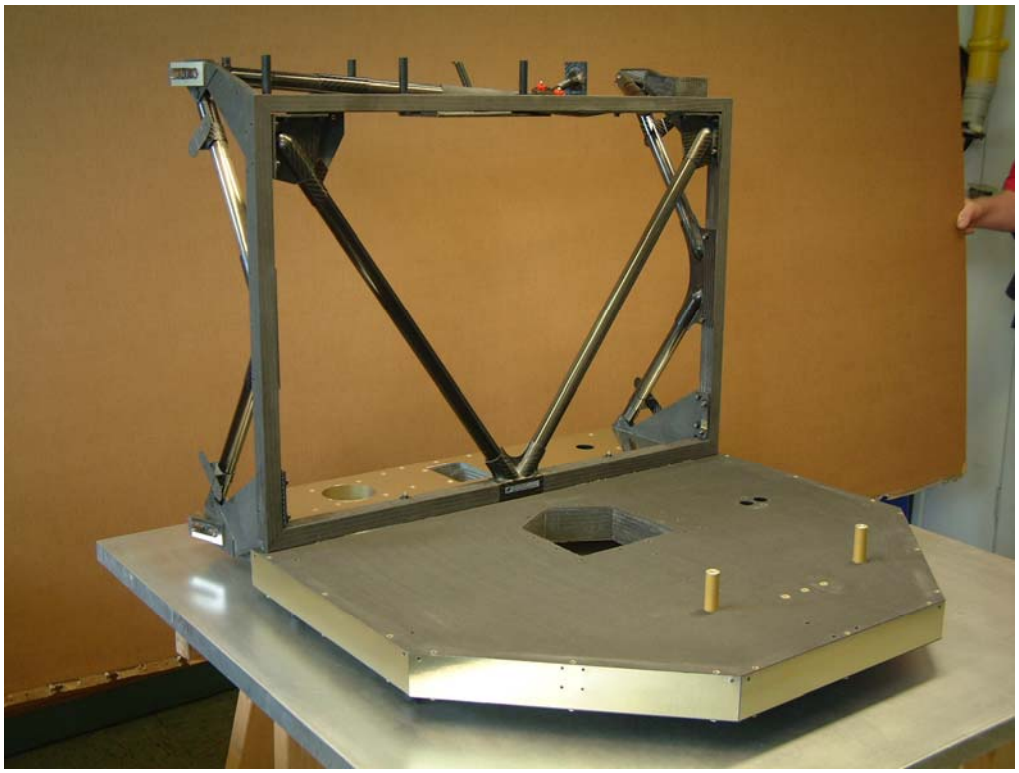

Figure 30.11-3 – Rosetta: View of base plate and support truss

30.11.4.4 Solar hood

In addition to providing a protective casing for the warm compartment, the solar hood acts as a carrier structure for:

- Solar cells,
- Two thermal absorbers,
- Five cameras,
- Locks for the three landing gear legs.

The solar hood consists of a lid, five side walls, and two balcony panels which are fixed to the support truss. The side walls are connected to each other and, together, are mounted on the base plate and the frame of the support truss. The lid is mounted on the upper edge of the side walls and support truss. It was an assembly, integration and verification (AIV) requirement that all the components could be integrated separately.

During transportation and most of the AIV operations, the solar hood was encased by a 'cover hood' consisting of lightweight sandwich plates which protected the sensitive solar cells.

Figure 30.11-4 – Rosetta: Solar hood inner side (view from bottom to top)

Figure 30.11.4 shows the camera holes in the side walls and the Kevlar frames around the thermal absorber holes in the lid. Their function is to hold the MLI on the top side of the warm compartment.

30.11.5 Construction details

30.11.5.1 Size

Both the length and width of the base plate are 850 mm. The overall height of the lander structure is 660 mm, not including protruding structural parts, payload adapters and landing gear.

30.11.5.2 Composite materials

The sandwich plates had to be as light and as stiff as possible. Therefore, high-modulus carbon-fibre fabric/epoxy laminates based on the Toray M40J carbon fibre were selected for the face sheets. These have an orthotropic modulus of elasticity of more than 90 GPa, and a density of about 1400 kg/m^3. Thin face sheets contain 0° and 90° plies only, but in all cases where the face sheet contains more than 4 fabric layers, ±45° plies are included as well. The CTE, coefficient of thermal expansion, of the carbon-fibre face sheets is negligible (close to zero) which makes the lander structure very insensitive to temperature variations. The outgassing rates are within the stipulated range, e.g. TML ≈ 0.7%, CVCM = 0 %.

The sandwich cores consist of aluminium honeycomb material (Hexcel Aeroweb 5052) with the cells perforated to ensure rapid evacuation (venting) during launch. The standard type is very low density, i.e. about 26 kg/m^3, and has medium longitudinal, transverse and shear stiffness values. Underneath the balcony section of the base plate, and in the instrument platform, a higher density honeycomb type is used, i.e. about 55 kg/m^3, which has higher stiffness properties.

The carbon-fibre struts, used mainly in the support truss, have excellent specific strength and stiffness (longitudinal: 200 GPa, shear: 80 GPa) because of UD carbon fibres in the longitudinal direction. To aid the manufacturing process, the carbon fibre is supported by a hard foam core and surrounded by a thin glass-fibre braided hose. The foam core is hermetically enclosed hence the outgassing rate of the free surface (carbon-fibre laminate with glass-fibre braided hose) is very similar to that of the sandwich face sheets.

Two types of Kevlar® stand-off element are used as thermal isolators:

- Cylindrical tubes,
- Shear webs (flat and angular).

The stand-off elements carry the normal and shear forces between the instrument carrier and the outer structure, i.e. the support truss and base plate.

Kevlar® is used because it it has the necessary mechanical properties and is a good thermal insulator. Perpendicular to the fibres the heat conductivity is 0.2 W/mK to 0.3 W/mK. The longitudinal and shear stiffness properties are 31 GPa and 11.9 GPa, respectively.

30.11.5.3 Metals

The insert caps are made from chromated aluminium alloy, Ref. [30-6].

The lander-orbiter interface adapters, the strut connectors in the upper corners of the support truss, and all of the screws for intra-structural connections are made of titanium alloy.

30.11.5.4 Surface layers and coatings

The substrate beneath the solar cells needs to be electrically insulating. Therefore, because of the uncertain electrical properties of carbon-fibre laminates, the outer surface of the solar hood has an additional glass-fibre layer.

The underside and edges of the base plate can face the sun during the cruise flight on the orbiter. As protection against solar and cosmic radiation, and to avoid local electrical charge concentrations, these are covered with chromated aluminium-alloy foil [See: Figure 30.11.3]. This metallic foil is laminated directly onto the carbon-fibre face sheets.

On the instrument carrier, the instrument-bearing surfaces of the sandwich plates are also coated in the same way to ensure electrical conductivity among the instrument feet [See: Figure 30.11.2].

30.11.5.5 Novel inserts

The design and accommodation demands of the ROSETTA lander structure led to the use of relatively thick sandwiches and a large number of inserts per unit area, including many through-the-thickness connections.

The mass constraints made it necessary to find a novel insert design with a better weight to load capacity ratio than conventional potted inserts. This resulted in the concept of the carbon fibre tube insert, which was qualified for the specific conditions and load cases on the Rosetta lander.

Subsequently the concept was investigated more thoroughly in the course of an ESA technology study Ref. [30-6].

[See also: ECSS-E-32-22 - Insert design handbook]

30.11.6 Loads

Design limit load (during the development phase) was 25 g (all axes).

Qualification test levels consisted of sine loads from 11 g (5Hz to 50 Hz) decreasing stepwise with frequency down to 4 g (90Hz to 100 Hz). Random loads up to 0.085 g^2/Hz were individually defined for the axes.

30.11.7 Eigenfrequencies

The original Eigenfrequencies stipulated in the development phase were >100 Hz for analysis, and >80 Hz to be verified in shaker tests with the fully equipped Rosetta lander. These demands were later relaxed by ESA because the lander had increased both in size and mass. The first eigenmode was verified experimentally as 72.8 Hz.

30.12 Mecabus central cylinder

30.12.1 Contractor

The Mecabus central cylinders for the Alcatel Spacebus series are manufactured by Saab Ericsson Space.

The development was a cooperative project between Alcatel Space and Saab Ericsson Space. The main aim was to provide a primary structure with increased load capability for the Alcatel Spacebus series.

30.12.2 Design

The Mecabus central tube is a cylindrical CFRP structure, composed of the blank shell and the connection hardware, as shown in Figure 30.12.1. The diameter is 1.2 m and the length is close to 4.0 m.

The blank shell is a co-cured sandwich structure, with internal and external M18/M55J carbon-fibre skins. The skin thicknesses range from 0.3 mm to 4 mm and various core densities and thicknesses are used in different areas.

Skin reinforcements are added, either co-cured with the blank shell or cold-bonded onto the cured skins.

The connection hardware consists of inserts, frames and corners. A total of more than 650 inserts are used for mounting equipment such as tanks, decks, corners and tubes.

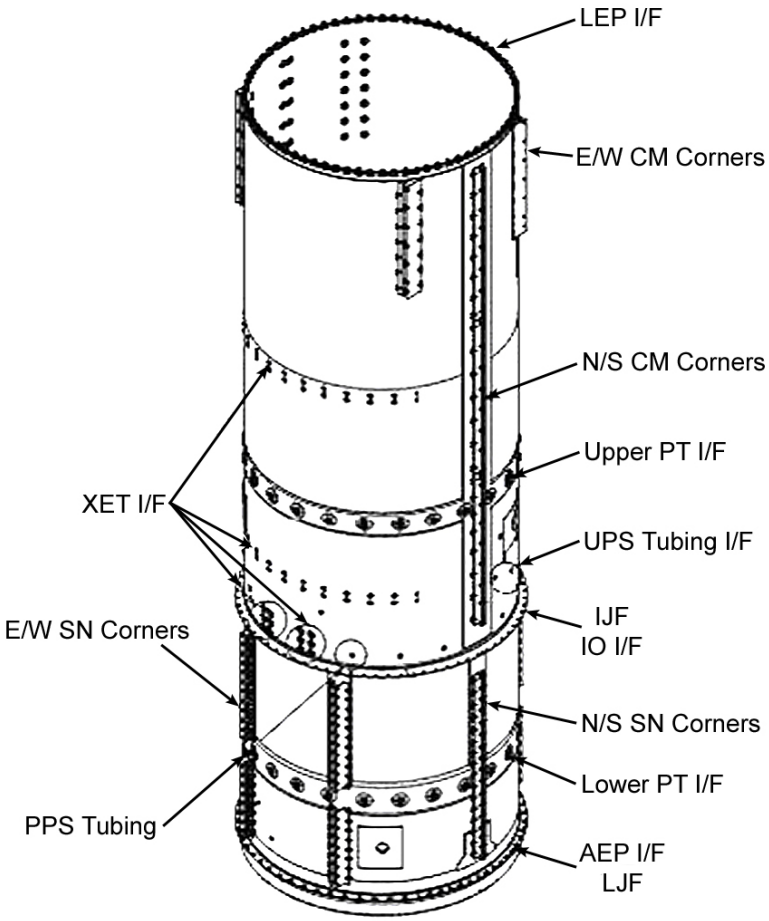

Figure 30.12-1 - Mecabus central cylinder: Overview

Two frames are implemented in the tube:

- The launcher junction frame (LJF) for launcher interfacing is attached using more than 170 screws.
- The intermediate junction frame (IJF) is bonded to the shell and is used for panel attachment.

In the final design, improvements were made in assembly methods, design of inserts (to give better stress distribution), core thickness optimisation and co-cured and cold-bonded reinforcements.

30.12.3 Manufacturing

The CFRP sandwich shell is co-cured with four, pre-manufactured, core assemblies.

Non-destructive inspection of the CFRP is based on air-coupled ultrasonics and X-ray inspection is used for the core-to-core junctions.

Hole drilling for the installation of inserts is performed using orbital drilling [See: 39.10].

All mechanical cleaning is done using a specially developed blasting method to improve quality and reduce the manufacturing cycle.

All inserts and interface surfaces on the central cylinder structure are mounted in their final positions with tight tolerances using an assembly jig. No final machining is performed.

30.13 Triax-fabric deployable antenna reflectors

30.13.1 Contractor

Developed by EADS Space Transportation, Les Mureaux, France.

30.13.2 Introduction

Ultra-Light Reflectors (ULR) are deployable antennas consisting of an open weave (triax fabric) thin shell linked by cleats to an independent, stiff, backing structure. At the end of 2005, such products were flight proven on the APSTAR 6 and SYRACUSE 3 GEO satellites and more than twenty have now been ordered. Figure 30.13.1 shows a membrane reflector from the STENTOR satellite which was qualified in 2001.

Figure 30.13-1 – STENTOR: Triax fabric membrane reflector

30.13.3 Design

30.13.3.1 General

Accuracy, stiffness, low mass and stability in an extreme environment are serious challenges for reflector design. Two programmes, which began in 1998, investigated the use of triax fabric in ULR ultra-light reflector architecture for large deployable reflectors:

- STENTOR: 2m diameter, membrane construction, [See: Figure 30.13.1].
- ASAS: 4m diameter, sandwich shell, Figure 30.13.2.

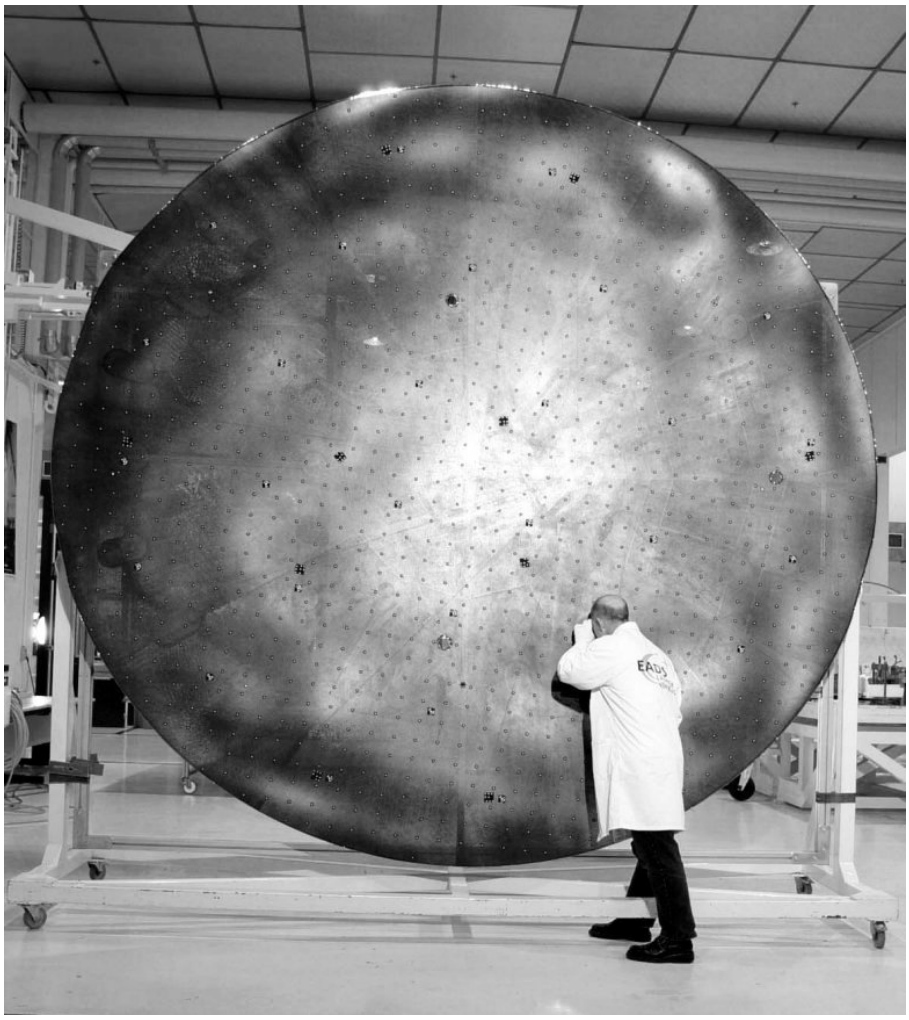

Figure 30.13-2 – ASAS: Reflector under inspection

30.13.3.2 Concept

The Ultra-Light Reflector (ULR) design consists of several elements:

- A thin shell, using a light, open-weave fabric.
- An independent rigid structure for interface with the spacecraft.
- Composite parts linking the shell with the structure, whilst mechanically and thermally decoupling the two elements.

A schematic diagram of an ultra-light reflector design is shown in Figure 30.13.3.

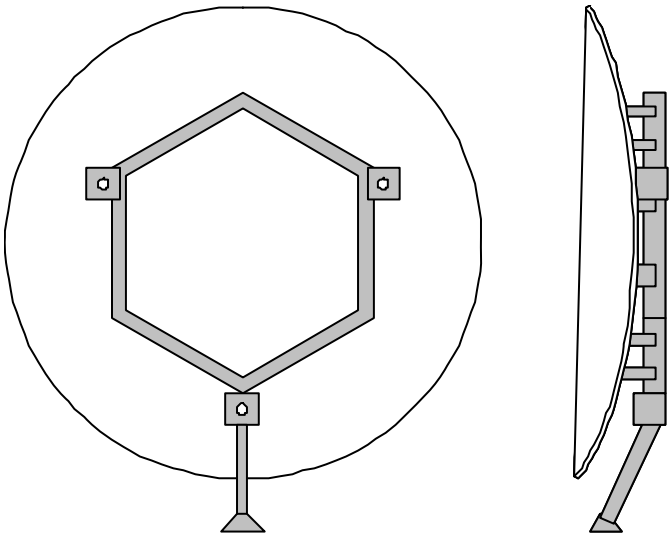

Figure 30.13-3 – Ultra-light reflector design

30.13.3.3 Reflector characteristics

The main reflector characteristics can be summarised as:

- Shell: to date (2006) diameters in the range 2.2 m to 3.8 m have been manufactured. The shell can be shaped with single curvature radii as small as 70 mm.
- Manufacturing accuracy: better than 130 μm RMS for 2.2 m diameter reflectors.
- Mass: less than 10 kg for 2.2 m diameter.
- Thermo-elastic stability: better than 120 μm for 2.2 m diameter reflector in a wide temperature range (-160°C to +140°C).
- Resonance tuning capability: It is possible to tune the resonant frequencies of the shell, after manufacture, to avoid interference with the spacecraft resonant frequencies.

30.13.3.4 Analysis

The various analyses conducted were:

- Mass, centre of gravity, inertia,
- Modal (stowed, deployed),
- Static (stowed),
- Thermal (stowed, deployed),
- Thermo-elastic distortions (deployed),
- Hygroscopic distortions (deployed),
- Thermo-elastic stresses (stowed, deployed),
- Sine vibrations (stowed),

30.13.4 Materials

30.13.4.1 Shell design details

Nominally, the shell skins are composed of high-modulus carbon triaxial woven fabric impregnated with an epoxy resin. The sandwich is manufactured by co-curing and self-adhesion, which optimises the manufacturing time and the material properties.

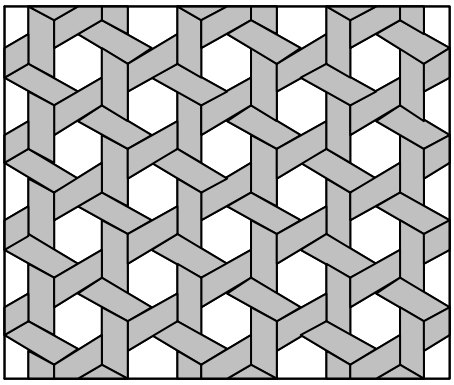

Figure 30.13-4 – Triaxial woven fabric

30.13.4.2 Backing structure design details

The backing structure is made of rectangular hollow section CFRP tubes, which provide stiffness and mechanical strength to the reflector. Currently the tubes are assembled using CFRP parts, which are standardised among all reflectors. The backing structure is shown in Figure 30.13.5.

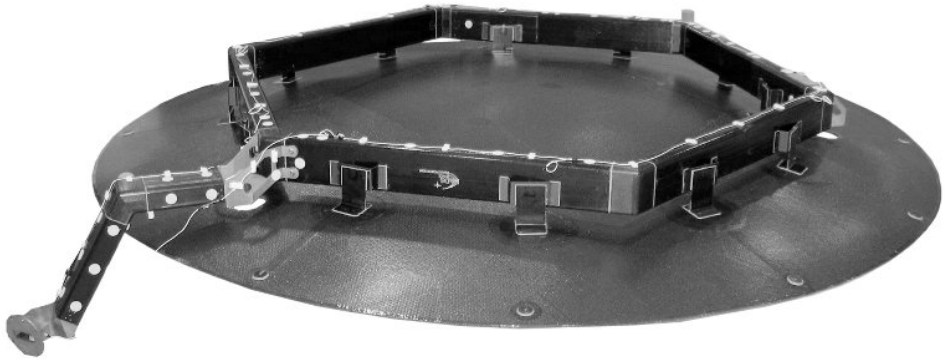

Figure 30.13-5 – Reflector backing structure (2.2 m diameter URL)

30.13.4.3 Structure-to-shell junctions

CFRP cleats are cold-bonded between the shell and the backing structure.

30.13.4.4 Manufacture

Hand lay-up processing is used for the manufacture of the sandwich shell and all the CFRP parts.

30.13.5 Testing and Inspection

Table 30.13.1 summarises the ULR qualification status for 2.2m diameter reflectors.

Ultrasonic inspection is used to evaluate the bonding of the composite parts.

Table 30.13-1 – Triax ULR: Qualification status of 2.2 m, 2nd generation reflector

Thermal environment	Thermal vacuum cycling between -185°C and +149°C.
Acoustic environment	148.8 dB levels reached.
Thermo-elastic distortion test	Temperatures -145°C and +135°C. Measured distortion ≤118µm RMS.
Hygroscopic distortion test	Measured distortion ≤54µm RMS.
Sine vibration environment	Excitation: 10g on out-of-plane axis, 15g on in-plane axes; Interface loads correspond to 20g quasi-static acceleration.
Profiles measurements	Measured accuracy ≤130µm RMS.
Mass measurements	Reflector mass (fully equipped including deployment arm) ≤9.9kg.

30.13.6 Comments

The use of triax fabric in sandwich shell construction gives a number of benefits, including:

- Low coefficients of thermal expansion and moisture expansion, which helps to provide high reflector stability.
- Low air resistance because of the open weave of the skins so the shell is fairly insensitive to acoustic loads.
- Low reflector mass.

The ULR design offers a high degree of standardisation with the 'off-the-shelf' backing structure, whilst offering maximum adaptability to meet customer demands.

30.13.7 Conclusions

The ULR design is successfully qualified for use on commercial programmes. The high performance is consistent with the launch environment, and on-station requirements for GEO satcoms. Standardisation and potential adaptability make this solution particularly attractive for antenna contractors.

30.14 Ariane 5: DIAS

30.14.1 Introduction

The design and development of DIAS 'dispositif assouplisseur' for Ariane 5 is an example of the use of elastomers in space structures.

SABCA is responsible for the development and the qualification of the JAV and DIAS. TECHLAM are responsible for LEC 'laminate elastomeric component' development and qualification. IABG are involved in qualification tests.

30.14.2 Need

30.14.2.1 Vibration

During the launch of Ariane 5, vibration loading, caused by thrust oscillations, is generated by the EAP solid rocket boosters, e.g. about 300kN in a frequency range from 15 Hz to 30 Hz.

In order to minimise the transmission of vibrations to the main stage, then to the upper stage and finally to the payload, it was decided to uncouple the dynamic behaviour of the EAP from the EPC - etage principal cryotechnique - by introducing a component with high longitudinal dynamic flexibility between the two stages. This led to a special flexible coupling device, known as DIAS - dispositif assouplisseur - being integrated to the JAV front skirt of the booster. Figure 30.14.1 shows the position of DIAS. It is linked to the forward attachment bracket of the DAAV - dispositif d'accrochage avant - on the EAP side.

Two additional design constraints taken into account by SABCA, were limiting the space and the mass, as far as possible.

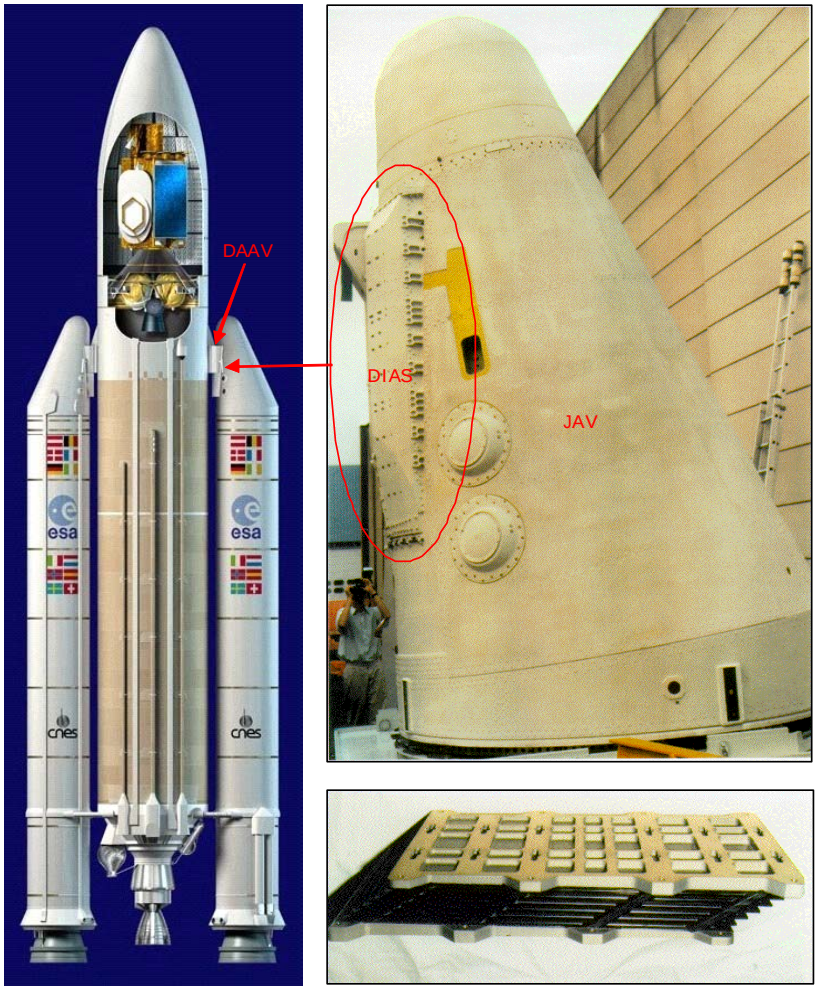

A: Position of DIAS (left),
B: DIAS implementation in the JAV (top right),
C: LEC - laminate elastomeric component (bottom right)

Figure 30.14-1 – Ariane 5: Position of DIAS and LEC

30.14.2.2 Considerations

The difficulty in the development was finding a system capable of:

- withstanding high quasi-static loadings with the smallest longitudinal displacements possible and,
- simultaneously avoiding transfer of quite low frequency vibrations (1Hz to 5Hz), whilst
- ensuring a low discrepancy of its longitudinal flexibility.
- Thus, the device chosen needs to:
- soften the connection in the longitudinal direction (axis of the booster thrust) whilst
- maintain transverse stiffness, in order to preserve the launcher attitude control in yaw, and
- to limit the excitability by wind on the launch pad.

All these criteria are linked to the high-reliability requirements.

30.14.2.3 Concept

To fulfil the set of demands, the connection consists of laminate elements, known as LEC laminate elastomeric components; developed by TECHLAM. These are a stack of rubber plates and metallic inserts oriented parallel to the thrust axis, which transmits thrust load by shear; as shown in Figure 30.14.1-C.

30.14.3 Definition

30.14.3.1 LEC laminate elastomeric components

The definition of the LECs aimed to meet the demand for longitudinal stiffness but at the same time provide high stiffness in the perpendicular direction.

Each laminate is parallelepiped (parallelogram-shaped), measuring 700mm × 300mm × 100 mm, made up of 6 layers of rubber, each 10 mm thick.

Under the thrust loading, the laminate elements sustain deformation that can be up to 200mm and the shear ratio is about 250% at j =1, i.e. under nominal loads; where shear ratio is determined by the shear displacement divided by thickness.

The complex multiaxial stiffness demands led to a final configuration of several laminates, i.e. 18 elements arranged in a metal box, as shown in Figure 30.14.2.

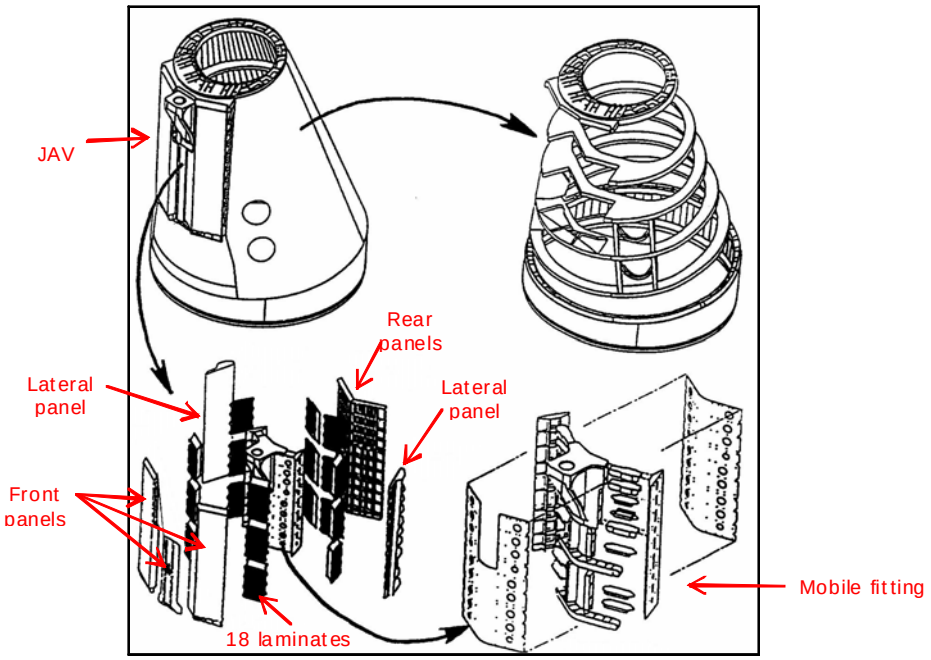

A: Position of DIAS in JAV with description

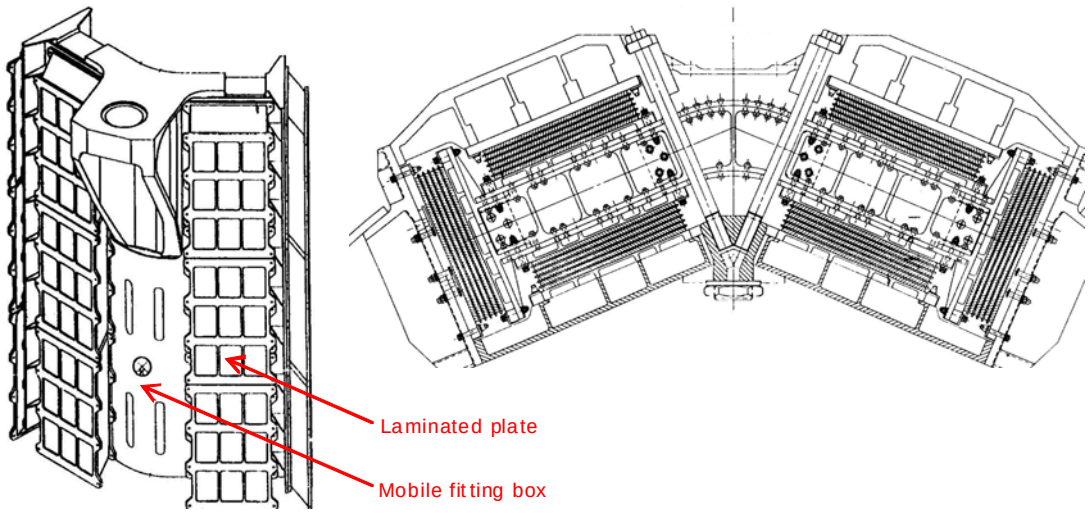

B: DIAS (overview)

C: DIAS (top-view)

Figure 30.14-2 – Ariane 5: Detail of DIAS construction

The stiff metal box containing the laminate is made of stiffened panels machined out of thick light-alloy plates; as shown in Figure 30.14.2 - B and Figure 30.14.2 - C. Its dimensions are about 2m long and 1.3m wide.

The box is closed by two frames on the JAV. This part transfers the thrust to the DAAV through the LEC to a mobile structure (fixed directly to the DAAV), which is composed of:

- an interface bracket machined out of a large, light alloy forged block;
- a V-shaped box made with two skin panels, two end spars and stiffened by internal ribs and spars, which are fixed to the LECs.

[See: Figure 30.14.2 for 'mobile fitting']

The advantage of the elastomer material is its high potential dynamic flexibility in a low volume. However, its dynamic performance is fixed once the design is frozen and is driven by the shear ratio through a non-linear response.

30.14.4 Development logic

30.14.4.1 Approach

The main concerns raised during the development of the system were:

- An incomplete knowledge of the elastomer materials, which led to numerous complementary analyses and specific adaptations for codes,
- The high safety factors imposed, i.e. $j = 2$ for failure; because of the multiaxial loading of the component, which led to high scatter in robustness.

30.14.4.2 Materials

The characterisation on different types of samples showed a decrease in shear strength with increasing tension. Therefore, the dimensioning case for the elastomer corresponds to the areas of the laminate where tension is the highest at iso-shear and where temperature and ageing are the highest.

For the laminates, the dimensioning parameters are the shear level, temperature and ageing, along with, as a second order of magnitude, transverse loading, bending and crack initiation.

30.14.4.3 Analysis

The stress analysis of the system was made with adapted finite element models for the LEC as well as for the structural parts of the JAV and of the DIAS.

One difficulty encountered was when the LEC non-linear model. i.e. large displacements and large deformations, had to be implemented in the already big structural linear model. It has been done through the use of super-elements for LEC which needed a high level of correlation.

The properties of the elastomer were established using a statistical analysis (both static and dynamic). This was necessary because the elastomer properties varied widely. This led to the development and validation of a code which enabled all sensitive parameters to be accounted for.

Furthermore, rubber formulation has been reviewed in order to guarantee more accurate strength and dynamic behaviours, but decreasing the robustness with respect to the damping.

30.14.4.4 Qualification tests

The qualification tests were performed in static and in dynamic for both parts, i.e. LEC and JAV-DIAS, on test benches specifically developed for the LEC and adapted for the JAV.

The qualification test campaign was conducted in steps:

- Determination of the shear static and dynamic stiffness during the ground and flight phases for LEC,
- Determination of the longitudinal loading effect on the transverse stiffness for the JAV,
- Damping test for aged and non-aged laminates for LEC,
- Strength up to rupture tests for LEC and JAV with a representative thermal environment.

One of the main conclusions is that temperature and ageing of LEC have an important impact on the rupture loading level; as previously demonstrated during characterisation tests. In order to limit the temperature of the rubber before the launch, a temporary cover component, known as COSYVE, is flushed by air-conditioned on the ground and placed on DIAS. This cover is disconnected at lift-off.

Thus, the development of such a highly constrained system led to a compromise with respect to the numerous and conflicting requirements and demand a high level of process control in production.

30.15 References

30.15.1 General

[30-1] 'Composites design for space applications'
ESA SP 243: Proceedings of Workshop, ESTEC, Noordwijk, (NL),15 18 Oct. 1985

[30-2] Fokker BV (NL)
'Final report of composite structural element (CSE) study'
TR R 86 CSE 080, ESA Contract No. 5928/84/NL/PB(SC)

[30-3] D.C.G. Eaton & E.J. Slachmuylders: ESTEC (NL)
'The use of advanced materials in space structure applications', IAF 87 305

[30-4] Unpublished report, courtesy of CASA Space Division, (E)

[30-5] ROSETTA Lander Subsystem Specification "Structure"
RO-LST-SP-3601, Issue 4/0 (Project documentation, 2001)

[30-6] J. Block, T. Brander, J. Lyytinen, K. Marjoniemi, L. Syvänen, R. Schütze
Study on Carbon Fibre Tube Inserts
ESTEC Contract No. 16822/02/NL/PA, DLR Braunschweig – Helsinki Univ. Technology – Patria , 2004

[30-7] M. Hofstetter et al.
"Static and dynamic tests of the Ariane 5 solid rocket booster flexible coupling system"
IAF-97-I.1.02, 48th International Astronautical Congress, October 6-10, 1997, Turin, Italy.

[30-8] P. Bara et al.
"Development and testing of Ariane 5 EAP skirts"
IAF-95-I.6.07, 46th International Astronautical Congress, October 2-6, 1995, Oslo, Norway.

[30-9] P. Bara et al.
"Ariane 5 : EAP solid rocket booster front skirt (JAV), design and dimensioning of DIAS flexible coupling system of the stage to the EPC cryogenic main stage"
ESA conference on Spacecraft structures, materials and mechanical testing, March 27-29, 1996, Noordwijk.

30.15.2 ECSS documents

ECSS-E-HB-32-22 Insert design handbook

31
Integrity control of composite structures

31.1 Introduction

Fibre-reinforced plastic structures exhibit very different fracture and failure characteristics to their conventional metallic counterparts. The objective is to ensure that the integrity of structures made from composite materials is commensurate with that realised by metallic structures throughout their operational life.

ECSS fracture control requirements for space systems are stated in ECSS-E-ST-32-01; previously ESA PSS-01-401, which covers both European requirements and those of NASA STS and ISS.

Guidelines are presented for the treatment of integrity control of composite structures produced in European-based programmes, [See: 31.2]. It covers the series of actions that are undertaken to demonstrate the structural integrity of a design; taking due account of operational conditions and design loads, in conjunction with defined damage tolerance and general safety requirements.

The guidelines are read in conjunction with normative ECSS standards ECSS-Q-ST-20; ECSS-Q-ST-40; ECSS-Q-ST-70 and the ECSS-E-ST-30 series.

Integrity control relates to structures irrespective of the materials of construction, in which materials are evaluated for approval, and components and structures are qualified. The associated subject matters are:

- Verification, [See: Chapter 32].
- Damage tolerance, [See: Chapter 33].
- Inspection and quality control, [Chapter 34].

31.2 Integrity control guidelines

31.2.1 Objective

The guidelines are intended to ensure that the integrity of composite structures is commensurate with that achieved with conventional metallic materials, and is maintained throughout their operational life.

The guidelines should be read in conjunction with normative ECSS standards.

31.2.2 Materials

31.2.2.1 Fibre-reinforced plastic composites

For the purposes of the guidelines, a composite structure is one manufactured from fibre-reinforced plastic material. The composite materials consist of carbon, aramid or glass continuous aligned fibres in a resin matrix. The structure is commonly manufactured from prepregs consisting of impregnated laminates or woven mats. Filament winding and pultrusions can also be used. Fibre-reinforced plastic face sheeted sandwich panels containing light alloy or composite material cores can also be contained in the definition of composite structural components.

31.2.2.2 Other materials

The guidelines presented do not apply to structural components manufactured from fibre-reinforced plastics containing discontinuous short fibres or those containing other materials, such as metal matrices, ceramics and carbon-carbon materials. A discussion of the integrity control aspects of structures made of metal matrix, ceramic-based and carbon-carbon materials includes:

- High-temperature structures, [See: Chapter 76].
- Defect types, [See: Chapter 77].
- Damage tolerance, [See: Chapter 78].
- Fracture control, [See: Chapter 79].
- Non-destructive testing techniques, [See: Chapter 80].

31.2.3 Special criteria for composites

The special criteria for fibre-reinforced plastic composites are due to the essential differences from metallic materials which include:

- Composites are inhomogeneous by nature.
- Composites exhibit small, Hookean strains to failure.
- The laminated composite has mechanical properties which are anisotropic. Anisotropy can also occur in thermal, electrical and permeability characteristics.
- The supply and control of composite materials is more complex, because the fibre, resin and pre-impregnation sources alter the supply route before the pre-impregnated material reaches the component manufacturer.
- A range of manufacturing processes is available which differ substantially from those used for metals. These can markedly influence the properties of a finished item. The properties are only achieved during the forming and curing process, are configuration-dependent and can also be influenced by the curing stresses.
- Environmental factors such a temperature, humidity and radiation can change properties, such as the strength of composites, significantly, as can fluids, such as solvents, hydraulic oils and propellants.
- Special precautions can be needed to avoid damage by lightning strike and to realise the necessary electrical return potential.
- Special consideration can be necessary regarding the differing flammability, smoke emission and toxicity characteristics.

- The failure modes of composite structures can differ substantially owing to the anisotropic and brittle characteristics of the laminated material involving the fibres, matrix and interface behaviour.
- The influence of repetitive loads and environmental ageing effects on composites differs substantially from that of metallic components. Composites have intrinsically good fatigue properties but the margin of static strength over fatigue strength is reduced and there can be greater scatter in the fatigue results.
- Typical manufacturing defects and the results of accidental damage, caused by low-energy impacts, differ markedly from those arising in metallic components, as can any damage propagation arising from subsequent loads. The issue can be com-plicated by the lack of visual clues such as are commonly found with metallic structures, e.g. surface cracks and other deformi-ties.
- The nature and extent of maintenance and inspection can differ substantially in consequence to any defects and damage present.
- Composite items can exhibit low coefficients of thermal expansion compared with metals. In the presence of large temperature excursions, high strains can be induced at composite-to-metal interfaces.
- In the case of moisture absorption and the associated swelling, composite items can exhibit large coefficients of expansion which can give rise to high strains at composite-to-metal interfaces.
- Galvanic corrosion can occur at composite-to-metal interfaces.
- Greater attention should be given to local, highly-loaded design features such as discrete attachment points and bonded joints, because composite material is susceptible to out of plane loads and little local load redistribution is possible owing to the virtual absence of plastic deformation.
- There are often differences in the constraints for drilling or bonding operations, when compared with those used for bolted, riveted or bonded metal structures.

[See also: Glossary for a description of terminology]

31.3 Integrity control programme

For a successful implementation, interdisciplinary control of all activities in all programme phases is necessary, where:

- Design development: The design of a safety-relevant structure is shown to be tolerant to:
  - general deviation, or
  - local imperfection

    NOTE These can be present due to the limited sensitivity of NDI, non destructive inspection.

An integrity control programme for composite structural elements is established in order to achieve the same objective as fracture control of metallic structures, given:

- Global deviations, and

- Local imperfections, inherent in fibre-reinforced plastics,
- Failure mechanisms of composites are significantly different from that of metals.

Figure 31.3.1 shows the logic of a structural integrity control programme applied during development, manufacturing and operation, Ref. [32-1].

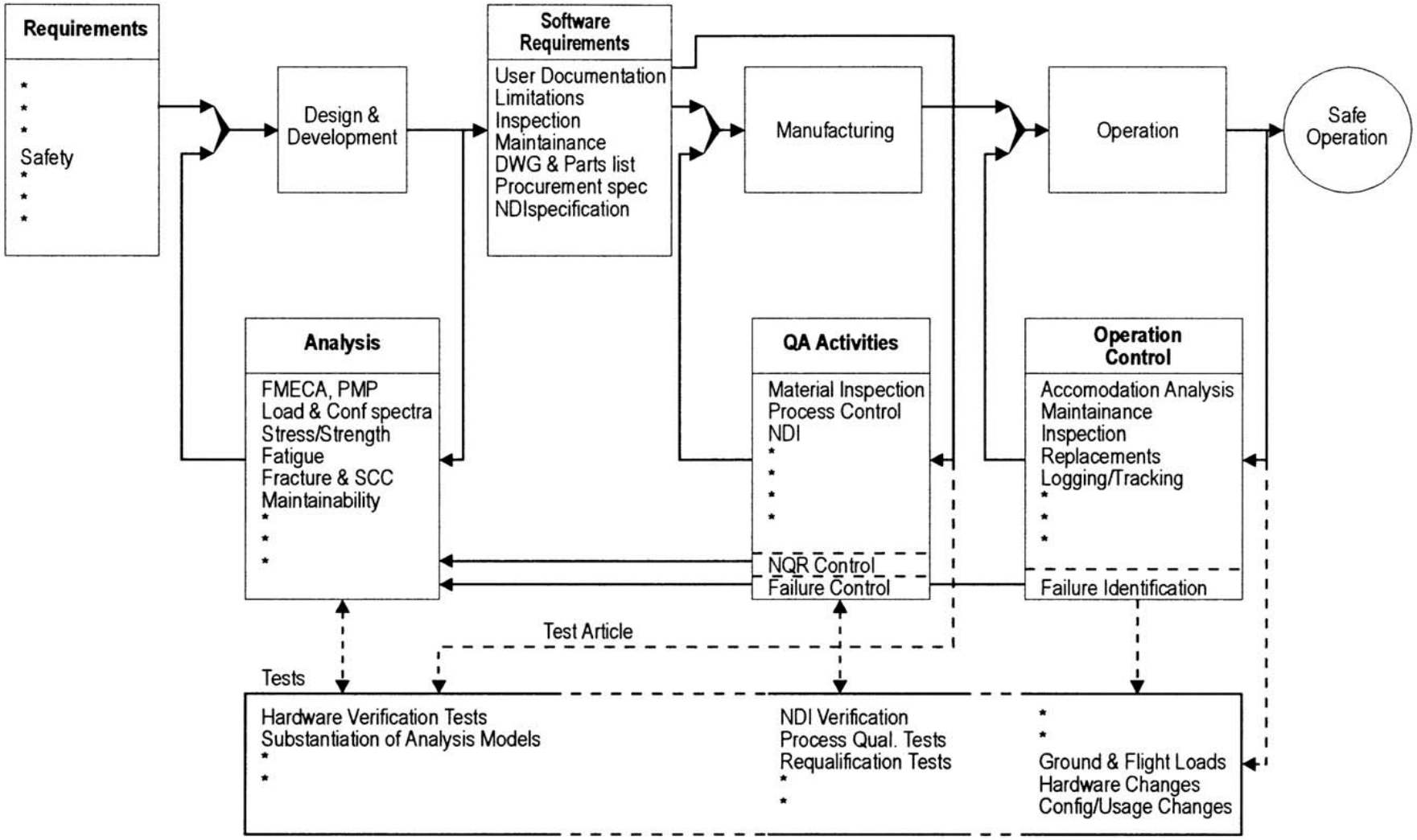

Figure 31.3-1 - Logic of a structural integrity control programme applied during development, manufacturing and operation

The structural capability cannot degrade below the minimum required performance in the design environment, within the operational interval required considering the maximum size of defect, or degree of deviation which might exist i.e.:

- Manufacture: Adequate non destructive inspection and control procedures need to be applied during manufacturing of the hardware to ensure that deviations or imperfections exceeding the tolerable level are reliably excluded.
- In-service: The operation of a structure relevant to a catastrophic failure mode needs further control to ensure that operation is maintained within the design envelopes and the structure is kept in adequate condition by the maintenance required, e.g. by inspection, repair or replacement.

31.4 Materials and design

31.4.1 Materials

31.4.1.1 Specification

The raw materials used in manufacturing composite structures, e.g. fibres, resins, prepregs, adhesives, are suitable for the intended application and be covered by adequate specifications, [See also: 34.2 for fabrication and quality assurance].

[See: ECSS-Q-ST-70 and ECSS-Q-70-71]

31.4.1.2 Availability

The availability of the specified materials is assured for the development and operational lifetime of the structure.

31.4.1.3 Allowables

The material allowables and their related acceptance level are based on statistical analysis of compared test results, unless otherwise agreed. The material properties used as design allowables make allowance for material process variation incurred in the establishment of production hardware, [See also: 37.3].

31.4.2 Design

31.4.2.1 Critical features

For all relevant design cases which include any interactive effects of different loading cases, e.g. effects arising as a result of first ply failure, structural analysis is undertaken to identify the critical structural design features using proven failure criteria.

31.4.2.2 Allowables

Multi-ply allowables are applied in failure criteria. Design allowables used in this analysis are established for each critical design feature by relevant tests taking into account:

- The material allowables are established at the laminate level by tests of the laminate or by tests of the lamina in conjunction with a test-validated analytical method to account for the:
  - orientation,
  - stacking sequence number, and
  - nature of the plies.
- The presence of any residual stresses due to the curing process.
- The effects of any stress concentrations, such as holes and joints.
- The effects of defects, [See also: 8.2; 33.2].
- The actual behaviour of finished components, which includes configuration-related coupon tests using specimens fully representative of the design and manufacture of the flight article.
- Any ageing, including repeated loading and other environmental degradation effects, [See: Chapter 4, Chapter 5 and Chapter 20].
- Existing test data can be used where it is shown to be directly related to the material system, laminate configuration and manufacturing processes.

31.5 Design procedure

31.5.1 General

The design procedure of fracture critical fibre-reinforced plastic elements is in general agreement with those of metallic systems, shown in Figure 31.5.1, Ref. [31-1].

The system layout design, dynamic response evaluation and the generation of design loads form the basis for stress, strength and fatigue life verification by analysis or test, [See: boxes 1 to 6 and 10 to 12 in Figure 31.5.1].

The determination of the maximum deviation or defect tolerable before losing limit load capability, box 7 in Figure 31.5.1, and the degradation of the structure being assumed as imperfect, box 8 in Figure 31.5.1, make it possible to define the necessary requirements for manufacturing and operation.

The activities detailed in boxes 7 and 8 in Figure 31.5.1 represent the major engineering effort with respect to integrity control.

The different design and verification procedures, i.e. safe-life or fail-safe, are used depending upon whether safety is maintained by sufficient slow degradation of the non perfect structure during operation, or by structural redundancy.

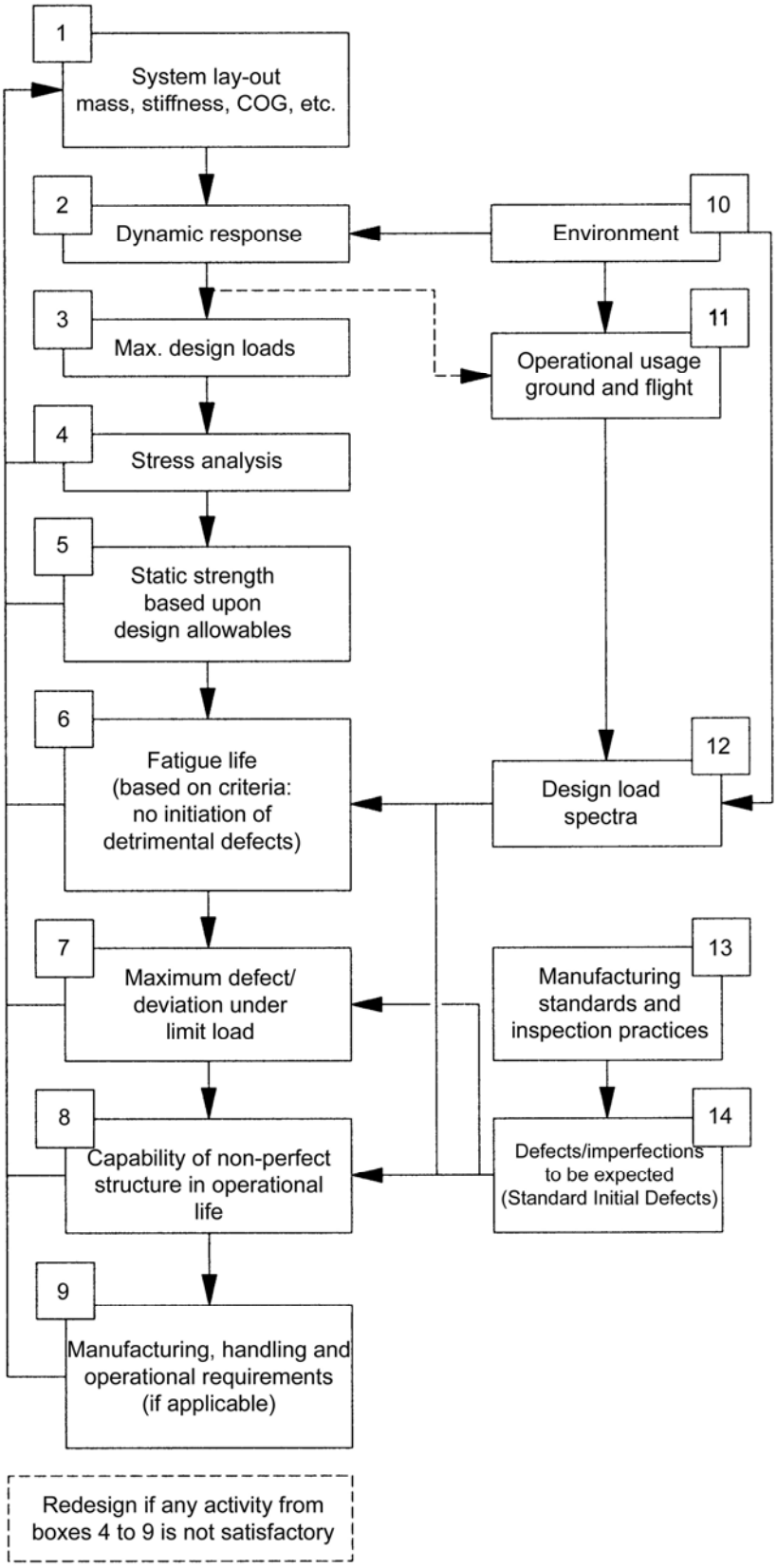

Figure 31.5-1 - Verification logic of potential fracture critical items (PFCI) with respect to integrity control

31.5.2 Test programme

The manufacturer needs to take into account numerous factors during the formulating of a test programme, [See: 32.2, 32.3, 32.4, 34.7 and 34.8].

31.5.3 Inspection and repair

The ability to inspect and repair structural components is established as part of the design process, [See: 34.3; 34.4; 34.5 and 34.6].

[See also: Chapter 8 for NDT and Chapter 41 for repair]

31.5.4 Stiffness charachteristics

The structure meets all stiffness requirements throughout its operational life.

31.5.5 Potentially fracture critical items

Throughout the design development, all potentially fracture critical items, PFCI, are identified that contribute significantly to carrying flight, ground, pressure or control loads and failure of which can alter the structural integrity. The damage tolerance characteristics are confirmed, [See also: 32.2].

Possible effects of impact damage are established and means of accommodating these are included in the design process, e.g. the design strain level can be limited.

[See: ECSS-E-ST-32-01]

31.6 References

31.6.1 General

[31-1] MBB/ERNO (D)
'Integrity control of carbon fibre-reinforced plastics (CFRP) structural elements - Executive summary'
ESA contract 4442/80/NL/AK (SC)

31.6.2 ECSS documents

[See: ECSS website]

ECSS-Q-ST-20	Space product assurance – Quality assurance
ECSS-Q-ST-40	Space product assurance – Safety
ECSS-Q-ST-70	Space product assurance – Materials, mechanical parts and processes.

ECSS-Q-70-71	Space product assurance – Data for the selection of space materials and processes; previously ESA PSS-01-701.
ECSS-E-30 series	Mechanical -
ECSS-E-ST-31	Thermal control general requirments
ECSS-E-ST-32	Structures general requirements
ECSS-E-ST-33-01	Mechanisms
ECSS-E-ST-34	Environmental contaol and life support (ECLS)
ECSS-E-ST-35	Propulsion general requirements
ECSS-E-ST-33-11	Explosive sytems and devices
ECSS-E-ST-32-08	Materials
ECSS-E-ST-32-01	Fracture control; previously ESA PSS-01-401

32
Verification of composite structures

32.1 Introduction

The materials of construction, components and assembled structure are evaluated to ensure that the structural design meets all the stipulated integrity and safety demands.

The evaluation is made using:

- Building block approach, [See: 32.2]
- Global and local structural analysis, [See: 32.3]
- Development tests, [See: 32.4]
- Qualification tests, [See: 32.5]
- Demonstration of damage tolerance, [See Chapter 33]

The guidelines should be read in conjunction with normative ECSS standards ECSS-Q-ST-20; ECSS-Q-ST-40; ECSS-Q-ST-70; ECSS-E-ST-30-series and ECSS-E-ST-32-01.

32.2 Building block approach

32.2.1 General

The design and testing of composite material structures often uses a 'building block' approach.

The overall approach involves progressively increasing the testing complexity and sample size, e.g. from coupon tests to structural tests on sub-assemblies and on full-scale structures.

[See: Figure 33.6.1 for 'building block' approach for test and analysis]

32.2.2 Testing aspects

The tests involved in the building block approach, particularly the larger structural tests, are expensive in terms of specimen production and test set-up. The results only help to provide qualitative empirical data to aid in understanding the response of the structure. The cost of development increases significantly if such tests are repeated in order to confirm an improvement due to the re-design of the geometry of the component.

32.2.3 Damage tolerance

32.2.3.1 General

Damage tolerance demands for many primary structural designs, involves determining the performance of the structural component when in a damaged state. Once the likely damage scenarios are established, the structural tests conducted in the design phase are repeated with the expected damage under the expected operating limits. From the information obtained, component life limitations can be established along with inspection and maintenance intervals.

32.2.3.2 Delamination

Delamination is one of the most serious damage modes in composite structures because it can produce a significant loss of stiffness properties. Delamination can occur from interlaminar stresses arising from geometric or material discontinuities from design features, such as an edge, a hole, a dropped ply or an out-of-plane load.

A delamination, once initiated, grows under fatigue loads. During growth, the structural loads can be redistributed such that another delamination occurs in another location. The delaminations can continue to grow and accumulate until a structural failure occurs, such as buckling or fibre failure. Additionally, a delamination can be arrested and the structure can maintain some integrity. Hence the incorporation of analysis for delaminations is needed for the design of durable and damage tolerant structures.

32.2.3.3 Interlaminar fracture mechanics

Efforts to predict delamination onset and growth have focused on interlaminar fracture mechanics. This approach needs to determine the change in strain energy for a unit area of delamination growth; known as the strain energy release rate, *G*.

The calculated values of *G* are compared with the critical values to determine if a delamination does or does not grow, [See: 14.11].

32.3 Global and local structural analysis

32.3.1 Design philosophy

Figure 32.3.1 is a flow diagram showing an overall global and local design philosophy, incorporating damage tolerance.

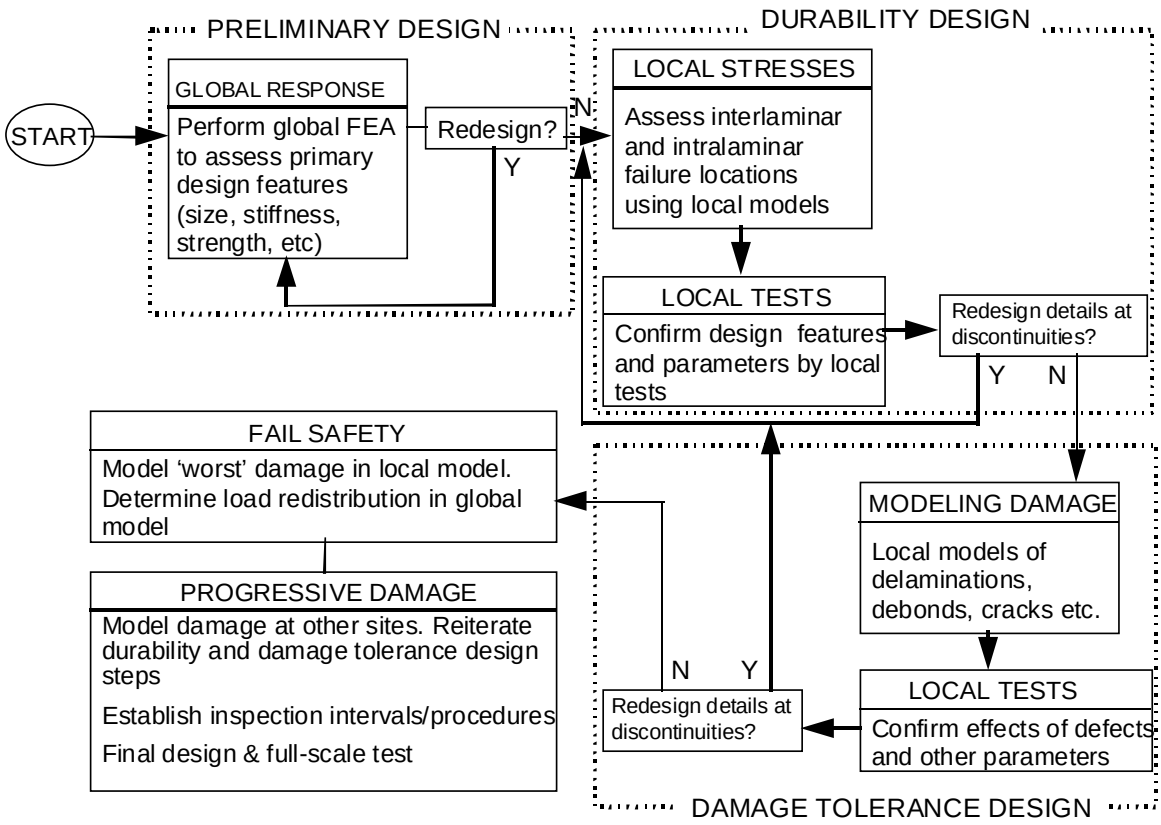

Figure 32.3-1 - The global and local design philosophy

32.3.2 Design steps

The main steps are shown in Figure 32.3.1:

- Preliminary design
- Durability design
- Damage tolerance design

The rationale for conductiong the different types of analyses and tests during these steps is described.

32.3.3 Preliminary design

For an undamaged component, the usual design tools and analyses are used in a global analysis. This is the preliminary design and enables a component to be sized to ensure that the stiffness and strength demands are met.

32.3.4 Durability design

32.3.4.1 General

Further FEA finite element analysis models are used to investigate the likelihood of matrix cracking or interlaminar failure in the durability design phase.

The FEA models used can be either 2-D or 3-D. Often there is a need to model the through-thickness properties. Usually these models are local, i.e. a model of an 'area of concern' with either idealised boundary conditions applied, or the actual boundary conditions from the global model. Global and local modelling techniques are used, Ref. [32-2], [32-3].

32.3.4.2 Local tests

Selection of an 'area of concern' is usually made based on engineering judgement. This is because the global finite element models invariably use 2-D shell elements that do not identify areas of high interlaminar stress. The results of analyses can be confirmed using local tests of such areas. At this level, different design features of the local region can be optimised.

32.3.4.3 Modelling damage

The stress outputs from the local models enable the interlaminar stresses away from any stress singularities associated with geometric discontinuities to be identified. These stresses or strains can be used with suitable failure criteria, such as maximum strain-stress, to determine if an interlaminar failure is likely to occur under static or fatigue loads.

If an interlaminar failure does occur, it appears as a delamination. The extent to which a delamination grows also needs to be determined.

If a delamination is not predicted to initiate, then other structural discontinuities need to be examined. The stresses at these locations are mesh-size dependent and, hence, are indefinite. Thus, the numerical values cannot be used to predict failure in or near such locations. However, the trend of the data is important. Delaminations primarily occur where the interlaminar tension or shear stresses are high. Such areas need to be identified for fracture analysis.

32.3.5 Damage tolerance design

32.3.5.1 Fracture analysis

The fracture analysis is conducted in the damage tolerance design phase. In a damaged structure, invariably the damage is the region where further delaminations can grow, so the type of damage needs to be modelled.

32.3.5.2 Delamination initiation and growth

A damage analysis is conducted for both a damaged component and for a component where damage is expected to initiate. Delamination onset and growth can be modelled using interlaminar fracture mechanics.

If a delamination is present or expected to initiate, then the parameters to determine are how far it grows and whether this amount of growth is critical, i.e. leading to component failure or rendering a component unservicable because of a significant reduction in stiffness.

If component failure does not occur, then the analysis can be stopped, or, another potential delamination site examined to investigate load transfer.

If the delamination does grow to a critical length, then several options are available, i.e.:

- Redesign: If the delamination is from a structural discontinuity, then that local area can be redesigned to prevent delamination initiation from that site.
- Inspection interval: If the delamination grows at a slow rate, then inspection intervals can be established to track the growth of the delamination.
- Repair: If the delamination grows to a critical length during the life of the component, then a repair will be instigated.

With a delamination present, loads can be redistributed causing delamination initiation in other locations.

32.3.5.3 Local tests

Local tests are conducted to help verify and optimise design changes in a damaged component. Both static and dynamic tests are conducted to determine a range of properties.

The static properties considered include:

- General strength, e.g.:
  - tension
  - compression
  - bending
  - torsion
- Structure-related, e.g.:
  - Panel buckling, e.g. shear, compression, bending
  - Strut and column buckling, e.g. compression, bending, torsion
  - Stiffeners and stringer instability, e.g. compression, bending, torsion
  - Attachment strength and gapping, under combined loads
  - Stiffness, alignment and function of systems.

NOTE Limit or ultimate loads are considered, as necessary.

The dynamic properties considered include:

- System response to excitation meets all requirements
- Interfaces to other systems meet all appropriate requirements.

32.3.6 Structural analysis

32.3.6.1 General

A structural analysis is confirmed by appropriate loading of a fully-instrumented structure or component.

The static strength of the composite design is demonstrated through a programme of component ultimate load tests in the appropriate environment. This applies unless experience with similar designs, material systems and loading is available to demonstrate the adequacy of the analysis supported by sub-component tests, or component tests to agreed lower levels.

32.3.6.2 Design load spectrum

The operational loads considered are those occurring during:

- Integration
- Check-out
- Transportation
- Launch
- Operation in orbit, and
- Re-entry.

Depending on the demonstration programme, which is approved by ESA or a delegated ESA authority, static strength and stiffness structural substantiation tests are conducted either on:

- As-produced new structures supported by the findings from tests.
- Structures that have been subjected to environmental exposure, which can include fatigue and standard repair schemes.

32.3.6.3 Coupon, element and sub-component

Test data is provided for coupon, element and sub-component to enable assessment of the possible degradation of static strength after repeated loading and environmental exposure.

The degradation is accounted for in the static test or in the analysis of the results of the static test of a new structure.

A component static test can be performed in an ambient atmosphere, if the effects of the environment are reliably predicted by sub-component or coupon tests, and are accounted for in the static test or in the analysis of the result of the static test.

In order that the test articles are fully representative of the production structure, all static-test items are fabricated and assembled in accordance with the production specifications and processes.

32.4 Development tests

32.4.1 General

32.4.1.1 Objectives

The tests are performed to define and validate data used for modelling and calculation. Furthermore, they are helpful for definition and validation of control and repair procedures, or, for identification of typical dispersions and typical defects on the product. The results can also contribute to the preparation of qualification tests, [See: 32.5].

In detail, the verifications to undertake are:

- Definition and validation of data used in calculation
- Definition and validation of calculation models
- Detection and repair of defects
- Definition and validation of typical dispersions and defects.

32.4.1.2 Data used in calculation

Definition and validation of data used in calculation includes the verification of:

- Static behaviour
- Fatigue behaviour
- Behaviour with defects
- Thermal behaviour
- Environmental effects.

32.4.1.3 Static behaviour

The verification of static behaviour includes:

- Measurement of engineering constants and strength allowables for tensile and compressive loads of typical materials (both ply and laminate), for:
  - running area (strength- and first-ply-failure allowable)
  - material with calibrated holes (strength allowable)
  - lay-ups with typical defects (strength allowable)
  - typical sandwich configurations (strength allowable)
  - laminates with typical bondings (shear allowable)
- Evaluation of allowable loads for:
  - bolted connections
  - bonded connections
- The influence of dynamic components of loads should be taken into account, as necessary
- The tests are such that the evaluation of dispersions (in agreement with a given reliability level) is possible. The dispersion effect is evaluated on many rolls

- The tests are also done for some points with tools and curing cycles identical to the fabrication ones.

32.4.1.4 Dynamic behaviour

The verification of dynamic fatigue behaviour includes:

- Assessment of typical fatigue curves for:
  - material with calibrated holes
  - material with typical defects which might propagate
  - bolted and bonded areas. On these areas, tests are done with *N*-times the real loading sequence; where *N* is stated)
  - evaluation of the delamination resistance of the material system

32.4.2 Behaviour with defects

32.4.2.1 General

The data is tested on representative samples. The models used can have different data.

32.4.2.2 Thermal

Thermal evaluation considers:

- Measurement of coefficient of thermal expansion, thermal capacity and conductivity
- Verification of temperature, thermal cycling and thermal shock effects on static data.
-

32.4.2.3 Environment

Environmental evaluation includes assessment of:

- humidity and ageing effects on static data
- effects of impacts on compressive behaviour, which are included in the global analysis of the structure.
- acoustic effects on parts using representative limit conditions, typical defects, representative noise spectra
- effects of other aggressive environments on the behaviour of the material, e.g. radiation, contact with propellant.

32.4.2.4 Models

Definition and validation of calculation models needs to include the verification of:

- Modelling the lay-up behaviour
- Areas with a hole

- Modelling of bonded areas
- Local loadings
- Load gradients
- Buckling and post-buckling behaviour
- Design allowables.

32.4.3 Modelling of the lay-up behaviour

The tests and analysis conducted to validate lay-up behaviour are:

- Tests to validate elastic calculation and rupture criteria used in models
- Statistical modelling of lay-up based on statistical behaviour of ply.

32.4.4 Areas with a hole

Critical initial defects should be detected with a given level of confidence, [See: 32.4.10].

Allowable initial defects are non-critical initial defects, and are not always repaired. The assessment of the structure with allowable initial defects and critical initial defects takes into account:

- Defects that can propagate, e.g. delamination, inclusions between plies
- Defects that can lead to rupture under given load case, e.g. through-thickness defects, porosity. The behaviour of defect is modelled using validated models.
- Other defects are assumed not to be dangerous, but tests are done in order to verify such statements.

The results are used in a global structural analysis in order to study global modes of failure.

32.4.5 Modelling of bonded areas

A model is used to assess the allowable loads; without and with defect in the bonding. This model is validated on some representative configuration, taking into account the orthotropy of both adherends.

32.4.6 Local loadings

Tests are performed on representative parts with representative limit conditions in order to assess the finite element model prediction.

32.4.7 Load gradients

Variations in loads can occur as a result of thermal gradients, stiffness step, local loading of a stiffener. Tests are performed on representative configurations in order to assess the results of finite-element models.

32.4.8 Buckling and post-buckling behaviour

Representative stiffened panels with representative limit conditions are tested in order to assess the buckling analysis and the post-buckling behaviour.

32.4.9 Design allowable

The design allowables used in the models are fully justified. The philosophy is shown in Figure 32.4.1

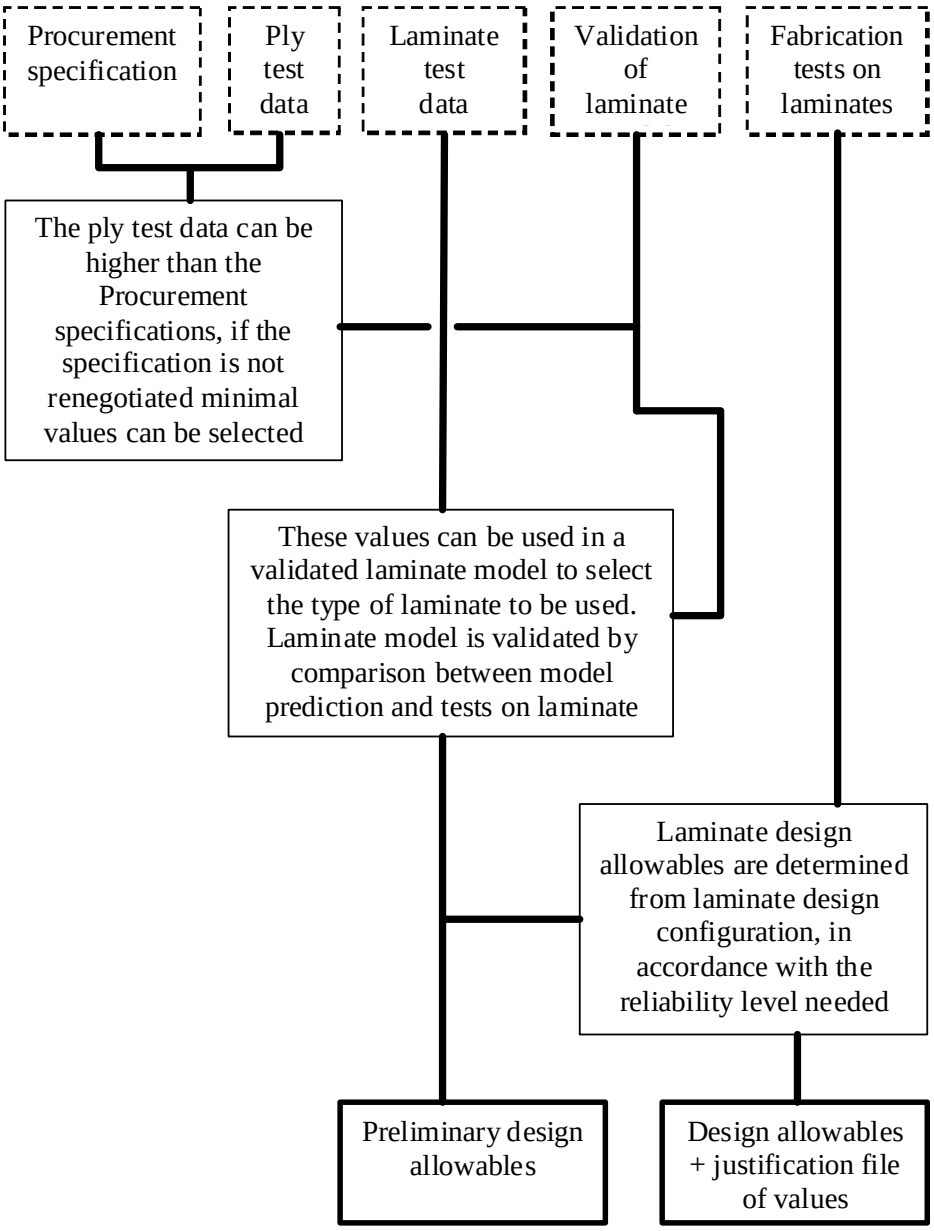

Figure 32.4-1 - Justification philosophy of design allowables

32.4.10 Detection and repair of defects

32.4.10.1 Detection

Allowable initial defects are detected with a given level of confidence. Critical initial defects are repaired. In the detection of defects, the factors to consider include:

- Certified operators are available for defect analysis
- Dedicated inspection tools are used
- Both operator level and tool capacity are checked during tests using representative areas of the structure with representative defects of each type
- A list of allowable initial defects of each type is established using results of the former tests.

32.4.10.2 Repair

When considering the repair of defects in composite structures, the factors that need to be considered include:

- Repair procedures are established with respect to the critical initial defects of each type
- Static and fatigue tests are performed on samples repaired with schemes developed in the procedures. These tests contribute to the validation of the procedures.

32.4.10.3 Defect dispersion

The development phase enables the designer to take into account validated dispersion data in the calculation. A clear understanding of the typical dispersions and defects on the product is needed. The validated dispersion data are also used in order to establish the load values of qualification tests. The dispersions considered include:

- Material dispersions, e.g.:
  - mechanical allowables
  - environmental effects
- Geometrical dispersions after fabrication, e.g.:
  - thickness
  - geometry
- Load repartition dispersions.

Specific testing is developed in order to validate the analysis of dispersions.

32.4.10.4 Typical defects

Typical defects are provided in a qualitative list. This includes:

- The typical defects that the structure can possibly include
- Classification and class descriptions of such defects.

Some main parameters are then defined and given for:

- The description of the given classes
- Some minimum and maximum expected values
- The probability to meet these values.

A production campaign validates the analysis.

32.5 Qualification tests

32.5.1 General

32.5.1.1 Objectives

The objective of qualification tests is to validate the global behaviour of the structure, i.e. whether the structure can sustain the specified mission. They also provide information on weak areas and the failure modes that to be taken into account. Furthermore, such tests are performed to validate the margins of safety and to update the models used for calculation. A procedure on how these subjects can be treated is described.

32.5.2 Validation of global behaviour, weak areas and modes of failure

The validation process covers:

- Among the given load cases, a selection of worst load cases or of envelope load cases are made and justified. This selection covers different modes of failure in order to validate the approach of each case. This selection also enables the designer to recover load distribution of every separate load case. The structure is then instrumented in such a way that a maximum amount of information is recorded regarding:
  - stresses
  - deformations
  - acoustic emission.
- The weakest areas are now carefully instrumented. The instrumentation enables the designer to obtain information concerning the expected mode of failure
- All the results are compared with a test prediction at each step of loading any discrepancies are explained, [See also: 32.5.3; 32.5.4].
- Since composite structures can exhibit very brittle behaviour, maximum use of camera recording devices is made. Internal areas are carefully instrumented.

32.5.3 Margins of safety

To establish margins of safety, the factors considered include:

- Loads to be applied during qualification tests are the design loads (with adequate safety factors), corrected to take into account:
  - discrepancies between the tested specimen and the specimen having the worst characteristics resulting from scattering
  - discrepancies between test conditions and actual working conditions, e.g. loads introduction, simulation of adjacent structures.
- Whereas the sequence of load cases can be done for each case at extreme load, this sequence can either lead to a new load case or to a rupture during the qualification process. Another possibility can be to select a factor k < 1 for the first load cases. The difference is then be covered by analysis performed with the updated model, [See: Updating of models].
- Some worst load cases can be increased up to the rupture of the structure. The rupture test can, for this load case, validate the rupture approach and can (if the case is really the worst one) show the ability of the structure to sustain the expected load (actual safety margins).
- The thermally-induced load cases can be covered by the application of a static load case and corrected, j factors covering the non-represented loads.

32.5.4 Updating of the models used for calculations

The updating of models includes:

- Test results after analysis are compared with test predictions and models are then updated.
- First pre-stacking areas are necessary for composite structures. Results in this load phase are ignored.
- Rigidity tests at rather low level (j = 0.4 to 0.8) are then performed, the results contributing to analysis of:
  - load distributions
  - deformation analysis
  - flexibility matrices.
- Static load tests are then performed and the test results enable the analysis of:
  - nonlinearity
  - stress distribution
  - local buckling
  - first ply ruptures.

These results are used to update the models' prediction behaviour at high loads (j = 1 to extreme). The updated models are then used to update the calculated safety margins of the structure.

32.5.5 Documentation

32.5.5.1 Fracture control

The damage tolerance evaluation of composite structures is based on the fracture control requirements of the normative standard ECSS-E-ST-32-01; previously ESA PSS-01-401.

[See also: 34.25]

32.5.5.2 Proof testing

The use of proof testing for flight articles, as a means of damage tolerance demonstration, can be considered on a case-by-case basis. In considering any such demonstration, it is necessary to review the test level and ensure that:

- The test does not introduce any unwarranted damage, and
- The worst limit load cases are covered by such a test.

[See also: Chapter 33 for aspects of damage tolerance]

32.6 References

32.6.1 General

[32-1] MBB/ERNO
'Integrity control of carbon fibre reinforced plastics (CFRP) structural elements - Executive summary'
ESA Contract 4442/80/NL/AK (SC)

[32-2] C.G. Davilla & E.R. Johnson
'Analysis for Delamination Initiation in Postbuckled Dropped-Ply Laminates'
AIAA Paper No. 92-2226-CP, AIAA, Washington, DC, 1992.

[32-3] R.H. Martin – MERL Ltd, (UK)
'Local Fracture Mechanics Analysis of Stringer Pull-Off and Delamination in a Post-Buckled Compression Panel'
Proceedings of the ICCM-10, Whistler, British Columbia, August 14-18 1995, Volume I, p.253.

32.6.2 ECSS documents

[See : ECSS website]

ECSS-Q-ST-20	Space product assurance – Quality assurance
ECSS-Q-ST-40	Space product assurance – Safety
ECSS-Q-ST-70	Space product assurance – Materials, mechanical parts and processes.
ECSS-Q-70-71	Space product assurance – Data for the

	selection of space materials and processes; previously ESA PSS-01-701.
ECSS-E-30 series	Mechanical -
ECSS-E-ST-31	Thermal control general requirments
ECSS-E-ST-32	Structures general requirements
ECSS-E-ST-33-01	Mechanisms
ECSS-E-ST-34	Environmental contaol and life support (ECLS)
ECSS-E-ST-35	Propulsion general requirements
ECSS-E-ST-33-11	Explosive sytems and devices
ECSS-E-ST-32-08	Materials
ECSS-E-ST-32-01	Fracture control; previously ESA PSS-01-401